

UNIVERSITA' DELLA CALABRIA



Dipartimento di Chimica e Tecnologie Chimiche

Dottorato di Ricerca in Medicina Traslazionale

CICLO XXXIII

**A COMPUTATIONAL MECHANISTIC STUDY OF
POTENTIALLY EVOLVING PLATINUM BASED
ANTICANCER DRUGS**

Settore Scientifico Disciplinare CHIM/03

Coordinatore: Ch.mo Prof. Sebastiano Ando

Supervisore: Prof.ssa Emilia Sicilia

Dottorando: Dott. Eslam Dabbish

Abstract

Metals are known to play a fundamental physiological role inside human body affecting many of the biological functions. Analogously, metal based drugs can also have a similar impact. Cisplatin, a simple platinum complex, is well known to be a cytotoxic agent and the first approved and most widely used metal based drug for fighting cancer. Currently, used platinum containing anticancer agents namely cisplatin, carboplatin and oxaliplatin suffer from serious toxic side effects as well as acquired and inherent drug resistance against many types of cancer. Consequently, new platinum anticancer drug families evolved to overcome the current limitations of traditional platinum drugs. Monofunctional platinum complexes, Pt(IV) complexes, platinum complexes targeting mitochondria, platinum iodido derivatives and photoactivated platinum compounds are examples of some of such newly developed platinum based cytotoxic families.

Computational chemistry has strongly grown over the past years with both the increase in computers capabilities and the development of new theories and efficient algorithms that can allow to handle bigger models in a reasonable time. Molecular modelling can give a wealth of information about the studied systems in terms of energies, electronic properties, geometries, conformations, structure/activity relationships, reaction mechanisms and many others. By using quantum mechanical methods like Density Functional Theory (DFT) and its time-dependant formulation TD-DFT and molecular dynamics (MD) computational tools, the mechanism of action of some selected examples of non-traditional platinum anticancer drug families have been studied in this thesis.

Phenanthriplatin is the most effective member of a new class of platinum anticancer agents (7-40 times more active than cisplatin) known as monofunctional platinum anticancer drugs. In addition, it has started its

clinical trials phase. Our computational mechanistic study of phenanthriplatin highlighted the importance of the role played by its unique chemical structure in the drug activation, interaction with DNA and transcription blockage.

Targeting of mitochondrial DNA by means of platinum drugs can lead to mitochondrial dysfunction in cancer cells that causes tumour cells growth inhibition and apoptosis. We have undertaken a comparative study between three different isomers of a recently prepared triphenyl phosphonium modified monofunctional platinum complexes for their mechanism of action.

Pt(IV) complexes are prodrugs that are reduced inside the body by means of abundant biological reducing agents like ascorbic acid to release the equivalent cytotoxic Pt(II) complexes. This reduction step is considered to be the limiting step for the activity of such class of drugs. In a series of studies, we have carried out a detailed mechanistic study to understand the relation between the nature of Pt(IV) complexes axial and equatorial ligands and the extent and mechanism of reduction by means of ascorbic acid at physiological pH. We highlighted the particular importance and impact of the nature of axial ligands on the reduction process.

Photoactivated chemotherapy (PACT) technique allows the localized activation of drugs by means of specific wavelength light. A recently synthesized complex named platicur is a cis-diammineplatinum(II) complex of curcumin in which the Pt(II) centre is bound to a curcumin molecule as the leaving ligand. Upon light irradiation curcumin molecule is released together with the doubly aquated Pt(II) complex that can exert the required cytotoxic effect. In our study, we have provided a deep insight in the photoactivated excited states and their role in the photocleavage mechanism with the release of curcumin.

Cycloplatinated complexes are known to be very rich in photophysical properties. Attempts are reported for the use of cycloplatinated platinum complexes in photodynamic therapy (PDT) where they act as cytotoxic photosensitizers upon illumination. Computational chemistry can represent a very important tool in studying the photoactivation and excited states properties that are normally not easily accessible experimentally. In this thesis, we have performed a thorough investigation of the behaviour of a model cycloplatinated drug upon light activation interacting with DNA aiming at highlighting the potential mechanisms of action.

Although Pt(II) iodido complexes have long been used as intermediates in the synthesis of several Pt(II) derivatives, they have always been considered not suitable as anticancer agents on the basis of old studies about the cytotoxic activity of cis-[Pt(NH₃)₂I₂] in comparison with cisplatin. More recently, platinum iodido derivatives have been reconsidered and of their cytotoxic effects have been re-evaluated as well as the interest in Pt(IV) iodido derivatives has been renewed as they can work as prodrugs that can be activated by photoreduction. In this thesis, the most relevant steps of iodido Pt(IV) complexes reduction and Pt(II) drugs mechanism of action and eventual deactivation have been computationally explored and compared with the chlorido analogues.

Bioorthogonal catalytic reactions are reactions that can be conducted in a biological system with good selectivity and minimal side reactions. This was the idea recently used to undertake the photoreduction of flavins using an electron source like NADH to lead to the formation of the active reduced catalytic form of flavin that can then cause a catalytic Pt(IV) complexes reduction, liberating the cytotoxic active Pt(II) species and the oxidised flavin that can repeat the cycle once again. This reaction was found to be a photoactivated bioorthogonal catalytic reaction. We have used DFT to study

the different reaction steps suggesting possible mechanisms that agree with the experimental findings.

To my supervisor, you have been always giving me support before I even ask for. Thanks.

To my colleagues, thanks for every personal chat or technical discussion we had, it really meant a lot to me.

To my family, the last but not the least, I couldn't have done this without your sacrifice and support.

Contents

Introduction	v
List of papers included in this thesis	x
I Platinum based Anticancer agents: A Background and Review	1
1.1 An Introduction for Classical Platinum based Chemotherapeutic agents.....	2
1.2 Emergence of non-classical platinum anticancer drugs.....	11
1.3 Monofunctional Platinum (II) drugs, a new era of platinum drugs.....	11
1.4 Platinum drugs targeting mitochondria, towards a smarter platinum drugs.....	16
1.5 Platinum (IV) complexes as prodrugs.....	20
1.6 Platinum drugs in photoactivated chemotherapy (PACT).....	24
1.7 Platinum drugs in photodynamic therapy (PDT).....	27
1.7.1 Cyclometalated platinum complexes and its use as photosensitizers.....	33
1.8 Iodido platinum (IV) and (II) complexes as a potential anticancer agents.....	36
1.9 Bioorthogonal photocatalytic reduction of platinum (IV) prodrugs.....	37
II Theoretical Concepts and Computational Methods	47
III Monofunctional Platinum (II) drugs	63
3.1 Rationalization of the superior anticancer activity of Phenanthriplatin. An in depth computational exploration.....	64
3.1.1 Introduction.....	64
3.1.2 Aim of study.....	66

3.1.3 Highlighting results.....	66
Paper I.....	70
IV Platinum Drugs Targeting Mitochondria.....	121
4.1 A comparative computational mechanistic study on derivatives of pyriplatin, modified with the $-\text{CH}_2\text{Ph}_3\text{P}^+$ group, as anticancer complexes targeting mitochondria.....	122
4.1.1 Introduction.....	122
4.1.2 Aim of study.....	123
4.1.3 Highlighting results.....	124
Paper II.....	126
V Platinum (IV) complexes as Prodrugs.....	143
5.1 Antitumor Pt(IV) prodrugs: a systematic computational exploration of their reduction mechanism by L-ascorbic acid.....	143
5.1.1 Introduction.....	143
5.1.2 Aim of study.....	144
5.1.3 Highlighting results.....	145
Paper III.....	149
5.2 Theoretical exploration of the reduction reaction of monofunctional phenanthriplatin Pt(IV) prodrugs.....	160
5.2.1 Introduction.....	160
5.2.2 Aim of study.....	161
5.2.3 Highlighting results.....	162
Paper IV.....	164
5.3 A multi-methodological inquiry of the behaviour of cisplatin-based Pt(IV) derivatives in the presence of bioreductants with a focus on the isolated encounter complexes.....	179
5.3.1 Introduction.....	179
5.3.2 Aim of study.....	180

5.3.3 Highlighting results.....	180
Paper V.....	183
VI Platinum drugs in Photoactivated Chemotherapy (PACT).....	216
6.1 Mechanism of Action of the Curcumin	
cis-Diammineplatinum(II) Complex as Photocytotoxic Agent....	217
6.1.1 Introduction.....	217
6.1.2 Aim of study.....	218
6.1.3 Highlighting results.....	218
Paper VI.....	222
VII Platinum drugs in Photodynamic Therapy (PDT).....	246
7.1 Anticancer activity, DNA-binding and photodynamic properties of	
a N ^C N-coordinated Pt(II) complex.....	247
7.1.1 Introduction.....	247
7.1.2 Aim of study.....	248
7.1.3 Highlighting results.....	249
Paper VII.....	254
VIII Iodido Platinum (IV) and (II) complexes as	
Potential anticancer agents.....	290
8.1 A computational study of iodido equatorial ligands	
influence on the mechanism of action of Pt(IV)	
and Pt(II) anti-cancer complexes.....	290
8.1.1 Introduction.....	290
8.1.2 Aim of study.....	292
8.1.3 Highlighting results.....	293
Paper VIII.....	296

IX Bioorthogonal Photocatalytic Reduction system

of Pt(IV) Prodrugs.....334

9.1 Riboflavin as a bioorthogonal photocatalyst for Pt(IV)
reduction.....334

9.1.1 Introduction.....334

9.1.2 Aim of study.....337

9.1.3 Highlighting results.....337

Paper IX.....346

Introduction

Since the discovery and FDA approval of cisplatin and its analogues, platinum based anticancer drugs became indispensable in many of the chemotherapeutic treatment protocols, with almost 50% of cancer patients assuming platinum based drugs. Owing to the severe limitations of those traditional Pt(II) anticancer drugs in terms of high toxicity and inherent and acquired drug resistance, a great deal of attention has been focused on the research aiming at overcoming such shortcomings. These efforts have led to the emergence of new non-classical classes of platinum drugs as will be illustrated in this thesis.

In short, the aim of this thesis is the computational study of the mechanism of action of different model systems taken as examples to represent each of these new non-classical classes of platinum drugs. To this aim, Density Functional Theory (DFT), its time-dependant approach TD-DFT and molecular dynamics (MD) have been used as computational tools to accomplish the aim of this thesis.

For a better understanding of traditional platinum (II) complexes and the emergence of the new non-classical potential drugs, a background will be given in **Chapter I** of this thesis. It will focus on cisplatin and its analogues mechanism of action as well as their limitations. A brief description as well as progress about each of these new classes of platinum drugs will be given, while clarifying the motivations of our interest for the systems whose investigation will be illustrated across this thesis.

In **Chapter II**, a concise theoretical background about the methodologies employed for carrying out this thesis will be provided.

The next chapters illustrate the outcomes of the investigations of one or more examples for each class of non-classical compounds taken into consideration in the present thesis.

Monofunctional platinum anticancer drugs differ from traditional cisplatin as they are positively charged and the leaving ligand, able to bind DNA at a single site, is only one. Phenanthriplatin is considered to be the prominent member of this class of drugs, being 7-40 times more active than cisplatin. From experimental findings it is possible to deduce that the drug acts by a mechanism that is different from that of cisplatin. In **Chapter III** of this thesis, the results of a comparative computational mechanistic study of phenanthriplatin and pyriplatin monofunctional complexes and cisplatin. How the nature of the only labile ligand in phenanthriplatin and pyriplatin impacts on the activation steps of the drugs, their interaction with the DNA and transcription blockage will be clarified.

Targeting of mitochondrial DNA is becoming one of the novel strategies for fighting cancer. Mitochondrial dysfunction in cancer cells cause inhibition of tumor cells growth and ultimately leads to apoptosis. The use of the monofunctional platinum drug pyriplatin as a backbone modified by means of the mitochondria directing cationic functional group triphenyl phosphonium, owing to its lipophilicity and cationic character, has been recently reported. Three different isomers have been prepared and have shown a difference in cytotoxic activity and mitochondrial localisation. In **Chapter IV**, we have undertaken a comparative study between the different isomers in their mechanism of action.

Pt(IV) complexes are considered to be prodrugs that, upon reduction inside the cell by means of biological reducing agents such as ascorbic acid and glutathione, release the corresponding active Pt(II) forms that exert the required cytotoxic effect. Pt(IV) pro-drugs have been developed to overcome the shortcomings of traditional Pt(II) drugs like high toxicity and unwanted side reactions with biomolecules. More inert Pt(IV) prodrugs with six-coordinate and octahedral geometries are designed to improve cytotoxicity and efficacy as well as flexibility in controlling drug properties by means of the

nature of axial ligands. Given the importance of Pt(IV) drugs reduction step, we have focused, in **Chapter V**, on the exploration of the reduction mechanism using ascorbic acid as reducing agent. In addition, the effect of changing the nature of axial and equatorial ligands on the reduction mechanism has been examined.

One of the strategies, when designing Pt(IV) complexes, is to use axial ligands that can help in directing the drug to a specific target or organ. A Pt(IV) derivative of phenanthriplatin with a hydroxido and a carboxylato axial ligands linked to a targeting group is one of the recent approaches. We have studied (**Chapter V**) the mechanism of reduction of phenanthriplatin Pt(IV) derivative having a hydroxido and acetate axial ligand by means of ascorbate.

The reduction process of $\text{Pt}(\text{Cl})_2(\text{NH}_3)_2(\text{OH})_2$ and $\text{Pt}(\text{Cl})_2(\text{NH}_3)_2(\text{OH})(\text{Ac})$ was studied (**Chapter V**) with both an experimental (mass spectrometry and ^{15}N -NMR) and a computational complementary work to understand the mechanism of reduction by means of ascorbate and the potential liberated moieties out of the reduction process.

Photoactivated platinum complexes and platinum complexes acting as photosensitizers are examples of novel approaches that allow localised activation of anticancer drugs by means of light of specific wavelength illumination for minimising the drug toxic side effects. A recently developed Pt(II) complex named platicur, a complex in which Pt(II) is bound to curcumin molecule as leaving group with two ammonias as a non-leaving ligand, shows cytotoxic activity only upon light activation with minimal dark toxicity. We have thoroughly explored the mechanism of action of platicur with special focus on the photoactivation mechanism and possibility of dark toxicity. DFT and TD-DFT approaches have been used to understand the photophysical properties of the new complex and the mechanism of curcumin release as described in **Chapter VI**.

Cyclometalated platinum complexes are known to have unique photophysical properties which makes them potential candidates to be used as photosensitizers, the presence of the platinum centre enabling control over intersystem crossing (ISC) efficiency, which is related to how easily spin-forbidden excited states can be accessed. A N[^]C[^]N cycloplatinated(II) complex has been studied (**Chapter VII**) as an example of potential platinum based photosensitizers.

Although on the basis of old studies Pt(II) iodido complexes have been considered to be not pharmacologically suitable as cytotoxic agents compared to corresponding chlorido analogues such as cisplatin, on the basis of recent investigations, they have been reconsidered as possible anticancer candidates. In addition, Pt(IV) iodido derivatives represent one of the very initial attempts of developing Pt(IV) complexes that can only be reduced by light. Further studies demonstrated that such complexes are toxic in dark because of their rapid reduction by endogenous reducing agents such as ascorbic acid. Based on the above mentioned renewed interest, we have investigated in **Chapter VIII** of this thesis the mechanism of reduction of Pt(IV) iodido derivatives relative to their chlorido analogues as well as the mechanism of action of the released Pt(II) iodido complexes relative to cisplatin.

Based on a novel pioneering work, a biorthogonal photoactivated catalytic system has been recently reported as a new approach for reducing dark stable Pt(IV) complexes. Riboflavin has been reduced in presence of light by means of NADH to liberate the reduced catalytically active form of riboflavin, which in turn undergoes the reduction of the studied Pt(IV) to liberate the Pt(II) form together with the regeneration of the riboflavin oxidised form that can then repeat the steps of the catalytic cycle. Aiming at rationalizing experimental findings and in combination with them, we have computationally studied in **Chapter IX** the mechanism of reaction between

NADH and oxidised riboflavin as well as Pt(IV) reduction mechanism upon reaction with the reduced form of riboflavin.

List of papers included in this thesis

I) Rationalization of the superior anticancer activity of Phenanthriplatin. An in depth computational exploration.

E. Dabbish, N. Russo, E. Sicilia, *Chem. Eur. J.*, **2020**, *26*, 259-268.

II) A comparative computational mechanistic study on derivatives of pyriplatin, modified with the $-\text{CH}_2\text{Ph}_3\text{P}^+$ group, as anticancer complexes targeting mitochondria

E. Dabbish, A. G. Ritacca, G. Mazzone, E. Sicilia, *Inorganica Chimica Acta*, **2020**, 119863.

III) Antitumor Pt(IV) prodrugs: a systematic computational exploration of their reduction mechanism by L-ascorbic acid

E. Dabbish, F. Ponte, N. Russo, E. Sicilia, *Inorg. Chem.*, **2019**, *58*, 3851-3860.

IV) Theoretical exploration of the reduction reaction of monofunctional phenanthriplatin Pt(IV) prodrugs.

E. Dabbish, D. Imbardelli, N. Russo, E. Sicilia, *Inorganica Chimica Acta*, **2019**, 118951.

V) A multi-methodological inquiry of the behavior of cisplatin-based Pt(IV) derivatives in the presence of bioreductants with a focus on the isolated encounter complexes.

D. Corinti, M. E. Crestoni, S. Fornarini, E. Dabbish, E. Sicilia, E. Gabano, E. Perin, D. Osella, *Journal of Biological Inorganic Chemistry*, **2020**, *25*, 655-670.

VI) Mechanism of Action of the Curcumin cis-Diammineplatinum(II) Complex as Photocytotoxic Agent

E. Dabbish, G. Mazzone, N. Russo, E. Sicilia, *Inorg. Chem. Front.*, **2020**, *7*, 2759-2769.

VII) Anticancer activity, DNA-binding and photodynamic properties of a N[^]C[^]N-coordinated Pt(II) complex

Eslam Dabbish, Stefano Scoditti, Nino Russo, Gloria Mazzone, Emilia Sicilia
Manuscript to be submitted (included)

VIII) A computational study of iodido equatorial ligands influence on the mechanism of action of Pt(IV) and Pt(II) anti-cancer complexes

Stefano Scoditti, Vincenzo Vigna, Eslam Dabbish and Emilia Sicilia
Manuscript submitted

IX) Bioorthogonal Photocatalytic Reduction system of Pt(IV) Prodrugs. Riboflavin as a bioorthogonal photocatalyst for Pt(IV) reduction.

Manuscript under preparation

Chapter I

**Platinum based
Anticancer agents: A
Background and
Review**

Chapter I Platinum based Anticancer agents: A Background and Review

This chapter provides a condensed review of classical and non-classical platinum anticancer drugs classes with a special emphasis on cases of interest in each class, whose properties and mechanism of action will be covered in later chapters as model systems.

1.1 An introduction for classical platinum based chemotherapeutic agents

Cancer is a widely spread disease worldwide and the second cause of death in the United states after heart disease. In 2020, 1.8 million new cancer cases and 606,520 cancer deaths are expected in the United States according to the American cancer society. Cancer is known to be the abnormal growth of cells that, instead of undergoing the normal cell cycle that ends with cell death, abnormally keep growing forming a lump named tumour. Many therapeutic approaches can be adopted to control the growth of cancer cells. One of these is the use of chemotherapeutic agents, which are expected to kill the cancer cells without harming the normal functioning ones.

Cisplatin is a simple neutral square planar compound with a divalent platinum centre covalently bound to two chlorido and two ammonia ligands in a *cis* configuration (**Figure 1.1**). It can be readily synthesised from potassium tetrachloroplatinate using a simple synthetic procedure. Chemical formula and structure were determined well before the discovery of its antineoplastic activity by the Italian scientist Michele Peyrone. Only in the early 1960s Rosenberg highlighted the potential antineoplastic activity of cisplatin carrying out an experiment with the original aim of studying the electric field effect on cells.¹⁻⁴ An alternating electric current was passed through a culture of Escherichia Coli and platinum was the, assumed inert, metal chosen for the electrodes. Coincidentally, the experiment resulting in

cell inhibition due to DNA damage, turned out to be a major breakthrough on how to control cancer cells growth that Rosenberg later supported by investigating the anticancer properties of cisplatin on a group of animal tumours including sarcoma 180 and Leukaemia L1210 with excellent results leading to preclinical and clinical studies and FDA drug approval in 1978.¹⁻⁴

Since the discovery and FDA approval of cisplatin and its analogues, platinum based anticancer drugs became indispensable in many of the chemotherapeutic treatment protocols with almost 50% of cancer patients assuming platinum based drugs.^{5,6} In spite of such widespread use, administration of platinum based drugs, including their lead compound cisplatin, is accompanied by many disadvantages such as the inherent and acquired drug resistance. That is, some types of cancer cells initially do not show any effect upon treatment with platinum drugs or some cancer cells, due to an evolutionary behaviour, start to develop a resistance against known platinum drugs. In addition, platinum based drugs show some severe toxic side effects damaging liver, kidneys, ears etc.^{5,7,8}

As a consequence, lots of research efforts have been focused on the deep understanding of the mechanism of action of the lead first metal based chemotherapeutic agent cisplatin and its analogues as well as the development of new platinum drugs that are more effective and less toxic than cisplatin..

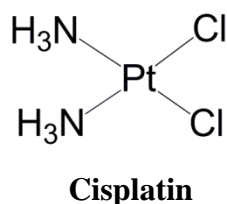


Figure 1.1 Chemical structure of cisplatin

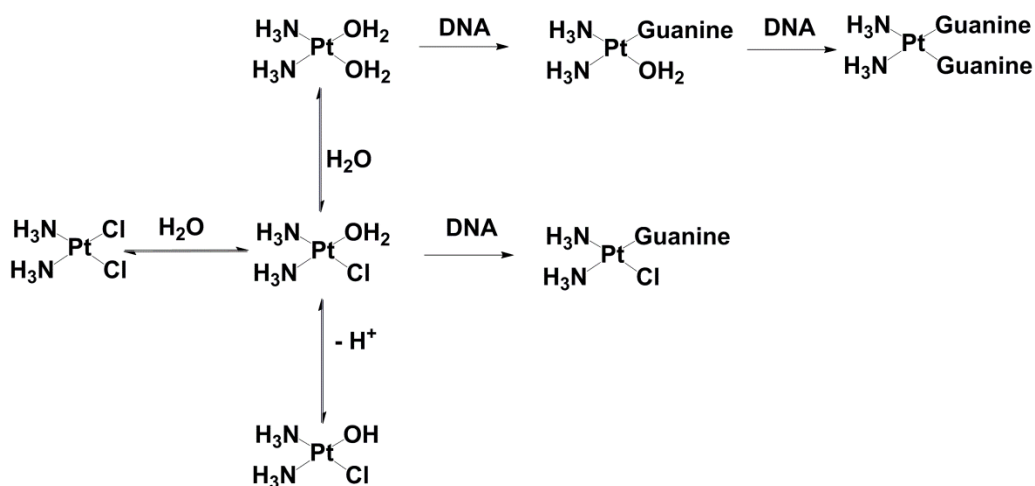
The first outcome of such efforts was that the nuclear DNA of the cancer cells is the main target for cisplatin to which it binds in a various binding modes leading to a strong perturbation and inhibition of many of the cell metabolic activities and preventing DNA transcription and replication processes. Regular cell metabolic pathways are disturbed, several apoptosis pathways are activated ultimately leading to cell death.⁹⁻¹³ Cisplatin showed anticancer activity in several types of cancer such as ovarian, lung, cervical, gastric and other types of cancer.

Although DNA is the ultimate target of cisplatin, before to reach this target, the travel of the drug through the bloodstream requires a detailed understanding of the mechanism of action, including drug transport, cellular uptake, aquation, DNA binding and resulting cellular implications, of the drug that can later help in drug improvement and development of more effective and less toxic new generations. Cisplatin is usually administered intravenously. In blood, chloride concentration is relatively high, 100 mM, protecting cisplatin by aquation, even if the risk exists of binding to sulphur or histidine containing peptides or proteins like plasma albumin.¹⁴⁻¹⁶ This off target binding of cisplatin to various proteins can correspond to an average of 80% of the administered dose of platinum.¹⁷ Beside the caused toxic effects, such off target bindings can be also responsible for the cisplatin-resistance for some types of cancer.

In order to penetrate into the cells, it was found that cisplatin is transported across the cell membrane by means of passive diffusion and CPT1 and CPT2 copper transporters.^{18,19} Some structurally related platinum drugs like Oxaliplatin might additionally use some other types of transporters known as organic cation transporters OCT. After cisplatin enters the cell, due to the much lower chloride concentration, 3-20 mM, labile chlorides coordinated to platinum start to be to be attacked and substituted by water molecules. The first chloride is replaced by one water molecule yielding a mono-aquated

cisplatin moiety. This reaction can be followed by a second aquation step in which the second chloride is substituted by another water molecule. It is still matter of debate whether monoaquated cisplatin is the active form of the drug capable to penetrate the nuclear membrane and to start exerting its action (**Scheme 1.1 and Figure 1.2**).

In fact, the monoaquated form is, likely, too reactive to allow the doubly aquated form to be observed. Inside the cell cytoplasm and upon aquation, cisplatin can still participate in side reactions of binding to free aminoacids, glutathione, peptides, proteins or free nucleotides. Indeed, the monoaquated cisplatin is about 10-70 times more reactive than intact cisplatin because of the increased possibility to replace water compared to chloride.¹⁹⁻²¹ Experimental evidence shows that only 1% approx. of administered platinum drug dose succeeds in reaching the nuclear DNA target.²²



Scheme 1.1 Cisplatin aquation reaction and interaction with guanine

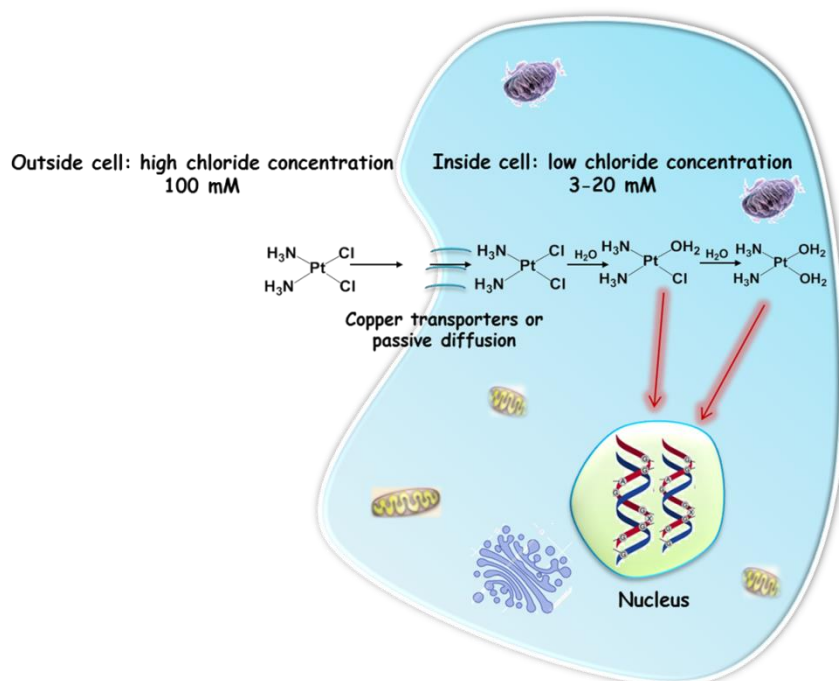


Figure 1.2 A schematic representation for the cisplatin entrance into the cell followed by aquation and penetration into cell nucleus

It is important to point out that the aquated forms of cisplatin can undergo deprotonation depending on its pka and pH of the medium where the deprotonated hydroxide form are relatively inert to substitution. The aquated form of cisplatin interacts with the DNA by covalently binding to DNA by means of active nitrogen atoms of several nucleotides which substitute the water molecules and bind to the platinum centre. Studies have revealed that the N7 of guanine is the most reactive site for platinum attack compared to adenine, thymine or cytosine.²³⁻²⁵ Being cisplatin bifunctional with two leaving groups, it can crosslink to DNA by binding to two different sites by same platinum centre with a prevalence of intrastrand crosslinks with about 95% in a 1,2-d(GpG) mode rather than 1,3-d(GpXpG) or interstrand modes accounting for about 2% each.^{24,26} As expected, most of the crosslinks are of guanine-guanine type owing to the binding preference for guanines followed by guanine-adenine types (**Figure 1.3**). Although bifunctional, cisplatin can bind to DNA in a monofunctional form even if the probability is very low.

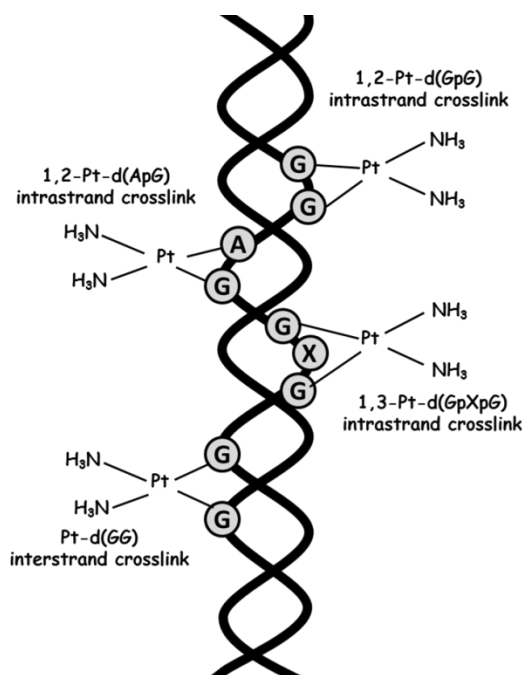


Figure 1.3 Different binding modes of cisplatin with DNA showing the 1,2-Pt-d(GpG), 1,2-Pt-d(ApG), 1,3-Pt-d(GpXpG) and Pt-d(GG) binding modes.

Cisplatin structure was, obviously, chosen to establish the classical structure activity relationship for platinum anticancer drugs. It was accepted for years that cisplatin features: divalent platinum, neutral, square planar with two cis leaving groups and two cis ammine groups allow a drug to manifest anticancer properties. At the same time, due to cisplatin and its derivatives shortcomings several platinum drugs were developed and fine-tuned to control aquation and leaving group lability and, thus, attempting to control the activity and toxicity of the newly potentially developed drugs.⁸ Two FDA approved cisplatin analogues Oxaliplatin and Carboplatin were developed in which the two chlorides are substituted by oxalic acid and cyclobutane dicarboxylic acid, respectively (**Figure 1.4**).⁸ While the two ammonias are replaced by diaminocyclohexane in oxaliplatin carboplatin retains the two ammonia ligands.⁸

As it can be expected, the aquation process of carboplatin is slower than that of cisplatin as the chlorides are better leaving groups compared to dicarboxylates. Carboplatin is a less potent drug in many types of cancer, like bladder and head and neck cancer, while comparable results were obtained for in few others like lung and ovarian cancer.^{27,18} At the same time, carboplatin resulted to have much less toxic side effects such as nephrotoxicity, ototoxicity and neurotoxicity while it is still suffering from myelosuppression side effect.^{27,28} Carboplatin has a similar behavior to cisplatin in terms of DNA binding and induced cell apoptosis.

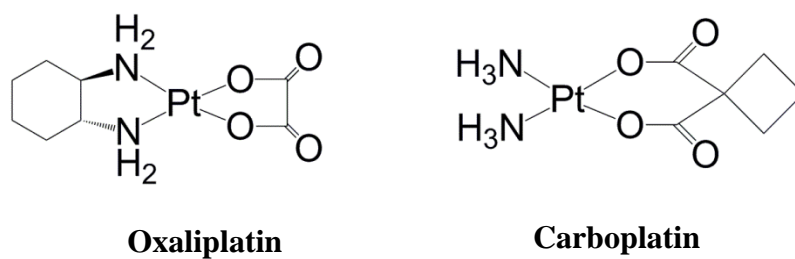


Figure 1.4 Chemical structures of Oxaliplatin and Carboplatin

Oxaliplatin, which is considered to be the third generation of classical anticancer drugs, is especially suitable in colon cancer cases not responding to cisplatin treatment. Owing to its carboxylate leaving groups, it shows a better stability compared to cisplatin. Oxaliplatin is thought to act through binding to DNA, but adopting a different mechanism that, with respect to cisplatin, leads to apoptosis more efficaciously affecting cell transcription and translation processes.⁷ Although less toxic than cisplatin, oxaliplatin suffers from neurotoxicity.⁷

Other than the three FDA approved drugs, cisplatin, carboplatin and oxaliplatin, some other drugs have been approved for their use in specific countries like heptaplatin (Korea), lobaplatin (China), miriplatin (Japan), and nedaplatin (Japan) (**Figure 1.5**).

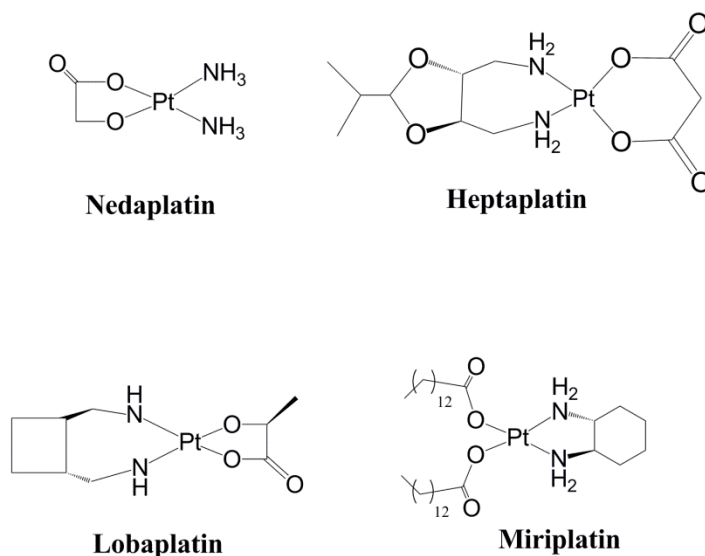


Figure 1.5 Chemical structures of Nedaplatin, Heptaplatin, Lobaplatin and Miriplatin

In the literature can be found many examples testifying the continuous research of new Pt(II) drugs according to classical SAR rules. In the next paragraphs a few cases are reported that represent steps forward. In an attempt to optimise the nature of the two amine ligands in cisplatin and inspired by the DACH moiety effect in Oxaliplatin, Natile et al synthesised a bicyclic based 1,4-diaminobutane like structure (**Figure 1.6**, complex **1**) and studied the effect of amine non-leaving group bound to the platinum centre. The bicyclic bulky nature of the amine group helped in increasing steric hindrance, structural flexibility with opportunity to fine tune the drug lipophilicity. A group of the synthesised drugs were found to be more active than cisplatin.²⁹

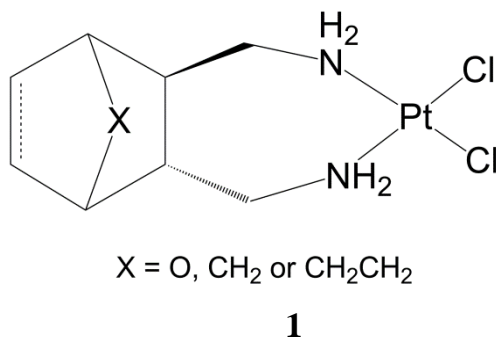


Figure 1.6 Chemical representation of the family of drugs prepared by Natile et al. (complex **1**)

Beside the dicarboxylate groups, the use of β -diketonate as the leaving group was also investigated by more than one research group. Lippard and his co-workers have studied the effect of using acetylacetonate and its fluoro and phenyl derivatives on the antineoplastic activity of a set of prepared platinum drugs with two regular ammonias as non-leaving groups (**Figure 1.7**, complex **2**).³⁰ It turned out that this class shows a chelating nature similar to that of carboplatin. Therefore, this potential group of platinum drugs merits, likely, to be further studied.

Out of many synthesised β -diketonate complexes, Fanizzi and Marsigliante found [Pt(*O,O'*-acac)(γ -acac)(DMS)] to be extremely promising compared to cisplatin in terms of chemotherapeutic effect, pharmacological properties and toxicological profile. [Pt(*O,O'*-acac)(γ -acac)(DMS)] was found to be 100 times more active than cisplatin against endometrial cancer cells, HeLa cells, with a mechanism of action expected to be different with respect to cisplatin owing to low reactivity towards nucleobases (**Figure 1.7**, complex **3**).^{31,32} On the other hand, the drug showed a specific reactivity to sulphur containing ligands like some amino acid residues in proteins.

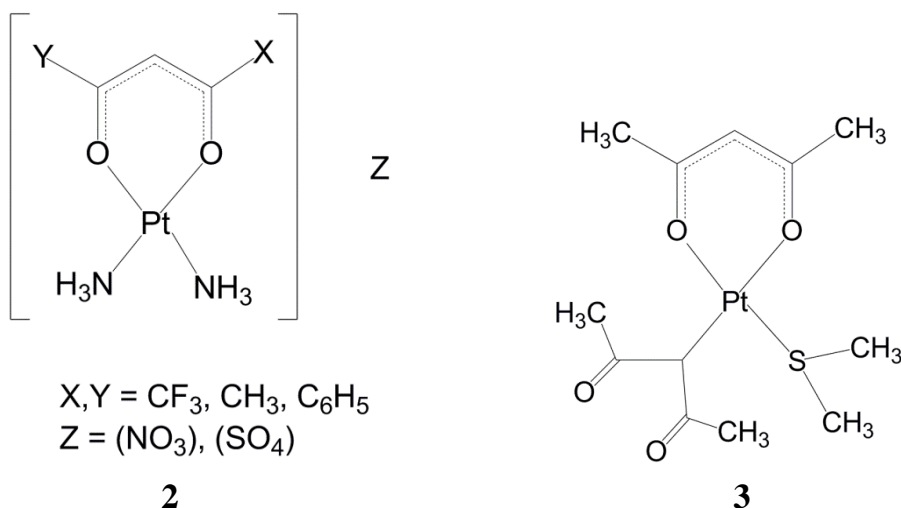


Figure 1.7 Chemical representation of the family of drugs prepared by Lippard (**2**) and Marsigliante (**3**)

1.2 Emergence of non-classical platinum anticancer drugs

Although the research illustrated here aimed at obtaining less toxic and more efficacious drugs, these efforts have led to the emergence of new non-classical classes of platinum drugs. A short review will be given for every class with a special focus on the potential drugs that will be studied in later chapters.

1.3 Monofunctional platinum (II) drugs, a new era for platinum drugs

This class of platinum drugs has been thought to be inactive as cytotoxic agents based on the early studies of the $\text{Pt}(\text{NH}_3)_3\text{Cl}$ and $\text{Pt}(\text{NH}_3)(\text{en})\text{Cl}$ complexes. Later, Hollis et al in 1989 prepared a long list of drugs having a N-heterocyclic donating ligand instead of one of the ammonias and, for the first time, an antineoplastic activity for this non classical class of platinum drugs was detected (**Figure 1.8**).^{33,34}

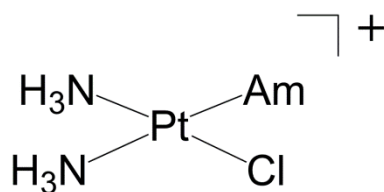


Figure 1.8 A general chemical structure of the monofunctional platinum complexes as presented by Holis and co-workers

On the other hand, Bierbach and co-workers thoroughly tested a new series of monofunctional platinum drugs with one ammonia replaced by an acridine moiety linked to the platinum by means of a diamine (**4**) or a thiourea (**5**) (PT-ACRAMTU) spacer that directly binds to platinum (**Figure 1.9**). This class of drugs was found to both bind to and intercalate into the DNA showing a high in vitro cytotoxicity and a potent inhibitory ability of DNA synthesis and transcription.³⁵⁻⁴⁰

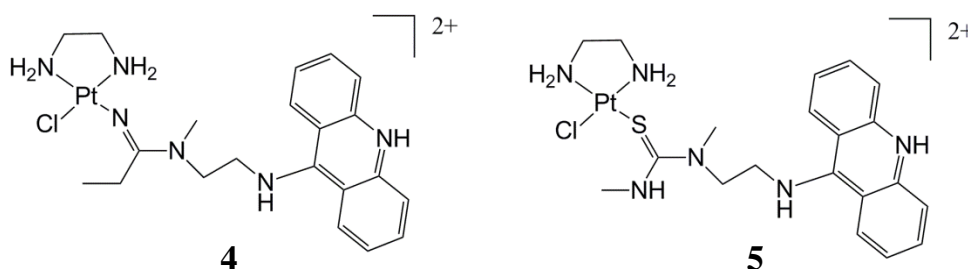
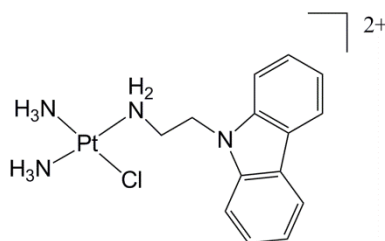


Figure 1.9 An example of monofunctional platinum complexes prepared by Bierbach with diamine (**4**) thiourea (**5**) spacer

In 2017, Lee et al have reported a monofunctional platinum complex having a carbazole group as an aromatic platinum binding ligand (**Figure 1.10**). It was revealed that the complex got the capability of both DNA intercalation and covalent binding however it doesn't cause a significant DNA distortion. The newly prepared complex given the name carbazoleplatin was found to be 8 times more cytotoxic than cisplatin against triple negative breast cancer (MDA-MB-231) cell lines.⁴¹



Carbazoleplatin

Figure 1.10 Chemical structure of carbazoleplatin

According to Hollis approach, Pyriplatin having a pyridine ring as the N-heterocyclic ligand, is the first known monofunctional platinum drug that was demonstrated to possess a significant antineoplastic activity with a different cellular profile comparable, even if still inferior, to cisplatin (**Figure 1.11**). Unlike cisplatin, this class of platinum drugs are positively charged with only one chloride leaving ligand and three amine donating ligands.^{33,42}

The Positively charged nature of those new complexes plays a role such that it was found that organic cation transporters play an important role in the mechanism by which the monofunctional platinum drugs are up taken by the cells supported by the fact that cancer cells having overexpressed OCTs are more efficiently killed than those that do not.⁴³

The opposite happens for cisplatin which relies more on copper transporters. Nevertheless, in analogy with cisplatin, monofunctional platinum drugs undergo aquation, that is prevented in blood due to the relatively high concentration of chlorido ions and promoted inside the cell where chloride concentration is much lower. Aquation is then followed by DNA binding which, contrary to cisplatin, involves only a DNA single site interaction due to the monofunctional nature of the complex without the possibility of inter or intra strand crosslinking.⁴⁴⁻⁴⁷

Pyriplatin, as well as other monofunctional drugs, was reported to bind to DNA at the N7 position of guanine base without causing significant distortion in DNA but inhibiting the transcription process. The hypothesis that this class of drugs adopt a different mechanism of action compared to classical platinum drugs difference in the mechanism of RNA polymerase II inhibition by pyriplatin-DNA adducts with respect to the inhibition observed with cisplatin-DNA adducts.^{42,44,46}

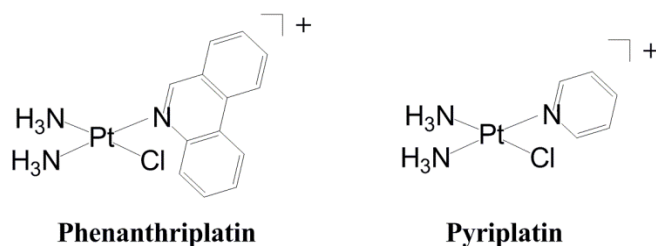


Figure 1.11 Chemical structures of Phenanthriplatin and Pyriplatin

Taking into consideration that Pyriplatin is more than 10 times less potent than cisplatin and the importance of the steric effect and aromatic nature of the pyridine ring in pyriplatin activity, Lippard et al systematically varied the N-heterocyclic ligand until the discovery of phenanthriplatin having phenanthridine ring as the N-heterocyclic ligand (**Figure 1.11**).^{44,45,47-52}

This result is also the fruit of many old efforts by Murray et al, back in 1998, to synthesize platinum complexes having phenanthridine ring in an indirect attachment to the platinum centre and thus conserving the traditional bifunctional structure (**Figure 1.12**, complex **6**). Murray's idea relied on the structural similarity between the DNA stain ethidium bromide, known to be a DNA polymerase inhibitor because of its ability to bind to DNA, and the phenanthridine ring which represents a part of the ethidium bromide structure (**Figure 1.12**).⁵³

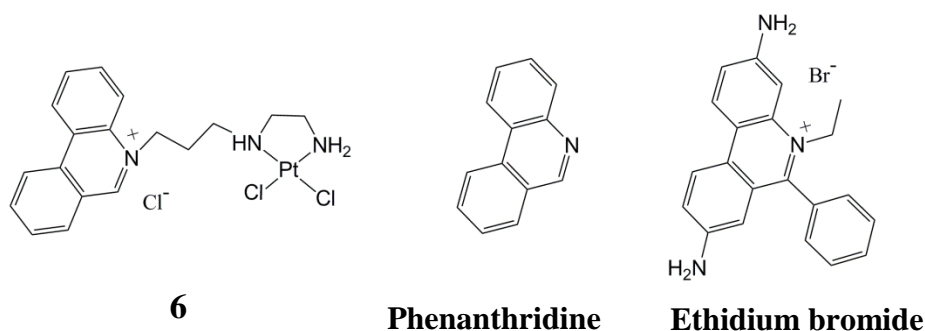


Figure 1.12 Chemical structure of Pt(II) complex with phenanthridine derivative side chain as prepared by Murray et al. (6) showing the structure similarity relative to phenanthridine ring and ethidium bromide.

Phenanthriplatin was found to be 7-40 times more active than cisplatin with a distinct pattern of activity. Phenanthriplatin was found to be able to covalently bind to the DNA at a single site without significant DNA distortion just like pyriplatin. However, the phenanthridine ring is known to have a DNA intercalating capability. At the same time, the substitution of the pyridine ring with phenanthridine caused a sharp increase in the drug cytotoxic effect which supports the assumption of the pivotal role played by the aromatic heterocyclic ligand in the drug mechanism of action including transcription.⁴⁷⁻⁵² Additionally, as phenanthriplatin is a chiral molecule, it has been also explored the possibility that chirality can have an impact on the drug mechanism of action.

In Chapter III of this thesis, the outcomes of our attempts to rationalise the high potency of phenanthriplatin and the investigation of the drug activation steps and mechanism of action with emphasis on the role of intercalation and transcription blockage in comparison to the less active analogue pyriplatin and the lead compound cisplatin.

1.4 Platinum drugs targeting mitochondria, towards a smarter platinum drugs

In previous studies, it has been suggested that sub-cellular compartments other than nuclear DNA can be the targets of platinum complexes.⁵⁴

Among those targets such as enzymes, proteins or non-nuclear cell organelles, mitochondria have been proved to be potential targets for platinum antineoplastic agents.^{55,56}

As a consequence, targeting mitochondria is attracting attention as one of the novel strategies for fighting cancer.⁵⁷

Mitochondria play a key role in the cells generating most of the chemical energy needed to power the cell biochemical reactions. Chemical energy produced by the mitochondria is stored in the small adenosine triphosphate (ATP) molecule. Since mitochondrial dysfunction in cancer cells cause damaging alterations in energy production pathways, mitochondrial metabolism can represent a potential target for cancer therapy to inhibit tumor cells growth and ultimately leading to apoptosis.^{58,59}

Complexes having mitochondria-targeting properties might result in a promising evolution in platinum-based anticancer drugs. Liang and co-workers have prepared a platinum complex of 8-substituted quinolone, named Mon-Pt-2 (**Figure 1.13**), targeting mitochondria and was found to be more effective than cisplatin and less toxic in a mouse model of cancer. This was attributed to the localization of the drug in mitochondria affecting ATP and ROS production by decreasing the former and increasing the latter.⁶⁰

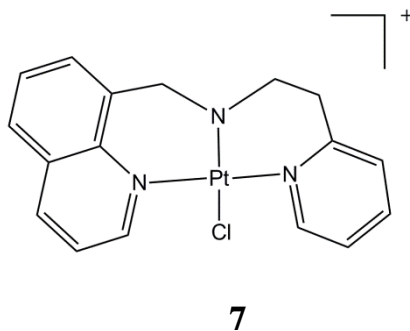


Figure 1.13 Chemical structure of Mon-Pt-2 (**7**) as prepared by Wang et al.

Based on the saccharinate capability of undergoing metal complexation and on the lipophilic and metal complexing nature of triphenyl phosphines, Ulukaya et al have synthesised and evaluated the anticancer properties of a family of platinum complexes (see **Figure 1.14**) targeting mitochondria. It was found that the trans isomers are having a good potential as anticancer agents with their mechanism of action relying on both DNA and mitochondrial damage as examined in MCF-7 cell lines.⁶¹

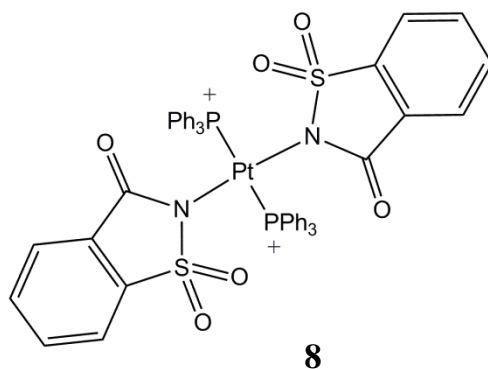


Figure 1.14 Chemical structure of platinum triphenyl phosphine saccharinate complex (**8**) as an example of mitochondria targeting platinum drugs

In a new dual targeting approach allowing to direct cisplatin towards mitochondria, Dhar et al have prepared a platinum(IV) prodrug known as Platin-M synthesized by appending two delocalized and lipophilic triphenylphosphonium (TPP) ligands targeting mitochondria by means of azadibenzocyclooctyne as a spacer. (**Figure 1.15**). Platin-M was further nano

formulated with a triphenyl phosphonium cation functionalised surface to further enhance the mitochondria targeting. Adopting this strategy, Platin-M was found to be 17 times more active than cisplatin in neuroblastoma cells.⁶²

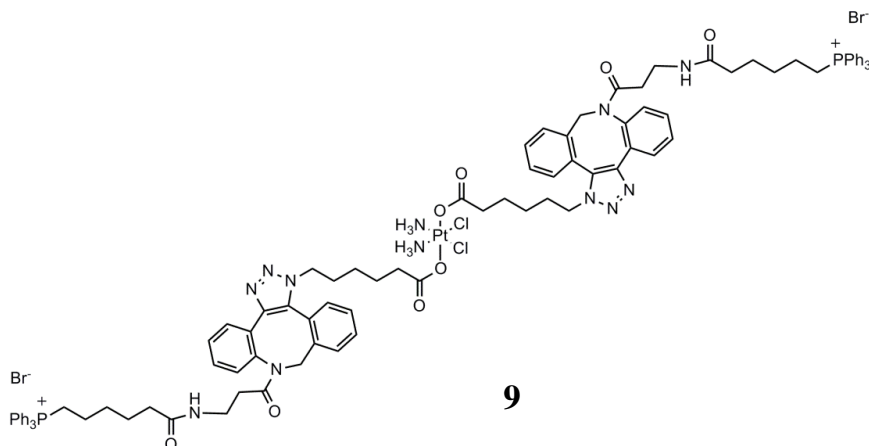


Figure 1.15 Chemical structure of Platin-M (**9**)

The same triphenyl phosphine containing axial ligands of platinum (IV) complexes (see **Figure 1.16**) were also adopted by Wang and his research team in 2018. Although the prepared drugs were found more destructive to the mitochondrial morphology compared to cisplatin, however, the overall cytotoxic effect resulted to be inferior to cisplatin.⁶³

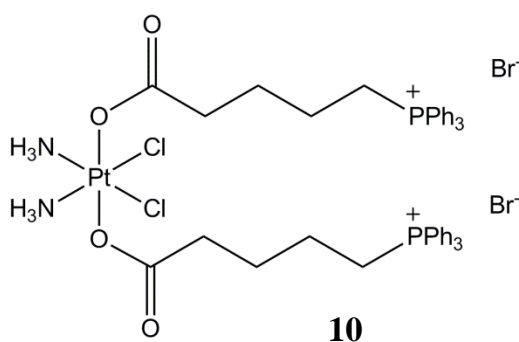


Figure 1.16 Chemical structure of platinum (IV) complex targeting mitochondria as prepared by Wang and co-workers (**10**)

Recently, a new set of platinum based anticancer drugs, designed to target mitochondria, has been synthesized and studied.⁶⁴ In their study, the authors

have combined the cytotoxic action of a new class of platinum based anticancer drugs, that is mono-functional platinum complexes having a pyriplatin backbone, with the introduction of a cationic functional group, $\text{CH}_2\text{Ph}_3\text{P}^+$, that allows the drug to be directed to and accumulate into mitochondria (see **Figure 1.17**). As mentioned before, monofunctional platinum anticancer drugs such as pyriplatin have significant antineoplastic action and a cellular response profile different with respect to those of the classic bifunctional, charge-neutral platinum-based drugs.⁴⁵ On the other hand, it has been demonstrated that lipophilic compounds with delocalized positive charge can easily penetrate the inner mitochondrial membrane due to their high impermeability and accumulate inside thanks to the negatively charged micro environment within the mitochondrial matrix. Combining the good of two worlds, this results into a group of monofunctional platinum complexes targeting mitochondria. Three monofunctional Pt(II) complexes have been synthesized by Wang et al.⁶⁴ The $-\text{CH}_2\text{Ph}_3\text{P}^+$ group was introduced into pyriplatin in ortho, meta and para positions of the pyriplatin pyridine ring.

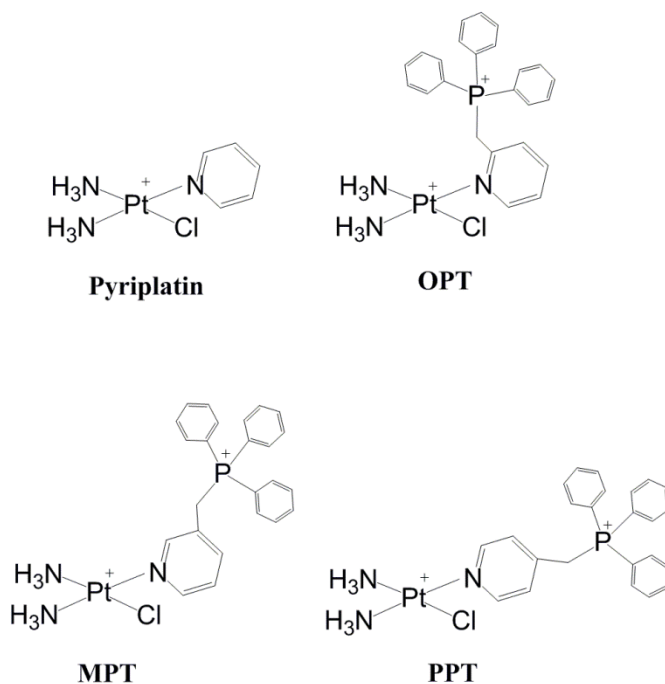


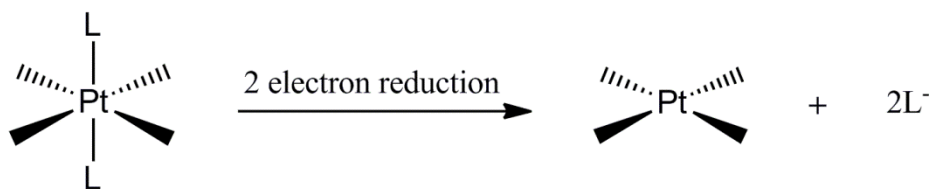
Figure 1.17 chemical structure of pyriplatin and its triphenyl phosphine derivatives in ortho (OPT), meta (MPT) and para (PPT) positions of pyridine ring

The corresponding complexes have been named OPT, MPT and PPT, respectively. The newly prepared complexes exhibited significant in vitro and in vivo antitumor efficacy and demonstrated to be able to penetrate mitochondria and accumulate in the mitochondrial matrix. In chapter IV of this thesis, we have studied the mechanism of action of this group of drugs and analysed the reasons behind the activity differences experimentally observed.

1.5 Platinum (IV) complexes as prodrugs

With the same aim of overcoming the shortcomings of cisplatin family of drugs like the toxic side effects, limited bioavailability with large amount of Pt(II) drugs loss in the bloodstream before arriving at the ultimate target.^{65,66}

and precluded oral administration, new strategies have emerged including the use of six-coordinate octahedral low spin d6 geometry Pt(IV) complexes, as inert prodrugs, which are shown to release the corresponding four-coordinate square planar active Pt(II) species upon reduction by cellular reducing agents or by photoactivation (see Scheme 1.2).⁶⁷⁻⁷¹



Scheme 1.2 The reduction of platinum (IV) complexes upon accepting two electrons together with the loss of the two axial ligands

Pt(IV) complexes are relatively inert to substitution.⁷²⁻⁷⁴ Reactions with biological nucleophiles, therefore, are disfavoured and lifetime in biological fluids is expected to increase making even oral administration feasible. The

administration of nontoxic Pt(IV) prodrugs might reduce unwanted reactions with biomolecules and consequently minimize undesired side effects. In addition, axial and equatorial ligands can be designed and fine-tuned to improve the pharmacological properties of the prodrug. The strong potential of this class of compounds, which was originally developed by Lippard, and co-workers has allowed many of them to be clinically tested reaching good stages although not accepted yet.^{67,75-78}

The most advanced of which is the orally active satraplatin that completed phase III clinical trials although not approved by FDA.⁷⁹

The great flexibility of the axial ligands of Pt(IV) complexes can allow a wide variety of additional drugs loading to platinum centre to have a dual action drugs as well as the utilisation of drug targeting approach directing the drug to particular sites or to nano formulate the platinum drugs in a particular micelles.

Ethacraplatin and mitaplatin are two Pt(IV) complexes having ethacrynic acid and dichloroacetate axial groups respectively (**Figure 1.18**). They are considered an example of dual action prodrugs that upon reduction liberate corresponding Pt(II) complexes as well as the free axial ligands which possess their own pharmacological effect.⁸⁰⁻⁸² As an example, ethacrynic acid is known to be a glutathione-S-transferase inhibitor which helps improving the effect of the released cisplatin. Dichloroacetate is a pyruvate dehydrogenase kinase inhibitor, which acts by inhibiting aerobic glycolysis and decreasing mitochondrial membrane potential allowing cancer cells to undergo apoptosis.

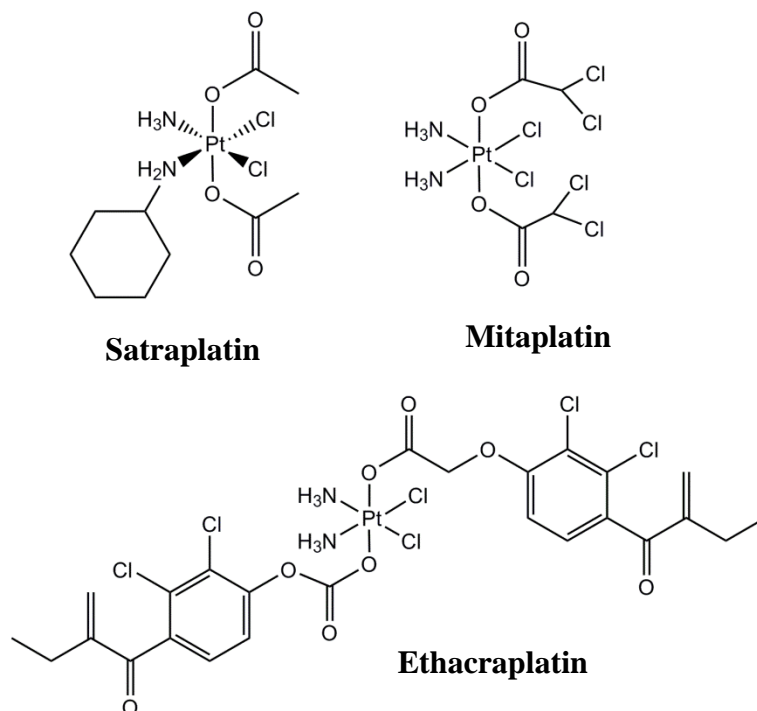


Figure 1.18 Chemical structures of satraplatin, mitaplatin and ethacraplatin

Intracellular reductive elimination represents the critical step of mechanism of the action of such compounds and, as a consequence, a great amount of attention has been focused on aspects such as the identity of the reducing agents, the ease, the rate and mainly the mechanism of the reduction process. If the reduction is too easy and occurs too early, the drug might be reduced before reaching the tumour location and, on the contrary, if the drug is too difficult to reduce it might reach the cancer cell and not be activated. Although many potential reducing agents are present both in plasma and cells and several hypotheses have been formulated.⁸³⁻⁸⁵

L-ascorbic acid (AscH₂) existing in its monodeprotonated form at physiological pH, and L-glutathione are commonly believed to be the biological species responsible for the reduction of Pt(IV) prodrugs and continue to be used for in vitro experiments (see **Figure 1.19**).⁸⁶⁻⁹⁴

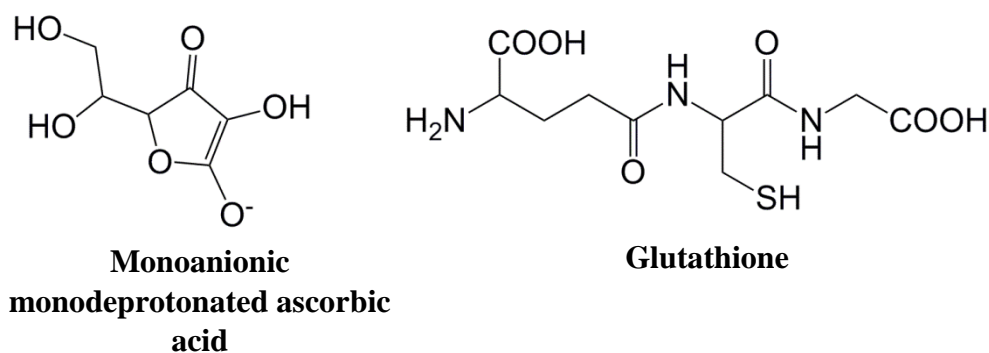


Figure 1.19 Chemical structure of monoanionic monodeprotonated ascorbic acid and glutathione

Several hypotheses on the mechanism by which Pt(IV) prodrugs are reduced have been formulated mainly on the basis of the information coming from kinetic measurements. Electron transfer mechanisms are generally classified as 1) ligand bridged inner-sphere, assuming that one of the axial ligands is able to form a bridge between the Pt(IV) center and the reductant mediating the flow of the electrons, and 2) outer sphere mechanism with no direct interaction between the complex and the reducing agent.⁶⁷

Reduction potential measurements by means of cyclic voltammetry can give indications about the ease of reduction, but in many cases the trend of the rates of drug reduction does not follow the reduction potential trend. Since the Pt(IV) reduction process involves both electron transfer chemical detachment of the two axial ligands the reaction rate depends on both steps.

In Chapter V of this thesis, the outcomes are reported of the investigation on a wide panel of Pt(IV) drugs having axial and equatorial ligands of different nature in an attempt to elucidate the mechanism of reduction by means of L-Ascorbic acid and cysteine amino acid at physiological.

1.6 Platinum drugs in photoactivated chemotherapy (PACT)

One of the main causes of the toxic side effects of regular platinum drugs is the inability of the drug to differentiate between normal and tumour cells.

The approach named Photoactivated chemotherapy (PACT) provides the opportunity for control over when and where a drug is activated, resulting in a greater specificity of drug action and remarkable potential for the treatment of cancer. Ideally, the non-irradiated form of the PACT compound should have no biological activity and low toxicity, while the irradiated form should have strong biological activity. This approach was adopted in platinum drugs in two ways.

The platinum (II) drug in its inactive form in the dark, due to the coordination of specially designed ligands, exerts its effect only upon light activation, which may or may not be accompanied by the ligand release. The increase in anticancer activity of both carboplatin and transplatin, known for long time to be inactive, upon light exposure spurred the development of novel cytotoxic compounds synthesized using such approach.^{95,96} The second approach involves the use of platinum tetravalent (IV) inactive prodrugs that are reduced by light to release active platinum(II) species. The released active form of the drug, then, exerts its anticancer action in the usual, well known, way. In the next paragraphs examples of both approaches will be given.

Examples of photoactivated platinum drugs having the platinum centre trapped by a special ligand are nitrophenyl substituted tetradentate platinum complexes, which liberate the active platinum upon light activation (**Figure 1.20**, complex **11**).⁹⁷ Chakravarty's group prepared a set of Pt(II) O,O-biphenolate (**12**) or β -diketonate (**13**) complexes that exhibit a marked photocytotoxicity together with low dark toxicity (**Figure 1.20**).^{98,99}

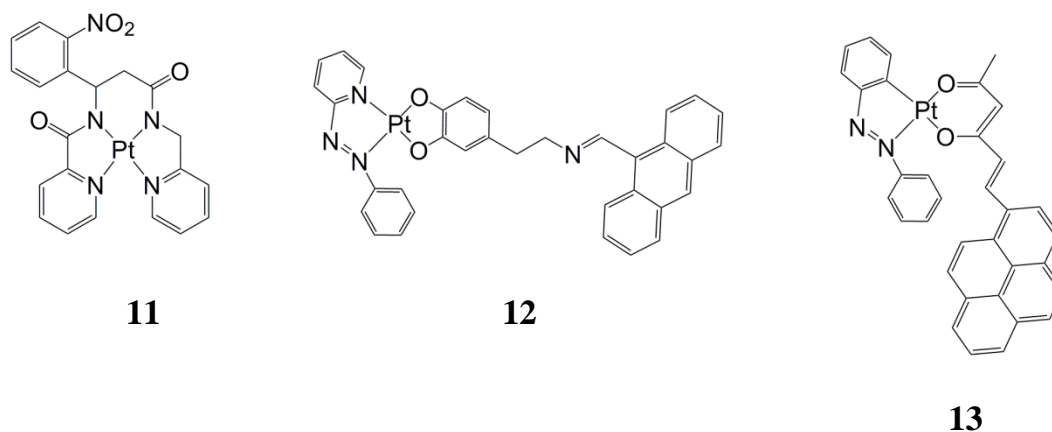


Figure 1.20 Chemical structure of an example of photoactivated platinum (II) complexes with nitrophenyl substituted tetradentate (**11**), O,O-biphenolate (**12**) and β -diketonate (**13**) ligands

Mitra et al. succeeded in synthesising a Pt(II) complex, named platicur, having a β -diketonate curcumin leaving ligand, being curcumin a known potential anticancer and photosensitizing molecule (see **Figure 1.21**). By coordination to the metal centre, as in platicur, through its monoanionic enolic form, curcumin instability and degradation can be prevented. At the same time, the use of the O,O-donor curcumin ligand allows to model oxaliplatin and carboplatin behaviour, which slowly release the O,O-donor ligand in the cellular medium in comparison with the two chlorido ligands of regular cisplatin.¹⁰⁰

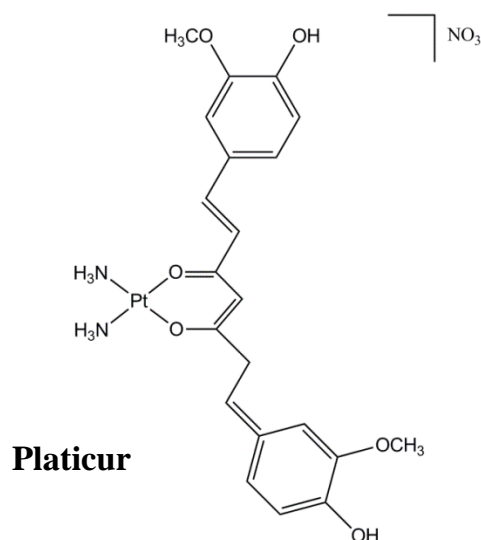


Figure 1.21 Chemical structure of platicur

Multiple benefits derive from the use of platinum(II) drug platicur, that is only activated upon irradiation at 430 nm. A water soluble form of curcumin is obtained concomitantly with the release upon light exposure of the active platinum(II) drug and curcumin photosensitizer. Experimentally, it was possible to detect the Pt-O bond cleavage upon light excitation and formation of the aquated free platinum(II) complex as well as free curcumin. The mechanism of activation of Platicur drug, with a particular emphasis on its photoactivation and photodissociation mechanism and dark stability as well, was thoroughly investigated. Obtained results will be illustrated in chapter VI of this thesis.

Initial attempts of the adoption of the second approach in the synthesis of photoactivated platinum drugs involving platinum in its tetravalent (IV) inactive form reduced by light light were carried out by Bendarski et al by preparing platinum(IV) complexes having diiodido groups (**14**) to be reduced by light (see **Figure 1.22**). Such complexes, nevertheless, turned out to be highly cytotoxic in dark because of their easy reduction by means of biological reducing agents.¹⁰¹⁻¹⁰³

Bendarski work, however, opened the door for further research carried out, for example, by Sadler et al who developed a set of platinum(IV) diazido complexes with cis and trans geometries and with multiple axial and equatorial ligands. Diazido platinum (IV) complexes (**15-18**) (**Figure 1.22**) have shown promising photoactivation properties with much better dark stability compared to diiodido substituents and a good potential for clinical evaluation.¹⁰⁴⁻¹¹³

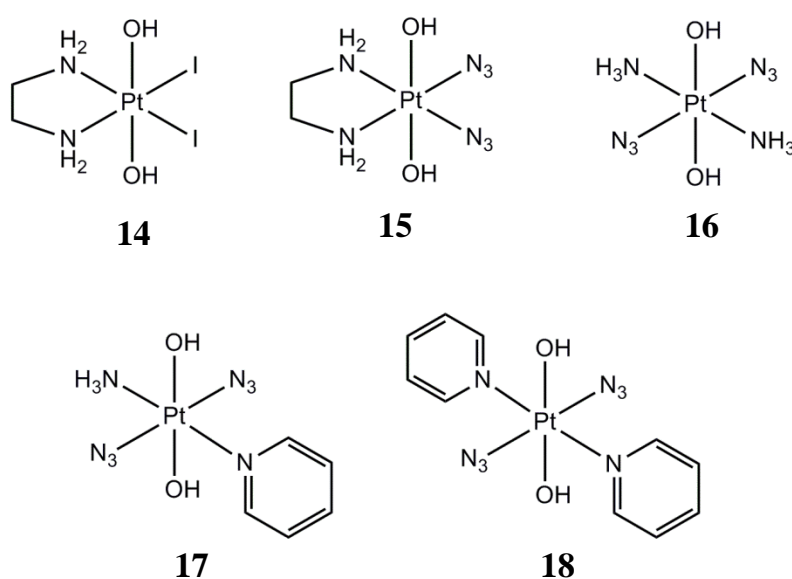


Figure 1.22 Chemical structure of a group of photoactivated platinum (IV) class with Iodido (**14**) and azido (**15-18**) equatorial ligands

1.7 Platinum drugs in photodynamic therapy

Platinum based drugs have found a place also in the field of photodynamic therapy (PDT) with the design of platinum complexes that can act as photosensitisers upon light absorption. Photosensitizers are known to exert their cytotoxic effect by generating active oxygen species (ROS) upon photoactivation with visible light at the appropriate wavelength leading to irreversible destruction of the treated tissues. The photosensitizer initially in

its ground state (S_0), following the absorption of light, is activated to a short-lived excited state (S_n) that may convert to a long-lived triplet state (T_n). The key role of the singlet state in the photosensitization process is to act as a precursor of the triplet state. Triplet state is the photoactive state, which may generate cytotoxic species by undergoing two main reactions. Type I reactions can produce free radicals or superoxide ions resulting from hydrogen or electron transfer. Type II reactions involve the interaction between oxygen and the triplet state of the sensitizer to mediate formation of singlet oxygen, which is generally believed to be the main cytotoxic species in PDT. These reactive oxygen species provoke irreversible damage to various cell membranes and protein modifications. For the photosensitizer to play its role, therefore, that photosensitive effect occurs only by irradiation at a specific wavelength and the maximum absorption of light should be at wavelengths from 600 nm to 800 nm to provide enough energy to stimulate oxygen in its singlet state. It is worth mentioning that oxygen concentration is generally low in cancer cells that are hypoxic in nature. For a better understanding of the PDT mechanisms Jablonski diagram is shown in **Figure 1.23**.

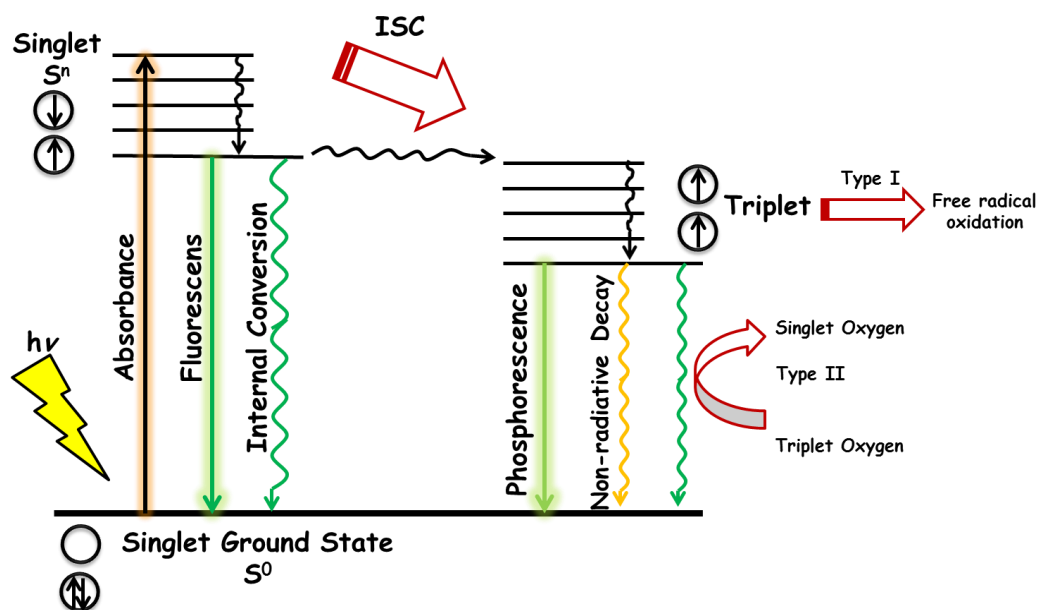


Figure 1.23 Jablonski diagram showing the photoexcitation from a singlet ground state to an excited singlet state followed by an intersystem crossing to the corresponding triplet state together with the mechanism of action of the photosensitizer by both Type I and Type II mechanisms.

Upon light excitation at specific wavelength, the photosensitizer is promoted to the first, or even higher, short lived excited singlet state, which can be deactivated to ground state by the release of heat (nonradiative decay), emitted as fluorescence of a wavelength equal to or longer than that of the excitation light, or by undergoing intersystem crossing (ISC). The excited triplet state can either decay back to ground state as phosphorescence or it can interact with the surrounding molecules with the modalities illustrated above. Photosensitizers are locally injected and activated with selected wavelength light initiating the activation processes leading to the selective destruction of the inappropriate cells. The photocytotoxic reactions occur only within the pathological tissues, in the area of photosensitizer distribution, enabling selective destruction, without harming healthy tissues.

Tetrapyrrole structures such as porphyrins, chlorins, bacteriochlorins and phthalocyanines with appropriate functionalization have received clinical approval (see **Figure 1.24**). Other molecular structures including the synthetic dyes classes as phenothiazinium, squaraine, DPP and BODIPY (boron-dipyrromethene) and natural products such as hypericin, riboflavin and curcumin have been investigated (**Figure 1.24**).¹¹⁴ Some drawbacks like poor water solubility and tendency to interact with biological media which alter photophysical properties and thus causing the loss of activity have to be overcome.

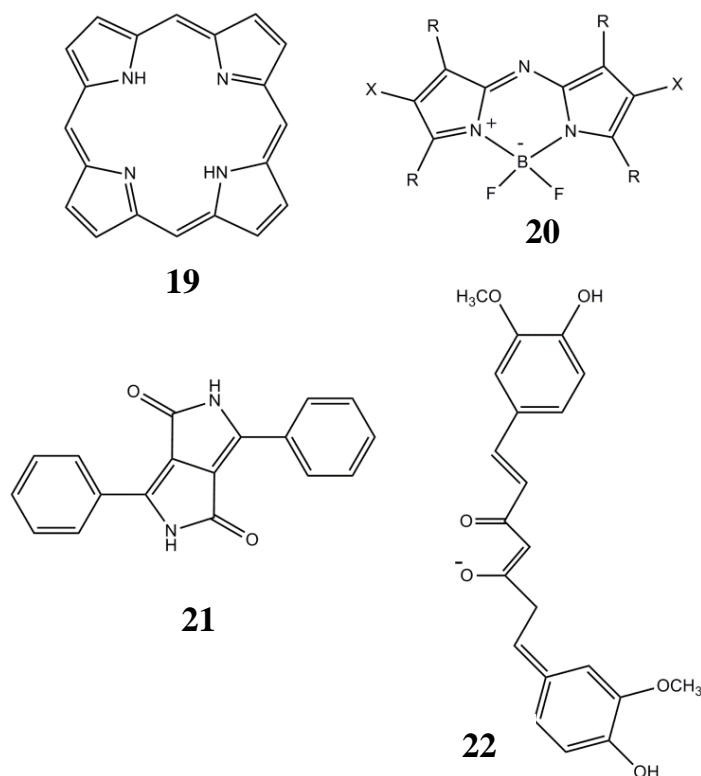


Figure 1.24 Chemical structure of a group of metal free photosensitizers. Porphyrin (**19**), BODIPY (**20**), DPP (**21**) and Curcumin (**22**)

Metals, especially platinum, use in photosensitizer design is very beneficial since they allow a wide flexibility of properties tuned by coordination of proper ligands. In addition, the presence of platinum enhances the triplet state population of the photo-excited complexes with sufficient lifetime owing to spin orbit coupling.

Combining two novel approaches, a platinum complex (**23**) developed by Chakravarty group to target mitochondria showed a good photocytotoxicity in-vitro with no dark toxicity. This complex was shown to cause a mitochondrial membrane disruption that leads to cell death by means of ROS and singlet oxygen generation phototoxic effect (see **Figure 1.25**).¹¹⁵

Upon substitution of one of the cisplatin ammonias with 1-methyl-7-azaindole (**24**), Brabec and co-workers succeeded in preparing platinum complexes, lacking dark toxicity, that showed a good phototoxic effect upon irradiation at 365 nm by means of singlet oxygen generation and DNA

crosslinks (**Figure 1.25**).¹¹⁶ The same was noticed upon substituting the two ammonias of carboplatin with 1-methyl-7-azaindole (**25**) as reported by Vanco et al.¹¹⁷

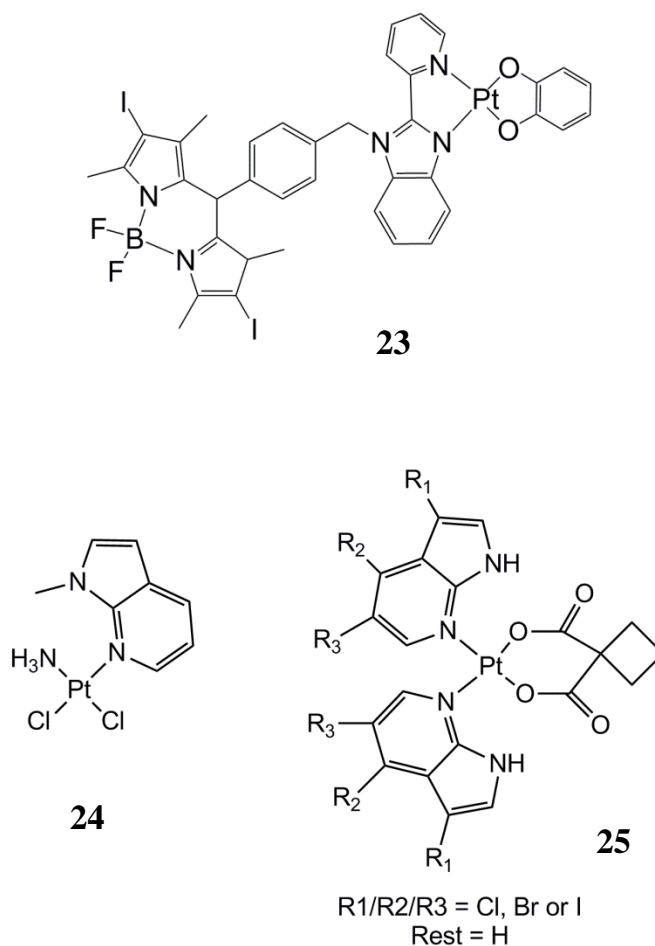


Figure 1.25 Chemical structure of photosensitizing complex targeting mitochondria as prepared by Chakravarty and co-workers (**23**). 7-Azaindole derivative of cisplatin and carboplatin as prepared by Brabec (**24**) and Vanco (**25**) respectively.

Some other platinum containing porphyrins (**26**), ferrocene derivatives (**27**) and N[^]N mono and bis acetylide complexes were also reported to have a significant cytotoxicity improvement by the effect of light although not fully inactive in darkness.^{118,119}

By preparing a platinum bound derivative of a known porphyrin skeleton, Spingler et al. found that the photosensitising effect was sharply increased

with a light wavelength of 420 nm and up to 575 nm. Such porphyrin derivatives (**26**) were found to successfully enter and localise into the cell nucleus.¹²⁰ In a close approach, Else et al. have reported a bimetallic zinc/platinum based porphyrazine photosensitizer (**28**) shown to induce a significant singlet oxygen production.¹²¹ Using oxaliplatin grafted to a porphyrin backbone (**29**), a newly photosensitising complex was prepared which was found to be effective against human bladder cell lines as reported by Brunnera and coworkers in 2004.¹²²

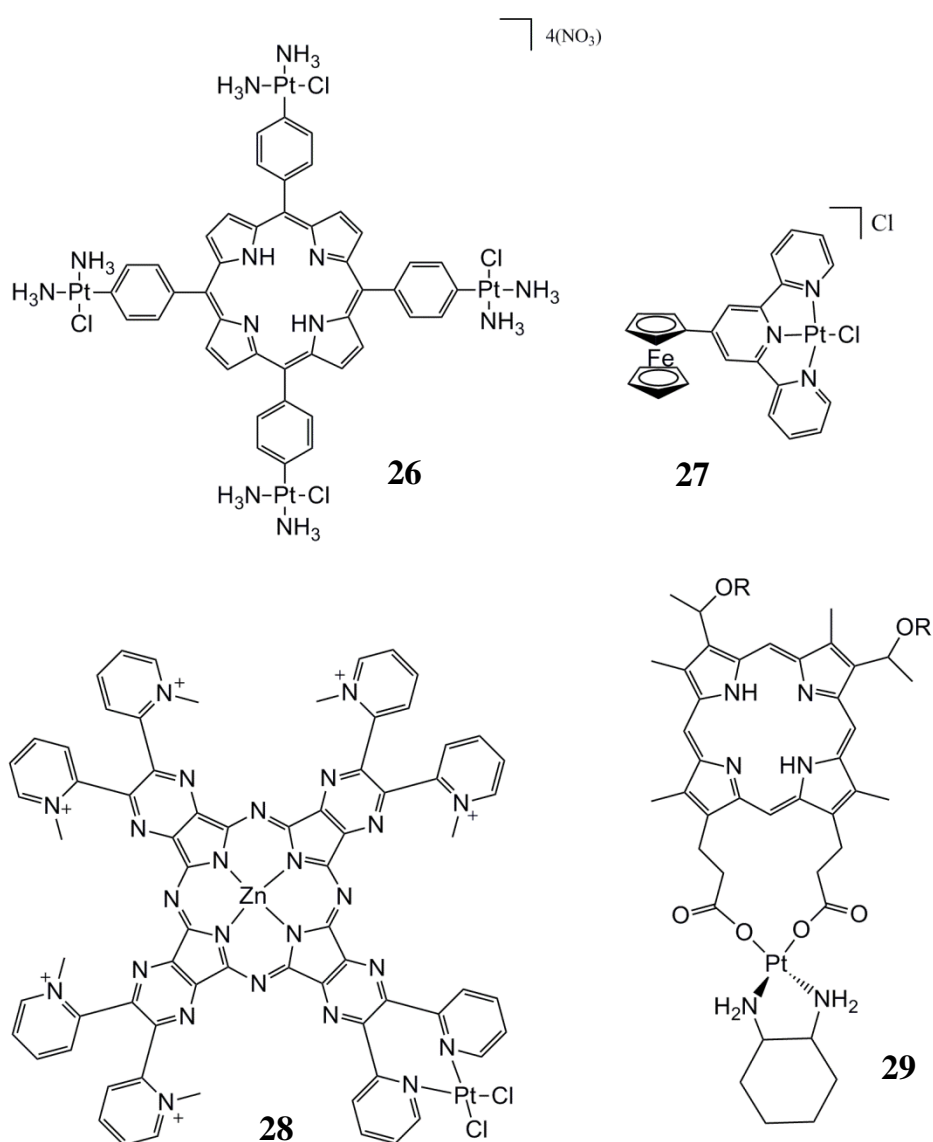


Figure 1.26 Chemical structure of photosensitising platinum porphyrin (**26**, **28**, **29**) and ferrocene (**27**) derivatives.

1.7.1 Cyclometalated platinum complexes and its use as photosensitizer

Cyclometalated metal complexes and especially those of platinum have attracted attention as a potential class of anticancer drugs capable to bind to DNA especially by intercalation owing to its planar ring structure. Such complexes are reported to have a pincer ligand of the tridentate π conjugated type (indicated as C^N^N , N^C^N , C^N^C or N^N^N) with a chloride leaving ligand that has been substituted (See **Figure 1.27**), in some cases, by ligands other than chloride in order to control the potential drug properties. Beside acting as traditional intercalating compounds and with the additional possibility of covalently bind to DNA, such complexes are known to have appropriate photophysical properties and, therefore, can act as photosensitizers causing a serious cellular damage.^{123,124}

Che et al prepared several variants of C^N^N based platinum complexes having an extra N-heterocyclic carbene (**32**) or acetylide (**33**) ligand bound to platinum centre which showed a good cytotoxic effect. The anticancer property of those newly prepared complexes were attributed to their DNA intercalation property and the stabilization of the topoisomerase II-DNA cleavage complex.^{125,126}

Similarly, the terpyridine N^N^N bound platinum complexes having a chloride leaving group (**34**) were found to initially intercalate in DNA followed by covalent binding to DNA nucleobases after the loss of the chloride.^{127,128} This covalent binding tendency can be inhibited by substituting the chloride with non-leaving ligands such as acetyl or sulfur based (**35**) groups allowing the drug to be solely acting by means of DNA intercalation.¹²⁷⁻¹²⁹

Inspired by Che's work, Huo and his group prepared a wide set of potential platinum anticancer complexes, mainly of N^C^N and N^N^C ligand type (See **Figure 1.27**, complex **30** and **31**). One of the very interesting findings

of Huo's work is the drastic difference in the cytotoxic activity of two of the prepared complexes, which differ in the position of the C atom in the ligand. Indeed, the N[^]C[^]N (**30**) based complex was found to possess a very good cytotoxic activity compared to the N[^]N[^]C (**31**) based complex which, instead, was found to be inactive.¹³⁰

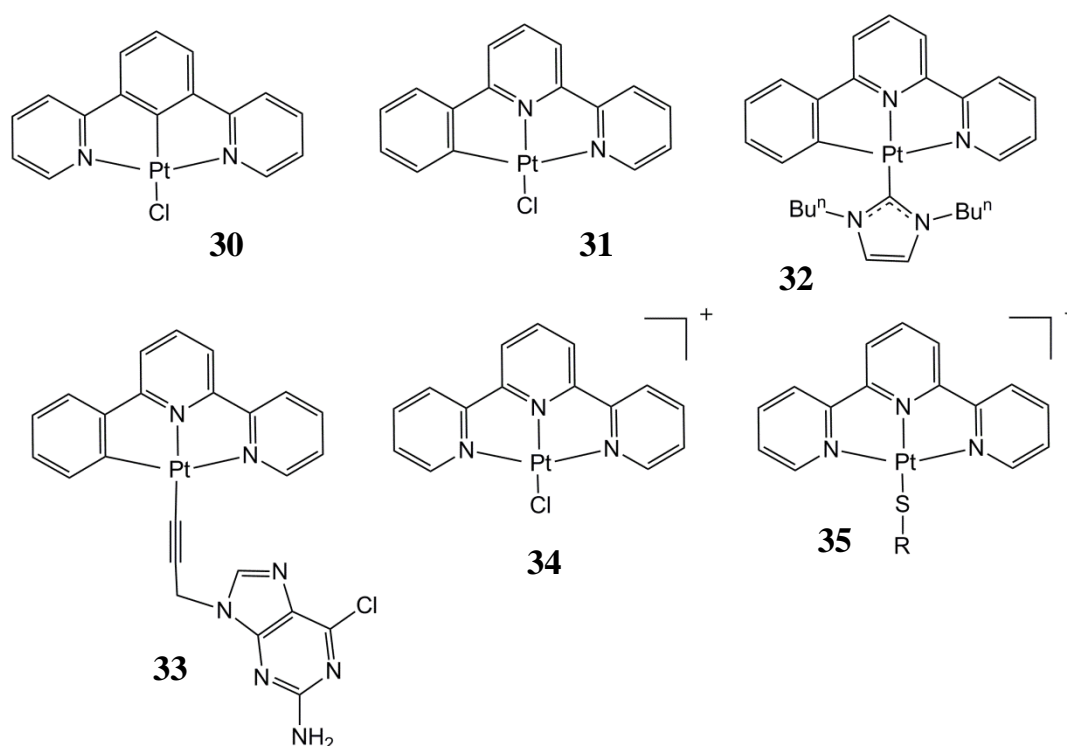
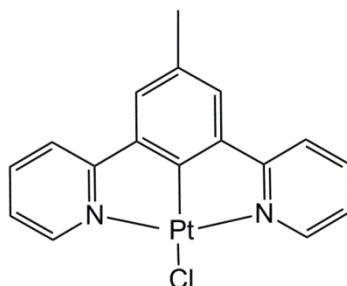


Figure 1.27 Chemical structure of a set of cyclometalated platinum complexes of N[^]C[^]N (**30**), C[^]N[^]N (**31**), C[^]N[^]N with heterocyclic carbene (**32**), C[^]N[^]N with acetylide (**33**), N[^]N[^]N (**34,35**) ligand types

It is worth mentioning that the complexes of general formula N[^]C[^]N (**30**) originally attracted attention as emission imaging agents for cells and were shown not to have cytotoxic effects for the short exposure time required for the cells treatment during the imaging application.¹³¹ Complex (30) was later re-characterised by Huo et al in 2014, as mentioned above, and was found to

have a cytotoxic effect, being the IC₅₀ concentration of 21.5 μ M and an incubation time 24 hours.¹³⁰



36

Figure 1.28 Chemical structure of cyclometalated platinum complex active as a photosensitizer as reported by Bryant and Weinstein (36)

Later in 2016, Bryant and Weinstein relied on their previous study of the emission imaging property of such complexes to study their photodynamic killing properties upon light excitation at 405nm. Unlike his old study, Weinstein investigated the long term dark and light induced toxicity at various micromolar concentrations of complex (36).¹³²

It was found that the studied complex (36) got an LD₅₀ values of 0.2 and 1.6 in light and dark respectively in HeLa cells. Although DNA is though not to be the only target of such type of drugs, however it represents a major site of action. It was found that this type of complexes are able to partially intercalate into DNA acting in a traditional way as an intercalator with a possibility of a non-intercalating part that is either covalently bound or binding to DNA grooves. Upon the action of light, the drug can induce its photosensitizing effect with both types I and II causing DNA strand breaks that are not repaired. Since the majority of such drugs were found to be in cytoplasm more than the nucleus, so there is possibility that the non-DNA drug bound targets may cause cell killing upon light effect. In chapter 5 of

this thesis, we will study the different activation and DNA interaction mechanism on a simplified models.¹³²

1.8 Iodido platinum (IV) and (II) complexes as a potential anticancer agents

Platinum iodido complexes have been mainly considered as one of the main intermediates in the synthetic pathways for the preparation of chlorido platinum-based drugs. The investigation of their biological properties and mechanism of action has been overlooked because iodido complexes have been historically regarded as biologically and pharmacologically unsuitable compared with chlorido analogues.¹³³

Recently, platinum iodido complexes have been reconsidered as possible anticancer drug candidates and for some of them it has been also suggested a different mechanism of action compared with their chlorido analogues. Given their unexpected prominent activity towards proteins, proteins were suggested as one of the potential targets of Pt(II) iodide complexes.¹³⁴⁻¹³⁸

With the severe side-effects and intrinsic and acquired resistance of Pt(II)-complexes and as previously discussed, Pt(IV) complexes have been designed and synthesized as prodrugs to be activated inside the cells by biological reducing agents that allow square planar active platinum(II) species to be formed by elimination of the axial ligands and the rates of reduction are one of the most important parameters determining the efficacy of the Pt(IV) complexes as anticancer agents.⁸⁷

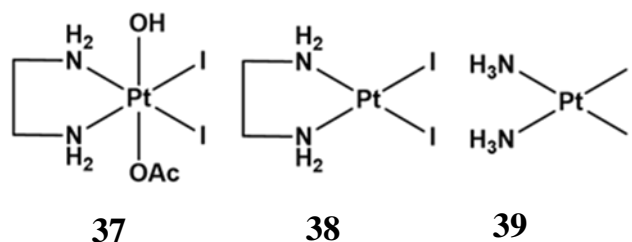


Figure 1.29 Chemical structure of a *trans,-cis*-[Pt(en)(OH)(OAc)I₂] (**37**) (en=ethylenediamine), *cis*-[Pt(en)I₂] (**38**) and *cis*-[Pt(NH₃)I₂] (**39**)

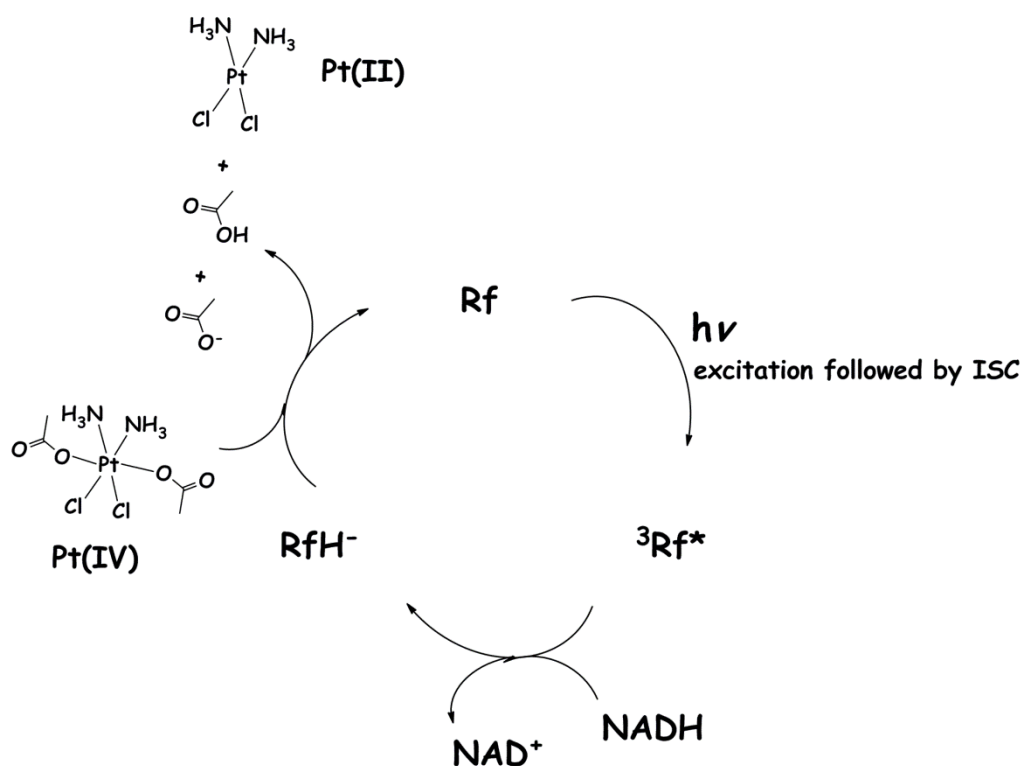
One alternative approach to activate the Pt(IV) pro-drug directly in tumors is by using light for inducing a photolytic reduction of a non-toxic but light-sensitive Pt(IV) complex to a cytotoxic Pt(II) species. This approach has been initially tried with diiodido-Pt(IV) diamines, which are activated by visible light to cytotoxic species that platinate DNA. However, the dark stability of these complexes in presence of biological reducing agents is poor and the complexes show relatively high dark activity.^{139,140}

With the renewed interest in Pt(II) iodide complexes, in chapter VIII of this thesis we have focused our attention on studying the reduction mechanism of a Pt(IV) iodido prodrug complexes (**Figure 1.29**, complex **37**) using ascorbate and cysteine as a reducing agent as well as a full mechanistic characterisation of the released Pt(II) iodido complex (**38**) and (**39**) in comparison with the chlorido Pt(IV) and Pt(II) analogues.

1.9 Bioorthogonal photocatalytic reduction of platinum (IV) complexes

If a reaction can be conducted in a biological system with a good degree of selectivity and minimal chance of side reactions, that reaction is known to be bioorthogonal. Using this approach in drug development would mean that the drug can undergo a certain selective catalytic or non-catalytic reaction in the living system leading to a final exact biological action resulting in its

therapeutic effect. In 2017, Salassa and co-workers have introduced a new concept of platinum (IV) complexes reduction by means of using the biological molecule riboflavin as a bioorthogonal photocatalyst.¹⁴¹ The reduction of riboflavin by means of light 460nm and in presence of electron donating source like NADH or MES (2-(N-morpholino)ethanesulfonic acid) will give the reduced form of riboflavin which will then act as a powerful reducing agent for platinum (IV) anticancer drugs (**Scheme 1.3**).



Scheme 1.3 A schematic representation of the photocatalytic cycle of Rf/NADH/Pt(IV)

To verify the model, a platinum (IV) complex with cisplatin backbone and two equatorial succinate ligands was used because of its known dark stability and low cytotoxicity in darkness. It is worth mentioning that riboflavin was effective in substoichiometric amounts relative to platinum (IV) indicating the catalytic effect that it plays where the generated oxidised form of riboflavin will re-enter the cycle again by receiving electrons from new NADH or MES

molecules where the cycle step involving the reduction of platinum (IV) was found to be the limiting step.¹⁴¹⁻¹⁴⁴

In collaboration with Salassa group, in chapter 6 of this thesis, we will be focusing on studying the mechanism of reaction between NADH and riboflavin. Although being a fundamental biological reaction, yet the reaction and its photophysical properties are not thoroughly studied either experimentally or computationally. In addition, the reduction mechanism of a set of platinum (IV) complexes using the reduced form of riboflavin will be explored. We will also try to rationalise the extent of reduction of this set of platinum(IV) complexes in relation with the suggested reduction mechanism shedding light on its kinetic and thermodynamic components.

References

- 1) B. Rosenberg, L. Van Camp, T. Krigas, *Nature* **1965**, *205*, 698–699.
- 2) B. Rosenberg, L. Van Camp, E. B. Grimley, A. J. Thomson, *J. Biol. Chem.* **1967**, *242*, 1347–1352.
- 3) B. Rosenberg, *Platin. Met. Rev.* **1971**, *15*, 42–51.
- 4) B. Rosenberg, L. Van Camp, J. E. Trosko, V. H. Mansour, *Nature* **1969**, *222*, 385–386.
- 5) S. Ghosh, *Bioorganic Chemistry*, **2019**, *88*, 102925
- 6) M. Galanski, M.A. Jakupec, B.K. Keppler, *Curr. Med. Chem.*, **2005**, *12*, 2075–2094.
- 7) I.A. Ridell, S. J. Lippard, *Met. Ions Life Sci.*, **2018**, *18*, 1–42 .
- 8) B. Tylkowski, R. Jastrzab, A. Odani, *Physical Sciences Reviews*, **2018**, 20160007
- 9) R. B. Ciccarelli, M. J. Solomon, A. Varshavsky, S. J. Lippard, *Biochemistry*, **1985**, *24*, 7533–7540.
- 10) P. Jordan, M. Carmo-Fonseca, *Cell. Mol. Life Sci.*, **2000**, *57* (8–9), 1229–1235.
- 11) Z. H. Siddik, *Oncogene*, **2003**, *22*, 7265–7279.
- 12) L. Imogen, A. Riddell, S. J. Lippard, Chapter-1: cisplatin and oxaliplatin: our current understanding of their actions, in: Astrid Sigel, Helmut Sigel, Eva Freisinger, Roland K.O. Sigel (Eds.), *Metallo-Drugs: Development and Action of Anticancer Agents*, De Gruyter, Berlin, Boston, **2018**, pp. 1–42, <https://doi.org/10.1515/9783110470734-007>.
- 13) I. W. Achkar, N. Abdulrahman, H. Al-Sulaiti, J. M. Joseph, S. Uddin, F. Mraiche, *J. Transl. Med.*, **2018**, *16*, 96.

- 14) R. A. Alderden, M. D. Hall, T. W. Hambley, *J. Chem. Educ.*, **2006**, 83 (5), 728–734.
- 15) M. Petrovic, D. Todorovic, *Med. Biol.*, **2016**, 18 (1), 12–18.
- 16) N. Nagai, R. Okuda, M. Kinoshita, H. Ogata, *J. Pharm. Pharmacol.*, **1996**, 48, 918–924.
- 17) A. I. Ivanov, J. Christodoulou, J.A. Parkinson, K.J. Barnham, A. Tucker, J. Woodrow, P.J. Sadler, *J. Biol. Chem.*, **1998**, 273, 14721–14730.
- 18) S. Ishida, J. Lee, D.J. Thiele, I. Herskowitz, *Proc. Natl. Acad. Sci. U S A.*, **2002**, 99, 14298–14302.
- 19) S. Dasari, P.B. Tchounwou, *Eur. J. Pharmacol.*, **2014**, 5, 364–378.
- 20) M. A. Fuertes, J. Castilla, C. Alonso, J. M. Perez, *Curr. Med. Chem. Anticancer Agents* , **2002**, 2, 539–551.
- 21) M. S. Davies, S. J. Berners-Price, T. W. Hambley, *Inorg. Chem.*, **2000**, 39, 5603–5613.
- 22) X. Lin, T. Okuda, A. Holzer, S.B. Howell, *Mol. Pharmacol.*, **2002**, 62, 1154–1159.
- 23) A.M. Fichtinger-Schepman, J. L. van der Veer, J. H. den Hartog, P. H. Lohman, J. Reedijk, *Biochemistry*, **1985**, 24, 707–713.
- 24) L. Kelland, *Nat. Rev. Cancer*, **2007**, 7 (8), 573–584.
- 25) M.-H. Baik, R.A. Friesner, S.J. Lippard, *J. Am. Chem. Soc.*, **2003**, 125 (46), 14082–14092.
- 26) R. A. Alderden, M. D. Hall, T. W. Hambley, *J. Chem. Educ.*, **2006**, 83 (5), 728–734.
- 27) J. Lokich, N. Anderson, *Annals of Oncology*, **1998**, 9, 13-21
- 28) R. Oun, Y. E. Moussa, N. J. Wheate, *Dalton Trans.*, **2018**, 47, 6645–6653
- 29) J. de Mier-Vinué, M. Gay, Á. M. Montaña , R.-I. Sáez, V. Moreno, V. Brabec, J. Kasparikova, O. Vrana, P. Heringova, A. Boccarelli, M. Coluccia, G. Natile., *Journal of Medicinal Chemistry*, **2008**, 51(3), 424–31.
- 30) J. J. Wilson, S. J. Lippard, *Journal of Medicinal Chemistry*, **2012**, 55(11), 5326-5336.
- 31) G. Antonaci, L. G. Cossa, A. Muscella, C. Vetrugno, S. A. De Pascali, F. P. Fanizzi, S. Marsigliante, *Biomolecules*, **2019**, 9(3), 92.
- 32) A.Muscella, C. Vetrugno, L. G. Cossa, G. Antonaci, F. De Nuccio, S. A. De Pascali, F. P. Fanizzi, S. Marsigliante, *PLOS ONE*, **2016**, 11(11), e0165154. <https://doi.org/10.1371/journal.pone.0165154>.
- 33) L. S. Hollis, A. R. Amundsen, E. W. Stern, *J. Med. Chem.* , **1989**, 32, 128-136.
- 34) L. S. Hollis, W.I. Sundquist, N. J. Burstyn, J. W. Heigher-Bernays, S. F. Bellon J. K. Ahmed, A. R. Amundsen, E. W. Stern, S. J. Lippard, *Cancer Res.* , **1991**, 51, 1875.
- 35) E. T. Martins, H. Baruah, J. Kramarczyk, G. Saluta, C. S. Day, G. L. Kucera, U. Bierbach, *J. Med. Chem.* , **2001**, 44, 4492-4496.

- 36) M. C. Ackley, C. G. Barry, A. M. Mounce, M. C. Farmer, B. E. Springer, C. S. Day, M. W. Wright, S. J. Berners-Price, S. M. Hess, U. Bierbach, *J. Biol. Inorg. Chem.*, **2004**, *9*, 453-461.
- 37) S. M. Hess, A. M. Mounce, R. C. Sequeira, T. M. Augustus, M. C. Ackley, U. Bierbach, *Cancer Chemother. Pharmacol.*, **2005**, *56*, 337-343.
- 38) H. Baruah, C. G. Barry, U. Bierbach, *Curr. Top. Med. Chem.*, **2004**, *4*, 1537-1549.
- 39) H. Baruah, M. W. Wright, U. Bierbach, *Biochemistry*, **2005**, *44*, 6059-6070.
- 40) S. Dutta, M. J. Snyder, D. Rosile, K. L. Binz, E. H. Roll, J. Suryadi, U. Bierbach, M. Guthold, *Cell Biochem. Biophys.*, **2013**, *67*, 1103-1113.
- 41) Y. Cheun, M.-C. Koag, Y. W. Naguib, H. O.-Shubeita, Z. Cui, D. Pakotiprapha, S. Lee, *Chem Biol Drug Des.*, **2018**, *91*, 116–125
- 42) D. Wang, G. Zhu, X. Huang, S. J. Lippard, *PNAS*, **2010**, *107*, 9584-9589.
- 43) A. Hucke, G. Y. Park, O. B. Bauer, G. Beyer, C. Köppen, D. Zeeh, C. A. Wehe, M. Sperling, R. Schröter, M. Kantauskaitė, Y. Hagos, U. Karst, S. J. Lippard, G. Ciarimboli, *Front Chem.*, **2018**, *6*, 180.
- 44) T. C. Johnstone, J. J. Wilson, S. J. Lippard, *Inorganic Chemistry*, **2013**, *52*, 12234-12239.
- 45) T. C. Johnstone, G. Y. Park, S. J. Lippard, *Anticancer research*, **2014**, 471-476.
- 46) K. S. Lovejoy, M. Serova, I. Bieche, S. Emami, M. D’Incalci, M. Broggin, E. Erba, C. Gespach, E. Cvitkovic, S. Faivre, E. Raymond, S. J. Lippard, *Mol Cancer Ther.*, **2011**, *10*, 1709-1719.
- 47) G. Y. Park, J. J. Wilson, Y. Song, S. J. Lippard, *PNAS*, **2012**, *109*, 11987-11992.
- 48) M. T. Gregory, G. Y. Park, T. C. Johnstone, Y. -S. Lee, W. Yang, S. J. Lippard, *PNAS*, **2014**, *111*, 9133-9138.
- 49) M. W. Kellinger, G. Y. Park, J. Chong, S. J. Lippard, D. Wang, *J. Am. Chem. Soc.*, **2013**, *135*, 13054-13061.
- 50) I. A. Riddell, T. C. Johnstone, G. Y. Park, S. J. Lippard, *Chem-Eur J.*, **2016**, *22*, 7574-7581.
- 51) C. Timothy, T. C. Johnstone, S. J. Lippard, *J. Am. Chem. Soc.*, **2014**, *136*, 2126-2134.
- 52) W. Zhou, M. Almeqdadi, M. E. Xifaras, I. A. Riddell, O. H. Yilmaz, S. J. Lippard, *Chem. Commun.*, **2018**, *54*, 2788-2791.
- 53) J. Whittaker, W. D. McFadyen, G. Wickham, L. P. Wakelin, V. Murray, *Nucleic Acids Res.*, **1998**, *26*(17), 3933–3939
- 54) L. Gatti, G. Cassinelli, N. Zaffaroni, C. Lanzi, P. Perego, *Drug Resist. Updates*, **2015**, *20*, 1-11.
- 55) S. P. Wisnovsky, J. J. Wilson, R. J. Radford, M. P. Pereira, M. R. Chan, R. R. Laposa, S. J. Lippard, S. O. Kelley, *Chem. Biol.*, **2013**, *20*, 1323-1328.
- 56) K. Suntharalingam, J. J. Wilson, W. Lin, S. J. Lippard, *Metall.*, **2014**, *6*, 437-443.

- 57) S. Fulda, L. Galluzzi, G. Kroemer, *Nat. Rev. Drug Discov.*, **2010**, *9*, 447-464.
- 58) S. E. Weinberg, N. S. Chandel, *Nat. Chem. Biol.*, **2015**, *11*, 9-15.
- 59) Y. H. Yang, S. Karakhanova, W. Hartwig, J. G. D'Haese, P. P. Philippov, J. Werner, A. V. Bazhin, *J. Cell. Physiol.*, **2016**, *231*, 2570-2581.
- 60) F.-Y. Wang, X.-M. Tang, X. Wang, K.-B. Huang, H.-W. Feng, Z.-F. Chen, Y.-N. Liu, H. Liang, *European Journal of Medicinal Chemistry*, **2018**, *155*, 639-650
- 61) V. T. Yilmaz, C. Icel, O. R. Turgut, M. Aygun, M. Erkisa, M. H. Turkdemir, E. Ulukaya, *European Journal of Medicinal Chemistry*, **2018**, *155*, 609-622.
- 62) S. Marrache, R. K. Pathak, S. Dhar, *PNAS*, **2014**, *111* (29), 10444-10449.
- 63) S. Jin, Y. Hao, Z. Zhu, N. Muhammad, Z. Zhang, K. Wang, Y. Guo, Z. Guo, X. Wang, *Inorg. Chem.*, **2018**, *57*, 17, 11135-11145
- 64) Z. Zhu, Z. Wang, C. Zhang, Y. Wang, H. Zhang, Z. Gan, Z. Guo, X. Wang, *Chem. Sci.*, **2019**, *10*, 3089-3095.
- 65) L. Galluzzi, L. Senovilla, I. Vitale, J. Michels, I. Martins, O. Kepp, M. Castedo, G. Kroemer, *Oncogene*, **2012**, *31*, 1869-1883.
- 66) E. Wexselblatt, E. Yavin, D. Gibson, *Inorg. Chim. Acta*, **2012**, *393*, 75-83.
- 67) N. Graf, S. J. Lippard, *Adv. Drug Delivery Rev.*, **2012**, *64*, 993-1004;
- 68) R. K. Pathak, S. Marrache, J. H. Choi, T. B. Berding, S. Dhar, *Angew. Chem. Int. Ed.*, **2014**, *53*, 1963-1967.
- 69) Q. Cheng, H. Shi, H. Wang, Y. Min, J. Wang, Y. Liu, *Chem. Commun.*, **2014**, *50*, 7427-7430.
- 70) E. Gabano, M. Ravera, D. Osella, *Dalton Trans.*, **2014**, *43*, 9813-9820.
- 71) J. S. Butler, P. J. Sadler, *Curr. Opin. Chem. Biol.*, **2013**, *17*, 175-188.
- 72) E. Wexselblatt, E. Yavin, D. Gibson, *Angew. Chem., Int. Ed.*, **2013**, *52*, 6059-6062.
- 73) I. Ritacco, G. Mazzone, N. Russo, E. Sicilia, *Inorg. Chem.*, **2016**, *55*, 1580-1586.
- 74) O. Bradáč, T. Zimmermann, J. V. Burda, *J. Mol. Model.*, **2013**, *19*, 4669-4680.
- 75) S. Dhar, F. X. Gu, R. Langer, O. C. Farokhzad, S. J. Lippard, *Proc. Natl. Acad. Sci. Acad. U. S. A.*, **2008**, *105*, 17356-17361.
- 76) J. J. Wilson, S. J. Lippard, *Chem. Rev.*, **2014**, *114*, 4470-4495.
- 77) K. Suntharalingam, Y. Song, S. J. Lippard, *Chem. Commun.*, **2014**, *50*, 2465-2468.
- 78) Y.-R. Zheng, K. Suntharalingam, T. C. Johnstone, H. Yoo, W. Lin, J. G. Brooks, S. J. Lippard, *J. Am. Chem. Soc.*, **2014**, *136*, 8790-8798.
- 79) D. P. Petrylak, O. Sartor, F. Witje, J. Ferrero, W. R. Berry, A. Koletsky, S. Falcon, F. E. Nathan, M. E. Petrone, C. A. Sternberg, *Proc. Am. Soc. Clin. Oncol.*, **2007**, 145s.
- 80) W. H. Ang, I. Khalaila, C. S. Allardyce, L. Juillerat-Jeanneret and P. J. Dyson, *J. Am. Chem. Soc.*, **2005**, *127*, 1382-1383.

- 81) W. H. Ang, S. Pilet, R. Scopelliti, F. Bussy, L. Juillerat-Jeanneret, P. J. Dyson, *J. Med. Chem.*, **2005**, *48*, 8060–8069.
- 82) M. G. Vander Heiden, L. C. Cantley, C. B. Thompson, *Science*, **2009**, *324*, 1029–1033
- 83) A. Nemirovski, Y. Kasherman, Y. Tzaraf, D. Gibson, *J. Med. Chem.*, **2007**, *50*, 5554-5556
- 84) U. Jungwirth, C. R. Kowol, B. K. Keppler, C. G. Hartinger, W. Berger, P. Heffeter, *Antioxid Redox Signal.*, **2011**, *15*, 1085-1127
- 85) A. Lasorsa, O. Stuchlikova, V. Brabec, G. Natile, F. Arnesano, *Mol. Pharm.*, **2016**, *13*, 3216-3223.
- 86) S. Choi, C. Filotto, M. Bisanzo, S. Delaney, D. Lagasee, J. L. Whitworth, A. Jusko, C. R. Li, N. A. Wood, J. Willingham, A. Schwenker, K. Spaulding, *Inorg. Chem.*, **1998**, *37*, 2500-2504.
- 87) K. Lemma, A. M. Sargeson, L. I. Elding, *J. Chem. Soc., Dalton Trans.*, **2000**, 1167-1172
- 88) K. Lemma, D. A. House, N. Retta, L. I. Elding, *Inorg. Chim. Acta*, **2002**, *331*, 98-108.
- 89) A. Nemirovski, I. Vinograd, K. Takrouri, A. Mijovilovich, A. Rompel, D. Gibson, *Chem. Commun.*, **2010**, *46*, 1842-1844.
- 90) J. Z. Zhang, E. Wexselblatt, T. W. Hambley, D. Gibson, *Chem. Commun.*, **2012**, *48*, 847-849.
- 91) E. Wexselblatt, D. Gibson, *J. Inorg. Biochem.* **2012**, *117*, 220-229.
- 92) M. Sinisi, F. P. Intini, G. Natile, *Inorg. Chem.*, **2012**, *51*, 9694-9704.
- 93) H. P. Varbanov, S. M. Valiahdi, C. R. Kowol, M. A. Jakupec, M. Galanski, B. K. Keppler, *Dalton Trans.*, **2012**, *41*, 14404-14415.
- 94) V. Pichler, S. Göschl, S. M. Meier, A. Roller, M. A. Jakupec, M. Galanski, B. K. Keppler, *Inorg. Chem.*, **2013**, *52*, 8151-8162.
- 95) P. Heringova, J. Woods, F. S. Mackay, J. Kasparkova, P. J. Sadler, V. Brabec, *J. Med. Chem.*, **2006**, *49*, 7792–7798.
- 96) J. Mlcouskova, J. Stepankova and V. Brabec, *J. Biol. Inorg. Chem.*, **2012**, *17*, 891–898.
- 97) K. L. Ciesiński, L. M. Hyman, D. T. Yang, K. L. Haas, M. G. Dickens, R. J. Holbrook, K. J. Franz, *Eur. J. Inorg. Chem.*, **2010**, 2224–2228.
- 98) K. Mitra, S. Patil, P. Kondaiah, A. R. Chakravarty, *Inorg. Chem.*, **2015**, *54*, 253–264.
- 99) Md. K. Raza, K. Mitra, A. Shettar, U. Basu, P. Kondaiah, A. R. Chakravarty, *Dalton Trans.*, **2016**, *45*, 13234–13243.
- 100) K. Mitra, S. Gautam, P. Kondaiah, A. R. Chakravarty, *Angew. Chem., Int. Ed.*, **2015**, *54*, 13989–13993
- 101) P. J. Bednarski, F. S. Mackay, P. J. Sadler, *Anticancer Agents Med. Chem.*, **2007**, *7*, 75–93.

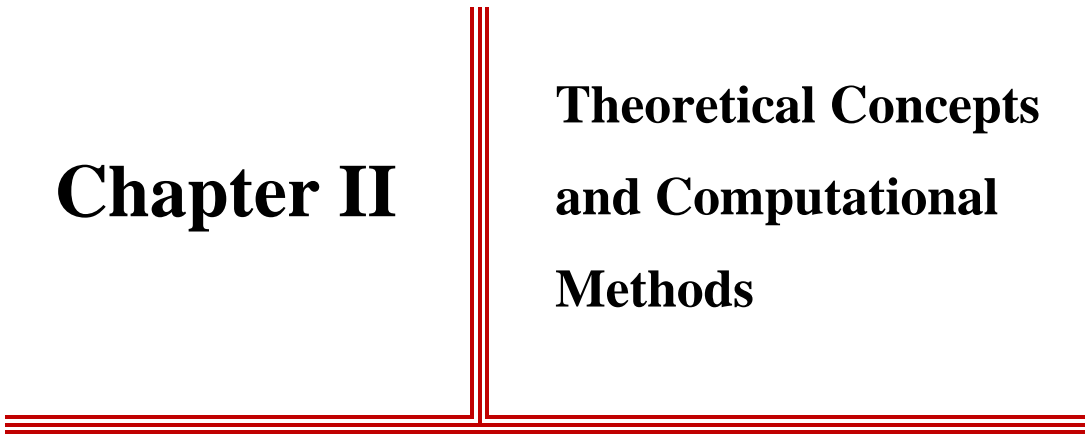
- 102) N. A. Kratochwil, M. Zabel, K.-J. Range, P. J. Bednarski, *J. Med. Chem.*, **1996**, *39*, 2499–2507.
- 103) N. A. Kratochwil, P. J. Bednarski, H. Mrozek, A. Vogler, J. K. Nagle, *Anticancer Drug Des.*, **1996**, *11*, 155–171
- 104) P. Müller, B. Schröder, J. A. Parkinson, N. A. Kratochwil, R. A. Coxall, A. Parkin, S. Parsons, P. J. Sadler, *Angew. Chem., Int. Ed.*, **2003**, *42*, 335–339.
- 105) P. J. Sadler, P. Müller, Photoreactive compounds and compositions, **2003**, International Patent Application, WO03/017993.
- 106) F. S. Mackay, J. A. Woods, H. Moseley, J. Ferguson, A. Dawson, S. Parsons, P. J. Sadler, *Chem. – Eur. J.*, **2006**, *12*, 3155–3161.
- 107) N. J. Farrer, J. A. Woods, V. P. Munk, F. S. Mackay, P. J. Sadler, *Chem. Res. Toxicol.*, **2010**, *23*, 413–421.
- 108) P. J. Bednarski, R. Grunert, M. Zielzki, A. Wellner, F. S. Mackay, P. J. Sadler, *Chem. Biol.*, **2006**, *13*, 61–67.
- 109) N. J. Farrer, P. Gierth, P. J. Sadler, *Chem. – Eur. J.*, **2011**, *17*, 12059–12066.
- 110) L. Ronconi, P. J. Sadler, *Dalton Trans.*, **2011**, *40*, 262–268.
- 111) A. F. Westendorf, J. A. Woods, K. Korpis, N. J. Farrer, L. Salassa, K. Robinson, V. Appleyard, K. Murray, R. Grünert, A. M. Thompson, P. J. Sadler, P. J. Bednarski, *Mol. Cancer Ther.*, **2012**, *11*, 1894–1904.
- 112) A. F. Westendorf, L. Zerzankova, L. Salassa, P. J. Sadler, V. Brabec, P. J. Bednarski, *J. Inorg. Biochem.*, **2011**, *105*, 652–662.
- 113) N. J. Farrer, J. A. Woods, L. Salassa, Y. Zhao, K. S. Robinson, G. Clarkson, F. S. Mackay, P. J. Sadler, *Angew. Chem., Int. Ed.*, **2010**, *49*, 8905–8908.
- 114) M. Lan, S. Zhao, W. Liu, C.-S. Lee, W. Zhang, P. Wang, *Adv. Healthcare Mater.*, **2019**, *8*, 1900132.
- 115) K. Mitra, S. Gautam, P. Kondaiah, A. R. Chakravarty, *ChemMedChem*, **2016**, *11*, 1956–1967.
- 116) P. Štarha, Z. Trávníček, A. Popa, T. Muchová, V. Brabec, *Journal of Inorganic Biochemistry*, **2012**, *115*, 57–63.
- 117) P. Štarha, Z. Trávníček, Z. Dvořák, T. Radošová-Muchová, J. Prachařová, J. Vančo J, et al., *PLOS ONE*, 2015, *10*(4), e0123595. doi:10.1371/journal.pone.0123595.
- 118) J. Zhao, W. Wu, J. Sun, S. Guo, *Chem. Soc. Rev.*, **2013**, *42*, 5323–5351.
- 119) L. K. Mckenzie, H. E. Bryant, J. A. Weinstein, *Coordination Chemistry Reviews*, 2019, *379*, 2-29.
- 120) Naik, R. Rubbiani, G. Gasser, B. Spingler, *Angew. Chem., Int. Ed.*, **2014**, *53*, 6938–6941.
- 121) I. Manet, F. Manoli, M.P. Donzello, E. Viola, A. Masi, G. Andreano, G. Ricciardi, A. Rosa, L. Cellai, C. Ercolani, S. Monti, *Inorg. Chem.*, 2013, *52*, 321–328.
- 122) C. Lottnera, R. Knuechelb, G. Bernhardt, H. Brunnera, *Cancer Lett.*, **2004**, *203*, 171–180.

- 123) N. Cutillas, G. S. Yellol, C. de Haro, C. Vincente, V. Rodriguez, J. Ruiz, *Coordination Chemistry Reviews*, **2013**, 257, 2784–2797.
- 124) W. Liu, R. Gust, *Chem. Soc. Rev.*, **2013**, 42, 755-773.
- 125) (a) R. W.-Y. Sun, A. L.-F. Chow, X.-H. Li, J. J. Yan, S. S.-Y. Chui, C.-M. Che, *Chem. Sci.*, **2011**, 2, 728-736. (b) P. Wang, C.-H. Leung, D.-L. Ma, W. Lu, C.-M. Che, *Chem. Asian J.*, **2010**, 5, 2271-2280.
- 126) P. Wang, C.-H. Leung, D.-L. Ma, R.W.-Y. Sun, S.-C. Yan, Q.-S. Chen, C.-M. Che, *Angew. Chem. Int. Ed.*, **2011**, 50, 2554-2558.
- 127) T. Lazarevic, A. Rilak, Z. D. Bugarcic, *European Journal of Medicinal Chemistry*, **2017**, 142, 8-31.
- 128) S. D. Cummings, *Coord. Chem. Rev.*, **2009**, 253, 1495-1516.
- 129) C. Yu, K.H.-Y. Chan, K.M.-C. Wong, V.W.-W. Yam, *Proc. Natl. Acad. Sci. U. S. A.*, **2006**, 103, 19652-19657.
- 130) D. A. K. Vezzu, Q. Lu, Y.-H. Chen, S. Huo, *Journal of Inorganic Biochemistry*, 2014, 134, 49–56.
- 131) S. W. Botchway, M. Charnley, J. W. Haycock, A. W. Parker, D. L. Rochester, J. A. Weinstein, J. A. G. Williams, *Natl Acad Sci*, **2008**, 105, 16071–16076.
- 132) R. E. Doherty, I. V. Sazanovich, L. K. McKenzie, A. S. Stasheuski, R. Coyle, E. Baggaley, S. Bottomley, J. A. Weinstein, H. E. Bryant, *Scientific Reports*, **2016**, 6, 22668.
- 133) M. J. Cleare, J. D. Hoeschele, *Bioinorganic Chemistry*, **1973**, 2 (3), 187–210.
- 134) D. Cirri, S. Pillozzi, C. Gabbiani, J. Tricomi, G. Bartoli, M. Stefanini, E. Michelucci, A. Arcangeli, L. Messori, T. Marzo, *Dalton Trans.*, **2017**, 46 (10), 3311–3317.
- 135) L. Messori, L. Cubo, C. Gabbiani, A. Álvarez-Valdés, E. Michelucci, G. Pieraccini, C. Ríos-Luci, L. G. León, J. M. Padrón, C. Navarro-Ranninger, A. Casini, A. G. Quiroga, *Inorg. Chem.*, **2012**, 51 (3), 1717–1726.
- 136) M. Navarro, A. R. Higuera-Padilla, M. Arsenak, P. Taylor, *Transition Met Chem*, **2009**, 34 (8), 869–875.
- 137) M. Navarro, W. Castro, A. R. Higuera-Padilla, A. Sierraalta, M. J. Abad, P. Taylor, R. A. Sánchez-Delgado, *Journal of Inorganic Biochemistry*, **2011**, 105 (12), 1684–1691.
- 138) L. Messori, T. Marzo, C. Gabbiani, A. A. Valdes, A. G. Quiroga, A. Merlino, *Inorg. Chem.*, **2013**, 52 (24), 13827–13829.
- 139) P. J. Bednarski, K. Korpis, A. F. Westendorf, S. Perfahl, R. Grünert, *Proc. R. Soc. A*, **2013**, 371 (1995), 20120118.
- 140) H. Shi, C. Imberti, P. J. Sadler, *Inorg. Chem. Front.*, **2019**, 6 (7), 1623–1638. <https://doi.org/10.1039/C9QI00288J>.
- 141) S. A.-de Castro, E. Ruggiero, A. R.-de-Angulo, E. Rezabal, J. C. M.- Rivas, X. Lopez, F. L. Gallego, L. Salassa, *Chem. Sci.*, **2017**, 8, 4619-4625.

- 142) S. A.-de Castro, A. Terenzi, S. Hager, B. Englinger, A. Faraone, J. C. Martinez, M. Galanski, B. K. Keppler, W. Berger, L. Salassa, *Scientific Reports*, **2018**, *8*, 17198.
- 143) S. A.-de Castro, A. L. Cortajarena, F. L. Gallego, L. Salassa, *Angew. Chem. Int. Ed.*, **2018**, *57*, 3143-3147.
- 144) J. G. Pereda, V. M. Martinez, E. Rezabal, X. Lopez, C. Garino, F. Mancin, A. L. Cortajarena, L. Salassa, *ACS Catal.*, **2020**, *10*, 1, 187-196.

Chapter II

**Theoretical Concepts
and Computational
Methods**



Chapter II Theoretical Concepts and Computational Methods

2.1 Quantum mechanics

The failure to describe several phenomena like photoelectric effect and blackbody radiation using the classical Newtonian mechanics led to the emergence of quantum mechanics. Quantum mechanics (QM) deals with the study of the microscopic systems stationary properties and their evolution over time. In quantum mechanics, particles have wavelike properties and, consequently, a particular wave equation, the Schrodinger equation, governs how these waves behave. Schrödinger equation (SE) can only be solved for simple systems, while for multielectronic systems it is impossible to exactly solve this equation. The wavefunction, is a function that depends on the space and spin coordinates of all electrons and time, $\Psi(r, t)$, and contains all the information regarding the behavior of microscopic particles such as the electrons¹.

Given the impossibility of solving the Schrödinger equation in the case of multielectronic systems approximations have to be introduced to bypass the exact solution of the SE. For example, an approach can be adopted that uses a function that is not directly related to the number of particles and able to describe the system as a whole. Starting from such premise the theoretical method that goes under the name of *Density Functional Theory (DFT)* has been developed. DFT uses a functional strictly dependent on only three spatial coordinates, but independent of the whole number of particles in the system. Supported by the introduction of the Thomas-Fermi model, the energy of a multi-electronic system is evaluated without the explicit use of the wavefunction. The use of this statistical model gives the possibility to derive, for a homogeneous electron gas, a medium potential (VTF) expressible simply through the density $\rho(r)$. The quantum mechanical DFT approach requires, for each energy contribution, a direct dependence on the density, but above all for a

solid theoretical foundation, it was necessary to univocally express all the properties of a system through the density $\rho(r)$ and formulate a variational principle allowing energy minimization. The DFT method is now considered the theoretical method that most effectively approximates real multielectronic systems behavior. In fact, the computational results, compared with those of traditional *ab initio* methods, also correlated, confirm the reliability of the method.

2.1.1 The Born-Oppenheimer approximation

A quantum system can be described by *non-relativistic time-independent Schrödinger equation*.²

$$\hat{H}\psi = E\psi \quad (2.1)$$

where \hat{H} is the Hamiltonian operator for a system of nuclei and electrons described by position vectors R_A and r_i , respectively.

In atomic units, for a general N electrons and M nuclei the Hamiltonian is:

$$\hat{H} = -\sum_{i=1}^N \frac{1}{2} \nabla_i^2 - \sum_{A=1}^M \frac{1}{2M_A} \nabla_A^2 - \sum_{i=1}^N \sum_{A=1}^M \frac{Z_A}{r_{iA}} + \sum_{i=1}^N \sum_{j>1}^N \frac{1}{r_{ij}} + \sum_{A=1}^M \sum_{B>A}^M \frac{Z_A Z_B}{R_{AB}} \quad (2.2)$$

The first term in Eq. (2.2) is the operator for the kinetic energy of the electrons while the second term is the operator for the kinetic energy of nuclei; the third term is the coulomb attraction between electrons and nuclei; the fourth and fifth terms are the repulsion between electrons and nuclei, respectively.

Due to the *Born-Oppenheimer* approximation,³ in equation (2.2), the second term can be neglected, and the last term can be considered constant. The remaining terms in (2.2) compose the electronic Hamiltonian, that is the Hamiltonian describing the motion of N electrons in the field of M point charges.

$$\hat{H}_{elec} = -\sum_{i=1}^N \frac{1}{2} \nabla_i^2 - \sum_{i=1}^N \sum_{A=1}^M \frac{Z_A}{r_{iA}} + \sum_{i=1}^N \sum_{j>1}^N \frac{1}{r_{ij}} \quad (2.3)$$

2.1.2 The Hartree-Fock approximation

To find and describe approximate solutions to the electronic Schrödinger equation is very difficult task. The first attempt to try to solve this problem without the introduction of empirical data coming from experiments is represented by the Hartree-Fock (HF) equations.⁵⁻⁸ The simplest antisymmetric wave function, which can be used to describe the ground state of an N-electron system, is a single Slater determinant.

The variational principle states that the best wave function, of this functional form, is the one which gives the lowest possible energy and, in the Slater Determinant wave function, the variational flexibility is in the choice of spin orbitals.

Minimizing the energy with respect to the choice of spin orbitals leads to the HF equations, that is an eigenvalue equation of the form:

$$f(i)\psi(r_i s_i) = \varepsilon\psi(r_i s_i) \quad (2.4)$$

where $f(i)$ is the Fock operator that includes a one-electron term for the kinetic energy of the i th electron and for the coulomb attraction between the i th electron and nucleus, and two-electron term that measures the “field” seen by the i th electron due to the presence of the other electrons in the other spin orbitals.

The Hartree-Fock equations depend on their eigenfunctions, so they are non-linear equations that must be solved iteratively, using the self-consistent-field (SCF) procedure. However, with the HF approach the motion of the electrons with opposite spins remains not correlated.

Electron correlation can be included explicitly with well-known extensions collectively called post-Hartree-Fock methods,⁹ like *Moller-Plesset perturbation theory (MP)*, the *generalized valence bond method (GVB)*, *configuration interaction (CI)*, *multiconfigurational self-consistent field (MCSCF)* and *coupled cluster theory (CC)*.

These approaches improve the level of accuracy, but become computationally much more demanding and thus are only suitable for relatively small systems. To handle larger systems, an alternative approach has been developed.

2.1.3 Density Functional Theory (DFT)

Density Functional Theory (DFT) allows to deal with large molecular systems, including the electron correlation, with a computational cost much lower than that required by post-HF methods. These DFT advantages are due to the use of the *electron density* $\rho(r)$ as basic variable.

$$\rho(r) = N \int \dots \int |\psi(x_1, x_2, \dots, x_N)|^2 dx_1 dx_2 \dots dx_N \quad (2.5)$$

In contrast to the wave function, ψ_N , that depends on $3N$ variable excluding the spin variable, the electron density $\rho(r)$ depends on 3 variables only, also for many-electron systems.

In 1964, Hohenberg-Kohn introduced the existence of a unique relationship between $\rho(r)$ and all fundamental properties of a given system.¹⁰

2.1.3.1 The Hohenberg-Kohn theorems

The *first theorem* of *Hohenberg-Kohn*¹⁰ affirms that every observable of a quantum mechanical system can be calculated exactly from the ground-state electron density $\rho(r)$, so every observable can be written as a functional of the ground-state electron density $\rho(r)$.

For a system defined by an external potential $v(r)$, acting on the electrons due to the nuclear charges, the energy E_v can be written as functional of the electron density.

Within the approximation of Born Oppenheimer, E_v can be splitted into three terms, which are kinetic energy T , electron-electron repulsion E_{ee} and the nuclei-electron attraction V :

$$E_v[\rho] = T[\rho] + E_{ee}[\rho] + V[\rho] = T[\rho] + E_{ee}[\rho] + \int \rho(r)v(r)dr \quad (2.6)$$

Since the terms T and E_{ee} depend exclusively on the coordinates of the electrons and their forms are the same for all systems, depending only on the number of electrons, they are grouped together into the universal Hohenberg and Kohn functional $F^{HK}[\rho]$.

$$F^{HK}[\rho] = T[\rho] + E_{ee}[\rho] \quad (2.7)$$

F^{HK} contains the functional for the kinetic energy $T[\rho]$ and that for the electron-electron interaction $E_{ee}[\rho]$. The explicit form of both these functionals are unknown.

However, from term $E_{ee}[\rho]$ can be extracted at least, analytically, the classical part $J[\rho]$ that measures the coulomb electron-electron interaction, whereas $Vq[\rho]$ is a measure of the non-classical electronic interaction:

$$E_{ee}[\rho] = J[\rho] + Vq[\rho] = \frac{1}{2} \iint \frac{\rho[r]\rho[r']}{|r-r'|} dr dr' + Vq[\rho] \quad (2.8)$$

The complete form of the ground state energy associated with the density $\rho(r)$, is the functional

$$\begin{aligned} E_v[\rho] &= F^{HK}[\rho] + \int \rho(r)v(r)dr = \\ &T[\rho] + \frac{1}{2} \iint \frac{\rho[r]\rho[r']}{|r-r'|} dr dr' + Vq[\rho] + \int \rho(r)v(r)dr \end{aligned} \quad (2.9)$$

The *second Hohenberg-Kohn theorem*,¹⁰ affirms that for a trial electron density $\tilde{\rho}(r)$, the energy is higher or equal to the real energy of system:

$$E_0 \leq E_v[\tilde{\rho}] \quad (2.10)$$

where E_0 is the correct energy and $E_v[\tilde{\rho}]$ is the energy, written as functional of trial electron density $\tilde{\rho}(r)$, of a system with an external potential $v(r)$.

So, this theorem states the variational principle for the DFT theory. The applicability of the variational principle is limited to the ground state. Hence the strategy cannot be easily transferred to the problem of excited states. According to the two theorems, the energy can be known exactly when the electron density of the system is exact.

2.1.3.2 The Kohn-Sham equations

The explicit form of the functional $F^{HK}[\rho]$ is the major challenge of DFT. Since only the $J[\rho]$ term is known, the main problem is to find the expression for $T[\rho]$ and $Vq[\rho]$.

In 1927 Thomas and Fermi provided the first example of density functional theory. However, the performance of their model presents a deficiency due to the poor approximation of the kinetic energy.

To solve this problem Kohn and Sham proposed, in 1965, a new approach.¹¹

They considered a reference system with non-interacting electrons, having the same density of the real, interacting one.

For the reference system, both the kinetic energy and ground-state electron density can be written using one-electron orbital:

$$T_s[\rho] = \sum_{i=1}^N \langle \psi_i | -\frac{1}{2} \nabla_i^2 | \psi_i \rangle \quad (2.11)$$

$$\rho[r] = \sum_{i=1}^N \sum_s |\psi_i(r, s)|^2 \quad (2.12)$$

The kinetic energy of the real system can be expressed as sum of two contributes: the kinetic energy of the reference system $T_s[\rho]$ and the kinetic energy that measures the electron correlation $T_c[\rho]$

$$T[\rho] = T_s[\rho] + T_c[\rho] \quad (2.13)$$

Consequently, a new redefinition of the universal functional can be introduced:

$$F[\rho] = T_s[\rho] + J[\rho] + E_{xc}[\rho] \quad (2.14)$$

Where $E_{xc}[\rho]$ is the exchange and correlation functional that represents the sum of the terms having an unknown analytically form: i) the difference between the exact kinetic energy and the kinetic energy of the reference system; ii) the non-classical electron-electron interaction; iii) the self-interaction correction.

So the exchange and correlation functional can be defined as

$$E_{xc}[\rho] = (T[\rho] - T_s[\rho]) + (E_{ee}[\rho] - J[\rho]) \quad (2.15)$$

Including all these considerations the expression of energy for the real, interacting system is

$$E_v[\rho] = T_s[\rho] + J[\rho] + E_{xc}[\rho] + \int \rho(r)v(r)dr \quad (2.16)$$

The only term for which no explicit form can be given is E_{xc} .

Applying the variational method, imposing the wave function orthogonality condition and using the Lagrange multipliers method, the Kohn-Sham equations have been obtained:

$$-\frac{1}{2}\nabla_i^2 + v_s(r)\psi_i^{KS} = \varepsilon_i\psi_i^{KS} \quad (2.17)$$

Where v_s is the local potential for the single particle that includes the exchange and correlation potential, v_{xc} , defined as the functional derivative of E_{xc} with respect to $\rho(r)$. So v_s depends on the density and therefore the Kohn-Sham equations have to be solved iteratively.

$$v_{xc} = \frac{\delta E_{xc}[\rho]}{\delta \rho(r)} \quad (2.18)$$

Kohn-Sham equations led to a formalism that is exact and computationally accessible. The only one lack is the fact that the explicit form of the functional E_{xc} is unknown. The major challenge in DFT is to find e improve approximate model for this unknown functional. Although there is no exact solution of this functional, an approximate functional have been proposed. One approach to calculate the functional E_{xc} is the *Local (Spin) Density Approximation* (L(S)DA). This approach is based on assuming that the density ρ varies very slowly and locally with position and can thus be treated as a homogeneous electron gas⁷. In fact, the exchange energy of an electron gas with uniform density can be calculated exactly. Unfortunately, the L(S)DA approximation cannot be used for systems with no uniform electronic distribution. In this case, to yield accurate chemical description, *Gradient Corrected or Generalized Gradient Approximation (GGA)* was introduced. This approximation depend not only on the density ρ , but also on the gradient $\Delta\rho$.

The development of GGA methods is based on two main lines. The first one, also credited *Semiempirical approach* was proposed by Becke.¹²⁻¹⁷ The basic idea is to choose a flexible mathematical functional form depending on one or more parameters extracted from molecular thermochemical data. Exchange functionals of this category are for example Becke88 (B), Perdew-Wang (PW) and modified-Perdew-Wang (MPW);¹⁸⁻²²

The second set of GGA method, nonempirical approach, was proposed by Perdew. This approach provides that the development of exchange- correlation functionals should depend on principles derived by quantum mechanics. Exchange functionals of this category are for example Perdew 86 (P), Perdew-Burke-Ernzerhof (PBE) and modified-Perdew-Burke- Ernzerhof (mPBE).²³⁻²⁵

GGA functionals have been shown to give more accurate predictions for thermochemistry than LSDA ones, but they still underestimate barrier heights. LSDAs and GGAs are “local” functionals because the electronic energy density

at a single spatial point depends only on the behaviour of the electronic density and kinetic energy at and near that point.²⁶

Local functional can be mixed with non-local HF exchange (calculated via Kohn-Sham orbitals) leading to the hybrid functionals, that are often more accurate than local functional especially for main group thermochemistry.

One popular group of hybrid methods is Becke 3 parameter functional (B3), with the three empirical fitted parameters A,B and C:

$$E_{XC}^{B3} = (1 - A)E_x^{Dirac-Slater} + AE_x^{HF} + BE_x^{B88} + E_c^{VWN} + C\Delta E_c^{GGA} \quad (2.19)$$

LSDA exchange, $E_x^{Dirac-Slater}$, is given by the Dirac-Slater formula for a uniform electron gas, and LSA correlation energy E_c^{VWN} is the functional by Vosko, Wilk an Nusair (VWN).²⁷

When ΔE_c^{GGA} gradient correction to correlation in eq. (2.19) is Lee, Yang and Parr functional (LYP),²⁸ the approximate functional is known as B3LYP. So A determines the extent of replacement of the Slater local exchange $E_x^{Dirac-Slater}$ by the exact HF exchange E_x^{HF} ; B controls the addition of Becke's gradient-correction to the exchange functional E_x^{B88} ; C defines the weight of the LYP correlation E_c^{LYP} and the VWN correlation E_c^{VWN} functionals.

In recent years, new density functionals have been developed, belonging to the M05-class and M06-class functionals (including M05, M052X, M06L, M06, M062X, M06HF).²⁹

In this thesis, the B3LYP functional is used to investigate the various reaction mechanisms.

2.1.4 Time-Dependent Density-Functional Theory (TD-DFT)

The fundamental ideas of DFT in the ground state are extended by means of time-dependent scheme to deal with the excitations or time-dependent phenomena in more general, so called TD-DFT. In the TD-DFT, the standard way to obtain the electron density, $\rho(r, t)$ is helped by a fictitious system with non-interacting electrons, i.e. the Kohn-Sham system. The equations for the systems are numerically simple to be solved. The scheme is general and there are two regimes as explained next. When the time dependent potential is weak, it is sufficient to resort to linear response theory and optical adsorption spectra can be calculated for instance. The spectra calculated within this framework agree with experimental results well, although the potential is approximated simply. If the TD potential is strong, full description of the Kohn Sham equations is required. The treatment of atoms or molecules in strong laser field is a canonical example for this regime. In such case, TD-DFT can describe non-linear phenomena (e.g. high harmonic generation or multi-photon ionization).^{30,31} The TD-DFT formulation is analogous derivation of the Kohn-Sham equation from the Schrödinger equation with time-independent regime, except for consideration of time-dependency.

2.1.4.1 Time dependent Kohn-Sham equations

The equations for a set of non-interacting electrons are described by single particle wavefunctions, $\{\phi_i(t)\}$ known as orbitals. The total electronic wavefunction in this context is taken to be a Slater determinant of the single particle orbitals as follow:

$$\psi(t) = \frac{1}{\sqrt{N!}} \begin{bmatrix} \phi_1(r_1, t) & \cdots & \phi_{1N}(r_1, t) \\ \vdots & \ddots & \vdots \\ \phi_1(r_N, t) & \cdots & \phi_N(r_N, t) \end{bmatrix}. \quad (2.20)$$

Herein, the time-dependent density of the interacting system can be computed from the following equation:

$$\rho(r, t) = \sum_{i=1}^N \phi_i^*(r, t) \phi_i(r, t). \quad (2.21)$$

The time-dependent Kohn Sham orbitals are obtained by solving the time-dependent Schrödinger equation of the non-interacting particle system shown below:

$$\left[-\frac{1}{2} \nabla^2 + v_s[\rho](r, t) \right] \phi_j(r, t) = i \frac{\partial \phi_j(r, t)}{\partial t}. \quad (2.22)$$

The single particle Kohn Sham potential is given by the following formula:

$$v_s[\rho](r, t) = \int dr' \frac{\rho(r', t)}{|r-r'|} + v_{ext}(r, t) + V_{XC}. \quad (2.23)$$

The first and second terms represent the Coulomb and the external potentials, respectively, while the third term represents the exchange-correlation potential which is approximated by the same exchange-correlation potential as in time-independent DFT. However, the time-dependent density at a particular time t is used in TD-DFT, rather than the time-independent density.

2.2 Molecular dynamics

Molecular Dynamics (MD) simulations is the method of choice to study the dynamical properties of a system in full atomic detail, condition that the properties are observable within the time scale of the simulations. To calculate the dynamics of the system, which the position of each atom as a function of time, Newton's classical equation of motion are solved iteratively for each atom:

$$F_i = m_i a_i = m_i \frac{d^2 r_i}{dt^2} \quad (2.24)$$

The force on each atom is the negative of the derivative of the potential energy with respect to the position of the atom:

$$F_i = -\frac{\partial V}{\partial r_i} \quad (2.25)$$

If the potential energy of the system is known, then, with the coordinates of a starting structure and a set of velocities, the force acting on each atom can be calculated and a new set of coordinates are generated, from which new forces can be calculated. Reiteration of the procedure will generate a trajectory corresponding to the evolution of the system in time. In molecular dynamics, a classical potential energy function is used that is defined as a function of the coordinates of each of the atoms. The potential energy function is separated into terms representing covalent interactions and non-covalent interactions. The covalent interactions may be described by the following terms:

$$V_{bond} = \sum_{i=1}^{Nb} \frac{k_{bi}}{2} (r_i - r_{i,0})^2 \quad (2.26)$$

$$V_{angle} = \sum_{i=1}^{N\theta} \frac{k_{\theta i}}{2} (\theta_i - \theta_{i,0})^2 \quad (2.27)$$

$$V_{dihedral} = \sum_{i=1}^{N\varphi} \frac{k_{\varphi i}}{2} \cos \left[n_i (\varphi_i - \varphi_{i,0}) \right] \quad (2.28)$$

$$V_{improper} = \sum_{i=1}^{N\xi} \frac{k_{\xi i}}{2} (\xi_i - \xi_{i,0})^2 \quad (2.29)$$

which correspond to two, three, four and four body interactions, respectively. These interactions are represented by harmonic potentials for the bond lengths r_i , for the bond angle θ_i , and for the improper dihedral (out of the plane) angle ξ_i and by a more complex potential for the dihedral angles φ_i . While the non-covalent interactions, which correspond to interactions between particles separated by more than three covalent bonds are usually described by Coulomb's law

$$V_{Coulumb} = \sum_i \sum_j \frac{a_i a_j}{r_{ij}} \quad (2.30)$$

for the electrostatic interactions and by a Lennard-Jones (V_{LJ}) potential

$$V_{LJ} = \sum_i \sum_j \frac{B_{ij}}{r_{ij}^{12}} - \frac{A_{ij}}{r_{ij}^6} \quad (2.31)$$

for the Van der Waals interactions where r_{ij} is the atomic distance between particle i and j . The complete set of parameters used in the potentials (force constants, ideal bond lengths, bond angles, improper dihedral angles, dihedral angles, partial charges and Van der Waals parameters) to describe the interactions between different particle types is called force field (FF). Molecular dynamics is a very in providing detailed information on the structure and dynamics of relatively big systems like proteins, peptides and DNA. MD is considered to be an important preliminary step that helps to have an optimum starting point in higher level of theory investigation like QM. However, MD simulation suffers certain limitations.³² First, it is computationally demanding. Simulation times are currently limited to hundreds of nanoseconds or a few microseconds. Also, the possibility to observe certain properties is directly related to the quality of the force field and, whether or not it has been parameterized for the system simulated. Examples of classical FFs are AMBER,³³ GROMOS,³⁴ CHARMM,³⁵ UFF,³⁶ and OPLS³⁷.

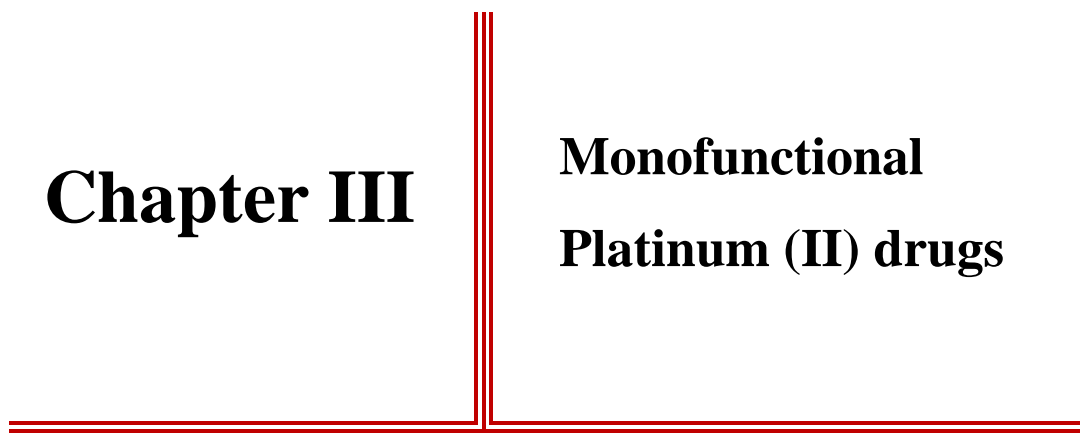
References

- 1) N. J. B. Green, *Quantum Mechanics I: Foundations*, Oxford University, **1997**, page 6.
- 2) E. Schrödinger, *Ann. Physik.*, **1926**, 79, 361-376.
- 3) M. Born, J. Oppenheimer, *Ann. Physik.*, **1927**, 84, 457-484.
- 4) W. Z. Pauli, *Physik.* **1925**, 31, 765-783.
- 5) A. Szabo, N. S. Ostlund, *Modern Quantum Chemistry*, Dover Publication: New York, **1989**.
- 6) D. Hartree, *Proc. Cambridge Phil. Soc.*, **1928**, 24, 89-110.
- 7) D. Hartree, *Proc. Cambridge Phil. Soc.*, **1928**, 24, 111-132.
- 8) D. Hartree, *Proc. Cambridge Phil. Soc.*, **1928**, 24, 426-437.
- 9) V. Z. Fock, *Physik.*, **1930**, 61, 126-148.
- 10) R. J. Bartlett, J. Stanton, *In Reviews in Computational Chemistry*; K. B. Lipkowitz, D. B. Boyd: Eds., VCH Publishers: New York, **1994**, Vol.V.
- 11) P. Hohenberg, W. Kohn, *Phys. Rev. B*, **1964**, 136, 864-871.
- 12) W. Kohn, L. Sham, *J. Phys. Rev. A* **1965**, 136, 1133.
- 13) A. D. Becke, *J. Chem. Phys.* **1986**, 84, 4524-4529.
- 14) A. D. Becke, *J. Chem. Phys.* **1992**, 96, 2155-2160.
- 15) A. D. Becke, *J. Chem. Phys.* **1992**, 97, 9173-9177.
- 16) A. D. Becke, *J. Chem. Phys.* **1993**, 98, 5648-5652.
- 17) A. D. Becke, *J. Chem. Phys.* **1996**, 104, 1040-1046.
- 18) A. D. Becke, *J. Chem. Phys.* **1997**, 107, 8544.
- 19) A. D. Becke, *Phys. Rev. A*, **1988**, 38, 3098-3100.
- 20) J. P. Perdew, Y. Wang, *Phys. Rev. B*, **1986**, 33, 8800.
- 21) C. Adamo, V. Barone, *J. Chem. Phys.*, **1998**, 108, 664-675.
- 22) N. C. Handy, A. Cohen, *J. Mol. Phys.*, **2001**, 99, 403-412.
- 23) X. Xu, W. A. Goddard, *Proc. Natl. Acad. Sci. U.S.A.*, **2004**, 101, 2673-2677.
- 24) J. P. Perdew, *Phys. Rev. B*, **1986**, 33, 8822-8824.
- 25) J. P. Perdew, K. Burke, M. Ernzerhof, *Phys. Rev. Lett.*, **1996**, 77, 3865-3868.
- 26) C. Adamo, V. Barone, *J. Chem. Phys.*, **2002**, 116, 5933-5940.
- 27) (a) R. van Leeuwen, E. J. Baerends, *Phys. Rev. A*, **1994**, 49, 2421-2431; b) A. D. Becke, *J. Chem. Phys.*, **1998**, 109, 2092-2098; c) P. Mori-Sanchez, A. J. Cohen, W. Yang, *J. Chem. Phys.*, **2006**, 124, 91102/1.
- 28) S. H. Vosko, L. Wilk, M. Nusair, *Can. J. Phys.*, **1980**, 58, 1200-1211.
- 29) C. Lee, W. Yang, R. G. Parr, *Phys. Rev. B*, **1988**, 37, 785-789.
- 30) W. Koch, M. C. Holthausen, *A Chemist's Guide to Density Functional Theory*, 2nd Edition, WILEY-VCH Verlag GmbH: Weinheim, **2001**.
- 31) P. Hohenberg, W. Kohn, *Phys. Rev.* **1964**, 136, B864-B871.
- 32) M. Karplus, A. McCammon, *Nature structural biology*, **2002**, 9, 646-652.

- 33) W. D. Cornell, P. Cieplak, C. I. Bayly, I. R. Gould, K. M. Jr Merz, D. M. Ferguson, D. C. Spellmeyer, T. Fox, J. W. Caldwell, P. A. Kollman, *J. Am. Chem. Soc.*, **1995**, *117*, 5179-5197.
- 34) C. Oostenbrink, A. Villa, A. E. Mark, W. F. Van Gunsteren, *J. Comp. Chem.*, **2004**, *25*, 1656-1676.
- 35) B. R. Brooks, R. E. Bruccoleri, B. D. Olafson, D. J. States, S. Swaminathan, M. Karplus, *J. Comp. Chem.*, **1983**, *4*, 187-217.
- 36) A. K. Rappe, C. J. Casewit, K. S. Colwell, W. A. Goddard, W. M. Skiff, *J. Am. Chem. Soc.*, **1992**, *114*, 10024-10035.
- 37) W. L. Jorgensen, J. Tirado-Rives, *J. Am. Chem. Soc.*, **1988**, *110*, 1657-1666.

Chapter III

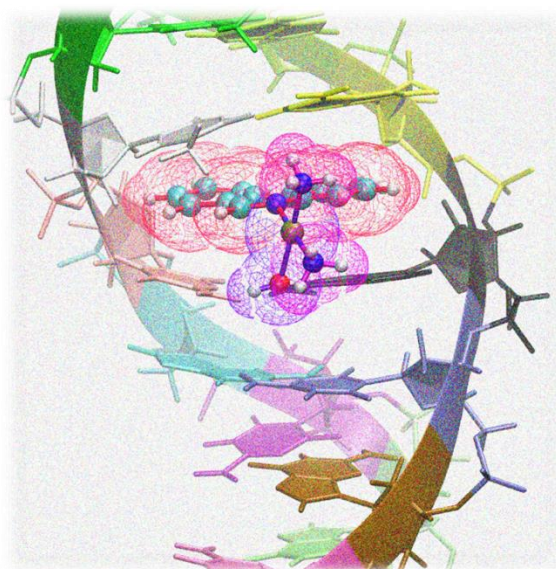
Monofunctional Platinum (II) drugs



Chapter III Monofunctional Platinum (II) drugs

3.1 Rationalization of the superior anticancer activity of phenanthriplatin. An in depth computational exploration.

3.1.1 Introduction



Since the discovery of the anticancer effects of cisplatin and the subsequent FDA approval of its carboplatin and oxaliplatin analogues,¹ research has focused on developing structural analogues belonging to the class of bifunctional platinum based anticancer drugs having the well-accepted classical structure activity relationship (SAR). In cisplatin and its alike, two coordination sites are occupied by labile ligands that can be displaced in the cytoplasm, allowing the formation of bifunctional DNA crosslinks of inter and intra strand types, mostly with guanine nucleobases.^{2,3} leading to an effective DNA distortion and cell apoptosis.

In the continuous research effort to develop more selective drugs with less toxic side effects and lower inherent or acquired resistance, new classes of platinum complexes such as mono-functional platinum drugs have been proposed as non-classical alternatives.⁴⁻⁶

Similar to cisplatin and its derivatives, mono-functional platinum drugs are subject to aquation, that is prevented in blood due to the relatively high concentration of chloride ions and is promoted inside the cell where chlorido concentration is much lower.⁴ Aquation is followed by DNA binding, which are known to be the two activation steps of platinum based drugs. Unlike cisplatin, instead, such drugs form a single bond with DNA as they contain only one labile ligand.

Although pyriplatin, the first monofunctional drug biologically and pharmacologically well characterised, is more than 10-fold less potent than cisplatin^{5,7,8} with the discovery of phenanthriplatin, that is 7-40 times more active than cisplatin, great attention is being focused on this new class of platinum drugs. This huge increase is possibly attributed to some of the characteristic unique features of phenanthriplatin (**Figure 3.1**).^{5,9-11} It is cationic, with a π rich phenanthridine ring that is perpendicular to the metal coordination plane and a steric hindrance created by the bulky asymmetric aromatic ring that might minimize the chance of side reactions with thiol containing deactivating molecules, possibility of DNA intercalation, proven DNA covalent binding and chirality of the complex. All these features as well as the capability of phenanthriplatin to inhibit the transcription process have inspired us to study the drug behaviour.^{5,9-11}

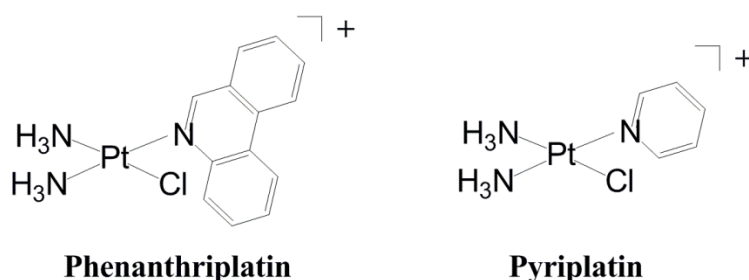


Figure 3.1 Chemical structure of phenanthriplatin and pyriplatin

3.1.2 Aim of study

In this paper, we have studied the activation and interaction mechanisms of a group of mono-functional platinum drugs phenanthriplatin and pyriplatin in comparison to cisplatin in an attempt to find a relationship between structures and anticancer activity especially that the three studied drugs shows a big difference in cytotoxic activity.

Aquation reaction, interaction with guanine and N-acetyl methionine as well as intercalation into, binding to and distortion of DNA have been investigated by using both quantum mechanical DFT and molecular mechanics (MM) and dynamics (MD) computations.

3.1.3 Highlighting results

Although the phenanthridine molecule is chiral, the energy barrier calculated for the two enantiomer interchange was found to be low enough to allow the rapid interconversion between the two enantiomers. The aquation step as well as the interaction with NAM of the three studied complexes and that of cisplatin didn't show any striking difference that can explain the great activity difference among them.

We have then turned our attention to the interaction of phenanthriplatin with DNA dodecamer model by means of intercalation that has revealed a preference for a specific site for the intercalation as calculated by means of MM-GBSA in the framework of the MD calculations (see **Figure 3.2**).

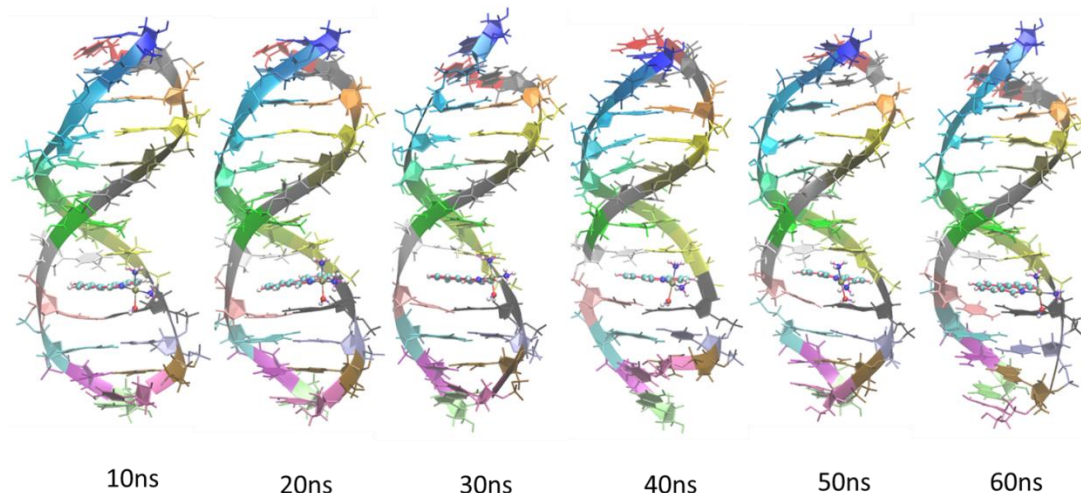


Figure 3.2 The DNA-phenanthriplatin intercalation complex corresponding to the best binding site at 10, 20, 30, 40, 50 and 60 ns

This preferred site was then used for creating a suitable four nucleotide QM model to study the possibility of phenanthriplatin interaction with guanine directly without intercalation *versus* the intercalation followed by covalent binding to guanine. It was found that the intercalation followed by guanine nucleophilic attack is more kinetically favoured, by $7.5 \text{ kcal mol}^{-1}$, compared to the direct guanine attack without intercalation. This result clarifies and supports the role played by the phenanthridine ring in intercalation that can further assist the drug covalent binding compared to pyriplatin, which has not the possibility to intercalate (see **Figure 3.3**).

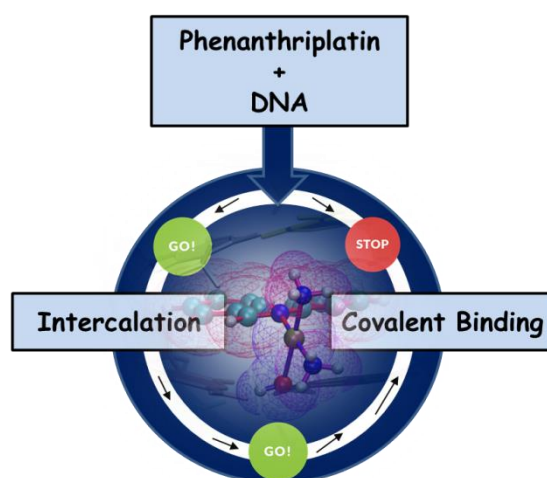


Figure 3.3 A graphical representation of the suggested preference of phenanthriplatin when interacting with DNA

Based on the X-ray crystal structure, as a starting point, of the phenanthriplatin stalled transcription process assisted by polymerase enzyme with phenanthriplatin covalently bound to a guanine nucleotide in the template DNA strand the MD modelling was carried out. It was demonstrated that the DNA template is greatly distorted causing the enzyme being not able to function properly. The MD study has revealed the critical importance played by the phenanthridine ring π - π interactions with the surrounding nucleotides of the template strand allowing a significant distortion, which was strong enough to cause a permanent distortion along the MD simulation, further supported by the calculated MMGBSA binding energies. Compared to pyriplatin, the pyridine ring interaction with surrounding nucleotides is not strong enough to allow a permanent distortion in the DNA template strand.

The above findings have revealed the critical role played by the phenanthridine ring that it is the major cause of the unique cytotoxic activity of phenanthriplatin compared to pyriplatin and cisplatin.

References

- 1) (a) B. Rosenberg, L. Camp, T. Krigas, *Nature*, **1965**, 205, 698-699 ; (b) B. Rosenberg, L. Camp, J. Trosko, V. H. Mansour, *Nature*, **1969**, 222, 385-386 ; (c) L. Kelland, *Nat. Rev. Cancer*, **2007**, 7, 573-584.
- 2) (a) C. F. Harrington, R. C. Le Pla, G. D. Jones, A. L. Thomas, P. B. Farmer, *Chem. Res. Toxicol.* **2010**, 23, 1313-1321; (b) S. Dasari, P. B. Tchounwou, *Eur. J. Pharmacol.* **2014**, 740, 364-378; (c) B. Behmand, J. L. Marignier, M. Mostafavi, J. R. Wagner, D. J. Hunting, L. Sanche, *J. Phys. Chem. B*, **2015**, 119, 9496-9500; (d) E. R. Jamieson, S. J. Lippard, *Chem. Rev.*, **1999**, 99, 2467-2498; (e) J. R. Masters, B. Koberle, *Nat. Rev. Cancer*, **2003**, 3, 517-525; (f) M. Enoiu, J. Jiricny, O. D. Scharer, *Nucleic Acids Res.*, **2012**, 40, 8953-8964; (g) D. Wang, S. J. Lippard, *Nat. Rev. Drug Discov.*, **2005**, 4, 307-320.
- 3) Z. H. Siddik, *Oncogene*, **2003**, 22, 7265-7279.

- 4) A. de Cózar, O. Larrañaga, F. M. Bickelhaupt, E. San Sebastián, E. OrtegaCarrasco, J.-D. Maréchal, A. Lledós, F. P. Cossío, *ChemPhysChem*, **2016**, *17*, 3932–3947.
- 5) a) T. C. Johnstone, J. J. Wilson, S. J. Lippard, *Inorganic Chemistry*, **2013**, *52*, 12234-12239; b) T. C. Johnstone, G. Y. Park, S. J. Lippard, *Anticancer research*, **2014**, 471-476.
- 6) K. S. Lovejoy, M. Serova, I. Bieche, S. Emami, M. D’Incalci, M. Broggin, E. Erba, C. Gespach, E. Cvitkovic, S. Faivre, E. Raymond, S. J. Lippard, *Mol Cancer Ther.*, **2011**, *10*, 1709-1719.
- 7) L. S. Hollis, A. R. Amundsen, E. W. Stern, *J. Med. Chem.*, **1989**, *32*, 128-136.
- 8) D. Wang, G. Zhu, X. Huang, S. J. Lippard, *PNAS*, **2010**, *107*, 9584-9589.
- 9) G. Y. Park, J. J. Wilson, Y. Song, S. J. Lippard, *PNAS*, **2012**, *109*, 11987-11992.
- 10) M. T. Gregory, G. Y. Park, T. C. Johnstone, Y. -S. Lee, W. Yang, S. J. Lippard, *PNAS*, **2014**, *111*, 9133-9138.
- 11) M. W. Kellinger, G. Y. Park, J. Chong, S. J. Lippard, D. Wang, *J. Am. Chem. Soc.*, **2013**, *135*, 13054-13061.

Paper I

Rationalization of the superior anticancer activity of Phenanthriplatin. An in depth computational exploration.

E. Dabbish, N. Russo, E. Sicilia, *Chem. Eur. J.*, **2020**, *26*, 259-268.

Anticancer Agents | Hot Paper |

Rationalization of the Superior Anticancer Activity of Phenanthriplatin: An In-Depth Computational Exploration

Eslam Dabbish, Nino Russo, and Emilia Sicilia*^[a]

Abstract: In the effort to overcome issues of toxicity and resistance inherent to treatment by the approved platinum anticancer agents, a large number of cisplatin variants continues today to be prepared and tested. One of the applied strategies is to use monofunctional platinum complexes that, unlike traditional bifunctional compounds, are able to form only a single covalent bond with nuclear DNA. Chirality, aquation reaction, interaction with guanine and *N*-acetyl methionine as well as, intercalation into, binding to and distortion


of DNA have been investigated by using both quantum mechanical DFT and molecular dynamics computations aiming at contributing to the elucidation of the molecular mechanism underlying the significantly enhanced spectrum of activity of the monofunctional Pt^{II} drug phenanthriplatin. Analogous calculations have been performed in parallel for other two less potent monofunctional Pt^{II} drugs, pyriplatin and enpyriplatin, which show very different cytotoxic effects.

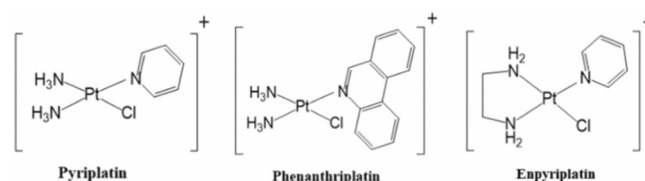
Introduction

Since the fundamental discovery of the anticancer effects of cisplatin and the subsequent clinical approval of its carboplatin and oxaliplatin analogues,^[1] research has focused on developing structural analogues belonging to the class of bifunctional platinum based anticancer drugs having a well-established structure activity relationship (SAR). In cisplatin and its analogues, indeed, two coordination sites are occupied by labile ligands that can be displaced in the cytoplasm, allowing the formation of bifunctional intra- and inter-strand DNA crosslinks, mostly with guanine nucleobases.^[2,3] These crosslinks distort the DNA helix, causing proteins to signal for apoptosis.^[3] In the continuous research effort to develop more selective drugs with less toxic side effects and lower inherent or acquired resistance, new classes of platinum complexes such as monofunctional platinum drugs^[4-6] have been proposed as non-classical alternatives. Similar to cisplatin and its derivatives, monofunctional platinum drugs are subject to aquation, that is prevented in blood due to the relatively high concentration of chloride ions and is promoted inside the cell where chlorido concentration is much lower.^[4] Aquation is followed by DNA binding, which are known to be the two activation steps of platinum-based drugs. Unlike cisplatin, instead, such drugs form a single bond with DNA as they contain only one labile ligand.^[5-7]

Early studies on the monofunctional cationic platinum(II) complexes activity have not been encouraging, as the initially studied monofunctional platinum(II) complexes [PtCl(NH₃)₃]⁺ and [PtCl(dien)]⁺ did not demonstrate to have cytotoxic properties.^[8] The interest in Pt^{II} monofunctional complexes has been renewed by the synthesis and screening activity of monofunctional complexes of general formula *cis*-[Pt(NH₃)₂(Am)Cl]⁺, where Am is an N-heterocyclic ligand.^[9] Such complexes have been synthesized as nitrate salts.^[10] No information has been given about the influence of the identity of the counterion and only the action of the cationic portion has been investigated here. The first synthesized complex of such class, *cis*-[Pt(NH₃)₂Cl(pyridine)]⁺ named pyriplatin (see Scheme 1), has significant antineoplastic action and a cellular response profile different with respect to those of the classic bifunctional, charge-neutral platinum-based drugs.^[5] It has been, indeed, reported that pyriplatin forms monofunctional DNA adducts binding to DNA at the N7 position of guanine residues and, even if no significant distortion is induced, transcription is inhibited.^[6,10] A X-ray crystal structure of pyriplatin interacting with the RNA polymerase II enzyme has revealed that steric hindrance of the pyridine ring and hydrogen bonds formation should reduce cellular repair via transcription, inducing apoptosis with a mechanism different than that of cisplatin.^[9,10] As pyriplatin is more than 10-fold less potent than

[a] E. Dabbish, Prof. N. Russo, Prof. Dr. E. Sicilia
Department of Chemistry and Chemical Technologies
Università della Calabria, Ponte P. Bucci Cubo 14c
87035 Arcavacata di Rende (CS) (Italy)
E-mail: emilia.sicilia@unical.it

 Supporting information and the ORCID identification number(s) for the author(s) of this article can be found under:
<https://doi.org/10.1002/chem.201903831>



Scheme 1. Structure of the cationic portion of the investigated drugs.

cisplatin,^[5,9,10] in the effort to search for analogues with improved activity, the information coming from such experiments has been used to systematically varying the N-heterocyclic ligand leading to the discovery of phenanthriplatin, that is *cis*-[Pt(NH₃)₂Cl(phenanthridine)]⁺, shown in Scheme 1.^[5,7,12,13] Phenanthriplatin has shown a 7–40-fold increase of the cytotoxicity with respect to cisplatin and has displayed a pattern of activity distinct from that of cisplatin and its analogues.^[5,7,12,13] A number of the features of the molecular structure of the cationic phenanthriplatin complex, possibly related to its observed huge increase of cytotoxicity, has been discussed. Phenanthridine ligand is coordinated to platinum such that the plane of the aromatic ligand is perpendicular to the metal coordination plane. The asymmetry of the ligand with respect to the metal coordination plane has been considered to be the cause of both some kind of steric block,^[7,12–15] that can reduce the rate of deactivation by biological thiols^[7,12,15] and chirality of the complex, that can influence the binding to DNA.^[7,12–16] Also the hypothesis that the large aromatic phenanthridine ligand might involve intercalation as a DNA binding mode for phenanthriplatin has been taken into consideration.^[7,12–15] Further studies proved that phenanthriplatin binds to DNA in a purely covalent manner, like cisplatin, being the N7 nucleophilic position of guanine the preferred site of coordination, and inhibits transcription by RNA polymerase II.^[7,12,13] The phenanthriplatin complex is able to block also DNA polymerases.^[12] Among all possible DNA polymerases, the enzymes able to catalyze the replication process, polymerase η is used to continue propagation even in presence of cisplatin-induced damages. Since it has been demonstrated that polymerase η also allows to bypass mutations caused by phenanthriplatin but with a significant low efficiency, the treatment of cancers that are, or can become, resistant to cisplatin can be successfully treated by phenanthriplatin.^[7,12,13] Very recently, a theoretical investigation^[17] and an experimental study^[18] have appeared in the literature dealing with the peculiar anticancer activity of phenanthriplatin, both underlining the key role played by intercalation and π – π stacking in DNA binding, even if from opposite points of view. Indeed, the former concludes that during DNA platination the phenanthridine ring is oriented outward from the double helix and is not intercalated between two base pairs. The latter, instead, suggests that the mechanism of binding of phenanthriplatin to DNA involves the rapid intercalation of the phenanthridine ring that localizes the platinum center on DNA where it irreversibly binds to DNA bases forming covalent bonds. All this information, even contradictory, coming from previous investigations of the specific cytotoxicity of phenanthriplatin compared to that of other Pt^{II} drugs has inspired us to study the activation and interaction mechanisms of a set of a mono-functional platinum drugs in an attempt to find a relationship between structures and anticancer activity. Phenanthriplatin (Phen), pyriplatin (Pyr) and enpyriplatin (Enpyr)^[9,19] mono-functional platinum drugs have been selected as they show very different cytotoxic effects. Enpyriplatin, ([PtCl(en)(py)]⁺, as reported in Scheme 1, is a structural analogous of pyriplatin characterized by the presence of an ethane-1,2-diamine (en) ligand, replacing the two *cis*-ammine ligands of

pyriplatin. In spite of this small structural difference, cytotoxicity of enpyriplatin is drastically reduced with respect to that of pyriplatin, such that this complex has not been tested further. Aquation reaction, interaction with guanine and *N*-acetyl methionine as well as intercalation into, binding to and distortion of DNA have been investigated by using both quantum mechanical DFT and molecular mechanics (MM) and dynamics (MD) computations.

Computational Details

All quantum mechanical calculations have been performed using Gaussian 09 package.^[20] Density functional theory has been employed using the hybrid Becke three parameter exchange functional^[21] and the Lee–Yang–Parr correlation functional,^[22] B3LYP. Grimme dispersion correction for nonbonding interactions has been included using atom pair-wise additive Scheme,^[23] DFT-D3 method. Stuttgart/Dresden effective core potential^[24] and corresponding split valence basis set have been used to describe platinum atom. 6-311+G** basis set has been employed to describe the atoms directly involved in the studied reactions, while the rest of the atoms have been described by the 6-311G** basis set. Frequency calculations have been performed at the same level of theory for all located stationary points to confirm their nature of minima and transition states and for zero-point energy corrections calculations. More details about the adopted protocol is included in the Supporting Information.

In order to study intercalation, using molecular mechanics and molecular dynamics calculations, a B-DNA dodecamer, with Protein Data Bank code 1BNA,^[25] has been used. The phenanthriplatin drug has been manually introduced into the different potential intercalation sites. The initial geometry for the transcription blockage study has been taken from the experimental X-ray structure of the platinum drug phenanthriplatin bound to the DNA with code 4Q8F from the Protein Data Bank.^[12] For the study of pyriplatin and enpyriplatin drugs bound to DNA in the transcription blockage step, phenanthriplatin has been substituted every time with the drug of interest.

For the molecular dynamics study of both of the above mentioned systems, topology and coordinate files have been generated by means of tleap in Amber^[17,26] using the standard DNA.bsc^[27] and gaff force fields^[28] together with the newly generated parameters for the metal center (refer to Supporting Information). A TIP3P solvation model^[29] has been used to construct an octahedral box of water around the DNA complex with a 14 Å buffer distance around the DNA in each direction. Sodium ions have been added to neutralize the system. Minimization and heating have been conducted at a constant volume periodic boundaries (details is in Supporting Information). Equilibration followed by production of molecular dynamics for 20 ns at 300 K have been ran under similar conditions with a 0.002 ps interval with no restraints on DNA. The SHAKE algorithm to constrain bonds involving hydrogen and the cutoff distance of 15.0 angstroms were all maintained. A constant pressure periodic boundary with an average pressure

of 1 atm and an isotropic position scaling with a relaxation time of 2 ps were used. Molecular dynamics production has been extended to 40 or 60 ns for some of the systems under investigation.

For evaluating the relative binding free energy between the different platinum complexes and DNA, MM-GBSA method,^[30] as implemented by MMPBSA.py script in Amber 16 package, has been used evaluating the whole production trajectory over 20 ns. VMD program has been used to generate the figures out of the dynamics trajectory.^[31] For quantum-mechanical calculations of some free energy profiles describing the displacement of water by DNA guanine, a downsized model has been used consisting of the intercalating complex and a B-DNA double helical dimer (2TA or 2CG), that is, four nucleosides and two phosphate residues. Both phosphate residues in the reduced model have been protonated in order to mimic the proximity of a sodium cation and reduced electrostatic charge of the phosphate. With the aim to reduce the required computational effort, the double- ζ 6-31G** basis set has been used for all the atoms, except platinum, given the large size of the model including 160 atoms.

Further detailed information about computations can be found in the Supporting Information.

Results and Discussion

In the next paragraphs the results of our quantum mechanical and MD exploration of the processes that mediate the cytotoxic activity of platinum-based drugs will be illustrated. It is worth mentioning that **Phen** is a chiral molecule.^[15] Then, the behavior of both M and P isomers has been preliminary examined for their interaction with both symmetric and asymmetric molecules such as water and guanine. By water coordination no new chiral center is generated. However, if the same position of water attack with respect to the two isomers is considered the different orientations of the phenanthridine ligand could influence the energetics. Guanine coordination to platinum through the N7, instead, generates a new center of chirality in the same manner as the Pt–N due to asymmetry of the molecule. According to what previously reported^[17] the aquation reaction free energy profiles for the two enantiomers are perfectly superimposable and for water displacement by guanine a very slight preference for the M isomer has been found. Therefore, in the next paragraphs only the results for the M isomer will be reported. Moreover, Lippard and co-workers have demonstrated that chirality does not impact DNA-binding properties of the drug as the rotation about the Pt–N bond of the phenanthridine ligand is fast enough at physiological conditions to racemize the complex.^[15] The energy barrier for the interconversion between the two enantiomers by rotation about the Pt–N (N of phenanthridine) bond has been calculated to be 17.4 kcal mol⁻¹ and the corresponding energy profile is reported in Figure S1 of the Supporting Information. This value of the activation free energy for the interconversion perfectly agrees with the experimentally estimated^[15] upper value of 16.7 kcal mol⁻¹ indicating a rapid enough interconversion between the two isomers, which makes useless to administer

an enantiomerically pure compound. Consistent with what underscored above, only the interaction of the phenanthriplatin M isomer with the right-handed helical conformation of the B-DNA dodecamer model has been examined.

QM simulation of aquation, guanine binding and *N*-acetyl methionine interaction

Quantum mechanical exploration of the following reactions have been carried out: activation by release of the chlorido labile ligand and aquation, binding to guanine, as model of a purine base site of DNA, and interaction with widely distributed in cellular systems sulfur-containing compounds, which can decrease platination levels thanks to their high binding affinity for DNA. Calculations have been carried out for the three selected complexes: pyriplatin (**Pyr**), enpyriplatin (**Enpyr**) and phenanthriplatin (**Phen**).

Aquation

The free energy profiles for the hydrolysis reaction of the monofunctional Pt^{II} complexes under examination are reported in Figure 1 together with a sketch of the located stationary point structures for **Phen**. Several water attack modes have

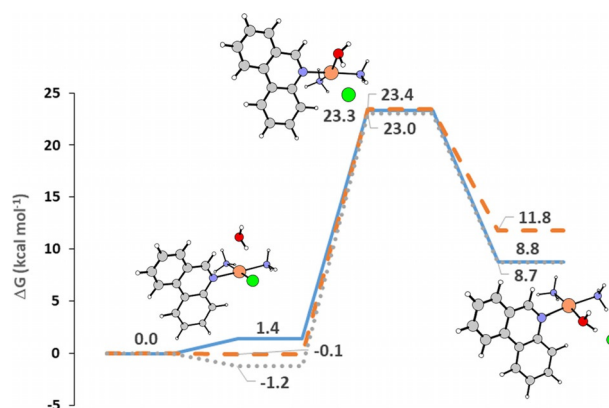


Figure 1. Free energy profiles describing the aquation reaction of **Phen** (solid line), **Pyr** (dashed line) and **Enpyr** (dotted line). Geometrical structures of the stationary points intercepted along the path for **Phen** are also reported. Relative energies are in kcal mol⁻¹ and calculated with respect to the zero-reference energy of separated reactants.

been explored and only one of them, the lowest energy one, has been reported. For the three complexes, the reaction proceeds by formation of a first adduct in which the water molecule interacts with the hydrogen atoms of ammonia molecules. The adducts formation from separated reactants is endergonic by 1.4 kcal mol⁻¹ for **Phen**, thermoneutral for **Pyr** and exergonic by 1.2 kcal mol⁻¹ for **Enpyr**. The reaction proceeds by second-order nucleophilic substitution (S_N2), that is an exchange of the chlorido anion with the water molecule. The transition states for the associative displacement of the chlorido ligand lie 23.3, 23.4 and 23.0 kcal mol⁻¹ above the reactants' reference energy for **Phen**, **Pyr** and **Enpyr**, respectively. That is,

the barrier that is necessary to overcome is $21.9 \text{ kcal mol}^{-1}$ for the displacement of the Cl^- from **Phen**, $23.5 \text{ kcal mol}^{-1}$ from **Pyr** and $24.2 \text{ kcal mol}^{-1}$ from **Enpyr**. The substitution reaction is calculated to be endergonic in all cases, that is by 8.8, 11.8 and $8.7 \text{ kcal mol}^{-1}$ for **Phen**, **Pyr** and **Enpyr**, respectively. The calculated value for the **Phen** complex barrier well compares with that experimentally estimated^[13] of $23.2 \text{ kcal mol}^{-1}$ even if it is slightly lower. No significant difference in the calculated energy barriers for the three studied complexes exists, although the trend agrees with the order of anticancer activity, being **Enpyr** the complex with the highest energy barrier and **Phen** the lowest one. Energy barrier heights can be compared with the values for the reference drug cisplatin. The theoretical value has been recently calculated to be $24.0 \text{ kcal mol}^{-1}$, whereas the experimentally estimated are 23.8 and $24.1 \text{ kcal mol}^{-1}$.^[32] It is, therefore, confirmed that the presence of a more or less extended π -system ligand does not affect the aquation process.

Only for **Phen** complex the impact of the presence of additional surrounding water molecules has been examined so as to include microsolvation effects. The outcomes of this analysis including 1, 2, 3 and 10 additional molecules have been summarized in Table S1 of the Supporting Information. 10 molecules have been added to create a uniform distribution less dependent on the specific position of the solvent molecules. From an inspection of the table, it appears that the presence of additional solvent molecules slightly changes the description of the aquation reaction causing an increase of the activation barrier height of about $1\text{--}2 \text{ kcal mol}^{-1}$.

Reaction with *N*-acetyl methionine

Low-molecular-weight sulfur containing molecules, very abundant in human cells, possess a high binding affinity for platinum and can cause inactivation of Pt complexes by forming stable adducts, thus preventing the drugs from reaching and binding to DNA and, then, decreasing their efficacy. Lippard and co-workers^[7] have examined the reactivity of both **Pyr** and **Phen** with *N*-acetyl methionine (NAM) as sulfur containing compound model. Indeed, the use of NAM allowed the direct comparison of the reactivities of the examined complexes. As a result of such investigation, **Phen** has been found to be more inert to NAM than **Pyr** and the products of such reaction, detected through ESI-MS, correspond to $[\text{Pt}(\text{NH}_3)(\text{Am})(\text{N-Ac-Met})\text{Cl}]^+$, where the Am group represents pyridine for **Pyr** and phenanthridine for **Phen**. Such inactive metabolites of the parent complexes should be obtained by displacement of a chlorido ligand by NAM, followed by release of ammonia and binding of chlorido due to the strong kinetic *trans* effect of the sulfur donor. The stepwise formation of the two $[\text{Pt}(\text{NH}_3)(\text{Am})(\text{N-AcMet})\text{Cl}]^+$ (Am = pyridine, phenanthridine) metabolites has been computationally examined. Free energy profiles for **Pyr** and **Phen** are shown in Figure 2 together with a sketch of the intercepted stationary point structures for the attack on **Phen**. Formation of the first adduct is equally exergonic for the two complexes by $14.6 \text{ kcal mol}^{-1}$. In analogy with the aquation reaction, the attack of NAM occurs out of

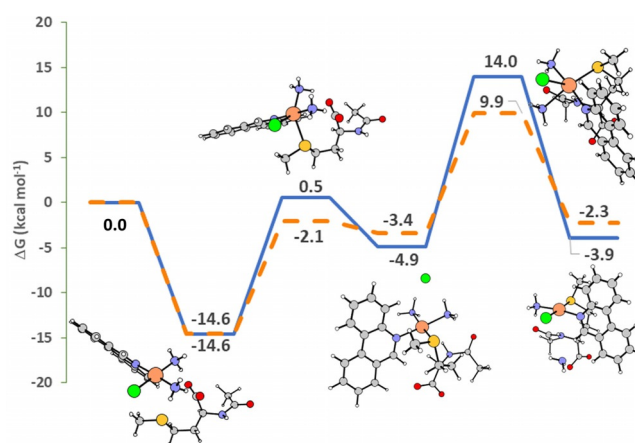


Figure 2. Free energy profiles describing the attack of NAM to **Phen** (solid line) and **Pyr** (dashed line). Geometrical structures of the stationary points intercepted along the path for **Phen** are also reported. Relative energies are in kcal mol^{-1} and calculated with respect to the zero-reference energy of separated reactants.

the molecular plane and in the transition state the S atom forms with Pt and Cl an angle of 82.2° and 80.6° for **Phen** and **Pyr**, respectively. The heights of the corresponding energy barriers for the displacement of the chlorido ligand are 15.1 and $12.5 \text{ kcal mol}^{-1}$. The formed products lay below the zero reactants' reference energy by $4.9 \text{ kcal mol}^{-1}$ for **Phen** and $3.4 \text{ kcal mol}^{-1}$ for **Pyr**. The subsequent second-order nucleophilic substitution ($\text{S}_{\text{N}}2$), which allows the exchange of the ammonia molecule in *trans* position to NAM with a chlorido ligand, proceeds surmounting an energy barrier of 18.9 and $13.3 \text{ kcal mol}^{-1}$ for **Phen** and **Pyr**, respectively. The whole reaction is calculated to be exergonic for both **Pyr** ($-2.3 \text{ kcal mol}^{-1}$) and for **Phen** ($-3.9 \text{ kcal mol}^{-1}$).

Analogous calculations have been carried out for cisplatin. The corresponding free energy profile is reported in the Supporting Information (see Figure S3).

The height of the energy barrier for the first attack of Pt to NAM to displace one of the chlorido ligands is $14.4 \text{ kcal mol}^{-1}$ and for the subsequent replacement of the ammonia *trans* to NAM the barrier is $19.4 \text{ kcal mol}^{-1}$. The products of the first and second substitution reactions lie 18.0 and $8.1 \text{ kcal mol}^{-1}$ below the reactants' reference energy. Therefore, the kinetics of the reaction of **Phen** is not significantly slower than that of cisplatin, whereas the large difference in thermodynamics, according to what has been underlined in ref. 6, should control the impact of the interaction of the drugs with sulfur-containing biomolecules. With respect to **Pyr**, instead, the presence of the bulky phenanthridine ligand appears to be decisive to slow down the involved rearrangements that could be responsible for the severe side effects accompanying platinum drugs intake.

Guanine binding

In analogy with the action of classical Pt^{II} drugs, the aquation step of monofunctional complexes is followed by the displacement of the water molecule due to the interaction with DNA

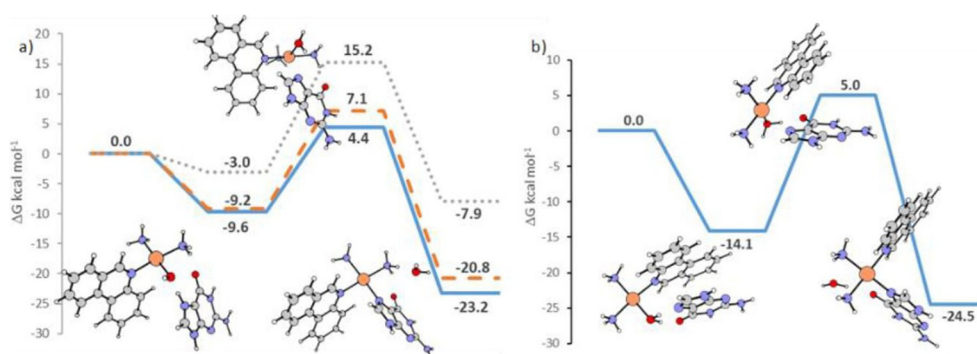


Figure 3. Free energy profiles describing the guanine interaction of a) **Phen** (solid line), **Pyr** (dashed line) and **Enpyr** (dotted line) and b) **Phen** when π - π stacking is taken into account. Geometrical structures of the stationary points intercepted along the path for **Phen** are also reported. Relative energies are in kcal mol⁻¹ and calculated with respect the zero reference energy of separated reactants.

bases. Therefore, the interaction of the aquated form of **Phen**, **Pyr** and **Enpyr** complexes with a purine base of DNA has been computationally investigated using guanine as model system. Corresponding free energy profiles are shown in Figure 3a). Also, in this case, geometrical structures of the stationary point for the **Phen** complex have been sketched, whereas structures for **Pyr** and **Enpyr** complexes can be found in Figure S4 and S5 of the Supporting Information. The interaction with guanine occurs via the N7 site and involves, as the first step, formation of a stable adduct that lies at -11.5 , -11.1 and -12.0 kcal mol⁻¹ below the reference energy of separated reactants for **Phen**, **Pyr** and **Enpyr**, respectively. It is worth mentioning that formation of the first adduct, as it appears in Figure 3a, is accompanied by the transfer of one of the water ligand protons to the guanine N7 position. This phenomenon, that has been already highlighted and discussed,^[33,34] does not seem to have a significant influence on the subsequent transition state formation. The transition state for the associative displacement of the water molecule and coordination of guanine lies 2.5 kcal mol⁻¹ above the reactants' zero reference energy for **Phen**, 5.3 kcal mol⁻¹ for **Pyr** and 3.2 kcal mol⁻¹ for **Enpyr**, whereas the whole process leading to the final N7-coordinated guanine complexes is exergonic for all the complexes ($\Delta G_{\text{Phen}} = -25.1$, $\Delta G_{\text{Enpyr}} = -22.7$, $\Delta G_{\text{Pyr}} = -26.5$ kcal mol⁻¹). The calculated barriers that is necessary to overcome for the substitution to occur are, therefore, 14.0, 16.4 and 15.2 kcal mol⁻¹ for **Phen**, **Pyr** and **Enpyr**, respectively. The heights are very similar amongst them and comparable with the values that have been calculated for the same substitution in cisplatin that is 16.8 kcal mol⁻¹^[33] and 17.8 kcal mol⁻¹.^[17] Moreover, it is confirmed^[7] that the increased steric hindrance of the phenanthridine ring does not affect the rate of the reaction. Once again, only for **Phen** an extra water molecule has been added. The calculated free energy profile is shown in Figure S2 of the Supporting Information. In this new arrangement the reciprocal positions of the leaving water ligand and the N7 atom of guanine do not allow the proton transfer to occur. The adduct at the entrance channel is stabilized and the height of corresponding energy barrier becomes 16.3 kcal mol⁻¹. However, the value of 14.0 kcal mol⁻¹, or eventually 16.3 kcal mol⁻¹, calculated for **Phen** is lower than the barrier experimentally estimat-

ed by Lippard and co-workers^[14] that is 23.5 kcal mol⁻¹. Such discrepancy has been rationalized by Cerón-Carrasco and co-workers^[17] as a consequence of the particular more stable arrangement adopted by the isolated base in the experiments. Indeed, when the phenanthridine ring is oriented parallel to guanine a favorable π - π interaction stabilizes the adduct formed between the complex and the base, whereas the energy of the corresponding transition state does not change, with a consequent increase of the barrier height. Our calculations, as shown in Figure 2b, confirm that the height of the barrier that is necessary to overcome increases and becomes 19.1 kcal mol⁻¹. The authors, however, claim that such arrangement is inaccessible in the real environment as, on the basis of computational outcomes,^[17] during DNA platination the phenanthridine ring is oriented outward from the double helix and is not intercalated between two base pairs.

Analogous calculations have been carried out to prove whether a similar arrangement can be assumed by the other two complexes under examination. However, the initial imposed parallel orientation of both **Pyr** and **Enpyr** pyridine ring and guanine is not retained during the optimization. This result can be considered a preliminary indication of the difference in intercalating propensity of the examined complexes that might influence the subsequent binding to DNA accordingly.^[18]

With the aim to further test how the possibility of establishing π - π interactions with additional bases can influence the metal attack on guanine to displace water, simulations have been carried out considering the presence of more than one guanine molecule. The presence of additional guanine molecules better reproduce the conditions used in the experiments from which the constants have been obtained.^[14] The free energy profiles describing the outcomes of these calculations are depicted in Figure 4. In the same Figure the structures of all the intercepted stationary points are reported. Three different situations have been simulated. Two additional guanine units are initially disposed parallel to the phenanthridine ligand to simulate a sort of intercalation. This arrangement is saved during the whole optimization. π - π stacking stabilizes equally well all the stationary points with respect to the energy profile reported in Figure 3a. The height of the energy

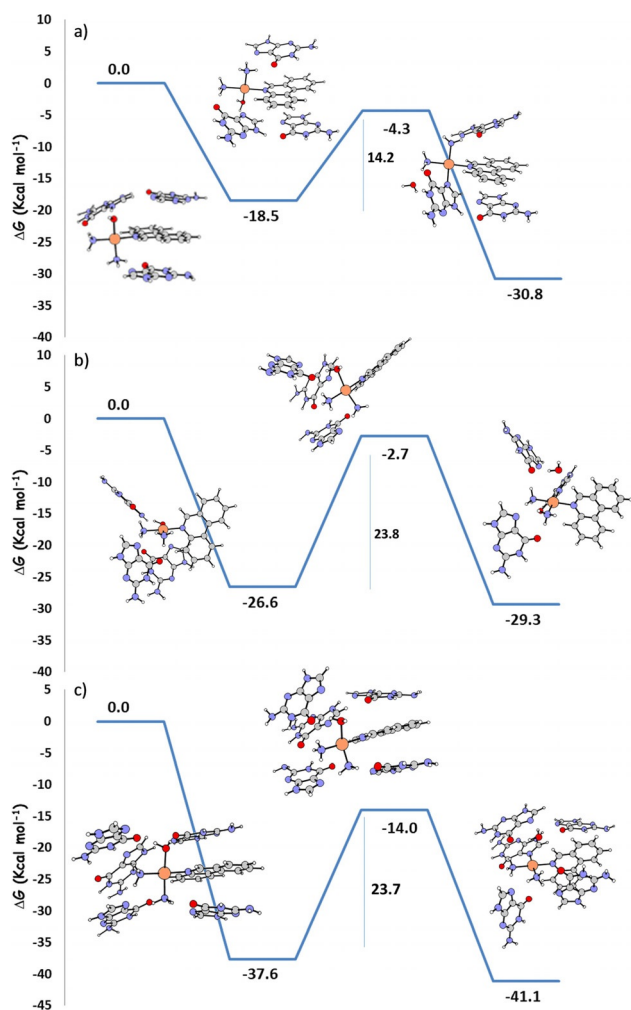


Figure 4. Free energy profiles describing guanine interaction of **Phen** including a) two additional guanine molecules interacting with the phenanthridine ligand, b) two additional guanine molecules interacting with the reacting guanine and c) four additional guanine molecules two of which interacting with the phenanthridine ligand and two with the reacting guanine. Geometrical structures of the intercepted stationary points are also reported. Relative energies are in kcal mol⁻¹ and calculated with respect the zero-reference energy of separated reactants.

barrier is 14.2 kcal mol⁻¹, that is very close to the value of 14.0 kcal mol⁻¹ calculated in absence of the two additional guanines. In the second situation the two additional molecules are disposed close to the reacting guanine to interact with it.

As shown in Figure 4b, such interaction is very stabilizing for the first adduct, but detrimental for the rearrangement required to occur in the transition state. As a consequence, the energy barrier increases and becomes 23.8 kcal mol⁻¹. In the third situation illustrated in Figure 4c, four additional guanine molecules have been included: two from the side of the phenanthridine ligand and two from the side of the reacting guanine. All the intercepted stationary points are stabilized by π - π interactions and the barrier for the substitution continues to be 23.7 kcal mol⁻¹ due to the hindered arrangement of the two molecules interacting with the reacting guanine. This value of the height of the barrier reproduces very well that reported by Lippard and co-workers.^[14] Therefore, when experi-

mental conditions entailing an excess of guanine molecules are reproduced, theoretical and experimental estimates of the rate of the reaction coincide. Mimicking intercalation and π - π stacking by additional guanine molecules causes a general stabilization of all the stationary points. Additional guanines interacting with the reacting base, instead, disturb the process and slow down the reaction rate according to what recorded by experiments.^[14] The former arrangement in some respects replicates the proposal by Lippard and co-workers^[18] of an intermediate intercalated state that allows phenanthriplatin to come in proximity of the N7 coordination site of a guanine base facilitating the formation of the covalent bond.

MD simulation of drugs interaction with DNA

On the basis of the results reported in the previous paragraphs it appears that none of the investigated aspects allows to explain the superior cytotoxic activity of phenanthriplatin with respect to both cisplatin and **Pyr** and **Enpyr** analogues. The asymmetry of the phenanthridine ligand causes the complex to be chiral. However, due to the rapid interconversion between the two enantiomers, the use of one of them does not give any advantage. Aquation reaction barrier does not significantly differ from those calculated and, when available, experimentally estimated for both **Pyr** and **Enpyr** complexes and cisplatin. The outcomes of the investigation about the interaction of **Phen** with sulfur-containing molecules show that its behavior is similar to that of cisplatin. Finally, when DNA platination is simulated by the attack to a single guanine molecule and ruling out the possibility that intercalation could occur, calculated heights of the barrier are very similar for all the complexes under investigation. However, the aspect of the interaction of the **Phen** drug with DNA merits further investigation, especially because of the conflicting results^[17,18] that, as already underscored above, have been reported concerning the role that should be played by intercalation in assisting formation of the bond between Pt and DNA bases.

Intercalation

Intercalators are compounds capable of inserting between adjacent base pairs of the double stranded DNA. The intercalation structure is usually stabilized by non-covalent interactions between the intercalator molecule and the surrounding nucleotides. Stacking effect as well as hydrogen bonding with surrounding nucleotides are the most important factors in governing the intercalation process, which, in turn, can induce conformational and functional changes in the DNA and ultimately lead to cell apoptosis. The stabilization energy of the cationic intercalators is reported to be considerably larger than that of the uncharged ones.^[36] Intercalation is believed to be a two-step process in which an outer complex is formed in the first step followed by the ligand insertion in the second step.^[35,36] Molecular dynamics simulations have been used to study the intercalation of the aquated cationic **Phen** complex into DNA. **Phen** intercalation, beside the induced structural changes in the DNA double helix, also might help bringing the

drug close to the DNA target bases, in particular guanine, facilitating the water ligand replacement and formation of strongly covalently bound Pt-DNA adducts. The estimation of the binding strength of the aquated phenanthriplatin at different potential sites of the adopted model DNA can give insights into the possible mechanism of action of the drug. The binding of aquated phenanthriplatin at different sites of the DNA dodecamer has been examined as shown in Figure 5. Several binding sites, in which the drug has been manually placed in all the studied cases, have been chosen across the major groove.

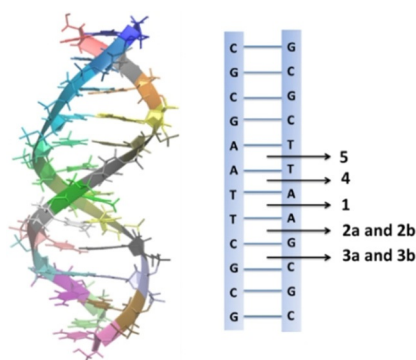


Figure 5. Possible intercalation positions in bare B-DNA dodecamer.

For all the investigated positions the phenanthridine ligand points towards the groove. For the 2 and 3 binding sites, different arrangements of the aquated **Phen** corresponding to different positions of the water molecule relative to the surrounding nucleotides have been taken into consideration as shown in Figure 6. The intercalation is found to cause a confor-

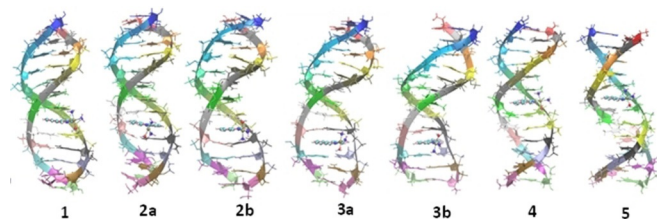


Figure 6. B-DNA dodecamer with the **Phen** complex intercalated at the different positions after 20 ns of dynamics simulation.

mational distortion in the modeled DNA with an initial stretching of the DNA length owing to the increased spacing between the base pairs at the intercalation site. The DNA length change calculated as the end-to-end distance of the helix, measured from the two terminal base pairs center of mass and taking drug-free DNA as a reference, is also reported in Figure S6 of the Supporting Information.

Binding free energy of the aquated phenanthriplatin at the different proposed intercalation sites has been calculated by means of the MM-GBSA approach. Detailed information about the results of the analysis, including the different MM-GBSA contributions to the total energy of each species are reported

in Table S2 of the Supporting Information. Position labeled **2a** is found to be the most preferred intercalation site with a binding energy of $-21.0 \text{ kcal mol}^{-1}$, even if very close to $-20.8 \text{ kcal mol}^{-1}$ for the next preferred **3b** and **2b** positions. The **2a** arrangement, besides being the most preferred in terms of binding energy, also shows the shortest distance, about 2.8 \AA , between the N7 guanine nitrogen atom and the platinum center throughout the dynamics which is expected to facilitate the potential attack of platinum on guanine replacing the water molecule.

In order to obtain better statistics, trajectories simulating the three arrangements labeled **2b**, **3a** and **3b** have been extended up to 40 ns, while for the most preferred site **2a** simulations have been extended up to 60 ns. Figure S6 shows the DNA-drug complex corresponding to the arrangement labeled **2a** at 10, 20, 30, 40, 50 and 60 ns. Figures for **2b**, **3a** and **3b** are included in the Supporting Information (Figure S7). Simulations show that the binding due to the intercalation is stable over the whole simulation time.

Transcription inhibition

As underlined above, in order to limit the amount of active platinum drugs in the cell and the number of platinum-DNA lesions, cancer cells adopt several strategies to survive. One of such mechanisms, at the origin of drug resistance, is to increase the rate at which they repair platinated DNA. For circumventing the induced DNA lesions, even if they are associated with large distortions of the double helix structure, cancer cells use polymerases. Among all DNA polymerases it has been established that tumors use the polymerase η enzyme to continue their propagation. Pol- η is significantly less efficacious in bypassing **Phen** mutations with respect to bifunctional Pt^{II} drugs and intercalation of **Phen** has been suggested to prelude and assist the platination step that causes a severe twist of the double helix. Molecular dynamics computations have been carried out to study the distortion in DNA induced by platination using as initial geometry the DNA-Phen complex portion, cutting the embedding enzyme (see Figure 7a) extracted from the X-ray structure deposited in the Protein Data Bank with code 4Q8F. Aiming at finding an explanation for the difference in activity between the studied monofunctional platinum drugs, analogous calculations have been carried out sub-

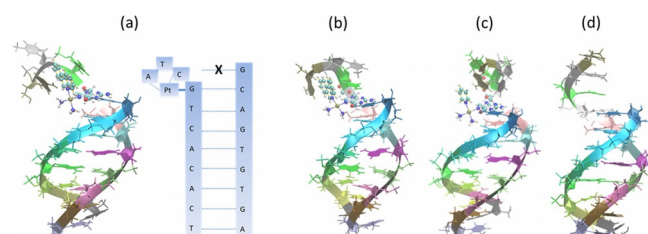


Figure 7. a) Portion of the X-ray structure (PDB code 4Q8F) of the phenanthriplatin-DNA adduct excluding the embedding Pol- η . b) Perturbed DNA conformation caused by the insertion of **Phen** at 20 ns. c) Perturbed DNA conformation caused by the insertion of **Pyr** at 20 ns. d) Unperturbed drug-free DNA structure at 20 ns.

stituting **Phen** with **Pyr** and **Enpyr** complexes. Additionally, in order to check the effect of the lack in the drug of an aromatic N-heterocyclic ligand, phenanthridine has been substituted with ammonia. The more the drug is strongly bound to DNA and the more it induces a conformational distortion, the greater the ability to hinder the transcription process and act effectively. Based on this assumption, the conformational distortion caused by the drug on the surrounding nucleotides has been evaluated by calculating the RMSD for the four different studied cases taking the drug free system as a reference. Perturbation of the DNA conformation due to **Phen** and **Pyr** insertion is reported in Figure 7b,c, respectively.

The drug that induces more conformational distortion is expected to have a greater RMSD. Calculations demonstrate that **Phen** is capable of inducing the most prominent degree of conformational distortion. Several forms of RMSD analysis are included in the Supporting Information and are reported in Figures S8 and S9.

Comparison of the conformation of the drug-DNA complex for both **Phen**, Figure 7b, and **Pyr**, Figure 7c, after 20 ns of molecular dynamics shows that, although the RMSD is very similar at the end of dynamics as reported in the Supporting Information, **Pyr** is totally not interacting with the terminal part of the DNA template single strand and thus expected to lose its activity. If **Phen** behavior is examined, instead, the distorted initial conformation, in which the DNA single strand is twisted and surrounds the N-heterocyclic ligand, remains intact. RMSD plots for both complexes shown in Figure S10 and S11 of the Supporting Information clearly confirm such behavior. Furthermore, relative binding energies of the four different complexes with respect to the modeled DNA have been estimated by means of MM-GBSA. Again, **Phen** is found to be the drug with the largest value of the binding energy followed, as expected, by **Pyr**, **Enpyr** and finally by the complex in which ammonia substitutes phenanthridine. The outcomes of the binding energy computations are reported in Table S3. In order to understand the nature of the interaction of the drugs with the surrounding nucleotides, van der Waals and electrostatic contributions have been comparatively evaluated. Although the electrostatic interaction represents the major contribution to the detected interaction, it is nearly similar for the different drugs. The most significant differences, instead, exist when the vdW contribution is examined, as shown in panel a of Figure 8 for **Phen** and **Pyr**, being the highest in case of **Phen** followed by both **Pyr** and **Enpyr** and finally the complex having an ammonia ligand. This trend depends on the ability of the phenanthridine ring to establish π - π interactions with the surrounding bases causing more significant and persistent distortions of the DNA template, thus allowing more effective transcription inhibition. The green surfaces reported in panel b of Figure 8, representing the contact due to weak interactions (see Supporting Information for more details), highlight the difference in behavior between **Phen** and **Pyr** drugs interacting with DNA. Interactions, mainly stacking in nature, that are established between **Phen** and the surrounding nucleotides, corresponding to an extended green surface, are lacking when **Pyr** is considered.

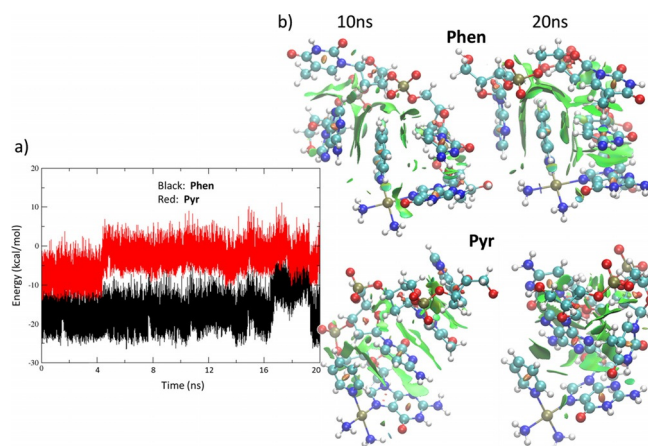


Figure 8. Van der Waals contribution a) extracted from decomposition analysis of the MM-GBSA DNA-drug complexes binding energy, and b) plot, shown as green surfaces, for the **Phen**-DNA and **Pyr**-DNA complexes at 10 and 20 ns.

QM description of the interaction with DNA of the intercalated and non-intercalated **Phen** drug

As a last step of our study, the role that should be played by intercalation in assisting DNA platination has been further examined performing quantum mechanical DFT computations. The displacement step of the bound water ligand by guanine base has been simulated by considering a DNA fragment of two base pairs. The attack of the guanine base has been simulated considering **Phen** complex in both intercalated and non-intercalated arrangements. One snapshot from the MD simulation of the binding site named 2a, in which the drug is stacked within the adenine-thymine (AT) and guanine-cytosine (GC) base pairs, has been selected to be used as the initial geometry to locate the stationary points along the pathway involving the intercalated **Phen** complex. Therefore, the region of interest, including 160 atoms, has cut and quantum-mechanically optimized at DFT level. In the selected geometry used to locate the transition state the distance between the platinum center and the N7 position of guanine is, at the beginning, about 2.8 Å. For the simulation of the adduct in which the phenanthridine ring is oriented outward from the double helix and is not intercalated between two base pairs, the fragment has been extracted from the MD simulation of the isolated DNA and optimized together with the **Phen** complex, in the same position indicated as 2a, for a total of 160 atoms in the downsized model. The outcomes of such computations are reported in Figure 9.

The path calculated for the guanine attack to the intercalated **Phen** complex involves a barrier of 11.4 kcal mol⁻¹, whereas the formation of the product is calculated to be almost thermoneutral. Along the free energy profile for the attack to the non-intercalated **Phen**, the intercepted transition state results to be higher in energy by 18.9 kcal mol⁻¹ than the adduct leading to it. The product of the substitution reaction is stabilized by 4.6 mol⁻¹ with respect to the initial adduct. Several possible favorable arrangements of the two interacting species have been taken into consideration and only one of them, besides

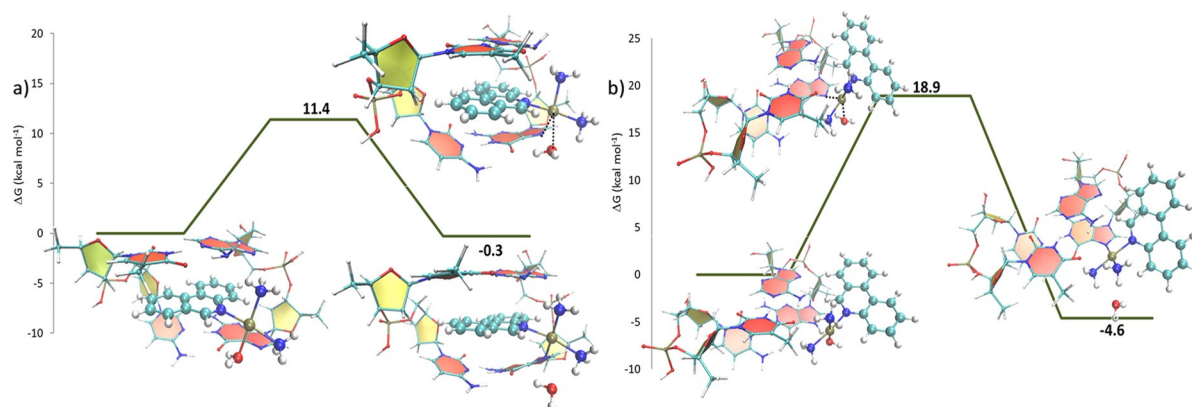


Figure 9. Free energy profiles describing the DNA guanine attack to a) intercalated, and b) non-intercalated **Phen**. Geometrical structures of the intercepted stationary points are also reported. Relative energies are in kcal mol⁻¹ and calculated with respect the zero-reference energy of the initial adduct.

that reported in Figure 9, has successfully led to a transition state that, however, involves a barrier of 20.1 kcal mol⁻¹, as reported in Figure S12 of the Supporting Information. Such results definitively support the hypothesis that DNA intercalation allows the labile water leaving ligand, in the intercalating moiety, to be optimally arranged to promote formation of new Pt-DNA bonds.

Conclusions

In the present paper many of the hypotheses that have been formulated to rationalize the superior cytotoxic activity of phenanthriplatin with respect to both cisplatin and **Pyr** and **Enpyr** analogues have been explored in detail using both quantum-mechanical DFT and molecular dynamics calculations. The investigation of the first aspect taken into consideration, that is the asymmetry of the phenanthridine ligand causing the complex to be chiral, has shown that both the two enantiomers have very similar activities. Moreover, due to the rapid interconversion between the two enantiomers, the use of one of them does not give any advantage. The energy barrier calculated along the hydrolysis path does not significantly differ from those calculated and, when available, experimentally estimated for both **Pyr** and **Enpyr** complexes and cisplatin. The outcomes of the investigation about the interaction of **Phen** with sulfur-containing molecules, using NAM as a model, show that its behavior is similar to that of cisplatin. Calculated barrier heights of DNA platination simulated by the attack to a single guanine molecule and excluding that intercalation could occur, are very similar for all the complexes under investigation. The presence of additional guanine molecules, instead, can influence the course of the reaction increasing or decreasing the rate as a function of the interactions that can be established. The interaction of the **Phen** complex with DNA has been thoroughly investigated as this aspect seems to be key factor in determining the peculiar anticancer activity of this drug. MD calculations of the binding energy have allowed to select the most favorable arrangement of the intercalating aquated drug in the double helix of a DNA dodecamer considering several possible alternatives. The conformational distortion caused by

strongly bound drugs to DNA and, as a consequence, the ability to hinder the transcription process and limit the development of drug resistance, has been evaluated for **Phen**, **Pyr**, **Enpyr** and an additional system in which the aromatic ring has been substituted by an ammonia. The most prominent conformational distortion on the surrounding nucleotides from MD calculation results to be caused by the **Phen** complex followed, as expected, by **Pyr**, **Enpyr** and finally by the complex in which ammonia substitutes phenanthridine. Finally, the role that should be played by intercalation in assisting DNA platination has been further examined performing quantum mechanical DFT computations considering a DNA fragment of two base pairs and the intercalating and non-intercalating drug. The barrier calculated for the non-intercalating drug is higher by 7.5 kcal mol⁻¹ than that for the intercalated drug demonstrating that DNA intercalation permits the labile water leaving ligand of the intercalating moiety to be properly arranged to promote displacement and formation of new bonds between Pt and DNA bases.

Acknowledgements

This research was supported by Università della Calabria.

Conflict of interest

The authors declare no conflict of interest.

Keywords: density functional calculations · intercalation · molecular dynamics · phenanthriplatin · platinum

- [1] a) B. Rosenberg, L. Camp, T. Krigas, *Nature* **1965**, *205*, 698–699; b) B. Rosenberg, L. Camp, J. Trosko, V. H. Mansour, *Nature* **1969**, *222*, 385–386; c) L. Kelland, *Nat. Rev. Cancer* **2007**, *7*, 573–584.
[2] a) C. F. Harrington, R. C. Le Pla, G. D. Jones, A. L. Thomas, P. B. Farmer, *Chem. Res. Toxicol.* **2010**, *23*, 1313–1321; b) S. Dasari, P. B. Tchounwou, *Eur. J. Pharmacol.* **2014**, *740*, 364–378; c) B. Behmand, J. L. Marignier, M. Mostafavi, J. R. Wagner, D. J. Hunting, L. Sanche, *J. Phys. Chem. B* **2015**, *119*, 9496–9500; d) E. R. Jamieson, S. J. Lippard, *Chem. Rev.* **1999**, *99*, 2467–2498; e) J. R. Masters, B. Koberle, *Nat. Rev. Cancer* **2003**, *3*, 517–

- 525; f) M. Enoiu, J. Jiricny, O. D. Schärer, *Nucleic Acids Res.* **2012**, *40*, 8953–8964; g) D. Wang, S. J. Lippard, *Nat. Rev. Drug Discovery* **2005**, *4*, 307–320.
- [3] Z. H. Siddik, *Oncogene* **2003**, *22*, 7265–7279.
- [4] A. de Cózar, O. Larrañaga, F. M. Bickelhaupt, E. S. Sebastián, E. Ortega-Carrasco, J.-D. Maréchal, A. Lledós, F. P. Cossio, *ChemPhysChem* **2016**, *17*, 3932–3947.
- [5] a) T. C. Johnstone, J. J. Wilson, S. J. Lippard, *Inorg. Chem.* **2013**, *52*, 12234–12239; b) T. C. Johnstone, G. Y. Park, S. J. Lippard, *Anticancer Res.* **2014**, *34*, 471–476.
- [6] K. S. Lovejoy, M. Serova, I. Bieche, S. Emami, M. D'Incalci, M. Broggin, E. Erba, C. Gespach, E. Cvitkovic, S. Faivre, E. Raymond, S. J. Lippard, *Mol. Cancer Ther.* **2011**, *10*, 1709–1719.
- [7] G. Y. Park, J. J. Wilson, Y. Song, S. J. Lippard, *Proc. Natl. Acad. Sci. USA* **2012**, *109*, 11987–11992.
- [8] a) M. J. Cleare, J. D. Hoeschele, *Bioinorg. Chem.* **1973**, *2*, 187–210; b) J.-P. Macquet, J.-L. Butour, *J. Natl. Cancer Inst.* **1983**, *70*, 899–905; c) A. L. Pinto, S. J. Lippard, *Proc. Natl. Acad. Sci. USA* **1985**, *82*, 4616–4619; d) V. Brabec, V. Boudny, *Met.-Based Drugs* **1994**, *1*, 195–200; e) V. Brabec, J. Reedijk, M. Leng, *Biochemistry* **1992**, *31*, 12397–12402; f) V. Bursova, J. Kasparkova, C. Hofr, V. Brabec, *Biophys. J.* **2005**, *88*, 1207–1214.
- [9] L. S. Hollis, A. R. Amundsen, E. W. Stern, *J. Med. Chem.* **1989**, *32*, 128–136.
- [10] D. Wang, G. Zhu, X. Huang, S. J. Lippard, *Proc. Natl. Acad. Sci. USA* **2010**, *107*, 9584–9589.
- [11] K. S. Lovejoy, R. C. Todd, S. Zhang, M. S. McCormick, J. A. D'Aquino, J. T. Reardon, A. Sancar, K. M. Giacomini, S. J. Lippard, *Proc. Natl. Acad. Sci. USA* **2008**, *105*, 8902–8907.
- [12] M. T. Gregory, G. Y. Park, T. C. Johnstone, Y.-S. Lee, W. Yang, S. J. Lippard, *Proc. Natl. Acad. Sci. USA* **2014**, *111*, 9133–9138.
- [13] M. W. Kellinger, G. Y. Park, J. Chong, S. J. Lippard, D. Wang, *J. Am. Chem. Soc.* **2013**, *135*, 13054–13061.
- [14] I. A. Riddell, T. C. Johnstone, G. Y. Park, S. J. Lippard, *Chem. Eur. J.* **2016**, *22*, 7574–7581.
- [15] T. C. Johnstone, S. J. Lippard, *J. Am. Chem. Soc.* **2014**, *136*, 2126–2134.
- [16] W. Zhou, M. Almeqdadi, M. E. Xifaras, I. A. Riddell, O. H. Yilmaz, S. J. Lippard, *Chem. Commun.* **2018**, *54*, 2788–2791.
- [17] D. Veclani, A. Melchior, M. Tolazzi, J. P. Cerón-Carrasco, *J. Am. Chem. Soc.* **2018**, *140*, 14024–14027.
- [18] A. A. Almaqwashi, W. Zhou, M. N. Nauffer, I. A. Riddell, A. H. Yilmaz, S. J. Lippard, M. C. Williams, *J. Am. Chem. Soc.* **2019**, *141*, 1537–1545.
- [19] M. E. Graziotto, M. C. Akerfeldt, A. P. Gunn, K. Yang, M. V. Somerville, N. V. Coleman, B. R. Roberts, T. W. Hambley, E. J. New, *J. Inorg. Biochem.* **2017**, *177*, 328–334.
- [20] Gaussian 09 (Revision D.01), M. J. Frisch, G. W. Trucks, H. B. Schlegel, G. E. Scuseria, M. A. Robb, J. R. Cheeseman, G. Scalmani, V. Barone, B. Mennucci, G. A. Petersson, H. Nakatsuji, M. Caricato, X. Li, H. P. Hratchian, A. F. Izmaylov, J. Bloino, G. Zheng, J. L. Sonnenberg, M. Hada, M. Ehara, K. Toyota, R. Fukuda, J. Hasegawa, M. Ishida, T. Nakajima, Y. Honda, O. Kitao, H. Nakai, T. Vreven, J. A. Montgomery, Jr., J. E. Peralta, F. Ogliaro, M. Bearpark, J. J. Heyd, E. Brothers, K. N. Kudin, V. N. Staroverov, T. Keith, R. Kobayashi, J. Normand, K. Raghavachari, A. Rendell, J. C. Burant, S. S. Iyengar, J. Tomasi, M. Cossi, N. Rega, J. M. Millam, M. Klene, J. E. Knox, J. B. Cross, V. Bakken, C. Adamo, J. Jaramillo, R. Gomperts, R. E. Stratmann, O. Yazyev, A. J. Austin, R. Cammi, C. Pomelli, J. W. Ochterski, R. L. Martin, K. Morokuma, V. G. Zakrzewski, G. A. Voth, P. Salvador, J. J. Dannenberg, S. Dapprich, A. D. Daniels, O. Farkas, J. B. Foresman, J. V. Ortiz, J. Cioslowski, D. J. Fox, Gaussian, Inc., Wallingford CT, **2010**.
- [21] A. D. Becke, *J. Chem. Phys.* **1993**, *98*, 5648–5652.
- [22] C. Lee, W. Yang, R. G. Parr, *Phys. Rev. B* **1988**, *37*, 785–789.
- [23] S. Grimme, J. Antony, S. Ehrlich, H. Krieg, *J. Chem. Phys.* **2010**, *132*, 154104.
- [24] D. Andrae, U. Häussermann, M. Dolg, H. Stoll, H. Preuss, *Theor. Chim. Acta* **1990**, *77*, 123–141.
- [25] H. R. Drew, R. M. Wing, T. Takano, C. Broka, S. Tanaka, K. Itakura, R. E. Dickerson, *Proc. Natl. Acad. Sci. USA* **1981**, *78*, 2179–2183.
- [26] D. A. Case, R. M. Betz, D. S. Cerutti, T. E. Cheatham, T. A. Darden, R. E. Duke, T. J. Giese, H. Gohlke, A. W. Goetz, N. Homeyer, S. Izadi, P. Janowski, J. Kaus, A. Kovalenko, T. S. Lee, S. LeGrand, P. Li, C. Lin, T. Luchko, R. Luo, B. Madej, D. Mermelstein, K. M. Merz, G. Monard, H. Nguyen, H. T. Nguyen, I. Omelyan, A. Onufriev, D. R. Roe, A. Roitberg, C. Sagui, C. L. Simmerling, W. M. Botello-Smith, J. Swails, R. C. Walker, J. Wang, R. M. Wolf, X. Wu, L. Xiao, P. A. Kollman, **2016**, AMBER 2016, University of California, San Francisco.
- [27] I. Ivani, P. D. Dans, A. Noy, A. Pérez, I. Faustino, A. Hospital, J. Walther, P. Andrio, R. Goñi, A. Balaceanu, G. Portella, F. Battistini, J. L. Gelpi, C. González, M. Vendruscolo, C. A. Laughton, S. A. Harris, D. A. Case, M. Orozco, *Nat. Methods* **2016**, *13*, 55–58.
- [28] a) J. Wang, W. Wang, P. A. Kollman, D. A. Case, *J. Mol. Graphics Modell.* **2006**, *25*, 247–260; b) J. Wang, R. M. Wolf, J. W. Caldwell, P. A. Kollman, D. A. Case, *J. Comput. Chem.* **2004**, *25*, 1157–1174.
- [29] a) M. W. Mahoney, W. L. Jorgensen, *J. Chem. Phys.* **2000**, *112*, 8910–8922; b) M. W. Mahoney, W. L. Jorgensen, *J. Chem. Phys.* **2001**, *114*, 363–366; c) W. L. Jorgensen, J. Chandrasekhar, J. D. Madura, R. W. Impey, M. L. Klein, *J. Chem. Phys.* **1983**, *79*, 926–935.
- [30] B. R. Miller, T. D. McGee, Jr., J. M. Swails, N. Homeyer, H. Gohlke, A. E. Roitberg, *J. Chem. Theory Comput.* **2012**, *8*, 3314–3321.
- [31] W. Humphrey, A. Dalke, K. Schulten, *J. Mol. Graphics Modell.* **1996**, *14*, 33–38.
- [32] S. Ahmad, *Polyhedron* **2017**, *138*, 109–124.
- [33] J. Raber, C. Zhu, L. A. Eriksson, *J. Phys. Chem. B* **2005**, *109*, 11006–11015.
- [34] F. Sebesta, J. V. Burda, *J. Inorg. Biochem.* **2017**, *172*, 100–109.
- [35] T. Kubar, M. Hanus, F. Ryjáček, P. Hobza, *Chem. Eur. J.* **2006**, *12*, 280–290.
- [36] M. L. D'Amico, V. Paiotta, F. Secco, M. Venturini, *J. Phys. Chem. B* **2002**, *106*, 12635.

Manuscript received: August 21, 2019

Revised manuscript received: October 11, 2019

Accepted manuscript online: October 15, 2019

Version of record online: December 9, 2019

CHEMISTRY

A **European** Journal

Supporting Information

Rationalization of the Superior Anticancer Activity of Phenanthriplatin: An In-Depth Computational Exploration

Eslam Dabbish, Nino Russo, and Emilia Sicilia*^[a]

chem_201903831_sm_miscellaneous_information.pdf

Computational details	S3-S4
Figure S1. Free energy profile for the interconversion between the two Phen enantiomers. Values are in kcal mol ⁻¹ .	S5
Table S1. Relative free energies in water for the Phen aquation reaction with different numbers of additional solvent molecules.	S6
Figure S2. Free energy profile in water describing the interaction of the Phen drug with guanine in presence of an additional water molecule. Geometrical structures of the stationary points intercepted along the path are also reported. Relative energies are in kcal mol ⁻¹ and calculated with respect the zero reference energy of separated reactants.	S7
Figure S3. Free energy profiles describing the attack of NAM to cisplatin. Geometrical structures of the stationary points intercepted along the path are also reported. Relative energies are in kcal mol ⁻¹ and calculated with respect the zero reference energy of separated reactants.	S8
Figure S5. Free energy profile describing the guanine interaction with Pyr . Geometrical structures of the stationary points intercepted along the path are reported. Relative energies are in kcal mol ⁻¹ and calculated with respect the zero reference energy of separated reactants.	S9
Figure S6. Free energy profile describing the guanine interaction with Enpyr . Geometrical structures of the stationary points intercepted along the path are reported. Relative energies are in kcal mol ⁻¹ and calculated with respect the zero reference energy of separated reactants.	S10
Figure S7. DNA length change due to the intercalated Phen complex calculated as the end-to-end distance of the helix, measured from the two terminal base pairs center of mass, taking the drug-free DNA as a reference.	S11
Figure S8. Structure of the B-DNA dodecamer and intercalating aquated Phen complex for the arrangement named 2a , at different times (10, 20, 30, 40, 50 and 60 ns) of the calculated dynamics.	S12
Figure S9. DNA- Phen complex corresponding to the arrangements labeled 2b , 3a and 3b at different times of the calculated dynamics.	S13
Table S2. Contributions to the MM-GBSA binding free energy for all the examined positions of the intercalated drug in the D NA- Phen complex. Van der Waals (VDWAALS), electrostatic (EEL), polar (EGB) and non-polar (ESURF) contributions to the solvation free energy, total gas phase (DELTA G gas) and solvation (DELTA G solv) binding energy, resulting MM-GBSA binding energy (DELTA TOTAL) and the estimation of the entropy term by quasi-harmonic analysis are reported. All the values are in kcal mol ⁻¹	S14
Figure S10. Plot of RMSD for the drug-surrounding nucleotides taking drug free DNA as a reference.	S15
Figure S11. Plot of the RMSD for the whole Phen -DNA complex taking drug free DNA as a reference.	S16
Figure S12. Free energy profile describing the DNA guanine attack to non-intercalated Phen . Geometrical structures of the intercepted stationary points are also reported. Relative energies are in kcal mol ⁻¹ and calculated with respect the zero reference energy of the initial adduct.	S17
Table S3. Contributions to the MM-GBSA binding free energy for all the examined DNA-drug complexes. Van der Waals (VDWAALS), electrostatic (EEL), polar (EGB) and non-polar (ESURF) contributions to the solvation free energy, total gas phase (DELTA G gas) and solvation (DELTA G solv) binding energy, resulting MM-GBSA binding energy (DELTA TOTAL) and the estimation of the entropy term by quasi-harmonic analysis are reported. All the values are in kcal mol ⁻¹ .	S18
Developed Parameters	S19-S39
References	S40

Computational details

All quantum mechanical calculations have been performed using Gaussian 09 package.¹ Density functional theory has been employed using the hybrid Becke three parameter exchange functional² and the Lee-Yang-Parr correlation functional,³ B3LYP. Grimme dispersion correction for nonbonding interactions has been included using atom pair-wise additive scheme,⁴ DFT-D3 method. Stuttgart/Dresden effective core potential⁵ and corresponding split valence basis set have been used to describe platinum atom. 6-311+G** basis set has been employed to describe the atoms directly involved in the studied reactions, while the rest of the atoms have been described by the 6-311G** basis set. Frequency calculations have been performed at the same level of theory for all located stationary points to confirm their nature of minima and transition states and for zero-point energy corrections calculations. All the located transition states have been checked to be properly connected to the corresponding minima by means of intrinsic reaction coordinate (IRC) analysis.⁶ Solvent effect has been included by using Tomasi's implicit Polarizable Continuum Model (PCM) as implemented in Gaussian 09.⁷ The UFF set of radii has been used to build up the cavity in which the solute molecules are accommodated. The solvation Gibbs free energy have been calculated in implicit water ($\epsilon = 78.4$) at the same level, performing single point calculations on all stationary point structures obtained from vacuum calculations. Enthalpies and Gibbs free energies have been obtained at 298 K at 1 atm from total energies, including zero-point, thermal and solvent corrections, using standard statistical procedures.⁸ As the free energy corrections in the Gaussian's default standard state corresponds to an ideal gas at a standard pressure of 1 atm, the computed free energies have been converted⁹ to yield Gibbs energies with a solution phase standard state of 1 mol L⁻¹ for all the species except water solvent. For water molecules a standard state of 55.5M has been used. That is, to the free energy of each species, as computed in Gaussian, a free energy correction term equal to $RT \ln(V_{\text{molar gas}}/V_{\text{molar solution}})$, (R =gas constant, T =absolute temperature) has been added, where $V_{\text{molar gas}}$ is the volume occupied by one mole of ideal gas at the considered temperature, and $V_{\text{molar solution}}$ is the volume occupied by one mole of species in a standard solution of concentration 1 mol L⁻¹. In order to study intercalation, using molecular mechanics and molecular dynamics calculations, a B-DNA dodecamer, with Protein Data Bank code 1BNA,¹⁰ has been used. The phenanthriplatin drug has been manually introduced into the different potential intercalation sites. The initial geometry for the transcription blockage study has been taken from the experimental X-ray structure of the platinum drug phenanthriplatin bound to the DNA with code 4Q8F from the Protein Data Bank.¹¹ For the study of pyrriplatin and enpyriplatin drugs bound to DNA in the transcription blockage step, phenanthriplatin has been substituted every time with the drug of interest.

For the molecular dynamics study of both of the above mentioned systems, hydrogens have been added to the model system using H++web-server.¹² The platinum metal center has been parametrized by using both Gaussian 09 and MCPB.py in Amber 16 package.^{1,13,14} Geometry optimization and frequency calculations have been carried out using Gaussian 09 for the metal center created model using Stuttgart/Dresden effective core potential⁵ and split valence basis set to describe platinum atom and 6-311G** basis set for the rest of the atoms. MCPB.py has been used to develop the parameters (reported below in Table S3) from the above quantum mechanical calculations using Seminario method. For the charges, Gaussian 09 has been used to calculate the Merz-Kollman ESP charge¹⁵ of the created metal center model. MCPB.py has been, then, used to perform RESP charge fitting. Topology and coordinate files have been generated by means of tleap in Amber 16¹⁴ using the standard DNA.bsc1¹⁶ and gaff force fields¹⁷ together with the newly generated parameters for the metal center. A TIP3P solvation model¹⁸ has been used to construct an octahedral box of water around the DNA complex with a 14 Å buffer distance around the DNA in each direction. Sodium ions have been added to neutralize the system. The system has been relaxed prior to the molecular dynamics by a 1000 minimization steps with a cutoff distance of 15.0 Å and a constant volume periodic boundaries. The DNA has been held fixed during this initial minimization by using a force constant of 500 kcal mol⁻¹. This has been followed by 2500 minimization steps for the whole system including the DNA with the same cutoff distance and constant volume periodic boundaries. The system has been, then, heated from 0 K to 300 K over 10000 steps for a total of 20 ps. SHAKE algorithm has been implemented to constrain bonds involving hydrogen. During the heating, the DNA has been weakly restrained by a force constant of 10 kcal mol⁻¹ while keeping the constant volume periodic boundaries and same cutoff distance. Equilibration followed by production of molecular dynamics for 20 ns at 300 K were ran under similar conditions with a 0.002 ps interval with no restraints on DNA. The SHAKE algorithm to constrain bonds involving hydrogen and the cutoff distance of 15.0 angstroms were all maintained. A constant pressure periodic boundary with an average pressure of 1 atm and an isotropic position scaling with a relaxation time of 2ps were used.

For evaluating the relative binding free energy between the different platinum complexes and the DNA, MM-GBSA method¹⁹ as implemented by MMPBSA.py script in Amber 16 package has been used evaluating the whole production trajectory over 20ns. Calculation of the interaction energy and solvation free energies for the drug-DNA adducts and DNA and drug alone has been followed by results averaging to obtain an estimate of the binding free energy as implemented in the MM-GBSA method in Amber 16. A quasi harmonic approximation has been used for entropy calculation. Cpptraj²⁰ in Amber 16 package has been used to generate data about the RMSD, distances between residues and conformational changes of the DNA in the drug-DNA complex either by taking the initial conformation or a simulated DNA alone without the bound drug as a reference. The electrostatic and vdW interactions have been also evaluated with the help of Cpptraj. VMD program was used to generate the figures out of the dynamics trajectory.²¹ The non covalent interactions have been represented by computing the electron density and reduced density gradient using NCIPLOT.^{22,23}

For the quantum-mechanical calculations of some of the free energy profiles describing the displacement of water by DNA guanine a downsized model consisting of the intercalating complex and a B-DNA double helical dimer (2TA or 2CG), that is, four nucleosides and two phosphate residues. Both phosphate residues in the reduced model have been protonated in order to mimic the proximity of a sodium cation and reduced electrostatic charge of the phosphate. With the aim to reduce the required computational effort, the double- ζ 6-31G** basis set has been used for all the atoms except platinum given the large size of the model including 160 atoms.

Figure S1

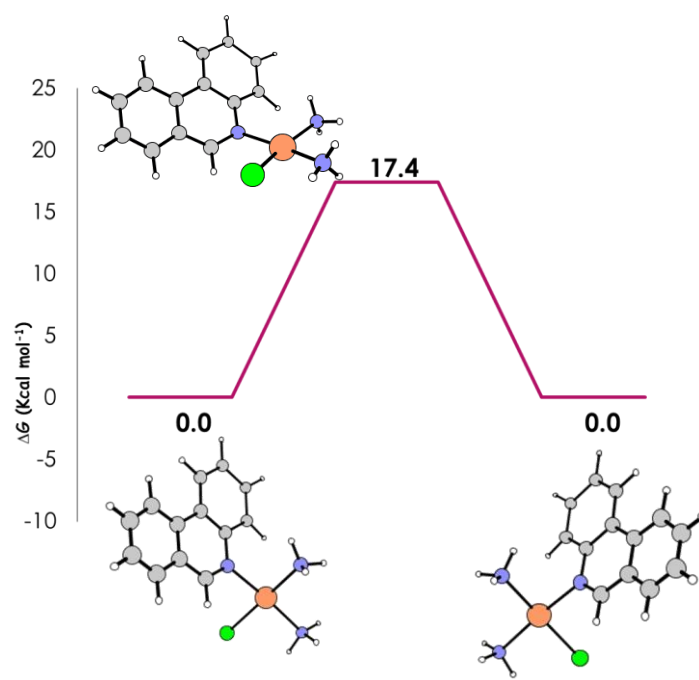


Table S1

	Reactant	TS	Product	Barrier
Aquation 1 water	1.4	23.3	8.8	21.9
Aquation 2 water	-1.2	21.9	7.6	23.1
Aquation 3 water	-1.4	21.6	5.9	23.1
Aquation 11 water	1.2	25.1	9.3	23.9

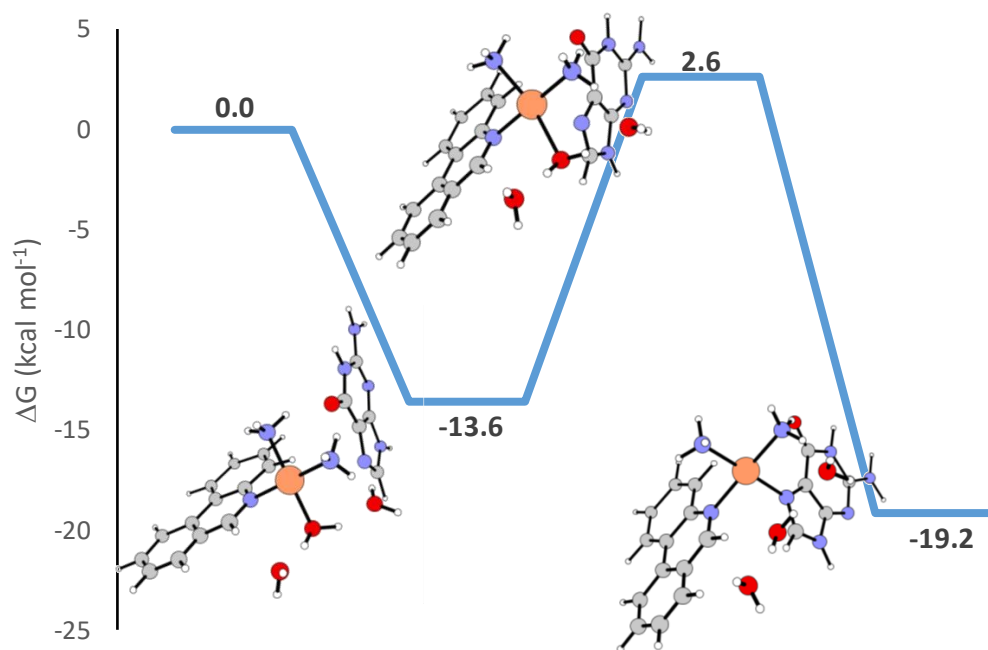


Figure S3

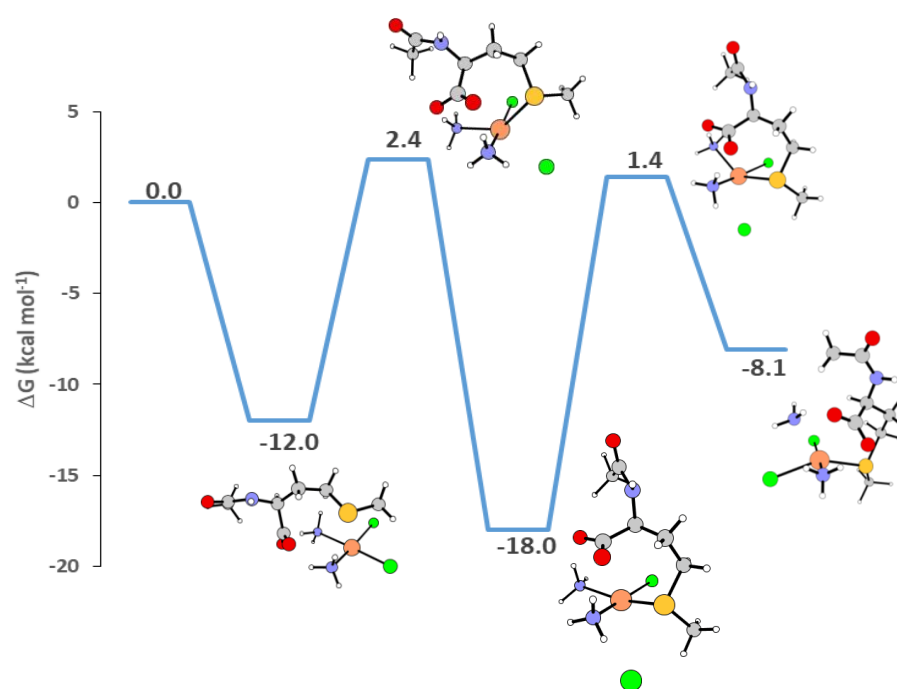


Figure S4

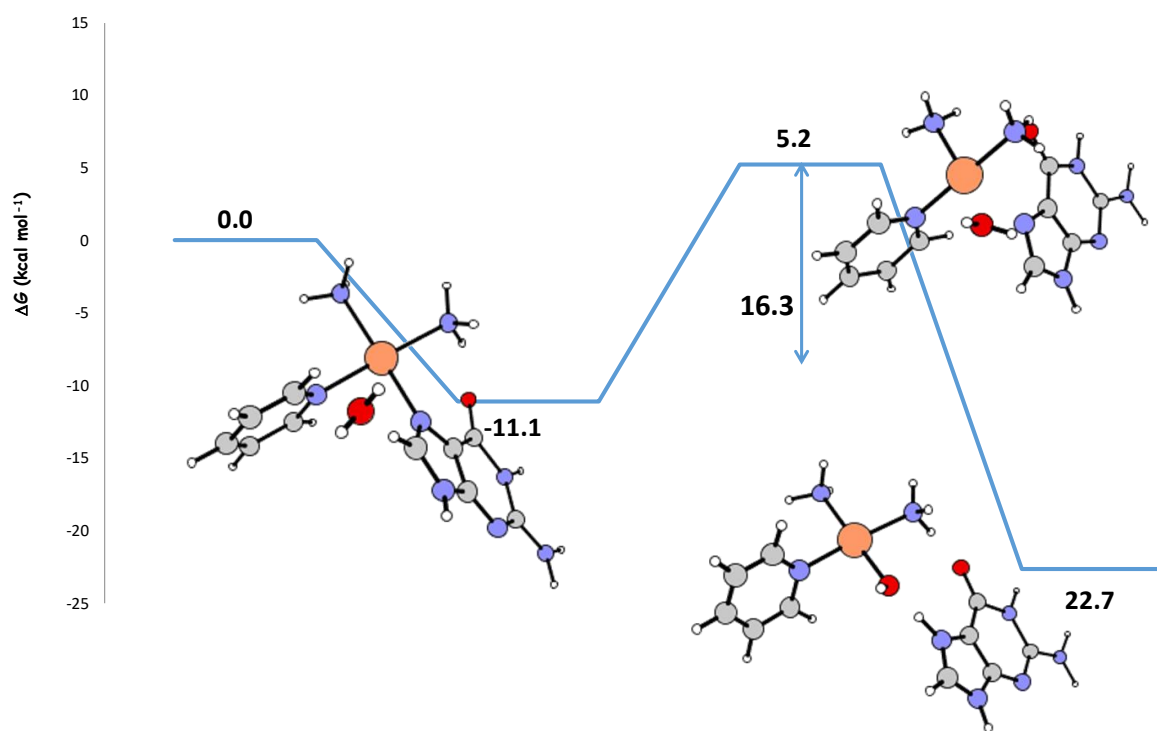


Figure S5

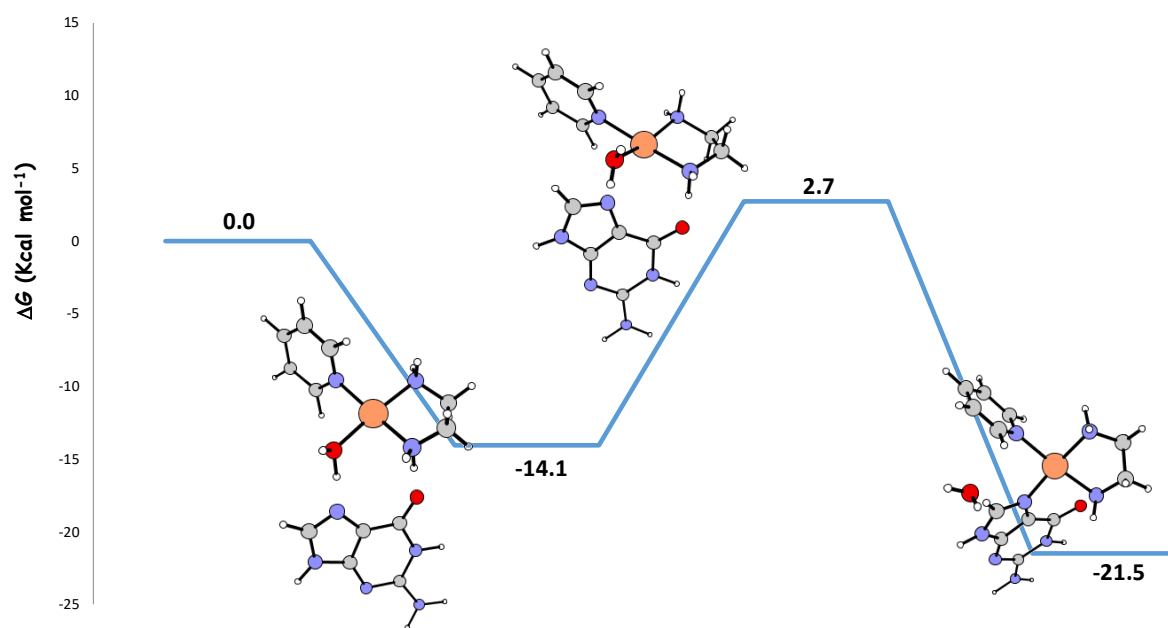


Figure S6

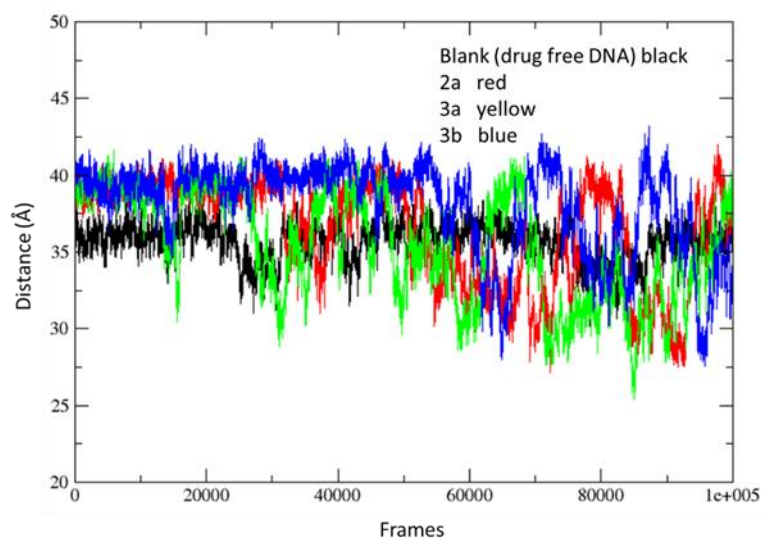


Figure S7

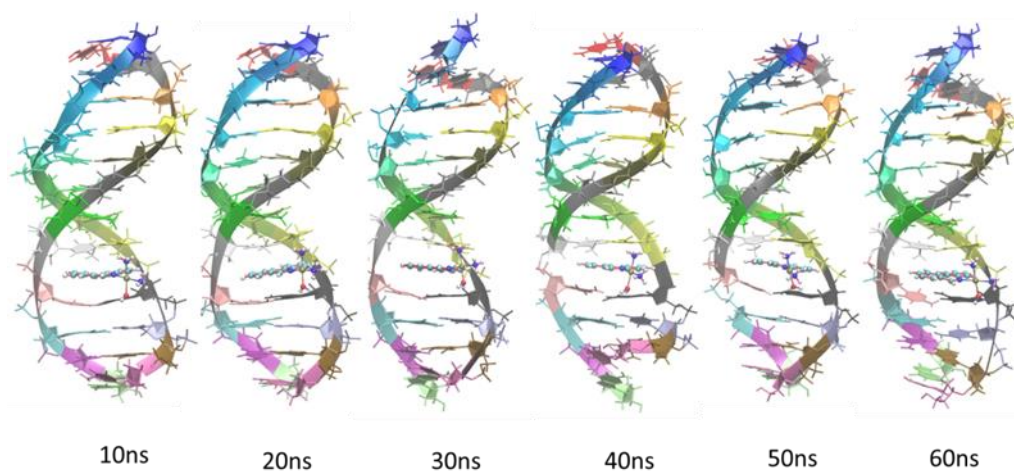


Figure S8

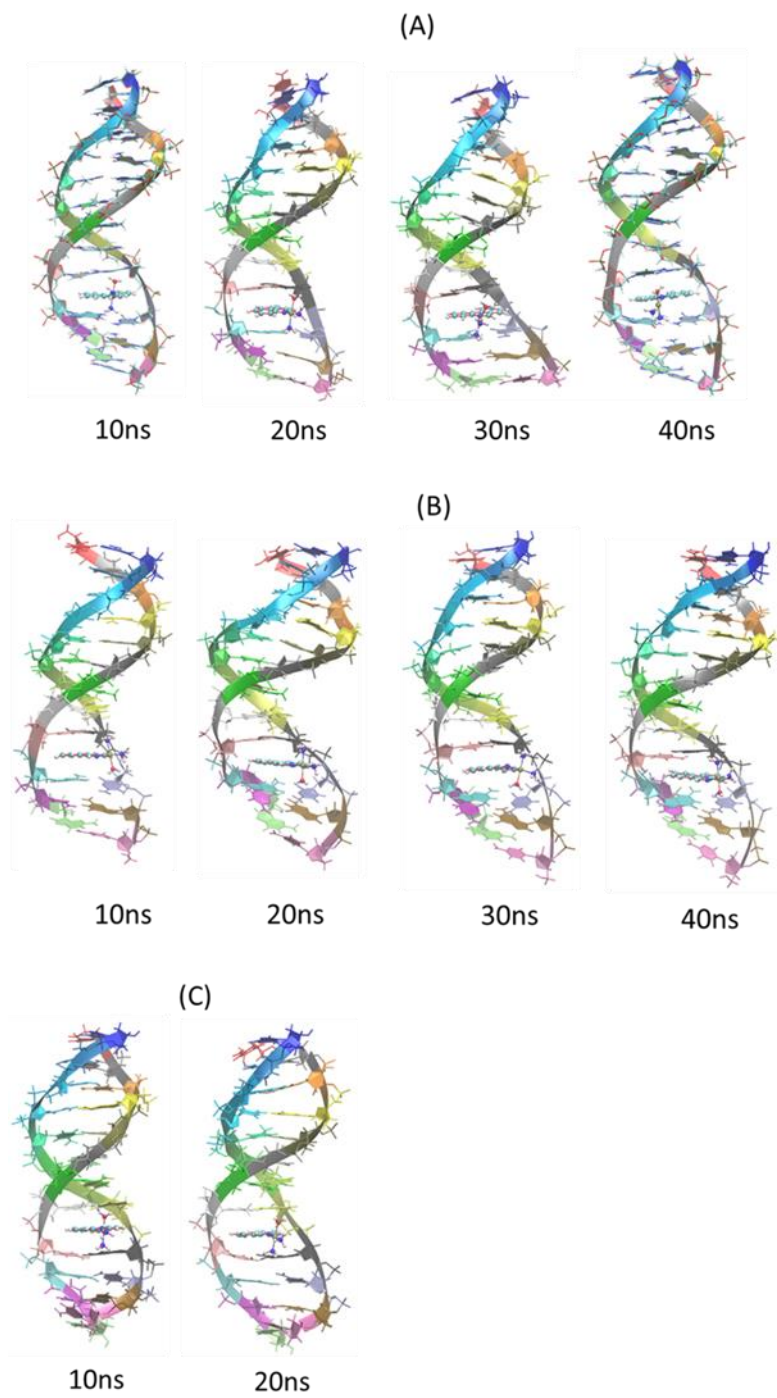


Table S2

Energy component	1	2a	2b	3a	3b	4	5
VDWAALS	-30.57	-32.06	-31.90	-32.21	-32.08	-31.30	-31.90
EEL	-1030.4	-1026.4	-1023.3	-975.1	-970.5	-1032.7	-1030.9
EGB	1036.7	1030.4	1026.9	980.6	975.2	1039.0	1035.0
ESURF	-2.62	-2.67	-2.71	-2.61	-2.59	-2.60	-2.74
DELTA G gas	-1061.0	-1058.4	-1055.2	-1007.3	-1002.5	-1064.0	-1062.8
DELTA G solv	1034.1	1027.8	1024.2	978.0	972.6	1036.4	1032.2
DELTA TOTAL	-26.89	-30.67	-31.02	-29.31	-29.89	-27.58	-30.55
Quasi-harmonic entropy approximation	-9.1	-9.7	-10.2	-9.4	-9.1	-8.3	-10.9
DELTA G binding	-17.8	-21.0	-20.8	-19.9	-20.8	-19.3	-19.6

Figure S9

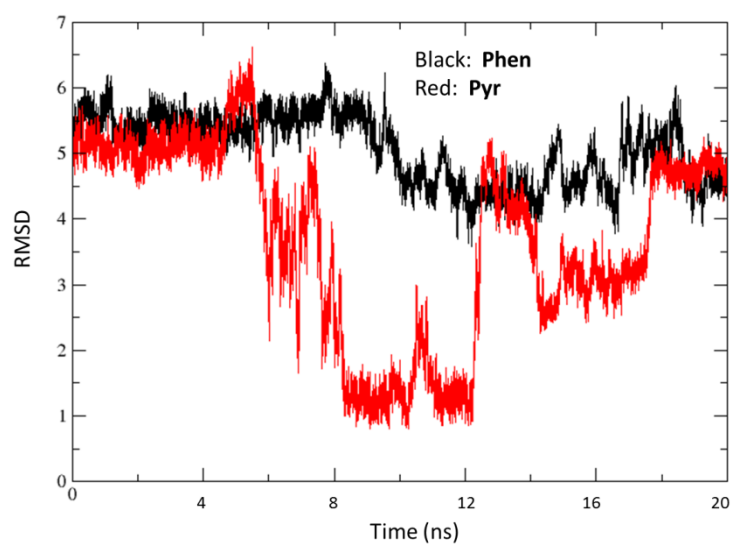


Figure S10

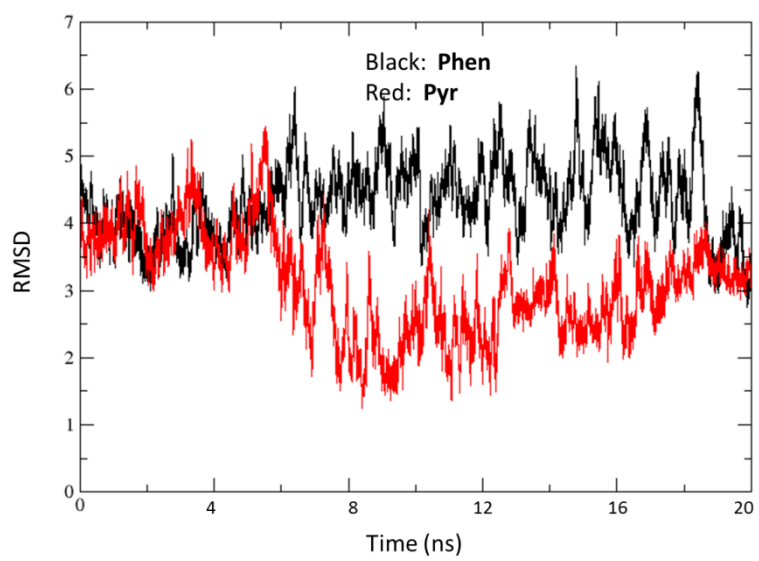


Figure S11

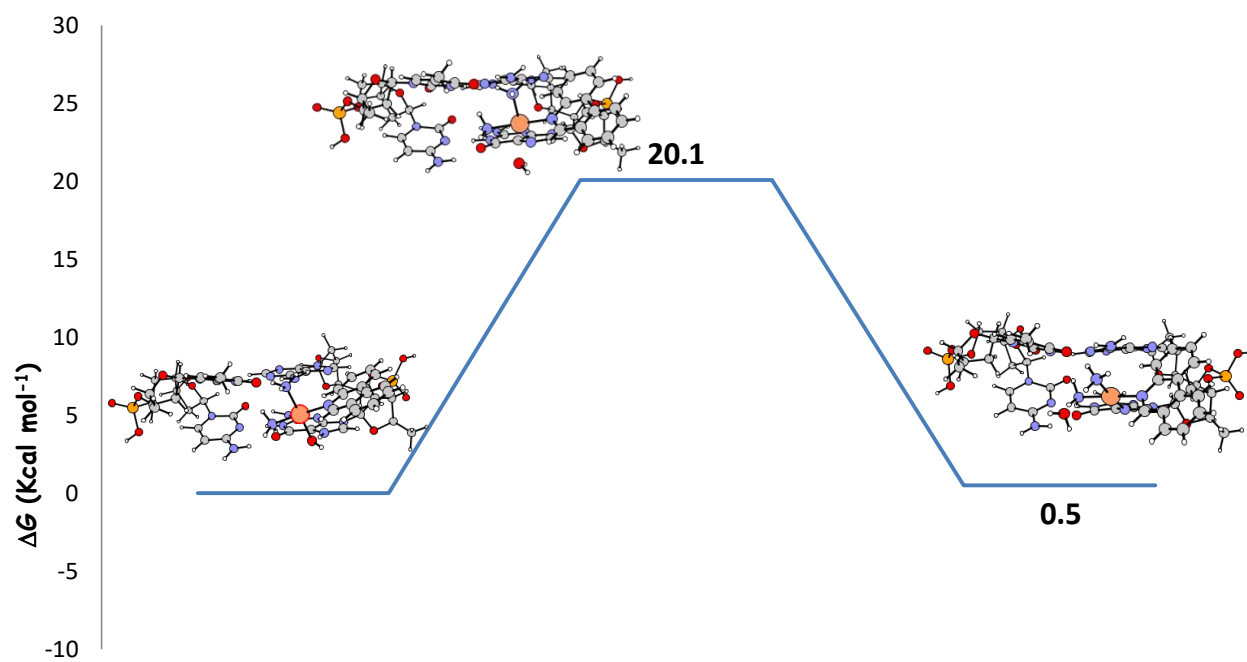


Table S3

Energy component	Phen	Pyr	Enpyr	Amn
BOND	0.31	0.31	0.30	0.34
ANGLE	1.03	1.11	1.11	1.16
DIHED	0.29	0.27	0.31	0.63
VDWAALS	-22.71	-9.44	-10.20	-2.19
EEL	-589.7	-606.6	-611.0	-583.1
1-4 VDW	-0.32	-0.35	-0.39	-0.29
1-4 EEL	-15.80	3.11	-13.88	-3.25
EGB	611.2	601.3	623.4	579.34
ESURF	-2.71	-1.77	-1.66	-1.01
DELTA G gas	-626.9	-611.6	-633.7	-586.7
DELTA G solv	608.5	599.7	621.8	578.3
DELTA TOTAL	-18.39	-11.99	-11.94	-8.33
Quasi-harmonic entropy approximation	-11.7	-10.6	-10.2	-9.0
DELTA G binding	-6.7	-1.3	-1.7	0.7

Developed parameters

In general the two ammonia residues bound to the platinum centers are named as AMN and AMO. Platinum center is named as PT. The ring attached to platinum or the third ammonia in case of **Amn** is named as MOL. Water residue bound to platinum center is named as FAT. Ethylene diamine portion of Enpyriplatin **Enpyr** as EMN while the guanine directly bound to platinum is named as DG2.

1.1 Phenanthriplatin Intercalation

1.1.1 Charges

a) Residue AMO prep file

0 0 2

This is a remark line

molecule.res

AMO INT 0

CORRECT OMIT DU BEG

0.0000

1	DUMM	DU	M	0	-1	-2	0.000	.0	.0	.00000
2	DUMM	DU	M	1	0	-1	1.449	.0	.0	.00000
3	DUMM	DU	M	2	1	0	1.523	111.21	.0	.00000
4	N12	Y3	M	3	2	1	1.540	111.208	-180.000	-0.547092
5	H82	hn	E	4	3	2	1.024	41.075	-168.773	0.307365
6	H83	hn	E	4	3	2	1.021	79.109	-36.241	0.342743
7	H84	hn	E	4	3	2	1.021	145.248	-140.787	0.345490

LOOP

IMPROPER

DONE

STOP

b) Residue AMN prep file

0 0 2

This is a remark line

molecule.res

AMN INT 0

CORRECT OMIT DU BEG

0.0000

1	DUMM	DU	M	0	-1	-2	0.000	.0	.0	.00000
2	DUMM	DU	M	1	0	-1	1.449	.0	.0	.00000
3	DUMM	DU	M	2	1	0	1.523	111.21	.0	.00000
4	N11	Y2	M	3	2	1	1.540	111.208	-180.000	-0.356937
5	H85	hn	E	4	3	2	1.022	107.076	74.256	0.272029
6	H86	hn	E	4	3	2	1.021	119.708	-165.102	0.281469
7	H87	hn	E	4	3	2	1.021	109.752	-40.737	0.269867

LOOP

IMPROPER

DONE

STOP

c) Residue FAT prep file

0 0 2

This is a remark line

```

molecule.res
FAT INT 0
CORRECT OMIT DU BEG
0.0000
 1 DUMM DU M 0 -1 -2 0.000 .0 .0 .00000
 2 DUMM DU M 1 0 -1 1.449 .0 .0 .00000
 3 DUMM DU M 2 1 0 1.523 111.21 .0 .00000
 4 O10 Y1 M 3 2 1 1.540 111.208 -180.000 -0.533606
 5 H81 HW E 4 3 2 0.970 67.375 19.042 0.437284
 6 H79 HW E 4 3 2 0.970 71.482 137.689 0.424345

```

LOOP

IMPROPER

DONE

STOP

d) Residue MOL prep file

0 0 2

This is a remark line

```

molecule.res
MOL INT 0
CORRECT OMIT DU BEG
0.0000
 1 DUMM DU M 0 -1 -2 0.000 .0 .0 .00000
 2 DUMM DU M 1 0 -1 1.449 .0 .0 .00000
 3 DUMM DU M 2 1 0 1.523 111.21 .0 .00000
 4 C11 ca M 3 2 1 1.540 111.208 -180.000 -0.123396
 5 H91 ha E 4 3 2 1.084 176.260 46.146 0.093329
 6 C10 ca M 4 3 2 1.380 62.743 177.991 -0.131368
 7 H90 ha E 6 4 3 1.084 119.969 -177.857 0.170692
 8 C15 ca M 6 4 3 1.404 119.933 1.664 -0.046570
 9 H93 ha E 8 6 4 1.083 119.935 -179.923 0.159993
10 C14 ca M 8 6 4 1.379 120.139 -0.447 -0.157351
11 H92 ha E 10 8 6 1.082 118.825 -179.492 0.166965
12 C13 ca M 10 8 6 1.412 121.686 0.465 0.027930
13 C12 ca M 12 10 8 1.423 117.554 0.099 0.103526
14 N10 Y4 M 13 12 10 1.404 119.955 179.323 -0.054505
15 C18 ca M 14 13 12 1.325 120.056 0.811 -0.103487
16 H94 h4 E 15 14 13 1.086 116.977 -179.122 0.146359
17 C17 ca M 15 14 13 1.409 123.873 0.208 0.114462
18 C16 ca M 17 15 14 1.426 118.763 -0.992 0.069723
19 C22 ca M 18 17 15 1.407 117.762 -179.393 -0.159712
20 H97 ha E 19 18 17 1.080 120.707 -179.975 0.156567
21 C21 ca M 19 18 17 1.383 120.495 0.013 -0.028664
22 H96 ha E 21 19 18 1.084 119.320 -179.954 0.156160
23 C20 ca M 21 19 18 1.410 121.408 0.067 -0.059346
24 H95 ha E 23 21 19 1.083 119.822 179.911 0.157012
25 C19 ca M 23 21 19 1.373 119.660 -0.016 -0.187160
26 H80 ha E 25 23 21 1.084 120.622 179.875 0.163334

```

LOOP

C12 C11

C16 C13

C19 C17

IMPROPER

C12 C10 C11 H91

C11 C15 C10 H90

C10 C14 C15 H93

C13 C15 C14 H92

C12 C16 C13 C14

C13 C11 C12 N10

C17 H94 C18 N10

C18 C16 C17 C19

C13 C17 C16 C22
C16 C21 C22 H97
C22 C20 C21 H96
C21 C19 C20 H95
C17 C20 C19 H80

DONE
STOP

e) Residue PT prepi file

0 0 2

This is a remark line

molecule.res

PT INT 0

CORRECT OMIT DU BEG

0.0000

1	DUMM	DU	M	0	-1	-2	0.000	.0	.0	.00000
2	DUMM	DU	M	1	0	-1	1.449	.0	.0	.00000
3	DUMM	DU	M	2	1	0	1.523	111.21	.0	.00000
4	PT	M1	M	3	2	1	1.540	111.208	-180.000	0.122550

LOOP

IMPROPER

DONE
STOP

1.1.2 Frcmod file of the phenanthriplatin

MASS

M1	195.08		Pt ion
Y1	16.00	0.000	oxygen in TIP3P water
Y2	14.01	0.530	Sp3 N with three connected atoms
Y3	14.01	0.530	Sp3 N with three connected atoms
Y4	14.01	0.530	Sp2 N in pure aromatic systems

BOND

M1-Y1	92.4	2.1344	Created by Seminario method using MCPB.py		
M1-Y2	92.7	2.1271	Created by Seminario method using MCPB.py		
M1-Y3	129.1	2.0624	Created by Seminario method using MCPB.py		
M1-Y4	124.6	2.0606	Created by Seminario method using MCPB.py		
Y1-HW	553.0	0.9572	! TIP3P water		
Y2-hn	392.4	1.0190	SOURCE3_SOURCE5	5944	0.0012
Y3-hn	392.4	1.0190	SOURCE3_SOURCE5	5944	0.0012
ca-Y4	488.0	1.3390	SOURCE3_SOURCE5	6806	0.0055

ANGL

M1-Y1-HW	57.84	116.55	Created by Seminario method using MCPB.py		
M1-Y2-hn	58.96	112.21	Created by Seminario method using MCPB.py		
M1-Y3-hn	55.63	111.81	Created by Seminario method using MCPB.py		
M1-Y4-ca	160.91	119.90	Created by Seminario method using MCPB.py		
Y2-M1-Y1	110.78	85.66	Created by Seminario method using MCPB.py		
Y3-M1-Y1	131.42	179.11	Created by Seminario method using MCPB.py		
Y3-M1-Y2	141.99	94.08	Created by Seminario method using MCPB.py		
Y4-M1-Y1	113.55	91.40	Created by Seminario method using MCPB.py		
Y4-M1-Y2	142.40	176.80	Created by Seminario method using MCPB.py		
Y4-M1-Y3	150.03	88.89	Created by Seminario method using MCPB.py		
HW-Y1-HW	100.	104.52	TIP3P water		
Y4-ca-h4	51.88	116.03	SOURCE3_SOURCE5	2217	0.2861
ca-Y4-ca	68.35	117.22	SOURCE3_SOURCE5	3343	1.0306
ca-ca-Y4	68.83	122.94	SOURCE3_SOURCE5	5507	1.1495
hn-Y2-hn	41.40	106.40	SOURCE3_SOURCE5	2019	0.9777

hn-Y3-hn 41.40 106.40 SOURCE3_SOURCE5 2019 0.9777

DIHE

X-ca-Y4-X 2 9.6 180.0 2.0 same as X-CA-NC-X
M1-Y4-ca-ca 3 0.00 0.00 3.0 Treat as zero by MCPB.py
M1-Y4-ca-h4 3 0.00 0.00 3.0 Treat as zero by MCPB.py
Y2-M1-Y1-HW 3 0.00 0.00 3.0 Treat as zero by MCPB.py
Y3-M1-Y1-HW 3 0.00 0.00 3.0 Treat as zero by MCPB.py
Y3-M1-Y2-hn 3 0.00 0.00 3.0 Treat as zero by MCPB.py
Y4-M1-Y1-HW 3 0.00 0.00 3.0 Treat as zero by MCPB.py
Y4-M1-Y2-hn 3 0.00 0.00 3.0 Treat as zero by MCPB.py
Y4-M1-Y3-hn 3 0.00 0.00 3.0 Treat as zero by MCPB.py
ca-Y4-M1-Y1 3 0.00 0.00 3.0 Treat as zero by MCPB.py
ca-Y4-M1-Y2 3 0.00 0.00 3.0 Treat as zero by MCPB.py
ca-Y4-M1-Y3 3 0.00 0.00 3.0 Treat as zero by MCPB.py
hn-Y2-M1-Y1 3 0.00 0.00 3.0 Treat as zero by MCPB.py
hn-Y3-M1-Y1 3 0.00 0.00 3.0 Treat as zero by MCPB.py
hn-Y3-M1-Y2 3 0.00 0.00 3.0 Treat as zero by MCPB.py

IMPR

Y4-ca-ca-ca 1.1 180.0 2.0 Using the default value
Y4-ca-ca-h4 1.1 180.0 2.0 Using the default value

NONB

M1 1.2660 0.0030764200 CM set for Pt2+ ion in TIP3P water from Li et al. JCTC, 2013, 9, 2733
Y1 1.7683 0.1520 TIP3P water model
Y2 1.8240 0.1700 OPLS
Y3 1.8240 0.1700 OPLS
Y4 1.8240 0.1700 OPLS

1.2 Transcription inhibition model

1.2.1 Phenanthriplatin (Phen)

1.2.1.1 Charges

a) Residue AMN prepri file

0 0 2

This is a remark line

molecule.res

AMN INT 0

CORRECT OMIT DU BEG

0.0000

1 DUMM DU M 0 -1 -2 0.000 .0 .0 .00000
2 DUMM DU M 1 0 -1 1.449 .0 .0 .00000
3 DUMM DU M 2 1 0 1.523 111.21 .0 .00000
4 N11 NF M 3 2 1 1.540 111.208 -180.000 -0.704275731
5 H85 H E 4 3 2 0.999 121.435 157.949 0.362357395
6 H86 H E 4 3 2 0.999 106.092 -76.325 0.428048644
7 H87 H E 4 3 2 1.000 100.140 37.569 0.431635219

LOOP

IMPROPER

DONE

STOP

b) Residue AMO prepri file

0 0 2

This is a remark line

molecule.res

```

AMO INT 0
CORRECT OMIT DU BEG
0.0000
 1 DUMM DU M 0 -1 -2 0.000 .0 .0 .00000
 2 DUMM DU M 1 0 -1 1.449 .0 .0 .00000
 3 DUMM DU M 2 1 0 1.523 111.21 .0 .00000
 4 N12 NL M 3 2 1 1.540 111.208 -180.000 -0.515489169
 5 H82 H E 4 3 2 1.000 121.408 157.974 0.350754522
 6 H83 H E 4 3 2 0.999 106.092 -76.325 0.389351038
 7 H84 H E 4 3 2 1.000 100.132 37.533 0.341593142

```

LOOP

IMPROPER

DONE

STOP

c) Residue MOL prep file

0 0 2

This is a remark line

molecule.res

MOL INT 0

```

CORRECT OMIT DU BEG
0.0000
 1 DUMM DU M 0 -1 -2 0.000 .0 .0 .00000
 2 DUMM DU M 1 0 -1 1.449 .0 .0 .00000
 3 DUMM DU M 2 1 0 1.523 111.21 .0 .00000
 4 N10 NK M 3 2 1 1.540 111.208 -180.000 0.051092611
 5 C18 CA M 4 3 2 1.355 39.856 -175.905 -0.105340898
 6 H90 H4 E 5 4 3 1.071 119.858 -55.530 0.16035839
 7 C13 CA M 5 4 3 1.384 120.209 124.450 0.039115986
 8 C12 CA M 7 5 4 1.387 120.042 -179.725 -0.212538402
 9 H91 HA E 8 7 5 1.071 119.992 0.252 0.236261997
10 C11 CA M 8 7 5 1.382 119.980 -179.768 -0.1849674
11 H92 HA E 10 8 7 1.070 119.996 179.542 0.238702423
12 C10 CA M 10 8 7 1.383 119.984 -0.479 -0.135124054
13 H93 HA E 12 10 8 1.070 119.987 -179.535 0.201400154
14 C9 CA M 12 10 8 1.384 119.970 0.461 -0.218508038
15 H98 HA E 14 12 10 1.070 120.099 179.742 0.185122348
16 C14 CA M 14 12 10 1.389 119.815 -0.262 0.108767732
17 C15 CA M 16 14 12 1.367 120.090 -179.923 0.064537089
18 C16 CA M 17 16 14 1.388 119.687 -179.966 0.175223682
19 C22 CA M 18 17 16 1.393 119.833 -179.973 -0.282599652
20 H94 HA E 19 18 17 1.070 119.968 179.971 0.232097779
21 C21 CA M 19 18 17 1.390 120.042 -0.003 -0.217101057
22 H95 HA E 21 19 18 1.070 119.945 -179.982 0.199897715
23 C20 CA M 21 19 18 1.390 119.970 0.064 -0.128877726
24 H96 HA E 23 21 19 1.069 119.992 179.831 0.187104848
25 C19 CA M 23 21 19 1.390 119.983 -0.132 -0.282036583
26 H97 HA E 25 23 21 1.069 120.050 -179.878 0.22411659

```

LOOP

C16 N10

C14 C13

C19 C15

IMPROPER

C13 H90 C18 N10

C14 C18 C13 C12

C13 C11 C12 H91

C10 C12 C11 H92

C9 C11 C10 H93

C10 C14 C9 H98

C9 C15 C14 C13

C14 C16 C15 C19

C15 C22 C16 N10
C16 C21 C22 H94
C22 C20 C21 H95
C21 C19 C20 H96
C15 C20 C19 H97

DONE
STOP

d) Residue DG2 prepri file

0 0 2

This is a remark line

molecule.res

MOL INT 0

CORRECT OMIT DU BEG

0.0000

1	DUMM	DU	M	0	-1	-2	0.000	.0	.0	.00000
2	DUMM	DU	M	1	0	-1	1.449	.0	.0	.00000
3	DUMM	DU	M	2	1	0	1.523	111.21	.0	.00000
4	N10	NK	M	3	2	1	1.540	111.208	-180.000	0.051092611
5	C18	CA	M	4	3	2	1.355	39.856	-175.905	-0.105340898
6	H90	H4	E	5	4	3	1.071	119.858	-55.530	0.16035839
7	C13	CA	M	5	4	3	1.384	120.209	124.450	0.039115986
8	C12	CA	M	7	5	4	1.387	120.042	-179.725	-0.212538402
9	H91	HA	E	8	7	5	1.071	119.992	0.252	0.236261997
10	C11	CA	M	8	7	5	1.382	119.980	-179.768	-0.1849674
11	H92	HA	E	10	8	7	1.070	119.996	179.542	0.238702423
12	C10	CA	M	10	8	7	1.383	119.984	-0.479	-0.135124054
13	H93	HA	E	12	10	8	1.070	119.987	-179.535	0.201400154
14	C9	CA	M	12	10	8	1.384	119.970	0.461	-0.218508038
15	H98	HA	E	14	12	10	1.070	120.099	179.742	0.185122348
16	C14	CA	M	14	12	10	1.389	119.815	-0.262	0.108767732
17	C15	CA	M	16	14	12	1.367	120.090	-179.923	0.064537089
18	C16	CA	M	17	16	14	1.388	119.687	-179.966	0.175223682
19	C22	CA	M	18	17	16	1.393	119.833	-179.973	-0.282599652
20	H94	HA	E	19	18	17	1.070	119.968	179.971	0.232097779
21	C21	CA	M	19	18	17	1.390	120.042	-0.003	-0.217101057
22	H95	HA	E	21	19	18	1.070	119.945	-179.982	0.199897715
23	C20	CA	M	21	19	18	1.390	119.970	0.064	-0.128877726
24	H96	HA	E	23	21	19	1.069	119.992	179.831	0.187104848
25	C19	CA	M	23	21	19	1.390	119.983	-0.132	-0.282036583
26	H97	HA	E	25	23	21	1.069	120.050	-179.878	0.22411659

LOOP

C16 N10

C14 C13

C19 C15

IMPROPER

C13 H90 C18 N10

C14 C18 C13 C12

C13 C11 C12 H91

C10 C12 C11 H92

C9 C11 C10 H93

C10 C14 C9 H98

C9 C15 C14 C13

C14 C16 C15 C19

C15 C22 C16 N10

C16 C21 C22 H94

C22 C20 C21 H95

C21 C19 C20 H96

C15 C20 C19 H97

DONE
STOP

e) Residue PT prep file

0 0 2

This is a remark line

molecule.res

PT INT 0

CORRECT OMIT DU BEG

0.0000

1	DUMM	DU	M	0	-1	-2	0.000	.0	.0	.00000
2	DUMM	DU	M	1	0	-1	1.449	.0	.0	.00000
3	DUMM	DU	M	2	1	0	1.523	111.21	.0	.00000
4	PT	PT	M	3	2	1	1.540	111.208	-180.000	-0.11609

LOOP

IMPROPER

DONE

STOP

1.2.1.2 Frcmod file for phenanthriplatin

Remark line goes here

MASS

NK	14.010	0.530	same as nc
CA	12.010	0.360	same as ca
H4	1.008	0.135	same as h4
HA	1.008	0.135	same as ha
NS	14.010	0.530	
NF	14.010	0.530	
NL	14.010	0.530	
PT	195.08		

BOND

CA-NK	467.70	1.352	same as ca-nc, penalty score=	0.0
CA-H4	341.50	1.089	same as ca-h4, penalty score=	0.0
CA-CA	461.10	1.398	same as ca-ca, penalty score=	0.0
CA-HA	345.80	1.086	same as ca-ha, penalty score=	0.0
PT-NF	101.6	2.1062	Created by Seminario method using	MCPB.py
PT-NL	106.0	2.1026	Created by Seminario method using	MCPB.py
PT-NK	107.7	2.0783	Created by Seminario method using	MCPB.py
NS-PT	113.7	2.0700	Created by Seminario method using	MCPB.py
NS-CB	441.1	1.3694	SOURCE1_SOURCE5	2269 0.0086
NF-H	392.4	1.0190	SOURCE3_SOURCE5	5944 0.0012
NL-H	392.4	1.0190	SOURCE3_SOURCE5	5944 0.0012
NK-CA	488.0	1.3390	SOURCE3_SOURCE5	6806 0.0055
CK-NS	525.4	1.3172	SOURCE3_SOURCE5	4612 0.0083

ANGLE

H4-CA-NK	51.000	118.360	same as h4-ca-nc, penalty score=	0.0
CA-CA-NK	69.460	119.720	same as ca-ca-nc, penalty score=	0.0
CA-NK-CA	69.910	109.950	same as ca-nc-ca, penalty score=	0.0
CA-CA-CA	66.620	120.020	same as ca-ca-ca, penalty score=	0.0
CA-CA-H4	48.060	120.340	same as ca-ca-h4, penalty score=	0.0
CA-CA-HA	48.180	119.880	same as ca-ca-ha, penalty score=	0.0
PT-NS-CB	171.01	128.41	Created by Seminario method using	MCPB.py
PT-NF-H	56.36	111.96	Created by Seminario method using	MCPB.py
PT-NL-H	63.49	111.05	Created by Seminario method using	MCPB.py
PT-NK-CA	164.04	120.13	Created by Seminario method using	MCPB.py
NS-PT-NF	128.60	178.47	Created by Seminario method using	MCPB.py
NS-PT-NL	160.63	89.36	Created by Seminario method using	MCPB.py
NS-PT-NK	166.14	90.91	Created by Seminario method using	MCPB.py
NL-PT-NF	152.94	91.59	Created by Seminario method using	MCPB.py
NK-PT-NF	158.20	88.14	Created by Seminario method using	MCPB.py
NK-PT-NL	179.53	179.65	Created by Seminario method using	MCPB.py
CK-NS-PT	138.99	125.31	Created by Seminario method using	MCPB.py
NS-CK-H5	50.58	125.52	SOURCE3_SOURCE5	1309 0.7276

NS-CB-C	66.22	123.32	CORR_SOURCE5	27	2.2025
NS-CB-CB	72.17	111.65	CORR_SOURCE5	1656	1.8430
NK-CA-CA	68.83	122.94	SOURCE3_SOURCE5	5507	1.1495
NK-CA-H4	51.88	116.03	SOURCE3_SOURCE5	2217	0.2861
CA-NK-CA	68.35	117.22	SOURCE3_SOURCE5	3343	1.0306
CK-NS-CB	71.76	105.49	CORR_SOURCE5	1810	1.9032
H-NF-H	41.40	106.40	SOURCE3_SOURCE5	2019	0.9777
H-NL-H	41.40	106.40	SOURCE3_SOURCE5	2019	0.9777
N*-CK-NS	74.90	112.22	SOURCE3_SOURCE5	2726	1.5103

DIHE

CA-CA-CA-NK	4	14.500	180.000	2.000	same as X -ca-ca-X , penalty score= 0.0
HA-CA-CA-NK	4	14.500	180.000	2.000	same as X -ca-ca-X , penalty score= 0.0
CA-CA-NK-CA	2	9.600	180.000	2.000	same as X -ca-nd-X , penalty score= 0.0
CA-CA-CA-HA	4	14.500	180.000	2.000	same as X -ca-ca-X , penalty score= 0.0
CA-CA-CA-CA	4	14.500	180.000	2.000	same as X -ca-ca-X , penalty score= 0.0
H4-CA-NK-CA	2	9.600	180.000	2.000	same as X -ca-nd-X , penalty score= 0.0
CA-CA-CA-H4	4	14.500	180.000	2.000	same as X -ca-ca-X , penalty score= 0.0
HA-CA-CA-HA	4	14.500	180.000	2.000	same as X -ca-ca-X , penalty score= 0.0
X-NS-CB-X	2	9.5	180.0	2.0	statistic value from parm94
X-NK-CA-X	2	9.6	180.0	2.0	same as X-CA-NC-X
X-CK-NS-X	2	9.5	180.0	2.0	statistic value from parm94
PT-NS-CK-H5	3	0.00	0.00	3.0	Treat as zero by MCPB.py
PT-NS-CB-C	3	0.00	0.00	3.0	Treat as zero by MCPB.py
PT-NS-CB-CK	3	0.00	0.00	3.0	Treat as zero by MCPB.py
PT-NK-CA-CA	3	0.00	0.00	3.0	Treat as zero by MCPB.py
PT-NK-CA-H4	3	0.00	0.00	3.0	Treat as zero by MCPB.py
NS-PT-NF-H	3	0.00	0.00	3.0	Treat as zero by MCPB.py
NS-PT-NL-H	3	0.00	0.00	3.0	Treat as zero by MCPB.py
NS-PT-NK-CA	3	0.00	0.00	3.0	Treat as zero by MCPB.py
NF-PT-NS-CB	3	0.00	0.00	3.0	Treat as zero by MCPB.py
NL-PT-NS-CB	3	0.00	0.00	3.0	Treat as zero by MCPB.py
NL-PT-NF-H	3	0.00	0.00	3.0	Treat as zero by MCPB.py
NK-PT-NS-CB	3	0.00	0.00	3.0	Treat as zero by MCPB.py
NK-PT-NF-H	3	0.00	0.00	3.0	Treat as zero by MCPB.py
NK-PT-NL-H	3	0.00	0.00	3.0	Treat as zero by MCPB.py
CA-NK-PT-NF	3	0.00	0.00	3.0	Treat as zero by MCPB.py
CA-NK-PT-NL	3	0.00	0.00	3.0	Treat as zero by MCPB.py
CK-NS-PT-NF	3	0.00	0.00	3.0	Treat as zero by MCPB.py
CK-NS-PT-NL	3	0.00	0.00	3.0	Treat as zero by MCPB.py
CK-NS-PT-NK	3	0.00	0.00	3.0	Treat as zero by MCPB.py
H-NL-PT-NF	3	0.00	0.00	3.0	Treat as zero by MCPB.py
N*-CK-NS-PT	3	0.00	0.00	3.0	Treat as zero by MCPB.py

IMPROPER

NS-H5-CK-N*	1.1	180.0	2.0	Using the default value
NK-CA-CA-CA	1.1	180.0	2.0	Using the default value
NK-CA-CA-H4	1.1	180.0	2.0	Same as X -X -ca-ha, penalty score= 44.3 (use general term))
NS-C -CB-CK	1.1	180.0	2.0	Using the default value
CA-H4-CA-NK	1.1	180.0	2.0	Same as X -X -ca-ha, penalty score= 44.3 (use general term))
CA-CA-CA-CA	1.1	180.0	2.0	Using the default value
CA-CA-CA-HA	1.1	180.0	2.0	Using general improper torsional angle X- X-ca-ha, penalty score= 6.0)
CA-CA-CA-NK	1.1	180.0	2.0	Using the default value

NONBON

CA	1.9080	0.0860	same as ca
H4	1.4090	0.0150	same as h4
HA	1.4590	0.0150	same as ha
PT	1.2660	0.0030764200	CM set for Pt2+ ion in TIP3P water from Li et al. JCTC, 2013, 9, 2733
NS	1.8240	0.1700	OPLS
NF	1.8240	0.1700	OPLS
NL	1.8240	0.1700	OPLS
NK	1.8240	0.1700	OPLS

1.2.2 Pyriplatin (Pyr)

1.2.2.1 Chrages

a) Residue AMN prepri file

0 0 2

This is a remark line

molecule.res

AMN INT 0

CORRECT OMIT DU BEG

0.0000

1	DUMM	DU	M	0	-1	-2	0.000	.0	.0	.00000
2	DUMM	DU	M	1	0	-1	1.449	.0	.0	.00000
3	DUMM	DU	M	2	1	0	1.523	111.21	.0	.00000
4	N11	NF	M	3	2	1	1.540	111.208	-180.000	-0.704275731
5	H85	H	E	4	3	2	0.999	121.435	157.949	0.362357395
6	H86	H	E	4	3	2	0.999	106.092	-76.325	0.428048644
7	H87	H	E	4	3	2	1.000	100.140	37.569	0.431635219

LOOP

IMPROPER

DONE

STOP

b) Residue AMO prepri file

0 0 2

This is a remark line

molecule.res

AMO INT 0

CORRECT OMIT DU BEG

0.0000

1	DUMM	DU	M	0	-1	-2	0.000	.0	.0	.00000
2	DUMM	DU	M	1	0	-1	1.449	.0	.0	.00000
3	DUMM	DU	M	2	1	0	1.523	111.21	.0	.00000
4	N12	NL	M	3	2	1	1.540	111.208	-180.000	-0.515489169
5	H82	H	E	4	3	2	1.000	121.408	157.974	0.350754522
6	H83	H	E	4	3	2	0.999	106.092	-76.325	0.389351038
7	H84	H	E	4	3	2	1.000	100.132	37.533	0.341593142

LOOP

IMPROPER

DONE

STOP

c) Residue MOL prepri file

0 0 2

This is a remark line

molecule.res

MOL INT 0

CORRECT OMIT DU BEG

0.0000

1	DUMM	DU	M	0	-1	-2	0.000	.0	.0	.00000
2	DUMM	DU	M	1	0	-1	1.449	.0	.0	.00000
3	DUMM	DU	M	2	1	0	1.523	111.21	.0	.00000
4	N10	NK	M	3	2	1	1.540	111.208	-180.000	0.051092611
5	C18	CA	M	4	3	2	1.355	39.856	-175.905	-0.105340898
6	H90	H4	E	5	4	3	1.071	119.858	-55.530	0.16035839
7	C13	CA	M	5	4	3	1.384	120.209	124.450	0.039115986
8	C12	CA	M	7	5	4	1.387	120.042	-179.725	-0.212538402
9	H91	HA	E	8	7	5	1.071	119.992	0.252	0.236261997

10	C11	CA	M	8	7	5	1.382	119.980	-179.768	-0.1849674
11	H92	HA	E	10	8	7	1.070	119.996	179.542	0.238702423
12	C10	CA	M	10	8	7	1.383	119.984	-0.479	-0.135124054
13	H93	HA	E	12	10	8	1.070	119.987	-179.535	0.201400154
14	C9	CA	M	12	10	8	1.384	119.970	0.461	-0.218508038
15	H98	HA	E	14	12	10	1.070	120.099	179.742	0.185122348
16	C14	CA	M	14	12	10	1.389	119.815	-0.262	0.108767732
17	C15	CA	M	16	14	12	1.367	120.090	-179.923	0.064537089
18	C16	CA	M	17	16	14	1.388	119.687	-179.966	0.175223682
19	C22	CA	M	18	17	16	1.393	119.833	-179.973	-0.282599652
20	H94	HA	E	19	18	17	1.070	119.968	179.971	0.232097779
21	C21	CA	M	19	18	17	1.390	120.042	-0.003	-0.217101057
22	H95	HA	E	21	19	18	1.070	119.945	-179.982	0.199897715
23	C20	CA	M	21	19	18	1.390	119.970	0.064	-0.128877726
24	H96	HA	E	23	21	19	1.069	119.992	179.831	0.187104848
25	C19	CA	M	23	21	19	1.390	119.983	-0.132	-0.282036583
26	H97	HA	E	25	23	21	1.069	120.050	-179.878	0.22411659

LOOP

C16 N10
C14 C13
C19 C15

IMPROPER

C13 H90 C18 N10
C14 C18 C13 C12
C13 C11 C12 H91
C10 C12 C11 H92
C9 C11 C10 H93
C10 C14 C9 H98
C9 C15 C14 C13
C14 C16 C15 C19
C15 C22 C16 N10
C16 C21 C22 H94
C22 C20 C21 H95
C21 C19 C20 H96
C15 C20 C19 H97

DONE

STOP

d) Residue DG2 prep file

0 0 2

This is a remark line

molecule.res

DG2 INT 1

CORR OMIT DU BEG

0.0

1	DUMM	DU	M	0	-1	-2	0.00	0.00	0.00	0.0000
2	DUMM	DU	M	1	0	-1	1.00	0.00	0.00	0.0000
3	DUMM	DU	M	2	1	0	1.00	90.00	0.00	0.0000
4	P	P	M	3	2	1	1.60	119.04	200.00	1.596763335
5	OP1	O2	E	4	3	2	1.48	109.61	150.00	-0.966829196
6	OP2	O2	E	4	3	2	1.48	109.58	20.00	-1.013874165
7	O5'	OS	M	4	3	2	1.60	101.43	-98.89	-0.643586644
8	C5'	CT	M	7	4	3	1.44	119.00	-39.22	-0.025366708
9	H5'	H1	E	8	7	4	1.09	109.50	60.00	0.129885567
10	H5''	H1	E	8	7	4	1.09	109.50	-60.00	0.129885567
11	C4'	CT	M	8	7	4	1.52	110.00	180.00	0.315344077
12	H4'	H1	E	11	8	7	1.09	109.50	-200.00	0.108140896
13	O4'	OS	S	11	8	7	1.46	108.86	-86.31	-0.520171766
14	C1'	CT	B	13	11	8	1.42	110.04	105.60	0.10210463
15	H1'	H2	E	14	13	11	1.09	109.50	-240.00	0.166728513
16	N9	N*	S	14	13	11	1.49	108.06	-127.70	0.154574353
17	C8	CK	B	16	14	13	1.38	129.20	81.59	-0.08797343
18	H8	H5	E	17	16	14	1.08	120.00	0.00	0.274686786
19	N7	NS	S	17	16	14	1.31	114.00	-179.90	-0.069058042
20	C5	CB	S	19	17	16	1.39	103.90	0.00	0.00766051
21	C6	C	B	20	19	17	1.42	130.40	180.00	0.453574993

```

22 O6 O E 21 20 19 1.23 128.80 0.00 -0.699343594
23 N1 NA B 21 20 19 1.40 111.38 180.00 -0.368320166
24 H1 H E 23 21 20 1.00 117.36 179.90 0.409476906
25 C2 CA B 23 21 20 1.38 125.24 -0.10 0.713429138
26 N2 N2 B 25 23 21 1.34 116.02 180.00 -1.065495796
27 H21 H E 26 25 23 1.01 127.00 -0.82 0.562667746
28 H22 H E 26 25 23 1.01 116.53 -179.44 0.543180968
29 N3 NC S 25 23 21 1.33 123.30 0.00 -0.599419381
30 C4 CB E 29 25 23 1.36 112.20 0.00 0.244144357
31 C3' CT M 11 8 7 1.53 115.78 -329.11 0.393641218
32 H3' H1 E 31 11 8 1.09 109.50 30.00 0.005239363
33 C2' CT B 31 11 8 1.53 102.80 -86.30 -0.080568869
34 H2' HC E 33 31 11 1.09 109.50 120.00 0.004500567
35 H2'' HC E 33 31 11 1.09 109.50 240.00 0.004500567
36 O3' OS M 31 11 8 1.42 116.52 -203.47 -0.685522301

```

IMPROPER

```

C8 C4 N9 C1'
C5 N1 C6 O6
C6 C2 N1 H1
C2 H21 N2 H22
N7 N9 C8 H8
N1 N3 C2 N2

```

LOOP CLOSING EXPLICIT

```

C1' C2'
C4 C5
C4 N9

```

DONE

STOP

e) Residue PT prep file

```
0 0 2
```

This is a remark line

molecule.res

PT INT 0

CORRECT OMIT DU BEG

0.0000

```

1 DUMM DU M 0 -1 -2 0.000 .0 .0 .00000
2 DUMM DU M 1 0 -1 1.449 .0 .0 .00000
3 DUMM DU M 2 1 0 1.523 111.21 .0 .00000
4 PT PT M 3 2 1 1.540 111.208 -180.000 -0.11609

```

LOOP

IMPROPER

DONE

STOP

1.2.2.2 Frcmod file of pyriplatin

Remark line goes here

MASS

```

NK 14.010 0.530 same as nc
CA 12.010 0.360 same as ca
H4 1.008 0.135 same as h4
HA 1.008 0.135 same as ha
NS 14.010 0.530
NF 14.010 0.530
NL 14.010 0.530
PT 195.08

```

BOND

CA-NK	467.70	1.352	same as ca-nc, penalty score=	0.0
CA-H4	341.50	1.089	same as ca-h4, penalty score=	0.0
CA-CA	461.10	1.398	same as ca-ca, penalty score=	0.0
CA-HA	345.80	1.086	same as ca-ha, penalty score=	0.0
PT-NF	101.6	2.1062	Created by Seminario method using	MCPB.py
PT-NL	106.0	2.1026	Created by Seminario method using	MCPB.py
PT-NK	107.7	2.0783	Created by Seminario method using	MCPB.py
NS-PT	113.7	2.0700	Created by Seminario method using	MCPB.py
NS-CB	441.1	1.3694	SOURCE1_SOURCE5	2269 0.0086
NF-H	392.4	1.0190	SOURCE3_SOURCE5	5944 0.0012
NL-H	392.4	1.0190	SOURCE3_SOURCE5	5944 0.0012
NK-CA	488.0	1.3390	SOURCE3_SOURCE5	6806 0.0055
CK-NS	525.4	1.3172	SOURCE3_SOURCE5	4612 0.0083

ANGLE

H4-CA-NK	51.000	118.360	same as h4-ca-nc, penalty score=	0.0
CA-CA-NK	69.460	119.720	same as ca-ca-nc, penalty score=	0.0
CA-NK-CA	69.910	109.950	same as ca-nc-ca, penalty score=	0.0
CA-CA-CA	66.620	120.020	same as ca-ca-ca, penalty score=	0.0
CA-CA-H4	48.060	120.340	same as ca-ca-h4, penalty score=	0.0
CA-CA-HA	48.180	119.880	same as ca-ca-ha, penalty score=	0.0
PT-NS-CB	171.01	128.41	Created by Seminario method using	MCPB.py
PT-NF-H	56.36	111.96	Created by Seminario method using	MCPB.py
PT-NL-H	63.49	111.05	Created by Seminario method using	MCPB.py
PT-NK-CA	164.04	120.13	Created by Seminario method using	MCPB.py
NS-PT-NF	128.60	178.47	Created by Seminario method using	MCPB.py
NS-PT-NL	160.63	89.36	Created by Seminario method using	MCPB.py
NS-PT-NK	166.14	90.91	Created by Seminario method using	MCPB.py
NL-PT-NF	152.94	91.59	Created by Seminario method using	MCPB.py
NK-PT-NF	158.20	88.14	Created by Seminario method using	MCPB.py
NK-PT-NL	179.53	179.65	Created by Seminario method using	MCPB.py
CK-NS-PT	138.99	125.31	Created by Seminario method using	MCPB.py
NS-CK-H5	50.58	125.52	SOURCE3_SOURCE5	1309 0.7276
NS-CB-C	66.22	123.32	CORR_SOURCE5	27 2.2025
NS-CB-CB	72.17	111.65	CORR_SOURCE5	1656 1.8430
NK-CA-CA	68.83	122.94	SOURCE3_SOURCE5	5507 1.1495
NK-CA-H4	51.88	116.03	SOURCE3_SOURCE5	2217 0.2861
CA-NK-CA	68.35	117.22	SOURCE3_SOURCE5	3343 1.0306
CK-NS-CB	71.76	105.49	CORR_SOURCE5	1810 1.9032
H-NF-H	41.40	106.40	SOURCE3_SOURCE5	2019 0.9777
H-NL-H	41.40	106.40	SOURCE3_SOURCE5	2019 0.9777
N*-CK-NS	74.90	112.22	SOURCE3_SOURCE5	2726 1.5103

DIHE

CA-CA-CA-NK	4	14.500	180.000	2.000	same as X-ca-ca-X, penalty score=	0.0
HA-CA-CA-NK	4	14.500	180.000	2.000	same as X-ca-ca-X, penalty score=	0.0
CA-CA-NK-CA	2	9.600	180.000	2.000	same as X-ca-nd-X, penalty score=	0.0
CA-CA-CA-HA	4	14.500	180.000	2.000	same as X-ca-ca-X, penalty score=	0.0
CA-CA-CA-CA	4	14.500	180.000	2.000	same as X-ca-ca-X, penalty score=	0.0
H4-CA-NK-CA	2	9.600	180.000	2.000	same as X-ca-nd-X, penalty score=	0.0
CA-CA-CA-H4	4	14.500	180.000	2.000	same as X-ca-ca-X, penalty score=	0.0
HA-CA-CA-HA	4	14.500	180.000	2.000	same as X-ca-ca-X, penalty score=	0.0
X-NS-CB-X	2	9.5	180.0	2.0	statistic value from parm94	
X-NK-CA-X	2	9.6	180.0	2.0	same as X-CA-NC-X	
X-CK-NS-X	2	9.5	180.0	2.0	statistic value from parm94	
PT-NS-CK-H5	3	0.00	0.00	3.0	Treat as zero by MCPB.py	
PT-NS-CB-C	3	0.00	0.00	3.0	Treat as zero by MCPB.py	
PT-NS-CB-CK	3	0.00	0.00	3.0	Treat as zero by MCPB.py	
PT-NK-CA-CA	3	0.00	0.00	3.0	Treat as zero by MCPB.py	
PT-NK-CA-H4	3	0.00	0.00	3.0	Treat as zero by MCPB.py	
NS-PT-NF-H	3	0.00	0.00	3.0	Treat as zero by MCPB.py	
NS-PT-NL-H	3	0.00	0.00	3.0	Treat as zero by MCPB.py	
NS-PT-NK-CA	3	0.00	0.00	3.0	Treat as zero by MCPB.py	
NF-PT-NS-CB	3	0.00	0.00	3.0	Treat as zero by MCPB.py	
NL-PT-NS-CB	3	0.00	0.00	3.0	Treat as zero by MCPB.py	
NL-PT-NF-H	3	0.00	0.00	3.0	Treat as zero by MCPB.py	
NK-PT-NS-CB	3	0.00	0.00	3.0	Treat as zero by MCPB.py	
NK-PT-NF-H	3	0.00	0.00	3.0	Treat as zero by MCPB.py	
NK-PT-NL-H	3	0.00	0.00	3.0	Treat as zero by MCPB.py	
CA-NK-PT-NF	3	0.00	0.00	3.0	Treat as zero by MCPB.py	
CA-NK-PT-NL	3	0.00	0.00	3.0	Treat as zero by MCPB.py	

CK-NS-PT-NF	3	0.00	0.00	3.0	Treat as zero by MCPB.py
CK-NS-PT-NL	3	0.00	0.00	3.0	Treat as zero by MCPB.py
CK-NS-PT-NK	3	0.00	0.00	3.0	Treat as zero by MCPB.py
H -NL-PT-NF	3	0.00	0.00	3.0	Treat as zero by MCPB.py
N*-CK-NS-PT	3	0.00	0.00	3.0	Treat as zero by MCPB.py

IMPROPER

NS-H5-CK-N*	1.1	180.0	2.0	Using the default value
NK-CA-CA-CA	1.1	180.0	2.0	Using the default value
NK-CA-CA-H4	1.1	180.0	2.0	Same as X -X -ca-ha, penalty score= 44.3 (use general term))
NS-C -CB-CK	1.1	180.0	2.0	Using the default value
CA-H4-CA-NK	1.1	180.0	2.0	Same as X -X -ca-ha, penalty score= 44.3 (use general term))
CA-CA-CA-CA	1.1	180.0	2.0	Using the default value
CA-CA-CA-HA	1.1	180.0	2.0	Using general improper torsional angle X- X-ca-ha, penalty score= 6.0)
CA-CA-CA-NK	1.1	180.0	2.0	Using the default value

NONBON

CA	1.9080	0.0860	same as ca
H4	1.4090	0.0150	same as h4
HA	1.4590	0.0150	same as ha
PT	1.2660	0.0030764200	CM set for Pt2+ ion in TIP3P water from Li et al. JCTC, 2013, 9, 2733
NS	1.8240	0.1700	OPLS
NF	1.8240	0.1700	OPLS
NL	1.8240	0.1700	OPLS

1.2.3 Enpyriplatin (Enpyr)

1.2.3.1 Charges

a) Residue EMN prepi file

0 0 2

This is a remark line

molecule.res

EMN INT 0

CORRECT OMIT DU BEG

0.0000

1	DUMM	DU	M	0	-1	-2	0.000	.0	.0	.00000
2	DUMM	DU	M	1	0	-1	1.449	.0	.0	.00000
3	DUMM	DU	M	2	1	0	1.523	111.21	.0	.00000
4	N11	NL	M	3	2	1	1.540	111.208	-180.000	-0.290658
5	H85	H	E	4	3	2	1.019	81.192	107.337	0.306558
6	H87	H	E	4	3	2	1.034	165.578	-17.872	0.355940
7	C81	CT	M	4	3	2	1.499	53.194	-16.109	-0.012428
8	H90	H1	E	7	4	3	1.093	107.967	20.391	0.113768
9	H91	H1	E	7	4	3	1.091	110.637	138.812	0.113768
10	C80	CT	M	7	4	3	1.520	108.326	-99.382	0.045742
11	H89	H1	E	10	7	4	1.092	110.813	-65.102	0.115623
12	H92	H1	E	10	7	4	1.092	111.456	173.661	0.115623
13	N12	NF	M	10	7	4	1.508	107.840	52.021	-0.456124
14	H86	H	E	13	10	7	1.020	109.977	-167.508	0.334440
15	H88	H	E	13	10	7	1.021	109.783	76.283	0.361008

LOOP

IMPROPER

DONE

STOP

b) Residue MOL prepi file

0 0 2

This is a remark line


```

molecule.res
MOL INT 0
CORRECT OMIT DU BEG
0.0000
 1 DUMM DU M 0 -1 -2 0.000 .0 .0 .00000
 2 DUMM DU M 1 0 -1 1.449 .0 .0 .00000
 3 DUMM DU M 2 1 0 1.523 111.21 .0 .00000
 4 C82 CA M 3 2 1 1.540 111.208 -180.000 -0.023212
 5 H94 H4 E 4 3 2 1.082 138.335 3.030 0.166119
 6 C83 CA M 4 3 2 1.385 85.072 -130.916 -0.201105
 7 H95 HA E 6 4 3 1.082 119.399 145.424 0.207515
 8 C84 CA M 6 4 3 1.394 119.158 -34.463 -0.068979
 9 H96 HA E 8 6 4 1.083 120.557 179.647 0.204878
10 C85 CA M 8 6 4 1.392 118.797 -0.583 -0.154314
11 H97 HA E 10 8 6 1.082 121.409 -179.720 0.239448
12 C86 CA M 10 8 6 1.387 119.326 0.487 -0.040404
13 H93 H4 E 12 10 8 1.082 121.262 -178.148 0.148134
14 N10 NK M 12 10 8 1.351 121.712 0.277 0.110746

```

```

LOOP
N10 C82

```

```

IMPROPER
C83 H94 C82 N10
C82 C84 C83 H95
C83 C85 C84 H96
C86 C84 C85 H97
C85 H93 C86 N10

```

```

DONE
STOP

```

c) Residue DG2 prepri file

```
0 0 2
```

This is a remark line

```

molecule.res
DG2 INT 1
CORR OMIT DU BEG
0.0
 1 DUMM DU M 0 -1 -2 0.00 0.00 0.00 0.0000
 2 DUMM DU M 1 0 -1 1.00 0.00 0.00 0.0000
 3 DUMM DU M 2 1 0 1.00 90.00 0.00 0.0000
 4 P P M 3 2 1 1.60 119.04 200.00 1.541752983
 5 OP1 O2 E 4 3 2 1.48 109.61 150.00 -0.940925943
 6 OP2 O2 E 4 3 2 1.48 109.58 20.00 -0.981357943
 7 O5' OS M 4 3 2 1.60 101.43 -98.89 -0.608722519
 8 C5' CT M 7 4 3 1.44 119.00 -39.22 -0.122174609
 9 H5' H1 E 8 7 4 1.09 109.50 60.00 0.168607546
10 H5'' H1 E 8 7 4 1.09 109.50 -60.00 0.168607546
11 C4' CT M 8 7 4 1.52 110.00 180.00 0.161850659
12 H4' H1 E 11 8 7 1.09 109.50 -200.00 0.143577197
13 O4' OS S 11 8 7 1.46 108.86 -86.31 -0.420466936
14 C1' CT B 13 11 8 1.42 110.04 105.60 0.020259997
15 H1' H2 E 14 13 11 1.09 109.50 -240.00 0.186673022
16 N9 N* S 14 13 11 1.49 108.06 -127.70 0.2062024
17 C8 CK B 16 14 13 1.38 129.20 81.59 -0.162506616
18 H8 H5 E 17 16 14 1.08 120.00 0.00 0.290887482
19 N7 NS S 17 16 14 1.31 114.00 -179.90 -0.07560968
20 C5 CB S 19 17 16 1.39 103.90 0.00 0.016440249
21 C6 C B 20 19 17 1.42 130.40 180.00 0.409325004
22 O6 O E 21 20 19 1.23 128.80 0.00 -0.679459188
23 N1 NA B 21 20 19 1.40 111.38 180.00 -0.370656887
24 H1 H E 23 21 20 1.00 117.36 179.90 0.408631716
25 C2 CA B 23 21 20 1.38 125.24 -0.10 0.698732583
26 N2 N2 B 25 23 21 1.34 116.02 180.00 -1.019304774
27 H21 H E 26 25 23 1.01 127.00 -0.82 0.546335967
28 H22 H E 26 25 23 1.01 116.53 -179.44 0.513290147
29 N3 NC S 25 23 21 1.33 123.30 0.00 -0.603385538

```

```

30 C4 CB E 29 25 23 1.36 112.20 0.00 0.251826058
31 C3' CT M 11 8 7 1.53 115.78 -329.11 0.408837036
32 H3' H1 E 31 11 8 1.09 109.50 30.00 0.020141338
33 C2' CT B 31 11 8 1.53 102.80 -86.30 -0.170627413
34 H2' HC E 33 31 11 1.09 109.50 120.00 0.037786841
35 H2'' HC E 33 31 11 1.09 109.50 240.00 0.037786841
36 O3' OS M 31 11 8 1.42 116.52 -203.47 -0.638301902

```

IMPROPER

```

C8 C4 N9 C1'
C5 N1 C6 O6
C6 C2 N1 H1
C2 H21 N2 H22
N7 N9 C8 H8
N1 N3 C2 N2

```

LOOP CLOSING EXPLICIT

```

C1' C2'
C4 C5
C4 N9

```

DONE

STOP

1.2.3.2 Frcmod file for Enpyriplatin

REMARK GOES HERE, THIS FILE IS GENERATED BY MCPB.PY

MASS

PT 195.08		Pt ion
NL 14.01	0.530	Sp3 N with three connected atoms
NF 14.01	0.530	Sp3 N with three connected atoms
NK 14.01	0.530	Sp2 N in pure aromatic systems
NS 14.01	0.530	Sp2 N in non-pure aromatic systems, identical to nc

BOND

PT-NL 112.1	2.0885	Created by Seminario method using MCPB.py
PT-NF 99.9	2.0989	Created by Seminario method using MCPB.py
PT-NK 105.7	2.0807	Created by Seminario method using MCPB.py
PT-NS 117.0	2.0690	Created by Seminario method using MCPB.py
NL-CT 325.9	1.4647	SOURCE1_SOURCE5 15206 0.0039
NL-H 392.4	1.0190	SOURCE3_SOURCE5 5944 0.0012
NF-CT 325.9	1.4647	SOURCE1_SOURCE5 15206 0.0039
NF-H 392.4	1.0190	SOURCE3_SOURCE5 5944 0.0012
NS-CB 441.1	1.3694	SOURCE1_SOURCE5 2269 0.0086
CA-NK 488.0	1.3390	SOURCE3_SOURCE5 6806 0.0055
CK-NS 525.4	1.3172	SOURCE3_SOURCE5 4612 0.0083

ANGL

PT-NL-CT	168.49	111.06	Created by Seminario method using MCPB.py		
PT-NL-H	65.70	108.18	Created by Seminario method using MCPB.py		
PT-NF-CT	158.47	108.49	Created by Seminario method using MCPB.py		
PT-NF-H	60.40	111.31	Created by Seminario method using MCPB.py		
PT-NK-CA	176.84	120.52	Created by Seminario method using MCPB.py		
PT-NS-CK	136.40	126.94	Created by Seminario method using MCPB.py		
PT-NS-CB	165.76	126.78	Created by Seminario method using MCPB.py		
NF-PT-NL	160.29	82.10	Created by Seminario method using MCPB.py		
NK-PT-NL	176.08	175.55	Created by Seminario method using MCPB.py		
NK-PT-NF	158.03	93.83	Created by Seminario method using MCPB.py		
NS-PT-NL	164.68	93.17	Created by Seminario method using MCPB.py		
NS-PT-NF	162.20	174.78	Created by Seminario method using MCPB.py		
NS-PT-NK	161.09	90.82	Created by Seminario method using MCPB.py		
NL-CT-CT	66.02	111.04	SOURCE3_SOURCE5	12086	1.5519
NL-CT-H1	49.53	109.88	SOURCE3_SOURCE5	20428	1.2681
NF-CT-CT	66.02	111.04	SOURCE3_SOURCE5	12086	1.5519
NF-CT-H1	49.53	109.88	SOURCE3_SOURCE5	20428	1.2681
NK-CA-CA	68.83	122.94	SOURCE3_SOURCE5	5507	1.1495
NS-CK-H5	50.58	125.52	SOURCE3_SOURCE5	1309	0.7276
NS-CB-C	66.22	123.32	CORR_SOURCE5	27	2.2025
NS-CB-CK	72.17	111.65	CORR_SOURCE5	1656	1.8430
CT-NL-H	47.42	109.29	SOURCE3_SOURCE5	6742	0.6614
CT-NF-H	47.42	109.29	SOURCE3_SOURCE5	6742	0.6614
CA-NK-CA	68.35	117.22	SOURCE3_SOURCE5	3343	1.0306
CK-NS-CB	71.76	105.49	CORR_SOURCE5	1810	1.9032
H4-CA-NK	51.88	116.03	SOURCE3_SOURCE5	2217	0.2861
H-NL-H	41.40	106.40	SOURCE3_SOURCE5	2019	0.9777
H-NF-H	41.40	106.40	SOURCE3_SOURCE5	2019	0.9777
N*-CK-NS	74.90	112.22	SOURCE3_SOURCE5	2726	1.5103
CB-CB-NS	69.460	119.720	same as ca-ca-nc, penalty score= 0.0		

DIHE

X-NK-CA-X	2	9.6	180.0	2.0	same as X-CA-NC-X
X-NS-CB-X	2	9.5	180.0	2.0	statistiv value from parm94
X-CT-NL-X	6	1.8	0.0	3.0	Junmei et al, 1999

X -CT-NF-X	6	1.8	0.0	3.0	Junmei et al, 1999
X -CK-NS-X	2	9.5	180.0	2.0	statistic value from parm94
PT-NL-CT-CT	3	0.00	0.00	3.0	Treat as zero by MCPB.py
PT-NL-CT-H1	3	0.00	0.00	3.0	Treat as zero by MCPB.py
PT-NF-CT-CT	3	0.00	0.00	3.0	Treat as zero by MCPB.py
PT-NF-CT-H1	3	0.00	0.00	3.0	Treat as zero by MCPB.py
PT-NK-CA-CA	3	0.00	0.00	3.0	Treat as zero by MCPB.py
PT-NK-CA-H4	3	0.00	0.00	3.0	Treat as zero by MCPB.py
PT-NS-CK-H5	3	0.00	0.00	3.0	Treat as zero by MCPB.py
PT-NS-CK-N*	3	0.00	0.00	3.0	Treat as zero by MCPB.py
PT-NS-CB-C	3	0.00	0.00	3.0	Treat as zero by MCPB.py
PT-NS-CB-CK	3	0.00	0.00	3.0	Treat as zero by MCPB.py
NF-PT-NL-CT	3	0.00	0.00	3.0	Treat as zero by MCPB.py
NF-PT-NL-H	3	0.00	0.00	3.0	Treat as zero by MCPB.py
NK-PT-NL-CT	3	0.00	0.00	3.0	Treat as zero by MCPB.py
NK-PT-NL-H	3	0.00	0.00	3.0	Treat as zero by MCPB.py
NK-PT-NF-CT	3	0.00	0.00	3.0	Treat as zero by MCPB.py
NK-PT-NF-H	3	0.00	0.00	3.0	Treat as zero by MCPB.py
NS-PT-NL-CT	3	0.00	0.00	3.0	Treat as zero by MCPB.py
NS-PT-NL-H	3	0.00	0.00	3.0	Treat as zero by MCPB.py
NS-PT-NF-CT	3	0.00	0.00	3.0	Treat as zero by MCPB.py
NS-PT-NF-H	3	0.00	0.00	3.0	Treat as zero by MCPB.py
NS-PT-NK-CA	3	0.00	0.00	3.0	Treat as zero by MCPB.py
CT-NF-PT-NL	3	0.00	0.00	3.0	Treat as zero by MCPB.py
CA-NK-PT-NL	3	0.00	0.00	3.0	Treat as zero by MCPB.py
CA-NK-PT-NF	3	0.00	0.00	3.0	Treat as zero by MCPB.py
CK-NS-PT-NL	3	0.00	0.00	3.0	Treat as zero by MCPB.py
CK-NS-PT-NF	3	0.00	0.00	3.0	Treat as zero by MCPB.py
CK-NS-PT-NK	3	0.00	0.00	3.0	Treat as zero by MCPB.py
CB-NS-PT-NL	3	0.00	0.00	3.0	Treat as zero by MCPB.py
CB-NS-PT-NF	3	0.00	0.00	3.0	Treat as zero by MCPB.py
CB-NS-PT-NK	3	0.00	0.00	3.0	Treat as zero by MCPB.py
H -NF-PT-NL	3	0.00	0.00	3.0	Treat as zero by MCPB.py

IMPR

NS-h5-CK-N*	1.1	180.0	2.0	Using the default value
-------------	-----	-------	-----	-------------------------

NK-CA-CA-H4	1.1	180.0	2.0	Same as X -X -CA-HA, penalty score= 44.3 (use general term))
NS-C -CB-CK	1.1	180.0	2.0	Using the default value

NONB

PT	1.2660	0.0030764200	CM set for Pt2+ ion in TIP3P water from Li et al. JCTC, 2013, 9, 2733
NL	1.8240	0.1700	OPLS
NF	1.8240	0.1700	OPLS
NK	1.8240	0.1700	OPLS
NS	1.8240	0.1700	OPLS

1.2.4 Amn

1.2.4.1 Charges

a) Residue AMN prep file

0 0 2

This is a remark line

molecule.res

AMN INT 0

CORRECT OMIT DU BEG

0.0000

1	DUMM	DU	M	0	-1	-2	0.000	.0	.0	.00000
2	DUMM	DU	M	1	0	-1	1.449	.0	.0	.00000
3	DUMM	DU	M	2	1	0	1.523	111.21	.0	.00000
4	N11	NF	M	3	2	1	1.540	111.208	-180.000	-0.337924897
5	H85	H	E	4	3	2	0.999	121.435	157.949	0.243952415
6	H86	H	E	4	3	2	0.999	106.092	-76.325	0.269372766
7	H87	H	E	4	3	2	1.000	100.140	37.569	0.234114716

LOOP

IMPROPER

DONE

STOP

b) Residue AMO prep file

0 0 2

This is a remark line

molecule.res

AMO INT 0

CORRECT OMIT DU BEG

0.0000

1	DUMM	DU	M	0	-1	-2	0.000	.0	.0	.00000
2	DUMM	DU	M	1	0	-1	1.449	.0	.0	.00000
3	DUMM	DU	M	2	1	0	1.523	111.21	.0	.00000
4	N12	NL	M	3	2	1	1.540	111.208	-180.000	-0.651310058
5	H82	H	E	4	3	2	1.000	121.408	157.974	0.418905137
6	H83	H	E	4	3	2	0.999	106.092	-76.325	0.386939126
7	H84	H	E	4	3	2	1.000	100.132	37.533	0.390777794

LOOP

IMPROPER

DONE

STOP

c) Residue MOL prep file

0 0 2

This is a remark line

molecule.res

MOL INT 0

CORRECT OMIT DU BEG

0.0000

1	DUMM	DU	M	0	-1	-2	0.000	.0	.0	.00000
2	DUMM	DU	M	1	0	-1	1.449	.0	.0	.00000
3	DUMM	DU	M	2	1	0	1.523	111.21	.0	.00000
4	N10	NK	M	3	2	1	1.540	111.208	-180.000	-0.45364247
5	H88	H	E	4	3	2	1.000	141.560	-78.491	0.341346027
6	H89	H	E	4	3	2	1.000	32.190	-71.157	0.340651084
7	H90	H	E	4	3	2	0.999	89.656	159.498	0.377436358

LOOP

IMPROPER

DONE

STOP

d) Residue DG2 prep file

0 0 2

This is a remark line

molecule.res

DG2 INT 1

CORR OMIT DU BEG

0.0

1	DUMM	DU	M	0	-1	-2	0.00	0.00	0.00	0.0000
2	DUMM	DU	M	1	0	-1	1.00	0.00	0.00	0.0000
3	DUMM	DU	M	2	1	0	1.00	90.00	0.00	0.0000
4	P	P	M	3	2	1	1.60	119.04	200.00	1.628273917
5	OP1	O2	E	4	3	2	1.48	109.61	150.00	-0.973788823
6	OP2	O2	E	4	3	2	1.48	109.58	20.00	-1.005989065
7	O5'	OS	M	4	3	2	1.60	101.43	-98.89	-0.648037079
8	C5'	CT	M	7	4	3	1.44	119.00	-39.22	-0.130509451
9	H5'	H1	E	8	7	4	1.09	109.50	60.00	0.17106121
10	H5''	H1	E	8	7	4	1.09	109.50	-60.00	0.17106121
11	C4'	CT	M	8	7	4	1.52	110.00	180.00	0.34793456
12	H4'	H1	E	11	8	7	1.09	109.50	-200.00	0.087886637
13	O4'	OS	S	11	8	7	1.46	108.86	-86.31	-0.483712293
14	C1'	CT	B	13	11	8	1.42	110.04	105.60	0.0411945
15	H1'	H2	E	14	13	11	1.09	109.50	-240.00	0.166629316
16	N9	N*	S	14	13	11	1.49	108.06	-127.70	0.231742584
17	C8	CK	B	16	14	13	1.38	129.20	81.59	-0.118279512
18	H8	H5	E	17	16	14	1.08	120.00	0.00	0.241825932
19	N7	NS	S	17	16	14	1.31	114.00	-179.90	-0.054696189
20	C5	CB	S	19	17	16	1.39	103.90	0.00	-0.00463378
21	C6	C	B	20	19	17	1.42	130.40	180.00	0.466433813
22	O6	O	E	21	20	19	1.23	128.80	0.00	-0.720492431
23	N1	NA	B	21	20	19	1.40	111.38	180.00	-0.385013044
24	H1	H	E	23	21	20	1.00	117.36	179.90	0.426866766
25	C2	CA	B	23	21	20	1.38	125.24	-0.10	0.71396064
26	N2	N2	B	25	23	21	1.34	116.02	180.00	-1.05664752
27	H21	H	E	26	25	23	1.01	127.00	-0.82	0.562531882

```

28 H22 H E 26 25 23 1.01 116.53 -179.44 0.53596112
29 N3 NC S 25 23 21 1.33 123.30 0.00 -0.562508534
30 C4 CB E 29 25 23 1.36 112.20 0.00 0.17978766
31 C3' CT M 11 8 7 1.53 115.78 -329.11 0.408069329
32 H3' H1 E 31 11 8 1.09 109.50 30.00 -0.006818826
33 C2' CT B 31 11 8 1.53 102.80 -86.30 -0.122682565
34 H2' HC E 33 31 11 1.09 109.50 120.00 0.020114508
35 H2'' HC E 33 31 11 1.09 109.50 240.00 0.020114508
36 O3' OS M 31 11 8 1.42 116.52 -203.47 -0.673955486

```

IMPROPER

```

C8 C4 N9 C1'
C5 N1 C6 O6
C6 C2 N1 H1
C2 H21 N2 H22
N7 N9 C8 H8
N1 N3 C2 N2

```

LOOP CLOSING EXPLICIT

```

C1' C2'
C4 C5
C4 N9

```

DONE

STOP

e) Residue PT prepi file

0 0 2

This is a remark line

molecule.res

PT INT 0

CORRECT OMIT DU BEG

0.0000

```

1 DUMM DU M 0 -1 -2 0.000 .0 .0 .00000
2 DUMM DU M 1 0 -1 1.449 .0 .0 .00000
3 DUMM DU M 2 1 0 1.523 111.21 .0 .00000
4 PT PT M 3 2 1 1.540 111.208 -180.000 -0.034293939

```

LOOP

IMPROPER

DONE

STOP

1.2.4.2 Frcmod file for Amn

REMARK GOES HERE, THIS FILE IS GENERATED BY MCPB.PY

MASS

PT 195.08

Pt ion

NS 14.01 0.530 Sp2 N in non-pure aromatic systems, identical to nc

NF 14.01 0.530 Sp3 N with three connected atoms

NL 14.01 0.530 Sp3 N with three connected atoms

NK 14.01 0.530 Sp3 N with three connected atoms

BOND

PT-NF 97.6 2.1153 Created by SemiN*rio method using MCPB.py

PT-NL 117.2 2.0845 Created by SemiN*rio method using MCPB.py

PT-NK 102.8 2.1146 Created by SemiN*rio method using MCPB.py

NS-PT 122.4 2.0641 Created by SemiN*rio method using MCPB.py

NS-CB	441.1	1.3694	SOURCE1_SOURCE5	2269	0.0086
NF-H	392.4	1.0190	SOURCE3_SOURCE5	5944	0.0012
NL-H	392.4	1.0190	SOURCE3_SOURCE5	5944	0.0012
NK-H	392.4	1.0190	SOURCE3_SOURCE5	5944	0.0012
CK-NS	525.4	1.3172	SOURCE3_SOURCE5	4612	0.0083

ANGL

PT-NS-CB	172.59	126.77	Created by SemiN*rio method using MCPB.py		
PT-NF-H	58.02	112.53	Created by SemiN*rio method using MCPB.py		
PT-NL-H	64.25	110.91	Created by SemiN*rio method using MCPB.py		
PT-NK-H	57.77	112.22	Created by SemiN*rio method using MCPB.py		
NS-PT-NF	163.56	178.80	Created by SemiN*rio method using MCPB.py		
NS-PT-NL	162.10	88.40	Created by SemiN*rio method using MCPB.py		
NS-PT-NK	159.04	89.96	Created by SemiN*rio method using MCPB.py		
NL-PT-NF	155.73	90.45	Created by SemiN*rio method using MCPB.py		
NK-PT-NF	156.40	91.17	Created by SemiN*rio method using MCPB.py		
NK-PT-NL	170.00	176.42	Created by SemiN*rio method using MCPB.py		
CK-NS-PT	142.51	126.90	Created by SemiN*rio method using MCPB.py		
NS-CK-H5	50.58	125.52	SOURCE3_SOURCE5	1309	0.7276
NS-CB-C	66.22	123.32	CORR_SOURCE5	27	2.2025
NS-CB-CK	72.17	111.65	CORR_SOURCE5	1656	1.8430
CK-NS-CB	71.76	105.49	CORR_SOURCE5	1810	1.9032
H -NF-H	41.40	106.40	SOURCE3_SOURCE5	2019	0.9777
H -NL-H	41.40	106.40	SOURCE3_SOURCE5	2019	0.9777
H -NK-H	41.40	106.40	SOURCE3_SOURCE5	2019	0.9777
N*-CK-NS	74.90	112.22	SOURCE3_SOURCE5	2726	1.5103
CB-CB-NS	69.460	119.720	same as ca-ca-nc, penalty score= 0.0		

DIHE

X -NS-CB-X	2	9.5	180.0	2.0	statistic value from parm94
X -CK-NS-X	2	9.5	180.0	2.0	statistic value from parm94
PT-NS-CK-H5	3	0.00	0.00	3.0	Treat as zero by MCPB.py
PT-NS-CB-C	3	0.00	0.00	3.0	Treat as zero by MCPB.py
PT-NS-CB-CK	3	0.00	0.00	3.0	Treat as zero by MCPB.py
NS-PT-NF-H	3	0.00	0.00	3.0	Treat as zero by MCPB.py
NS-PT-NL-H	3	0.00	0.00	3.0	Treat as zero by MCPB.py
NS-PT-NK-H	3	0.00	0.00	3.0	Treat as zero by MCPB.py
NF-PT-NS-CB	3	0.00	0.00	3.0	Treat as zero by MCPB.py
NL-PT-NS-CB	3	0.00	0.00	3.0	Treat as zero by MCPB.py
NL-PT-NF-H	3	0.00	0.00	3.0	Treat as zero by MCPB.py
NK-PT-NS-CB	3	0.00	0.00	3.0	Treat as zero by MCPB.py
NK-PT-NF-H	3	0.00	0.00	3.0	Treat as zero by MCPB.py
NK-PT-NL-H	3	0.00	0.00	3.0	Treat as zero by MCPB.py
CK-NS-PT-NF	3	0.00	0.00	3.0	Treat as zero by MCPB.py
CK-NS-PT-NL	3	0.00	0.00	3.0	Treat as zero by MCPB.py
CK-NS-PT-NK	3	0.00	0.00	3.0	Treat as zero by MCPB.py
H -NL-PT-NF	3	0.00	0.00	3.0	Treat as zero by MCPB.py
H -NK-PT-NF	3	0.00	0.00	3.0	Treat as zero by MCPB.py
H -NK-PT-NL	3	0.00	0.00	3.0	Treat as zero by MCPB.py
N*-CK-NS-PT	3	0.00	0.00	3.0	Treat as zero by MCPB.py

IMPR

NS-H5-CK-N*	1.1	180.0	2.0	Using the default value
NS-C -CB-CK	1.1	180.0	2.0	Using the default value

NONB

PT	1.2660	0.0030764200	CM set for Pt ²⁺ ion in TIP3P water from Li et al. JCTC, 2013, 9, 2733	
NS	1.8240	0.1700	OPLS	
NF	1.8240	0.1700	OPLS	
NL	1.8240	0.1700	OPLS	
NK	1.8240	0.1700	OPLS	

References

- (1) Gaussian 09, Revision D.01, M. J. Frisch, G. W. Trucks, H. B. Schlegel, G. E. Scuseria, M. A. Robb, J. R. Cheeseman, G. Scalmani, V. Barone, B. Mennucci, G. A. Petersson, H. Nakatsuji, M. Caricato, X. Li, H. P. Hratchian, A. F. Izmaylov, J. Bloino, G. Zheng, J. L. Sonnenberg, M. Hada, M. Ehara, K. Toyota, R. Fukuda, J. Hasegawa, M. Ishida, T. Nakajima, Y. Honda, O. Kitao, H. Nakai, T. Vreven, J. A. Montgomery-Jr., J. E. Peralta, F. Ogliaro, M. Bearpark, J. J. Heyd, E. Brothers, K. N. Kudin, V. N. Staroverov, T. Keith, R. Kobayashi, J. Normand, K. Raghavachari, A. Rendell, J. C. Burant, S. S. Iyengar, J. Tomasi, M. Cossi, N. Rega, J. M. Millam, M. Klene, J. E. Knox, J. B. Cross, V. Bakken, C. Adamo, J. Jaramillo, R. Gomperts, R. E. Stratmann, O. Yazyev, A. J. Austin, R. Cammi, C. Pomelli, J. W. Ochterski, R. L. Martin, K. Morokuma, V. G. Zakrzewski, G. A. Voth, P. Salvador, J. J. Dannenberg, S. Dapprich, A. D. Daniels, O. Farkas, J. B. Foresman, J. V. Ortiz, J. Cioslowski, D. J. Fox, Gaussian, Inc., Wallingford CT, 2010.
- (2) A. D. Becke, *J. Chem. Phys.*, **1993**, *98*, 5648-5652.
- (3) C. Lee, W. Yang, R. G. Parr, *Phys. Rev. B*, **1988**, *37*, 785-789.
- (4) S. Grimme, J. Antony, S. Ehrlich, H. Krieg, *J. Chem. Phys.*, **2010**, *132*, 154104-154122.
- (5) D. Andrae, U. Häussermann, M. Dolg, H. Stoll, H. Preuss, *Theor. Chim. Acta*, **1990**, *77*, 123-141.
- (6) (a) K. Fukui, *J. Phys. Chem.*, 1970, **74**, 4161-4163. (b) C. Gonzalez, H. B. Schlegel, *J. Chem. Phys.*, **1989**, *90*, 2154-2161.
- (7) (a) S. Miertuš, E. Scrocco, J. Tomasi, *Chem. Phys.*, 1981, **55**, 117-129; (b) S. Miertuš, J. Tomasi, *Chem. Phys.*, **1982**, *65*, 239-245; (c) J. L. Pascual-Ahuir, E. Silla, I. Tuñón, *J. Comp. Chem.*, **1994**, *15*, 1127-1138.
- (8) D. A. McQuarrie, J. D. Simon, *Molecular Thermodynamics*, University Science Books: Sausalito, CA, **1999**.
- (9) R.W. Ashcraft, S. Raman, H.W. Green, *J. Phys. Chem. B* **111** (2007) 11968-11971.
- (10) H. R. Drew, R. M. Wing, T. Takano, C. Broka, S. Tanaka, K. Itakura, R. E. Dickerson, *Proc. Natl. Acad. Sci., USA*, **1981**, *78*, 2179-2183.
- (11) M. T. Gregory, G. Y. Park, T. C. Johnstone, Y. -S. Lee, W. Yang, S. J. Lippard, *PNAS*, **2014**, *111*, 9133-9138.
- (12) (a) A. R. Anandakrishnan, B. Aguilar, A. V. Onufriev, *Nucleic Acids Res.*, **2012**, *40*, 537-541; (b) J. Myers, G. Grothaus, S. Narayanan, A. Onufriev, *Proteins*, **2006**, *63*, 928-938; (c) J. C. Gordon, J. B. Myers, T. Folta, V. Shoja, L. S. Heath, A. Onufriev, *Nucleic Acids Res.*, **2005**, *33*, 368-371.
- (13) P. Li, K. M. Merz-Jr., *J. Chem. Inf. Model.*, **2016**, *56*, 599-604.
- (14) D. A. Case, R. M. Betz, D. S. Cerutti, T. E. Cheatham, T. A. Darden, R. E. Duke, T. J. Giese, H. Gohlke, A. W. Goetz, N. Homeyer, S. Izadi, P. Janowski, J. Kaus, A. Kovalenko, T. S. Lee, S. LeGrand, P. Li, C. Lin, T. Luchko, R. Luo, B. Madej, D. Mermelstein, K. M. Merz, G. Monard, H. Nguyen, H. T. Nguyen, I. Omelyan, A. Onufriev, D. R. Roe, A. Roitberg, C. Sagui, C. L. Simmerling, W. M. Botello-Smith, J. Swails, R. C. Walker, J. Wang, R. M. Wolf, X. Wu, L. Xiao, P. A. Kollman, 2016, AMBER 2016, University of California, San Francisco.
- (15) (a) U. C. Singh, P. A. Kollman, *J. Comp. Chem.*, **1984**, *5*, 129-145; (b) B. H. Besler, K. M. Merz, P. A. Kollman, *J. Comput. Chem.*, **1990**, *11*, 431-439.
- (16) I. Ivani, P. D. Dans, A. Noy, A. Pérez, I. Faustino, A. Hospital, J. Walther, P. Andrio, R. Goñi, A. Balaceanu, G. Portella, F. Battistini, J. L. Gelpí, C. González, M. Vendruscolo, C. A. Lughton, S. A. Harris, D. A. Case, M. Orozco, *Nat. Methods*, **2016**, *13*, 55-58.
- (17) (a) J. Wang, W. Wang, P. A. Kollman, D. A. Case, *J. Mol. Graph. Mod.*, **2006**, *25*, 247-260; (b) J. Wang, R. M. Wolf, J. W. Caldwell, P. A. Kollman, D. A. Case, *J. Comput. Chem.*, **2004**, *25*, 1157-1174.
- (18) (a) M. W. Mahoney, W. L. Jorgensen, *J. Chem. Phys.*, **2000**, *112*, 8910-8922; (b) M. W. Mahoney, W. L. Jorgensen, *J. Chem. Phys.*, 2001, **114**, 363-366; (c) W. L. Jorgensen, J. Chandrasekhar, J. D. Madura, R. W. Impey, M. L. Klein, *J. Chem. Phys.*, **1983**, *79*, 926-935.
- (19) B. R. Miller, T. D. McGee Jr., J. M. Swails, N. Homeyer, H. Gohlke, A. E. Roitberg, *J. Chem. Theory Comput.* **2012**, *8*, 3314-3321.
- (20) D. R. Roe, T. E. Cheatham, *J. Chem. Theory Comput.*, **2013**, *9*, 3084-3095.
- (21) W. Humphrey, A. Dalke, K. J. Schulten, *Molec. Graphics*, **1996**, *14*, 33-38.
- (22) E. R. Johnson, S. Keinan, P. Mori-Sanchez, J. Contreras-Garcia, A. J. Cohen, W. Yang, *J. Am. Chem. Soc.*, **2010**, *132*, 6498-6506.
- (23) J. Contreras-Garcia, E. R. Johnson, S. Keinan, R. Chaudret, J-P. Piquemal, D. N. Beratan, W. Yang, *J. Chem. Theory Comput.*, **2011**, *7*, 625-632.

Chapter IV

Platinum Drugs

Targeting

Mitochondria

Chapter IV Platinum drugs Targetting Mitochondria

4.1 A comparative computational mechanistic study on derivatives of pyriplatin, modified with the $-\text{CH}_2\text{Ph}_3\text{P}^+$ group, as anticancer complexes targeting mitochondria

4.1.1 Introduction

In previous studies, it has been suggested that sub-cellular compartments other than nuclear DNA can be the targets of platinum complexes.¹ Those targets can be enzymes, proteins or non-nuclear cell organelles. Amongst the possible alternatives, mitochondria have been proved to be potential targets for platinum chemotherapeutics toxic to cancer cells.^{2,3} As a consequence, mitochondria targeting can become a novel strategy for fighting cancer.⁴ Mitochondria are the crucial players of the cell in which oxygen is consumed in the oxidative phosphorylation process to supply energy to the cell in the form of the bioenergetic intermediate ATP, producing reactive oxygen species (ROS) as byproducts.⁵ Mitochondrial dysfunction in cancer cells manifests with various alterations in energy-production pathways, which makes mitochondrial metabolism a potential target for cancer therapy to inhibit tumor cells growth and ultimately leading to their apoptosis.^{6,7}

Delivering Pt(II) complexes to the mitochondria to attack mitochondrial genome which lacks a repair machinery can lead to rationally designed cytotoxic drugs that might overcome the problems associated with conventional cisplatin and its derivatives treatment.

Three monofunctional Pt(II) complexes have been synthesized by Wang et al., starting from the monofunctional drug pyriplatin as the backbone and introducing the $-\text{CH}_2\text{Ph}_3\text{P}^+$ group in ortho, meta and para positions of the pyriplatin pyridine ring. The corresponding complexes have been named OPT, MPT and PPT, respectively (**Figure 4.1**).⁸ The newly prepared

complexes exhibited significant in vitro and in vivo antitumor efficacy and demonstrated to be able to penetrate mitochondria with some characterised differences among them although they are all cationic and possess the same degree of lipophilicity.

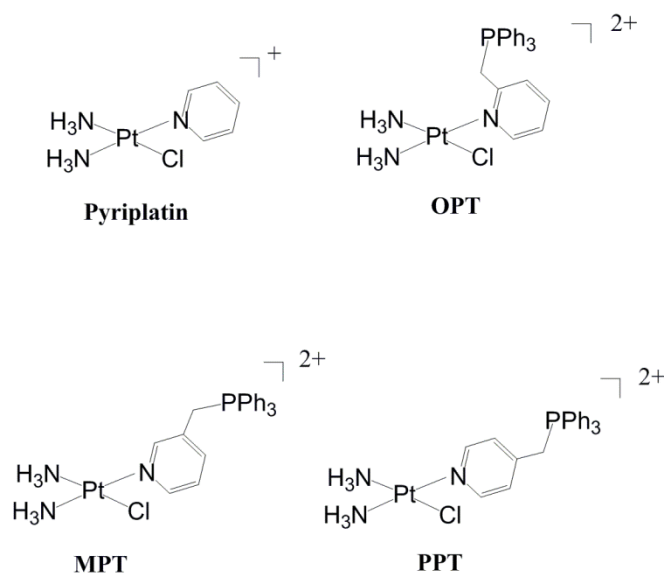


Figure 4.1 Structures of the Pt(II) complexes under investigation

OPT complex showed to be more efficacious than cisplatin, but less toxic toward normal cells. Further, the experimental study of the cellular distribution of those platinum complexes in different cell compartments as well as the degree of binding of nuclear DNA showed that the OPT complex is the most concentrated complex in mitochondria among the studied complexes and in comparison with cisplatin, which is mainly concentrated in nucleus. In addition, there is a strong evidence for the possibility of non-DNA targets for the OPT complex

4.1.2 Aim of study

The purpose of the computational analysis in this paper is to verify whether the experimentally observed differences in cytotoxic activity, DNA binding ability and potential interactions with non-DNA targets can be rationalized by examining the reactions that are considered to be key steps for cisplatin

and its derivatives mechanism of action. Aquation reaction, DNA attack, modeled by the interaction with the guanine nucleobase, as well as reaction with N-acetyl methionine and imidazole as a model for proteins such as histidine- and methionine-rich compounds, have been computationally investigated for the three complexes and compared with analogous interactions of pyriplatin and cisplatin.

4.1.3 Highlighting results

Aquation process appears to be thermodynamically favored especially for the OPT complex, whereas the PPT one is calculated to be the best suited to bind guanine when the aquated complexes are taken into consideration. The calculated trend for tendency to be aquated, prior to DNA binding, of the three OPT, MPT and PPT complexes together with Pyr and cisplatin reproduces the experimentally detected DNA binding ability and should explain the observed behaviour (**Figure 4.2**).

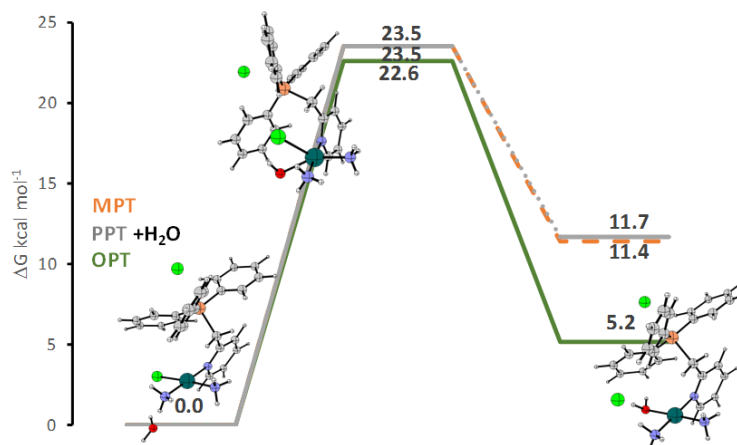


Figure 4.2 Free energy profiles describing the aquation reaction in water solvent of OPT (green solid line), MPT (orange dashed line) and PPT (grey dotted line) complexes. Relative energies are in kcal mol⁻¹ and calculated with respect to the reference energy of the initial adduct.

Reactions with N-acetyl methionine and imidazole show that reaction of OPT, MPT and PPT are less favourable than those of Pyr and cisplatin, with

the PPT complex the least prone to react with the examined off-target model system.

Although the outcomes of the present investigation confirm that the presence of the cationic $-\text{CH}_2\text{Ph}_3\text{P}^+$ group, introduced to allow the complexes to penetrate and accumulate in mitochondria, affects the reactivity as a function of its position on the pyridine ligand, however there is not a full agreement with the experimental results.

Thus it can be anticipated that some other factors, that are not taken into consideration in our simplified model, might affect the DNA binding capability of the drugs such as the steric hindrance of the bulky $-\text{CH}_2\text{Ph}_3\text{P}^+$ group while approaching the double stranded DNA to affect the covalent binding or some other modes of interaction that can be involved in drug binding to DNA that are influenced by the position of the cationic group. This information could further be helpful for designing and synthesizing new Pt(II) complexes as potent anticancer drugs or to undergo a more intensive mechanistic investigation for such complexes taking into consideration the possibility of non-conventional mechanisms of action.

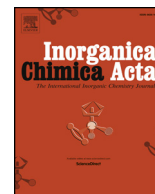
References

- 1) L. Gatti, G. Cassinelli, N. Zaffaroni, C. Lanzi, P. Perego, *Drug Resist. Updates*, **2015**, *20*, 1-11.
- 2) S. P. Wisnovsky, J. J. Wilson, R. J. Radford, M. P. Pereira, M. R. Chan, R. R. Laposa, S. J. Lippard, S. O. Kelley, *Chem. Biol.*, **2013**, *20*, 1323-1328.
- 3) K. Suntharalingam, J. J. Wilson, W. Lin, S. J. Lippard, *Metall.*, **2014**, *6*, 437-443.
- 4) S. Fulda, L. Galluzzi, G. Kroemer, *Nat. Rev. Drug Discov.*, **2010**, *9*, 447-464.
- 5) D. Stock, A. G. Leslie, J. E. Walker, *Science*, **1999**, *286*, 1700-1705.
- 6) S. E. Weinberg, N. S. Chandel, *Nat. Chem. Biol.*, **2015**, *11*, 9-15.
- 7) Y. H. Yang, S. Karakhanova, W. Hartwig, J. G. D'Haese, P. P. Philippov, J. Werner, A. V. Bazhin, *J. Cell. Physiol.*, **2016**, *231*, 2570-2581.
- 8) Z. Zhu, Z. Wang, C. Zhang, Y. Wang, H. Zhang, Z. Gan, Z. Guo, X. Wang, *Chem. Sci.*, **2019**, *10*, 3089-3095.

Paper II

A comparative computational mechanistic study on derivatives of pyriplatin, modified with the $-\text{CH}_2\text{Ph}_3\text{P}^+$ group, as anticancer complexes targeting mitochondria

E. Dabbish, A. G. Ritacca, G. Mazzone, E. Sicilia, *Inorganica Chimica Acta*, **2020**, 119863.



Research paper

A comparative computational mechanistic study on derivatives of pyriplatin, modified with the $-\text{CH}_2\text{Ph}_3\text{P}^+$ group, as anticancer complexes targeting mitochondria



Eslam Dabbish, Alessandra G. Ritacca, Gloria Mazzone, Emilia Sicilia*

Dipartimento di Chimica e Tecnologie Chimiche, Università della Calabria, 87036 Rende, (CS), Italy

ARTICLE INFO

Keywords:

DFT
 Pyriplatin derivatives
 Mitochondria DNA targeting
 Biological reactivity
 Reactivity tuning

ABSTRACT

Chemoresistance of Pt(II) based therapy is related to the extensive repair of modified DNA in the nucleus as a consequence of the nucleotide excision repair mechanism. Delivering Pt(II) complexes to the mitochondria to attack mitochondrial genome lacking repair machinery can lead to a rationally designed therapy for chemoresistant cancers and might overcome the problems associated with conventional cisplatin and its derivatives treatment. Here the outcomes of a computational investigation on the behavior of three monofunctional Pt(II) complexes synthesized starting from the monofunctional drug pyriplatin is reported. Owing to the introduction of the $-\text{CH}_2\text{Ph}_3\text{P}^+$ group in ortho, meta and para positions of the pyridine ligand of pyriplatin, the newly prepared complexes exhibited significant *in vitro* and *in vivo* antitumor efficacy and demonstrated to be able to penetrate mitochondria and accumulate in the mitochondrial matrix. Aquation reaction, DNA attack, modeled by the interaction with the guanine nucleobase, as well as reaction with *N*-acetyl methionine and imidazole as a model for proteins such as histidine- and methionine-rich compounds, have been computationally investigated for the three complexes and compared with analogous interactions of intact pyriplatin and cisplatin.

1. Introduction

Classical platinum anticancer drugs, cisplatin and its analogues, exert their anticancer activity interacting with nuclear DNA as main target forming intra- and inter-strand DNA crosslinks and inducing cell apoptosis and/or necrosis [1]. However, such drugs suffer from serious side effects and limited clinical efficacy in many types of cancer owing to developed and acquired drug resistance, which results primarily from the decrease of cellular drug accumulation and increase of cellular self-repairment [2,3]. In previous studies, it has been suggested that sub-cellular compartments other than nuclear DNA can be the targets of platinum complexes [4]. Those targets can be enzymes, proteins or non-nuclear cell organelles. Amongst the possible alternatives, mitochondria have been proved to be potential targets for platinum chemotherapeutics toxic to cancer cells [5,6]. As a consequence, targeting them can become a novel strategy for fighting cancer [7]. Mitochondria are the crucial players of the cell in which oxygen is consumed in the oxidative phosphorylation process to supply energy to the cell in the form of the bioenergetic intermediate ATP producing reactive oxygen species (ROS) as byproducts [8]. Mitochondrial dysfunction in cancer cells manifests with various alterations in energy-production pathways,

which makes mitochondrial metabolism a potential target for cancer therapy to inhibit tumor cells growth and ultimately leading to their apoptosis [9,10]. Complexes having mitochondria-targeting properties might result in an advance in the design of platinum-based anticancer drugs. Recently, the action of a new set of platinum based anticancer drugs, designed to target mitochondria, has been synthesized and studied [11]. In their study, the authors have combined the cytotoxic action of a new class of platinum based anticancer drugs, that is monofunctional platinum complexes, with the introduction of a cationic functional group, $-\text{CH}_2\text{Ph}_3\text{P}^+$, that allows the drug to be directed to and accumulate into mitochondria. Monofunctional platinum anticancer drugs such as pyriplatin have significant antineoplastic action and a cellular response profile different with respect to those of the classic bifunctional, charge-neutral platinum-based drugs [12]. It has been, indeed, reported that pyriplatin (Pyr) forms monofunctional DNA adducts binding to DNA at the N7 position of guanine residues and, even if no significant distortion is induced, transcription is inhibited likely due to cellular repair reduction as consequence of steric hindrance and hydrogen bonds formation [13,14]. On the other hand, it has been demonstrated that lipophilic compounds with delocalized positive charge can easily penetrate the inner mitochondrial membrane due to

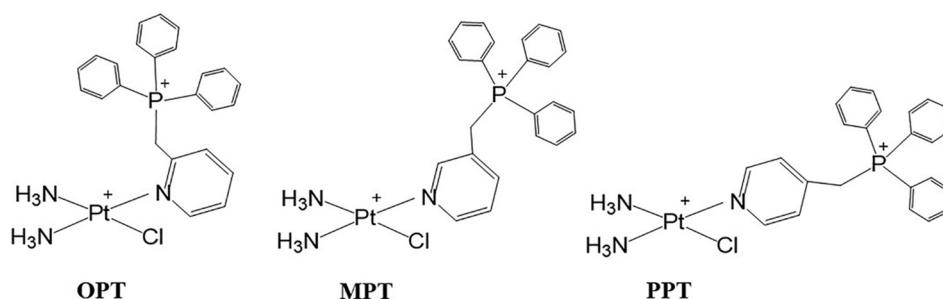
* Corresponding author.

E-mail address: emilia.sicilia@unical.it (E. Sicilia).<https://doi.org/10.1016/j.ica.2020.119863>

Received 13 April 2020; Received in revised form 22 June 2020; Accepted 26 June 2020

Available online 02 July 2020

0020-1693/© 2020 Elsevier B.V. All rights reserved.



Scheme 1. Structures of the Pt(II) complexes under investigation.

their high impermeability and accumulate thanks to the negatively charged microenvironment within the mitochondrial matrix.

Three monofunctional Pt(II) complexes have been synthesized by Wang et al. [11], see Scheme 1, starting from the monofunctional drug pyriplatin as the backbone and introducing the $-\text{CH}_2\text{Ph}_3\text{P}^+$ group in ortho, meta and para positions of the pyriplatin pyridine ring. The corresponding complexes have been named here **OPT**, **MPT** and **PPT**, respectively. The newly prepared complexes exhibited significant *in vitro* and *in vivo* antitumor efficacy and demonstrated to be able to penetrate mitochondria and accumulate in the mitochondrial matrix.

Among them the **OPT** complex showed to be more efficacious than cisplatin, but less toxic toward normal cells. Further, the experimental study of the cellular distribution of those platinum complexes in different cell compartments as well as the degree of binding of nuclear DNA showed that the **OPT** complex is the most concentrated complex in mitochondria among the studied complexes and in comparison with cisplatin, which is mainly concentrated in nucleus. In addition, there is a strong evidence for the possibility of non-DNA targets for the **OPT** complex. Although the three studied complexes are all cationic in nature and equally lipophilic they behave differently especially in terms of mitochondrial versus nuclei localization as well as DNA binding capability, which follows the order **MPT** < **PPT** < **OPT**. Intrigued by such results we have decided to computationally study, by means of quantum mechanical DFT calculations, the activation mechanistic steps of platinum anticancer drugs for such three complexes in comparison with cisplatin and pyriplatin previously investigated by some of us [15].

The purpose of the computational analysis reported here is to verify whether the experimentally observed differences in cytotoxic activity, DNA binding ability and potential interactions with non-DNA targets can be rationalized examining the reactions that are considered to be key steps for cisplatin and its derivatives mechanism of action. To this aim aquation reaction and DNA attack, modeled by the interaction with the purine guanine nucleobase, as well as reaction with sulfur and imidazole containing residues, taking *N*-acetyl methionine and imidazole as a model, respectively, have been explored.

2. Computational methodology

All DFT calculations have been performed using Gaussian 09 package [16]. The hybrid Becke three parameter exchange functional [17] and the Lee-Yang-Parr correlation functional B3LYP [18], have been employed. To properly take into account nonbonding interactions, Grimme dispersion correction have been included using atom pair-wise additive scheme [19], DFT-D3 method. Stuttgart/Dresden effective core potential [20] and corresponding split valence basis set have been used to describe platinum atom. 6–311 + G** basis set has been employed to describe the atoms directly involved in the studied reactions, while the rest of the atoms have been described by the 6-311G** basis set. In order to properly balance the charge of the cationic $-\text{CH}_2\text{Ph}_3\text{P}^+$ group introduced in ortho, meta and para positions of pyridine, an additional chloride has been included as counterion. Preliminary calculations have been carried out to check the influence of the presence of both a second

chloride and one and two nitrates that are the counterions used in the reference paper [11]. The identity of the counterion does not influence the energetics, while the presence of the second ion slows down the convergence, but does not change the reported behaviors. For all the located stationary points, frequency calculations have been performed at the same level of theory to both calculate zero-point energy corrections and confirm the nature of minima and transition states. All the located transition states have been checked by means of intrinsic reaction coordinate (IRC) analysis to be properly connected to the corresponding minima [21,22]. Solvent effect has been included by using Tomasi's implicit Polarizable Continuum Model (PCM) as implemented in Gaussian 09 [23–25]. To build up the cavity in which the solute molecules are accommodated, the UFF set of radii has been used. On all stationary point structures obtained from vacuum calculations, single point calculations at the same level have been performed to calculate solvation Gibbs free energy in implicit water ($\epsilon = 78.4$). Enthalpies and Gibbs free energies have been obtained at 298 K at 1 atm from total energies, including zero-point, thermal and solvent corrections, using standard statistical procedures [26]. Several water molecules have been added to reactants, transition state and products located along the aquation pathway and treated explicitly to check whether hydrogen bond interactions can influence the energetics.

3. Results and discussion

3.1. Aquation reaction

Similar to cisplatin and its derivatives, monofunctional platinum drugs undergo hydrolysis inside the cell where chlorido concentration is much lower than outside. Aquation followed by DNA binding are known to be the two activation steps of platinum-based drugs. However, such drugs, unlike cisplatin, form a single bond with DNA as they contain only one labile ligand.

The free energy profiles for the hydrolysis reaction of the three complexes under examination are reported in Fig. 1 together with the located stationary points for the **OPT** complex. Geometrical structures of all the remaining stationary points can be found in Fig. S1 of the Supplementary Material (SM). The hydrolysis reaction starts from water complex adducts stabilised by hydrogen bonds established between the water molecule and the ammonia ligands. The water molecule attacks the platinum centre replacing the chlorido ligand in a $\text{S}_{\text{N}}2$ fashion leading to the formation of pseudo trigonal bipyramid platinum transition state geometries. Calculated free energy barriers are 22.6 kcal mol⁻¹ for the **OPT** complex and 23.5 kcal mol⁻¹ for the two **MPT** and **PPT** complexes.

The aquation process results to be endergonic: 11.7 and 11.4 kcal mol⁻¹ are the very similar values for the **MPT** and **PPT** complexes, respectively; 5.2 kcal mol⁻¹ is the value calculated for the **OPT** complex. The effect of the inclusion of additional explicit water molecules on the energetics of the aquation process was also taken into consideration. Up to three solvating water molecules, excluding the nucleophilic one, were included. Results clearly show that the values of

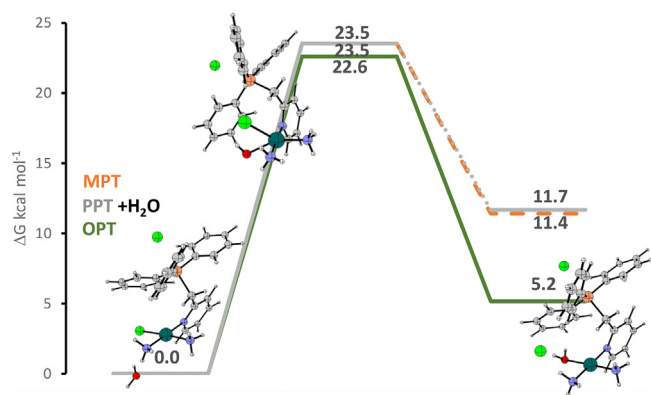


Fig. 1. Free energy profiles describing the aquation reaction in water solvent of **OPT** (green solid line), **MPT** (orange dashed line) and **PPT** (grey dotted line) complexes. Relative energies are in kcal mol⁻¹ and calculated with respect to the reference energy of the initial adduct. (For interpretation of the references to colour in this figure legend, the reader is referred to the web version of this article.)

the computed activation and reaction energies do not significantly change in presence of additional explicit water molecules. The only exception is the reaction energy of the **OPT** complex hydrolysis that results to be even less endergonic, by only 1.9 and 1.2 kcal mol⁻¹ if one and two additional water molecules, respectively are included. The energy profiles computed for the chloride displacement by water in presence of both one and two additional solvent molecules are reported in Figs. S2 and S3 of the SM together with the structures of the located stationary points. The first cisplatin chloro/aqua ligand exchange is reported to be endergonic (3.6 kcal mol⁻¹ and 4.2 kcal mol⁻¹) and the experimentally estimated values of the energy barrier range from 19 to 24.1 kcal mol⁻¹ [27–33] for an average value of 21.6 kcal mol⁻¹. Regarding **Pyr**, previous calculations showed that the chlorido ligand displacement by water proceeds by overcoming an energy barrier of 23.5 kcal mol⁻¹ and the reaction products lie 11.9 kcal mol⁻¹ above the zero reference energy of the initial adduct [15]. Additional calculations carried out also for **Pyr** complex, for the sake of comparison, including explicit water solvent molecules show that the positions of the located stationary points along the free energy profiles are not notably influenced. Results are summarized in Fig. S4 of SM. Therefore, the barriers computed for the three complexes under examination and, as a consequence, the aquation rates are comparable to those of the reference drug cisplatin. Aquation reaction, instead, appears to be more

endergonic than the values suggested for cisplatin except for the **OPT** complex. The calculated values of the activation and reaction energy for **OPT**, **MPT** and **PPT** are very close to those suggested for the **Pyr** complex and once again the only difference that is worth mentioning is the increased stability of the formed products when the **OPT** complex hydrolysis is analysed. This phenomenon can be explained by the charge redistribution due to the presence of the positively charged -CH₂Ph₃P⁺ group on pyridine. When this group is in ortho position more favorable electrostatic and hydrogen bonding interactions cause a larger stabilization of the reaction products with respect to the other two isomers. Therefore, calculations suggest that is the thermodynamics that drives the aquation reaction. This trend calculated for the aquation reaction, precluding DNA binding, of the three **OPT**, **MPT** and **PPT** complexes together with **Pyr** and cisplatin is in good agreement with the experimentally reported [11] DNA binding ability trend.

3.2. Guanine binding

The aquation step of platinum anticancer drugs preludes to the interaction with DNA especially through guanine nucleobases in a monodentate fashion at the N7 position. The free energy profiles that describe the interaction of the aquated form of the studied complexes, named **aquaOPT**, **aquaMPT** and **aquaPPT** with guanine as a model are depicted in Fig. 2 panel a. A sketch of the geometrical structure of the located stationary points along the aquated **OPT** energy profile is reported in the same figure. Stationary point geometries for the **MPT** and **PPT** complexes can be found in the SM in Fig. S5. The initial adducts formed by the complexes and the interacting guanine are stabilized by hydrogen bonds formed between the guanine N7 and the water molecule to be displaced as well as the guanine oxygen with the ammonia ligands. Such interactions create a proper arrangement that favors the guanine attack on platinum causing water displacement in a nucleophilic substitution reaction. The transition states for the associative displacement of water and coordination of guanine through the N7 binding site lie 20.0, 18.2 and 12.2 kcal mol⁻¹ above the reference energy of the corresponding adducts for the aquated **OPT**, **MPT** and **PPT** complexes, respectively. The associative displacement of the water molecule and coordination of the guanine base is calculated to be exergonic for all the examined complexes. The reaction is exergonic by 8.9 kcal mol⁻¹ relative to the entrance channel for the **OPT** complex. The stability of the formed products increases for **MPT** and **PPT** complexes being 11.1 and 16.9 kcal mol⁻¹, respectively.

Analogous calculations carried out to describe the water/guanine exchange in **Pyr** [15] give 16.4 kcal mol⁻¹ for the barrier and

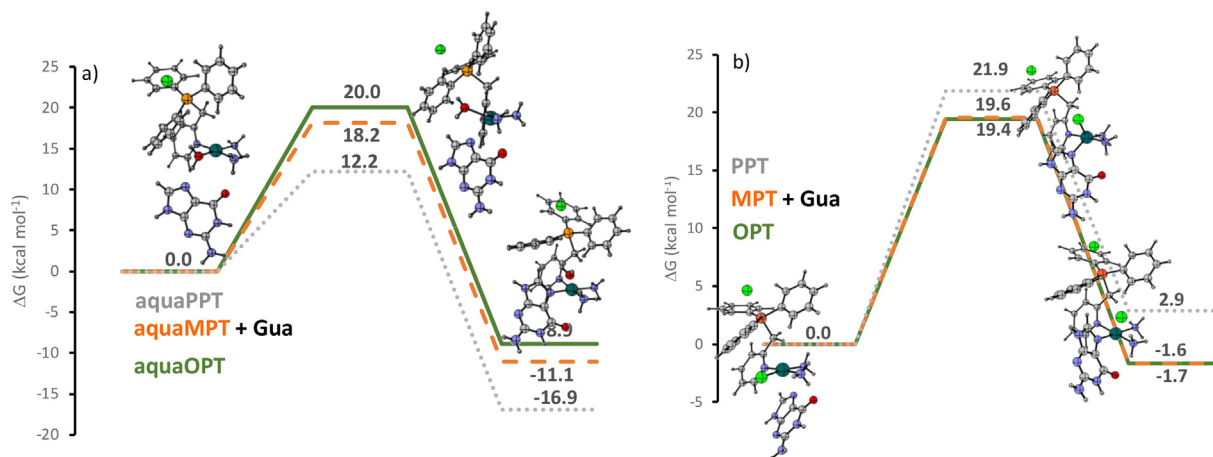


Fig. 2. Free energy profiles describing interaction with Gua, in water solvent, of a) aquated and b) intact **OPT** (green solid line), **MPT** (orange dashed line) and **PPT** (grey dotted line) complexes. Relative energies are in kcal mol⁻¹ and calculated with respect to the reference energy of the initial adduct. (For interpretation of the references to colour in this figure legend, the reader is referred to the web version of this article.)

– 11.6 kcal mol⁻¹ for the reaction energy. For the same substitution to occur in cisplatin we have calculated, as shown in Fig. S5 of the SM, a barrier of 17.6 kcal mol⁻¹ and a product stabilization of 9.4 kcal mol⁻¹ with respect to the initial cisplatin guanine adduct. From a comparison with such data it appears that whereas for aquated OPT and MPT complexes the barriers are even higher and the reaction energies are comparable, the PPT complex behaves differently. The substitution reaction involves a low energy barrier and is about 7 kcal mol⁻¹ more exergonic. It seems, therefore, that the PPT complex is the best suited for the guanine attack. As underlined above, the initial adducts are stabilized by hydrogen bonds established between one of the NH₃ moieties and the carbonyl group as well as the water and the carbonyl group of the incoming guanine. It is this latter interaction that, due the charge redistribution caused by the presence in para position of the -CH₂Ph₃P⁺ group on the pyridine, causes a partial detachment of the water molecule precluding to its substitution by guanine and lowering the energy barrier for the PPT complex. Also stabilizing hydrogen bonding interactions lower the energy of the products more than for MPT and OPT complexes.

The interaction of the non aquated OPT, MPT and OPT complexes with guanine has been also explored. The corresponding free energy profiles are shown in panel b of the same Fig. 2 together with the optimized structures of intercepted stationary points for the OPT isomer. Analogous stationary point structures for MPT and PPT complexes are collected in Fig. S6 of the SM. The presence of the charged -CH₂Ph₃P⁺ group should, indeed, influence the charge distribution and make viable a direct attack of guanine on the chlorido ligand. Displacement of the chloride by guanine requires to occur that a barrier of 19.4, 19.6 and 21.9 kcal mol⁻¹ is overcome for the OPT, MPT and PPT isomers, respectively. The reaction is slightly endergonic, by 1.7 and 1.6 kcal mol⁻¹ for the two OPT and MPT complexes, whereas for the PPT isomer the reaction is endergonic by 2.9 kcal mol⁻¹. Such results show that the attack on guanine of the intact complexes is competitive with the aquation reaction as the barriers are, even if by a small quantity, lower and the reaction energies are more favorable.

3.3. Reaction with *N*-Acetyl methionine and imidazole

In spite of the proved preference for guanine adducts formation, Pt (II) drugs interactions are too unspecific to afford selective therapies. Inside the body, the drug also interacts with many biomolecules and participates to a cascade of molecular events that ultimately lead to severe side effects and the emergence of resistance. According with the growing attention devoted to the off-target interactions of Pt(II) drugs with proteins such as histidine- and methionine-rich compounds, here substitution reactions by *N*-acetyl methionine and imidazole as a model for histidine were computationally investigated.

The abundant sulfur containing biological molecules, which are known to possess a high affinity for soft platinum, can cause the deactivation of Pt containing complexes forming stable adducts and, thus, preventing the drug from reaching the DNA target. *N*-acetyl methionine (NAM) was used here as a simplified model to study the tendency of the examined complexes to interact with sulfur containing species. The free energy profiles for the interaction of NAM with the three complexes under examination are reported in Fig. 3. Stationary point geometrical structures are reported for the OPT complex, whereas for MPT and PPT geometries can be found in the SM (Fig. S7).

The chlorido ligand displacement by NAM occurs, once again, following a second-order nucleophilic substitution (SN₂) mechanism. The transition states for the associative displacement of the chlorido ligand lie 13.2, 15.3 and 17.4 kcal mol⁻¹ above the first adduct reference energy for OPT, MPT and PPT, respectively. The NAM substitution reaction is endergonic for all the examined complexes. For the OPT complex, formed products are less stable than the initial adduct by 3.3 kcal mol⁻¹, while for MPT and PPT products result to be less stable by 6.3 and 7.3 kcal mol⁻¹, respectively.

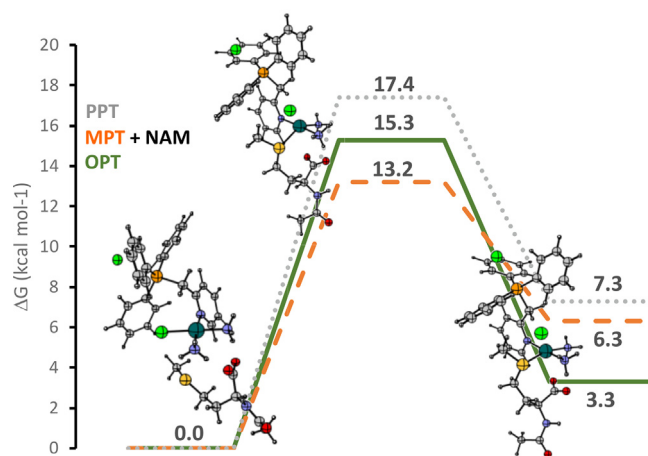


Fig. 3. Free energy profiles describing the interaction with NAM, in water solvent, of OPT (green solid line), MPT (orange dashed line) and PPT (grey dotted line) complexes. Relative energies are in kcal mol⁻¹ and relative to the reference energy of the initial adduct. (For interpretation of the references to colour in this figure legend, the reader is referred to the web version of this article.)

Such outcomes can be compared with those previously reported for Pyr and cisplatin [15]. The height of the energy barrier for the attack of NAM to Pt for displacing the chlorido ligand in Pyr is 12.5 kcal mol⁻¹ and the products lie 9.7 kcal mol⁻¹ above the initial adduct reference energy.

The analogous values for cisplatin are: 14.4 kcal mol⁻¹ for the barrier and –6.0 kcal mol⁻¹ for the reaction energy. Therefore, the kinetics of the reaction of OPT and MPT are slightly less favorable than those of Pyr and cisplatin, whereas from a thermodynamic point of view, in analogy with Pyr, the products of the interaction with NAM are less stable than the initial adduct, while for cisplatin the reaction is exergonic. The PPT complex due to the higher activation barrier, that controls the interaction of the drug, and the unfavorable thermodynamics results to be less prone to be deactivated by sulphur-containing biomolecules. Very favorable hydrogen bonding interactions are established between the hydrogen atom of the ammonia ligands with the carbonyl groups of NAM. Such interactions in the case of the PPT complex hamper to a greater extent the rearrangement, which through the transition state leads to the substitution products, and cause a minor stabilization of the products.

The reaction of mitochondria targeted monofunctional complexes with imidazole (Im) as a simple model for the interaction with histidine residues has been next examined. The results of this computational analysis are summarized in Fig. 4 and the geometric structures of the minima and transition state for the OPT isomer are reported in the same figure. The rest of the structures are gathered in Fig. S8 of the SM. The initial adducts are characterized by stabilizing hydrogen bond interactions between the Im N1 nitrogen atom and the hydrogen atoms of one of the ammonia ligands. Once again substitution of the chlorido ligand by imidazole occurs by an associative displacement mechanism and the transition states allowing the displacement to occur lie 18.2, 20.0 and 20.9 kcal mol⁻¹ above the zero reference energy of the initial adducts. Products formation is calculated to be exergonic, but large differences in stabilization are displayed in Fig. 4 between the values of –2.1 kcal mol⁻¹ for MPT, –0.2 kcal mol⁻¹ for PPT and –11.2 kcal mol⁻¹ for the OPT isomer.

Comparison with Pyr and cisplatin behaviours (results are reported in Fig. S9 of the SM) show that the MPT and PPT complexes are somewhat less inclined to react with the imidazole model compound, whereas for OPT both kinetics and thermodynamics are more favourable.

The obtained results demonstrate that the propensity of the

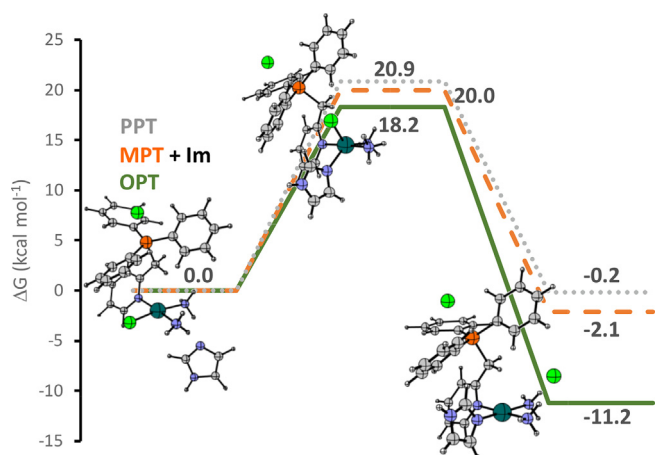


Fig. 4. Free energy profiles describing the interaction with Im, in water solvent, of **OPT** (green solid line), **MPT** (orange dashed line) and **PPT** (grey dotted line) complexes. Relative energies are in kcal mol⁻¹ and relative to the reference energy of the initial adduct. (For interpretation of the references to colour in this figure legend, the reader is referred to the web version of this article.)

examined complexes to react with off-target compounds is modulated by the cationic $-\text{CH}_2\text{Ph}_3\text{P}^+$ group as a function of its position on the pyridine ligand. The relatively low energy barriers of NAM and imidazole attack on **OPT** supports the hypothesis of non DNA targets of such new complexes.

4. Conclusions

The present paper reports the outcomes of a computational investigation of the reactivity behaviour of three newly synthesized Pt(II) complexes that have demonstrated to possess significant *in vitro* and *in vivo* antitumor efficacy and to be able to penetrate mitochondria and accumulate in the mitochondrial matrix. Indeed, delivering Pt(II) complexes to the mitochondria to attack mitochondrial genome lacking nucleotide excision repair machinery can represent an alternative strategy to overcome the problems associated with conventional cisplatin and its derivatives treatment. The complexes have been prepared starting from the monofunctional pyriplatin introducing in its backbone the $-\text{CH}_2\text{Ph}_3\text{P}^+$ group in ortho, **OPT**, meta, **MPT** and para, **PPT**, positions of the pyridine ring. Due to the presence of such positively charged group a charge redistribution is induced that influences in different ways the reactivity as a function of its position. Aquation reaction, DNA binding, modeled by the interaction with the guanine nucleobase, as well as reaction with *N*-acetyl methionine and imidazole, as a model for proteins such as histidine- and methionine-rich compounds, have been explored and compared with analogous interactions of intact pyriplatin and cisplatin. Aquation process appears to be more thermodynamically favored especially for the **OPT** complex, whereas the **PPT** one is calculated to be the best suited to bind guanine when the aquated complexes are taken into consideration. The calculated trend in propensity to be aquated, that preludes DNA binding, of the three **OPT**, **MPT** and **PPT** complexes together with **Pyr** and cisplatin reproduces the experimentally detected DNA binding ability and should explain the observed behavior. If the attack of intact complexes on guanine is examined, instead, the reaction appears to be viable, competitive with respect to aquation and there are not significant differences, that is worth mentioning, in behavior among the examined complexes.

Since there is not a full agreement with the experimental results, it can be inferred that some other factors, that are not taken into consideration in our simplified model, might affect the DNA binding capability of the drugs such as the steric hindrance of the bulky $-\text{CH}_2\text{Ph}_3\text{P}^+$ group approaching the double stranded DNA. Other modes of interaction can be involved in drug binding to DNA that are influenced by the

position of the cationic group.

Reactions with *N*-acetyl methionine and imidazole show that reaction of **OPT** and **MPT** are less favorable than those of **Pyr** and cisplatin, but is the **PPT** complex the least prone to react with the examined off-target compounds.

The outcomes of the present investigation confirm that the presence of the cationic $-\text{CH}_2\text{Ph}_3\text{P}^+$ group, introduced to allow the complexes to penetrate and accumulate in mitochondria, modulates the reactivity as a function of its position on the pyridine ligand. This information could further be helpful for designing and synthesizing new Pt(II) complexes as potent anticancer drugs. Nevertheless, for a complete rationalization of the detected behaviors, due to peculiar nature of such complexes, it should be required, very likely, the exploration of mechanistic aspects not commonly taken into consideration.

CRedit authorship contribution statement

Eslam Dabbish: Conceptualization, Methodology, Writing - original draft. **Alessandra G. Ritacca:** Data curation. **Gloria Mazzone:** Investigation, Validation. **Emilia Sicilia:** Investigation, Validation.

Declaration of Competing Interest

The authors declare that they have no known competing financial interests or personal relationships that could have appeared to influence the work reported in this paper.

Acknowledgment

This work is supported by Università della Calabria.

Appendix A. Supplementary data

Geometrical structures of the stationary points located for **MPT** and **PPT** complexes along the free energy profiles for: hydrolysis reaction, chloride displacement by water in presence of one and two additional solvent molecules, interaction with *N*-acetyl Methionine and imidazole, interaction in both their aquated and non-aquated form with guanine; free energy profiles for a) the aquation reaction in water of **Pyr** complex, even in presence of b) one, c) two and d) three additional solvent molecules; free energy profiles for **Pyr** and cisplatin complexes for their interaction with Im. Supplementary data associated with this article can be found, in the online version, at <http://dx.doi.org/>. Supplementary data to this article can be found online at <https://doi.org/10.1016/j.ica.2020.119863>.

References

- [1] E.R. Jamieson, S.J. Lippard, *Chem. Rev.* 99 (1999) 2467–2498.
- [2] K. Cheung-Ong, G. Gaefer, C. Nislow, *Chem Biol.* 20 (2013) 648–659.
- [3] A. Ruggiero, G. Trombatore, S. Triarico, R. Arena, P. Ferrara, M. Scalzone, F. Pierri, R. Riccardi, *Drugs* 24 (2013) 1007–1019.
- [4] L. Gatti, G. Cassinelli, N. Zaffaroni, C. Lanzi, P. Perego, *Drug Resist. Updates* 20 (2015) 1–11.
- [5] S.P. Wisnovsky, J.J. Wilson, R.J. Radford, M.P. Pereira, M.R. Chan, R.R. Laposa, S.J. Lippard, S.O. Kelley, *Chem. Biol.* 20 (2013) 1323–1328.
- [6] K. Suntharalingam, J.J. Wilson, W. Lin, S.J. Lippard, *Metall.* 6 (2014) 437e443.
- [7] S. Fulda, L. Galluzzi, G. Kroemer, *Nat. Rev. Drug Discov.* 9 (2010) 447–464.
- [8] D. Stock, A.G. Leslie, J.E. Walker, *Science* 286 (1999) 1700–1705.
- [9] S.E. Weinberg, N.S. Chandel, *Nat. Chem. Biol.* 11 (2015) 9–15.
- [10] Y.H. Yang, S. Karakhanova, W. Hartwig, J.G. D'Haese, P.P. Philippov, J. Werner, A.V. Bazhin, *J. Cell. Physiol.* 231 (2016) 2570–2581.
- [11] Z. Zhu, Z. Wang, C. Zhang, Y. Wang, H. Zhang, Z. Gan, Z. Guo, X. Wang, *Chem. Sci.* 10 (2019) 3089–3095.
- [12] T.C. Johnstone, G.Y. Park, S.J. Lippard, *Anticancer Res.* 34 (2014) 471–476.
- [13] K.S. Lovejoy, M. Serova, I. Bieche, S. Emami, M. D'Incalci, M. Broggin, E. Erba, C. Gespach, E. Cvitkovic, S. Faivre, E. Raymond, S.J. Lippard, *Mol. Cancer Ther.* 10 (2011) 1709–1719.
- [14] D. Wang, G. Zhu, X. Huang, S.J. Lippard, *Proc. Natl. Acad. Sci. USA* 107 (2010) 9584–9589.
- [15] E. Dabbish, N. Russo, *E. Sicilia Chem.-Eur. J.* 26 (2020) 259.

- [16] M.J. Frisch, G.W. Trucks, H.B. Schlegel, G.E. Scuseria, M.A. Robb, J.R. Cheeseman, G. Scalmani, V. Barone, G.A. Petersson, H. Nakatsuji, X. Li, M. Caricato, A. Marenich, J. Bloino, B.G. Janesko, R. Gomperts, B. Mennucci, H.P. Hratchian, J.V. Ortiz, A.F. Izmaylov, J.L. Sonnenberg, D. Williams-Young, F. Ding, F. Lipparini, F. Egidi, J. Goings, B. Peng, A. Petrone, T. Henderson, D. Ranasinghe, V.G. Zakrzewski, J. Gao, N. Rega, G. Zheng, W. Liang, M. Hada, M. Ehara, K. Toyota, R. Fukuda, J. Hasegawa, M. Ishida, T. Nakajima, Y. Honda, O. Kitao, H. Nakai, T. Vreven, K. Throssell, J.A. Montgomery Jr., J.E. Peralta, F. Ogliaro, M. Bearpark, J.J. Heyd, E. Brothers, K.N. Kudin, V.N. Staroverov, T. Keith, R. Kobayashi, J. Normand, K. Raghavachari, A. Rendell, J.C. Burant, S.S. Iyengar, J. Tomasi, M. Cossi, J.M. Millam, M. Klene, C. Adamo, R. Cammi, J.W. Ochterski, R. L. Martin, K. Morokuma, O. Farkas, J.B. Foresman, D.J. Fox, Gaussian 09, Revision D.01, Gaussian, Inc., Wallingford CT, 2016.
- [17] A.D. Becke, *J. Chem. Phys.* 98 (1993) 5648–5652.
- [18] C. Lee, W. Yang, R.G. Parr, *Phys. Rev. B* 37 (1988) 785–789.
- [19] S. Grimme, J. Antony, S. Ehrlich, H. Krieg, *J. Chem. Phys.* 132 (2010) 154104–154122.
- [20] D. Andrae, U. H-ussermann, M. Dolg, H. Stoll, H. Preuss, *Theor. Chim. Acta* 77 (1990) 123–141.
- [21] K. Fukui, *J. Phys. Chem.* 74 (1970) 4161–4163.
- [22] C. Gonzalez, H.B. Schlegel, *J. Chem. Phys.* 90 (1989) 2154–2161.
- [23] Miertuš, E. Scrocco, J. Tomasi, *Chem. Phys.* 55 (1981) 117–129.
- [24] S. Miertuš, J. Tomasi, *Chem. Phys.* 65 (1982) 239–245.
- [25] J.L. Pascual-Ahuir, E. Silla, I. Tuñón, *J. Comput. Chem.* 15 (1994) 1127–1138.
- [26] D.A. McQuarrie, J.D. Simon, *Molecular Thermodynamics*, University Science Books, Sausalito, CA, 1999.
- [27] J.R. Perumareddi, A.W. Adamson, *J. Phys. Chem.* 72 (1978) 414–420.
- [28] Coe, J. S. *MTP Int. Rev. Sci.: Inorg. Chem., Ser. 2* (1974) 45.
- [29] A.I. Stetsenko, L.B. Sci'derkhanova, *Zh. Neorg. Khim.* 25 (1981) 164.
- [30] R.N. Bose, R.D. Cornelius, R.E. Viola, *J. Am. Chem. Soc.* 106 (1984) 3336–3343.
- [31] K. Hindmarsh, D.A. House, M.M. Turnbull, *Inorg. Chim. Acta* 257 (1997) 11–18.
- [32] S.E. Miller, D.A. House, *Inorg. Chim. Acta* 166 (1989) 189–197.
- [33] S. Ahmad, *Polyhedron* 138 (2017) 109–124.

Supplementary Material

A comparative computational mechanistic study on derivatives of pyriplatin, modified with the $-\text{CH}_2\text{Ph}_3\text{P}^+$ group, as anticancer complexes targeting mitochondria

Eslam Dabbish, Alessandra Ritacca, Gloria Mazzone, Emilia Sicilia*

Dipartimento di Chimica e Tecnologie Chimiche, Università della Calabria, 87036 Rende (CS), Italy

Table of Content

- **Figure S1:** Geometrical structures of the stationary points located for **MPT** and **PPT** complexes along the free energy profiles for the hydrolysis reaction S2
- **Figure S2:** Free energy profiles for chloride displacement by water in presence of one additional solvent molecule and geometrical structures of the located stationary points for **OPT**, **MPT** and **PPT** complexes S3
- **Figure S3:** Free energy profiles for chloride displacement by water in presence of two additional solvent molecule and geometrical structures of the located stationary points for **OPT**, **MPT** and **PPT** complexes S4
- **Figure S4:** Free energy profiles for a) the aquation reaction in water of **Pyr** complex, even in presence of b) one, c) two and d) three additional solvent molecules S5
- **Figure S5:** Geometrical structures of the stationary points located for **MPT** and **PPT** complexes along the free energy profiles for the interaction of their aquated forms with guanine S6
- **Figure S6:** Geometrical structures of the stationary points located for **MPT** and **PPT** complexes along the free energy profiles for their interaction with N-acetyl Methionine S7
- **Figure S7:** Geometrical structures of the stationary points located for **MPT** and **PPT** complexes along the free energy profiles for their interaction with Imidazole S8
- **Figure S8:** Free energy profiles for **Pyr** and cisplatin complexes for their interaction with Im S9

Figure S1

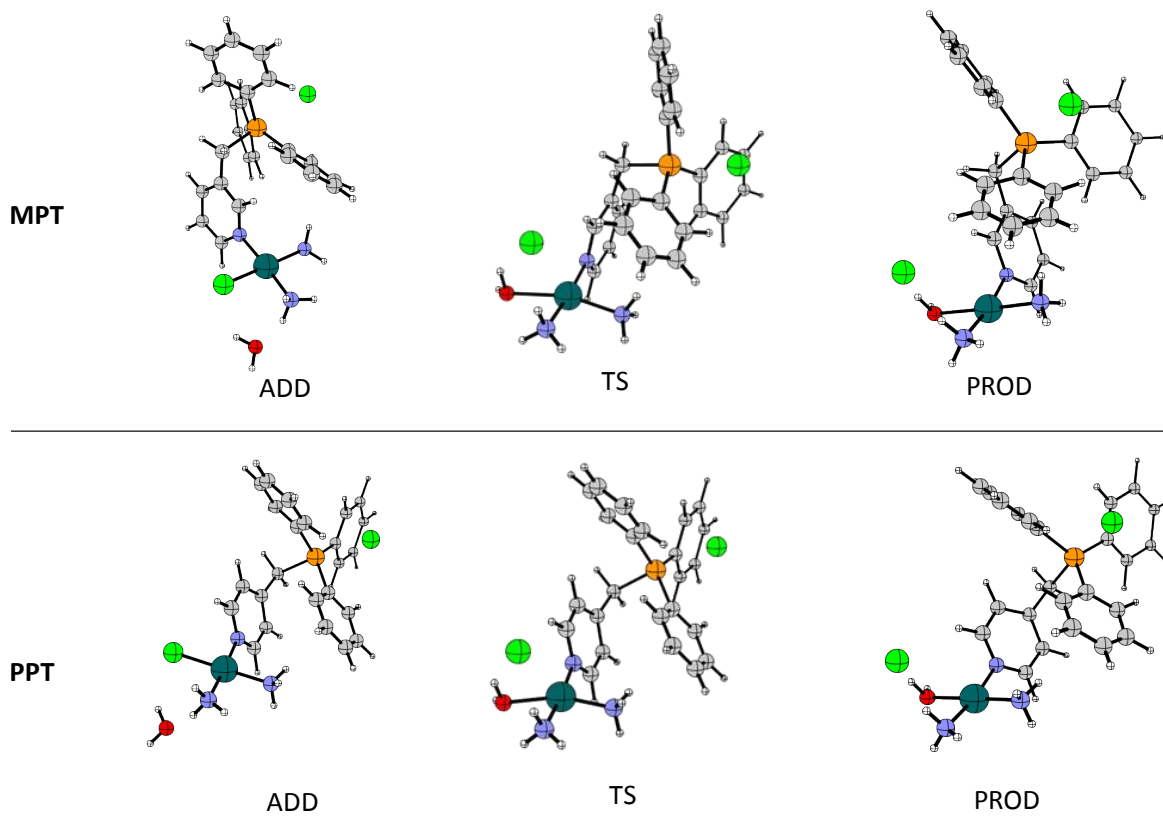


Figure S2

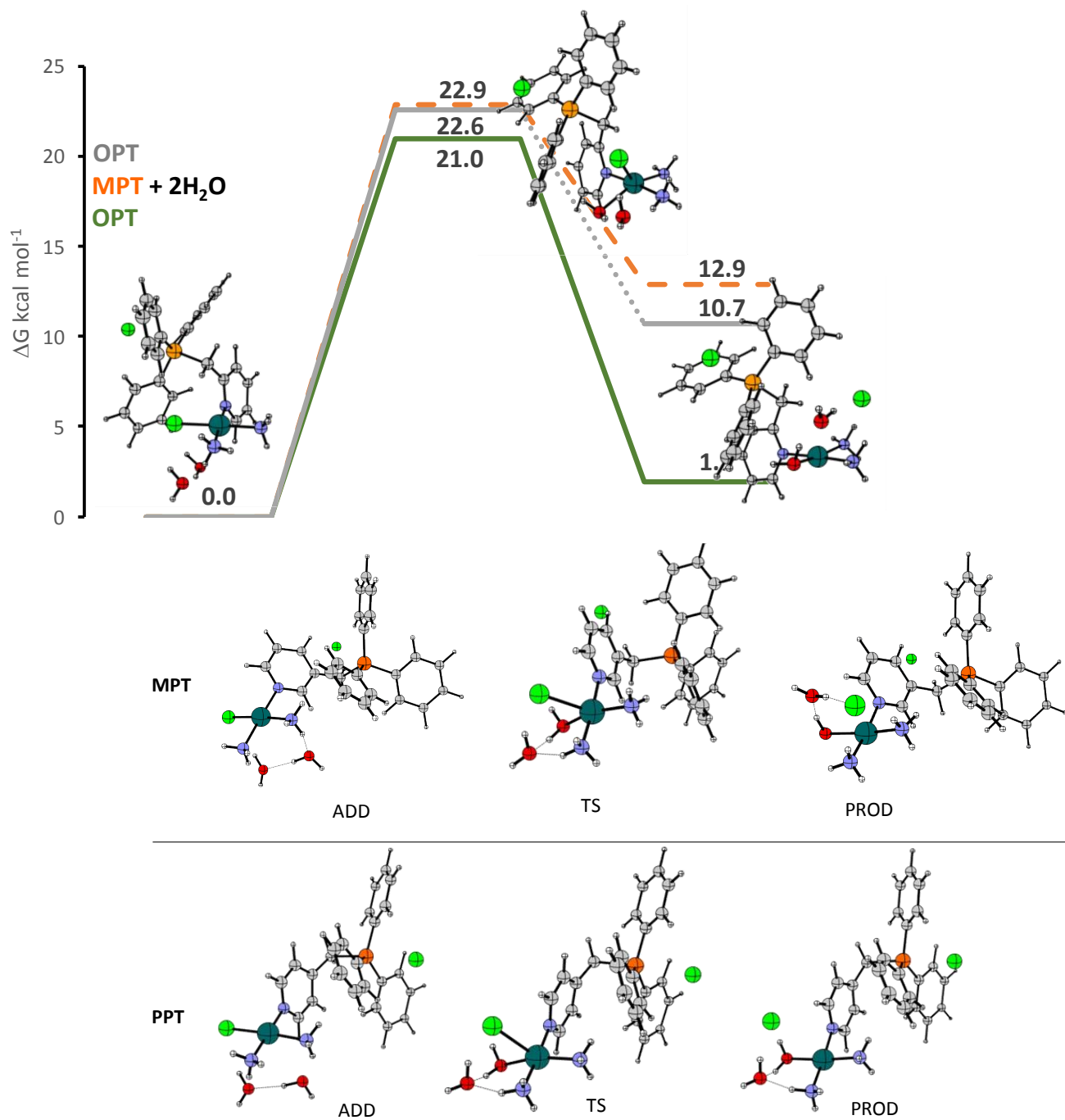


Figure
S3

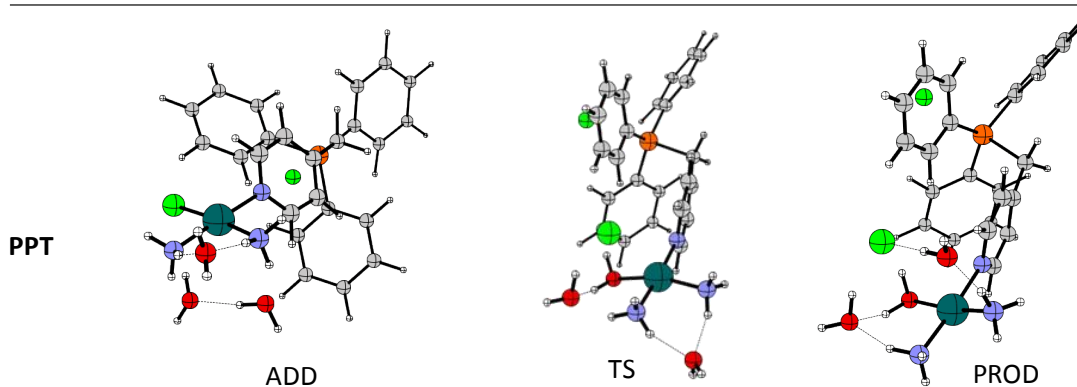
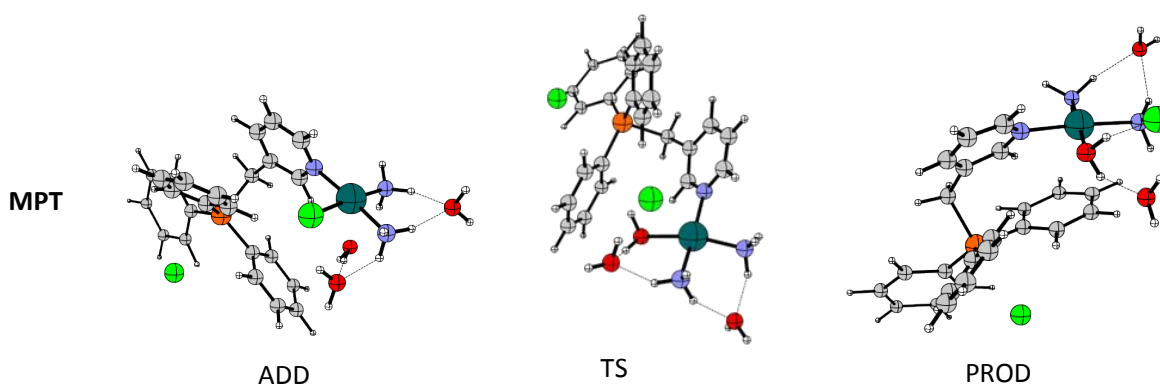
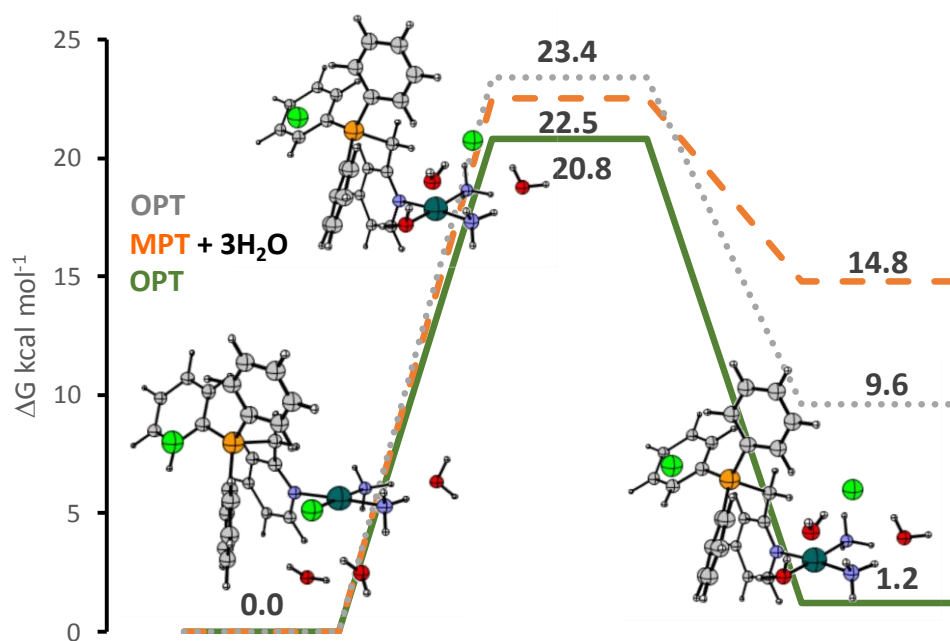


Figure S4

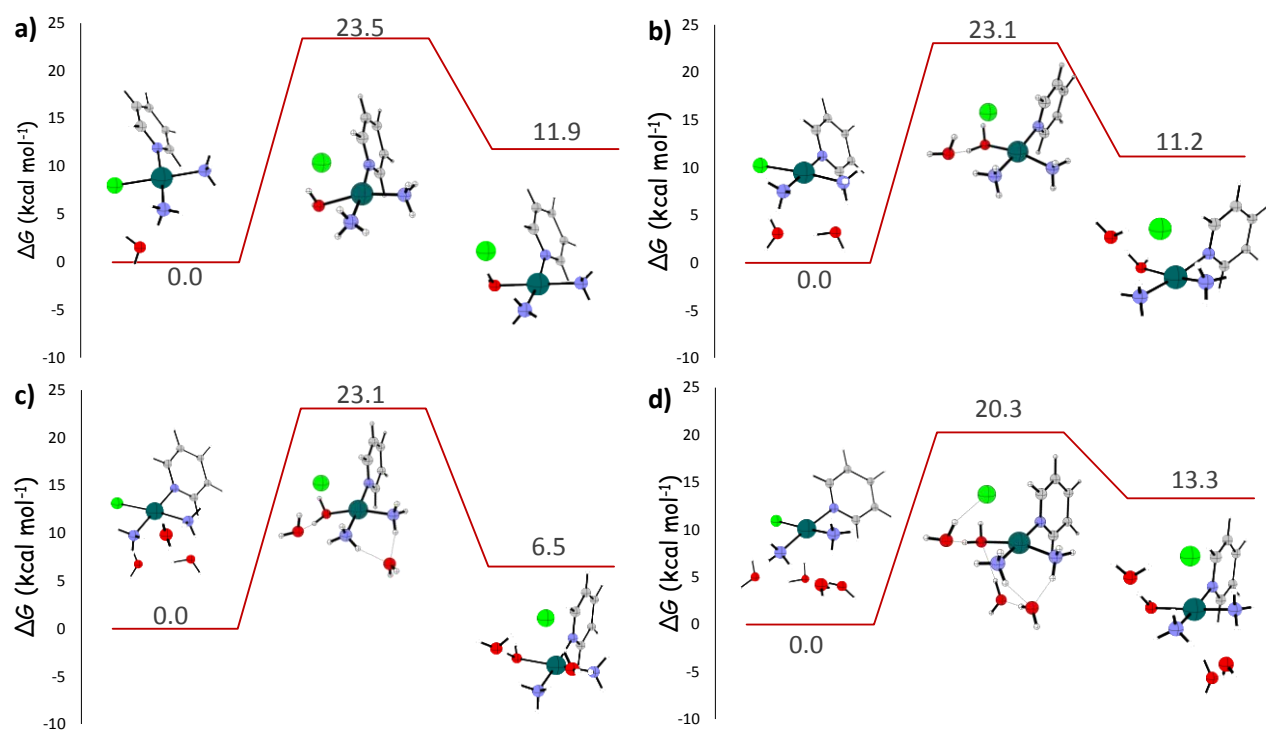


Figure S5

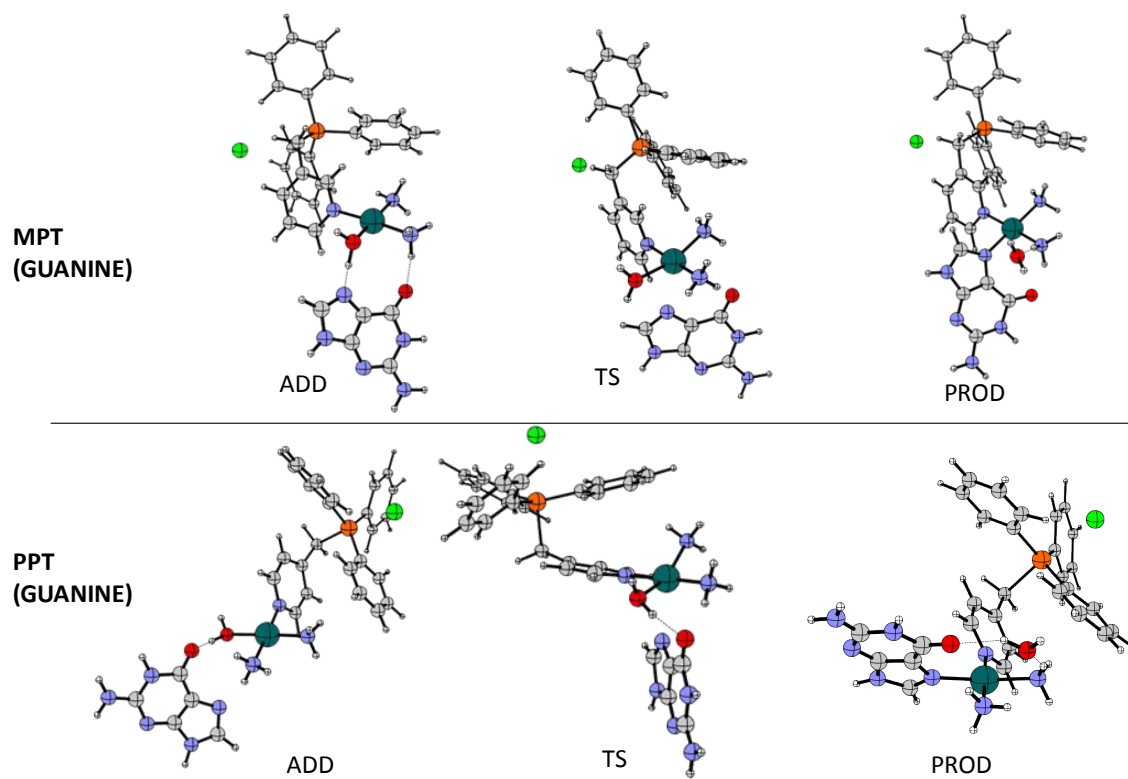


Figure S6

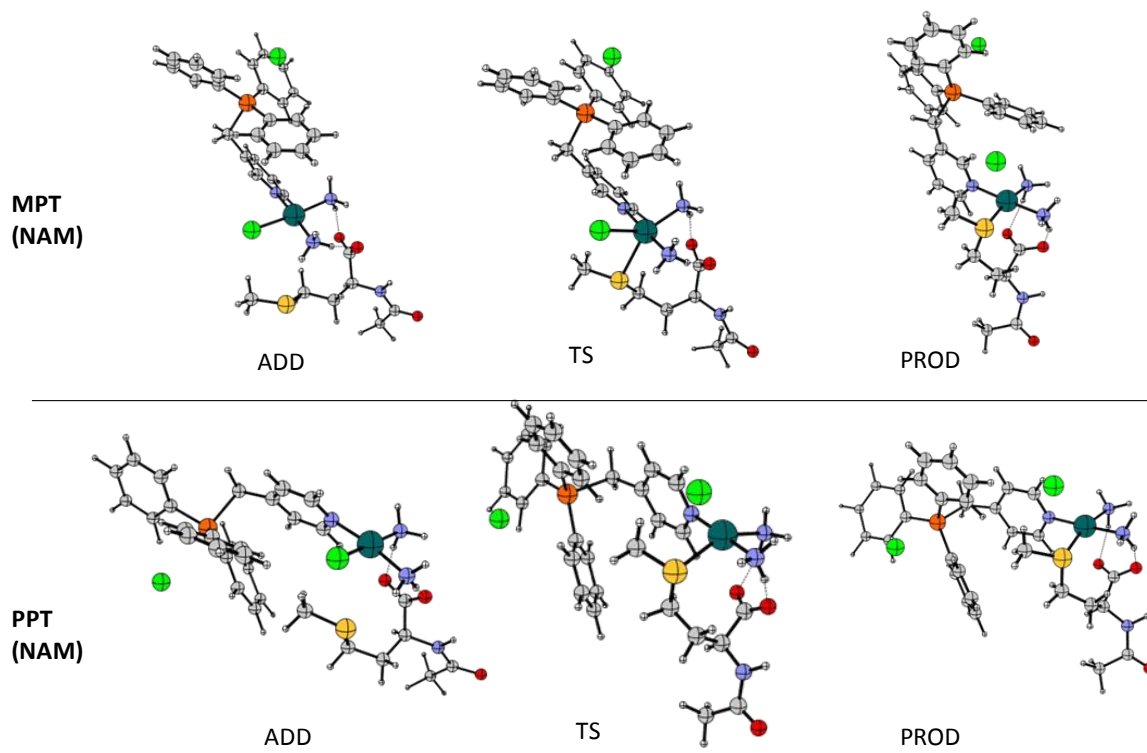


Figure S7

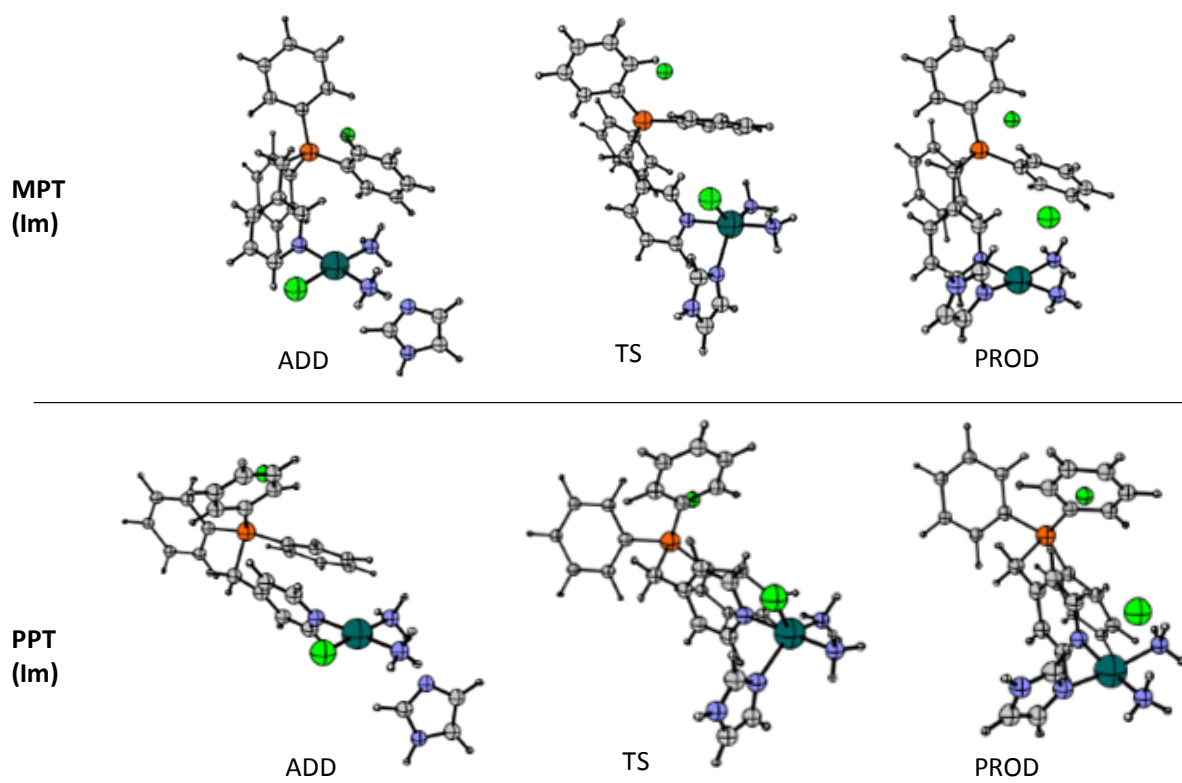
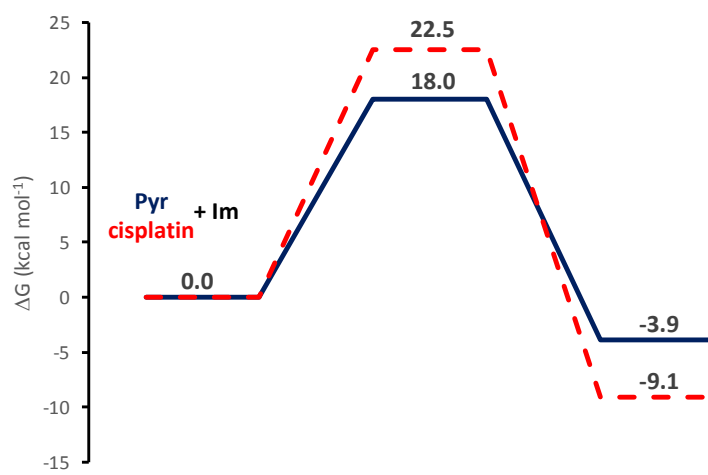


Figure S8



Chapter V

Platinum (IV)

Complexes as Prodrugs

Chapter V Platinum (IV) Complexes as Prodrugs

5.1 Antitumor Pt(IV) prodrugs: a systematic computational exploration of their reduction mechanism by L-ascorbic acid

5.1.1 Introduction

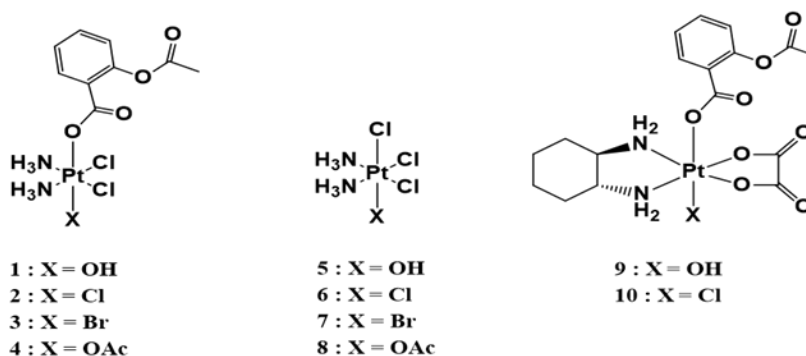
With the known shortcomings of the traditional FDA approved anticancer platinum drugs cisplatin, oxaliplatin and carboplatin such as toxic side effects, limited bioavailability and precluded oral administration, new strategies have emerged including the use of six-coordinate Pt(IV) complexes.¹⁻² Pt(IV)-based drugs are more inert and can act as prodrugs able to release the corresponding four-coordinate active Pt(II) species upon reduction. As prodrugs, Pt(IV) complexes are converted inside the body into the active Pt(II) forms by means of a two electron reduction process with the aid of the biologically abundant reducing agents such as ascorbic acid and glutathione.³⁻¹⁰

Some of the additional benefits deriving from the use of Pt(IV) complexes is that, as inertness to reactions with biological nucleophiles and lifetime in biological fluids are expected to increase, even oral administration becomes feasible.¹¹⁻¹³ Furthermore, unwanted reactions with biomolecules and their resulting side-effects can be minimized. The six coordinate nature, additionally, gives a high flexibility in designing ligands, especially the axial ones, to tune the pharmacological properties of the prodrug in the desired way.

5.1.2 Aim of study

Since the reduction step is the most critical step for the activity of such complexes, we have focused our attention in this paper on the study of the reduction mechanism by means of mono deprotonated ascorbic acid and the impact of having different axial and equatorial ligand on the tendency to undergo reduction and its mechanism.

A wide panel of Pt(IV) complexes with cisplatin and oxaliplatin backbone while varying the ligands in axial position has been investigated. OH, OAc, Cl and Br ligands have been tested as bridging/leaving ligands, whereas Cl and aspirin have been used as *trans* labile and less labile ligands, respectively as shown in **Scheme 5.1**.



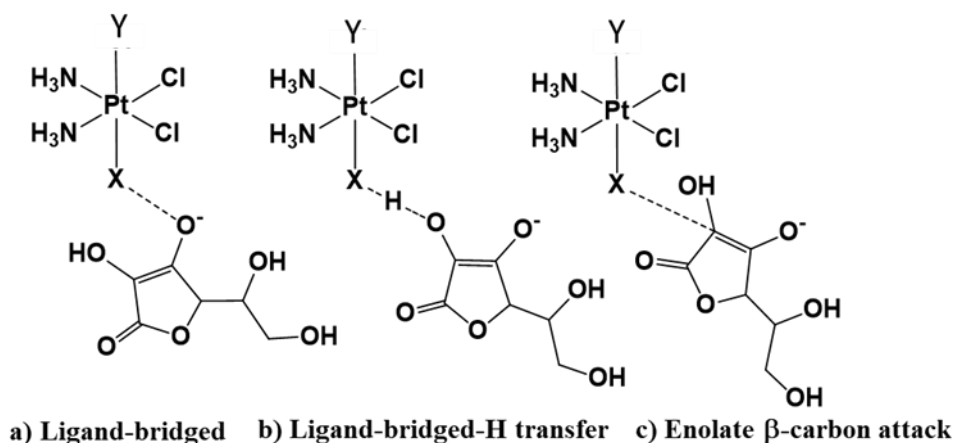
Scheme 5.1 Pt(IV) complexes investigated for reduction

5.1.3 Highlighting results

On the basis of both experimental and theoretical investigations, reduction mechanisms are classified into two main types, that is inner- and outer-sphere as a function of the electron transfer mode.

For each of the studied complexes, three different inner sphere mechanisms were investigated including a) ligand-bridged, b) ligand-bridged-H transfer and c) enolate β -carbon attack. For the outer sphere mechanism, redox potential was theoretically calculated for every complex. In addition, based on the possibility of having an outer sphere mechanism that involves the formation of Pt(III) intermediates and eventual crossings between singlet and triplet states, we have also investigated the possibility of a base assisted outer sphere mechanism in both singlet and triplet states.

Results reported here show that for the *inner sphere mechanism* (**Scheme 5.2**),



Scheme 5.2 Inner-sphere mechanistic alternatives

for both OH and OAc ligands, the inner sphere two-electron transfer, classified as ligand-bridged-H transfer, is the preferred mechanism. The rate of the process is not influenced by the identity of the ligands in both axial and equatorial positions. The enolate β -carbon attack can occur for the OH group, but overcoming higher energy barriers, whereas it does not take place when the OAc ligand is involved.

For Cl and Br ligands, the preferred mechanism is a function of the nature of the ligands in trans-axial and equatorial positions. When cisplatin derivatives are taken into consideration and the trans ligand is Cl⁻ the inner-sphere ligand-bridged is the most favourable mechanism. When the ligand in trans is the aspirinate, the calculated barriers become significantly higher and the enolate β -carbon attack becomes the preferred mechanism.

For the Cl oxaliplatin derivative having aspirinate in trans axial position, the reduction occurs by the ligand-bridged-H transfer mechanism involving the aspirinate ligand. Very likely the mechanism changes due to the equatorial ligands steric hindrance. The enolate β -carbon attack can occur, but it is not competitive.

The exploration of the so called *base-assisted outer-sphere mechanism* for Pt(NH₃)₂(Cl)₄ shows that both singlet and triplet multiplicities are involved.

The apparently spin conserving process starts in a singlet state, the spin is changed to triplet to avoid the very high energy singlet transition state and continues along the singlet energy profile, due to a second spin crossing, to form the final products (**Figure 5.1**). The spin inversions allow the base-assisted outer-sphere mechanism to be accessible and competitive with respect to inner-sphere alternatives.

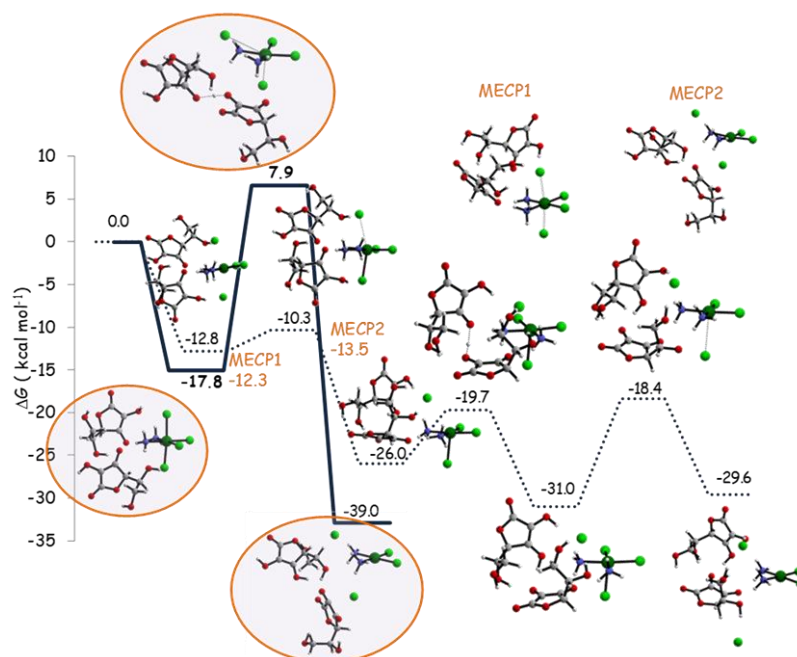


Figure 5.1 Singlet (solid) and triplet (dotted) crossing free energy profiles for the $\text{Pt}(\text{NH}_3)\text{Cl}_4$ complex describing the “base-assisted” outer-sphere electron transfer mechanism in presence of ascorbate as reducing agent. Energies are in kcal mol^{-1} and relative to separated reactants.

Redox potential calculations of the studied complexes, show that the propensity to be reduced by an **outer-sphere mechanism** depends principally on the nature of axial ligands. Such propensity increases in the order: $\text{OH} < \text{OAc} < \text{Cl} < \text{Br}$ and the rate of the reduction decreases in going from cisplatin derivatives to oxaliplatin ones.

References

- 1) L. Galluzzi, L. Senovilla, I. Vitale, J. Michels, I. Martins, O. Kepp, M. Castedo, G. Kroemer, *Oncogene* **2012**, *31*, 1869-1883.
- 2) E. Wexselblatt, E. Yavin, D. Gibson, *Inorg. Chim. Acta* **2012**, *393*, 75-83.
- 3) S. Choi, C. Filotto, M. Bisanzo, S. Delaney, D. Lagasee, J. L. Whitworth, A. Jusko, C. R. Li, N. A. Wood, J. Willingham, A. Schwenker, K. Spaulding, *Inorg. Chem.*, **1998**, *37*, 2500-2504.
- 4) K. Lemma, A. M. Sargeson, L. I. Elding, *J. Chem. Soc., Dalton Trans.*, **2000**, 1167-1172.
- 5) K. Lemma, D. A. House, N. Retta, L. I. Elding, *Inorg. Chim. Acta*, **2002**, *331*, 98-108.
- 6) A. Nemirovski, I. Vinograd, K. Takrouri, A. Mijovilovich, A. Rompel, D. Gibson, *Chem. Commun.*, **2010**, *46*, 1842-1844.
- 7) J. Z. Zhang, E. Wexselblatt, T. W. Hambley, D. Gibson, *Chem. Commun.*, **2012**, *48*, 847-849.
- 8) E. Wexselblatt, D. Gibson, *J. Inorg. Biochem.* **2012**, *117*, 220-229.
- 9) M. Sinisi, F. P. Intini, G. Natile, *Inorg. Chem.*, **2012**, *51*, 9694-9704.
- 10) H. P. Varbanov, S. M. Valiahdi, C. R. Kowol, M. A. Jakupec, M. Galanski, B. K. Keppler, *Dalton Trans.*, **2012**, *41*, 14404-14415.
- 11) E. Wexselblatt, E. Yavin, D. Gibson, *Angew. Chem., Int. Ed.*, **2013**, *52*, 6059-6062.
- 12) I. Ritacco, G. Mazzone, N. Russo, E. Sicilia, *Inorg. Chem.*, **2016**, *55*, 1580-1586.
- 13) O. Bradáč, T. Zimmermann, J. V. Burda, *J. Mol. Model.*, **2013**, *19*, 4669-4680.

Paper III

Antitumor Pt(IV) prodrugs: a systematic computational exploration of their reduction mechanism by L-ascorbic acid

E. Dabbish, F. Ponte, N. Russo, E. Sicilia, *Inorg. Chem.*, **2019**, *58*, 3851-3860.

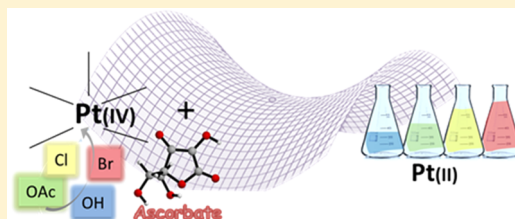
Antitumor Platinum(IV) Prodrugs: A Systematic Computational Exploration of Their Reduction Mechanism by L-Ascorbic Acid

Eslam Dabbish, Fortuna Ponte, Nino Russo, and Emilia Sicilia*¹

Department of Chemistry and Chemical Technologies, Università della Calabria, 87036, Arcavacata di Rende, CS, Italy

ABSTRACT: The reduction mechanism of Pt(IV) anticancer prodrugs, still today a matter of debate, assisted by one of the dominant reductants in human plasma, that is L-ascorbic acid in its monodeprotonated form, has been computationally examined in this work. In order to check what should be the influence on the reduction rate of the identity of the ligands in axial and equatorial position, both cisplatin and oxaliplatin derivatives have been studied, varying the ligands in axial position in connection with the role they should play as bridges, *trans* leaving species, and proton acceptors. OH, OAc, Cl, and Br ligands have been tested as bridging/

leaving ligands, whereas Cl and aspirin have been used as *trans* labile and less labile ligands, respectively. The most recent theoretical and experimental investigations have demonstrated that the generally adopted grouping of reduction mechanisms into inner- and outer-sphere does not properly take into account all the viable alternatives. Therefore, inner-sphere mechanisms, classified as ligand-bridged, ligand-bridged-H transfer and enolate β -carbon attack, have been explored for all the complexes under investigation. Concerning the outer-sphere mechanism, redox potentials have been calculated adopting a recently proposed procedure based on the separation between electrochemical and chemical events to evaluate their propensity to be reduced. Moreover, according to the hypothesis that the outer-sphere reduction mechanism involves the sequential addition of two electrons causing the formation of a Pt(III) intermediate, the possibility that singlet and triplet pathways can cross for the Pt(IV) cisplatin derivative having two chlorido ligands in axial position has been explored in detail. Results show that the mechanism indicated as base-assisted outer sphere can become competitive with respect to the inner one if two singlet–triplet spin inversions occur. Results presented here are helpful in addressing synthetic strategies as they show that Pt(IV) prodrugs propensity to be reduced can be properly tuned and give indications on how this aim can be accomplished.



1. INTRODUCTION

Platinum complexes, notwithstanding the fact that only a relatively small number of metal-containing drugs are currently in clinical use, have proven to be invaluable and are the pillars of cancer chemotherapy.¹ Only three Pt(II)-based anticancer drugs are approved by the FDA and used worldwide: cisplatin, carboplatin, and oxaliplatin, which are square-planar d^8 Pt(II) complexes, whose mechanism of action (MoA) involves water substitution of ligands for the formation of the corresponding “aquated” complexes acting as transcription inhibitors by binding to nuclear DNA and distorting its structure.^{2–4} Although very efficacious, cisplatin and related Pt(II) complexes suffer from side-effects. Furthermore, bioavailability is limited and oral administration is precluded, since a large amount of Pt(II) drugs is lost in the bloodstream before arriving at the ultimate target.⁵ Aiming at overcoming such shortcomings new strategies have emerged including the use of six-coordinate Pt(IV) complexes, as inert prodrugs, which are shown to release the corresponding four-coordinate active Pt(II) species upon reduction by cellular reducing agents or by photoactivation.⁶

Pt(IV) complexes are relatively inert to substitution.⁷ Reactions with biological nucleophiles, therefore, are disfavored and lifetime in biological fluids is expected to increase making even oral administration feasible. The administration of nontoxic Pt(IV) prodrugs might reduce unwanted reactions

with biomolecules and consequently minimize undesired side-effects. In addition, axial ligands can be designed to improve in different ways the pharmacological properties of the prodrug. Intracellular reductive elimination represents the critical and decisive step of the MoA of such compounds and, as a consequence, a great amount of attention has been focused on aspects such as the identity of the reducing agents, the ease, the rate and mainly the mechanism of the reduction process. Although many potential reducing agents are present both in plasma and cells and several hypotheses have been formulated,⁸ L-ascorbic acid ($AscH_2$) and L-glutathione are commonly believed to be the biological species responsible for the reduction of Pt(IV) prodrugs and continue to be used for *in vitro* experiments.^{9–13}

Several hypotheses on the mechanism by which Pt(IV) prodrugs are reduced have been formulated mainly on the basis of the information coming from kinetic measurements. Electron transfer mechanisms are generally classified as ligand-bridged inner-sphere, assuming that one of the axial ligands is able to form a bridge between the Pt(IV) center and the reductant mediating the flow of the electrons, and outer-sphere.^{6a,11c,14} However, such classification does not properly account for all the proposed mechanistic alternatives. The

Received: December 14, 2018

Published: March 7, 2019



inner-sphere mechanism could involve the Pt(II) complex catalytic action¹⁵ or the enolate β -carbon of the monodeprotonated form of L-ascorbic acid (AsCH^-) attack to the axial ligands.¹⁶ Outer-sphere reduction can take place through a two steps electron transfer encompassing formation of a metastable six-coordinate Pt(III) intermediate,¹⁷ and intersystem singlet–triplet crossings.¹⁶ Very recently, we have shown that when one of the axial ligands is an OH group and AsCH^- is the reducing agent, the inner-sphere electron transfer proceeds by the direct participation of the ligand, leading to the release of a water molecule and formation of dehydroascorbic acid (DHA), the oxidized form of L-ascorbic acid.¹⁸

Experimental information on the ease of reduction is usually obtained by cyclic voltammetry, which allows to measure the peak potential for the irreversible reduction, but not the standard redox potential. Since the electron transfer is accompanied by the release of the two axial ligands, the measured peak potentials do not necessarily correlate with the rate of the reduction process¹⁹ that depends both on the rate of the electron transfer and on strength of the bonds between the ligands and the metal center. Theoretical procedures for the elucidation of the reduction mechanism and calculation of redox potential have been proposed.^{17,20} Baik and co-workers¹⁷ have demonstrated that reduction occurs in two steps. The first step involves one electron transfer accompanied by the formation of a six-coordinate Pt(III) complex and, being less exergonic than the second one, determines the magnitude of the redox potential as it has been confirmed by computations.^{18,21}

Motivated by the attention devoted to the design of novel antineoplastic agents based on Pt(IV) prodrugs and the contradictory information coming from experimental and theoretical investigations, we have undertaken a thorough computational analysis of the chief reduction step using several platinum complexes and L-ascorbic acid as reducing agent. The Pt(IV) model complexes have been selected to check what is the influence on the reduction rate of the nature of the equatorial and, mostly, axial ligands owing to the role they should play as bridges, *trans* leaving species and proton acceptors.

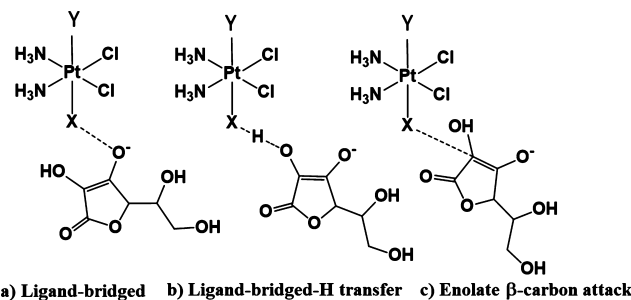
2. RESULTS AND DISCUSSION

A systematic examination of the inner- and outer-sphere reduction mechanisms for all the Pt(IV) complexes, shown in Scheme 1 has been carried out. Ascorbic acid, in its monoanionic form, AsCH^- , at physiological pH (pK_a ca. 3.8), has been used as reducing agent. The reduction mechanism of Asplatin complex, c,c,t -[PtCl₂(NH₃)₂(OH)(aspirin)], a dual-action drug with the ability to release cisplatin and aspirin for their

respective biological actions,^{6b,c} has been recently investigated by us.¹⁸ For comparison with the outcomes of our study on Asplatin and its analogues, obtained by substituting the OH (1) group with either Cl (2) or Br (3), the corresponding acetate (OAc) complex (4) has been examined. Furthermore, in order to check the influence on the reaction rate of the nature of the ligand in *trans* with respect to bridging/leaving ligands, the behavior of the Pt(IV) complexes c,c,t -[PtCl₂(NH₃)₂(X)(Cl)] (X = OH⁻ (5), Cl⁻ (6), Br⁻ (7), Ac⁻ (8)) has been analyzed, with the chlorido ligand being both a better leaving ligand than aspirinate and unable to accept a proton. The influence of the nature of the ligands in equatorial position has been examined by considering Pt(IV) derivatives of oxaliplatin, that is [Pt(dach)(Ox)] (dach = (1*R*,2*R*)-1,2-diaminocyclohexane, Ox = oxalate). Calculations have been carried out for two complexes in which one of the axial ligands is the aspirinate having in the *trans* position a hydroxido (9) and a chlorido (10) ligand.

The explored alternatives are shown in Scheme 2. The inner-sphere mechanistic alternative involving Pt(II) as catalyst has

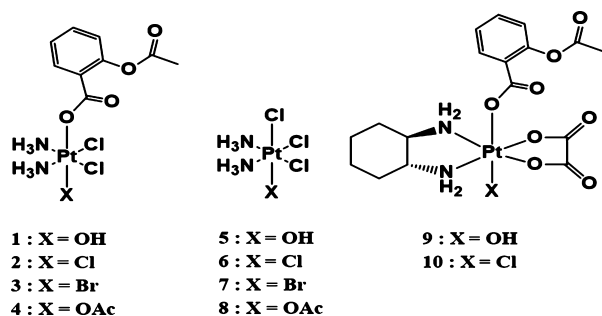
Scheme 2. Inner-Sphere Mechanistic Alternatives



not been explored because of both the previously calculated¹⁸ high energy barriers for the reduction and the low viability of this path as a consequence of the low cellular concentration of Pt(II).

2.1. Inner-Sphere Reduction of c,c,t -[PtCl₂(NH₃)₂(X)- (aspirin)], X = OH⁻, Cl⁻, Br⁻, OAc⁻. The detailed investigation of the inner-sphere reduction reaction of Asplatin (1) and its chlorido (2) and bromido (3) derivatives in the presence of AsCH^- has highlighted¹⁸ the peculiar behavior of the OH⁻ ligand. Indeed, for the (1) complex, the reduction mechanism involves formation and release of a water molecule due to the shift of a H⁻ unit from the OH group of the ascorbate to the hydroxido ligand. Therefore, the hydroxido ligand not only plays the role of bridge to allow the transfer of the electrons, but directly participates in the reduction process leading to formation of the oxidized form of the ascorbic acid DHA. Simultaneously, the *trans* aspirinate ligand detaches and the cisplatin drug is formed. When the reduction mechanism of 2 and 3 complexes is taken into consideration, the electrons are transferred thanks to the bridging Cl and Br ligands that interact with the deprotonated oxygen of the AsCH^- reducing species and concurrently a proton shift occurs from the OH group of the ascorbate to the *trans* aspirinate. As a result, the chlorido or bromido, ligands are released along with aspirin. Cisplatin and DHA are formed. However, for (2) and (3) complexes the most favorable mechanism is that involving the nucleophilic attack of the enolate β -carbon of ascorbate on the X (X = Cl, Br) ligand leading to the formation of a new C–X bond and the release of the ligand in *trans* position. Since many

Scheme 1. Pt(IV) Complexes Investigated for Reduction



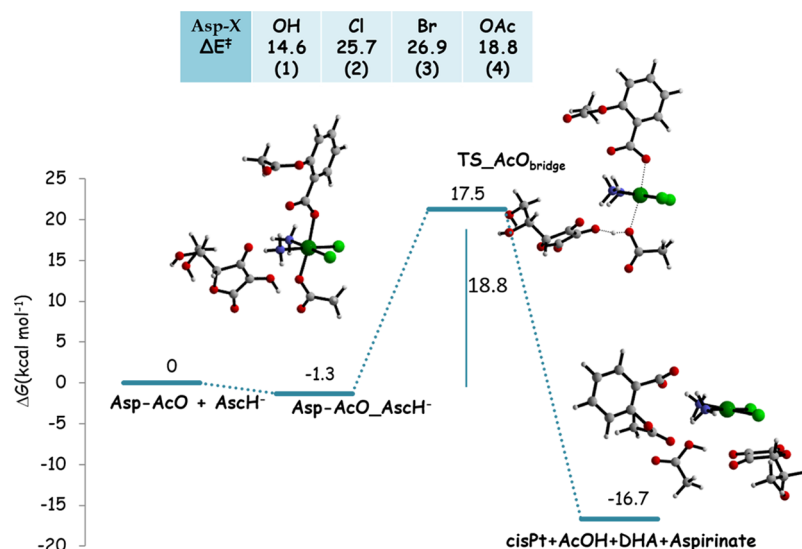


Figure 1. Calculated B3LYP-D3 free energy profile in water describing the OAc-bridged-H electron transfer mechanism for the reduction of complex 4 by ascorbate. Energies are in $\text{kcal}\cdot\text{mol}^{-1}$ and relative to separated reactants.

Pt(IV) cisplatin and oxaliplatin derivatives have been prepared by tethering carboxylate axial ligands to the metal center, also the behavior of a possible Asplatin derivative obtained by substituting the OH ligand with an acetate (OAc) (4) one has been investigated. The calculated energy profile together with the structures of intercepted stationary points describing the ascorbate assisted reduction of complex 4 is reported in Figure 1.

In the same figure, for the sake of comparison, the heights of the analogous free energy barriers for complexes 1, 2, and 3 are reported. The interaction between the reducing agent and complex 4 leads to the formation of the adduct named **Asp-OAc_AscH⁻**, which is slightly more stable than the reactants by $1.3 \text{ kcal mol}^{-1}$. In analogy with the mechanism operative for the hydroxido ligand and as already suggested,²² the two-electron transfer occurs in one step through the shift of a H^+ unit from the OH group of the ascorbate to the acetate oxygen coordinated to the metal center. Formed acetic acid detaches and, simultaneously, the *trans*-aspirinate ligand is released and dehydroascorbic acid is formed. The Pt(IV) to Pt(II) reduction caused by such rearrangement takes place overcoming an energy barrier of $18.8 \text{ kcal mol}^{-1}$ for the corresponding concerted transition state, **TS_OAc_{bridge}**, characterized by an imaginary frequency of $142i \text{ cm}^{-1}$. Formation of separated products is calculated to be exergonic by $16.7 \text{ kcal mol}^{-1}$.

The possibility that the reduction reaction can occur by a nucleophilic attack of the enolate β -carbon of ascorbate (mechanism c in Scheme 2) on the acetate ligand has been also unsuccessfully explored, very likely due to steric hindrance of the acetate ligand.

2.2. Inner-Sphere Reduction of *c,c,t*-[PtCl₂(NH₃)₂(X)(Cl)], X = OH, Cl, Br, OAc. Aiming at analyzing what should be the role played by the ligands in *trans* with respect to the bridging ligands that allow the Pt(IV) reduction to occur, Pt(IV) cisplatin derivatives *c,c,t*-[PtCl₂(NH₃)₂(X)(Cl)] (X = OH (5), Cl (6), Br (7), OAc (8)) have been examined. With respect to aspirin, chlorido ligand both is a better leaving ligand and is not able to accept protons. It is worth underlining that for complex (6), recently, Dong et al.^{19b} have studied the reduction process by ascorbic acid in a wide range of pH and

proposed a halide-bridged inner-sphere electron transfer mode for the rate-determining steps. The outer-sphere electron transfer mode practically has been excluded and activation parameters have been measured at physiological pH. The energy profiles describing the reduction of complexes 5–8 by ascorbate are depicted in Figure 2.

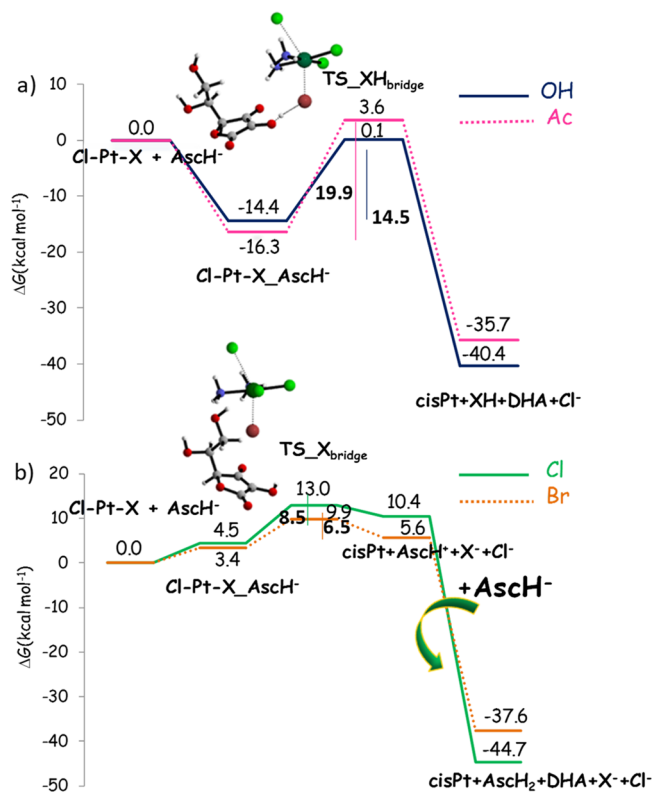


Figure 2. Calculated B3LYP-D3 free energy profiles in water describing the X-bridged electron transfer mechanism in the presence of ascorbate as reducing agent for (a) 5 (X = OH), solid line, and 8 (X = OAc), dotted line, and (b) 6 (X = Cl), solid line, and 7 (X = Br), dotted line. Energies are in $\text{kcal}\cdot\text{mol}^{-1}$ and are relative to separated reactants.

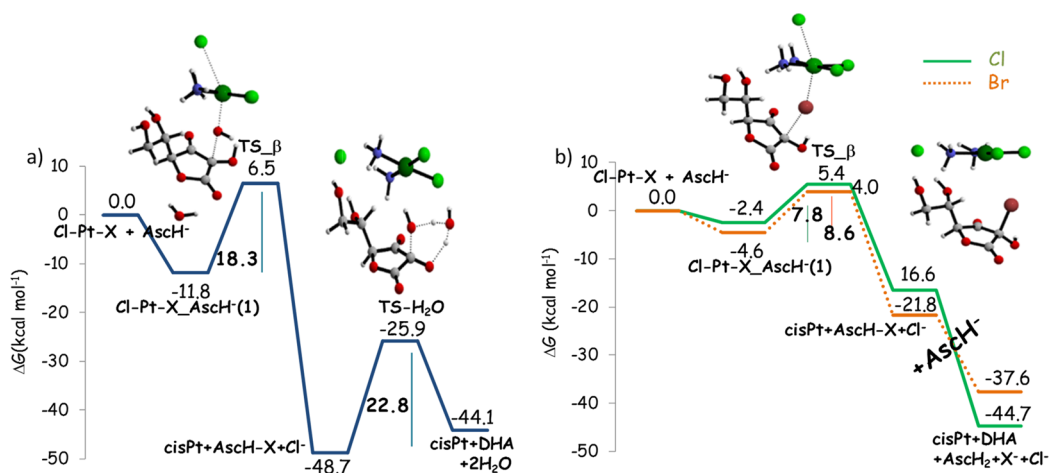


Figure 3. Calculated B3LYP-D3 free energy profiles in water describing the enolate β -carbon attack mechanism in the presence of ascorbate as reducing agent for (a) 5 ($X = \text{OH}$) and (b) 6 ($X = \text{Cl}$), solid line, and 7 ($X = \text{Br}$), dotted line. Energies are in kcal mol⁻¹ and are relative to separated reactants.

The two (5 and 8) cisplatin derivatives undergo the two-electrons reduction reaction following a mechanism that, in analogy with complexes 1 and 4, involves the transfer of a H⁻ unit from the OH group of the ascorbate to the bridging hydroxido and acetato ligands, respectively, to form the oxidized form of ascorbic acid, DHA. Formed water and acetic acid molecules detach from the platinum center inducing the simultaneous detachment of the *trans* chlorido ligand. After the exergonic formation of the first adduct (−14.4 and −16.3 kcal mol⁻¹ for OH and OAc, respectively), for the subsequent rearrangement to take place it is required that a barrier of 14.5 kcal mol⁻¹ for the OH ligand and 19.9 kcal mol⁻¹ for the OAc ligand is overcome. The corresponding transition states are characterized by 94i and 172i cm⁻¹ imaginary frequencies, respectively.

The whole process is calculated to be exergonic by 40.4 and 35.7 kcal mol⁻¹ for complexes 5 and 8, respectively. Comparison with the results obtained for complexes 1 and 4, shows that the reduction process is not greatly affected by the identity of the *trans* ligand. When the reduction behavior of 6 and 7 complexes is examined, Cl and Br only act as bridging ligands allowing two-electron transfer after the endergonic formation of the initial adducts (4.5 and 3.4 kcal mol⁻¹ for Cl and Br, respectively). In the subsequent transition state, chlorido and bromido ligands interact with the deprotonated oxygen of the ascorbate reducing agent causing the detachment of the *trans* chlorido ligand. The imaginary frequencies are 65i and 68i cm⁻¹ for chlorido and bromido, respectively. Such rearrangement has an energetic cost of 8.5 kcal mol⁻¹ for Cl and 6.5 kcal mol⁻¹ for Br and leads to the release of the anionic axial ligands, the reduced platinum complex and protonated dehydroascorbate. Products lie 10.4 and 5.6 kcal mol⁻¹, respectively above the zero reference energy.

The Pt(IV) to Pt(II) reduction is completed by the intervention of a species, that we have imagined to be a second AscH⁻ unit, capable to accept the proton from the OH group of the dehydroascorbate. DHA together with the cisplatin complex and the detached axial ligands are afforded. Such step is barrierless and exergonic by 44.7 kcal mol⁻¹ for the 6 complex and 37.6 kcal mol⁻¹ for the 7 one. With respect to our previous investigation,¹⁸ the presence in *trans* position of the chlorido ligand, which is a good leaving group unable to

accept the proton from the ascorbate, has a beneficial effect on the kinetics of the process as the calculated activation barriers significantly lower. Moreover, the assistance of an additional basic species is required in order to accomplish the reduction process.

The main conclusion of such analysis is that when the *trans* living ligand is the labile chlorido the rate of the reaction depends on the bridging ability that follows the expected trend (Br > Cl > OAc > OH) even if the role played by hydroxido and acetato is different with respect to that of chlorido and bromido ligands.

The outcomes of the examination of the alternative β -carbon inner-sphere mechanism involving the attack of the enolate β -carbon on the X = OH, Cl, Br ligands, of complexes 5–7, are shown in Figure 3. Once again the β -carbon attack does not take place when X = OAc.

In the first step the adduct, Cl–Pt–X–AscH⁻ (1), which favorably orients the ascorbate to facilitate the nucleophilic attack of the enolate β -carbon on the X ($X = \text{OH}, \text{Cl}, \text{Br}$) ligand, is formed. All the intermediates lie lower in energy with respect to reactants: −11.8, −2.4, and −4.8 kcal mol⁻¹ for OH, Cl and Br, respectively. As a consequence of the attack a new C–X bond is formed and simultaneously the *trans* chlorido ligand is released. The intercepted concerted transition states, are identified by a negative frequency (120i cm⁻¹ for the hydroxido and 85i cm⁻¹ for both chlorido and bromido ligands) corresponding to such rearrangement and the calculated barriers are 18.3 kcal mol⁻¹ for the hydroxido complex and 7.8 and 8.6 kcal mol⁻¹ for the chlorido and bromido ones, respectively. The reaction is calculated to be exergonic for all the examined complexes, as shown in Figure 3, and leads to the release of the cisplatin complex, the free chlorido *trans* ligand and the intermediate species in which the X atom is bonded to the enolate β -carbon in geminal position to the OH. In the case of the hydroxido complex (5), elimination of a water molecule requires an auxiliary water molecule that assists the process acting as a proton shuttle. The calculated barrier height for the corresponding transition state is 22.8 kcal mol⁻¹ and leads to the exergonic formation of the final products. For the chlorido and bromido complexes (6 and 7), instead, the action of a second AscH⁻ unit causes the OH group deprotonation and the final products formation in a

barrierless process. The whole process results to be exergonic by 44.7 and 37.6 kcal mol⁻¹ for the chlorido and bromido complexes, respectively.

The height of the calculated barriers for both inner sphere ligand-bridging and β -carbon mechanisms for complex **6**, even if lower than the value which can be obtained using the activation parameters measured by Dong et al.^{19b} ($\Delta H^\ddagger = 46.7 \pm 1.5$ kJ mol⁻¹, $\Delta S^\ddagger = -34 \pm 9$ J K⁻¹ mol⁻¹), support the hypothesis that the electron transfer occurs in an inner-sphere fashion.

2.3. Inner-Sphere Reduction of [Pt(dach)(Ox)(X)(aspirin)], X = OH, Cl. As anticipated above, in order to understand how the nature of the ligands in equatorial position can influence the Pt(IV) complexes reduction, two possible oxaliplatin derivatives have been considered: with one aspirinate and one hydroxido ligand (**9**), with one aspirinate and one chlorido ligand (**10**). For each complex, both inner bridging and β -carbon mechanisms have been examined. Outcomes for the bridging mechanism are shown in Figure 4.

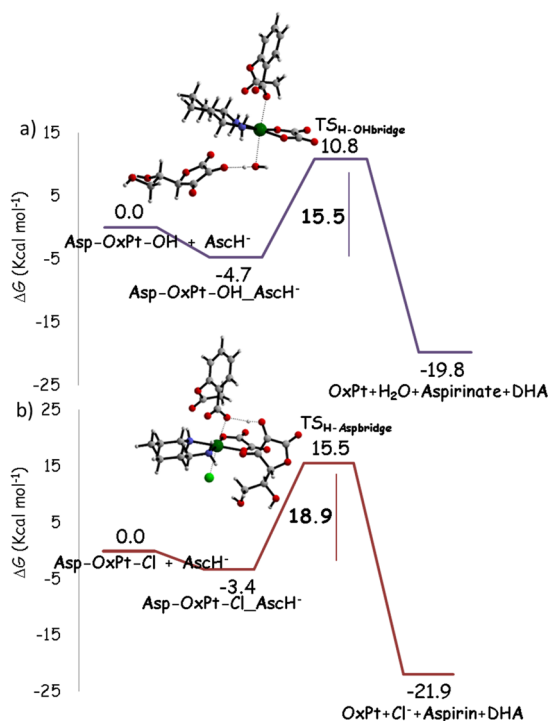


Figure 4. Calculated B3LYP-D3 free energy profiles in water describing the bridging reduction mechanism in the presence of ascorbate as reducing agent for (a) **9** (X = OH) and (b) **10** (X = Cl), complexes. Energies are in kcal mol⁻¹ and relative to separated reactants.

Along the calculated pathways the structures of the intercepted transition states are sketched. For the oxaliplatin derivative (**9**) having a hydroxido group in *trans* position to the aspirinate ligand, the reaction proceeds following the same steps already illustrated above, and the drawn energy profile strictly mirrors those of **1** and **5** complexes. After the formation of the first adduct ($\Delta G = -4.7$ kcal mol⁻¹), reduction takes place by the transfer of a H⁻ unit to the OH group causing the contemporaneous detachment of a water molecule and the *trans* aspirinate ligand. The active Pt(II) species and the DHA oxidized form of ascorbic acid are formed. The intercepted transition state lies 10.8 kcal mol⁻¹ above the zero reference

energy of reactants for a calculated barrier of 15.5 kcal mol⁻¹, and is characterized by an imaginary frequency of 75i cm⁻¹. The whole reaction is exergonic by 19.8 kcal mol⁻¹. The behavior of complex (**10**), having in axial position a chlorido in *trans* position to the aspirinate, significantly differs with respect to the similar situations already examined.

Indeed, many unsuccessful attempts have been carried out to locate a transition state for the formation of a bridge between the negatively charged ascorbate oxygen atom and the Cl ligand to allow two-electron transfer. Due to the steric hindrance of the ligands in equatorial position, the two-electron transfer through the Cl bridging ligand accompanied by the proton shift from the OH group of the ascorbate to the *trans* aspirinate cannot occur. The only intercepted transition state, named TS_{H-Aspbridge}, involves the shift of a H⁻ unit from the OH group of the ascorbate to the aspirinate ligand leading to the detachment of an aspirin molecule. The *trans* chlorido ligand is released and oxaliplatin and DHA reduction products are formed. The height of the energy barrier that is necessary to overcome is 18.9 kcal mol⁻¹. The imaginary frequency that confirms the nature of this stationary point is 59i cm⁻¹.

The pathways describing the alternative inner-sphere mechanism comprising the nucleophilic attack of the enolate β -carbon to the OH and Cl ligand are shown in Figure 5. Once again the two (**9** and **10**) complexes behave differently as a consequence of the presence of a hydroxido and chlorido ligand in *trans* to the aspirinate. Indeed, after the slightly exergonic formation of the first adduct (-0.4 kcal mol⁻¹ for OH and -3.3 kcal mol⁻¹ for Cl), the reaction proceeds with the β -carbon attack of the ascorbate on the living ligand forming new C–O and C–Cl bonds and causing the *trans* aspirinate ligand release. The calculated barrier is 21.5 kcal mol⁻¹ for both complexes, whereas the reaction is exergonic by 18.9 and 1.9 kcal mol⁻¹ for the Asp-OxPt–OH and Asp-OxPt–Cl, respectively. The oxaliplatin complex, the free aspirinate ligand and the intermediate species in which the OH and Cl moieties are bonded to the enolate β -carbon in germinal position to the OH are formed. The imaginary frequencies characterizing these TSs are 247i for Asp-OxPt–OH and 122i cm⁻¹ for Asp-OxPt–Cl. The reaction is completed by the release of a water molecule for complex (**9**) assisted by an additional water molecule and surpassing a barrier of 20.0 kcal mol⁻¹. The transition state structure is characterized by an imaginary frequency of 1177i cm⁻¹. Detachment of the Cl⁻ ion and deprotonation of the OH group to yield the oxidized DHA product occurs in the presence of a second AscH⁻ unit in a barrierless fashion according to what observed in all analogous situations.

2.4. Calculated Two-Electron Reduction Potentials of Complexes 1–10. Although standard cyclic voltammetry has been routinely used to characterize redox behavior of Pt(IV) antitumor compounds, the study of the reduction process involving transfer of two electrons and release of the two axial ligands is challenging owing to the intrinsic irreversibility of the reduction and the influence that the rate of the ligand loss can have on the thermodynamics and kinetics of the process. The two-electron redox process is commonly observed as a single irreversible reduction event, and the peak potential for the cathodic wave obtained in cyclic voltammetric measurements is usually used to measure the ease of reduction instead of the standard redox potential. Peak potentials, however, strongly depend on the experimental conditions. Therefore, it is matter

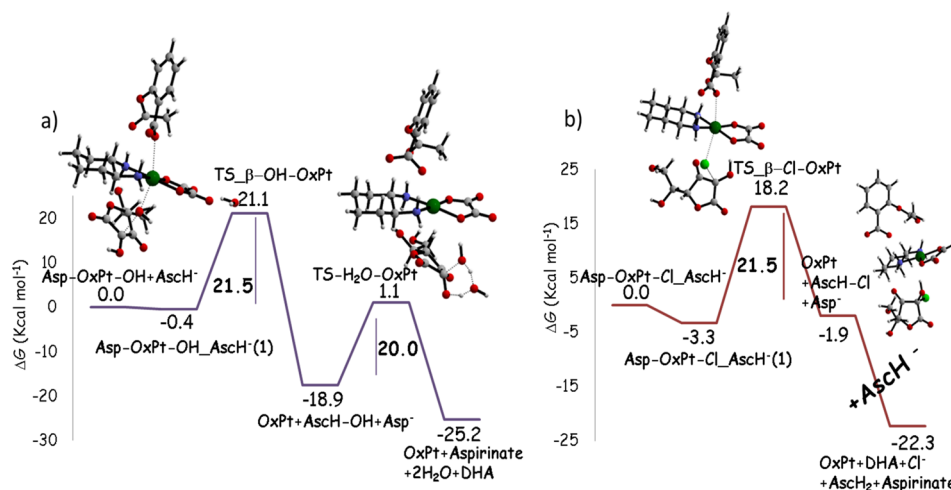
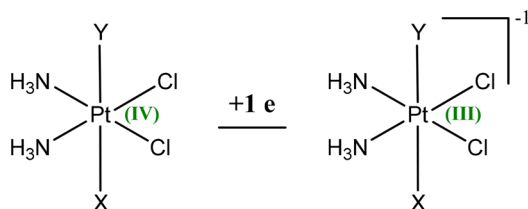


Figure 5. Calculated B3LYP-D3 free energy profiles in water describing the enolate β -carbon attack mechanism in the presence of ascorbate as reducing agent for (a) **9** ($X = \text{OH}$) and (b) **10** ($X = \text{Cl}$) complexes. Energies are in $\text{kcal}\cdot\text{mol}^{-1}$ and relative to those of separated reactants.

of debate the possibility to extract information about the redox behavior of Pt(IV) prodrugs from such measurements.

Baik and co-workers in a recent study,¹⁷ have carried out a series of electrochemical experiments to study the mechanism of the two-electron reduction of Pt(IV) cisplatin derivatives demonstrating that electron transfer and Pt–ligand bond cleavage occur in a stepwise fashion, thus leading to the formation of a metastable six-coordinate Pt(III) intermediate upon the first electron addition. From this intermediate the two axial ligands are removed sequentially, being the second ligand released as a consequence of the second electron addition. Furthermore, density functional calculations have been performed to elucidate the reduction mechanism and estimate standard reduction potentials. Indeed, on the basis of the adopted decomposition scheme the reduction potential can be calculated as the energy change that accompanies the one electron transfer for the reduction of the six-coordinate Pt(IV) complex to the corresponding six-coordinate Pt(III) (see Scheme 3) species with the axial ligand remaining in the coordination sphere of the metal center as it is illustrated in the Computational Details section.

Scheme 3. First Step of the Decomposition Scheme Proposed by Baik et al. for the First Electron Transfer



The reduction potential is computed as $E_{\text{first}}^{\circ} = -\Delta G_{(\text{sol})} - 4.43 \text{ V}$, where $\Delta G_{(\text{sol})}$ is the Gibbs free energy change in solution for the one electron transfer to the Pt(IV) complex and 4.43 V is the absolute potential of the standard hydrogen electrode (SHE) in water used as a reference. The values of the calculated redox potential for all the examined complexes are collected in Table 1. The difference in behavior between the Asplatin complex (**1**) and its Asp-Cl (**2**) and Asp-Br (**3**) derivatives has been already underlined.¹⁸ Indeed, the addition of one electron to **2** and **3** complexes causes the spontaneous release of the aspirinate ligand that, according to the results reported by Baik and co-workers,¹⁷ remains in the primary coordination sphere of the metal center forming hydrogen bonds with the equatorial ammonia ligands.

As formation of such bonds is unrealistic in solvent, explicit water molecules have to be included for a more reliable simulation. Aspirinate detachment from complex **1**, instead, takes place, overcoming an energy barrier. In analogous way, full optimization of the structure of six coordinate Pt(III) anionic complexes obtained by adding an electron to neutral (**4**–**10**) complexes has been carried out in gas-phase without imposing any geometrical constrain. Spontaneous release of the first ligand as a consequence of one electron addition has been observed for **6**, **7**, and **8** cisplatin derivatives. Thus, explicit water molecules, which have been removed for subsequent calculations in implicit solvent, have been added around the axial ligands. For the rest of complexes, the electrochemical and chemical events occur in two separate steps.

The calculated standard reduction potentials allow to estimate the propensity of the examined complexes to be reduced. Therefore, the possibility that the reduction occurs, if an outer-sphere mechanism is assumed to be operative, depends principally on the nature of axial ligands and increases

Table 1. Standard Reduction Potentials, in eV, Calculated as the Energy Change That Accompanies the First Step One-Electron Transfer for the Reduction of the Six-Coordinate Pt(IV) Complexes in the Proposed by Baik et al.¹⁷ Decomposition Scheme

E_{first}°	(1) Asp-OH −0.241	(2) Asp-Cl 0.127	(3) Asp-Br 0.279	(4) Asp-OAc −0.051
E_{first}°	(5) Cl–Pt–OH −0.163	(6) Cl–Pt–Cl 0.374	(7) Cl–Pt–Br 0.439	(8) Cl–Pt–OAc 0.431
E_{first}°	(9) Asp-Oxpt–OH −0.536	(10) Asp-Oxpt–Cl 0.132		

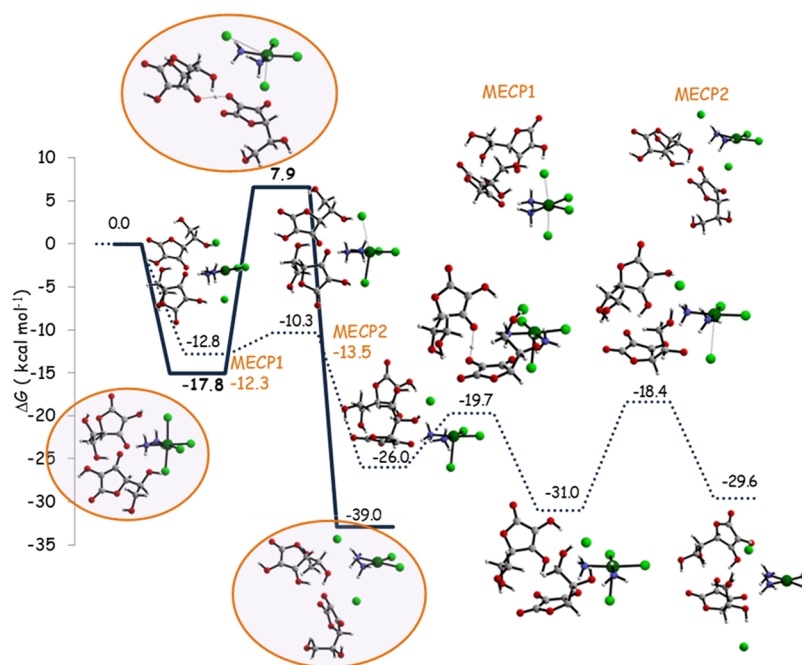


Figure 6. Singlet (solid) and triplet (dotted) crossing free energy profiles for the Cl–Pt–Cl (**6**) complex describing the “base-assisted” outer-sphere electron transfer mechanism in presence of ascorbate as reducing agent. Energies are in kcal mol⁻¹ and relative to separated reactants.

in the order: OH < OAc < Cl < Br. Moreover, the tendency to be reduced increases when in cisplatin derivatives the aspirinate ligand is substituted by the chlorido one. Concerning the influence of the nature of the equatorial ligands, it appears that the rate of the reduction for cisplatin derivatives is generally higher than oxaliplatin ones. The trend in the tendency to be reduced by an outer-sphere mechanism does not necessarily correspond to the trend in the rate of reduction by an inner-sphere mechanism. This disagreement can explain the observed lack of correlation between the measured rates of reaction and the reduction potentials.^{10b,11c}

The calculated value of 0.374 eV of the standard reduction potential for complex (**6**) compared with the measured value -0.206 eV,²³ versus the normal hydrogen electrode, confirms the already reported trends.^{17,18} That is, redox potentials calculated adopting such procedure are considerably different from those reported in the literature, corresponding to a redox-stability higher than the real one.

2.5. Potential Energy Surface Description of the Outer-Sphere Electron Transfer Mechanism. According to the hypothesis that the outer-sphere reduction mechanism involves the sequential addition of two electrons causing the formation of a Pt(III) intermediate, the possibility that singlet and triplet pathways can cross has been recently computationally examined for the [Pt(dach)Cl₄] (dach = diaminocyclohexane) model complex.¹⁶ Here, the results of an analogous calculation carried out for complex (**6**) having two axial chlorido ligands are reported. Free energy profiles for both singlet and triplet multiplicities are drawn in Figure 6. Relative free energies in solution have been calculated with respect to the ground-state singlet reactants' asymptote (**6**) + 2AscH⁻. The adduct formed by the Cl–Pt–Cl (**6**) complex and two ascorbate molecules has been optimized in both singlet and triplet multiplicities. The singlet and triplet adducts lie 17.8 and 12.8 kcal mol⁻¹, respectively below the entrance channel. The reduction reaction, along the singlet pathway directly leads to the formation of the products: cisplatin, two chlorido

ligands, ascorbic acid and dehydroascorbic acid. The concerted transition state, that is necessary to overcome for the reduction to occur, lies 7.9 kcal mol⁻¹ above the reactants' reference energy for a barrier of 25.7 kcal mol⁻¹. The imaginary frequency is 59.2i cm⁻¹. The rearrangement of the reactants involves the elimination of the two axial chlorido ligands as a consequence of the outer-sphere two-electrons transfer and the proton shift from one of the ascorbates to the other, leading to the formation of both ascorbic and dehydroascorbic acids. The reaction is calculated to be exergonic by 39.0 kcal mol⁻¹. The presence of two ascorbate units is required for the proton shift to occur simultaneously with the electron transfer. Indeed, a very huge number of attempts carried out in presence of only one ascorbate unit all failed. It is worth underlining that such mechanism corresponds to the mechanism classified as “base assisted outer-sphere” by Ejeji and Ariafard, found to be the preferred one for the reduction of the [Pt(dach)Cl₄] complex.¹⁶ Along the triplet surface the reaction takes place going through several intermediates. Once the first adduct is formed the reaction proceeds with the transfer of one electron leading to the release of one chlorido ligand and formation of a penta-coordinated intermediate more stable than the previous one by 13.2 kcal mol⁻¹. The barrier for the corresponding transition state is only 2.5 kcal mol⁻¹ and the imaginary frequency is 38.5i cm⁻¹. In the next step the transfer of the proton from one ascorbate to the other occurs surmounting an energy barrier of 6.3 kcal mol⁻¹, and forming a stable intermediate at -31.0 kcal mol⁻¹. The TS is characterized by an imaginary frequency of 391.0i cm⁻¹.

In the last step the second electron is transferred causing the detachment of the second axial Cl ligand and therefore the exergonic ($\Delta G = -29.6$ kcal mol⁻¹) formation of the final products.

A careful search of the minimum energy crossing points (MECPs) has allowed to identify the structure and the energy of the points where the singlet and triplet PESs cross along

with the calculation of the frequencies within the seam of crossing for both MECPs.

The reaction starts in a singlet state and, immediately after, a crossing occurs avoiding the high energy barrier for the singlet transition state. In going from the singlet state adduct to the triplet transition state it is necessary to overcome a barrier of 7.5 kcal mol⁻¹. As it is evident from both geometry and energy of this point, the crossing occurs in the vicinity of the triplet minimum with the MECP1 structure that lies only 0.5 kcal mol⁻¹ higher in energy. In the framework of the two-state reactivity (TSR) paradigm, this kind of spin crossing occurring before formation of the transition state has to be considered a rate-limiting factor.²⁴ The second surface spin crossing occurs after the triplet transition state is surpassed and due to the spin change the reaction finishes with the formation of the products in a singlet spin multiplicity. Looking at the energy of the MECP2 reported in Figure 6, it appears that it is closer to the triplet transition state and, as it is located after the transition states, does not play a key role. This process is a typical example of the TSR paradigm²⁴ as a reaction that is not viable becomes accessible thanks to a spin change and products formation arises from an interplay of spin inversion and the respective barrier heights on both spin surfaces. Moreover, the reaction is formally spin conserving as reactants and products ground states have the same spin multiplicity. Along the reaction path, the reaction starts in a singlet state, the spin is changed to triplet to avoid the very high energy singlet transition state and continues to form the final products in a singlet state. It is worth mentioning that only if the spin inversions are taken into consideration do the so-called base-assisted outer-sphere path become viable and competitive with respect to the described inner-sphere alternatives.

3. SUMMARY AND CONCLUSIONS

In this paper, the outcomes of a systematic investigation of the key reduction step of Pt(IV) antiproliferative complexes have been illustrated. In order to obtain information on the influence of the identity of ligands in axial and equatorial position, both cisplatin and oxaliplatin derivatives have been examined and compared varying involved ligands. Mono-deprotonated ascorbic acid has been used as reducing agent model. The usually invoked classification of Pt(IV) into Pt(II) complexes reduction mechanisms as inner- and outer-sphere does not properly account for all the possible alternatives. Indeed, beside the possible involvement of Pt(II) as catalyst that has been considered to be not viable, the inner-sphere mechanisms have been classified as (a) ligand-bridged, (b) ligand-bridged-H transfer, and (c) enolate β -carbon attack. Results reported here show that (i) for both OH and OAc ligands the inner sphere two-electron transfer, classified as ligand-bridged-H transfer, is the preferred mechanism. The rate of the process is not influenced by the identity of the ligands in both axial and equatorial positions. The enolate β -carbon attack can occur for the OH group but overcoming higher energy barriers, whereas it does not take place when the OAc ligand is involved. (ii) For Cl and Br ligands, the preferred mechanism is a function of the nature of the ligands in *trans*-axial and equatorial positions. When cisplatin derivatives are taken into consideration and the *trans* ligand is Cl the inner-sphere ligand-bridged is the most favorable mechanism. When the ligand in *trans* is the aspirinate, the calculated barriers become significantly higher and the enolate β -carbon attack becomes the preferred mechanism. (iii) For

the Cl oxaliplatin derivative having aspirinate in *trans* axial position, the reduction occurs by the ligand-bridged-H transfer mechanism involving the aspirinate ligand. Very likely the mechanism changes due to the equatorial ligands steric hindrance. The enolate β -carbon attack can occur, but it is not competitive.

The exploration of the so-called base-assisted outer-sphere mechanism shows that both singlet and triplet multiplicities are involved. The apparently spin conserving process starts in a singlet state, the spin is changed to triplet to avoid the very high energy singlet transition state and continues along the singlet energy profile, due to a second spin crossing, to form the final products. The spin inversions allow the base-assisted outer-sphere mechanism to be accessible and competitive with respect to inner-sphere alternatives.

Finally, redox potentials calculated for all the Pt(IV) complexes under examination by separating the steps for the electron transfer from those for the axial ligand release, show that the propensity to be reduced by an outer-sphere mechanism depends principally on the nature of axial ligands. Such propensity increases in the order: OH < OAc < Cl < Br and the rate of the reduction decreases in going from cisplatin derivatives to oxaliplatin ones. Calculated values for the cisplatin derivative (6) having two chlorido ligands in axial position confirms that generally used peak potentials are significantly more negative than redox potentials computed adopting this method.

In conclusion, results demonstrate that the propensity of Pt(IV) prodrugs to be reduced can be appropriately modulated. The inner-sphere, in its different mechanistic alternatives, is the preferred mode of reduction, when monoanionic ascorbate is the reducing agent, for some of the examined cases. Very low calculated energy barriers strongly support the thesis, already formulated, that these prodrugs can hardly reach the target before reduction and the reduction takes place extracellularly.

4. COMPUTATIONAL DETAILS

All molecular geometry optimizations have been carried out with the Gaussian09 software package,²⁵ at density functional level of theory employing the B3LYP functional^{26,27} and including dispersion corrections for nonbonding interaction through the Grimme approach²⁸ that uses an atom pairwise additive scheme denoted as DFT-D3.

For the Pt atom, the relativistic compact Stuttgart/Dresden effective core potential has been used²⁹ in conjunction with the split valence basis set. For the atoms directly participating in the process the standard triple- ζ quality 6-311+G** basis sets of Pople and co-workers have been used, while to reduce the computational effort, for peripheral atoms, the 6-311G** basis sets have been employed.

Calculation of vibrational frequencies at the same level of theory has been carried out to both establishing the nature of intercepted stationary points as minima and transition states and calculating both zero-point energy (ZPE) and Gibbs free energy corrections. The involved transition states have been carefully checked to be properly connected to the correct minima by IRC (intrinsic reaction coordinate) analysis.³⁰

With the purpose of characterizing the MECPs, geometries and corresponding frequencies have been calculated with the help codes developed for the localization of MECPs³¹ and the vibrational frequency analysis at these points (GlowFreq).^{32,33}

In the decomposition scheme proposed by Baik and co-workers,¹⁷ it is assumed that electron transfer occurs separately with respect to ligand release. However, it can happen that in Pt(III) anionic intermediates ligands are released and remain in the metal coordination sphere as a consequence of the bonding interactions with the equatorial ligands. As these structures are unrealistic in solvent, explicit water molecules in proximity of the axial ligands have been included for the gas-phase optimizations and removed for subsequent calculations in implicit solvent.

The effects due to the presence of the solvent have been taken into consideration by using the Tomasi's implicit polarizable continuum model (PCM)³⁴ as implemented in Gaussian09. The UFF set of radii has been used to build-up the cavity in which solute molecules are accommodated. Single-point calculations on all stationary points structures obtained in vacuum have been carried out in implicit water ($\epsilon = 78.4$) at the same level for obtaining solvation Gibbs free energies. Using standard statistical procedures,³⁵ enthalpies and Gibbs free energies have been obtained at 298 K at 1 atm from total energies, including zero-point, thermal and solvent corrections. However, mainly when association and dissociation steps are involved, the entropic change that occurs when a solute is transferred from the gas- to the condensed-phase is not properly taken into consideration the following correction scheme has been adopted. Since the Gaussian's default standard state corresponds to an ideal gas at a standard pressure of 1 atm, the computed free energies have been converted³⁶ to yield Gibbs energies with a solution phase standard state of 1 mol L⁻¹ for all the species. For water molecules a standard state of 55.5 M has been used. That is, to the free energy of each species, as computed in Gaussian, a free energy correction term equal to $RT \ln(V_{\text{molar gas}}/V_{\text{molar solution}})$, (R = gas constant, T = absolute temperature) has been added, where $V_{\text{molar gas}}$ is the volume occupied by one mole of ideal gas at the considered temperature, and $V_{\text{molar solution}}$ is the volume occupied by one mole of species in a standard solution of concentration 1 mol L⁻¹.

AUTHOR INFORMATION

Corresponding Author

*(E.S.) E-mail: emilia.sicilia@unical.it

ORCID

Emilia Sicilia: 0000-0001-5952-9927

Notes

The authors declare no competing financial interest.

REFERENCES

- (1) (a) Johnstone, T. C.; Suntharalingam, K.; Lippard, S. J. The Next Generation of Platinum Drugs: Targeted Pt(II) Agents, Nanoparticle Delivery, and Pt(IV) Prodrugs. *Chem. Rev.* **2016**, *116*, 3436–3486. (b) Dilruba, S.; Kalayda, G. V. Platinum-based drugs: past, present and future. *Cancer Chemother. Pharmacol.* **2016**, *77*, 1103–1124.
- (2) (a) Klein, A. V.; Hambley, T. W. Platinum Drug Distribution in Cancer Cells and Tumors. *Chem. Rev.* **2009**, *109*, 4911–4920. (b) Benedetti, M.; Ducani, C.; Migoni, D.; Antonucci, D.; Vecchio, V. M.; Ciccarese, A.; Romano, A.; Verri, T.; Ciccarella, G.; Fanizzi, F. P. Experimental evidence that a DNA polymerase can incorporate N7-platinated guanines to give platinated DNA. *Angew. Chem.* **2008**, *120*, 517–520. (c) Carrisi, C.; Romano, A.; Lunetti, P.; Antonucci, D.; Verri, T.; De Benedetto, G. E.; Dolce, V.; Fanizzi, F. P.; Benedetti, M.; Capobianco, L. Platinated nucleotides are substrates for the human mitochondrial deoxynucleotide carrier (DNC) and DNA polymerase. Relevance for the development of new platinum based drugs. *Chemistry SELECT* **2016**, *1*, 4633–4637. (d) Benedetti, M.; Romano, A.; De Castro, F.; Girelli, C. R.; Antonucci, D.; Migoni, D.; Verri, T.; Fanizzi, F. P. N7-platinated ribonucleotides are not incorporated by RNA polymerases. New perspectives for a rational design of platinum antitumor drugs. *J. Inorg. Biochem.* **2016**, *163*, 143–146.
- (3) Gibson, D. The mechanism of action of platinum anticancer agents—what do we really know about it? *Dalton Trans* **2009**, 10681–10689.
- (4) Bugarčić, Ž. D.; Bogojeski, J.; Petrović, B.; Hochreuther, S.; van Eldik, R. Mechanistic studies on the reactions of platinum(II) complexes with nitrogen- and sulfur-donor biomolecules. *Dalton Trans* **2012**, *41*, 12329–12345.
- (5) (a) Galluzzi, L.; Senovilla, L.; Vitale, I.; Michels, J.; Martins, I.; Kepp, O.; Castedo, M.; Kroemer, G. Molecular mechanisms of cisplatin resistance. *Oncogene* **2012**, *31*, 1869–1883. (b) Wexselblatt, E.; Yavin, E.; Gibson, D. Cellular interactions of platinum drugs. *Inorg. Chim. Acta* **2012**, *393*, 75–83.
- (6) (a) Graf, N.; Lippard, S. J. Redox activation of metal-based prodrugs as a strategy for drug delivery. *Adv. Drug Delivery Rev.* **2012**, *64*, 993–1004. (b) Pathak, R. K.; Marrache, S.; Choi, J. H.; Berding, T. B.; Dhar, S. The Prodrug Platin-A: Simultaneous Release of Cisplatin and Aspirin. *Angew. Chem., Int. Ed.* **2014**, *53*, 1963–1967. (c) Cheng, Q.; Shi, H.; Wang, H.; Min, Y.; Wang, J.; Liu, Y. The ligation of aspirin to cisplatin demonstrates significant synergistic effects on tumor cells. *Chem. Commun.* **2014**, *50*, 7427–7430. (d) Gabano, E.; Ravera, M.; Osella, D. Pros and cons of bifunctional platinum(IV) antitumor prodrugs: two are (not always) better than one. *Dalton Trans* **2014**, *43*, 9813–9820. (e) Butler, J. S.; Sadler, P. J. Targeted delivery of platinum-based anticancer complexes. *Curr. Opin. Chem. Biol.* **2013**, *17*, 175–188.
- (7) (a) Wexselblatt, E.; Yavin, E.; Gibson, D. Platinum(IV) Prodrugs with Haloacetato Ligands in the Axial Positions can Undergo Hydrolysis under Biologically Relevant Conditions. *Angew. Chem., Int. Ed.* **2013**, *52*, 6059–6062. (b) Ritacco, I.; Mazzone, G.; Russo, N.; Sicilia, E. Investigation of the Inertness to Hydrolysis of Platinum(IV) Prodrug. *Inorg. Chem.* **2016**, *55*, 1580–1586. (c) Bradáč, O.; Zimmermann, T.; Burda, J. V. Can Satraplatin be hydrated before the reduction process occurs? The DFT computational study. *J. Mol. Model.* **2013**, *19*, 4669–4680.
- (8) (a) Nemirovski, A.; Kasherman, Y.; Tzaraf, Y.; Gibson, D. Reduction of cis,trans,cis-[PtCl₂(OCOCH₃)₂(NH₃)₂] by aqueous extracts of cancer cells. *J. Med. Chem.* **2007**, *50*, 5554–5556. (b) Jungwirth, U.; Kowol, C. R.; Keppler, B. K.; Hartinger, C. G.; Berger, W.; Heffeter, P. Anticancer activity of metal complexes: involvement of redox processes. *Antioxid. Redox Signaling* **2011**, *15*, 1085–1127. (c) Lasorsa, A.; Stuchlikova, O.; Brabec, V.; Natile, G.; Arnesano, F. Activation of Platinum(IV) Prodrugs by Cytochrome c and Characterization of the Protein Binding Sites. *Mol. Pharmaceutics* **2016**, *13*, 3216–3223.
- (9) Choi, S.; Filotto, C.; Bisanzo, M.; Delaney, S.; Lagasee, D.; Whitworth, J. L.; Jusko, A.; Li, C. R.; Wood, N. A.; Willingham, J.; Schwenker, A.; Spaulding, K. Reduction and Anticancer Activity of Platinum(IV) Complexes. *Inorg. Chem.* **1998**, *37*, 2500–2504.
- (10) (a) Lemma, K.; Sargeson, A. M.; Elding, L. I. Kinetics and mechanism for reduction of oral anticancer platinum(IV) dicarboxylate compounds by L-ascorbate ions. *J. Chem. Soc., Dalton Trans.* **2000**, 1167–1172. (b) Lemma, K.; House, D. A.; Retta, N.; Elding, L. I. Kinetics and mechanism for reduction of halo- and haloam(m)ine platinum(IV) complexes by L-ascorbate. *Inorg. Chim. Acta* **2002**, *331*, 98–108.
- (11) (a) Nemirovski, A.; Vinograd, I.; Takroui, K.; Mijovilovich, A.; Rempel, A.; Gibson, D. New reduction pathways for ctc-[PtCl₂(CH₃CO₂)₂(NH₃)(Am)] anticancer prodrugs. *Chem. Commun.* **2010**, *46*, 1842–1844. (b) Zhang, J. Z.; Wexselblatt, E.; Hambley, T. W.; Gibson, D. Pt(IV) analogs of oxaliplatin that do not follow the expected correlation between electrochemical reduction potential and rate of reduction by ascorbate. *Chem. Commun.* **2012**, *48*, 847–849.

(c) Wexselblatt, E.; Gibson, D. What do we know about the reduction of Pt(IV) pro-drugs? *J. Inorg. Biochem.* **2012**, *117*, 220–229.

(12) Sinesi, M.; Intini, F. P.; Natile, G. Dependence of the reduction products of platinum(IV) prodrugs upon the configuration of the substrate, bulk of the carrier ligands, and nature of the reducing agent. *Inorg. Chem.* **2012**, *51*, 9694–9704.

(13) (a) Varbanov, H. P.; Valiahdhi, S. M.; Kowol, C. R.; Jakupec, M. A.; Galanski, M.; Keppler, B. K. Novel tetracarboxylatoplatinum(IV) complexes as carboplatin prodrugs. *Dalton Trans* **2012**, *41*, 14404–14415. (b) Pichler, V.; Göschl, S.; Meier, S. M.; Roller, A.; Jakupec, M. A.; Galanski, M.; Keppler, B. K. Bulky N,N-(di)alkylethane-1,2-diamineplatinum(II) Compounds as Precursors for Generating Unsymmetrically Substituted Platinum(IV) Complexes. *Inorg. Chem.* **2013**, *52*, 8151–8162. (c) Chen, C. K. J.; Zhang, J. Z.; Aitken, J. B.; Hambley, T. W. Influence of Equatorial and Axial Carboxylato Ligands on the Kinetic Inertness of Platinum(IV) Complexes in the Presence of Ascorbate and Cysteine and within DLD-1 Cancer Cells. *J. Med. Chem.* **2013**, *56*, 8757–8764. (d) Pichler, V.; Göschl, S.; Schreiber-Brynzak, E.; Jakupec, M. A.; Galanski, M.; Keppler, B. K. Influence of reducing agents on the cytotoxic activity of platinum(IV) complexes: induction of G₂/M arrest, apoptosis and oxidative stress in A2780 and cisplatin resistant A2780cis cell lines. *Metallomics* **2015**, *7*, 1078–1090.

(14) (a) Hall, M. D.; Hambley, T. W. Platinum(IV) antitumor compounds: their bioinorganic chemistry. *Coord. Chem. Rev.* **2002**, *232*, 49–67. (b) Reisner, E.; Arion, V. B.; Keppler, B. K.; Pombeiro, A. J. L. Electron-transfer activated metal-based anticancer drugs. *Inorg. Chim. Acta* **2008**, *361*, 1569–1583.

(15) Weaver, E. L.; Bose, R. N. Platinum(II) catalysis and radical intervention in reductions of platinum(IV) antitumor drugs by ascorbic acid. *J. Inorg. Biochem.* **2003**, *95*, 231–239.

(16) Ejeji, Z.; Ariafard, A. A computational mechanistic investigation into the reduction of Pt(IV) prodrugs with two axial chlorides by biological reductants. *Chem. Commun.* **2017**, *53*, 1413–1416.

(17) McCormick, M. C.; Keijzer, K.; Polavarapu, A.; Schultz, F. A.; Baik, M. H. Understanding Intrinsically Irreversible, Non-Nernstian, Two-Electron Redox Processes: A Combined Experimental and Computational Study of the Electrochemical Activation of Platinum(IV) Antitumor Prodrugs. *J. Am. Chem. Soc.* **2014**, *136*, 8992–9000.

(18) Ponte, F.; Russo, N.; Sicilia, E. Insights from Computations on the Mechanism of Reduction by Ascorbic Acid of Pt^{IV} Prodrugs with Asplatin and Its Chlorido and Bromido Analogues as Model Systems. *Chem. - Eur. J.* **2018**, *24*, 9572–9580.

(19) (a) Zhang, J. Z.; Wexselblatt, E.; Hambley, T. W.; Gibson, D. Pt(IV) analogs of oxaliplatin that do not follow the expected correlation between electrochemical reduction potential and rate of reduction by ascorbate. *Chem. Commun.* **2012**, *48*, 847–849. (b) Dong, J.; Ren, Y.; Huo, S.; Shen, S.; Xu, J.; Tian, H.; Shi, T. Reduction of ormaplatin and cis-diamminetetrachloroplatinum(IV) by ascorbic acid and dominant thiols in human plasma: kinetic and mechanistic analyses. *Dalton Trans* **2016**, *45*, 11326–11337.

(20) Šebesta, F.; Baxová, K.; Burda, J. V. Redox Potentials for Tetraplatin, Satraplatin, Its Derivatives and Ascorbic Acid; Computational Study. *Inorg. Chem.* **2018**, *57*, 951–962.

(21) Tolbatov, I.; Coletti, C.; Marrone, A.; Re, N. Insight into the Electrochemical Reduction Mechanism of Pt(IV) Anticancer Complexes. *Inorg. Chem.* **2018**, *57*, 3411–3419.

(22) Šebesta, F.; Burda, J. V. Interactions of Ascorbic Acid with Satraplatin and Its Trans Analog JMS76; DFT Computational Study'. *Eur. J. Inorg. Chem.* **2018**, *2018*, 1481–1491.

(23) Gramatica, P.; Papa, E.; Luini, M.; Monti, E.; Gariboldi, M. B.; Ravera, M.; Gabano, E.; Gaviglio, L.; Osella, D. Antiproliferative Pt(IV) complexes: synthesis, biological activity, and quantitative structure-activity relationship modeling. *JBIC, J. Biol. Inorg. Chem.* **2010**, *15*, 1157–1169.

(24) Schröder, D.; Shaik, S.; Schwarz, H. Two-State Reactivity as a New Concept in Organometallic Chemistry. *Acc. Chem. Res.* **2000**, *33*, 139–145.

(25) Frisch, M. J.; Trucks, G. W.; Schlegel, H. B.; Scuseria, G. E.; Robb, M. A.; Cheeseman, J. R.; Scalmani, G.; Barone, V.; Mennucci, B.; Petersson, G. A.; Nakatsuji, H.; Caricato, M.; Li, X.; Hratchian, H. P.; Izmaylov, A. F.; Bloino, J.; Zheng, G.; Sonnenberg, J. L.; Hada, M.; Ehara, M.; Toyota, K.; Fukuda, R.; Hasegawa, J.; Ishida, M.; Nakajima, T.; Honda, Y.; Kitao, O.; Nakai, H.; Vreven, T.; Montgomery, Jr., J. A.; Peralta, J. E.; Ogliaro, F.; Bearpark, M.; Heyd, J. J.; Brothers, E.; Kudin, K. N.; Staroverov, V. N.; Keith, T.; Kobayashi, R.; Normand, J.; Raghavachari, K.; Rendell, A.; Burant, J. C.; Iyengar, S. S.; Tomasi, J.; Cossi, M.; Rega, N.; Millam, J. M.; Klene, M.; Knox, J. E.; Cross, J. B.; Bakken, V.; Adamo, C.; Jaramillo, J.; Gomperts, R.; Stratmann, R. E.; Yazyev, O.; Austin, A. J.; Cammi, R.; Pomelli, C.; Ochterski, J. W.; Martin, R. L.; Morokuma, K.; Zakrzewski, V. G.; Voth, G. A.; Salvador, P.; Dannenberg, J. J.; Dapprich, S.; Daniels, A. D.; Farkas, O.; Foresman, J. B.; Ortiz, J. V.; Cioslowski, J.; Fox, D. J. *Gaussian 09*, Revision D.01; Gaussian, Inc.: Wallingford CT, 2010.

(26) Becke, A. D. Density-functional thermochemistry. III. The role of exact exchange. *J. Chem. Phys.* **1993**, *98*, 5648–5652.

(27) Lee, C.; Yang, W.; Parr, R. G. Development of the Colle-Salvetti correlation-energy formula into a functional of the electron density. *Phys. Rev. B: Condens. Matter Mater. Phys.* **1988**, *37*, 785–789.

(28) Grimme, S.; Antony, J.; Ehrlich, S.; Krieg, H. A consistent and accurate ab initio parameterization of density functional dispersion correction (DFT-D) for the 94 elements H-Pu. *J. Chem. Phys.* **2010**, *132*, 154104–154122.

(29) Andrae, D.; Häussermann, U.; Dolg, M.; Stoll, H.; Preuss, H. Energy-adjusted ab initio pseudopotentials for the second and third row transition elements. *Theor. Chim. Acta* **1990**, *77*, 123–141.

(30) (a) Fukui, K. Formulation of the reaction coordinate. *J. Phys. Chem.* **1970**, *74*, 4161–4163. (b) Gonzalez, C.; Schlegel, H. B. An improved algorithm for reaction path following. *J. Chem. Phys.* **1989**, *90*, 2154–2161.

(31) Harvey, J. N.; Aschi, M.; Schwarz, H.; Koch, W. The Singlet and Triplet States of Phenyl Cation. A Hybrid Approach for Locating Minimum Energy Crossing Points between Non-interacting Potential Energy Surfaces. *Theor. Chem. Acc.* **1998**, *99*, 95–99.

(32) Gannon, K. L.; Blitz, M. A.; Liang, C.-H.; Pilling, M. J.; Seakins, P. W.; Glowacki, D. R.; Harvey, J. N. An experimental and theoretical investigation of the competition between chemical reaction and relaxation for the reactions of ICH₂ with acetylene and ethene: implications for the chemistry of the giant planets. *Faraday Discuss.* **2010**, *147*, 173–188.

(33) Plane, J. M. C.; Whalley, C. L.; Frances-Soriano, L.; Goddard, A.; Harvey, J. N.; Glowacki, D. R.; Viggiano, A. A. O₂(a¹Δg) + Mg, Fe, and Ca: Experimental kinetics and formulation of a weak collision, multiwell master equation with spin-hopping. *J. Chem. Phys.* **2012**, *137*, 014310–20.

(34) (a) Miertuš, S.; Scrocco, E.; Tomasi, J. Electrostatic interaction of a solute with a continuum. A direct utilization of AB initio molecular potentials for the prevision of solvent effects. *Chem. Phys.* **1981**, *55*, 117–129. (b) Miertuš, S.; Tomasi, J. Approximate evaluations of the electrostatic free energy and internal energy changes in solution processes. *Chem. Phys.* **1982**, *65*, 239–245. (c) Pascual-Ahuir, J. L.; Silla, E.; Tuñón, I. GEPOL: An improved description of molecular surfaces. III. A new algorithm for the computation of a solvent-excluding surface. *J. Comput. Chem.* **1994**, *15*, 1127–1138.

(35) McQuarrie, D. A.; Simon, J. D. *Molecular Thermodynamics*; University Science Books: Sausalito, CA, 1999.

(36) Ashcraft, R. W.; Raman, S.; Green, H. W. Ab initio aqueous thermochemistry: application to the oxidation of hydroxylamine in nitric acid solution. *J. Phys. Chem. B* **2007**, *111*, 11968–11983.

5.2 Theoretical exploration of the reduction reaction of monofunctional phenanthriplatin Pt(IV) prodrugs.

5.2.1 Introduction

Severe side effects and toxicity, due to high chemical reactivity and anticipated aquation, as well as inherent and acquired resistance to platinum treatment are some of the limitations associated to the use of classical FDA approved anticancer agents cisplatin, carboplatin and oxaliplatin. In order to overcome these shortcomings, alternative metal-based therapeutics are being developed.¹⁻⁵

Combining two of the new previously discussed approaches, a Pt(IV) complex of a monofunctional platinum complex is reported.⁶

Unlike traditional bifunctional platinum compounds, monofunctional complexes are able to form only a single covalent bond with nuclear DNA and, therefore, do not typically cause bending or unwinding of its structure. Phenanthriplatin, $\text{Pt}(\text{NH}_3)_2(\text{phenanthridine})\text{Cl}^+$, a cationic monofunctional platinum complex that has been synthesized by replacing one of the chlorido ligands with a sterically hindered phenanthridine group,⁷ is actually intensively investigated as it appears to be considerably more active than cisplatin and more potent than analogous monofunctional Pt-based complexes. On the other hand, the advantages in the use of platinum compounds having a Pt(IV) core, instead, rely on their inertness and stability in the bloodstream so reducing the incidence of undesired toxic side effects and allowing for oral administration.

Phenanthriplatin(IV) has been proposed as a prodrug that has been prepared by tethering to the metal center carboxylate ligands, which have to be released upon reduction by cellular reducing agents when the drug enters the cell releasing the monofunctional phenanthriplatin in its Pt(II) form.

The key step of the mechanism of action (MoA) of Pt(IV) prodrugs is the reductive elimination, which allows the release of the corresponding four-coordinate active Pt(II) species, a great deal of attention has been devoted to the theoretical and experimental investigation of such process.

5.2.2 Aim of study

Our aim is to undergo a computational DFT investigation of the reduction process of Pt(IV) phenanthriplatin derivatives, one having in axial position a hydroxido and an acetate, named PhenPt(IV)(OH)(OAc) and one having two acetate ligands, named PhenPt(IV)(OAc)₂ using the ascorbic acid in its monodeprotonated form (AscH⁻) as reducing agent model.

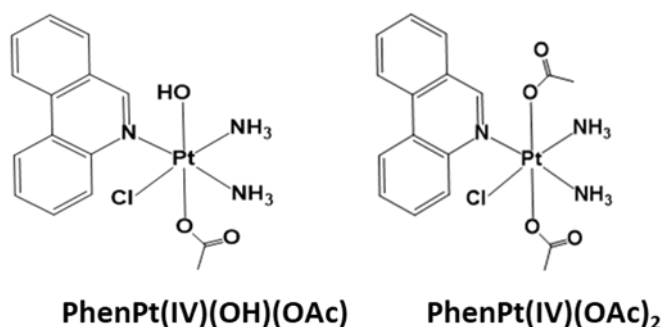


Figure 5.2 Chemical structure of the two studied complexes PhenPt(IV)(OH)(OAc) and PhenPt(IV)(OAc)₂

According to previous investigations, for the inner-sphere reduction the ligand-bridged-H transfer, that is a H- unit transfer from the OH group of the ascorbate to the axial ligand and the enolate β -carbon attack, involving the attack of the carbon of the monodeprotonated form of ascorbic acid to the axial ligand, have been studied.

The influence of several possible arrangements of reacting Pt(IV) prodrugs and the reducing agents as well as site of attack can have on the rate of the reduction reaction has been studied.

5.2.3 Highlighting results

The most relevant conclusion concerning the inner-sphere mechanism is that, in analogy with previously examined cisplatin and oxaliplatin Pt(IV) prodrugs the heights of the calculated barriers are low, especially for the asymmetric hydroxido acetato exa-coordinated complex and reduction appears to be facile.

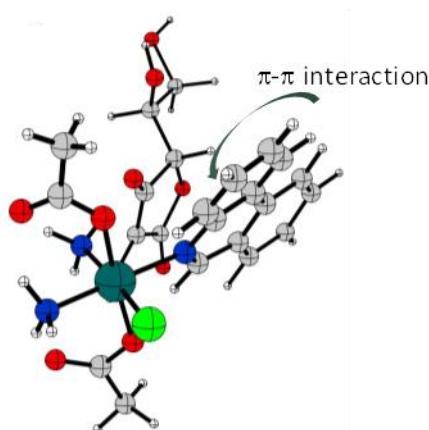


Figure 5.3 A representation of the π - π interaction created between the AscH⁻ and PhenPt(IV)(OAc)₂

The presence of the sterically hindered phenanthridine ligand does not influence the course of the reaction except that for the possibility that π - π interactions are established between the ligand and the ascorbate (**Figure 5.3**). When such interactions can be created during the reaction, the effect on the reduction rate is opposite for the examined complexes. Indeed, for the asymmetric complex the heights increase and decrease for the symmetric one.

References

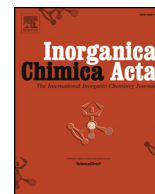
- 1) L. Kelland, Nat. Rev. Cancer 7 (2007) 573-584.
- 2) A. Horwich, J. Shipley, R. Huddart, Lancet 367 (2006) 754-765.
- 3) J. C. Timothy, K. Suntharalingam, S. J. Lippard, Chem. Rev. 116 (2016) 3436-3486.

- 4) K. Cheung-Ong, G. Giaever, C. Nislow, *Chem Biol.* 20 (2013) 648-659.
- 5) A. Ruggiero, G. Trombatore, S. Triarico, R. Arena, P. Ferrara, M. Scalzone, F. Pierri, R. Riccardi, *Drugs* 24 (2013) 1007-1019.
- 6) B. Teng, Y. Han, X. Zhang, H. Xiao, C. Yu, H. Li, Z. Cheng, D. Jin, P. Ma, K. L. Wong J. Lin, *J. Mater. Chem. B*, **2018**, 6, 5059-5068.
- 7) G. Y. Park, J. J. Wilson, Y. Song, S. J. Lippard, *PNAS*, **2012**, 109, 11987-11992.

Paper IV

Theoretical exploration of the reduction reaction of monofunctional phenanthriplatin Pt(IV) prodrugs.

E. Dabbish, D. Imbardelli, N. Russo, E. Sicilia, *Inorganica Chimica Acta*, **2019**, 118951.



Theoretical exploration of the reduction reaction of monofunctional phenanthriplatin Pt(IV) prodrugs



Eslam Dabbish, Daniela Imbardelli, Nino Russo, Emilia Sicilia*

Dipartimento di Chimica e Tecnologie Chimiche, Università della Calabria, 87036 Rende, CS, Italy

ARTICLE INFO

Keywords:

DFT
Phenanthriplatin (IV) prodrugs
Reduction reaction
Ascorbic acid reductant

ABSTRACT

Phenanthriplatin is a cationic monofunctional anticancer agent derived from cisplatin, with a phenanthridine ligand instead of a chlorido one, that has shown significantly enhanced cytotoxic activity compared to its parent complex. Moreover, phenanthriplatin has been derivatized to its prodrug using carboxylate ligands in the axial positions to decrease side effects and improve the therapeutic index. Here are reported the results of a computational investigation of the key step of the mechanism of action of Pt(IV) prodrugs, that is activation by reduction leading to the release of the active Pt(II) species. Results of both inner-sphere reduction mechanism exploration and quantum-mechanical calculation of the reduction potentials are reported. Only one of the two enantiomeric forms of Phenanthriplatin, originating from the asymmetry of the phenanthridine ligand, has been taken into consideration. For such isomer the influence that several possible arrangements of reacting Pt(IV) prodrugs and the monodeprotonated ascorbic acid reducing agent as well as site of attack can have on the rate of the reduction reaction has been studied. It is worth underscoring that the presence of the sterically hindered phenanthridine ligand does not influence the course of the reaction except that for the possibility that π - π interactions are established between the ligand and the ascorbate.

1. Introduction

Cisplatin, carboplatin, and oxaliplatin, are the platinum(II) anticancer drugs approved by the Food and Drug Administration (FDA) widely used to treat and manage cancer [1–3]. Nevertheless, severe side effects and toxicity, due to high chemical reactivity and anticipated aquation, are associated to the use of such anticancer agents, as well as inherent and acquired resistance to platinum treatment [4,5] requiring the development of new compounds that operate with novel mechanisms of action. In order to overcome these shortcomings, alternative metal-based therapeutics are being developed. Current research efforts are focused on a variety of non-classical metal anticancer drug candidates [3,6–8], including non-platinum complexes, Pt(IV) compounds, multinuclear compounds, and monofunctional Pt(II) complexes. Monofunctional platinum complexes have emerged as a promising class of non-classical platinum drug candidates [9–11] that, unlike traditional bifunctional platinum compounds, are able to form only a single covalent bond with nuclear DNA and, therefore, do not typically cause bending or unwinding of its structure. The advantages in the use of platinum compounds having a Pt(IV) core, instead, rely on their inertness and stability in the bloodstream so reducing the incidence of undesired toxic side effects and allowing for oral administration

[3,12–14]. Since the key step of the mechanism of action (MoA) of Pt(IV) prodrugs is the reductive elimination, which allows the release of the corresponding four-coordinate active Pt(II) species, a great deal of attention has been devoted to the theoretical and experimental investigation of such process [15–19]. Phenanthriplatin, $\text{Pt}(\text{NH}_3)_2(\text{phenanthridine})\text{Cl}^+$, a cationic monofunctional platinum complex that has been synthesized by replacing one of the chlorido ligands with a sterically hindered phenanthridine group [10], is actually intensively investigated as it appears to be considerably more active than cisplatin and more potent than analogous monofunctional Pt-based complexes. Very recently, an anticancer drug delivery system based on phenanthriplatin(IV) has been proposed aiming at increasing the cytotoxicity of the drug [20]. Phenanthriplatin(IV) prodrug has been prepared by tethering to the metal center carboxylate ligands, which have to be released upon reduction by cellular reducing agents when the drug enters the cell. The mechanism by which such prodrugs are reduced, as already underlined, is still matter of debate and seems to change as a function of the nature of both axial and equatorial ligands. In particular, for the equatorial ligands the steric hindrance can significantly influence the course of the reduction reaction [21]. Here are reported the outcomes of a computational DFT investigation of the reduction process of Pt(IV) Phenanthriplatin derivatives using the

* Corresponding author.

E-mail address: siciliae@unical.it (E. Sicilia).

<https://doi.org/10.1016/j.ica.2019.06.002>

Received 14 April 2019; Received in revised form 29 May 2019; Accepted 3 June 2019

Available online 04 June 2019

0020-1693/© 2019 Elsevier B.V. All rights reserved.

ascorbic acid in its monodeprotonated form (AsCH^-) as reducing agent model.

2. Computational details

Gaussian 09 suite of programs [22], has been employed to carry out all calculations in the framework of the density functional theory employing the hybrid Becke three-parameter exchange functional [23] and the Lee–Yang–Parr correlation functional, B3LYP [24]. Dispersion corrections for nonbonding interaction have been included through the Grimme approach using atom pair-wise additive schemes [25], denoted as DFT-D3 method.

The relativistic compact Stuttgart/Dresden effective core potential has been used for the Pt atom [26], along with the split valence basis set. The standard triple- ζ quality 6-311 + G** basis sets of Pople and coworkers have been used for the atoms directly participating in the process, whereas in order to reduce the computational effort, the 6-311G** basis sets have been employed for peripheral atoms.

Vibrational frequencies at the same level of theory have been calculated for both establishing the nature of intercepted stationary points as minima and transition states and calculating zero-point energy (ZPE) and Gibbs free energy corrections. The intercepted transition states are first order saddle points on a potential energy surface (PES) and their vibrational spectrum is characterized by one imaginary frequency, corresponding to a negative force constant, which means that in one direction, in the nuclear configuration space, the energy has a maximum, while in all the other directions the energy has a minimum. Furthermore, transition states have been carefully checked to be properly connected to the correct minima by IRC (intrinsic reaction coordinate) analysis [27,28].

The Tomasi's implicit Polarizable Continuum Model (PCM) [29–31] as implemented in Gaussian09 has been used to include the effects due to the presence of the solvent and the UFF set of radii has been used to build-up the cavity in which the solute molecules are accommodated. Solvation Gibbs free energies have been calculated performing single-point calculations for all *in vacuo* stationary points structures in implicit water ($\epsilon = 78.4$) at the same level of theory. Enthalpies and Gibbs free energies have been obtained using standard statistical procedures [32] at 298 K and 1 atm from total energies, including zero-point, thermal and solvent corrections. As the free energy corrections in the Gaussian's default standard state corresponds to an ideal gas at a standard pressure of 1 atm, the computed free energies have been converted [33] to yield Gibbs energies with a solution phase standard state of 1 mol L⁻¹ for all the species except water solvent. For water molecules a standard state of 55.5 M has been used. That is, to the free energy of each species, as computed in Gaussian, a free energy correction term equal to $RT \ln(V_{\text{molar gas}}/V_{\text{molar solution}})$, (R = gas constant, T = absolute temperature) has been added, where $V_{\text{molar gas}}$ is the volume occupied by one mole of ideal gas at the considered temperature, and $V_{\text{molar solution}}$ is the volume occupied by one mole of species in a standard solution of concentration 1 mol L⁻¹.

3. Results and discussion

Previous theoretical investigations, dealing with the mechanism of reduction of Pt(IV) prodrugs into corresponding Pt(II) complexes occurring inside the cell, [10,18,19,21,34,35] have demonstrated that the usually invoked classification into inner- and outer-sphere mechanisms does not properly account for all the viable alternatives, that depend on the nature of, principally, the axial and, less, the equatorial ligands. Therefore, the propensity of Pt(IV) prodrugs to be reduced can be modulated by properly choosing ligands. Both theoretical and experimental studies have demonstrated that, in some cases, prodrugs stability should be even increased and reduction rate decreased to avoid premature extracellular reduction [21,36]. Moreover, the synthesis of asymmetric Pt(IV) prodrugs can represent a means for ascribing to the

prodrugs specific properties as a consequence of the presence of two different ligands. Here, it has been computationally investigated the reduction process of two Pt(IV) Phenanthriplatin derivatives (see Scheme): one having in axial position a hydroxido and an acetate, named **PhenPt(IV)(OH)(OAc)** and one having two acetate ligands, named **PhenPt(IV)(OAc)₂**.

Inner-sphere mechanistic alternatives can be classified as a) *ligand-bridged* when one of the axial ligands is able to form a bridge between the Pt(IV) center and the reductant mediating the flow of the electrons, b) *ligand-bridged-H transfer* if the two-electron reduction occurs through a H⁻ unit transfer from the OH group of the ascorbate to the axial ligand and c) *enolate β -carbon attack* that involves the nucleophilic attack of the enolate β -carbon of the ascorbate on the axial ligand. The inner-sphere, in its different mechanistic alternatives, seems to be the preferred mode of reduction, when monoanionic ascorbate is the reducing agent. If the barrier that is necessary to surmount for the reduction to occur is too low these prodrugs can hardly reach the target before reduction and the reduction takes place extracellularly. Concerning the reduction process of the Pt(IV) Phenanthriplatin derivatives, on the basis of our previous experience [19,21], for the complex with two acetate axial ligands only the *ligand-bridged-H transfer* mechanism, that resulted to be the most viable for OAc, has been explored. For the complex having one OH and one OAc, both *ligand-bridged-H transfer* and *enolate β -carbon attack* mechanisms have been examined. We expect that the presence in equatorial position of the sterically hindered phenanthridine ligand, also able to establish π interactions, can influence the course of the reaction.

It is well known that, due to the asymmetry of the phenanthridine ligand about the platinum coordination plane, the complex exists in two enantiomeric forms [37]. However, as preliminary calculations have clearly demonstrated that pathways for the two isomers coincide, in terms of both structures and energies, only one of the two isomers has been taken into consideration. Therefore, for the isomer denoted as P, according to the conventions of axial chirality [37], several possible reciprocal orientations of the complex and the ascorbate anion have been examined, including the possibility that the π system of the phenanthridine ligand can interact with that of the ascorbate with the two cyclic moieties oriented parallel to each other.

3.1. Reduction of PhenPt(IV)(OH)(OAc) complex

The calculated energy profiles together with the structures of intercepted stationary points illustrating the ascorbate assisted inner-sphere reduction of the **PhenPt(IV)(OH)(OAc)** complex are reported in Fig. 1. The phenanthridine ligand is oriented perpendicular to the coordination plane of the Pt center. Therefore, due to the asymmetric structure of the phenanthridine ligand the two axial positions are not equivalent and for the P enantiomer two conformers have been investigated, one for the axial OH ligand lying above the coordination plane and the acetate below, denoted as **A**, and one for the two ligands exchanging their positions, denoted as **B**. In addition, for the *ligand-bridged-H transfer* mechanism, among all the possible different reciprocal orientations of the two reactants, only two are shown being those corresponding to different heights of the transition state barrier. Indeed, for both **A** and **B** isomers the ascorbate can assume, during the reaction, an orientation parallel to the phenanthridine ligand, due to the interaction between the π systems, or not as shown in Fig. 1. For all the isomers, in analogy with the mechanism previously described, the two-electron transfer occurs in one step through the shift of a H⁻ unit from the OH group of the ascorbate to the hydroxido ligand. The formed water molecule detaches and, simultaneously, the *trans*-acetate ligand is released and a dehydroascorbic acid molecule is formed. Formation of separated products is calculated to be exergonic in all cases, in an energy range going from 24.9 to 27.6 kcal mol⁻¹. What is worth mentioning is how the height of the energy barrier that is necessary to overcome for such Pt(IV) to Pt(II) reduction to occur changes

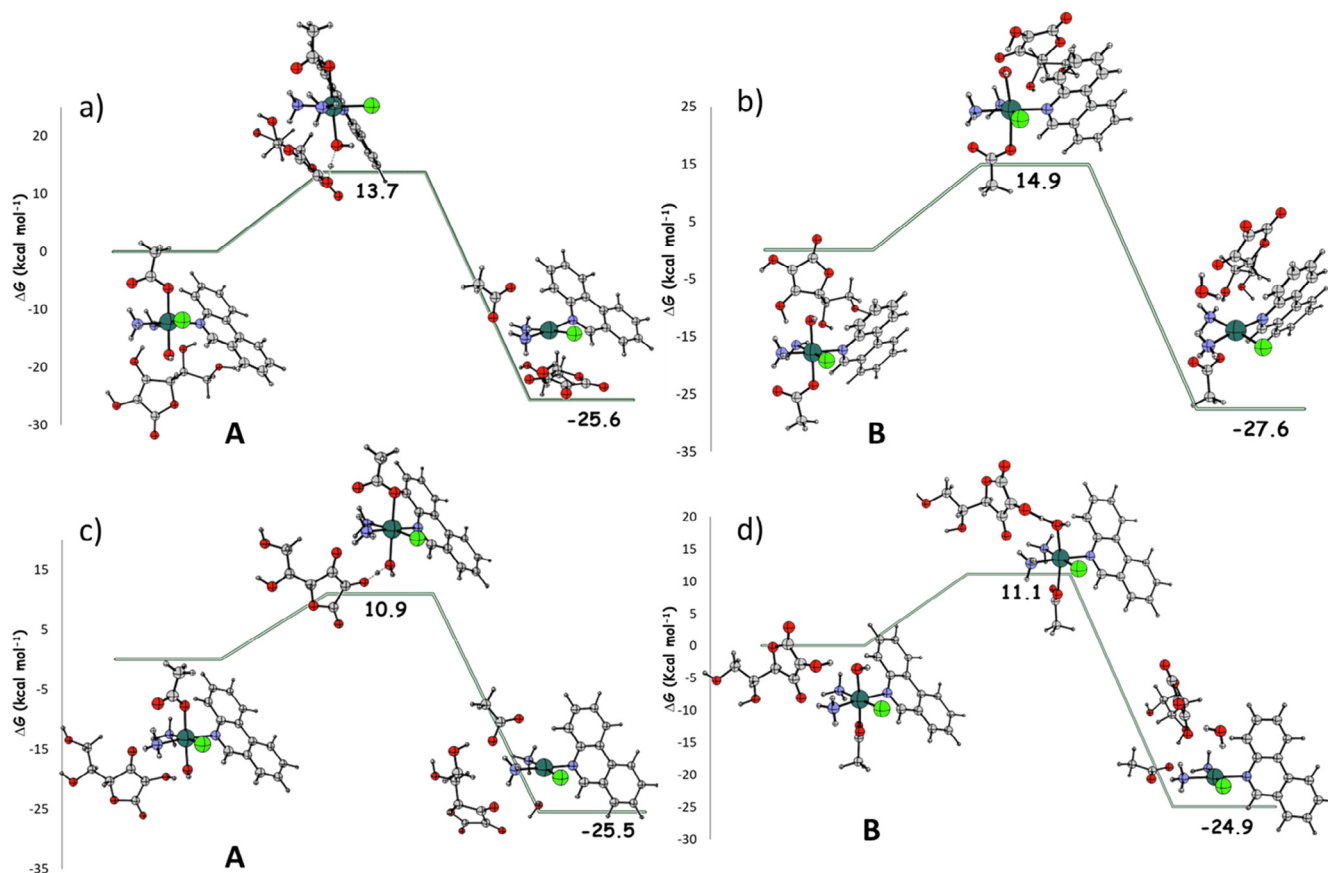


Fig. 1. Free energy profiles in water describing the *ligand-bridged-H transfer* mechanism in presence of ascorbate as reducing agent for the a) **A** and b) **B** isomers involving π - π interactions and c) **A** and d) **B** isomers not involving π - π interactions of the **PhenPt(IV)(OH)(OAc)** complex. Energies are in kcal mol^{-1} and relative to separated reactants.

if the π systems of the ascorbate and the phenanthridine ligand assume a parallel orientation with respect to each other. Indeed, it clearly appears, from Fig. 1, that the difference is not significant when the two isomers **A** and **B** are considered. Instead, for each of the two **A** or **B** isomers (Fig. 1a-c and 1b-1d) the ascorbate can approach the complex in such a way that in the transition state a π - π interaction is established that is conserved in the final products. Such arrangement is not accessible in the initial adduct, whereas in the transition state the ascorbate can be both oriented parallel to the phenanthridine ligand and in a proper position to transfer the H^+ unit to the OH ligand. The result is that the energy barrier for the corresponding transition states increases. For the **A** and **B** isomers the barriers are 13.7 and 14.9 kcal mol^{-1} , respectively that is 2.8 and 3.8 kcal mol^{-1} higher than the barriers for the same isomers when π interactions are not involved. The attention devoted to

this aspect derives from the hypotheses, even contradictory, which have been formulated [38,39] about the role that π - π stacking interactions can play in favoring or disfavoring the bond breaking and forming steps involved in the mechanism of action of phenanthriplatin and analogous monofunctional Pt complexes having ligands with less extended π systems. Low barriers correspond to a high propensity of the prodrug to be reduced and, as a consequence, to a low probability that it can reach intact the target before reduction takes place. Therefore, for the system under investigation the possibility to establish additional π interactions should be beneficial once it is assumed that such arrangement is accessible and more favorable in the real biological environment [39].

For the sake of completeness, also the *ligand-bridged-H transfer* mechanism involving the transfer of the H^+ unit from the ascorbate to the acetate ligand has been examined. Results can be found in the

Supplementary Data. Calculated barriers, as expected, are higher than those involved in the attack to the OH moiety due to the low lability of the *trans* hydroxido ligand. The low propensity of OH^- to be released is confirmed by the rearrangements occurring in the intercepted transition state structures. Indeed, the leaving hydroxido ligand, in all the examined cases, abstracts a proton from one of the coordinated ammonia molecules to form water.

The outcomes of the exploration of the mechanism denoted as *enolate β -carbon attack*, entailing the attack of the enolate β -carbon on the OH ligand, are reported in Fig. 2 for both **A** and **B** isomers. The nucleophilic attack of the ascorbate enolate β -carbon on the OH group leads to the formation of a new C-O bond and to the simultaneous release of the *trans* acetate ligand. For the **A** isomer, the intercepted concerted transition state is identified by an imaginary frequency of 1861 cm^{-1} corresponding to such rearrangement and the calculated barrier is 17.5 kcal mol^{-1} . The reaction is exergonic by 30.6 kcal mol^{-1} for the formation of the free active Pt(II) complex, the acetate and the geminal diol species from which a water molecule should be eliminated to generate the oxidized dehydroascorbic acid. In an analogous way the reaction takes place for the **B** isomer, being the height of the energy barrier 17.1 kcal mol^{-1} and 25.1 kcal mol^{-1} the energy released to form the final products. It is possible to conclude, then, that the enolate β -carbon attack, even if viable, is not the preferred one, in analogy with preceding investigations [19,21].

3.2. Reduction of **PhenPt(IV)(OAc)₂** complex

In this section the outcomes of the exploration of the pathways describing how the reduction of the **PhenPt(IV)(OAc)₂** complex should occur are reported. The only viable *ligand-bridged-H transfer* mechanism

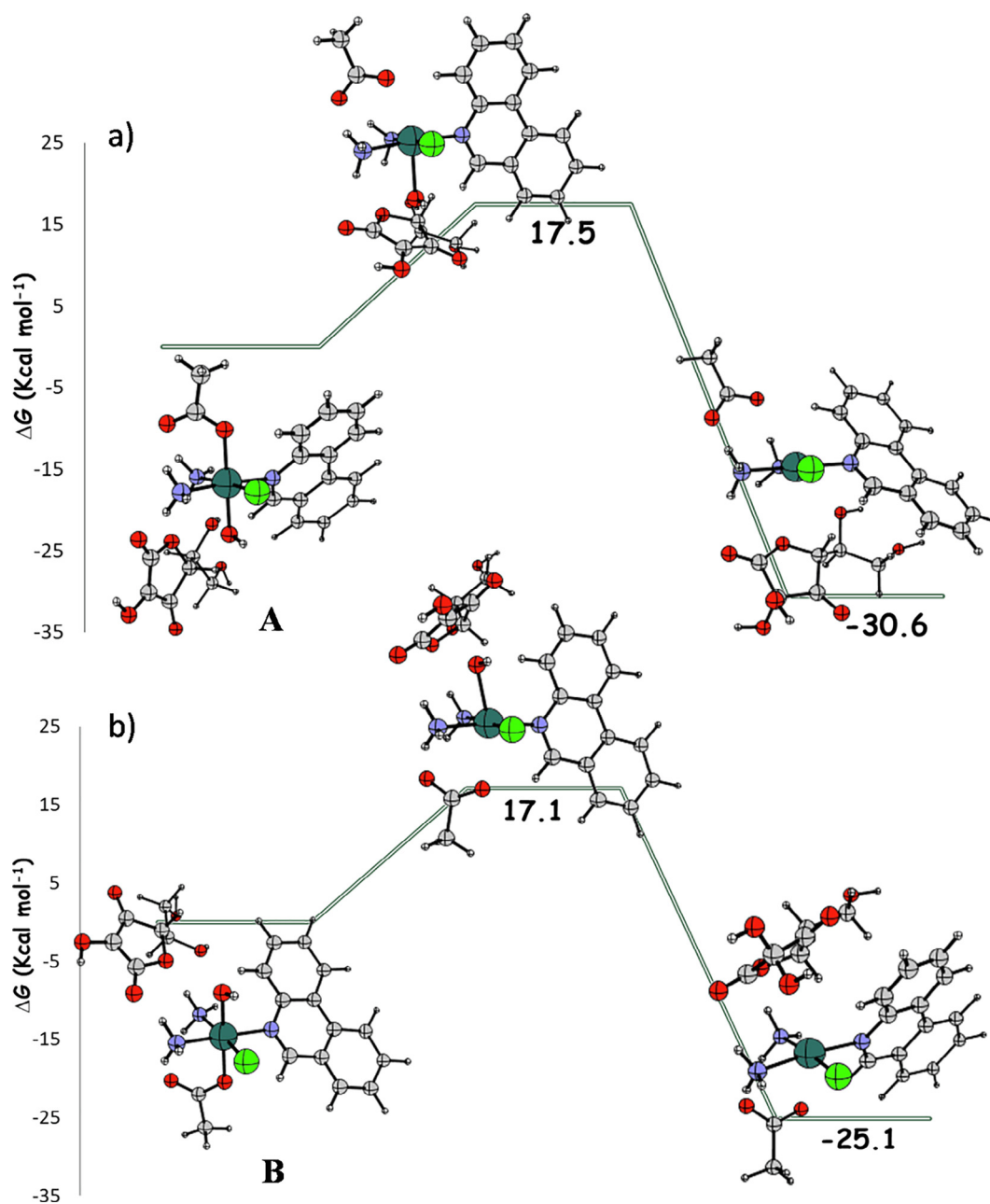
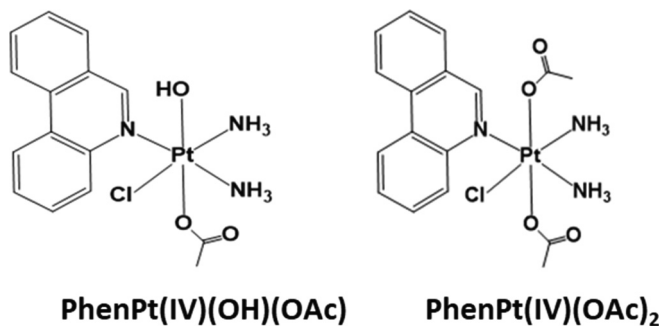
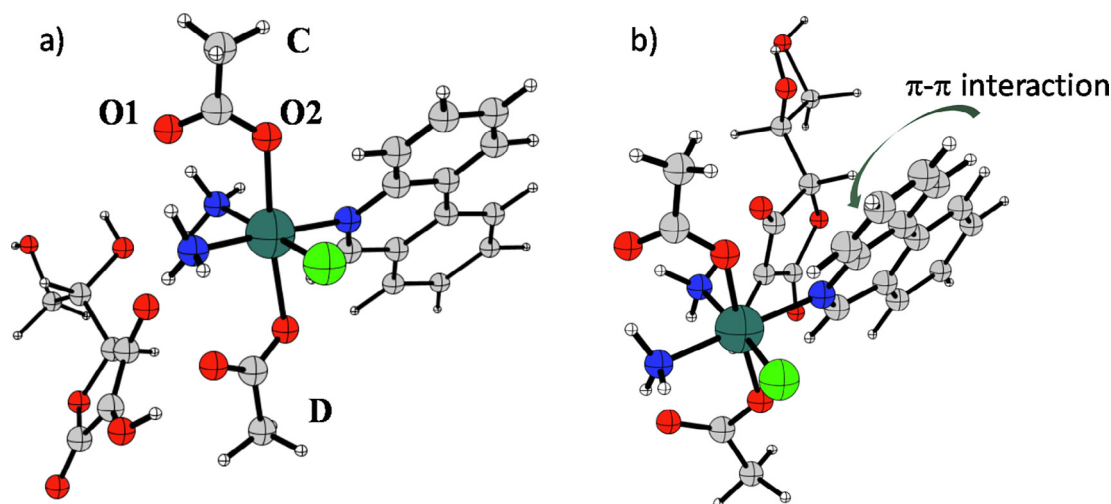


Fig. 2. Free energy profiles in water describing the *enolate* β -carbon attack mechanism in presence of ascorbate as reducing agent for a) A and b) B isomers of the $\text{PhenPt(IV)(OH)(OAc)}$ complex. Energies are in kcal mol^{-1} and relative to separated reactants.



Scheme 1. Phenanthriplatin Pt(IV) complexes investigated for reduction.

has been examined. In this case, owing again to the asymmetric nature of the phenanthridine ligand, the two acetate ligands are not equivalent and the H^+ transfer to both of them has been examined. The acetate coordinated above the Pt coordination plane is indicated as C and that below as D and Pt non-coordinated and coordinated oxygen atoms are labeled O1 and O2, respectively. In Scheme 1 the labels for the different possible arrangements precluding to the transfer of the H^+ unit to the acetates of the M isomer are shown. Moreover, as shown in Scheme 2 and illustrated in the previous paragraph, the π system of the ascorbate can be aligned parallel to the π system of the phenanthridine ligand. The reduction reaction, once the reactants are properly assembled, proceeds by the transfer of the H^- unit to one of the acetates above or below the coordination plane of platinum. The transfer can involve either the coordinated or the not coordinated oxygen atoms causing the simultaneous release of the *trans* ligand. The most significant results are summarized in Table 1, whereas energy profiles together with



Scheme 2. a) Labeling of isomers and oxygen atoms involved in the reduction reaction and b) optimized structure of an adduct showing π - π interactions.

Table 1

Activation free energies (ΔG^\ddagger) and reaction free energies (ΔG_R), in kcal mol⁻¹, calculated with respect initial adducts.

Side oxygen	ΔG^\ddagger (TS)	ΔG_R (Products)
C...O...1 π - π interaction	19.0	-16.3
D...O...1 π - π interaction	17.6	-17.7
D...O2... π - π interaction	17.0	-16.1
C...O1	21.2	-22.2
C...O2	20.6	-23.0
D...O1	24.9	-25.5
D...O2	23.6	-23.3

structures of intercepted minima and transition states are reported in the [Supplementary Data](#).

Reported energies, in kcal mol⁻¹, are relative energies calculated with respect to the zero reference energy of the adducts assembled by the ascorbate and phenanthriplatin(IV) complex reacting species.

At a first glance, from the data reported in [Table 1](#), it appears that the main difference in behavior exists between the adducts in which π - π interactions can be established and those that can be defined non-stacking adducts. With respect to the **PhenPt(IV)(OH)(OAc)** complex, the π - π interaction is established yet in the initial adducts and conserved in the transition states and products. For such stacking adducts, the energy barriers are lower and the reduction reactions are less exergonic, that is the products are less stabilized with respect the corresponding adducts zero reference energy. Differences are less significant if the H⁺ transfer to the acetate above or below the complex as well as the transfer to the coordinated or non-coordinated oxygen is taken into consideration.

Moreover, with respect to the asymmetric **PhenPt(IV)(OH)(OAc)** complex the reduction reaction is hampered by higher energy barriers for both stacking and non-stacking arrangements, reducing the risk for the prodrugs to be reduced before to reach the target.

Comparing these results with those of previous investigations of the reduction by ascorbic acid of cisplatin and oxaliplatin Pt(IV) prodrugs, it is confirmed that for the complex with an hydroxido axial ligand reduction is facile and even faster. For the symmetric complex with two acetato axial ligands barriers are comparable to those previously calculated.

The presence of the sterically hindered phenanthridine ligand does not influence the course of the reaction except that for the possibility that π - π interactions are established between the ligand and the ascorbate. When such interactions can be established during the course of the reaction, opposite trends are found. Indeed, for the asymmetric

PhenPt(IV)(OH)(OAc) complex the height of the barriers to overcome increases, whereas for the symmetric **PhenPt(IV)(OAc)₂** one the height decreases. Examining the structures of the located transition states these behaviors can be rationalized considering that for the **PhenPt(IV)(OAc)₂** complex such interactions facilitate an optimal arrangement of the ascorbate and the drug for the transfer of the H⁺ unit to the more preferred inner oxygen atom.

3.3. Quantum chemically calculated reduction potentials

The redox behavior of Pt(IV) prodrugs has been extensively investigated by using electrochemical approaches, mainly by cyclic voltammetry. Nevertheless, due to the irreversibility of the process, a standard redox potential cannot be obtained as the mid-point potential from a typical cyclic voltammogram of a chemically reversible process. The peak potential of the irreversible cathodic response is, therefore, used to approximate the ease of reduction of Pt(IV) complexes and to estimate reduction rates in solution even if it is well known that such potential does not depend only on the thermodynamics of reduction, but is influenced by other factors such as the energy barrier for the loss of the two axial ligands. It is, therefore, not surprisingly that redox potential does not always correlate with the rate of reduction of Pt(IV) complexes. A series of electrochemical experiments have been employed by Baik and collaborators to study the mechanism of Pt(IV) two electron reduction and to show that electron transfer and Pt-ligands bond cleavage occur in a stepwise fashion, thus suggesting the formation of a metastable six-coordinate Pt(III) intermediate as a consequence of the first electron addition. The authors have demonstrated that the redox potential value for the examined two-electron chemistry is dominated by the more difficult one-electron first reduction, whereas the second one-electron transfer corresponds to a more positive reduction potential not changing the value of the total reduction potential [17]. The adopted decomposition scheme allows the reduction potential to be calculated as the energy change that accompanies the first one-electron transfer for the reduction of the six-coordinate Pt(IV) complex to the corresponding six-coordinate Pt(III) as shown in [Scheme 2](#).

Such approach has been used to estimate the reduction potential of the Phenanthriplatin Pt(IV) derivatives investigated here. The following formula has been used: $E_{1st} = -\Delta G_{(sol)} - 4.43$ V, where $\Delta G_{(sol)}$ is the Gibbs free energy change in solution for the one electron transfer to the Pt(IV) complex and 4.43 V is the absolute potential of the standard hydrogen electrode (SHE) in water used as a reference. The values of the calculated redox potential are reported in [Table 2](#). The addition of one electron to the complexes under investigation here, does not cause

Table 2

Standard reduction potentials, in eV, calculated as the energy change that accompanies the first step one electron transfer for the reduction of the six-coordinate phenanthriplatin derivatives.

Complex	$\Delta G_{\text{(sol)}}$	$E_{1\text{st}}^{\circ}$
PhenPt(IV)(OH)(OAc) A	-4.332	-0.098
PhenPt(IV)(OH)(OAc) B	-4.358	-0.072
PhenPt(IV)(OAc) ₂	-4.602	0.172

the spontaneous detachment of one of the axial ligands confirming once again [19,21] that for acetate and hydroxido ligands the electrochemical and chemical events occur in two separate steps.

From the calculated standard reduction potentials the propensity of the examined complexes to be reduced can be estimated. The ease to be reduced considering an outer-sphere reduction mechanism increases when the OH ligand is substituted with the OAc one. Therefore, it is further confirmed that the rate of the reaction calculated by considering the height of the barriers for the inner-sphere mechanism does not correspond to the trend in redox potentials [19,21]. Such disagreement can explain why experimentally measured redox potentials do not always correlate with the rate of reduction [16,40,41]. It is also worth mentioning that for the two **A** and **B** isomers of the **PhenPt(IV)(OH)(OAc)** complex the values of the estimated redox potential are not exactly the same due to the slightly different electronic charge distribution.

4. Conclusions

The present paper reports the outcomes of a DFT computational exploration of the possibility to use Phenanthriplatin (IV) prodrugs as more inert complexes than Phenanthriplatin (II) and, therefore, able to decrease platinum deactivation in transit towards the tumor cells. Calculations have been carried out for two kinds of Phenanthriplatin (IV) derivatives: one asymmetric having in axial position a hydroxido and an acetate and one symmetric having two acetate ligands. Both inner- and outer-sphere mechanisms have been examined in presence of monodeprotonated ascorbic acid as reducing agent. According to previous investigations, for the inner-sphere reduction the ligand-bridged-H transfer, that is a H⁺ unit transfer from the OH group of the ascorbate to the axial ligand and the enolate β -carbon attack, involving the attack of the carbon of the monodeprotonated form of ascorbic acid to the axial ligand, have been studied. For the outer-sphere it has been considered that reduction can take place through a two steps electron transfer encompassing formation of a metastable six-coordinate Pt(III) intermediate. Only one of the two enantiomeric forms of Phenanthriplatin, originating from the asymmetry of the phenanthridine ligand, have been taken into consideration and for such isomer the influence that several possible arrangements of reacting Pt(IV) prodrugs and the reducing agents as well as site of attack can have on the rate of the reduction reaction has been studied. The most relevant conclusion concerning the inner-sphere mechanism is that, in analogy with previously examined cisplatin and oxaliplatin Pt(IV) prodrugs the heights of the calculated barriers are low, especially for the asymmetric hydroxido acetato exa-coordinated complex and reduction appears to be facile.

The presence of the sterically hindered phenanthridine ligand does not influence the course of the reaction except that for the possibility that π - π interactions are established between the ligand and the ascorbate. When such interactions can be created during the reaction, the effect on the reduction rate is opposite for the examined complexes. Indeed, for the asymmetric complex the heights increase and decrease for the symmetric one.

From the estimated reduction potentials, it results that the ease to be reduced following an outer-sphere reduction mechanism increases

when the OH ligand is substituted with the OAc one. According to previous investigations it is confirmed that the values of the reduction potentials do not correspond to the propensity to be reduced measured by the heights of the barriers that is necessary to overcome along an inner-sphere reduction pathway.

Acknowledgment

This work is supported by Universit  della Calabria.

Appendix A. Supplementary data

Supplementary data to this article can be found online at <https://doi.org/10.1016/j.ica.2019.06.002>.

References

- [1] L. Kelland, *Nat. Rev. Cancer* 7 (2007) 573–584.
- [2] A. Horwich, J. Shipley, R. Huddart, *Lancet* 367 (2006) 754–765.
- [3] J.C. Timothy, K. Suntharalingam, S.J. Lippard, *Chem. Rev.* 116 (2016) 3436–3486.
- [4] K. Cheung-Ong, G. Giaefer, C. Nislow, *Chem. Biol.* 20 (2013) 648–659.
- [5] A. Ruggiero, G. Trombatore, S. Triarico, R. Arena, P. Ferrara, M. Scalzone, F. Pierri, R. Riccardi, *Drugs* 24 (2013) 1007–1019.
- [6] A.G. Quiroga, *Curr. Top. Med. Chem.* 11 (2011) 2613–2622.
- [7] I. Romero-Canel n, P.J. Sadler, *Inorg. Chem.* 52 (2013) 12276–12291.
- [8] K. Wang, E. Gao, *Anticancer Agents Med. Chem.* 14 (2014) 147–169.
- [9] K.S. Lovejoy, R.C. Todd, S. Zhang, M.S. McCormick, J.A. D'Aquino, J.T. Reardon, A. Sancar, K.M. Giacomini, S.J. Lippard, *Proc. Natl. Acad. Sci. U.S.A.* 105 (2008) 8902–8907.
- [10] G.Y. Park, J.J. Wilson, Y. Song, S.J. Lippard, *Proc. Natl. Acad. Sci. U.S.A.* 109 (2012) (1992) 11987–11991.
- [11] L. Cerasino, F.P. Intini, J. Kobe, E. de Clercq, G. Natlie, *Inorg. Chim. Acta* 344 (2003) 174–182.
- [12] M.D. Hall, T.W. Hambley, *Coord. Chem. Rev.* 232 (2002) 49–67.
- [13] E. Wexselblatt, D. Gibson, *J. Inorg. Biochem.* 117 (2012) 220–229.
- [14] G. Ermondi, G. Caron, M. Ravera, E. Gabano, S. Bianco, J.A. Platts, D. Osella, *Dalton Trans.* 42 (2013) 3482–3489.
- [15] E.L. Weaver, R.N. Bose, *J. Inorg. Biochem.* 95 (2003) 231–239.
- [16] J.Z. Zhang, E. Wexselblatt, T.W. Hambley, D. Gibson, *Chem. Commun.* 48 (2012) 847–849.
- [17] M.C. McCormick, K. Keijzer, A. Polavarapu, F.A. Schultz, M.H. Baik, *J. Am. Chem. Soc.* 136 (2014) 8992–9000.
- [18] Z. Ejechia, A. Ariafard, *Chem. Commun.* 53 (2017) 1413–1416.
- [19] F. Ponte, N. Russo, E. Sicilia, *Chem. Eur. J.* 24 (2018) 9572–9580.
- [20] B. Teng, Y. Han, X. Zhang, H. Xiao, C. Yu, H. Li, Z. Cheng, D. Jin, P. Ma, K.L. Wong, *J. Lin. J. Mater. Chem. B* 6 (2018) 5059–5068.
- [21] E. Dabbish, F. Ponte, N. Russo, E. Sicilia, *Inorg. Chem.* 58 (2019) 3851–3860.
- [22] Gaussian 09, Revision D.01, M. J. Frisch, G. W. Trucks, H. B. Schlegel, G. E. Scuseria, M. A. Robb, J. R. Cheeseman, G. Scalmani, V. Barone, B. Mennucci, G. A. Petersson, H. Nakatsuji, M. Caricato, X. Li, H. P. Hratchian, A. F. Izmaylov, J. Bloino, G. Zheng, J. L. Sonnenberg, M. Hada, M. Ehara, K. Toyota, R. Fukuda, J. Hasegawa, M. Ishida, T. Nakajima, Y. Honda, O. Kitao, H. Nakai, T. Vreven, J. A. Montgomery, Jr., J. E. Peralta, F. Ogliaro, M. Bearpark, J. J. Heyd, E. Brothers, K. N. Kudin, V. N. Staroverov, T. Keith, R. Kobayashi, J. Normand, K. Raghavachari, A. Rendell, J. C. Burant, S. S. Iyengar, J. Tomasi, M. Cossi, N. Rega, J. M. Millam, M. Klene, J. E. Knox, J. B. Cross, V. Bakken, C. Adamo, J. Jaramillo, R. Gomperts, R. E. Stratmann, O. Yazyev, A. J. Austin, R. Cammi, C. Pomelli, J. W. Ochterski, R. L. Martin, K. Morokuma, V. G. Zakrzewski, G. A. Voth, P. Salvador, J. J. Dannenberg, S. Dapprich, A. D. Daniels, O. Farkas, J. B. Foresman, J. V. Ortiz, J. Cioslowski, and D. J. Fox, Gaussian, Inc., Wallingford CT, 2010.
- [23] A.D. Becke, *J. Chem. Phys.* 98 (1993) 5648–5652.
- [24] C. Lee, W. Yang, R.G. Parr, *Phys. Rev. B* 37 (1988) 785–789.
- [25] S. Grimme, J. Antony, S. Ehrlich, H. Krieg, *J. Chem. Phys.* 132 (2010) 154104–154122.
- [26] D. Andrae, U. HUSSERMANN, M. Dolg, H. Stoll, H. Preuss, *Theor. Chim. Acta* 77 (1990) 123–141.
- [27] K. Fukui, *J. Phys. Chem.* 74 (1970) 4161–4163.
- [28] C. Gonzalez, H.B. Schlegel, *J. Chem. Phys.* 90 (1989) 2154–2161.
- [29] S. Miertu , E. Scrocco, J. Tomasi, *Chem. Phys.* 55 (1981) 117–129.
- [30] S. Miertu , J. Tomasi, *Chem. Phys.* 65 (1982) 239–245.
- [31] J.L. Pascual-Ahuir, E. Silla, I. Tu n, *J. Comput. Chem.* 15 (1994) 1127–1138.
- [32] D.A. McQuarrie, J.D. Simon, *Molecular Thermodynamics*, University Science Books, Sausalito, CA, 1999.
- [33] R.W. Ashcraft, S. Raman, H.W. Green, *J. Phys. Chem. B* 111 (2007) (1983) 11968–11971.
- [34] I. Tolbatov, C. Coletti, A. Marrone, N. Re, *Inorg. Chem.* 57 (2018) 3411–3419.
- [35] F.  sebasta, J.V. Burda, *Eur. J. Inorg. Chem.* (2018) 1481–1491.
- [36] S.Q. Yap, C.F. Chin, A.H. Hong Thng, Y.Y. Pang, H.K. Ho, W.H. Ang, *ChemMedChem* 12 (2017) 300–311.
- [37] T.C. Johnstone, S.J. Lippard, *J. Am. Chem. Soc.* 136 (2014) 2126–2134.

- [38] D. Veclani, A. Melchior, M. Tolazzi, J.P. Cerón-Carrasco, *J. Am. Chem. Soc.* 140 (2018) 14024–14027.
- [39] A.A. Almaqwashi, W. Zhou, M.N. Nauffer, I.A. Riddell, Ö.H. Yilmaz, S.J. Lippard, M.C. Williams, *J. Am. Chem. Soc.* 141 (2019) 1537–1545.
- [40] R.K. Pathak, S. Marrache, J.H. Choi, T.B. Berding, S. Dhar, *Angew. Chem. Int. Ed.* 53 (2014) 1963–1967.
- [41] Q. Cheng, H. Shi, H. Wang, Y. Min, J. Wang, Y. Liu, *Chem. Commun.* 50 (2014) 7427–7430.

Supplementary data

Theoretical exploration of the reduction reaction of monofunctional phenanthriplatin Pt(IV) prodrugs.

Eslam Dabbish, Daniela Imbardelli, Nino Russo and Emilia Sicilia*

Dipartimento di Chimica e Tecnologie Chimiche, Università della Calabria, 87036 Rende (CS), Italy

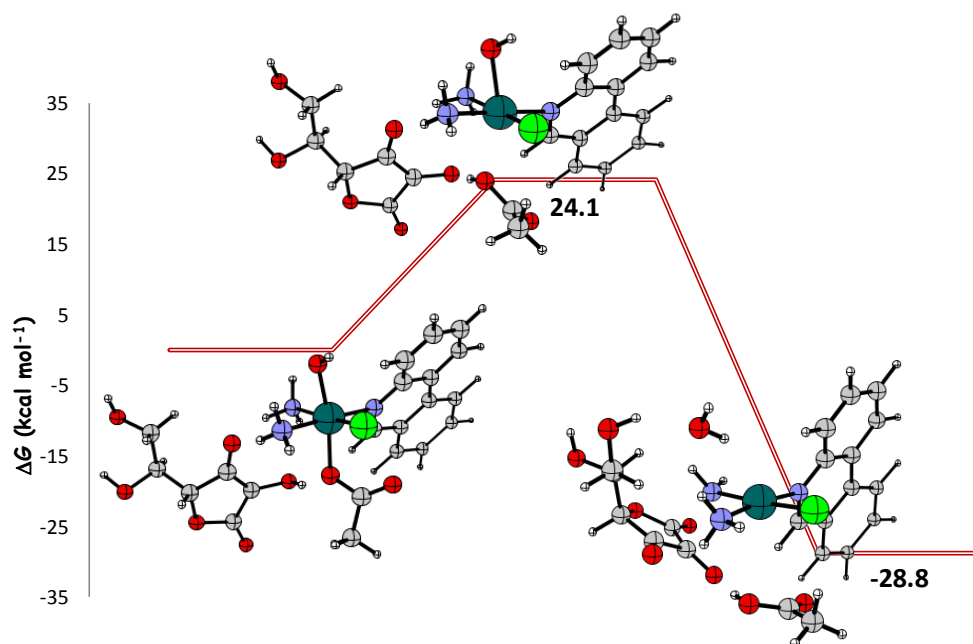


Figure S1. Free energy profile in water describing the ligand-bridged-H transfer mechanism in presence of ascorbate as reducing agent for the attack to the acetate ligand of the **PhPt(IV)(OH)(OAc)** complex to the oxygen bound to the metal center. Energies are in kcal mol^{-1} and relative to separated reactants.

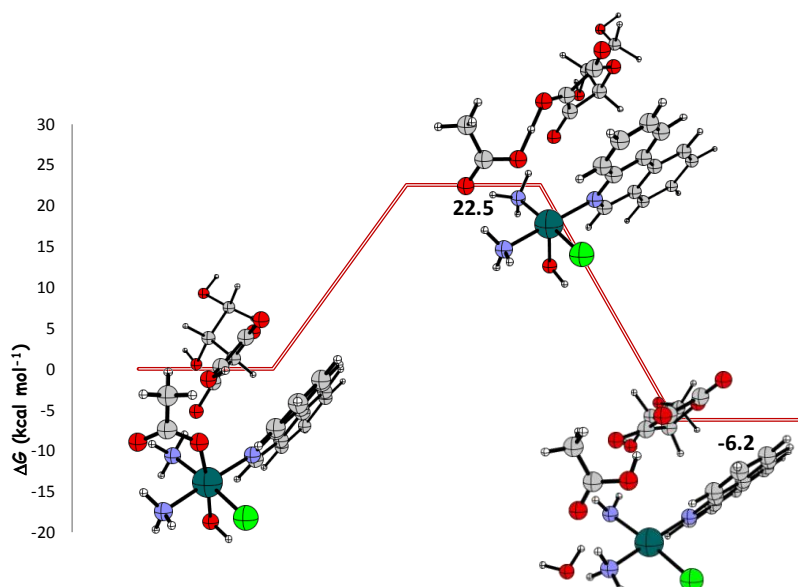


Figure S2. Free energy profile in water describing the ligand-bridged-H transfer mechanism in presence of ascorbate as reducing agent for the attack, involving π - π interactions, on the acetate ligand of the **PhPt(IV)(OH)(OAc)** complex to the oxygen atom bound to the metal center. Energies are in kcal mol^{-1} and relative to separated reactants.

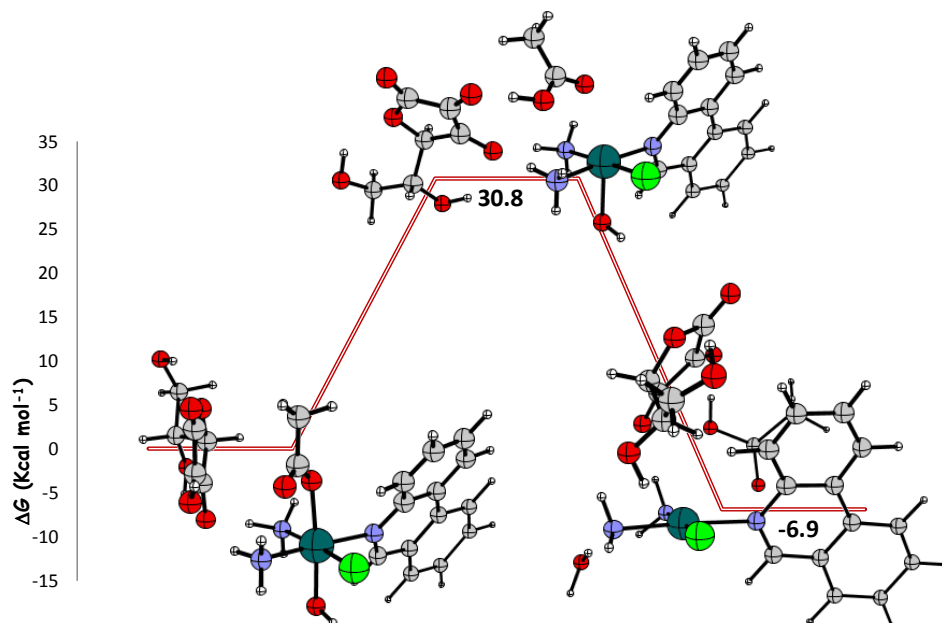


Figure S3. Free energy profile in water describing the ligand-bridged-H transfer mechanism in presence of ascorbate as reducing agent for the attack to the acetate ligand of the **PhPt(IV)(OH)(OAc)** complex to the oxygen not bound to the metal center. Energies are in kcal mol⁻¹ and relative to separated reactants.

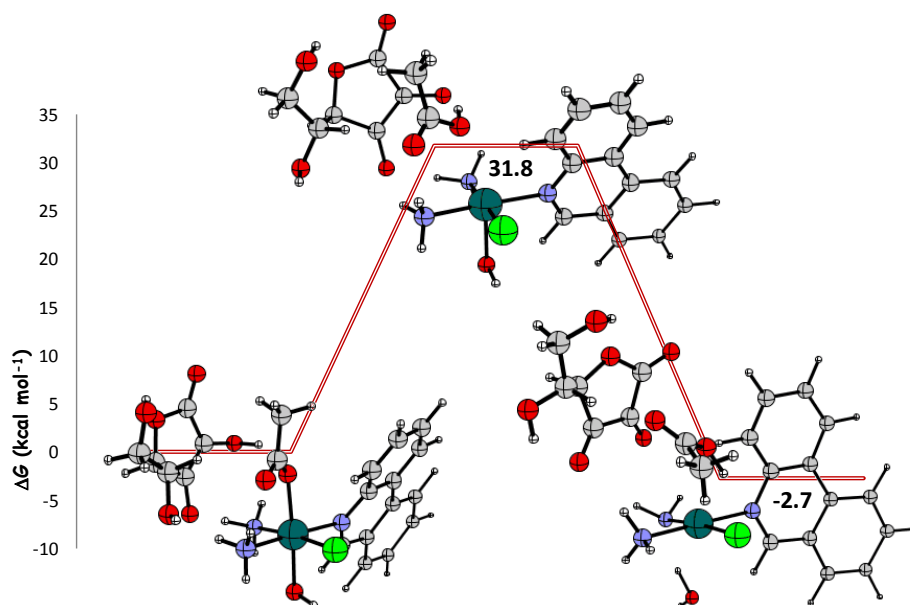


Figure S4. Free energy profile in water describing the ligand-bridged-H transfer mechanism in presence of ascorbate as reducing agent for the attack, on the acetate ligand of the **PhPt(IV)(OH)(OAc)** complex to the oxygen atom bound to the metal center. Energies are in kcal mol⁻¹ and relative to separated reactants.

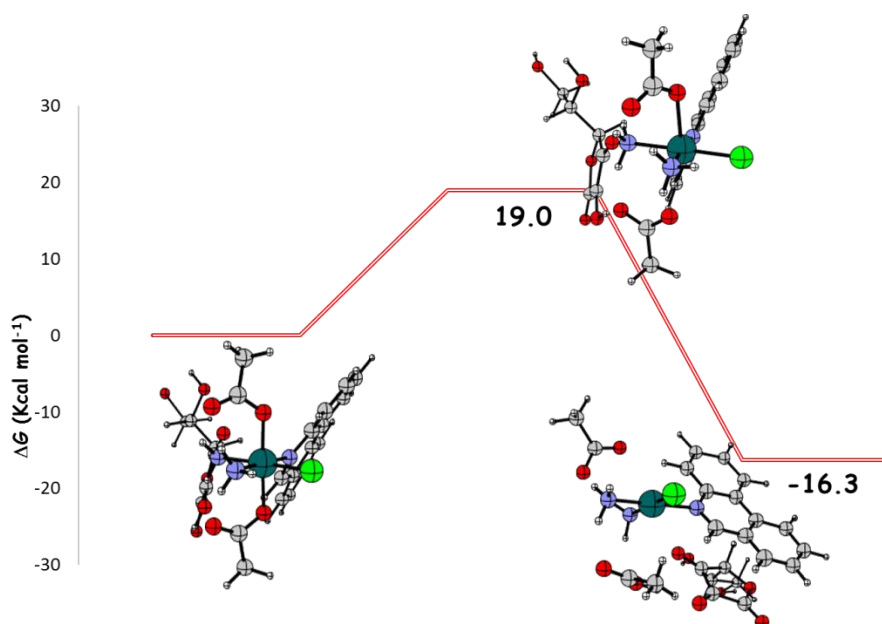


Figure S5. Free energy profile in water describing the ligand-bridged-H transfer mechanism in presence of ascorbate as reducing agent for the attack, involving π - π interactions, from the **C** side of the **PhPt(IV)(OAc)₂** complex to the **O1** oxygen atom. Energies are in kcal mol⁻¹ and relative to separated reactants.

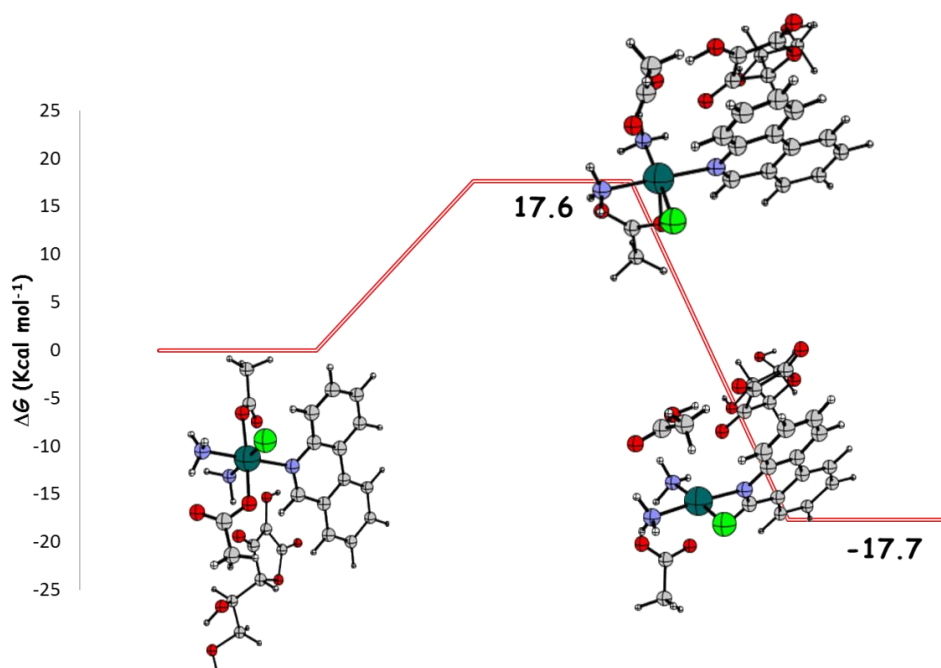


Figure S6. Free energy profile in water describing the ligand-bridged-H transfer mechanism in presence of ascorbate as reducing agent for the attack, involving π - π interactions, from the **D** side of the **PhPt(IV)(OAc)₂** complex to the **O1** oxygen atom. Energies are in kcal mol⁻¹ and relative to separated reactants.

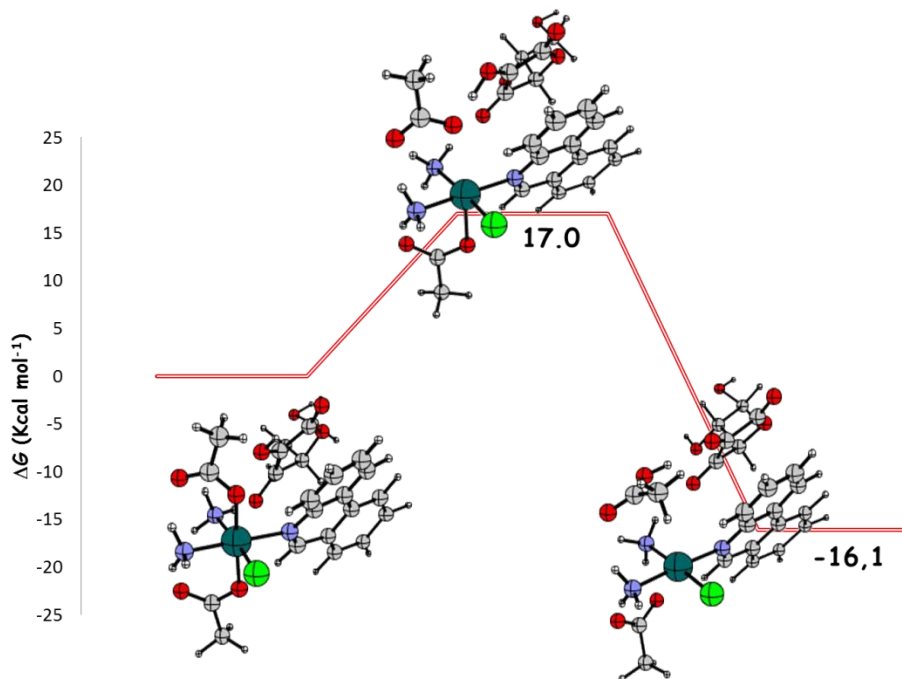


Figure S7. Free energy profile in water describing the ligand-bridged-H transfer mechanism in presence of ascorbate as reducing agent for the attack, involving π - π interactions, from the **D** side of the **PhPt(IV)(OAc)₂** complex to the **O₂** oxygen atom. Energies are in kcal mol⁻¹ and relative to separated reactants.

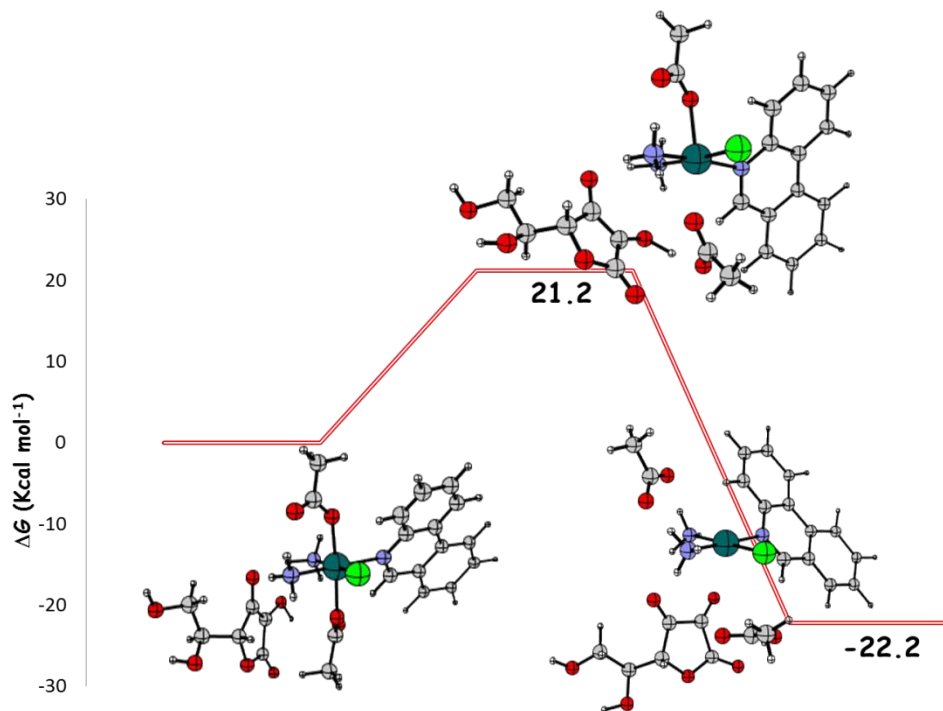


Figure S8. Free energy profile in water describing the ligand-bridged-H transfer mechanism in presence of ascorbate as reducing agent for the attack, not involving π - π interactions, from the **C** side of the **PhPt(IV)(OAc)₂** complex to the **O₁** oxygen atom. Energies are in kcal mol⁻¹ and relative to separated reactants.

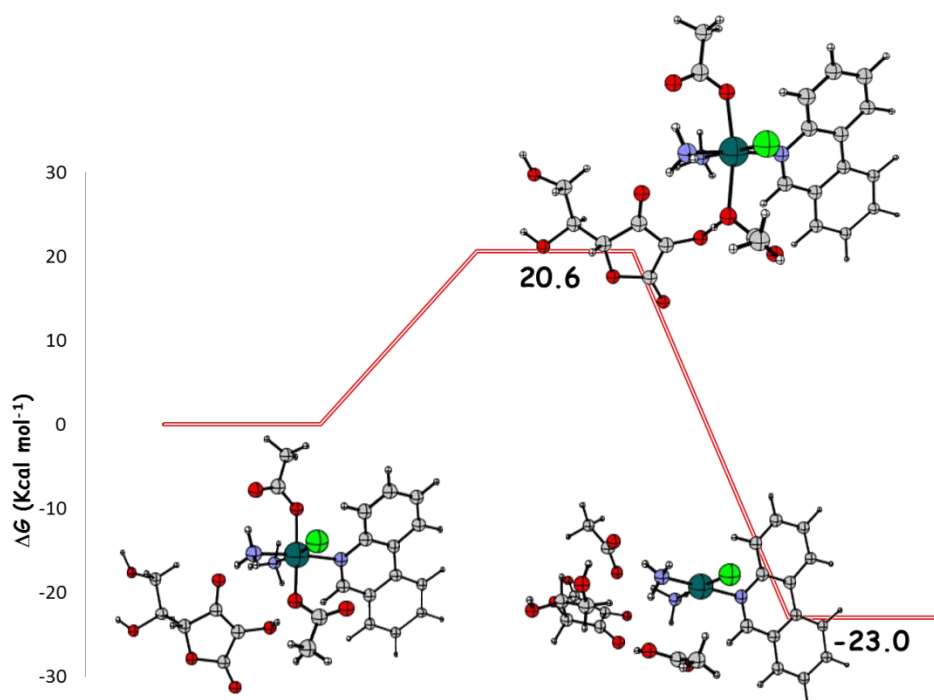


Figure S9. Free energy profile in water describing the ligand-bridged-H transfer mechanism in presence of ascorbate as reducing agent for the attack, not involving π - π interactions, from the **C** side of the **PhPt(IV)(OAc)₂** complex to the **O2** oxygen atom. Energies are in kcal mol⁻¹ and relative to separated reactants.

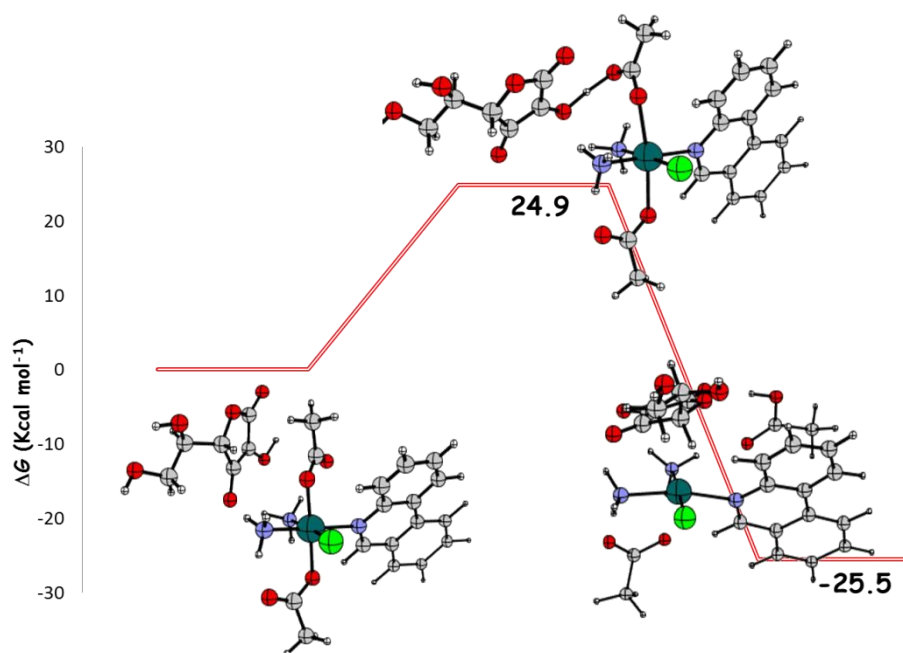


Figure S10. Free energy profile in water describing the ligand-bridged-H transfer mechanism in presence of ascorbate as reducing agent for the attack, not involving π - π interactions, from the **D** side of the **PhPt(IV)(OAc)₂** complex to the **O1** oxygen atom. Energies are in kcal mol⁻¹ and relative to separated reactants.

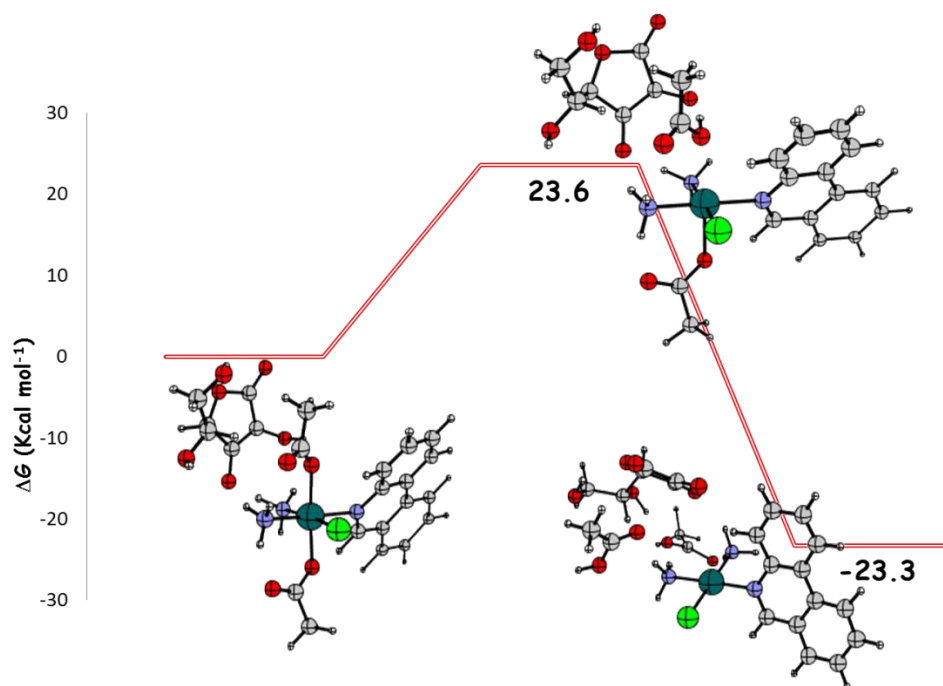


Figure S11. Free energy profile in water describing the ligand-bridged-H transfer mechanism in presence of ascorbate as reducing agent for the attack, not involving π - π interactions, from the **D** side of the **PhPt(IV)(OAc)₂** complex to the **O2** oxygen atom. Energies are in kcal mol^{-1} and relative to separated reactants.

5.3 A multi-methodological inquiry of the behavior of cisplatin-based Pt(IV) derivatives in the presence of bioreductants with a focus on the isolated encounter complexes

5.3.1 Introduction

Unsuccessful chemotherapeutic responses were often related to tumor hypoxia, since cells surviving in such conditions exhibit high chemoresistance. However, tumor hypoxia could be exploited to enhance the selectivity of anticancer drugs, if they become active in such conditions.¹ In this framework, the octahedral Pt(IV) complexes act as prodrugs, being *per se* quite substitution-inert. They can be selectively transformed in the tumor environment via a Pt(IV) \rightarrow Pt(II) 2e-reduction to the corresponding cytotoxic square planar Pt(II) complexes. Usually the reduction involves the loss of the axial ligands and thus the main product is the parent Pt(II) complex that maintains the equatorial groups, even though some cases of ligand rearrangements have been reported.²⁻⁴

The first systematic studies on the reduction potentials of Pt(IV) complexes by Hambley and coworkers, mainly focused on the role of the axial ligands, concluded that reduction occurs more easily (i.e. at less negative potentials) in the case of axial chlorido ligands, less easily for hydroxido substituents, with intermediate potentials for carboxylato groups.^{5,6}

Since the electron transfer is accompanied by the release of the two axial ligands (electrochemical mechanism), the potential does not necessarily correlate with the rate of the reduction process that depends both on the rate of the electron transfer and on strength of the bonds to be broken.^{7,8} This is particularly proper when an inner-sphere reduction mechanism is operating.^{9,10} Thus, the kinetic features of the chemical reduction play an important role.

5.3.2 Aim of study

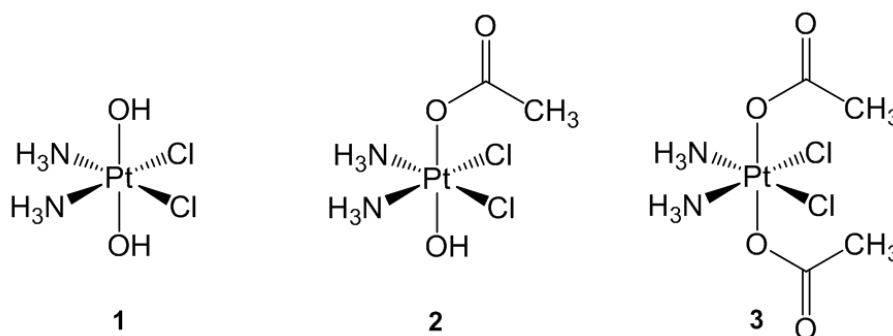


Figure 5.4 Chemical structure of studied complexes **1** cis,trans,cis-[PtCl₂(OH)₂(NH₃)₂], **2** cis,trans,cis-[PtCl₂(CH₃COO)(OH)(NH₃)₂] and **3** cis,trans,cis-PtCl₂(CH₃COO)₂(NH₃)₂]

The purpose of this work is to shed more light on the reduction of three cisplatin-based Pt(IV) complexes **1** cis,trans,cis-[PtCl₂(OH)₂(NH₃)₂], **2** cis,trans,cis-[PtCl₂(CH₃COO)(OH)(NH₃)₂] and **3** cis,trans,cis-PtCl₂(CH₃COO)₂(NH₃)₂] in the presence of H₂Asc at controlled pH by means of reduction kinetics, electrochemical measurements, tandem mass spectrometry (MS), infrared multiple photon dissociation (IRMPD) spectroscopy and *theoretical calculations at DFT level*. This multi-methodological approach is expected to unveil the reactivity behavior in solution, to relate these findings with peak reduction potentials and to ascertain what the behavior would be in an isolated encounter complex of the reactant pair. Structural and reactivity features of the latter species are interpreted by DFT calculations.

5.3.3 Highlighting results

The reduction kinetics of 1-3, in the presence of ascorbic acid, that were recorded by resorting to ¹⁵N-NMR spectroscopy of ¹⁵N-enriched samples, have displayed the 1 > 2 >> 3 order, pointing to a key role of an axial hydroxido ligand. The trend of reduction peak potentials (E_p values: 1 < 2 < 3) is not in this case a reliable predictor for the corresponding chemical

reductions, rather suggesting 3 to be the most susceptible to be electrochemically reduced. This missing correlation has been already documented and ascribed to the mechanistic complexity of the reaction involving not only electron transfer to the metal center but also elimination of two axial ligands.

An ESI-MS study of the breakdown pattern of positively and negatively charged ions delivered from 1-3 solutions in the presence of the bio-reductant models H₂Asc and GSH has been carried out. The ESI process delivers ionic non-covalent complexes of 1-3 with a bio-reductant (H₂Asc or GSH) molecule as isolated species in the gas phase. The structure of these adducts has been assayed by IR ion spectroscopy and their reactivity has been evaluated by collision induced dissociation. The results show the adducts of 1 and 2 with ascorbic acid to be prone to reduction, releasing Pt(II) species as major products. In particular, the [1+H₂Asc+H]⁺ adduct yields [Pt(II)Cl₂(NH₃)₂+H]⁺ and the [1+HAsc]⁻ adduct yields [Pt(II)Cl₂(NH₃)₂+OH]⁻ as prominent products, while the [2+HAsc]⁻ adduct yields [Pt(II)Cl₂(NH₃)₂+AcO]⁻ in somewhat lower extent. In contrast, the non-covalent adduct of 3 and H₂Asc does not yield any reduced product. The reactivity trend from reduction kinetics in solution is thus confirmed by the reactivity behavior of the isolated encounter complex.

Quantum-mechanical DFT exploration of the corresponding fragmentation pathways in the presence of H₂Asc/HAsc⁻ have provided a theoretical support to the proposed dissociation patterns and mechanistic hypotheses.

References

- 1) N. Graf, S. J. Lippard, *Adv. Drug Delivery Rev.*, **2012**, *64*, 993-1004.
- 2) E. Wexselblatt, D. Gibson, *J. Inorg. Biochem.* **2012**, *117*, 220-229.
- 3) A. Nemirovski, I. Vinograd, K. Takrouri, A. Mijovilovich, A. Rompel, D. Gibson, *Chem. Commun.*, **2010**, *46*, 1842-1844.

- 4) M. Ravera M, E. Gabano, I. Zanellato, I. Bonarrigo, E. Escribano, V. Moreno, M. Font-Bardia, T. Calvet, D. Osella, *Dalton Trans*, **2012**, 41(11), 3313-3320.
- 5) M. D. Hall, T. W. Hambley, *Coord Chem Rev*, **2002**, 232 (1-2), 49-67.
- 6) M. D. Hall, H. R. Mellor, R. Callaghan, T. W. Hambley, *J Med Chem*, **2017**, 50 (15), 3403-3411.
- 7) I. Tolbatov , C. Coletti, A. Marrone, N. Re, *Inorg Chem*, **2018**, 57 (6), 3411-3419.
- 8) M. C. McCormick, K. Keijzer, A. Polavarapu, F. A. Schultz, M. H. Baik, *J Am Chem Soc*, **2014**, 136 (25), 8992-9000.
- 9) I. Zanellato, I. Bonarrigo, D. Colangelo, E. Gabano, M. Ravera, M. Alessio, D. Osella, *J Inorg Biochem*, 2014, 140, 219-227.
- 10) J. Z. Zhang, E. Wexselblatt, T. W. Hambley, D. Gibson, *Chem. Commun.*, **2012**, 48, 847-849.

Paper V

A multi-methodological inquiry of the behavior of cisplatin-based Pt(IV) derivatives in the presence of bioreductants with a focus on the isolated encounter complexes.

D. Corinti, M. E. Crestoni, S. Fornarini, E. Dabbish, E. Sicilia, E. Gabano, E. Perin, D. Osella, *Journal of Biological Inorganic Chemistry*, **2020**, 25, 655-670.



A multi-methodological inquiry of the behavior of cisplatin-based Pt(IV) derivatives in the presence of bioreductants with a focus on the isolated encounter complexes

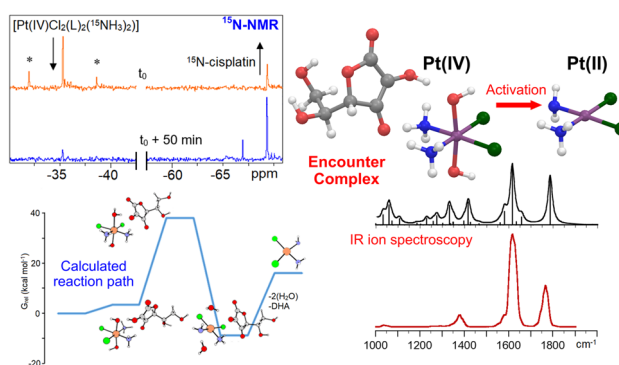
Davide Corinti¹ · Maria Elisa Crestoni¹ · Simonetta Fornarini¹ · Eslam Dabbish² · Emilia Sicilia² · Elisabetta Gabano³ · Elena Perin³ · Domenico Osella³

Received: 19 February 2020 / Accepted: 31 March 2020 / Published online: 15 April 2020
© Society for Biological Inorganic Chemistry (SBIC) 2020

Abstract

The study of Pt(IV) antitumor prodrugs able to circumvent some drawbacks of the conventional Pt(II) chemotherapeutics is the focus of a lot of attention. This paper reports a thorough study based on experimental methods (reduction kinetics, electrochemistry, tandem mass spectrometry and IR ion spectroscopy) and quantum–mechanical DFT calculations on the reduction mechanism of cisplatin-based Pt(IV) derivatives having two hydroxido (**1**), one hydroxido and one acetato (**2**), or two acetato ligands (**3**) in axial position. The biological reductants glutathione and ascorbic acid were taken into consideration. The presence of a hydroxido ligand resulted to play an important role in the chemical reduction with ascorbic acid, as verified by ¹⁵N-NMR kinetic analysis using ¹⁵N-enriched complexes. The reactivity trend (**1** > **2** > **3**) does not reflect the respective reduction peak potentials (**1** < **2** < **3**), an inverse relationship already documented in similar systems. Turning to a simplified environment, the Pt(IV) complexes associated with a single reductant molecule (corresponding to the encounter complex occurring along the reaction coordinate in bimolecular reactions in solution) were characterized by IR ion spectroscopy and sampled for their reactivity under collision-induced dissociation (CID) conditions. The complexes display a comparable reduction reactivity ordering as that observed in solution. DFT calculations of the free energy pathways for the observed fragmentation reactions provide theoretical support for the CID patterns and the mechanistic hypotheses on the reduction process are corroborated by the observed reaction paths. The bulk of these data offers a clue of the intricate pathways occurring in solution.

Graphic abstract



Electronic supplementary material The online version of this article (<https://doi.org/10.1007/s00775-020-01789-w>) contains supplementary material, which is available to authorized users.

Extended author information available on the last page of the article

Keywords Antitumor prodrug · Mass spectrometry · IR ion spectroscopy · Reduction kinetics · ^{15}N -NMR spectroscopy · DFT calculations

Introduction

Tumors are characterized by uncontrolled proliferation, inadequate angiogenesis and, then, low oxygen level resulting in a more reducing environment than that of healthy tissue. Unsuccessful chemotherapeutic responses were often related to tumor hypoxia, since cells surviving in such conditions exhibit high chemoresistance. However, tumor hypoxia could be exploited to enhance the selectivity of anticancer drugs, if they become active in such conditions [1]. In this framework, the octahedral Pt(IV) complexes act as prodrugs, being per se quite substitution inert. They can be selectively transformed in the tumor environment via a Pt(IV) \rightarrow Pt(II) 2e-reduction to the corresponding cytotoxic square planar Pt(II) complexes. Usually, the reduction involves the loss of the axial ligands and thus, the main product is the parent Pt(II) complex that maintains the equatorial groups, even though some cases of ligand rearrangements have been reported [2–4].

Cyclic voltammetry (CV) was employed to obtain information on this chemically irreversible reduction process, affording the reduction peak potentials (not exactly coincident with standard redox potentials) [5]. The first systematic studies on the reduction potentials of Pt(IV) complexes by Hambley and coworkers, mainly focused on the role of the axial ligands, concluded that reduction occurs more easily (i.e., at less negative potentials) in the case of axial chlorido ligands, less easily for hydroxido substituents, with intermediate potentials for carboxylato groups [5, 6]. This scenario reproduces the overall biological response shown by the Pt(IV) complexes that exhibited enough promise to enter clinical trials. Indeed, iproplatin, *cis,cis,trans*-[PtCl₂(isopropylamine)₂(OH)₂] (hardly reduced to the active Pt(II) metabolite), was found to be less active than cisplatin. On the contrary, tetraplatin or ormaplatin, *cis,trans,cis*-[PtCl₄(dach)] (easily reduced to the active Pt(II) metabolite), was highly active but caused severe neurotoxicity; therefore, for opposite reasons, both were abandoned. Only the diacetato satraplatin, *trans,cis,cis*-[Pt(Ac)₂Cl₂(cyclohexylamine)(NH₃)] (Ac = acetato), is still involved in several clinical trials. Quantitative structure–activity relationship (QSAR) studies confirmed the importance of electronic (linked to reduction) as well as lipophilic (linked to cellular uptake) features at least for the in vitro activity of these complexes [7–11].

Since the electron transfer is accompanied by the release of the two axial ligands (EC mechanism), the potential does not necessarily correlate with the rate of the reduction process that depends both on the rate of the

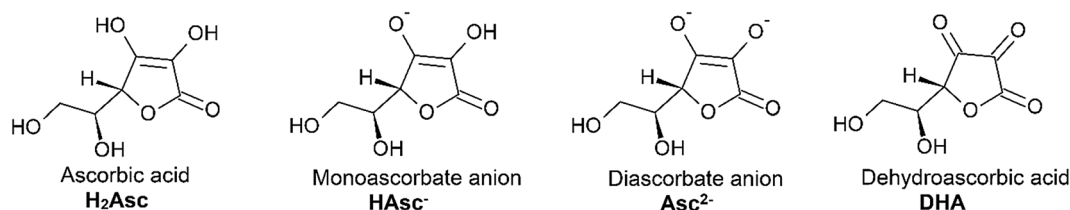
electron transfer and on strength of the bonds to be broken [12, 13]. This is particularly proper when an inner-sphere reduction mechanism is operating [14, 15]. Thus, the kinetic features of the chemical reduction play an important role [2, 5, 16–18].

The tumor reducing microenvironment is due to the high cellular concentrations of several bioreductants, the more abundant being glutathione, GSH, and ascorbic acid, H₂Asc [1]. The glutathione (GSH)/glutathione disulphide (GSSG) couple is the most abundant redox buffer in cells, with an average cytosolic GSH concentration of 1–11 mM [19]. Indeed, the GSH/GSSG ratio is used to estimate the cell redox environment. The GSH level has been found sixfold higher in tumor tissue than in healthy one [20]. The axially *trans*-dichlorido Pt(IV) complexes are prone to be reduced by thiol-containing molecules, such as GSH or L-cysteine, and these prodrugs are too reactive in plasma to enter cancerous cells intact [21]. On the contrary, a number of Pt(IV) complexes (especially dicarboxylato) is not reduced at all by GSH [22–30]. In particular, satraplatin was found to be stable in solution in the presence of GSH. Very recently, Ang et al. investigated the intracellular reduction of Pt(IV) prodrugs based on the cisplatin scaffold with GSH employing a radiometric fluorescence probe. The conclusion of this fluorescence resonance energy transfer (FRET) study, able to distinguish between Pt(IV)/Pt(II) oxidation states in the multifaceted cellular *milieu* without altering their redox equilibrium, was: “contrary to conventional thinking, GSH is not the main cellular reductant for Pt(IV) prodrugs based on cisplatin” [31]. Also, H₂Asc is present at higher concentration in the cytoplasm (about 1 mM) than in blood (40–80 μM). Similar to GSH, differences between tumor and non-tumor tissues have been also observed for H₂Asc (tumor levels were greater than those of the adjacent normal tissue in a 2.4:1 molar ratio) [20, 32]. Because H₂Asc proved to be a good reductant for Pt(IV) derivatives, experimental data on Pt(IV) \rightarrow Pt(II) reduction with such a reagent are then abundant in the literature. Studies with H₂Asc have indicated that the reduction of Pt(IV) complexes follows either outer- or inner-sphere mechanisms, depending on the nature and geometry of the complexes [33]. Inner-sphere is operating especially for compounds with axial chlorido or hydroxido [2, 26, 34–36]. On the contrary, carboxylate functionalities proved to be not efficient bridging groups in a reductive *trans* elimination process [33]. In addition, the equatorial ligands play a role. Equatorial dicarboxylate groups lead to slower reduction rates than equatorial chlorides [37, 38]. Indeed, a tetracarboxylato Pt(IV) derivative proved to be hardly reduced at least in vitro. In addition, both σ -donor

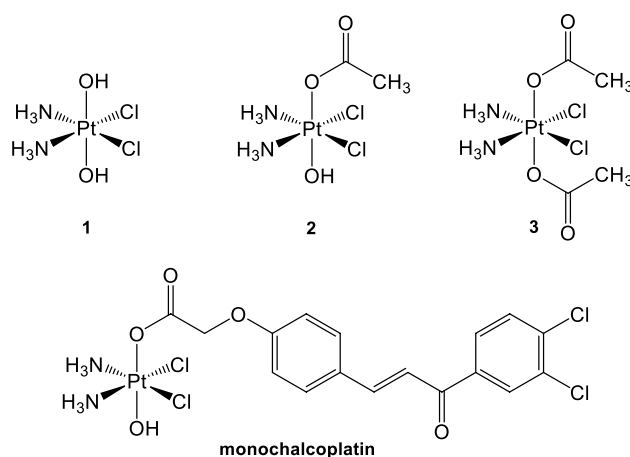
ability and steric hindrance of the amines (as equatorial carrier groups) affect the kinetics of reduction [4, 39].

An important point in understanding the role of H_2Asc for the reduction of Pt(IV) concerns the pH of the solution (Scheme 1). The reduction is faster moving to higher pH [26, 40, 41]. The neutral H_2Asc seems in fact to be not involved in the reduction of Pt(IV) prodrugs, while Asc^{2-} is by far more reactive than the HAsc^- species [26, 40]. However, mono-deprotonated ascorbic acid (HAsc^-) is definitely the most abundant at physiological pH and, therefore, is considered the active species for Pt(IV)-reduction [2]. Recently, the reduction of Pt(IV) derivatives of cisplatin, oxaliplatin and phenanthriplatin with HAsc^- was theoretically investigated showing that the naïve classification into inner- and outer-sphere mechanisms does not accurately take into account all the feasible alternatives [42, 43]. For hydroxido and acetato, the inner-sphere operative mechanism is that named “ligand-bridged-H transfer” that involves the transfer of a H^- unit, causing the reduction of the Pt core and leading to the release of water and acetic acid molecules, respectively. For chlorido and bromido, the mechanism depends on the nature of the axially *trans* ligand and can proceed via ligand-bridged or via enolate β -carbon attack. Equatorial bulky ligands can influence the course of the reaction due to their steric hindrance. The alternative mechanism involving the participation of Pt(II) as catalyst can be considered not viable owing to both the previously calculated high-energy barriers [42] and the low cellular concentration of Pt(II) in pharmacological conditions. Despite the above-reported considerations, the mechanism of the reduction of Pt(IV) complexes with model bioreductants is not completely deciphered [2, 37, 44]. It is worth mentioning that other bioreductants present in the high MW fraction of cytosol proved able to reduce and then activate Pt(IV) prodrugs [2, 45–51].

The purpose of this work is to shed more light on the reduction of three cisplatin-based Pt(IV) complexes **1**, **2** and **3** (Scheme 2) in the presence of GSH and H_2Asc at controlled pH by means of reduction kinetics, electrochemical measurements, tandem mass spectrometry (MS), infrared multiple photon dissociation (IRMPD) spectroscopy and theoretical calculations at DFT level. This multi-methodological approach is expected to unveil the reactivity behavior in solution, to relate these findings with peak reduction potentials and to ascertain what the behavior would be in an



Scheme 1 Structure of ascorbic acid and its deprotonation and dehydrogenation products



Scheme 2 Pt(IV) complexes under investigation and the cisplatin-based Pt(IV) prodrug monochalcoptatin [52]

isolated encounter complex of the reactant pair. Structural and reactivity features of the latter species are interpreted by DFT calculations. Interestingly, the basic elements of compound **2** (hydroxido and carboxylato axial ligands on a Pt(IV) derivative of cisplatin) are found also in monochalcoptatin (Scheme 2), a recently discovered Pt(IV) prodrug that is among the most cytotoxic Pt(IV) complexes to date [48].

Materials and methods

Synthesis and sample preparation for mass analysis

The complexes oxoplatin or *cis,trans,cis*-[PtCl₂(OH)₂(NH₃)₂], **1** [7, 14, 46, 53] *cis,trans,cis*-[PtCl₂(CH₃COO)(OH)(NH₃)₂], **2** [47, 53] and *cis,trans,cis*-[PtCl₂(CH₃COO)₂(NH₃)₂], **3** [14, 53] were prepared according to literature reports. Stock aqueous solutions of **1–3** (10^{-3} M) were used to obtain 5×10^{-5} M solutions of the complexes in 1:1 molar ratio with the selected reducing agent (GSH or H_2Asc) in 1:1 MeOH/ H_2O , which have been directly infused in the ESI source of the mass spectrometer. To enhance the intensity of the protonated species, formic acid was added; while, ammonia was employed for the analyses of the deprotonated ones. The final concentrations

of formic acid and ammonia were 5×10^{-3} M and 0.1 M, respectively.

Synthesis of $^{15}\text{NH}_3$ -labeled complexes $^{15}\text{N-1}$, $^{15}\text{N-2}$, and $^{15}\text{N-3}$

The syntheses of ^{15}N -labeled complexes started with the preparation of *cis*-[PtCl₂($^{15}\text{NH}_3$)₂] as previously reported [64]. ^{15}N -cisplatin was then oxidized with hydrogen peroxide in water to get the dihydroxido complex $^{15}\text{N-1}$ (with a microwave-assisted heating) [46] or in acetic acid to get the monoacetato complex $^{15}\text{N-2}$ [48]. Finally, the diacetato complex $^{15}\text{N-3}$ was obtained from the reaction between the ^{15}N -labeled dihydroxido complex and acetic anhydride [14].

$^{15}\text{N-1}$. Yield: 90% (from 100 mg of ^{15}N -cisplatin). ^{15}N -NMR (50.70 MHz, H₂O/D₂O 9/1): δ – 33.8 ppm with satellite peaks at – 31.2 ppm and – 36.6 ppm ($^1J_{\text{Pt-N}} = 274$ Hz and $^2J_{\text{Pt-H}} = 52$ Hz). ESI-MS (positive ion mode): 336 *m/z* [M+H]⁺. Calc. for [Cl₂H₉ $^{15}\text{N}_2\text{O}_2\text{Pt}$]⁺ 336 *m/z* [M+H]⁺.

$^{15}\text{N-2}$. Yield: 85% (from 100 mg of ^{15}N -cisplatin). ^{15}N -NMR (50.70 MHz, H₂O/D₂O 9/1): δ – 35.6 ppm with satellite peaks at – 32.9 ppm and – 38.2 ppm ($^1J_{\text{Pt-N}} = 273$ Hz and $^2J_{\text{Pt-H}} = 54$ Hz). ESI-MS (positive ion mode): 379 *m/z* [M+H]⁺. Calc. for [C₂H₁₁Cl₂ $^{15}\text{N}_2\text{O}_3\text{Pt}$]⁺ 379 *m/z* [M+H]⁺.

$^{15}\text{N-3}$. Yield: 80% (from 100 mg of $^{15}\text{N-1}$). ^{15}N -NMR (50.70 MHz, H₂O/D₂O 9/1): δ – 39.6 ppm with satellite peaks at – 37.0 ppm and – 42.5 ppm ($^1J_{\text{Pt-N}} = 265$ Hz and $^2J_{\text{Pt-H}} = 54$ Hz). ESI-MS (negative ion mode): 418 *m/z* [M–H][–]. Calc. for [C₄H₁₁Cl₂ $^{15}\text{N}_2\text{O}_4\text{Pt}$][–] 418 *m/z* [M–H][–].

Kinetics of reduction

^{15}N -labeled complexes **1–3** (6 mM) and ascorbic acid (60 mM) were dissolved in HEPES (4-(2-hydroxyethyl) piperazine-1-ethanesulfonic acid) buffer (2 mM, pH 7.4) and diluted to a final H₂O/D₂O 9:1 nominal solvent ratio. The resulting solutions were monitored at 37 °C by ^{15}N -NMR spectroscopy. ^{15}N -NMR spectra were recorded using a solution of $^{15}\text{NH}_4\text{Cl}$ in 1 M HCl as the external reference. $^{15}\text{N}\{^1\text{H}\}$ DEPT-45 (Distortionless Enhanced by Polarization Transfer) spectra were recorded at 37 °C with 140 scans, 3.5-s relaxation delay, 0.5-s acquisition time and 75 Hz for $^1\text{J}(^{15}\text{N}, ^1\text{H})$ using a NMR-Bruker Avance III instrument operating at 500 MHz and 50.70 MHz for ^1H and ^{15}N , respectively.

Electrochemistry

An Autolab PGSTAT12 electrochemical analyzer (Eco Chemie, Utrecht, The Netherlands) interfaced to a personal computer running GPES 4.9 electrochemical software was used for the electrochemical measurements. A standard three-electrode cell was designed to allow the tip of the

reference electrode (Ag/AgCl, 3-M KCl) to closely approach the working electrode (a glassy carbon, GC, disk, diameter 0.1 cm, sealed in epoxy resin). The GC working electrode was polished with alumina, then rinsed with distilled water and dried. This process yielded an almost completely reproducible surface for all CV experiments. All measurements were carried out at 0.2 V s^{–1} scan rate under nitrogen in ethanol solutions containing 0.1 M [NBu₄][ClO₄] as supporting electrolyte and 0.50 mM of metal complex. The temperature of the solution was kept constant (25 ± 1 °C) by circulation of a water/ethanol mixture through a jacketed cell connected to a thermostatic bath. Positive-feedback iR compensation was applied routinely.

Mass analyses

Mass spectrometric analyses were carried out in a Paul ion-trap (Esquire 6000, Bruker) equipped with an electrospray ionization (ESI) source, through direct infusion of the solutions prepared as stated above at a flow rate of 180 $\mu\text{L h}^{-1}$. Typical parameters used for the analyses include drying gas (N₂) fluxed with a flow rate of 7 L min^{–1} at 300 °C, capillary voltage set at 3.8 kV, capillary exit and skimmer voltages at 60 V and 40 V, respectively (negative values were used to analyze anions). Mass selected ions were submitted to collision-induced dissociation (CID) experiments with an activation amplitude of 0.20–0.35 V and an activation time of 0.50 ms.

IRMPD experiments

The complexes of interest were submitted to IRMPD spectroscopy in the fingerprint region of the IR spectrum (800–2000 cm^{–1}) using the free-electron laser (FEL) of the Centre Laser Infrarouge d’Orsay (CLIO). The FEL beam-line (operated at 44 MeV for the present experiments) was coupled with a hybrid Fourier transform-ion cyclotron resonance (FT-ICR) tandem mass spectrometer (APEX-Qe Bruker Daltonics) [54], equipped with a 7.0-T actively shielded magnet and a quadrupole–hexapole interface allowing to mass select and accumulate ions prior to irradiation. All the ions were produced by ESI and source conditions are as reported in “[Mass analyses](#)”. The isolated ions were irradiated for 210–500 ms with the IR FEL light operating at a repetition rate of 25 Hz. When needed, optical attenuators were employed, each reducing the laser power by ca. 25%. IRMPD spectra are obtained by plotting the photofragmentation yield $R = -\log(I_p/(I_p + \Sigma I_f))$, where I_p and ΣI_f are the integrated intensities of the precursor and sum of the product ions, respectively, as a function of the photon energy [55].

Computational details

All calculations were performed in the framework of the density functional theory (DFT) employing the hybrid Becke three-parameter exchange functional [56] and the Lee–Yang–Parr correlation functional, B3LYP [57] as implemented in the Gaussian 09 program [58] and including dispersion corrections for nonbonding interaction through the Grimme approach using atom pair-wise additive schemes [59], denoted as DFT-D3 method. The relativistic compact Stuttgart/Dresden effective core potential was used for the Pt atom [60], along with the split valence basis set. Standard Pople basis sets of triple- ζ quality, 6-311 + G**, were used for the atoms directly bound to the Pt center and oxygen and hydrogen atoms directly involved in the reduction reaction. For the rest of the atoms, to reduce the computational effort, the, 6-311G** basis sets was used. Vibrational frequencies at the same level of theory were calculated to both ascertain the nature of intercepted stationary points as minima and transition states, and calculate zero-point energy (ZPE) and Gibbs free energy corrections. Calculated IR spectra have been scaled by a factor of 0.974. Furthermore, transition states have been carefully checked to be properly connected to the correct minima by IRC (intrinsic reaction coordinate) analysis [61, 62]. Enthalpies and Gibbs free energies were computed using standard statistical procedures [63] at 298 K and 1 atm from total energies, including zero-point and thermal corrections.

Results and discussion

Kinetics of reduction with ascorbic acid in aqueous solution: role of the hydroxido ligand

Aiming to shed light on the kinetics of the reduction reaction of **1–3** with ascorbic acid in HEPES buffer at 37 °C, different approaches have been assayed in turn. The RP-HPLC technique with ESI-MS detector was first chosen. However, due to overlapping of signals, it was not possible to quantitatively monitor the reactions. NMR spectroscopy was then taken into consideration, but the aqueous medium hampered the use of $^1\text{H-NMR}$. A C-containing ligand such as acetate (Ac) was not present in all the complexes; thus, $^{13}\text{C-NMR}$ was not viable for sampling compound **1**. $^{195}\text{Pt-NMR}$ spectroscopy can distinguish between complexes in different oxidation state and with a different coordination environment. However, the Pt(IV) and Pt(II) complexes involved in the reduction reaction have $^{195}\text{Pt-NMR}$ signals differing by 2–3 thousand ppm and each spectrum to be recorded separately requires a long acquisition time, depending on sample concentration and spectrometer sensitivity. So, it is not a suitable method to record relatively fast kinetics. On the

contrary, comparatively high reduction rates (as in the actual case) can be monitored by $^{15}\text{N-NMR}$ spectroscopy using ^{15}N -enriched samples. The $^{15}\text{N-NMR}$ signals of the ammine groups coordinated to the Pt center have a different chemical shift depending on the metal oxidation state (II or IV) [65]. Recording a $^{15}\text{N}\{^1\text{H}\}$ DEPT-45 (Distortionless Enhanced by Polarization Transfer) spectrum, it is possible to observe in the same spectrum the $^{15}\text{N-NMR}$ signals of both Pt(IV) and Pt(II) species. The reaction of $^{15}\text{N-1}$, $^{15}\text{N-2}$ and $^{15}\text{N-3}$ with HAsc^- was monitored with $^{15}\text{N}\{^1\text{H}\}$ DEPT-45 in NMR tube as shown in Figure S1 in the Electronic Supplementary Material (SM). The results showed that the reduction rate follows the order: $^{15}\text{N-1} > ^{15}\text{N-2} \gg ^{15}\text{N-3}$. Since the molar ratio between HAsc^- and each Pt(IV) complex is 10:1, the data (i.e., the decreasing area of the peak of the Pt(IV) species under observation) were analyzed according to pseudo-first-order kinetics and gave half-times of 8.6 min, 20.5 min and 8.8 h for $^{15}\text{N-1}$, $^{15}\text{N-2}$ and $^{15}\text{N-3}$, respectively (Table 1). Interestingly enough, this kinetic behavior is opposite to the trend of the reduction peak potentials (E_p) measured by linear sweep voltammetry (LSV) at a glassy carbon working electrode in ethanol solutions. The E_p values obtained at a scan rate of 0.2 V s^{-1} were -0.815 V , -0.618 V , and -0.486 V vs. Ag/AgCl , $\text{KCl } 3 \text{ M}$, for **1**, **2**, and **3**, respectively (Table 1). This trend shows that the Pt(IV) derivatives are increasingly prone to electrochemical reduction following the order **1** < **2** < **3** (gradually less negative reduction potentials) but rather display faster (more diagnostic) chemical reduction with HAsc^- in the order **1** > **2** > **3**. It is reasonable to ascribe the observed behavior to the role played by hydroxido ligand(s). The overall scenario is in tune with that previously reported by Gibson for similar complexes [2, 15].

Reactivity of Pt(IV) complexes emerging from mass spectrometric analysis

ESI-MS of Pt(IV) complexes in the presence of ascorbic acid and glutathione

Reaction intermediates and products from the interaction of **1**, **2** and **3** with H_2Asc and GSH in aqueous methanol solution have been examined by ESI-MS.

Table 1 Kinetics and electrochemical data for the reduction of **1–3**

Compound	$t_{1/2} (\text{s} \times 10^2)^a$	$E_p (\text{V})^b$
1	5.2	-0.815
2	12.3	-0.618
3	320	-0.486

^aHalf-life (s) at 37 °C in the presence of a tenfold excess HAsc^-

^bReduction peak potential (V vs Ag/AgCl), GC electrode, scan rate 0.2 V s^{-1}

The mass spectra of the solution of **1** with ascorbic acid in positive ion mode at pH 4, recorded either right after mixing or following 12-h incubation time, are reported in panel A and B, respectively, of Figure S2 in the SM. Despite the acidic environment, that reduces the concentration of HAsc^- , which is considered the active species [2], an almost quantitative reduction of **1** to cisplatin is observed after one night incubation time. The reduction product is observed as aqua complex, $[\text{PtCl}(\text{NH}_3)_2(\text{H}_2\text{O})]^+$, yielding the isotopic cluster at m/z 281–285 shown in panel B of Figure S2. Because all platinum complexes reported in this work present a broad isotopic distribution, for the sake of simplicity, from now on, only the m/z value of the first intense peak of the cluster, namely the one containing ^{194}Pt and ^{35}Cl isotopes, is referred to. In this way, the isotopic cluster at m/z 281–285 becomes just m/z 281. The higher mass region of the positive ion mass spectrum (Figure S3A) shows the presence of a protonated putative non-covalent adduct of **1** and H_2Asc , $[\mathbf{1} + \text{H}_2\text{Asc} + \text{H}]^+$, at m/z 509. In an analogous way, a basic solution (pH ca. 9) analyzed in negative ion mode shows as the most important signal, apart from the ones related to ascorbic acid, a deprotonated non-covalent adduct $[\mathbf{1} + \text{HAsc}]^-$ at m/z 507 (Figure S3B). The putative non-covalent adducts of **1** and ascorbic acid are an interesting finding because these species represent the coming together of the two reactants forming the non-covalent intermediate named encounter complex in bimolecular reactions in solution. In the ESI isolated ions, this complex is freed from the solvent and obtained as naked species, void of any solvation interaction. The ESI process is, thus, a valuable route to investigate these significant (though elusive to any direct assay) intermediates in bimolecular reactivity in solution. The gas phase has recently been proven to be a suitable

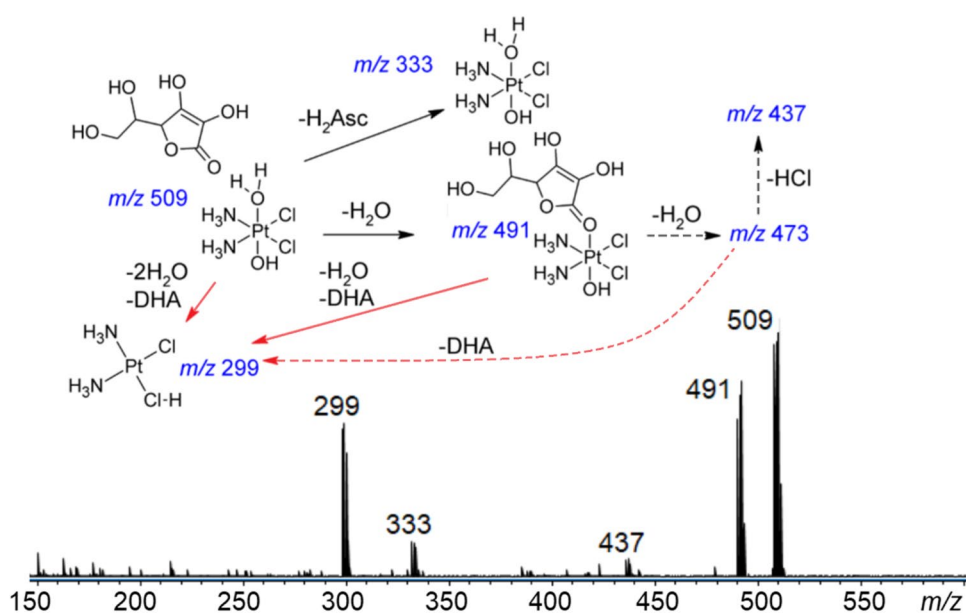
medium to reveal structural features and reactivity properties of the encounter complexes involved in ligand exchange reactions between cisplatin derived complexes and biological targets [66, 67].

The reaction with glutathione (GSH) was also tested. The mass spectrum of **1** in the presence of GSH is reported in Figure S4 either right after mixing (panel A) or after 12-h incubation time (panel B). In the latter condition, it is possible to observe the formation of the aqua complex of cisplatin, though the reaction is far from complete at variance with the reactivity behavior observed in the presence of ascorbic acid under comparable conditions. This evidence is in agreement with kinetic studies in solution which highlight that the reduction of Pt(IV) by GSH is less efficient than by ascorbic acid [68]. In acidic solution, a non-covalent adduct, $[\mathbf{1} + \text{GSH} + \text{H}]^+$ at m/z 640, is observed.

Behavior of activated non-covalent adducts of Pt(IV) complexes with ascorbic acid or glutathione

As reported in “ESI-MS of Pt(IV) complexes in the presence of ascorbic acid and glutathione”, adducts of the Pt(IV) prodrugs and ascorbic acid are observed in both positive and negative ion modes. These isolated encounter complexes are, thus, amenable to be assayed for their intrinsic reactivity, unaffected by the presence of solvent or counter ions. These adducts were, thus, assayed upon activation using either collision-induced dissociation (CID) or IRMPD. The mass spectrum of activated $[\mathbf{1} + \text{H}_2\text{Asc} + \text{H}]^+$ ions is reported in Fig. 1 together with a proposed fragmentation pathway. The dissociation products obtained by IRMPD are entirely consistent with the CID behavior. In particular, the release of the two non-covalently bound units yields $[\mathbf{1} + \text{H}]^+$ rather

Fig. 1 Mass spectrum of $[\mathbf{1} + \text{H}_2\text{Asc} + \text{H}]^+$ ions activated by IR multiple photon absorption at 1300 cm^{-1} . A proposed interpretation of the dissociation pathways leading to the reduced fragment, protonated cisplatin at m/z 299, are highlighted in red. The ion at m/z 473 does not grow to any significant abundance and its role in the fragmentation scheme could not be verified by MS/MS experiments (dashed arrows). All species in the scheme are singly charged. Charges are not made explicit



than $[\text{H}_2\text{Asc} + \text{H}]^+$, meaning that the gas phase basicity of **1** is higher than $202 \text{ kcal mol}^{-1}$, the experimentally reported value for H_2Asc at 298 K [69].

The spectrum in Fig. 1 contains dissociation paths that involve the reduction of the platinum core, suggesting that the sampled non-covalent complex is in fact involved in the reduction process of Pt(IV)-containing prodrugs. The ion at m/z 299, corresponding to protonated cisplatin, is in fact a major product. A CID experiment (MS^3) on the fragment at m/z 491, namely the product of water-loss from the reactant ionic adduct at m/z 509, was performed to unveil its role in the formation of the reduced species at m/z 299. Indeed, the CID spectrum of this ion contains the reduced complex as the most abundant CID product (Figure S5). Given that the ion at m/z 491 has likely undergone substitution of a water molecule by ascorbic acid, the formation of reduced complex, formally protonated cisplatin, from this species suggests an inner-sphere mechanism to be prominent in the reduction of Pt(IV) complexes by neutral ascorbic acid.

Because no $[\mathbf{3} + \text{H}_2\text{Asc} + \text{H}]^+$ and $[\mathbf{2} + \text{H}_2\text{Asc} + \text{H}]^+$ adducts could be observed from acidic solutions of either **3** or **2** with ascorbic acid, their reactivity behavior could not be explored.

In the negative ESI mode, the non-covalent adduct $[\mathbf{1} + \text{HAsc}]^-$ has been assayed by IR activation and the ensuing spectrum is reported in Fig. 2.

The negatively charged complex $[\mathbf{1} + \text{HAsc}]^-$ yields reduced fragments reminiscent of the behavior of its protonated counterpart. In particular, the dissociation products observed at m/z 315 and m/z 297 are formally accounted for by $[\text{Pt}(\text{II})\text{Cl}_2(\text{NH}_3)_2(\text{OH})]^-$ and $[\text{Pt}(\text{II})\text{Cl}_2(\text{NH}_2)(\text{NH}_3)]^-$, respectively. Once again, these reduced species represent the most important dissociation channel.

A negatively charged non-covalent adduct of **2** with ascorbic acid, $[\mathbf{2} + \text{HAsc}]^-$, was also identified in the solution with added ammonia. Figure 3 shows the fragmentation mass spectrum of $[\mathbf{2} + \text{HAsc}]^-$. Interestingly, the fragmentation process yields two reduced species at m/z 357 and m/z 297 along a similar process as observed by activation of the $[\mathbf{1} + \text{HAsc}]^-$ complex. In fact, the ion at m/z 357 still retains an acetate unit following reduction and formal loss of $\text{DHA} + \text{H}_2\text{O}$; while, the complex at m/z 297 corresponds to the same end product observed previously ($[\text{PtCl}_2(\text{NH}_2)(\text{NH}_3)]^-$). However, one may note that the reduced species are not the major Pt-containing products, as instead observed in the reaction of $[\mathbf{1} + \text{HAsc}]^-$.

With regard to complex **3**, the $[\mathbf{3} + \text{HAsc}]^-$ adduct was identified at m/z 591, as reported in panel A of Figure S6 in the SM. However, contrary to the behavior displayed by $[\mathbf{1} + \text{HAsc}]^-$ and $[\mathbf{2} + \text{HAsc}]^-$, this ion does not yield reduction products when activated towards dissociation, releasing only HAsc^- at m/z 175 (panel B of Figure S6). Therefore, the comparative reactivity behavior of the three assayed deprotonated complexes suggests that the presence of a hydroxido ligand in axial position is important to allow reduction of the isolated activated complexes.

The fragmentation behavior of the adduct of **1** with glutathione in acidic environment, $[\mathbf{1} + \text{GSH} + \text{H}]^+$, was also assayed. However, activated $[\mathbf{1} + \text{GSH} + \text{H}]^+$ ions yield mainly protonated glutathione (Figure S7). The only other pathway involves stepwise loss of two water molecules and Pt(II) containing species are by no means observed. This result is not surprising, though, because GSH acts as a single-electron reducing agent, thus the two-electron reduction from Pt(IV) to Pt(II) is inhibited in the

Fig. 2 Mass spectrum of $[\mathbf{1} + \text{HAsc}]^-$ ions activated by IR multiple photon absorption at 1780 cm^{-1} . A proposed interpretation of the dissociation pathways is reported in the scheme. The dissociation channel leading to the reduced fragments at m/z 315 and 297 is highlighted in red. All the species in the scheme are singly charged. Charges are not made explicit

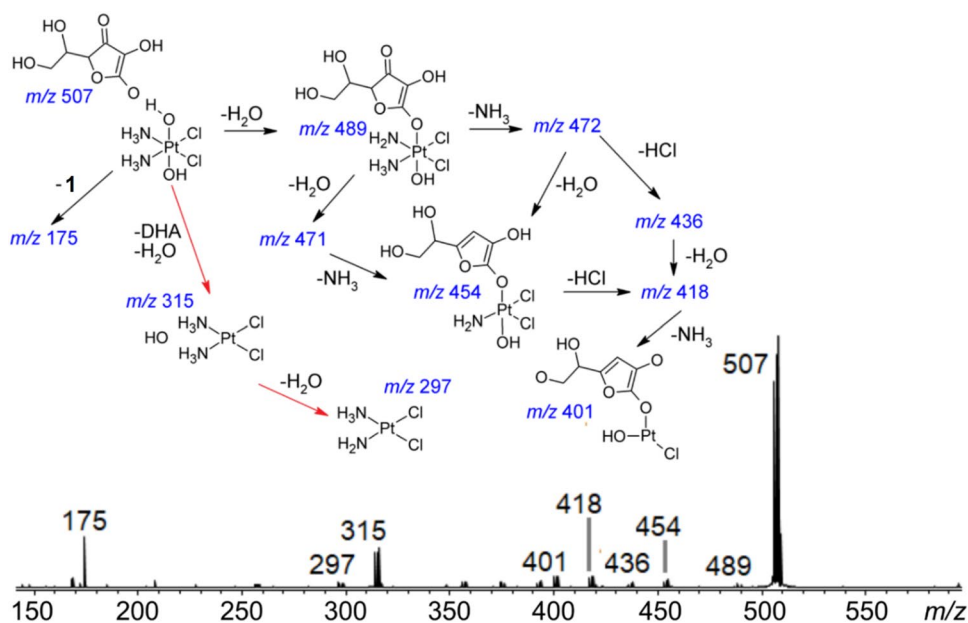
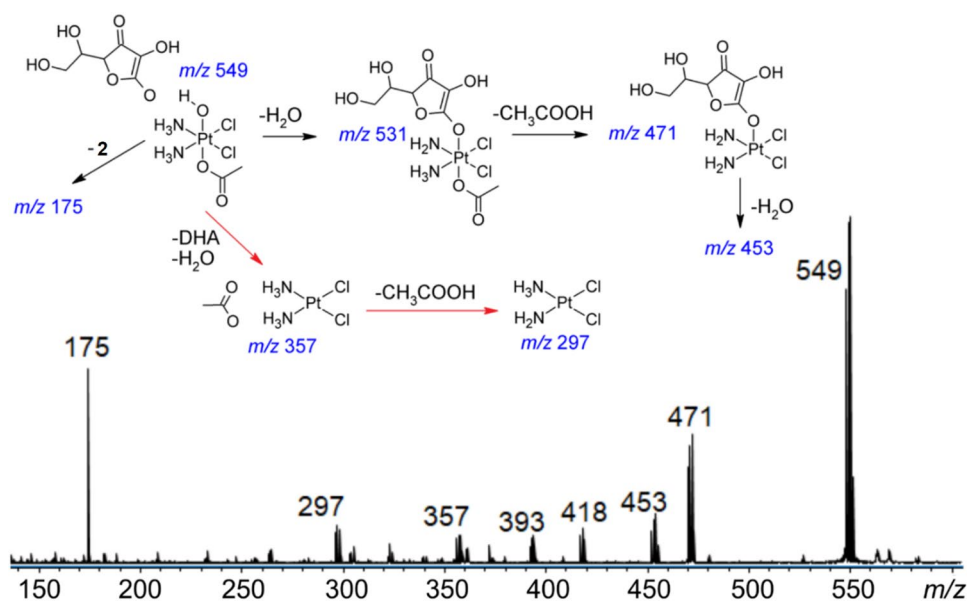


Fig. 3 Mass spectrum of $[2 + \text{HAsc}]^-$ activated by multiple photon absorption at 1420 cm^{-1} . A proposed interpretation of the dissociation pathways is reported in the scheme. The dissociation channel leading to the reduced fragments at m/z 357 and 297 is highlighted in red. All the species in the scheme are singly charged. Charges are not made explicit



isolated complex that does not allow for the participation of another reductant molecule.

IRMPD spectroscopy and structural characterization of ionic encounter complexes

To probe the structure of the sampled ions and verify any correspondence with the complexes depicted in the schemes of Figs. 1, 2 and 3, the IR spectrum has been recorded for $[1 + \text{H}_2\text{Asc} + \text{H}]^+$, $[1 + \text{HAsc}]^-$ and $[2 + \text{HAsc}]^-$, using IRMPD spectroscopy in the fingerprint range. IRMPD spectroscopy has already successfully provided a structural characterization of platinum complexes of biological interest [67, 70, 71]. Figure 4 displays the IRMPD spectrum of $[1 + \text{H}_2\text{Asc} + \text{H}]^+$ together with the calculated IR spectra of conformers **509_1** and **509_1b**.

The agreement between the experimental spectrum and the calculated ones confirms the sampled ions as non-covalently bound adducts of neutral ascorbic acid and $[1 + \text{H}]^+$. The calculated structures are characterized by a H-bond interaction between the donor aqua ligand of protonated **1** and either a hydroxyl or carbonyl oxygen atom of H_2Asc , in **509_1** and **509_1b**, respectively. The shared proton is covalently bound to the water oxygen of **1** (at ca. 0.98 \AA) and lies at 1.7 \AA from the acceptor oxygen of H_2Asc in both conformers. The assignment of the experimental IRMPD bands to calculated vibrational modes is reported in Table S1 in the SM.

The anionic adduct of **1** and ascorbic acid was also assayed by IRMPD spectroscopy, in view of the interest attached to ascorbate, known to be more active than neutral

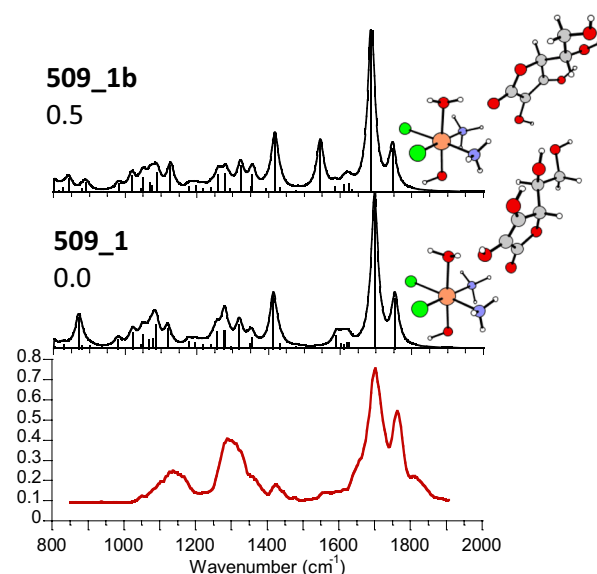


Fig. 4 IRMPD spectrum of $[1 + \text{H}_2\text{Asc} + \text{H}]^+$ (red profile) compared with the calculated IR spectra of **509_1** and **509_1b**, whose optimized structures are reported on the right. Relative free energies (298 K) are reported in kcal mol^{-1}

H_2Asc in reducing Pt(IV) complexes [2]. The IRMPD spectrum of $[1 + \text{HAsc}]^-$ and calculated IR spectra of the optimized most stable structures **507_1** and **507_1b** are reported in Fig. 5, while Table S2 in the SM provides a list of the experimental bands and assigned vibrational modes. The two isomers are similar in energy, **507_1b** lying $1.9 \text{ kcal mol}^{-1}$ higher. However, they present a rather different arrangement of the ascorbate anion interacting with **1**.

In the lowest lying isomer **507_1**, the furanone moiety is oriented toward the ammine ligands of **1** and a hydroxido

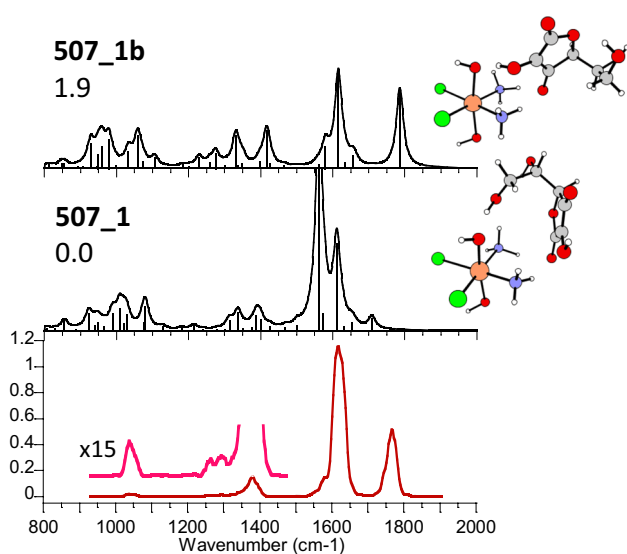


Fig. 5 IRMPD spectrum of $[1+\text{HAsc}]^-$ (red profile) compared with the calculated IR spectra of **507_1** and **507_1b**, whose optimized structures are reported on the right. Relative free energies (298 K) are reported in kcal mol^{-1}

oxygen atom is involved as H-bond acceptor with the primary alcohol functionality of HAsc^- . Within **507_1b**, the hydrogen of the hydroxyl group in the furanone cycle is directed toward the hydroxido ligand of **1**; while, protons on the ammine ligands interact with a carbonyl oxygen.

The comparison of the experimental spectrum with the theoretical ones suggests a significant contribution of **507_1b** in the gas-phase population. In fact, the IR spectrum of **507_1b** presents two major bands at 1786 cm^{-1} (free CO stretching) and 1615 cm^{-1} (furanone CC stretching) which are in good agreement with the experimental signals at 1767 and 1620 cm^{-1} . However, the presence of the species lowest in energy (**507_1**) cannot be excluded based on the spectroscopic data. Actually, while it does not possess any vibrational mode around 1800 cm^{-1} , **507_1** shows an important absorption at 1611 cm^{-1} , corresponding to the asymmetric bending of NH_3 coupled with the stretching of the CO group involved in H-bonding with the NH_3 ligands, which may contribute to the pronounced experimental band at 1620 cm^{-1} . In addition, a shoulder feature is observed at 1573 cm^{-1} that is where **507_1** shows its most intense vibrational mode (1561 cm^{-1}). However, this mode corresponds to the OH bending of the primary alcohol H-bonded to the hydroxido ligand. This particular vibration is known to be typically poorly active in IRMPD spectra, thus in contrast with the theoretically predicted intensity [72–74]. In conclusion, both **507_1** and **507_1b** are likely to both contribute to the gas-phase population of $[1+\text{HAsc}]^-$, confirming its attribution to the non-covalent encounter complex of **1** and deprotonated ascorbic acid. The contribution of **507_1b**

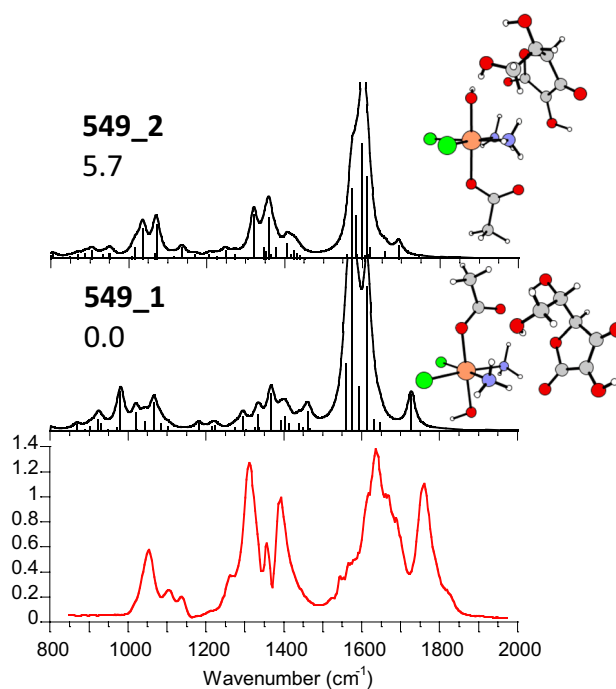


Fig. 6 IRMPD spectrum of $[2+\text{HAsc}]^-$ (red profile) and calculated IR spectra of **549_1** and **549_2** whose optimized structures are reported on the right. Relative free energies (298 K) are reported in kcal mol^{-1}

lying at 1.9 kcal mol^{-1} relative to **507_1** may be ascribed to the kinetic trapping of a species that is energetically favored in solution although, in view of the moderate energy difference between the two species, this result may also underline an uncertainty in the theoretical estimate exceeding the typically accepted $\pm 1\text{ kcal mol}^{-1}$.

Finally, in Fig. 6, the IRMPD spectrum of $[2+\text{HAsc}]^-$ is reported and compared with the calculated IR spectra of **549_1** and **549_2**. The lowest lying geometry, **549_1**, in a survey of potential isomers presents HAsc^- non-covalently bound to the acetato ligand. In isomer **549_2**, ascorbate anion is oriented toward the hydroxido ligand. The theoretical spectrum of **549_1** shows several features which appear also in the IRMPD spectrum, assessing the importance of this isomer in the sampled population. In particular, the experimental band at 1754 cm^{-1} can be assigned to the coupled CO stretching of both carbonyl groups of ascorbate at 1727 cm^{-1} . The broad experimental feature centered at 1637 cm^{-1} is likely to encompass several vibrational modes calculated at $1550\text{--}1650\text{ cm}^{-1}$, including NH_3 asymmetric bending modes coupled with either OH bendings or CO stretches of the ascorbate unit.

The absorptions below 1450 cm^{-1} are conserved among the whole set of calculated isomers and are described in detail together with the other calculated modes in Table S3 in the SM. It is, however, clear from the comparison in Fig. 6

that the presence of other isomers in the gas-phase population cannot be ruled out based on the spectroscopic evidence. In fact, isomer **549_2**, lying 5.7 kcal mol⁻¹ higher in energy relative to **549_1**, shares most features with the lowest lying isomer. The CO stretches, however, are red-shifted at 1692 cm⁻¹. This finding suggests that **549_1** makes anyway the major part of the population due to the high intensity of the band at 1754 cm⁻¹. The reported results concur in confirming the non-covalent character for the complex of **2** and HAsc⁻, where the latter ion is oriented toward either the hydroxido or acetato ligands, in overall agreement with the structural features of both [1 + HAsc]⁻ and the corresponding cation [1 + H₂Asc + H]⁺.

Calculated free energy profiles for the gas-phase fragmentation

Preliminarily to the presentation and discussion of the fragmentation pathways assisted by the computational study, one may underline that CID processes do not occur at thermal energies. Rather, they require appropriate excitation of the reactant species by kinetic to internal energy conversion occurring in an energetic collision event. Calculated B3LYP-D3 free energy profiles for the fragmentation of the [1 + H₂Asc + H]⁺ adduct are reported in Fig. 7. The first event in the dissociation of [1 + H₂Asc + H]⁺ is either water or ascorbic acid elimination causing a bifurcation of the fragmentation path. Water elimination occurs simultaneously with the coordination of ascorbic acid to the metal center, surmounting an energy barrier of 18.4 kcal mol⁻¹. Subsequently, a hydrogen transfer from one of the ammonia molecules to the OH group in *trans* position leads to the formation of a second water molecule that can be released leading to the penta-coordinated ion at *m/z* 473. The two involved intercepted transition states lie at 29.4 and 44.1 kcal mol⁻¹ above the zero-reference energy. Fragmentation can proceed by the elimination of a chlorido ligand that, in turn, can abstract a proton from the remaining ammonia to form a HCl molecule releasing the ion at *m/z* 437, in a process endergonic by 55.1 kcal mol⁻¹. The most significant path, however, regards the formation of the ion at *m/z* 299, as reported in panel b of Fig. 7. Starting from the penta-coordinated ion at *m/z* 473, a H₂Asc molecule is released and, subsequently, two formal hydrogen atom transfer from H₂Asc to the amino and chlorido ligands, ultimately yield DHA and protonated cisplatin. Elimination of a HCl unit completes the process (Fig. 7b and Figure S5).

The pathway that involves the elimination of neutral H₂Asc from the [1 + H₂Asc + H]⁺ adduct is depicted in Figure S8 of the SM. 24.6 kcal mol⁻¹ are required for the release to occur.

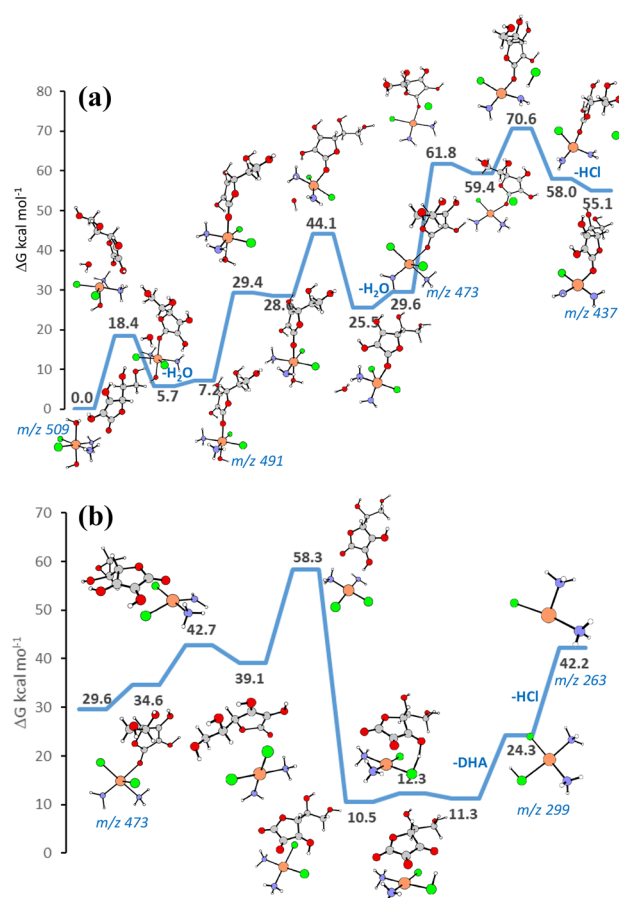


Fig. 7 Free energy profiles for the breakdown pattern of [1 + H₂Asc + H]⁺. The neutral losses for all the examined dissociations are indicated along the paths. Relative free energies at 298 K in kcal mol⁻¹ are calculated with respect to the most stable isomer of the initial ionic adduct. The *m/z* values for each species are also reported

The free energy profiles regarding the [1 + HAsc]⁻ breakdown pattern are illustrated in Fig. 8. Several alternative fragmentation pathways are displayed. First, let us consider the path (Fig. 8a) that through the formation of the ion at *m/z* 315, consistent with the species [PtCl₂(NH₃)₂](OH)⁻, leads to the formation of the ion at *m/z* 297 corresponding to the species [PtCl₂(NH₂)(NH₃)]⁻, both ions representing reduced cisplatin related species. The calculated PES shows that, for the process to occur, a conformational rearrangement is required to transform the lowest intercepted isomer of the [1 + HAsc]⁻ ion into the one, indicated as *m/z* 507_2, less stable by 7.9 kcal mol⁻¹. Formation of the ion at *m/z* 315 involves the attack of the ascorbate enolate β-carbon to the OH ligand, leading to the formation of a new C-O bond simultaneously with the release of the *trans* hydroxido ligand which remains in a non-covalently bound adduct with neutral cisplatin. The corresponding concerted transition state lies at 39.4 kcal mol⁻¹ above the zero-reference energy and the products are cisplatin, the OH⁻ ligand and ascorbic

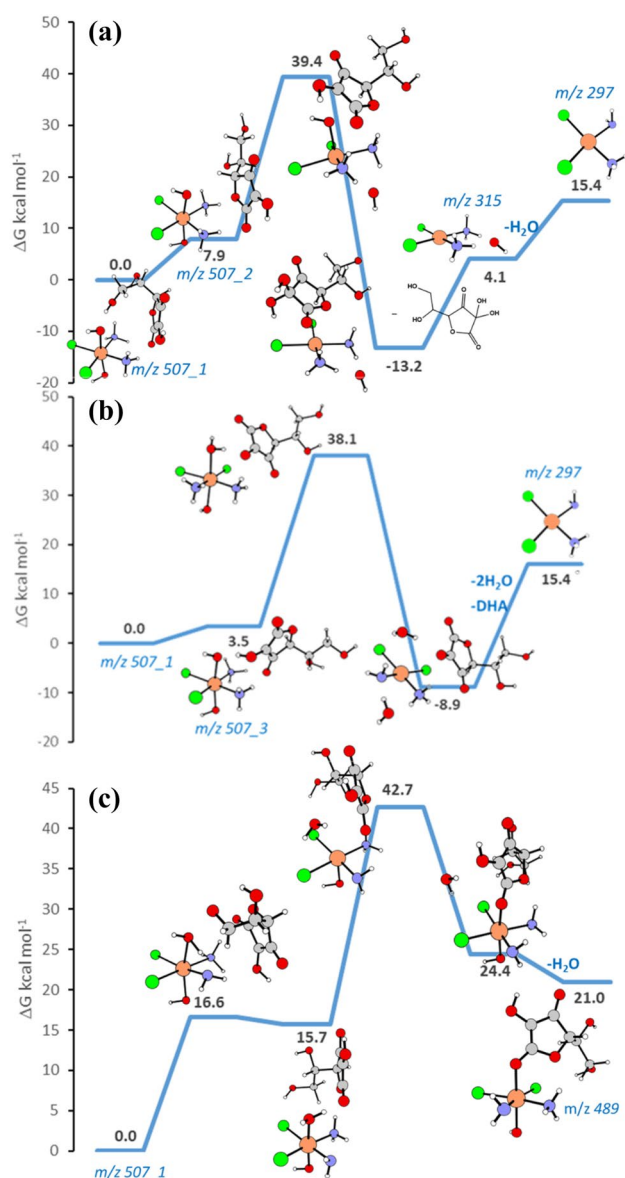


Fig. 8 Free energy profiles for the breakdown pattern of $[1 + \text{HAsc}]^-$. The neutral losses for all the examined dissociations are indicated along the paths. Relative free energies at 298 K in kcal mol^{-1} are calculated with respect to the most stable isomer (m/z 507_1) of the initial ionic adduct. The m/z values for each species are also reported

acid with an additional OH moiety on the enolate β -carbon. The abstraction of a proton from one of the NH_3 molecules with formation and release of a water molecule concludes the process, leading to deprotonated cisplatin, that results to be endergonic by $15.4 \text{ kcal mol}^{-1}$. The same $[\text{PtCl}(\text{NH}_2)(\text{NH}_3)]^-$ complex could be produced by the concerted elimination of two water molecules and formation of a DHA unit as reported in panel b of Fig. 8. The isomer properly arranged to start the process, indicated as m/z 507_3, is less stable by $3.5 \text{ kcal mol}^{-1}$ relative to the most stable conformer. The transition state involving the transfer of a

formal H^- unit from HAsc^- to a hydroxido ligand, triggering a proton migration from NH_3 to the second *trans* hydroxido ligand, lies at $38.1 \text{ kcal mol}^{-1}$ above the entrance channel. The whole process is endergonic by $15.4 \text{ kcal mol}^{-1}$.

The third alternative path does not present any reduction reactivity. It involves the transfer of a proton from NH_3 to one of the hydroxido ligands forming a water molecule bound to the metal center (see panel c of Fig. 8). The displacement of such H_2O molecule by the ascorbate and consequent elimination of the formed water leads to the ion at m/z 489. The two involved transition states are higher in energy than the initial complex by 16.6 and $42.7 \text{ kcal mol}^{-1}$, respectively. The whole reaction is calculated to be endergonic by $21.0 \text{ kcal mol}^{-1}$.

The ion at m/z 489 can further fragment and two interconnected pathways are generated differing in the moiety released first, as shown in Figures S9 and S10 of the SM.

The third Pt(IV) complex investigated by DFT calculations, $[2 + \text{HAsc}]^-$, presents several alternative fragmentation pathways, accounting for the formation of Pt(II) species at m/z 357 and m/z 297, as reported in Fig. 9.

In analogy with the fragmentation pathways calculated for the $[1 + \text{HAsc}]^-$ complex, there are two viable routes leading to the ion at m/z 357, formally corresponding to an adduct of cisplatin, $\text{PtCl}_2(\text{NH}_3)_2$, still interacting with an acetato unit. The conformer m/z 549_2, lying at $8.9 \text{ kcal mol}^{-1}$ relative to the most stable species, is the starting reactant, as shown in panel a of Fig. 9, for hydroxyl transfer to the ascorbate enolate β -carbon, causing the simultaneous cleavage of the *trans* acetato ligand. The release of acetate then occurs following a proton transfer from NH_3 to form acetic acid, completing the process calculated to be endergonic by $31.0 \text{ kcal mol}^{-1}$. The same outcome can be accomplished along the path depicted in panel b of Fig. 9, whereby a H^- unit is transferred from ascorbate to the hydroxido ligand to release a water molecule and the *trans* acetate. The ion at m/z 357 is formed by loss of H_2O and DHA. A third path (panel c of Fig. 9) is activated from an additional isomer lying at $10.3 \text{ kcal mol}^{-1}$ above the entrance channel. The H^- unit is transferred from ascorbate to the acetate ligand causing the concomitant detachment of an acetic acid molecule and OH^- . The transition state for this process is $43.4 \text{ kcal mol}^{-1}$ higher in energy than the reference complex, representing the highest value among the sampled free energy profiles. The formed ion at m/z 315 releases water after proton transfer to OH^- from NH_3 (see also path a in Fig. 8) forming the product ion at m/z 297. This last path (c) is, however, less likely in view of the missing evidence about the intermediate complex at m/z 315, which is consistent with the highest energy transition state among the three routes.

Additional calculations have addressed the paths that lead to the formation of the ions at m/z 514 and m/z 471.

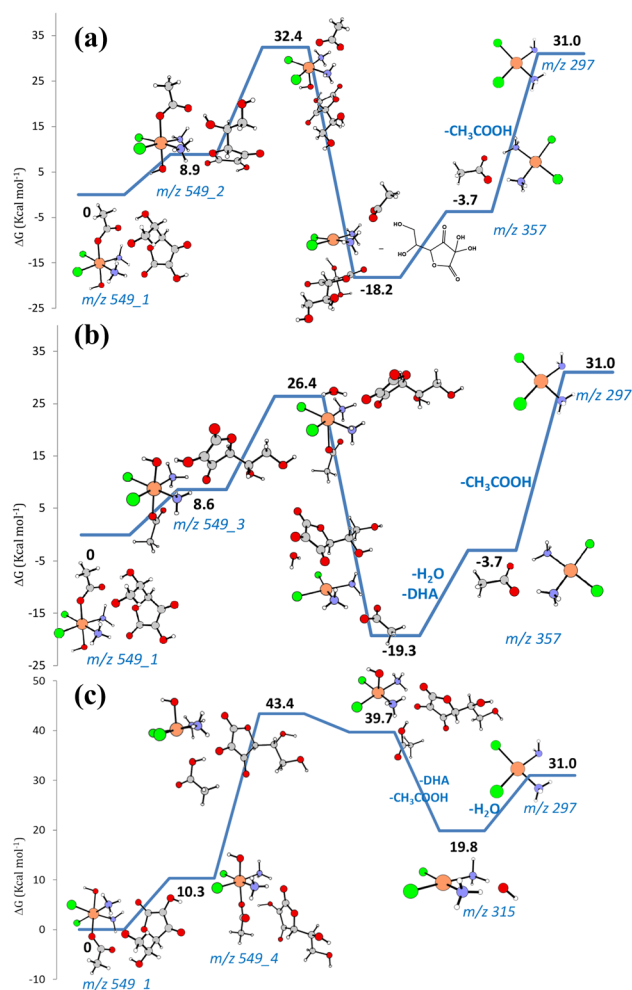


Fig. 9 Free energy profiles for the breakdown pattern of $[2 + \text{HAsc}]^-$. The neutral losses for all the examined dissociations are indicated along the paths. Relative free energies at 298 K in kcal mol^{-1} are calculated with respect to the most stable isomer of the initial ionic adduct. The m/z values for each species are also reported

These ions do not imply any reduction to Pt(II) and the free energy profiles are reported in Figure S11 in the SM.

Conclusions

Understanding some aspects of the reduction process leading to the release of the active Pt(II) species from their Pt(IV) prodrugs is the goal motivating this work. Indeed, the efficacy of Pt(IV) drug candidates requires their reduction to be neither too fast to avoid premature (extracellular) activation nor too slow to allow cytotoxic Pt(II) metabolite to be released effectively in tumor cells [38].

Interestingly enough, unsymmetrical Pt(IV) complexes containing a biologically active compound and one OH group in axial positions (dual-action prodrugs)

often exhibit in vitro and in vivo much better performance with respect to the symmetrically disubstituted counterparts. For instance, monochalcoptatin, a cisplatin-based unsymmetrical monocarboxylated Pt(IV) (Fig. 2) prodrug showed higher cytotoxicity than chalcoptatin, the symmetrical dicarboxylated homologue, despite the latter being more lipophilic and affording upon reduction two molecules of chalcone, a potent p53 agonist, instead of one. Although monochalcoptatin and chalcoptatin have similar reduction potentials, only the former is quickly reduced by HAsc^- and this immediate activation contributes to its higher cytotoxicity.

In the present contribution, the reduction reactivity behavior of the three exemplary Pt(IV) complexes, 1–3, has been assayed by the integration of quite diverse, though complementary, approaches. The reduction kinetics of 1–3, in the presence of ascorbic acid, that were recorded by resorting to ^{15}N -NMR spectroscopy of ^{15}N -enriched samples, have displayed the $1 > 2 \gg 3$ order, pointing to a key role of an axial hydroxido ligand. The trend of reduction peak potentials (E_p values: $1 < 2 < 3$) is not in this case a reliable predictor for the corresponding chemical reductions, rather suggesting 3 to be the most susceptible to be electrochemically reduced. This missing correlation has been already documented and ascribed to the mechanistic complexity of the reaction involving not only electron transfer to the metal center but also elimination of two axial ligands.

The mechanistic complexity prompted the gas phase study where the encounter complexes lying on the reaction coordinate for the reduction reaction can be isolated and studied at a molecular level. Thus, aiming to gain alternative evidence on the ease of reduction of 1–3, an ESI-MS study of the breakdown pattern of positively and negatively charged ions delivered from solutions in the presence of the bioreductant models H_2Asc and GSH has been carried out. The ESI process delivers ionic non-covalent complexes of 1–3 with a bioreductant (H_2Asc or GSH) molecule, namely the encounter complex lying on the reaction coordinate for the reduction in solution, as isolated species in the gas phase. The structure of these adducts has been assayed by IR ion spectroscopy and their reactivity has been evaluated by collision-induced dissociation. The results show the adducts of 1 and 2 with ascorbic acid to be prone to reduction, releasing Pt(II) species as major products. In particular, the $[1 + \text{H}_2\text{Asc} + \text{H}]^+$ adduct yields $[\text{Pt(II)Cl}_2(\text{NH}_3)_2 + \text{H}]^+$ and the $[1 + \text{HAsc}]^-$ adduct yields $[\text{Pt(II)Cl}_2(\text{NH}_3)_2 + \text{OH}]^-$ as prominent products, while the $[2 + \text{HAsc}]^-$ adduct yields $[\text{Pt(II)Cl}_2(\text{NH}_3)_2 + \text{AcO}]^-$ in somewhat lower extent. In contrast, the non-covalent adduct of 3 and H_2Asc does not yield any reduced product. The reactivity trend from reduction kinetics in solution is, thus, confirmed by the reactivity behavior of the isolated encounter complex. As expected, the GSH 1:1 complex with 1–3 does not allow the formation

of Pt(II) products, lacking the required two electron donor ability.

Quantum–mechanical DFT exploration of the corresponding fragmentation pathways in the presence of $H_2Asc/HAsc^-$ has provided a theoretical support to the proposed dissociation patterns and mechanistic hypotheses.

In conclusion, this work highlights the role of an axially coordinated hydroxido ligand in promoting the reduction of Pt(IV) prodrugs and suggests ESI-MS as a means to obtain an overview of reduction reactivity at the level of the isolated encounter complex of the reaction partners.

Acknowledgements The authors acknowledge financial support by Università della Calabria, Università del Piemonte Orientale, and Università di Roma “La Sapienza” (Dipartimenti di Eccellenza-L. 232/2016), and by the project CALIPSO plus under the Grant Agreement No. 730872 from the EU Framework Programme for Research and Innovations HORIZON 2020. The support of Philippe Maitre, Jean-Michel Ortega, Debora Scuderi, and Estelle Loire for the experiments at CLIO (IC 19-002) is also gratefully acknowledged. The authors were indebted to Inter-University Consortium for Research on the Chemistry of Metals in Biological Systems (CIRCMSB, Bari) for providing opportunities of stimulating discussions during the annual meetings.

Compliance with ethical standards

Conflict of interest The authors declare that they have no conflict of interest.

References

- Graf N, Lippard SJ (2012) Redox activation of metal-based prodrugs as a strategy for drug delivery. *Adv Drug Deliv Rev* 64(11):993–1004. <https://doi.org/10.1016/j.addr.2012.01.007>
- Wesselblatt E, Gibson D (2012) What do we know about the reduction of Pt(IV) pro-drugs? *J Inorg Biochem* 117:220–229. <https://doi.org/10.1016/j.jinorgbio.2012.06.013>
- Nemirovski A, Vinograd I, Takroui K, Mijovilovich A, Rompel A, Gibson D (2010) New reduction pathways for *cis*-PtCl₂(CH₃CO₂)₂(NH₃)(Am) anticancer prodrugs. *Chem Commun* 46(11):1842–1844. <https://doi.org/10.1039/b925721g>
- Ravera M, Gabano E, Zanellato I, Bonarrigo I, Escribano E, Moreno V, Font-Bardia M, Calvet T, Osella D (2012) Synthesis, characterization and antiproliferative activity on mesothelioma cell lines of bis(carboxylato)platinum(IV) complexes based on picoplatin. *Dalton Trans* 41(11):3313–3320. <https://doi.org/10.1039/c2dt11874b>
- Hall MD, Hambley TW (2002) Platinum(IV) antitumour compounds: their bioinorganic chemistry. *Coord Chem Rev* 232(1–2):49–67. [https://doi.org/10.1016/s0010-8545\(02\)00026-7](https://doi.org/10.1016/s0010-8545(02)00026-7)
- Hall MD, Mellor HR, Callaghan R, Hambley TW (2007) Basis for design and development of Platinum(IV) anticancer complexes. *J Med Chem* 50(15):3403–3411. <https://doi.org/10.1021/jm070280u>
- Gramatica P, Papa E, Luini M, Monti E, Gariboldi MB, Ravera M, Gabano E, Gaviglio L, Osella D (2010) Antiproliferative Pt(IV) complexes: synthesis, biological activity, and quantitative structure–activity relationship modeling. *J Biol Inorg Chem* 15(7):1157–1169. <https://doi.org/10.1007/s00775-010-0676-4>
- Platts JA, Ermondi G, Caron G, Ravera M, Gabano E, Gaviglio L, Pelosi G, Osella D (2011) Molecular and statistical modeling of reduction peak potential and lipophilicity of platinum(IV) complexes. *J Biol Inorg Chem* 16(3):361–372. <https://doi.org/10.1007/s00775-010-0731-1>
- Ermondi G, Caron G, Ravera M, Gabano E, Bianco S, Platts JA, Osella D (2013) Molecular interaction fields vs. quantum-mechanical-based descriptors in the modelling of lipophilicity of platinum(IV) complexes. *Dalton Trans* 42(10):3482–3489. <https://doi.org/10.1039/c2dt32360e>
- Varbanov HP, Jakupec MA, Roller A, Jensen F, Galanski M, Keppler BK (2013) Theoretical investigations and density functional theory based quantitative structure–activity relationships model for novel cytotoxic platinum(IV) complexes. *J Med Chem* 56(1):330–344. <https://doi.org/10.1021/jm3016427>
- Tetko IV, Varbanov HP, Galanski M, Talmaciu M, Platts JA, Ravera M, Gabano E (2016) Prediction of logP for Pt(II) and Pt(IV) complexes: comparison of statistical and quantum-chemistry based approaches. *J Inorg Biochem* 156:1–13. <https://doi.org/10.1016/j.jinorgbio.2015.12.006>
- Tolbatov I, Coletti C, Marrone A, Re N (2018) Insight into the electrochemical reduction mechanism of Pt(IV) anticancer complexes. *Inorg Chem* 57(6):3411–3419. <https://doi.org/10.1021/acs.inorgchem.8b00177>
- McCormick MC, Keijzer K, Polavarapu A, Schultz FA, Baik MH (2014) Understanding intrinsically irreversible, non-Nernstian, two-electron redox processes: a combined experimental and computational study of the electrochemical activation of platinum(IV) antitumor prodrugs. *J Am Chem Soc* 136(25):8992–9000. <https://doi.org/10.1021/ja5029765>
- Zanellato I, Bonarrigo I, Colangelo D, Gabano E, Ravera M, Alesio M, Osella D (2014) Biological activity of a series of cisplatin-based aliphatic bis(carboxylato) Pt(IV) prodrugs: how long the organic chain should be? *J Inorg Biochem* 140:219–227. <https://doi.org/10.1016/j.jinorgbio.2014.07.018>
- Zhang JZ, Wesselblatt E, Hambley TW, Gibson D (2012) Pt(IV) analogs of oxaliplatin that do not follow the expected correlation between electrochemical reduction potential and rate of reduction by ascorbate. *Chem Commun* 48(6):847–849. <https://doi.org/10.1039/c1cc16647f>
- Chaney SG, Wyrick S, Till GK (1990) In vitro biotransformations of tetrachloro-(D, L-trans)-1,2-diaminocyclohexaneplatinum(IV) (tetraplatin) in rat plasma. *Cancer Res* 50(15):4539–4545
- Chaney SG, Gibbons GR, Wyrick SD, Podhasky P (1991) An unexpected biotransformation pathway for tetrachloro-(D, L-trans)-1,2-diaminocyclohexaneplatinum(IV) (tetraplatin) in the L1210 cell-line. *Cancer Res* 51(3):969–973
- Pendyala L, Cowens JW, Chheda GB, Dutta SP, Creaven PJ (1988) Identification of cis-dichloro-bis-isopropylamine platinum(II) as a major metabolite of iproplatin in humans. *Cancer Res* 48(12):3533–3536
- Schafer FQ, Buettner GR (2001) Redox environment of the cell as viewed through the redox state of the glutathione disulfide/glutathione couple. *Free Radic Biol Med* 30(11):1191–1212. [https://doi.org/10.1016/s0891-5849\(01\)00480-4](https://doi.org/10.1016/s0891-5849(01)00480-4)
- Fiaschi AI, Cozzolino A, Ruggiero G, Giorgi G (2005) Glutathione, ascorbic acid and antioxidant enzymes in the tumor tissue and blood of patients with oral squamous cell carcinoma. *Eur Rev Med Pharmacol Sci* 9:361–367
- Liu Y, Tian HW, Xu LY, Zhou L, Wang JH, Xu BY, Liu CL, Elding LI, Shi TS (2019) Investigations of the kinetics and mechanism of reduction of a carboplatin Pt(IV) prodrug by the major small-molecule reductants in human plasma. *Int J Mol Sci* 20(22):5660. <https://doi.org/10.3390/Ijms20225660>
- Kostrhunova H, Kasparkova J, Gibson D, Brabec V (2010) Studies on cellular accumulation of satraplatin and its major metabolite

- JM118 and their interactions with glutathione. *Mol Pharm* 7(6):2093–2102. <https://doi.org/10.1021/mp100080e>
23. Ravera M, Gabano E, Bianco S, Ermondi G, Caron G, Vallaro M, Pelosi G, Zanellato I, Bonarrigo I, Cassino C, Osella D (2015) Host-guest inclusion systems of Pt(IV)-bis(benzoato) anticancer drug candidates and cyclodextrins. *Inorg Chim Acta* 432:115–127. <https://doi.org/10.1016/j.ica.2015.03.039>
 24. Ravera M, Perin E, Gabano E, Zanellato I, Panzarasa G, Sparnacci K, Laus M, Osella D (2015) Functional fluorescent nonporous silica nanoparticles as carriers for Pt(IV) anticancer prodrugs. *J Inorg Biochem* 151:132–142. <https://doi.org/10.1016/j.jinorgbio.2015.08.001>
 25. Dong JR, Huo SY, Shen SG, Xu JZ, Shi TS, Elding LI (2016) Reactivity of the glutathione species towards the reduction of ormaplatin (or tetraplatin). *Bioorg Med Chem Lett* 26(17):4261–4266. <https://doi.org/10.1016/j.bmcl.2016.07.046>
 26. Dong JR, Ren YL, Huo SY, Shen SG, Xu JZ, Tian HW, Shi TS (2016) Reduction of ormaplatin and cis-diamminetetrachloroplatinum(IV) by ascorbic acid and dominant thiols in human plasma: kinetic and mechanistic analyses. *Dalton Trans* 45(28):11326–11337. <https://doi.org/10.1039/c6dt01804a>
 27. Dong JR, Tian HW, Song CY, Shi TS, Elding LI (2018) Reduction of ormaplatin by an extended series of thiols unravels a remarkable correlation. *Dalton Trans* 47(16):5548–5552. <https://doi.org/10.1039/c8dt00852c>
 28. Lemma K, Shi TS, Elding LI (2000) Kinetics and mechanism for reduction of the anticancer prodrug trans, trans, trans-PtCl₂(OH)₂(c-C₆H₁₁NH₂)(NH₃) (JM335) by thiols. *Inorg Chem* 39(8):1728–1734. <https://doi.org/10.1021/ic9913511>
 29. Ravera M, Gabano E, Pelosi G, Fregonese F, Tinello S, Osella D (2014) A new entry to asymmetric platinum(IV) complexes via oxidative chlorination. *Inorg Chem* 53(17):9326–9335. <https://doi.org/10.1021/ic501446b>
 30. Chipman A, Yates BF, Canty AJ, Ariafard A (2018) Reduction of a platinum(IV) prodrug model by sulfur containing biological reductants: computational mechanistic elucidation. *Chem Commun* 54(74):10491–10494. <https://doi.org/10.1039/c8cc05682j>
 31. Ong JX, Lim CSQ, Le HV, Ang WH (2019) A Ratiometric fluorescent probe for cisplatin: investigating the intracellular reduction of platinum(IV) prodrug complexes. *Angew Chem Int Edit* 58(1):164–167. <https://doi.org/10.1002/anie.201810361>
 32. Moriarty MJ, Mulgrew S, Malone J, O'Connor M (1977) Results and analysis of tumour levels of ascorbic acid. *Iran J Med Sci* 146:74–78
 33. Lemma K, Sargeson AM, Elding LI (2000) Kinetics and mechanism for reduction of oral anticancer platinum(IV) dicarboxylate compounds by L-ascorbate ions. *J Chem Soc Dalton Trans* 7:1167–1172. <https://doi.org/10.1039/a909484i>
 34. Bose RN, Weaver EL (1997) A long-lived ascorbate radical in the platinum(II) catalysed reductions of platinum(IV) antitumor drugs. *J Chem Soc Dalton Trans* 11:1797–1799. <https://doi.org/10.1039/a700196g>
 35. Hindmarsh K, House DA, van Eldik R (1998) The redox kinetics of platinum(II)/(IV) complexes. *Inorg Chim Acta* 278(1):32–42. [https://doi.org/10.1016/S0020-1693\(97\)06171-9](https://doi.org/10.1016/S0020-1693(97)06171-9)
 36. Weaver EL, Bose RN (2003) Platinum(II) catalysis and radical intervention in reductions of platinum(IV) antitumor drugs by ascorbic acid. *J Inorg Biochem* 95(4):231–239. [https://doi.org/10.1016/s0162-0134\(03\)00136-3](https://doi.org/10.1016/s0162-0134(03)00136-3)
 37. Chen CKJ, Zhang JZ, Aitken JB, Hambley TW (2013) influence of equatorial and axial carboxylato ligands on the kinetic inertness of platinum(IV) complexes in the presence of ascorbate and cysteine and within DLD-1 cancer cells. *J Med Chem* 56(21):8757–8764. <https://doi.org/10.1021/jm401218n>
 38. Chen CKJ, Kappen P, Hambley TW (2019) The reduction of cis-platinum(IV) complexes by ascorbate and in whole human blood models using H-1 NMR and XANES spectroscopy. *Metallomics* 11(3):686–695. <https://doi.org/10.1039/c9mt00003h>
 39. Peloso A (1984) An investigation on the influence of coordinated aliphatic amines on the rates of reduction of tetrachlorodiamineplatinum(IV) complexes. *J Chem Soc Dalton Trans* 2:249–254. <https://doi.org/10.1039/DT9840000249>
 40. Lemma K, House DA, Retta N, Elding LI (2002) Kinetics and mechanism for reduction of halo- and haloam(m)ine platinum(IV) complexes by L-ascorbate. *Inorg Chim Acta* 331:98–108. [https://doi.org/10.1016/s0020-1693\(01\)00762-9](https://doi.org/10.1016/s0020-1693(01)00762-9)
 41. Choi S, Filotto C, Bisanzo M, Delaney S, Lagasee D, Whitworth JL, Jusko A, Li CR, Wood NA, Willingham J, Schwenker A, Spaulding K (1998) Reduction and anticancer activity of platinum(IV) complexes. *Inorg Chem* 37(10):2500–2504. <https://doi.org/10.1021/ic971047x>
 42. Dabbish E, Ponte F, Russo N, Sicilia E (2019) Antitumor platinum(IV) prodrugs: a systematic computational exploration of their reduction mechanism by L-ascorbic acid. *Inorg Chem* 58(6):3851–3860. <https://doi.org/10.1021/acs.inorgchem.8b03486>
 43. Ponte F, Russo N, Sicilia E (2018) insights from computations on the mechanism of reduction by ascorbic acid of Pt-IV prodrugs with asplatin and its chlorido and bromido analogues as model systems. *Chem Eur J* 24(38):9572–9580. <https://doi.org/10.1002/chem.201800488>
 44. Sinisi M, Intini FP, Natile G (2012) Dependence of the reduction products of platinum(IV) prodrugs upon the configuration of the substrate, bulk of the carrier ligands, and nature of the reducing agent. *Inorg Chem* 51(18):9694–9704. <https://doi.org/10.1021/ic300957v>
 45. Gabano E, Ravera M, Zanellato I, Tinello S, Gallina A, Rangone B, Gandin V, Marzano C, Bottone MG, Osella D (2017) An unsymmetric cisplatin-based Pt(IV) derivative containing 2-(2-propynyl) octanoate: a very efficient multi-action antitumor prodrug candidate. *Dalton Trans* 46(41):14174–14185. <https://doi.org/10.1039/c7dt02928d>
 46. Gabano E, Ravera M, Trivero F, Tinello S, Gallina A, Zanellato I, Gariboldi MB, Monti E, Osella D (2018) The cisplatin-based Pt(IV)-diclorofibrato multi-action anticancer prodrug exhibits excellent performances also under hypoxic conditions. *Dalton Trans* 47(25):8268–8282. <https://doi.org/10.1039/c7dt04614f>
 47. Ravera M, Gabano E, Tinello S, Zanellato I, Osella D (2017) May glutamine addiction drive the delivery of antitumor cisplatin-based Pt(IV) prodrugs? *J Inorg Biochem* 167:27–35. <https://doi.org/10.1016/j.jinorgbio.2016.11.024>
 48. Ravera M, Gabano E, Zanellato I, Fregonese F, Pelosi G, Platts JA, Osella D (2016) Antiproliferative activity of a series of cisplatin-based Pt(IV)-acetylamo/carboxylato prodrugs. *Dalton Trans* 45(12):5300–5309. <https://doi.org/10.1039/c5dt04905a>
 49. Nemirovski A, Kasherman Y, Tzaraf Y, Gibson D (2007) Reduction of *cis*, *trans*, *cis*-Pt₂I₂(OCO₂C₂H₃)₂(NH₃)₂ by aqueous extracts of cancer cells. *J Med Chem* 50(23):5554–5556. <https://doi.org/10.1021/jm070740j>
 50. Carr JL, Tingle MD, McKeage MJ (2006) Satraplatin activation by haemoglobin, cytochrome *c* and liver microsomes in vitro. *Cancer Chemother Pharmacol* 57(4):483–490. <https://doi.org/10.1007/s00280-005-0069-5>
 51. Lasorsa A, Stuchlíková O, Brabec V, Natile G, Arnesano F (2016) Activation of platinum(IV) prodrugs by cytochrome *c* and characterization of the protein binding sites. *Mol Pharm* 13(9):3216–3223. <https://doi.org/10.1021/acs.molpharmaceut.6b00438>
 52. Ma LL, Wang N, Ma R, Li C, Xu ZF, Tse MK, Zhu GY (2018) Monochalcoplatin: an actively transported, quickly reducible, and highly potent Pt-IV anticancer prodrug. *Angew Chem Int Ed* 57(29):9098–9102. <https://doi.org/10.1002/anie.201804314>

53. Corinti D, Crestoni ME, Fornarini S, Ponte F, Russo N, Sicilia E, Gabano E, Osella D (2019) Elusive intermediates in the breakdown reactivity patterns of prodrug platinum(IV) complexes. *J Am Soc Mass Spectrom*. <https://doi.org/10.1007/s13361-019-02186-7>
54. Bakker JM, Besson T, Lemaire J, Scuderi D, Maître P (2007) Gas-phase structure of a π -allyl–palladium complex: efficient infrared spectroscopy in a 7 T Fourier transform mass spectrometer. *J Phys Chem A* 111(51):13415–13424. <https://doi.org/10.1021/jp074935e>
55. Lemaire J, Boissel P, Heninger M, Mauclaire G, Bellec G, Mestdagh H, Simon A, Caer SL, Ortega JM, Glotin F, Maître P (2002) Gas phase infrared spectroscopy of selectively prepared ions. *Phys Rev Lett* 89(27):273002. <https://doi.org/10.1103/PhysRevLett.89.273002>
56. Becke AD (1993) Density-functional thermochemistry. 3. The role of exact exchange. *J Chem Phys* 98(7):5648–5652. <https://doi.org/10.1063/1.464913>
57. Lee C, Yang W, Parr RG (1988) Development of the Colle–Salvetti correlation-energy formula into a functional of the electron density. *Phys Rev B* 37(2):785–789
58. Frisch MJ, Trucks GW, Schlegel HB, Scuseria GE, Robb MA, Cheeseman JR, Scalmani G, Barone V, Mennucci B, Petersson GA, Nakatsuji H, Caricato M, Li X, Hratchian HP, Izmaylov AF, Bloino J, Zheng G, Sonnenberg JL, Hada M, Ehara M, Toyota K, Fukuda R, Hasegawa J, Ishida M, Nakajima T, Honda Y, Kitao O, Nakai H, Vreven T, Montgomery Jr. JA, Peralta JE, Ogliaro F, Bearpark MJ, Heyd J, Brothers EN, Kudin KN, Staroverov VN, Kobayashi R, Normand J, Raghavachari K, Rendell AP, Burant JC, Iyengar SS, Tomasi J, Cossi M, Rega N, Millam NJ, Klene M, Knox JE, Cross JB, Bakken V, Adamo C, Jaramillo J, Gomperts R, Stratmann RE, Yazyev O, Austin AJ, Cammi R, Pomelli C, Ochterski JW, Martin RL, Morokuma K, Zakrzewski VG, Voth GA, Salvador P, Dannenberg JJ, Dapprich S, Daniels AD, Farkas Ö, Foresman JB, Ortiz JV, Cioslowski J, Fox DJ (2009) Gaussian 09. Revision D.01 edn. Gaussian, Inc., Wallingford
59. Grimme S, Antony J, Ehrlich S, Krieg H (2010) A consistent and accurate ab initio parametrization of density functional dispersion correction (DFT-D) for the 94 elements H–Pu. *J Chem Phys*. <https://doi.org/10.1063/1.3382344>
60. Andrae D, Haussermann U, Dolg M, Stoll H, Preuss H (1990) Energy-adjusted ab initio pseudopotentials for the second and third row transition elements. *Theor Chim Acta* 77(2):123–141. <https://doi.org/10.1007/bf01114537>
61. Fukui K (1970) Formulation of the reaction coordinate. *J Phys Chem* 74(23):4161–4163. <https://doi.org/10.1021/j100717a029>
62. Gonzalez C, Schlegel H (1989) An improved algorithm for reaction-path following. *J Chem Phys* 90:2154–2161. <https://doi.org/10.1063/1.456010>
63. McQuarrie DA, Simon JD (1999) Molecular thermodynamics. University Science Books, Sausalito
64. Davies MS, Hall MD, Berners-Price SJ, Hambley TW (2008) (1)H, (15)N heteronuclear single quantum coherence NMR study of the mechanism of aquation of platinum(IV) ammine complexes. *Inorg Chem* 47(17):7673–7680. <https://doi.org/10.1021/ic8006734>
65. Ronconi L, Sadler PJ (2008) Applications of heteronuclear NMR spectroscopy in biological and medicinal inorganic chemistry. *Coord Chem Rev* 252(21–22):2239–2277. <https://doi.org/10.1016/j.ccr.2008.01.016>
66. Corinti D, Coletti C, Re N, Chiavarino B, Crestoni ME, Fornarini S (2016) Cisplatin binding to biological ligands revealed at the encounter complex level by IR action spectroscopy. *Chem Eur J* 22(11):3794–3803. <https://doi.org/10.1002/chem.201504521>
67. Corinti D, Coletti C, Re N, Paciotti R, Maitre P, Chiavarino B, Crestoni ME, Fornarini S (2019) Short-lived intermediates (encounter complexes) in cisplatin ligand exchange elucidated by infrared ion spectroscopy. *Int J Mass Spectrom* 435:7–17. <https://doi.org/10.1016/j.ijms.2018.10.012>
68. Lemma K, Berglund J, Farrell N, Elding LI (2000) Kinetics and mechanism for reduction of anticancer-active tetrachloroam(m)ine platinum(IV) compounds by glutathione. *J Biol Inorg Chem* 5(3):300–306. <https://doi.org/10.1007/pl00010658>
69. Ricci A, Pepi F, Cimino P, Troiani A, Garzoli S, Salvitti C, Di Rienzo B, Barone V (2016) Vitamin C: an experimental and theoretical study on the gas-phase structure and ion energetics of protonated ascorbic acid. *J Mass Spectrom* 51(12):1146–1151. <https://doi.org/10.1002/jms.3848>
70. He CC, Kimutai B, Bao X, Hamlow L, Zhu Y, Strobehn SF, Gao J, Berden G, Oomens J, Chow CS, Rodgers MT (2015) Evaluation of hybrid theoretical approaches for structural determination of a glycine-linked cisplatin derivative via infrared multiple photon dissociation (IRMPD) action spectroscopy. *J Phys Chem A* 119(44):10980–10987. <https://doi.org/10.1021/acs.jpca.5b08181>
71. Corinti D, Paciotti R, Re N, Coletti C, Chiavarino B, Crestoni ME, Fornarini S (2020) Binding motifs of cisplatin interaction with simple biomolecules and amino acid targets probed by IR ion spectroscopy. *Pure Appl Chem* 92(1):3–13. <https://doi.org/10.1515/pac-2019-0110>
72. Oomens J, Steill JD, Redlich B (2009) Gas-phase IR spectroscopy of deprotonated amino acids. *J Am Chem Soc* 131(12):4310–4319. <https://doi.org/10.1021/ja807615v>
73. Paciotti R, Coletti C, Re N, Scuderi D, Chiavarino B, Fornarini S, Crestoni ME (2015) Serine O-sulfation probed by IRMPD spectroscopy. *Phys Chem Chem Phys* 17(39):25891–25904. <https://doi.org/10.1039/c5cp01409c>
74. Paciotti R, Corinti D, De Petris A, Ciavardini A, Piccirillo S, Coletti C, Re N, Maitre P, Bellina B, Barran P, Chiavarino B, Crestoni ME, Fornarini S (2017) Cisplatin and transplatin interaction with methionine: bonding motifs assayed by vibrational spectroscopy in the isolated ionic complexes. *Phys Chem Chem Phys* 19(39):26697–26707. <https://doi.org/10.1039/c7cp05203k>

Publisher's Note Springer Nature remains neutral with regard to jurisdictional claims in published maps and institutional affiliations.

Affiliations

Davide Corinti¹  · Maria Elisa Crestoni¹  · Simonetta Fornarini¹  · Eslam Dabbish² · Emilia Sicilia² · Elisabetta Gabano³  · Elena Perin³  · Domenico Osella³ 

✉ Davide Corinti
davide.corinti@uniroma1.it

✉ Eslam Dabbish
eslammoustafa6@gmail.com

✉ Elisabetta Gabano
elisabetta.gabano@uniupo.it

¹ Dipartimento di Chimica e Tecnologie del Farmaco,
Università di Roma “La Sapienza”, P.le A. Moro 5,
00185 Rome, Italy

² Department of Chemistry and Chemical Technologies,
Università della Calabria, Ponte P. Bucci Cubo 14c,
87035 Arcavacata di Rende (CS), Italy

³ Dipartimento di Scienze e Innovazione Tecnologica,
Università del Piemonte Orientale, Viale T. Michel 11,
15121 Alessandria, Italy

Supplementary Material

A multi-methodological inquiry of the behavior of cisplatin-based Pt(IV) derivatives in the presence of bioreductants with a focus on the isolated encounter complexes

Davide Corinti,¹ Maria Elisa Crestoni,¹ Simonetta Fornarini,¹ Eslam Dabbish,² Emilia Sicilia,² Elisabetta Gabano,³ Elena Perin,³ and Domenico Osella³

¹ Dipartimento di Chimica e Tecnologie del Farmaco, Università di Roma “La Sapienza”, P.le A. Moro 5, I-00185 Roma, Italy.

² Department of Chemistry and Chemical Technologies Università della Calabria, Ponte P. Bucci Cubo 14c, 87035 Arcavacata di Rende (CS), Italy.

³ Dipartimento di Scienze e Innovazione Tecnologica, Università del Piemonte Orientale, Viale T. Michel 11, 15121 Alessandria, Italy.

Table of contents

Figure S1. $^{15}\text{N}\{^1\text{H}\}$ DEPT-45 (Distortionless Enhanced by Polarization Transfer) spectra of ^{15}N -**2** in HEPES/D₂O 9:1 at 37°C.

Figure S2. Mass spectrum of a solution of **1** and ascorbic acid in aqueous methanol at pH 4. The solution was analyzed A) just after mixing and B) after a night incubation time.

Figure S3. ESI mass spectra of a solution of **1** in the presence of ascorbic acid analyzed right after mixing. Panel A displays the positive ion spectrum of a pH 4 solution, while panel B shows the negative ion spectrum of a pH 9 solution.

Figure S4. Mass spectrum of a solution of **1** and glutathione. The solution was analyzed A) just after the mixing and B) after a night of incubation time.

Figure S5. MS³ for the ion at m/z 491-495, generated by CID of $[\mathbf{1}+\text{H}_2\text{Asc}+\text{H}]^+$, at 15 V activation energy.

Figure S6. A) Negative ESI mass spectrum of a solution of **3** and ascorbic acid. B) CID of the complex at m/z 591, corresponding to $[\mathbf{3}+\text{HAsc}]^-$.

Figure S7. CID mass spectrum of $[\mathbf{1}+\text{GSH}+\text{H}]^+$.

Table S1. Experimental IRMPD features and calculated vibrational frequencies for **509_1** and **509_1b** isomers of $[1+H_2Asc+H]^+$.

Table S2. Experimental IRMPD features and calculated vibrational frequencies for **507_1** and **507_1b** isomers of $[1+HAsc]^-$.

Table S3. Experimental IRMPD features and calculated vibrational frequencies for the **549_1** and **549_2** isomers of $[2+HAsc]^-$.

Figure S8. Free energy profile for the step that along the breakdown pattern of $[1+H_2Asc+H]^+$ leads from the m/z 509 ion to the formation of the m/z 263 ion by the elimination of the H_2Asc molecule.

Figure S9. Free energy profile describing the alternative steps for the further fragmentation the m/z 489 ion along the breakdown pattern of $[1+HAsc]^-$.

Figure S10. Free energy profile describing the alternative steps for the further fragmentation the m/z 489 ion along the breakdown pattern of $[1+HAsc]^-$.

Figure S11. Free energy profiles describing alternative fragmentation pathways of $[2+HAsc]^-$ that, following an initial water loss (m/z 531), leads to the formation of either m/z 514 or m/z 471.

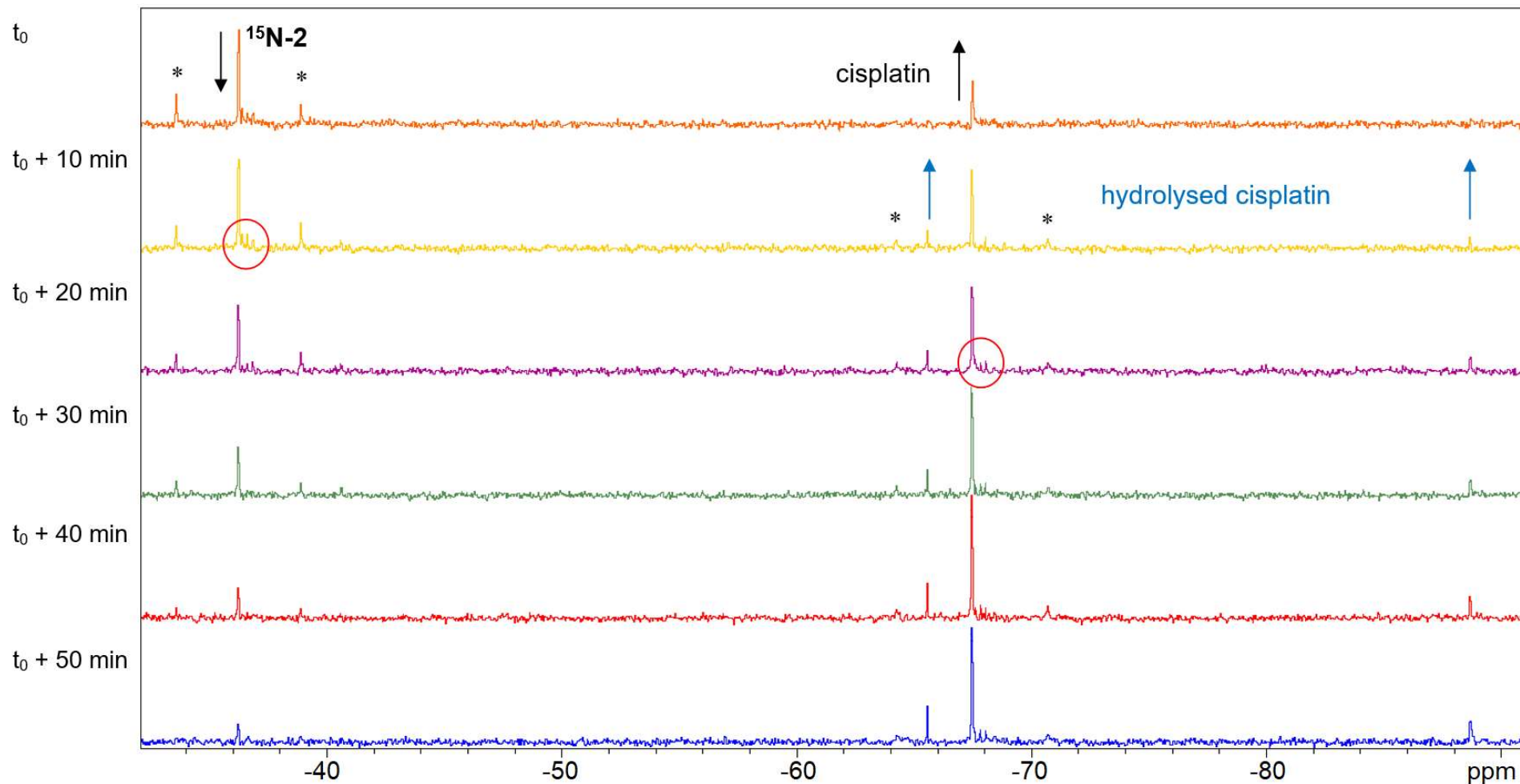


Figure S1. $^{15}\text{N}\{^1\text{H}\}$ DEPT-45 (Distortionless Enhanced by Polarization Transfer) spectra of $^{15}\text{N-2}$ in HEPES/ D_2O 9:1 at 37°C . Besides the peak of $^{15}\text{N-2}$ at -35.5 ppm, already in the first spectrum the signal of cisplatin (the product of reduction of $^{15}\text{N-2}$) is visible at -67.8 ppm. The former decreases and the latter grows in the following spectra. Additionally, the signals of the hydrolyzed cisplatin (two signals corresponding to $^{15}\text{NH}_3$ trans to Cl and to O, respectively) become visible from the second spectrum. Satellite peaks (*) around the main signals are due to the $^{15}\text{N-}^{195}\text{Pt}$ coupling, while additional peaks at the right foot of the main signals (red circles) are due to the formation of deuterated ammonia by chemical H/D exchange from D_2O .

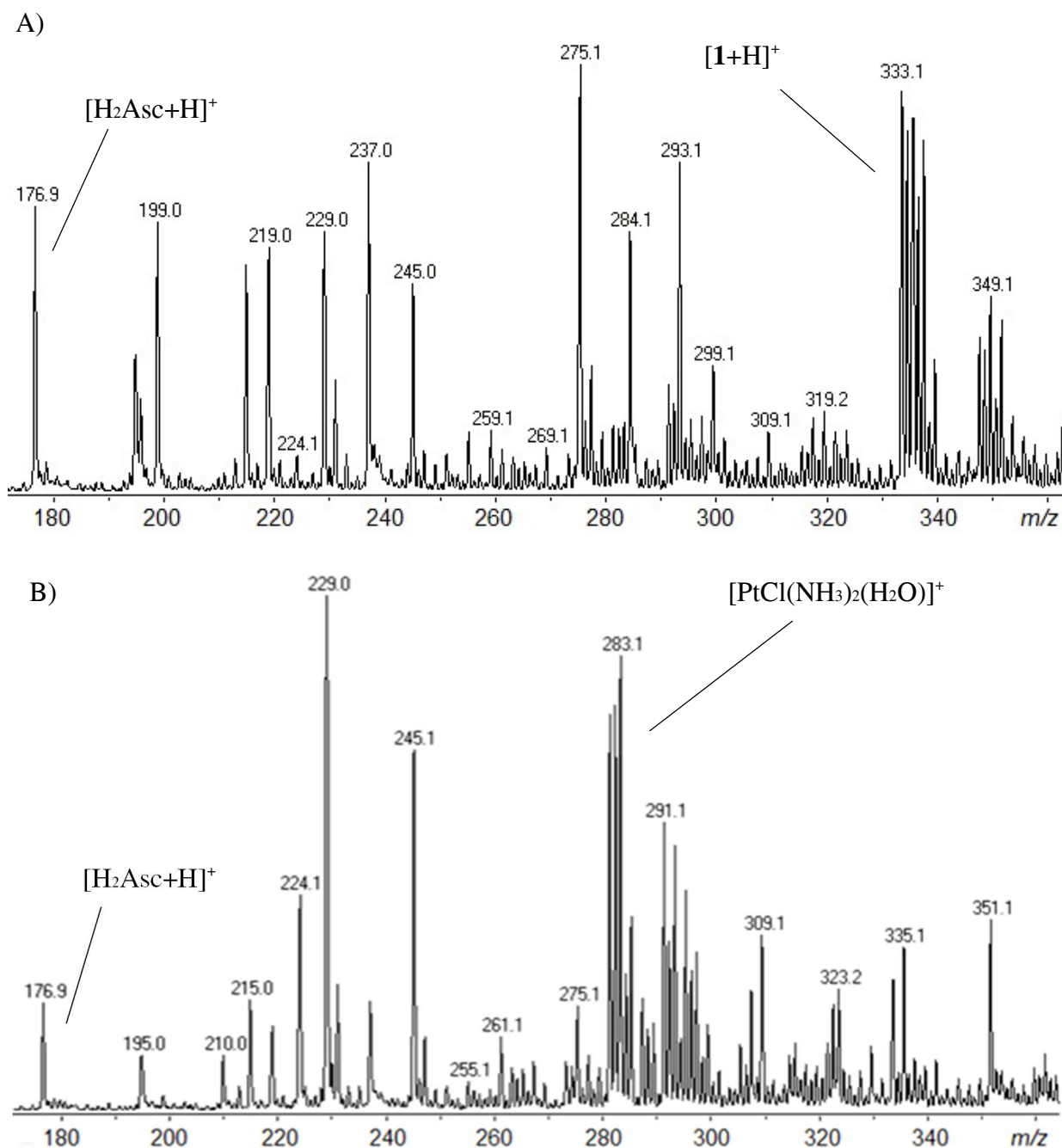


Figure S2. Mass spectrum of a solution of **1** and ascorbic acid in aqueous methanol at pH 4. The solution was analyzed A) just after mixing and B) after a night incubation time.

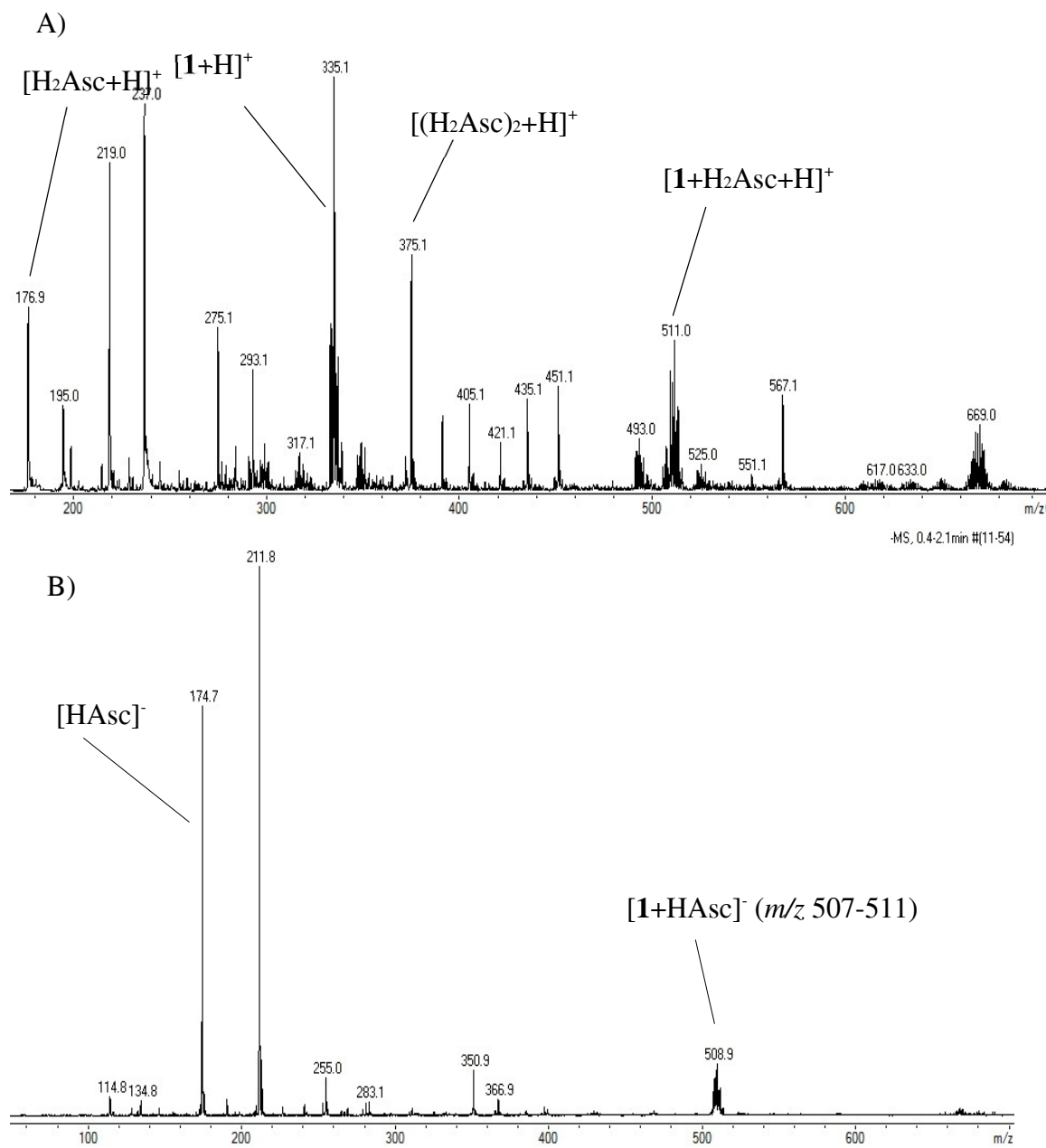


Figure S3. ESI mass spectra of a solution of **1** in the presence of ascorbic acid analyzed right after mixing. Panel A displays the positive ion spectrum of a pH 4 solution, while panel B shows the negative ion spectrum of a pH 9 solution.

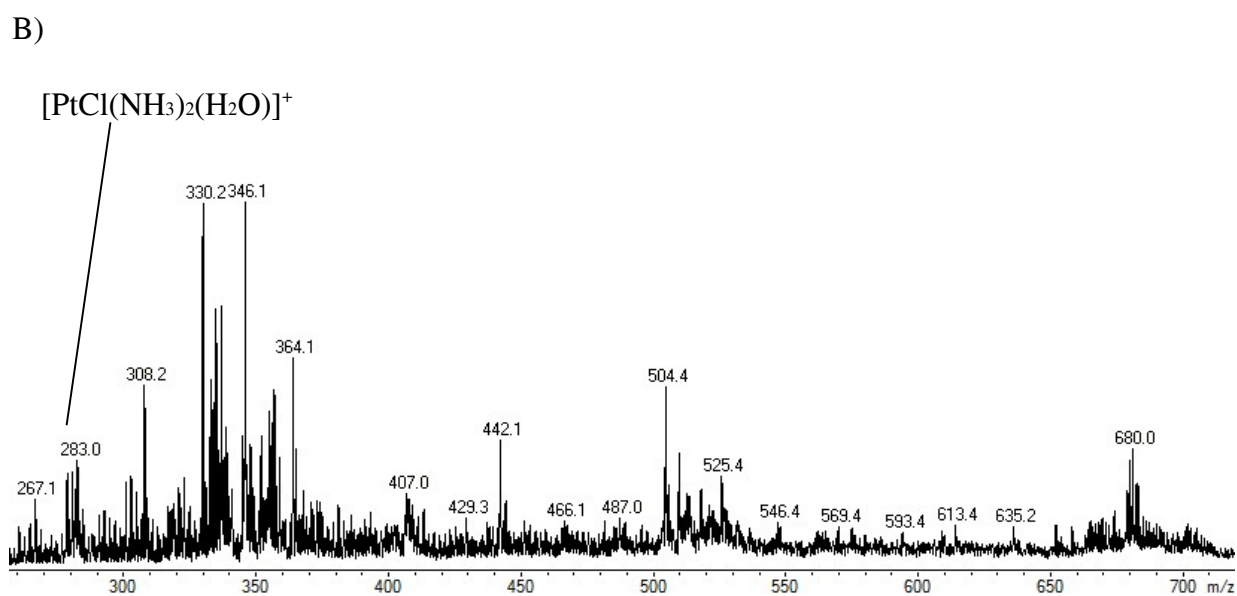
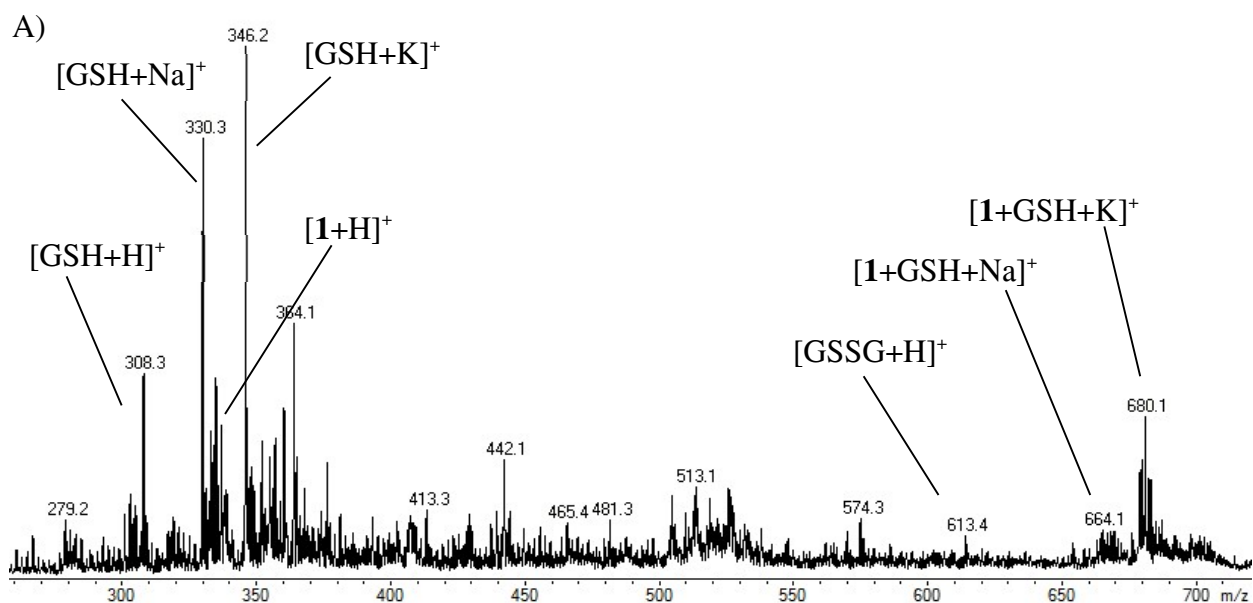


Figure S4. Mass spectrum of a solution of **1** and glutathione. The solution was analyzed A) just after the mixing and B) after a night of incubation time.

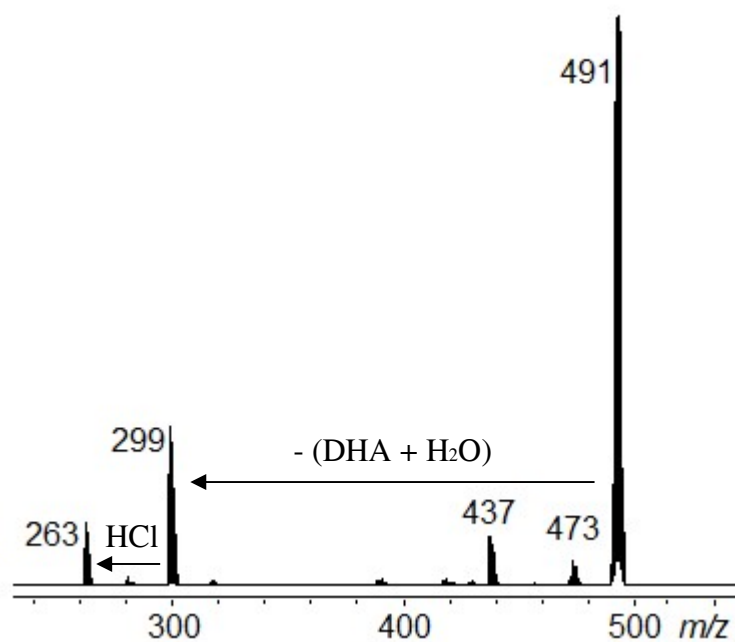


Figure S5. MS³ for the ion at m/z 491-495, generated by CID of $[1+H_2Asc+H]^+$, at 15 V activation energy.

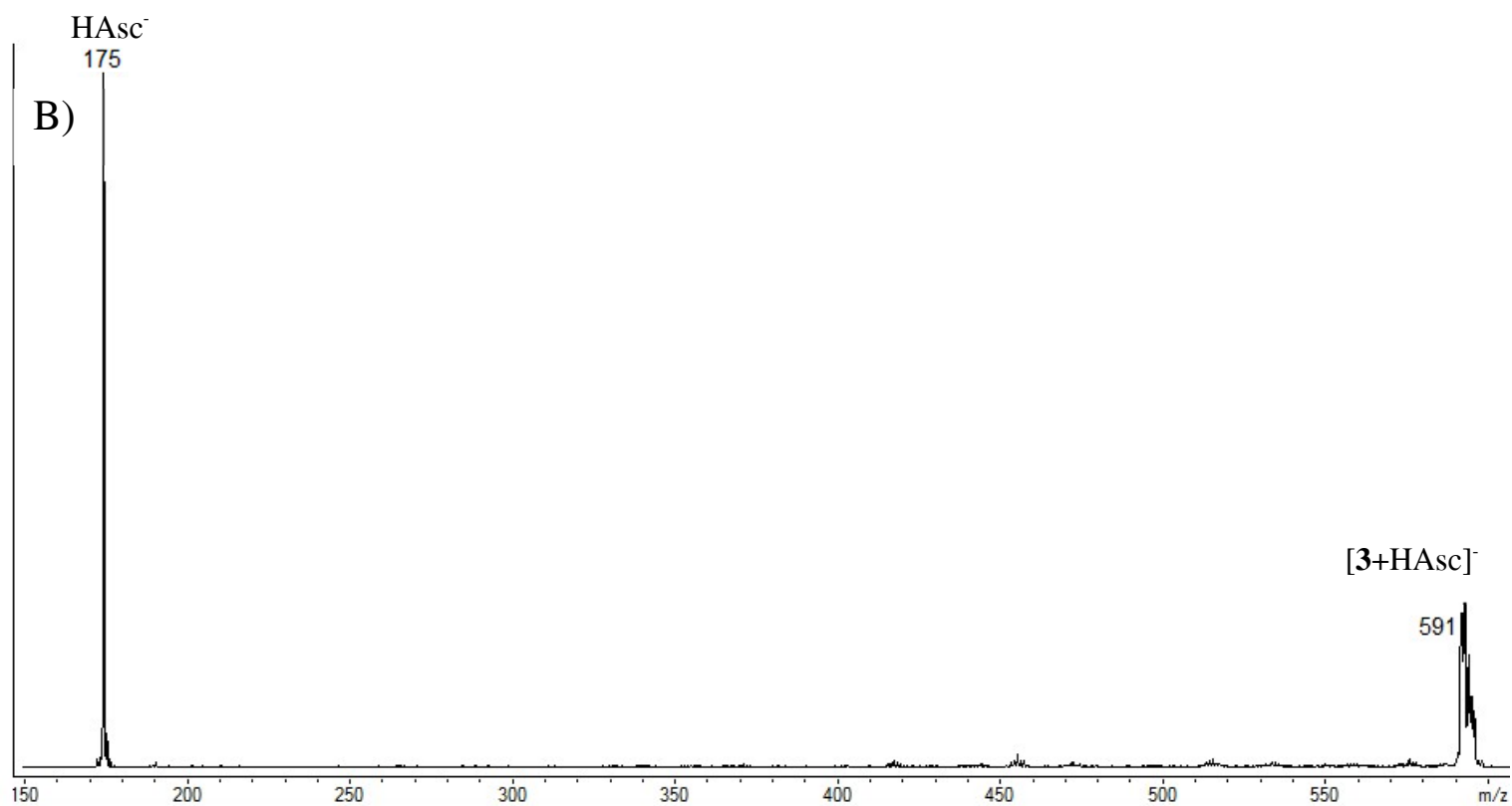
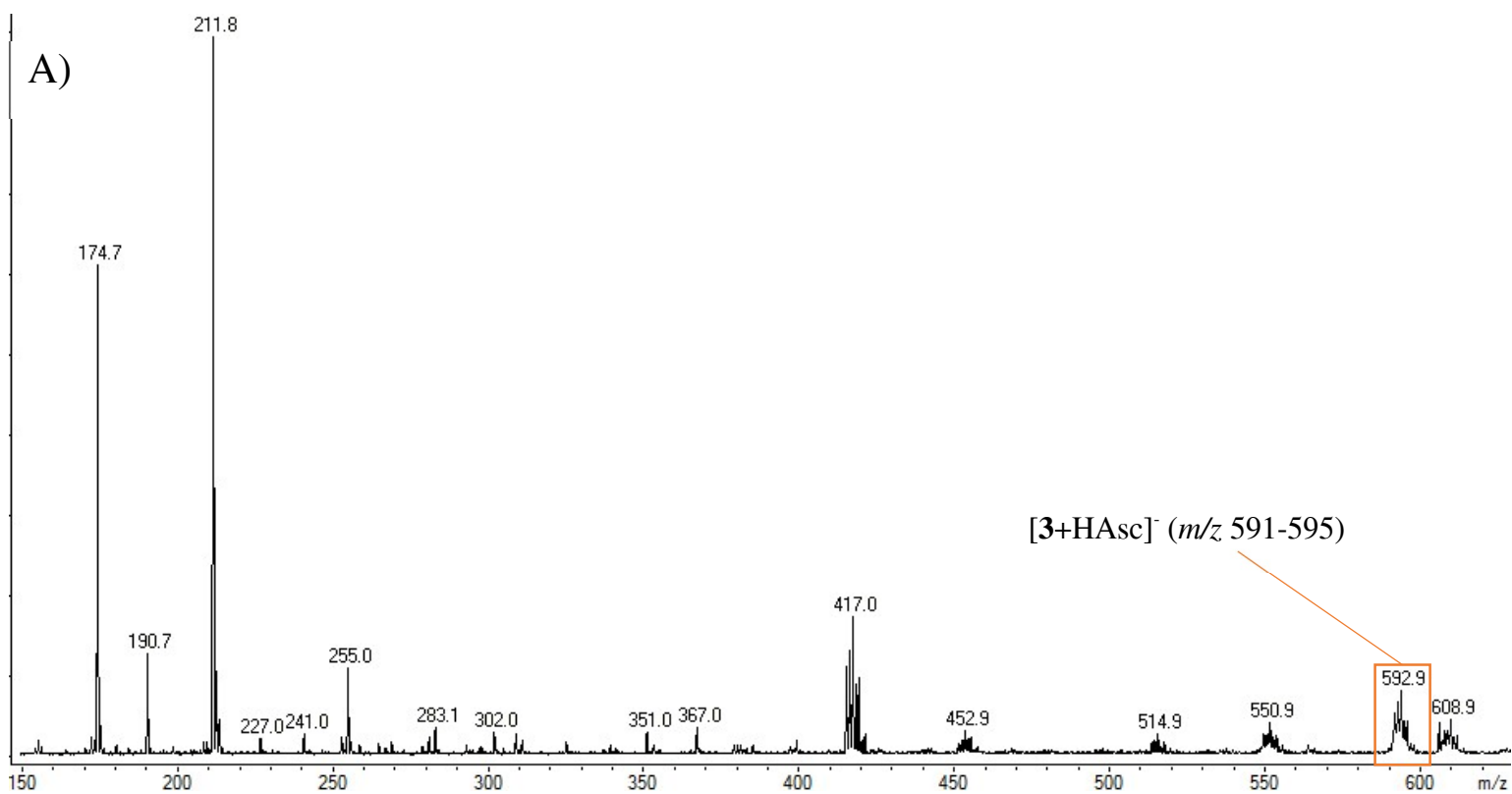


Figure S6. A) Negative ESI mass spectrum of a solution of **3** and ascorbic acid. B) CID of the complex at m/z 591, corresponding to $[3+HAsc]^-$.

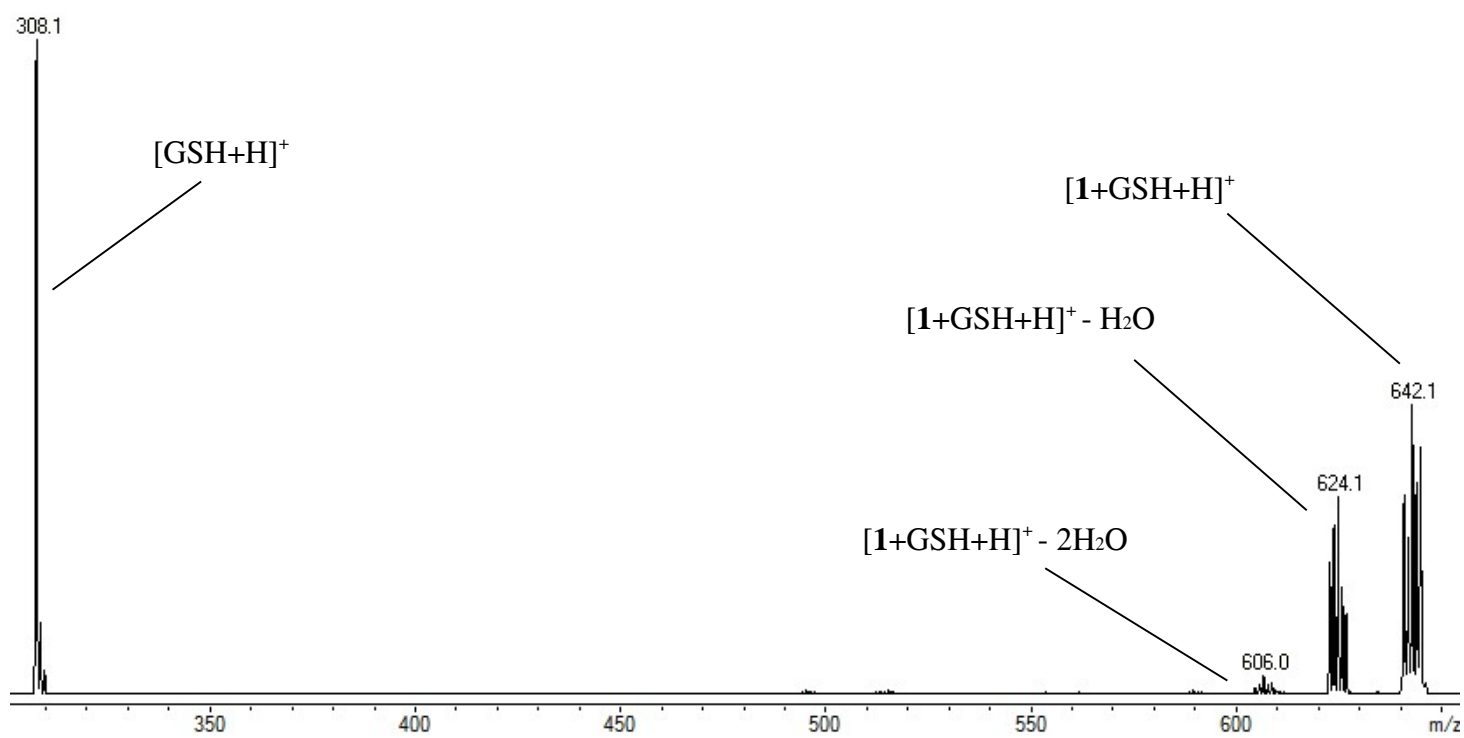


Figure S7. CID mass spectrum of $[\text{1}+\text{GSH}+\text{H}]^+$.

Table S1. Experimental IRMPD features and calculated vibrational frequencies for **509_1** and **509_1b** isomers of $[1+H_2Asc+H]^+$.

$[1+H_2Asc+H]^+$			
Experimental IRMPD ^a	Calculated IR ^{a,b}		Vibrational mode assignment
	509_1	509_1b	
	869 (193)	841 (79)	NH bend
	1020 (96)	1018 (99)	furanone OH bend + C-OC stretch
	1045 (82)	1049 (85)	CC stretch + primary OH bend
	1084 (148)	1087 (114)	CH ₂ rocking + ring breathing
1133	1118 (118)	1125 (157)	furanone OH bend + ring breathing
	1254 (101)	1260 (104)	NH ₃ umbrella
	1275 (107)		NH ₃ umbrella
	1278 (106)		furanone CH bend + furanone OH bend
		1279 (109)	NH ₃ umbrella + furanone CH bend
1287	1318 (148)	1321 (157)	furanone OH bend + CH bend
	1353 (64)		CH bend
		1356 (102)	CH bend + furanone OH bend
1425	1413 (326)	1417 (342)	furanone OH bend + C-OH stretch
1558	1589 (76)	1544 (309)	H ₂ O scissoring
1705	1696 (944)	1687 (1042)	CO stretch + C=C stretch
1762	1752 (306)	1746 (266)	CO stretch + ring breathing

^a In cm⁻¹. ^b Intensities are reported in parentheses (km mol⁻¹). Modes with an intensity lower than 70 km mol⁻¹ are not included. Frequencies are scaled by a factor of 0.974.

Table S2. Experimental IRMPD features and calculated vibrational frequencies for **507_1** and **507_1b** isomers of $[1+\text{HAsc}]^-$.

Experimental IRMPD ^a	$[1+\text{HAsc}]^-$		Vibrational mode assignment
	Calculated IR ^{a,b}		
	507_1	507_1b	
		928 (149)	C-OC stretch + CH bend
	922 (107)	949 (81)	NH bend
	988 (101)	959 (130)	PtO-H bend
	1008 (137)	978 (174)	furanone CH bend + C-OC stretch
	1027 (101)		secondary OH bend
		1032 (100)	C-OC stretch + primary C-OH stretch
1043	1079 (146)	1058 (197)	CH bend + CC stretch
		1274 (89)	NH ₃ umbrella
	1336 (110)	1330 (194)	NH ₃ umbrella + furanone OH bend
	1389 (90)		furanone OH bend
1377		1416 (227)	ascorbate OH bend
	1561 (1253)		primary OH bend
1573		1580 (133)	NH ₂ scissoring of NH ₃
	1611 (540)		NH ₂ scissoring of NH ₃
1620		1615 (581)	furanone C=C stretch
		1657 (75)	NH bend
	1708 (74)		CO stretch + ring breathing
1767		1786 (491)	CO stretch

^a In cm^{-1} . ^b Intensities are reported in parentheses (km mol^{-1}). Modes with an intensity lower than 70 km mol^{-1} are not included. Frequencies are scaled by a factor of 0.974.

Table S3. Experimental IRMPD features and calculated vibrational frequencies for the **549_1** and **549_2** isomers of $[2+\text{HAsc}]^-$.

Experimental IRMPD ^b	[2+HAsc] ⁻		Vibrational mode assignment
	549_1	549_2	
	980 (221)		C-OH stretch + furanone OH bend
	1019 (101)		C-OH stretch + CC stretch + CH ₃ twisting
1054		1035 (170)	C-OH stretch + secondary OH bend + ring breathing
1104	1066 (158)	1070 (192)	C-OH stretch + CC stretch + ring breathing
1141			
1258	1294 (80)		NH ₃ umbrella
1312		1320 (246)	CH ₃ umbrella + acetate CO stretch
	1333 (91)		CH ₃ umbrella + NH ₃ umbrella
1356	1367 (211)	1359 (230)	CH ₃ umbrella + acetate CO stretch
1392	1402 (78)	1406 (79)	secondary OH bend + primary OH bend
	1461 (105)		primary OH bend + secondary OH bend
	1560 (380)		NH ₂ scissoring of NH ₃ + acetate CO stretch
1550	1575 (1134)	1572 (394)	NH ₂ scissoring of NH ₃ + furanone CO stretch
	1593 (251)	1584 (241)	NH ₂ scissoring of NH ₃ + acetate CO stretch
		1599 (654)	NH ₂ scissoring of NH ₃
1637	1613 (821)	1610 (463)	NH ₂ scissoring of NH ₃ + acetate CO stretch
		1692 (73)	furanone CO stretch
1754	1727 (202)		furanone CO stretch

^a In cm^{-1} . ^b Intensities are reported in parentheses (km mol^{-1}). Modes with an intensity lower than 70 km mol^{-1} are not included. Frequencies are scaled by a factor of 0.974.

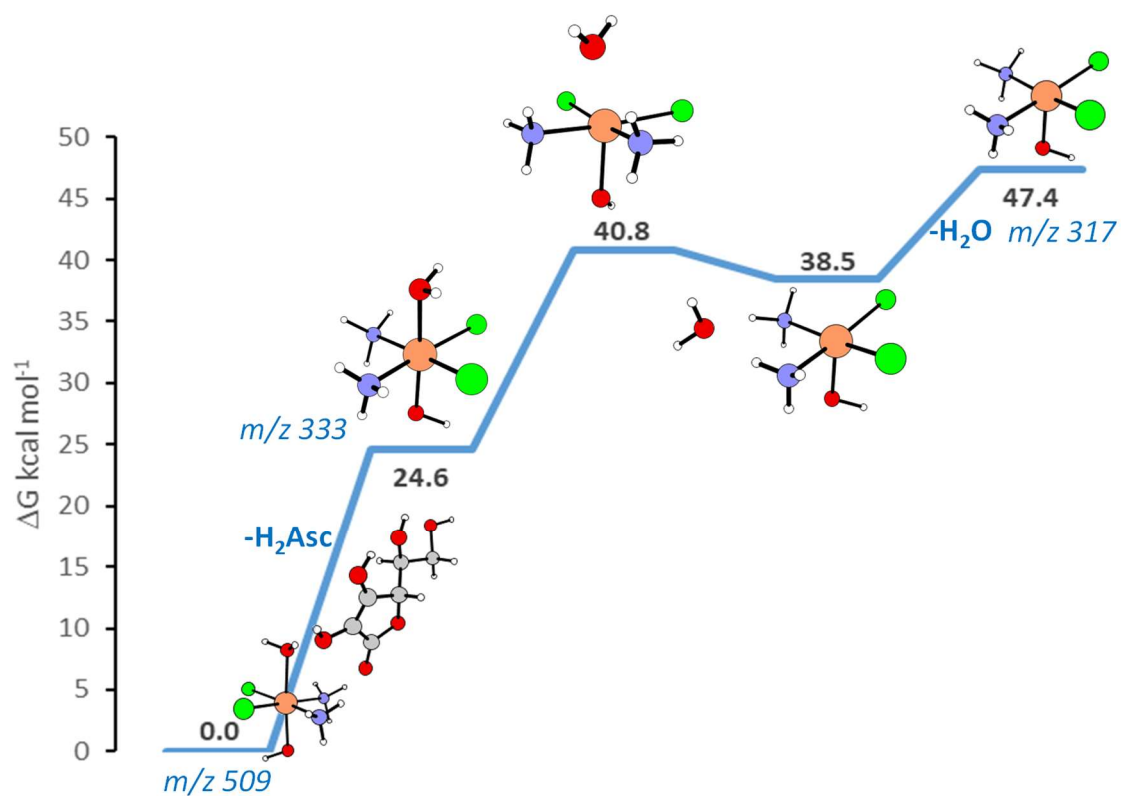


Figure S8. Free energy profile for the step that along the breakdown pattern of $[1+H_2Asc+H]^+$ leads from the m/z 509 ion to the formation of the m/z 263 ion by the elimination of the H_2Asc molecule. The neutral losses for all the examined dissociations are indicated along the paths. Relative free energies at 298 K in kcal mol⁻¹ are calculated with respect to the most stable isomer of the initial ionic adduct. The m/z values for each species are also reported.

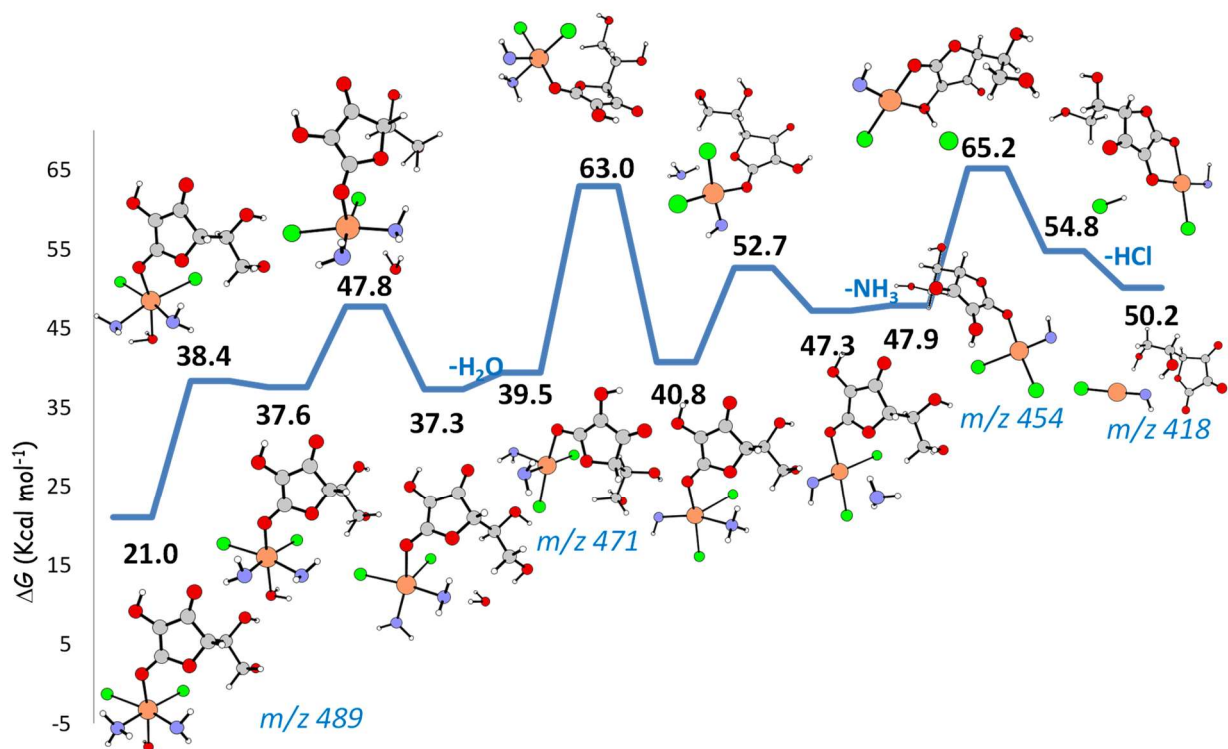


Figure S9. Free energy profile describing the alternative steps for the further fragmentation the m/z 489 ion along the breakdown pattern of $[\mathbf{1}+\text{HAsc}]^-$. The neutral losses for all the examined dissociations are indicated along the paths. Relative free energies at 298 K in kcal mol^{-1} are calculated with respect to the most stable isomer of the initial ionic adduct. The m/z values for each species are also reported.

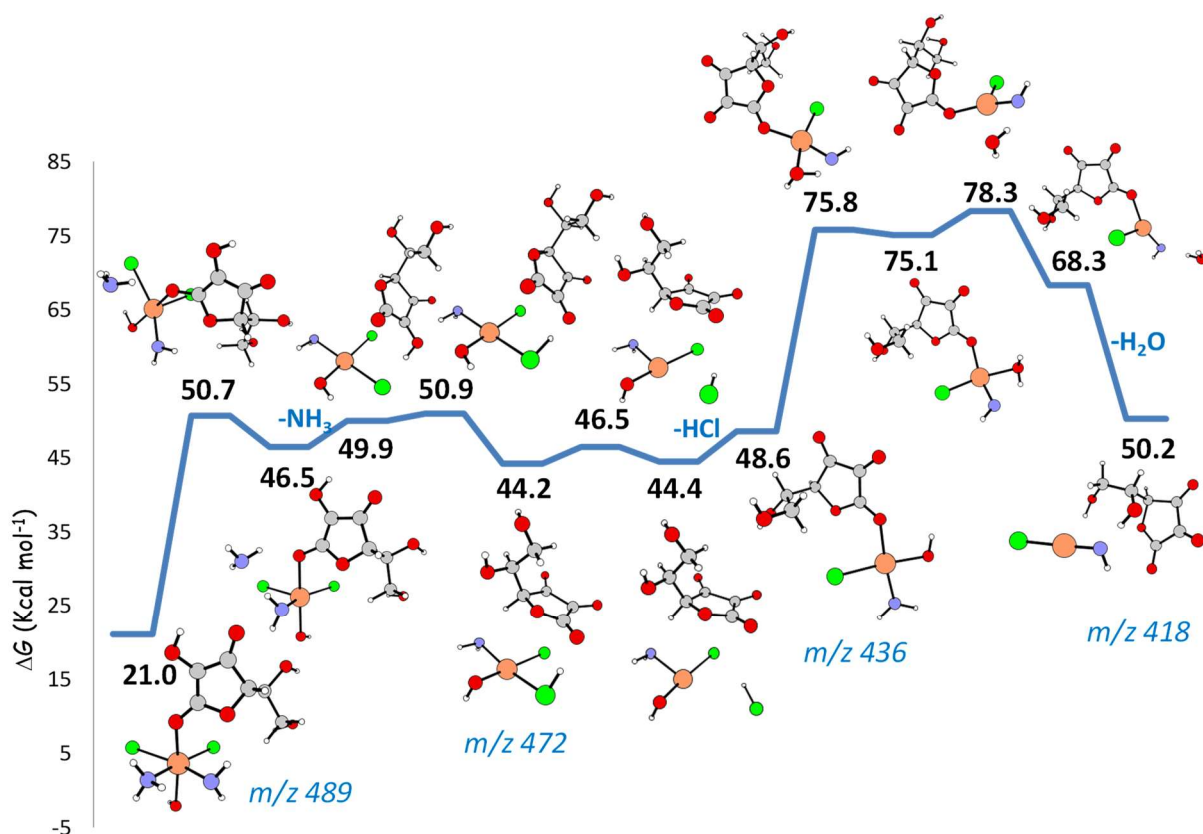


Figure S10. Free energy profile describing the alternative steps for the further fragmentation the m/z 489 ion along the breakdown pattern of $[1+\text{HAsc}]^-$. The neutral losses for all the examined dissociations are indicated along the paths. Relative free energies at 298 K in kcal mol^{-1} are calculated with respect to the most stable isomer of the initial ionic adduct. The m/z values for each species are also reported.

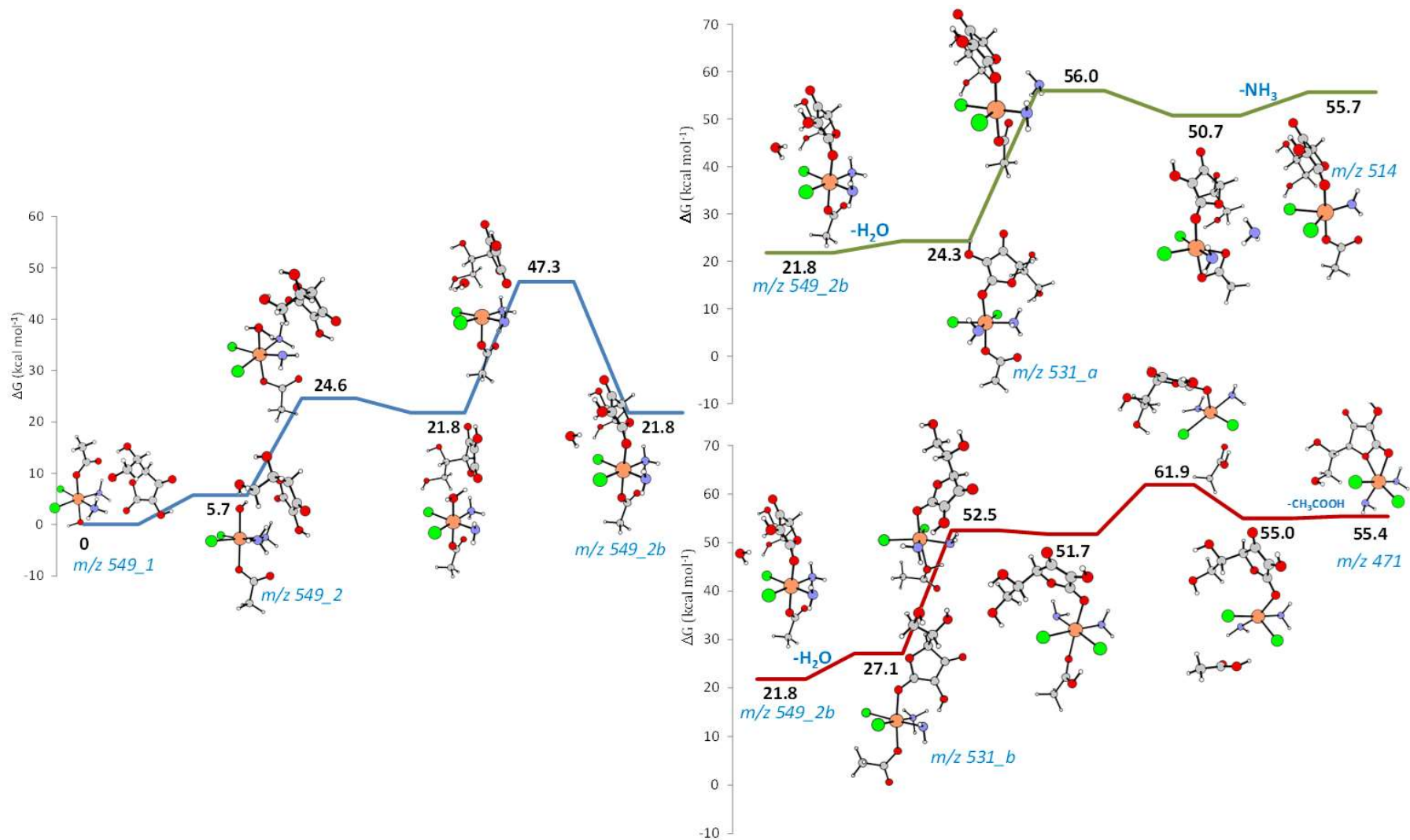


Figure S11. Free energy profiles describing alternative fragmentation pathways of [2+HAsc]⁺ that, following an initial water loss (*m/z* 531), leads to the formation of either *m/z* 514 or *m/z* 471. The neutral losses for all the examined dissociations are indicated along the paths. Relative free energies at 298 K in kcal mol⁻¹ are calculated with respect to the most stable isomer of the initial ionic adduct. The *m/z* values for each species are also reported.

Chapter VI

**Platinum drugs in
Photoactivated
Chemotherapy (PACT)**

Chapter VI Platinum drugs in Photoactivated Chemotherapy (PACT)

6.1 Mechanism of action of the curcumin cis-diammineplatinum(II) complex as photocytotoxic agent

6.1.1 Introduction

Platinum(II) complexes are on the frontline of inorganic anticancer agents and are indispensable in chemotherapeutic treatment protocols.¹⁻⁴ Cisplatin, the lead Pt(II) based drug, carboplatin and oxaliplatin have been approved by the FDA and are used globally for the treatment of various cancers.⁵⁻⁷ Their therapeutic ability involves water substitution of ligands for the formation of the corresponding “aquated” complexes acting as transcription inhibitors by binding to nuclear DNA and distorting its structure.^{1,8-11} However, cisplatin and its analogues suffer from severe side-effects associated with the intake of anticancer drugs which usually lack specificity and kill both cancer and healthy cells. In this respect, Photodynamic Therapy (PDT) is known to be a very interesting alternative to chemotherapy.¹²⁻¹⁵ in which a photosensitizer (PS) is used to generate toxic reactive oxygen species (ROS) upon light irradiation which in turn induces severe oxidative damage to various biological molecules, resulting in cell death. This medical technique dramatically reduces the side-effects as the toxic species, which destroy the cancer cells, are produced only in the illuminated regions.^{15,16} One of the drawbacks of effective PDT is that it relies on the presence of oxygen in target tissue, whereas tumors are hypoxic by nature. On the other hand, photoactivated chemotherapy (PACT) can overcome many of such limitations. PACT causes cell death due to the action of cytotoxic species produced in a controlled manner by exposure to light of specific wavelength of metal complexes that are inert in darkness thus reducing toxicity in healthy tissues.^{14,17-21}

Cis-diammineplatinum(II) complex of curcumin, named platicur (see **Figure 6.1**),²² has been synthesized and proposed for its use in PACT as it exhibits photodegradation, upon irradiation with visible light, leading to the controlled release of diammine-platinum(II) species as a DNA-crosslinking agent and curcumin as a potential photosensitizer thus working as a dual action anticancer agent.

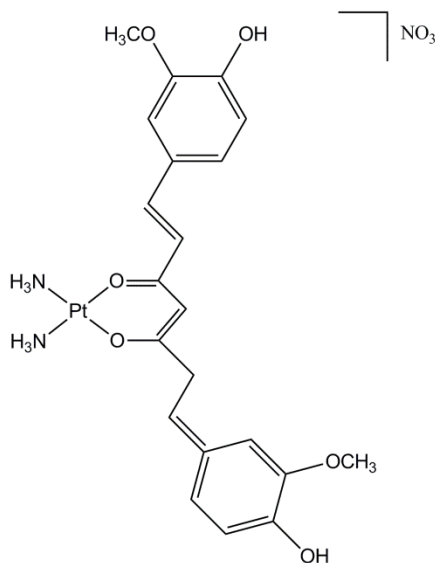


Figure 6.1 Chemical structure of platicur

6.1.2 Aim of study

The purpose of this work has been the investigation of the photochemistry of the parent platicur Pt(II) curcumin complex, the rate and extent of dissociation of the curcumin ligand upon irradiation with visible light by means of DFT and TD-DFT calculations. Both singlet and triplet excited states have been investigated to identify and characterize the states involved in the photochemical process and the ligand dissociation mechanism.

6.1.3 Highlighting results

The inspection of the photophysical properties including electronic transitions, spin-orbit coupling constants, singlet triplet states energy gaps, have revealed that the light exposure leads to the population of a mixed

singlet state $^1\text{LC}/^1\text{LMCT}$, from which the radiationless electronic transition (ISC) to T_4 , whose character is entirely centred on the metal (^3MC), definitively yields one of the most active species of platicur. All the plausible pathways starting from this state have been fully explored which are the direct curcumin release as well as the relaxation (IC) to triplet states, T_1 - T_3 , lying below it and the successive implication of such states in the ligand detachment. From the **energy** profiles for the curcumin detachment computed for the two triplet states with ^3MC character, T_1 and T_4 , it emerges that the ligand release is favoured along the T_1 PES. If the triplet states T_2 and T_3 , that closely resembles the GS geometry, are formed can trigger type II photoprocesses (see **Figure 6.2**).

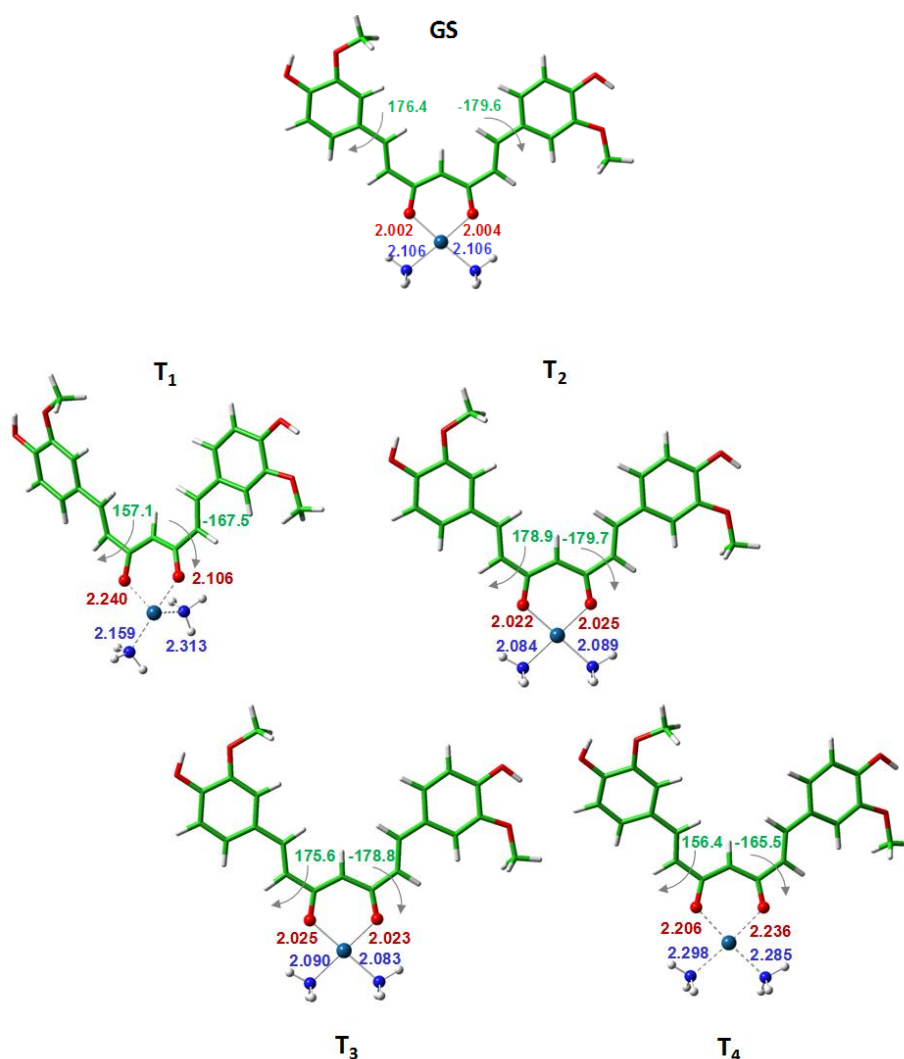


Figure 6.2 Optimized structures and selected geometric parameters of the ground (GS) and triplet excited states ($T_1 - T_4$) lying below the energy of S_1 . Importantly, the two effects can be cumulative, platicur may generate 1O_2 and ROS species (through T_4-T_2 states) until it undergoes ligand dissociation (through T_1) serving as a DNA binding agent and releasing a compound able to act as a photosensitizer. Furthermore, the complete description of the aquation mechanism leading to curcumin cleavage in the dark, even assisted by GSH, supports the inactivity of platicur until light exposure. The deep understanding of the photoprocesses involved in the activation of prodrugs, like the case of platicur, is of pivotal importance for the design of new and effective drugs to be used in the clinical treatments of cancer.

References

- 1) T. C. Johnstone, K. Suntharalingam, S. J. Lippard, *Chem. Rev.*, **2016**, *116*, 3436-3486.
- 2) S. Dilruba, G. V. Kalayda, *Cancer Chemother Pharmacol*, **2016**, *77*, 1103-1124.
- 3) Q.-Q. Deng, X.-E. Huang, L.-H. Ye, Y.-Y. Lu, Y. Liang, J. Xiang, *Asian Pacific Journal of Cancer Prevention*, **2013**, *14*, 413-417.
- 4) A.-M. Florea and D. Busselberg, *Cancers*, **2011**, *3*, 1351-1371.
- 5) G. J. Bosl, R. J. Motzer, *New England Journal of Medicine*, **1997**, *337*, 242-254.
- 6) M. Morris, P. J. Eifel, J. Lu, P. W. Grigsby, C. Levenback, R. E. Stevens, M. Rotman, D. M. Gershenson, D. G. Mutch, *New England Journal of Medicine*, **1999**, *340*, 1137-1143.
- 7) J. H. Schiller, D. Harrington, C. P. Belani, C. Langer, A. Sandler, J. Krook, J. Zhu, D. H. Johnson, *New England Journal of Medicine*, **2002**, *346*, 92-98.
- 8) T. C. Johnstone, G. Y. Park, S. J. Lippard, *Anticancer Res*, **2014**, *34*, 471-476.
- 9) J. J. Wilson, S. J. Lippard, *Chem. Rev.*, **2014**, *114*, 4470-4495.
- 10) R. K. Pathak, S. Marrache, J. H. Choi, T. B. Berding, S. Dhar, *Angewandte Chemie International Edition*, **2014**, *53*, 1963-1967.
- 11) S. Marrache, R. K. Pathak, S. Dhar, *PNAS*, **2014**, *111*, 10444-10449.
- 12) A. Naik, R. Rubbiani, G. Gasser, B. Spingler, *Angewandte Chemie International Edition*, **2014**, *53*, 6938-6941.
- 13) A. Frei, R. Rubbiani, S. Tubafard, O. Blacque, P. Anstaett, A. Felgentrager, T. Maisch, L. Spiccia, G. Gasser, *J. Med. Chem.*, **2014**, *57*, 7280-7292.
- 14) E. Shaili, *Science Progress*, **2014**, *97*, 20-40.

- 15) T. J. Dougherty, C. J. Gomer, B. W. Henderson, G. Jori, D. Kessel, M. Korbelik, J. Moan, Q. Peng, *J Natl Cancer Inst*, **1998**, *90*, 889-905.
- 16) D. Phillips, *Pure and Applied Chemistry*, **1995**, *67*, 117-126.
- 17) J. D. Knoll, C. Turro, *Coordination Chemistry Reviews*, **2015**, 282-283, 110-126.
- 18) B. S. Howerton, D. K. Heidary, E. C. Glazer, *J. Am. Chem. Soc.*, **2012**, *134*, 8324-8327.
- 19) R. Bonnett, in *Comprehensive Coordination Chemistry II*, eds. J. A. McCleverty and T. J. Meyer, Pergamon, Oxford, **2003**, pp. 945-1003.
- 20) K. Mitra, S. Patil, P. Kondaiah, A. R. Chakravarty, *Inorg. Chem.*, **2015**, *54*, 253-264.
- 21) K. Mitra, A. Shettar, P. Kondaiah, A. R. Chakravarty, *Inorg. Chem.*, **2016**, *55*, 5612-5622.
- 22) K. Mitra, S. Gautam, P. Kondaiah, A. R. Chakravarty, *Angewandte Chemie International Edition*, **2015**, *54*, 13989-13993.

Paper VI

**Mechanism of Action of the Curcumin cis-Diammineplatinum(II)
Complex as Photocytotoxic Agent**

E. Dabbish, G. Mazzone, N. Russo, E. Sicilia, *Inorg. Chem. Front.*,
2020, *7*, 2759-2769.

RESEARCH ARTICLE



Cite this: *Inorg. Chem. Front.*, 2020, **7**, 2759

Received 7th May 2020,
Accepted 9th June 2020
DOI: 10.1039/d0qi00503g

rsc.li/frontiers-inorganic

Mechanism of action of the curcumin *cis*-diammineplatinum(II) complex as a photocytotoxic agent†

Eslam Dabbish, Gloria Mazzone, * Nino Russo and Emilia Sicilia

In the search for new and more active anticancer drugs, light-activated compounds are emerging as effective drugs to be used in photodynamic therapy (PDT) and photoactivated chemotherapy (PACT). These clinical treatments are able to overcome severe side effects caused by the conventional Pt(II) complexes in chemotherapy, since the cytotoxic species are released directly into the target regions, reducing toxicity in healthy tissues. The curcumin *cis*-diammineplatinum(II) complex has been proposed for PACT as it allows the controlled release of aquated diammine–platinum(II) species as a DNA cross-linking agent and curcumin as a potential photosensitizer, thus working as a dual action anticancer agent. The curcumin ligand dissociation upon irradiation with visible light was examined by means of DFT and TD-DFT calculations. The outcomes clearly unraveled the metal-centered triplet states 3MC as active species involved in the photocleavage of curcumin that lead to the formation of aquated platinum species and ruled out the potential activity of such a complex in the dark.

Introduction

Platinum(II) complexes are on the frontline of inorganic anti-cancer agents and still the most effective therapeutic agents in clinical medicines.^{1–4} Among these chemotherapeutics, cisplatin, carboplatin and oxaliplatin have been approved by the FDA and are used transnationally for the treatment of various cancers.^{5–7} Their therapeutic ability involves water substitution of ligands for the formation of the corresponding “aquated” complexes acting as transcription inhibitors by binding to nuclear DNA and distorting its structure.^{1,8–11} Cisplatin and related Pt(II) complexes, although very efficacious, suffer from severe side effects associated with the intake of anticancer drugs which usually lack specificity and kill both cancer and healthy cells. In spite of the enormous progress made in this field, less invasive and more tumor-specific therapies continue

to be a need. In this respect, photodynamic therapy (PDT) is a very interesting alternative to chemotherapy.^{12–15} The mechanism of action involves a photosensitizer (PS), a species able to generate toxic reactive oxygen species (ROS) upon light irradiation that induce severe oxidative damage to cellular biological molecules, resulting in cell death. This medical technique typically results in fewer side effects as the toxic species which destroy the cancer cells are produced only in the regions where the light source is applied.^{15,16} One of the drawbacks of effective PDT is that it relies on the presence of oxygen in the target tissue, whereas tumors are hypoxic. Photoactivated chemotherapy (PACT), as a complementary approach to photodynamic therapy, can overcome such limitations.^{14,17–21} PACT, indeed, causes cell death due to the action of cytotoxic species produced in a controlled manner by exposure to light of a specific wavelength of otherwise inert metal complexes.^{15,16} This approach significantly reduces toxicity in healthy tissues. One potential objective in the context of PACT is the development of complexes capable of killing cancer cells by binding to DNA as a target. Dissociation of one or more ligands from the coordination sphere of the metal might occur upon photoinduction leading to the release of active metal fragments directly into cancer cells.

The *cis*-diammineplatinum(II) complex of curcumin, named Platicur, has been synthesized and proposed for its use in PACT as it exhibits photodegradation, upon irradiation with visible light, leading to the controlled release of diammine–platinum(II) species as a DNA cross-linking agent and curcu-

Department of Chemistry and Chemical Technologies, Università della Calabria, 87036 Arcavacata di Rende, CS, Italy. E-mail: gloria.mazzone@unical.it

† Electronic supplementary information (ESI) available: Additional curcumin and Platicur absorption details; energy diagram of the molecules involved in the electronic transitions of Platicur; EDDMs and NTOs of Platicur excited singlet states; TDDFT singlet excited energies from relaxed scan calculations along the Pt–O distance reaction coordinate; optimized structures of ground and lowest singlet excited states and their adiabatic energy gaps; optimized structures of the triplet excited states (T_1 – T_4) lying below the energy of S_1 ; energy profile for the conversion of $ADD_{(1)}$ in $ADD_{(4)}$; photophysical properties of curcumin (excited states, adiabatic energies, SOC, $\Delta E(S_m-T_n)$, VEA, VIP and MO); PES for the GS curcumin release. See DOI: 10.1039/d0qi00503g

min as a potential photosensitizer, thus working as a dual action anticancer agent.²² Therapeutic properties of both cisplatin and curcumin are retained, whereas drawbacks associated with their use are avoided. Enormous attention has been dedicated to curcumin in the past two decades due to its bio-functional properties such as anti-tumor, antioxidant, and anti-inflammatory activities.^{23–25} Anticancer properties of curcumin are principally ascribed to its antioxidant and free-radical scavenging properties that, however, are limited by low bioavailability and hydrolytic instability.²⁶ Furthermore, more recently research studies have been devoted to the photosensitization properties of curcumin showing its excellent therapeutic power *in vitro*.^{27–30} On the other hand, lability of cisplatin chlorido ligands results in non-specific interactions enroute to the targeted tumors. By coordination to transition metal ions, as in Platicur, through its monoanionic enolic form curcumin instability and degradation can be prevented, whereas the use of the O,O-donor curcumin ligand allows to model oxaliplatin and carboplatin, which slowly release the O,O-donor ligand in the cellular medium in comparison with the two chlorido ligands.^{31,32} Moreover, Platicur has shown to be localized in cytosol in preference to the nuclear uptake. Subsequently, in order to further improve the therapeutic properties of Pt(II) curcumin conjugates, amine ligands have been properly modulated and new modified Pt(II) curcumin complexes have been synthesized.³¹ The analysis of the toxicity profiles both in the dark and upon irradiation has shown that modifications in the structure can have a significant impact on the visible-light-activated dual-action anticancer properties of these complexes and stimulated additional investigations directed towards a rational design of new complexes for improving stability, selectivity and efficacy.

Given such premises, the purpose of this work has been the investigation of the photochemistry of the parent Pt(II) curcumin complex, Platicur. More specifically, the extent of dissociation of the curcumin ligand upon irradiation with visible light has been examined by means of DFT and TD-DFT calculations. Both singlet and triplet excited states have been investigated, so that, by identifying and characterizing the states involved in the photochemical process, the ligand dissociation mechanism can be unraveled.

Results and discussion

Photophysical properties

The optimized structure of the Platicur complex, synthesized and spectroscopically characterized by Mitra *et al.*,^{22,31} shows the typical square planar geometry around the metal centre. The ammonia ligands lie at 2.106 Å from the platinum, while the curcumin, in approximately planar conformation, chelates the metal centre at a mean distance of 2.003 Å. In the structure of the curcumin ligand, hydroxyl and methoxyl groups of both phenyl rings are arranged in order to maximize their interaction by establishing H-bonds. The experimental absorption spectrum in DMSO/DPBS is dominated by a shoulder band at

385 nm and two bands with equal intensities at 460 and 435 nm.²² The computed spectrum (Fig. 1 and Table S1 of the ESI†) agrees with this behaviour; the band at the long wavelength results from two diverse transitions: the HOMO(H) → LUMO(L) and H-1 → L transitions located at 473 and 411 nm, respectively. Light absorption occurs essentially due to the charge transfer from one orbital to another orbital with a ligand-like character (LC). However, looking at the molecular orbital compositions (Fig. S1†), the former transition can be ascribed also to the transfer of electrons from an orbital primarily on the ligand to one primarily located on the metal ion, ligand-to-metal charge transfer (LMCT), while, in contrast, the latter is generated to a small extent by the charge transfer from the metal centre to the curcumin ligand (MLCT). To confirm this assignment, the electron density difference maps, EDDMs, namely the representation of the changes in the electron density upon electronic transition between the ground (GS) and the excited singlet states S_n , have been analysed and shown in Fig. S2 of the ESI,† together with the natural transition orbitals, NTOs, computed for each singlet excited state generating the two bands shown in Fig. 1. These confirm the localization of the transition on the curcumin ligand for both states with a small amount of LMCT and MLCT for S_1 and S_2 , respectively. Also the absorption band at a shorter wavelength is primarily generated by two transitions, at 330 and 319 nm. Similar to the transition at the lowest energy, the former is ruled by the curcumin ligand (LC) with a small amount of MLCT, while the latter involves, almost exclusively, the charge transfer from the metal to the O,O ligand (MLCT).

The comparison with the absorption spectrum of the free ligand (HCur) shows a slight bathochromic shift (from 452 to 473 nm) of the maximum absorption wavelength, reproducing what has been experimentally observed,²² and showing that the well-known photosensitizing properties of curcumin dominate the absorption spectrum of the platinum complex. Nevertheless, compared with the curcumin alone, the examination of the absorption bands revealed the involvement of LMCT and MLCT which give access to other cell-killing modes, with respect to classical PDT photosensitizers, that will be discussed in detail below.

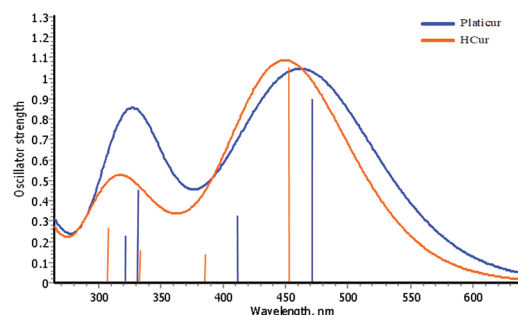


Fig. 1 Computed absorption spectra of the free ligand (HCur) and curcumin *cis*-diammineplatinum(II) complex, Platicur. Only transitions with an oscillator strength greater than 0.1 are shown.

Excited state characterization

To gain an insight into the active species of the Platicur complex potentially involved in the curcumin photocleavage, we firstly applied one of the procedures reported in the literature to ascertain that a chemical bond break can occur once the drug is activated by light.^{33,34} It consists of a semi-relaxed scan calculation along the selected reaction coordinate representing the detachment of the curcumin ligand. The Pt–O distance of a keto group of the curcumin ligand, chosen as a suitable reaction coordinate, was increased starting from the equilibrium distance of 2.002 Å, in ten steps of 0.1 Å. Each step in this scan provided a set of atomic coordinates in the ground state, which has been then subjected to TDDFT calculations. Though the ten singlet excited states taken into consideration are all dissociative, as they do not exhibit any minimum along the chosen reaction coordinate, their behaviour shows only a small variation (see Fig. S3 of the ESI†) with respect to the ground state. This suggests that none of these excited states shows an accelerating profile towards the ligand release in the non-adiabatic description. Moreover, even the TDDFT optimized structures of both bright states, S_1 and S_2 , which, very likely, could be involved, show very modest differences in their structure compared with that of the ground state, GS (see Fig. S4†). The Pt–O bond distances are a little bit elongated, contrariwise to the Pt–N ones, confirming their dissociative nature along the O,O-donor ligand detachment, while the permanence of the planar conformation of curcumin structure surely prevents its removal. Keeping in mind that, generally, the lifetime of singlet excited states is five-fold less than that of a triplet one (10^{-8} vs. 10^{-3} s), it appears reasonable to hypothesize that the main route for converting Platicur into diaquo species can involve an excited triplet state rather than a singlet one.

To properly locate and characterize the plausible triplet states, the most stable geometries of the first six triplet excited states (found within the vertical approximation) have been primarily determined at the TD-B3LYP level of theory, then optimized within the unrestricted DFT formalism.^{35,36} With this procedure, four different triplet excited states have been obtained, while the other trials ended up in the wells of the four excited-state minima. The intercepted optimized struc-

tures are reported in the ESI (Fig. S5†), while the relative energies and the spin density distribution used to determine their character, together with the spin density on the Pt atom, are shown in Fig. 2.

Triplet states, named T_2 and T_3 , have very similar structural and electronic features. The only difference relies on the localization of the spin density on one or the other phenyl ring of the curcumin chromophore. In both the optimized structures, curcumin maintains its planar conformation with Pt–O distances slightly elongated compared to the ground state minimum, though they are the triplet excited states mostly GS-like. A similar distribution of the spin density on the curcumin ligand is reflected in the energy of the two triplet states (1.94 and 1.96 eV, respectively) and the same spin density on the metal atom.

In contrast, the highest triplet state (labelled T_4) is characterized by a substantial elongation of the Pt–O bonds with a consequent distortion of curcumin planarity (see Fig. S5†), which breaks the conjugation on the π ligand making the state essentially centred on the metal 3MC , as a result from the spin density (1.64) highly localized on Pt.

The lowest triplet state (T_1) shows the largest deviations from the GS structure, since the coordination sphere of the metal results in strong distortion. One ancillary ammonia ligand now lies in a nearly perpendicular position (85.9 degrees) with respect to the plane of the metal, curcumin and other ammonia. Looking at the bond distances (Fig. S5†) between the metal and both oxygen and nitrogen atoms, all the ligands appear to be less bound to the Pt atom. Thus, even this state was found to be centred on platinum (3MC) with a localized spin density of 1.53.

Though all the optimized triplet excited states have been found to be dissociative with respect to the curcumin ligand detachment, as witnessed by the elongation of the Pt–O distances in all the intercepted triplet states (see Fig. S5†) with respect to the ground state, this behaviour is much more evident in both T_1 and T_4 , whose Pt–O distances increase by up to approximately 0.2 Å. Therefore, though in principle the cleavage of the ligand could occur along all the triplet state potential energy surfaces, this structural feature suggests that only T_1 and T_4 can be really involved in the ligand detachment. In order to confirm this hypothesis, the accessibility to the plausible channels for triplets' population must be taken into

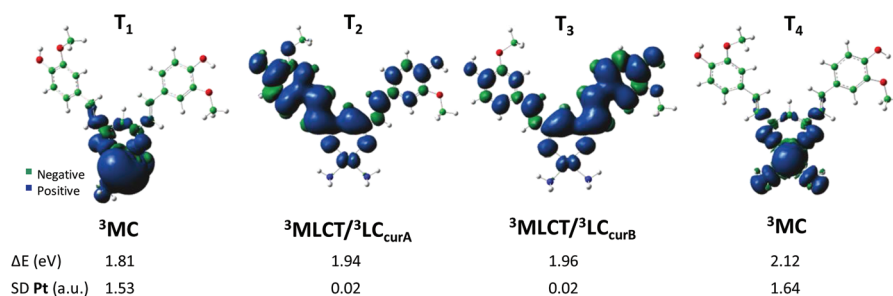


Fig. 2 Computed spin density distributions of the intercepted triplet states. Spin densities on the metal centre and the adiabatic energy gap ΔE with respect to the GS are also provided.

account. It is well known that the population probability of the triplet states depends on the possibility that an efficient intersystem spin crossing (ISC) from the bright state to the triplets lying below could occur. According to the Fermi Golden Rule,³⁷ the ISC kinetics is directly related to the spin-orbit matrix elements and the adiabatic singlet-triplet energy gap. Thus, both spin-orbit coupling constants (SOCs) and S-T adiabatic energy differences (ΔE) have been computed and plotted in Fig. 3. Looking at the TDDFT outcomes, once the photon is absorbed, both singlet states S_1 and S_2 can be, in principle, populated. However, keeping in mind the Kasha rules, it seems reasonable hypothesizing that, if the higher energy state S_2 is that involved in the absorption, a primary internal conversion should occur before the ISC process can start. The relative adiabatic energies of the photoactivated excited states follow the order S_1 ($^1LC/{}^1LMCT$) > T_4 (3MC) > T_3 (${}^3MLCT/LC_{curB}$) > T_2 (${}^3MLCT/LC_{curA}$) > T_1 (3MC). Based on these energies, the bright state deactivation can, thus, involve all the four triplet states. Therefore, the coupling between S_1 and all the triplet states T_n (with $n = 1-4$), lying below it, has been explored.

Looking at Fig. 3a, it is worth noting that the triplet states show a common behaviour in pairs, depending on their character. The small SOC values computed for both $S_1 \rightarrow T_2$ and $S_1 \rightarrow T_3$ energy transfer (27.0 and 17.7 cm^{-1} , respectively) suggest a lower probability that an intersystem crossing between the bright state and both the triplets T_2 and T_3 occurs, if compared with those calculated for T_1 and T_4 triplet states, one order of magnitude larger (297.8 and 281.7 cm^{-1} , respectively). This behaviour can be easily rationalized by recalling the El-Sayed rules, according to which the rate of intersystem crossing, from the lowest singlet state to the triplet manifold, strongly depends on changing of the molecular orbital type between the coupled states. The character of both T_2 and T_3 states is responsible for the smallest SOC values, as they are essentially localized on the O,O donor ligand, likewise the S_1 , with only a little participation of the metal. In contrast, the significant change in the composition of the molecular orbitals of the states coupled for the ISC from S_1 to both T_1 and T_4 states, both localized on the metal centre, explains the large values of the SOC.

Combining all the data discussed so far, the population of the photoactivation-pertinent excited states should follow the

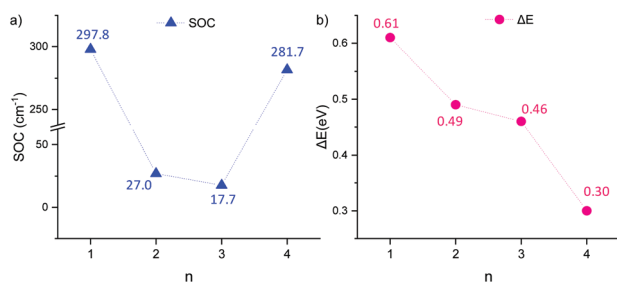


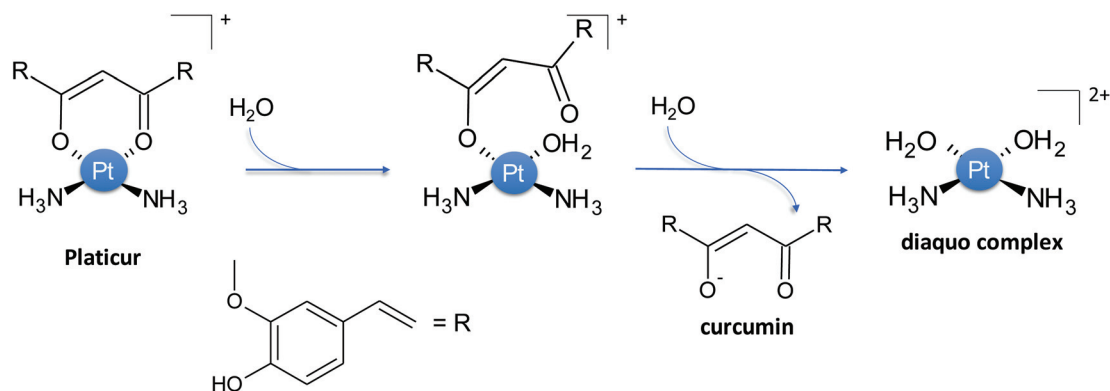
Fig. 3 (a) Spin orbit coupling constants (SOC, cm^{-1}) between the excited singlet S_1 and triplet n states and (b) their adiabatic energy difference (ΔE , eV).

absorption to S_1 (${}^1LC/{}^1LMCT$), then the ISC to T_4 (3MC) from which the internal conversion processes can lead to the three triplet states lying below, named T_3 , T_2 and T_1 . The nature of both T_1 and T_4 states, 3MC , can facilitate ligand photodissociation, contrariwise to triplet states T_2 and T_3 , characterized by a spin density essentially localized on the ligand (Fig. 2), which cannot easily trigger the detachment of curcumin. Notwithstanding looking at the energy gaps S_1-T_n , both triplet states T_2 and T_3 lie at an energy close to the bright state. Thus, if populated, they will either decay *via* 3MC (T_1) leading to ligand dissociation or directly decay to the ground state transferring their energy to the molecular oxygen eventually present into the target tissues, triggering type II photoreactions characterizing the PDT action. Indeed, they have enough energy to promote the ${}^3\Sigma_g^- \rightarrow {}^1A_g$ transition, 0.98 eV, yielding the cytotoxic singlet oxygen species, 1O_2 .

Curcumin photorelease

Belonging to the class of drugs active in PACT, the antiproliferative activity of Platicur does not primarily rely on the generation of the cytotoxic 1O_2 . It represents a non-toxic precursor that, activated by light, can promote the formation of a cytotoxic species exhibiting a specific mechanism toward cancer cells. Thus, Platicur is expected to be inert until it is converted into the active aquated form, by the photorelease of curcumin, according to a hydrolysis mechanism, following the typical behaviour of most square-planar $Pt(II)$ -based anticancer drugs.¹ It is well known that the hydrolysis process of square-planar d^8 complexes, belonging to the class of second-order nucleophilic substitution (S_N2) reactions, occurs according to a classical associative mechanism in which the displacement of the leaving groups by water passes through a five-coordinated transition state.³⁸ Likewise, the curcumin release takes place in two steps: the detachment of one arm of β -diketone ligand in favour of a water molecule coordination, and the complete release of the ligand, by substitution with another water molecule, to afford the diaquo species (Scheme 1). Basically, the detachment of the ligand can occur in the dark or upon irradiation, which implies the involvement of the excited states in the aquation process. According to the experimental evidence, the hydrolysis in the dark should be unfavourable since Platicur does not show any significant activity in the absence of a light source, considering its hydrolysis is very slow.²² This suggests, as desired, that Platicur remains essentially inert until exposure to light. Aiming at supporting this proposal, the mechanism leading to curcumin release in the dark will be discussed in detail in the next section in order to discard its implication in the anticancer activity of Platicur.

As underlined above, combining the experimental evidence^{22,31} with the photophysical properties explored here, it is reasonable to hypothesize that light excitation to the lowest-lying singlet excited state (S_1) is followed by efficient intersystem crossings (ISCs) to the triplet manifold. The ultrafast nature of the ISC processes is assured by the largest spin-orbit couplings (SOC) computed for both T_1 and T_4 (see



Scheme 1 Schematic of the Platicur hydrolysis process affording curcumin and the diaquodiamminePt(II) complex.

Fig. 3), whose spin densities are essentially localized on the metal centre (Fig. 2).

An excited state with a MC character surely cannot be involved in the emissive processes, while it can play a role as an active species toward the reactive ligand release.^{35,39,40} Therefore, the curcumin detachment in favour of aquated species formation has been investigated along both T_1 and T_4 potential energy surfaces (PESs), disregarding both T_2 and T_3 because of the small SOCs computed for the radiationless ISC processes leading to their population. The entire reaction has been explored considering the assistance by a critical number of solvent molecules, six water molecules, along all the investigated PESs. All the minima and transition states intercepted along the explored pathways have been labelled with subscripts (1) and (4), indicating the process occurring along the T_1 and T_4 state PESs, respectively. The free energy profiles and a cut-out of the optimized structures for all the intercepted stationary points are shown in Fig. 4. The relative free energies have been determined with respect to the singlet ground state with the same microsolvation environment.

The formation of the first adduct, named ADD, in which the six water molecules surround the platinum complex, leads to different scenarios depending on the state taken into consideration. While the solvent molecules simply establish a network of hydrogen bonds with the ancillary ligands and oxygen atoms of curcumin in $ADD_{(4)}$, starting from the T_1 state two water molecules approach the metal occupying positions in the first coordination sphere to afford an octahedral arrangement around the $ADD_{(1)}$ metal centre. These two molecules have been, thus, considered part of such a triplet state, so that the coordination pattern of platinum results to be significantly different from that of T_4 . These adducts lie 46.4 and 45.5 kcal mol⁻¹ above the reference energy of the adduct in the ground state, respectively. For both T_1 and T_4 states, the entering water molecule in the first transition state approaches the metal centre essentially in the same way, with a valence angle, between the leaving and the entering groups of 52 and 62 degrees in $TS1_{(1)}$ and $TS1_{(4)}$, respectively. Nevertheless, the height of the barriers that is necessary to overcome in the two cases are substantially different. Along the T_1 PES, the first

transition state lies 23.3 kcal mol⁻¹ above $ADD_{(4)}$, similar to the barriers that are expected for the canonical hydrolysis process in the dark. While, the energy required for the T_1 state is only 7.5 kcal mol⁻¹. The product of the first aquation, named INT, is characterized by the loss of curcumin planarity and results to be less stable by 4.5 and 11.9 kcal mol⁻¹ for T_1 and T_4 , respectively, compared to the corresponding first adduct. Thus, from both kinetic and thermodynamic points of view, the first step of the hydrolysis process along the T_1 surface was more favourable than T_4 . In the second step, a second aquation occurs passing through the TS2: the activation barrier is less than 10 kcal mol⁻¹ in both cases (5.4 and 8.2 kcal mol⁻¹, along T_4 and T_1 , respectively). The formation of the aquated product results to be endergonic in both cases (3.3 and 8.5 kcal mol⁻¹, respectively). The pathway that requires overcoming the lowest energy barriers is surely that involving T_1 . Nevertheless, based on the rationalization of the photophysical properties reported above (see Fig. 3), T_4 state has a higher probability to be populated than T_1 because of smaller energy gap between the coupled states, in spite of similar SOCs. Thus, we have found of interest estimating the energy expense for the conversion of $ADD_{(4)}$ into $ADD_{(1)}$, which results to be only 6.5 kcal mol⁻¹ (see Fig. S6†). The imaginary frequency (133i cm⁻¹) characterizing the TS connecting the two minima essentially involves the torsion of ammonia with respect to the square plane to pass from the square-planar geometry of $ADD_{(4)}$ to the octahedral structure of $ADD_{(1)}$. The associated energy barrier is significantly lower than the energy required to afford the mono-aquated species along the T_1 PES (Fig. 4). Hence, it can be reasonably hypothesized that, if the T_4 state is populated through ISC from S_1 , it is rapidly converted into T_1 before undergoing the aquation process. Following the most probable pathway, once the final product, $PROD_{(1)}$, is formed, the canonical square-planar diaquo complex is yielded by the release of the water molecules labelled as W1 and W2 in Fig. 4, when the complex comes back to the ground state. The planar complex can, thus, interact with nucleobases, mainly the N7 position of guanine, through water displacement allowing the formation of intra- and inter-strand DNA cross-links.⁴¹ On the other hand, the

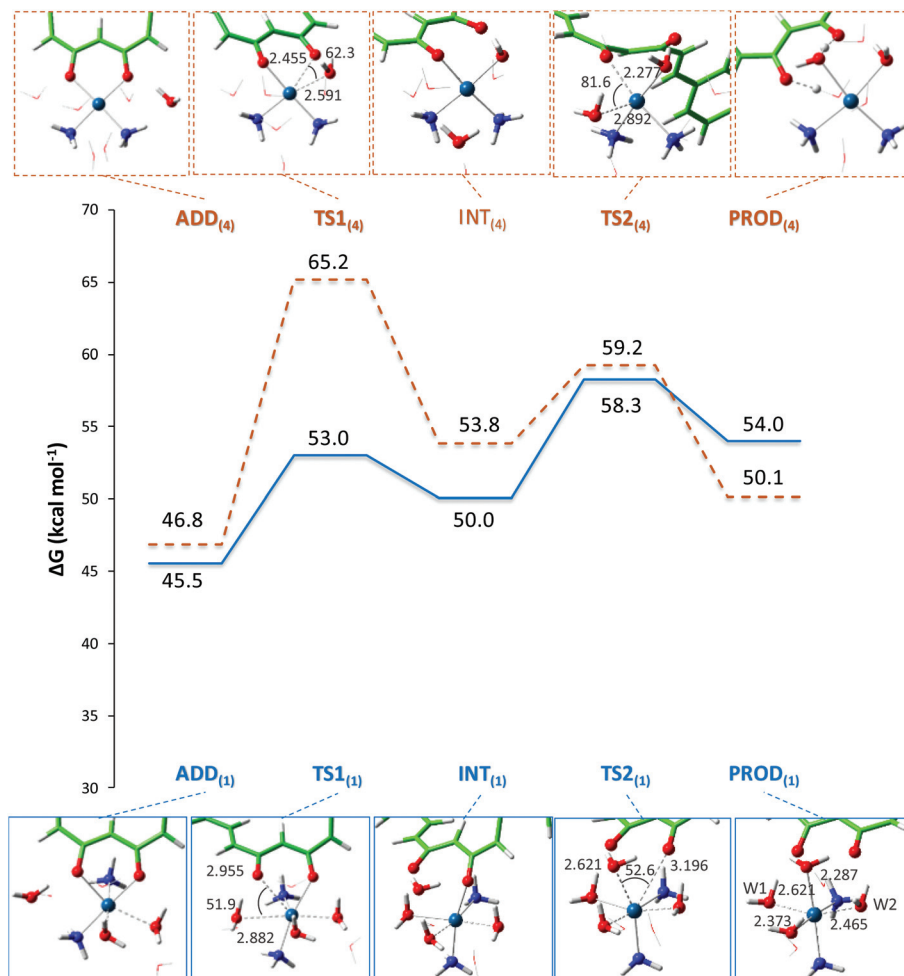


Fig. 4 Potential energy surfaces and a cut-out of the optimized structures of all the stationary points intercepted along the surfaces of both T₁ (solid blue line) and T₄ (dashed orange line) triplet states for the whole aquation process. The water molecules not directly involved in the process have been represented in the wireframe for clarity. Some key structural parameters have been also reported.

released curcumin can act as a phototoxin. Its release directly into the target tissues allows some of its limitations to be overcome and, being able to absorb in the same region of the complex from which it is derived, it can be easily activated once formed. Besides the absorption properties (Fig. 1 and Table S1†), even the factors influencing the promotion of type I and type II photoreactions (provided in the ESI, Fig. S7†) confirm its possible implication in PDT-related photoprocesses leading to ¹O₂ and ROS formation.

Dark curcumin release

To give a complete description of the conditions leading to the most favourable pathway, the aquation mechanism along the ground state PES has also been completely characterized. In analogy to what has been done for the reaction mechanism involving the triplet states, six explicit water molecules have been added around the Platicur complex. The outcomes of these calculations are shown in Fig. S8 of the ESI.† It is worth mentioning that the activation barriers computed for the first and second hydrolysis are 26.1 and 22.0 kcal mol⁻¹,

respectively, while both the steps are found to be endergonic by more than 10 kcal mol⁻¹ (15.8 and 23.1 kcal mol⁻¹, respectively). Looking at the available data for the leading chemotherapeutic agent cisplatin, for which the first chloro/aqua ligand exchange is reported to be the rate limiting step, the formation of the monoquo complex is endergonic by only few kcal mol⁻¹ (less than 5) and the estimated values of the energy barrier go from 19 to 23.32 kcal mol⁻¹.^{42–45} Therefore, it appears reasonable to consider Platicur inactive in the dark, supporting the slow hydrolysis experimentally observed.²²

Moreover, another possibility to activate Platicur in the absence of a light source was taken into consideration, which is related to a possible implication of glutathione (GSH) in the aquation process. It is well known that GSH plays an important role in the main biological processes, and due to its presence in excess within the tumour cells, it is used as an indicator for cancer onset.^{46–48} Recent works have reported a GSH-triggered drug release according to different reaction mechanisms, most of which exploit its reducing power.^{20,49,50}

Furthermore, thiols generally have a strong affinity for the platinum centre moiety, which may result in Pt-GSH adduct formation.⁵¹ Therefore, GSH can attack the platinum centre to replace a good leaving group, such as oxygen of the curcumin ligand. Aiming at completely excluding the activation of Platicur in the dark, the possibility that a GSH-triggered release of curcumin to afford an active DNA cross-linker could occur has been investigated. The outcomes of these calculations are shown in Fig. 5, in which both the free energy profile and the optimized structures of the located stationary points have been included. Starting from the initial interaction of GSH with the Platicur complex, ADD1_{GSH} , the reaction between them leads to the detachment of one curcumin arm to afford the complex $[\text{Pt}(\text{NH}_3)_2(\eta^1\text{-cur})(\text{GSH})]$, named INT_{GSH} . This reaction step requires the overcoming of an activation barrier of $29.1 \text{ kcal mol}^{-1}$. The formed INT_{GSH} lies at $6.5 \text{ kcal mol}^{-1}$ above the ADD1_{GSH} and it is characterized by a distorted structure because of the formation of the Pt-SH coordination bond. The complete curcumin release requires the intervention of a water molecule, whose entrance does not perturb the structural arrangement of INT_{GSH} , since ADD2_{GSH} lies almost at the same energy. The aquation step involves the overcoming of a lower activation barrier ($16.4 \text{ kcal mol}^{-1}$) and the formation of the monoquo complex is found to be only slightly

endergonic ($2.8 \text{ kcal mol}^{-1}$). On the basis of such results, considering the first step of the GSH triggered aquation of Platicur is highly unfavourable, it can be excluded that GSH could play any role in the activation of Platicur in the dark.

Computational details

All molecular geometry optimizations were carried out with the Gaussian09 software package,⁵² at the density functional level of theory, employing the B3LYP functional^{53,54} and including the dispersion corrections for the non-bonding interaction through the Grimme approach,⁵⁵ which uses an atom pairwise additive scheme denoted as DFT-D3.

For the Pt atom, the relativistic compact Stuttgart/Dresden effective core potential has been used⁵⁶ in conjunction with the split valence basis set. The standard triple- ζ 6-311G** basis sets have been used for all the atoms except for oxygen atoms directly bound to the metal centre (β -diketone moiety of curcumin), for which a diffuse function was included, 6-311+G**. The impact of the aqueous solvent has been taken into account by considering the dielectric constant of 78.4, within the Tomasi implicit polarizable continuum model,^{57,58} as implemented in Gaussian09.

The electronic spectra have been obtained, within the non-equilibrium time-dependent (TD) DFT approach, as vertical

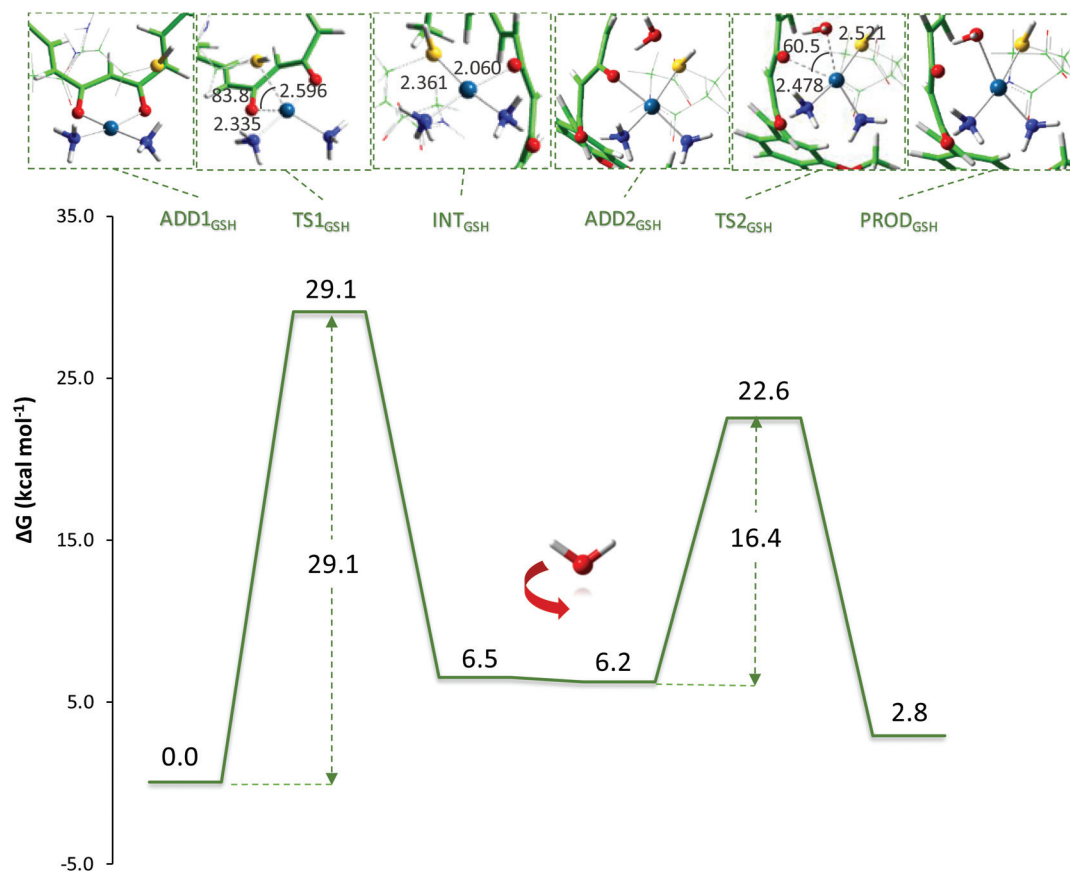


Fig. 5 Potential energy surface and a cut-out of the optimized structures of all the stationary points intercepted along the GSH-triggered curcumin release mechanism. The structure of GSH is almost entirely depicted in the wireframe for clarity; only the SH group has been drawn down in ball and stick. Some key structural parameters have been also reported.

electronic excitations on the ground-state structure, at the same level of theory used for other calculations. The optimized structures of all the excited states potentially involved in the curcumin photocleavage have been searched using the TDDFT in a condensed phase. In the case of triplet states, the obtained guesses have then been used as starting points for the optimization within the unrestricted Kohn–Sham formalism with UB3LYP. This procedure was suggested to avoid the instability of excited states involving charge transfer.³⁶

Since the characterization of the stationary points along the potential energy surface of the hydrolysis process along the triplet states has been possible only taking into consideration a critical number of explicit solvent water molecules, the same approach has been used for describing all the plausible hydrolysis pathways investigated here. Local minima and transition states have been identified by the number of imaginary vibrational frequencies (0 or 1, respectively). These calculations have been also used for calculating zero-point energy (ZPE). The involved transition states have been carefully checked to be properly connected to the correct minima by IRC (intrinsic reaction coordinate) analysis.^{59,60} Single-point calculations on all stationary point structures obtained in a vacuum have been carried out in implicit water at the same level for obtaining solvation Gibbs free energies. For this purpose, the UFF set of radii has been used to build-up the cavity holding solute molecules. Final Gibbs free energies have been thus obtained at 298 K at 1 atm from total energies, including zero-point, thermal and solvent corrections.⁶¹ However, as the free energy corrections in the Gaussian's default standard state corresponds to an ideal gas at a standard pressure of 1 atm, the computed free energies have been corrected, using a scheme already applied on similar systems,^{62,63} to yield the free energies with a solution-phase standard state of 1 mol L⁻¹ for all the species, while for water a standard state of 55.5 M has been used.

To ascertain the probability that a triplet state could be populated, spin–orbit matrix elements have been computed using the quadratic-response TD-DFT approach, as implemented in the Dalton code,⁶⁴ at the involved singlet excited state optimized geometry, as shown below:

$$\text{SOC}_{nm} = \sqrt{\sum_i \left| \langle \psi_{T_i,n} | \hat{H}_{\text{SO}} | \psi_{S_m} \rangle \right|^2}; \quad i = x, y, z$$

where \hat{H}_{SO} is the spin–orbit Hamiltonian. For this purpose, TD-B3LYP/cc-pVDZ in conjunction with the SDD pseudopotential for a Pt atom have been used within the spin–orbit coupling operators for effective core potentials with an effective nuclear charge.⁶⁵

Conclusions

This work provides an insight into the photoactivation-pertinent excited states of *cis*-[Pt(NH₃)₂(Cur)]⁺ towards curcumin release. The complete characterization of both singlet and

triplet excited states has allowed identification of the active species involved in the photoactivation pathway towards the controlled release of aquated diammine–platinum(II) species, as a DNA cross-linking agent, and curcumin, as a potential photosensitizer. The inspection of the photophysical properties, which are electronic transitions, spin–orbit coupling constants, and singlet–triplet states energy gaps, has revealed that the light exposure leads to the population of a mixed singlet state ¹LC/¹LMCT, from which the radiationless electronic transition (ISC) to T₄, whose character is entirely centred on the metal (³MC), definitively yields one of the most active species of Platicur. All the plausible pathways starting from this state have been fully explored: the direct curcumin release as well as the relaxation (IC) to triplet states lying below it, T₁–T₃, and the successive implication of such states in the ligand detachment. From the energy profiles of the curcumin detachment computed for the two triplet states with ³MC character, T₁ and T₄, it emerges that the ligand release is favoured along the T₁ PES. The triplet states formed, T₂ and T₃, which closely resemble the GS geometry, can trigger type II photoprocesses. Importantly, the two effects can be cumulative, and Platicur may generate ¹O₂ and ROS species (through T₄–T₂ states) until it undergoes ligand dissociation (through T₁) serving as a DNA binding agent and releasing a compound able to act as a photosensitizer. Furthermore, the complete description of the aquation mechanism leading to curcumin cleavage in the dark, even assisted by GSH, supports the inactivity of Platicur until light exposure.

It is worth noting that a deep understanding of the photoprocesses involved in the activation of prodrugs, such as that reported here, is of pivotal importance for the design of new and effective drugs to be used in the clinical treatments of cancer.

Conflicts of interest

There are no conflicts to declare.

Acknowledgements

This work is supported by Università della Calabria.

Notes and references

- 1 T. C. Johnstone, K. Suntharalingam and S. J. Lippard, The Next Generation of Platinum Drugs: Targeted Pt(II) Agents, Nanoparticle Delivery, and Pt(IV) Prodrugs, *Chem. Rev.*, 2016, **116**, 3436–3486.
- 2 S. Dilruba and G. V. Kalayda, Platinum-based drugs: past, present and future, Platinum-based drugs: past, present and future, *Cancer Chemother. Pharmacol.*, 2016, **77**, 1103–1124.
- 3 Q.-Q. Deng, X.-E. Huang, L.-H. Ye, Y.-Y. Lu, Y. Liang and J. Xiang, Phase II Trial of Loubo ® (Lobaplatin) and

- Pemetrexed for Patients with Metastatic Breast Cancer not Responding to Anthracycline or Taxanes, *Asian Pac. J. Cancer Prev.*, 2013, **14**, 413–417.
- 4 A.-M. Florea and D. Büsselberg, Cisplatin as an Anti-Tumor Drug: Cellular Mechanisms of Activity, Drug Resistance and Induced Side Effects, *Cancers*, 2011, **3**, 1351–1371.
- 5 G. J. Bosl and R. J. Motzer, Testicular Germ-Cell Cancer, *N. Engl. J. Med.*, 1997, **337**, 242–254.
- 6 M. Morris, P. J. Eifel, J. Lu, P. W. Grigsby, C. Levenback, R. E. Stevens, M. Rotman, D. M. Gershenson and D. G. Mutch, Pelvic Radiation with Concurrent Chemotherapy Compared with Pelvic and Para-Aortic Radiation for High-Risk Cervical Cancer, *N. Engl. J. Med.*, 1999, **340**, 1137–1143.
- 7 J. H. Schiller, D. Harrington, C. P. Belani, C. Langer, A. Sandler, J. Krook, J. Zhu and D. H. Johnson, Comparison of Four Chemotherapy Regimens for Advanced Non-Small-Cell Lung Cancer, *N. Engl. J. Med.*, 2002, **346**, 92–98.
- 8 T. C. Johnstone, G. Y. Park and S. J. Lippard, Understanding and Improving Platinum Anticancer Drugs – Phenanthriplatin, *Anticancer Res.*, 2014, **34**, 471–476.
- 9 J. J. Wilson and S. J. Lippard, Synthetic Methods for the Preparation of Platinum Anticancer Complexes, *Chem. Rev.*, 2014, **114**, 4470–4495.
- 10 R. K. Pathak, S. Marrache, J. H. Choi, T. B. Berding and S. Dhar, The Prodrug Platin-A: Simultaneous Release of Cisplatin and Aspirin, *Angew. Chem., Int. Ed.*, 2014, **53**, 1963–1967.
- 11 S. Marrache, R. K. Pathak and S. Dhar, Detouring of cisplatin to access mitochondrial genome for overcoming resistance, *Proc. Natl. Acad. Sci. U. S. A.*, 2014, **111**, 10444–10449.
- 12 A. Naik, R. Rubbiani, G. Gasser and B. Spingler, Visible-Light-Induced Annihilation of Tumor Cells with Platinum-Porphyrin Conjugates, *Angew. Chem., Int. Ed.*, 2014, **53**, 6938–6941.
- 13 A. Frei, R. Rubbiani, S. Tubafard, O. Blacque, P. Anstaett, A. Felgenträger, T. Maisch, L. Spiccia and G. Gasser, Synthesis, Characterization, and Biological Evaluation of New Ru(II) Polypyridyl Photosensitizers for Photodynamic Therapy, *J. Med. Chem.*, 2014, **57**, 7280–7292.
- 14 E. Shaili, Platinum Anticancer Drugs and Photochemotherapeutic Agents: Recent Advances and Future Developments, *Sci. Prog.*, 2014, **97**, 20–40.
- 15 T. J. Dougherty, C. J. Gomer, B. W. Henderson, G. Jori, D. Kessel, M. Korbek, J. Moan and Q. Peng, Photodynamic Therapy, *J. Natl. Cancer Inst.*, 1998, **90**, 889–905.
- 16 D. Phillips, The photochemistry of sensitizers for photodynamic therapy, *Pure Appl. Chem.*, 1995, **67**, 117–126.
- 17 J. D. Knoll and C. Turro, Control and utilization of ruthenium and rhodium metal complex excited states for photo-activated cancer therapy, *Coord. Chem. Rev.*, 2015, **282–283**, 110–126.
- 18 B. S. Howerton, D. K. Heidary and E. C. Glazer, Strained Ruthenium Complexes Are Potent Light-Activated Anticancer Agents, *J. Am. Chem. Soc.*, 2012, **134**, 8324–8327.
- 19 R. Bonnett, in *Comprehensive Coordination Chemistry II*, ed. J. A. McCleverty and T. J. Meyer, Pergamon, Oxford, 2003, pp. 945–1003.
- 20 K. Mitra, S. Patil, P. Kondaiah and A. R. Chakravarty, 2-(Phenylazo)pyridineplatinum(II) Catecholates Showing Photocytotoxicity, Nuclear Uptake, and Glutathione-Triggered Ligand Release, *Inorg. Chem.*, 2015, **54**, 253–264.
- 21 K. Mitra, A. Shettar, P. Kondaiah and A. R. Chakravarty, Biotinylated Platinum(II) Ferrocenylterpyridine Complexes for Targeted Photoinduced Cytotoxicity, *Inorg. Chem.*, 2016, **55**, 5612–5622.
- 22 K. Mitra, S. Gautam, P. Kondaiah and A. R. Chakravarty, The cis-Diammineplatinum(II) Complex of Curcumin: A Dual Action DNA Crosslinking and Photochemotherapeutic Agent, *Angew. Chem., Int. Ed.*, 2015, **54**, 13989–13993.
- 23 T. Esatbeyoglu, P. Huebbe, I. M. A. Ernst, D. Chin, A. E. Wagner and G. Rimbach, Curcumin—From Molecule to Biological Function, *Angew. Chem., Int. Ed.*, 2012, **51**, 5308–5332.
- 24 M. Salem, S. Rohani and E. R. Gillies, Curcumin, a promising anti-cancer therapeutic: a review of its chemical properties, bioactivity and approaches to cancer cell delivery, *RSC Adv.*, 2014, **4**, 10815–10829.
- 25 S. Prasad, A. K. Tyagi and B. B. Aggarwal, Recent Developments in Delivery, Bioavailability, Absorption and Metabolism of Curcumin: the Golden Pigment from Golden Spice, *Cancer Res. Treat.*, 2014, **46**, 2–18.
- 26 K. I. Priyadarsini, Photophysics, photochemistry and photobiology of curcumin: Studies from organic solutions, bio-mimetics and living cells, *J. Photochem. Photobiol., C*, 2009, **10**, 81–95.
- 27 A. Kielbik, P. Wawryka, D. Przystupski, J. Rossowska, A. Szewczyk, J. Saczko, J. Kulbacka and A. Chwiłkowska, Effects of Photosensitization of Curcumin in Human Glioblastoma Multiforme Cells, *In Vivo*, 2019, **33**, 1857–1864.
- 28 K. T. Kazantzis, K. Koutsonikoli, B. Mavroidi, M. Zachariadis, P. Alexiou, M. Pelecanou, K. Politopoulos, E. Alexandratou and M. Sagnou, Curcumin derivatives as photosensitizers in photodynamic therapy: photophysical properties and in vitro studies with prostate cancer cells, *Photochem. Photobiol. Sci.*, 2020, **19**, 193–206.
- 29 H. H. Buzzá, L. C. Fialho de Freitas, L. T. Moriyama, R. G. Teixeira Rosa, V. S. Bagnato and C. Kurachi, Vascular Effects of Photodynamic Therapy with Curcumin in a Chorioallantoic Membrane Model, *Int. J. Mol. Sci.*, 2019, **20**, 1084.
- 30 H. B. Strazzi Sahyon, P. P. da Silva, M. S. de Oliveira, L. T. A. Cintra, E. Dezan-Júnior, J. E. Gomes-Filho, R. C. de Jacinto, P. H. dos Santos and G. Sivieri-Araujo, Influence of curcumin photosensitizer in photodynamic therapy on the mechanical properties and push-out bond strength of glass-fiber posts to intraradicular dentin, *Photodiagn. Photodyn. Ther.*, 2019, **25**, 376–381.
- 31 K. Mitra, S. Gautam, P. Kondaiah and A. R. Chakravarty, Platinum(II) Complexes of Curcumin Showing

- Photocytotoxicity in Visible Light, *Eur. J. Inorg. Chem.*, 2017, **2017**, 1753–1763.
- 32 A. Upadhyay, S. Gautam, V. Ramu, P. Kondaiah and A. R. Chakravarty, Photocytotoxic cancer cell-targeting platinum(II) complexes of glucose-appended curcumin and biotinylated 1,10-phenanthroline, *Dalton Trans.*, 2019, **48**, 17556–17565.
- 33 L. Salassa, H. I. A. Phillips and P. J. Sadler, *Phys. Chem. Chem. Phys.*, 2009, **11**, 10311–10316.
- 34 J. C. Manton, S. Amirjalayer, A. C. Coleman, S. McMahon, E. C. Harvey, G. M. Greetham, I. P. Clark, W. J. Buma, S. Woutersen, M. T. Pryce and C. Long, Excited state evolution towards ligand loss and ligand chelation at group 6 metal carbonyl centres, *Dalton Trans.*, 2014, **43**, 17797–17805.
- 35 D. Escudero, E. Heuser, R. J. Meier, M. Schäferling, W. Thiel and E. Holder, Unveiling Photodeactivation Pathways for a New Iridium(III) Cyclometalated Complex, *Chem. – Eur. J.*, 2013, **19**, 15639–15644.
- 36 D. Escudero and W. Thiel, Assessing the density functional theory-based multireference configuration interaction (DFT/MRCI) method for transition metal complexes, *J. Chem. Phys.*, 2014, **140**, 194105.
- 37 C. M. Marian, Spin–Orbit Coupling and Intersystem Crossing in Molecules, *Wiley Interdiscip. Rev.: Comput. Mol. Sci.*, 2012, **2**, 187–203.
- 38 Y. Zhang, Z. Guo and X.-Z. You, Hydrolysis Theory for Cisplatin and Its Analogues Based on Density Functional Studies, *J. Am. Chem. Soc.*, 2001, **123**, 9378–9387.
- 39 B. A. Albani, B. Peña, K. R. Dunbar and C. Turro, Hydrolysis Theory for Cisplatin and Its Analogues Based on Density Functional Studies, *Photochem. Photobiol. Sci.*, 2014, **13**, 272–280.
- 40 Y. Chen, W. Lei, G. Jiang, Y. Hou, C. Li, B. Zhang, Q. Zhou and X. Wang, Fusion of Photodynamic Therapy and Photoactivated Chemotherapy: A Novel Ru(II) Arene Complex with Dual Activities of Photobinding and Photocleavage toward DNA, *Dalton Trans.*, 2014, **43**, 15375–15384.
- 41 M.-H. Baik, R. A. Friesner and S. J. Lippard, Theoretical Study of Cisplatin Binding to Purine Bases: Why Does Cisplatin Prefer Guanine over Adenine?, *J. Am. Chem. Soc.*, 2003, **125**, 14082–14092.
- 42 J. R. Perumareddi and A. W. Adamson, Photochemistry of complex ions. V. Photochemistry of some square-planar platinum(II) complexes, *J. Phys. Chem.*, 1968, **72**, 414–420.
- 43 R. N. Bose, R. E. Viola and R. D. Cornelius, Phosphorus-31 NMR and kinetic studies of the formation of ortho-, pyro-, and triphosphato complexes of cis-dichlorodiammineplatinum(II), *J. Am. Chem. Soc.*, 1984, **106**, 3336–3343.
- 44 K. Hindmarch, D. A. House and M. M. Turnbull, The hydrolysis products of cis-diamminedichloroplatinum(II) 9. Chloride and bromide anation kinetics for some $[\text{Pt}^{\text{II}}(\text{N})_2(\text{OH}_2)_2]^{2+}$ complexes and the structures of $[\text{Pt}^{\text{IV}}\text{Br}_4(\text{N})_2]$ ($(\text{N})_2 = \text{en}, \text{tn}$), *Inorg. Chim. Acta*, 1997, **257**, 11–18.
- 45 S. E. Miller and D. A. House, The hydrolysis products of cis-dichlorodiammineplatinum(II) 2. The kinetics of formation and anation of the cis-diamminedi(aqua)platinum(II) cation, *Inorg. Chim. Acta*, 1989, **166**, 189–197.
- 46 S. Banerjee, S. Kar, J. M. Perez and S. Santra, Quantum Dot-Based OFF/ON Probe for Detection of Glutathione, *J. Phys. Chem. C*, 2009, **113**, 9659–9663.
- 47 A. L. Ortega, S. Mena and J. M. Estrela, Glutathione in Cancer Cell Death, *Cancers*, 2011, **3**, 1285–1310.
- 48 X. Wu, X. Sun, Z. Guo, J. Tang, Y. Shen, T. D. James, H. Tian and W. Zhu, In Vivo and in Situ Tracking Cancer Chemotherapy by Highly Photostable NIR Fluorescent Theranostic Prodrug, *J. Am. Chem. Soc.*, 2014, **136**, 3579–3588.
- 49 S. J. Dougan, M. Melchart, A. Habtemariam, S. Parsons and P. J. Sadler, Phenylazo-pyridine and Phenylazo-pyrazole Chlorido Ruthenium(II) Arene Complexes: Arene Loss, Aquation, and Cancer Cell Cytotoxicity, *Inorg. Chem.*, 2006, **45**, 10882–10894.
- 50 Y. Fu, A. Habtemariam, A. M. Pizarro, S. H. van Rijt, D. J. Healey, P. A. Cooper, S. D. Shnyder, G. J. Clarkson and P. J. Sadler, Organometallic Osmium Arene Complexes with Potent Cancer Cell Cytotoxicity, *J. Med. Chem.*, 2010, **53**, 8192–8196.
- 51 X. Wang and Z. Guo, The Role of Sulfur in Platinum Anticancer Chemotherapy, *Anti-Cancer Agents Med. Chem.*, 2007, **7**, 19–34.
- 52 M. Frisch, G. Trucks, H. Schlegel, G. Scuseria, M. Robb, J. Cheeseman, G. Scalmani, V. Barone, B. Mennucci, G. Petersson, H. Nakatsuji, M. Caricato, X. Li, H. Hratchian, A. Izmaylov, J. Bloino, G. Zheng, J. Sonnenberg, M. Hada, M. Ehara, K. Toyota, R. Fukuda, J. Hasegawa, M. Ishida, T. Nakajima, Y. Honda, O. Kitao, H. Nakai, T. Vreven, J. Montgomery, J. Peralta, F. Ogliaro, M. Bearpark, J. Heyd, E. Brothers, K. Kudin, V. Staroverov, R. Kobayashi, J. Normand, K. Raghavachari, A. Rendell, J. Burant, S. Iyengar, J. Tomasi, M. Cossi, N. Rega, J. Millam, M. Klene, J. Knox, J. Cross, V. Bakken, C. Adamo, J. Jaramillo, R. Gomperts, R. Stratmann, O. Yazyev, A. Austin, R. Cammi, C. Pomelli, J. Ochterski, R. Martin, K. Morokuma, V. Zakrzewski, G. Voth, P. Salvador, J. Dannenberg, S. Dapprich, A. Daniels, O. Farkas, J. Foresman, J. Ortiz, J. Cioslowski and D. Fox, *Gaussian 09, Revision D.01*, Gaussian, Inc., Wallingford, CT.
- 53 A. D. Becke, Density-functional Thermochemistry., III. The Role of Exact Exchange, *J. Chem. Phys.*, 1998, **98**, 5648.
- 54 C. Lee, W. Yang and R. G. Parr, Development of the Colle-Salvetti Correlation-Energy Formula into a Functional of the Electron Density, *Phys. Rev. B: Condens. Matter Mater. Phys.*, 1988, **37**, 785–789.
- 55 S. Grimme, J. Antony, S. Ehrlich and H. Krieg, Consistent and Accurate Ab Initio Parametrization of Density Functional Dispersion Correction (DFT-D) for the 94 Elements H–Pu, *J. Chem. Phys.*, 2010, **132**, 154104.
- 56 D. Andrae, U. Häußermann, M. Dolg, H. Stoll and H. Preuß, Energy-Adjusted ab Initio Pseudopotentials for

- the Second and Third Row Transition Elements, *Theor. Chim. Acta*, 1990, **77**, 123–141.
- 57 S. Miertuš and J. Tomasi, Approximate Evaluations of the Electrostatic Free Energy and Internal Energy Changes in Solution Processes, *Chem. Phys.*, 1982, **65**, 239–245.
- 58 S. Miertuš, E. Scrocco and J. Tomasi, Electrostatic Interaction of a Solute with a Continuum. A Direct Utilizaion of AB Initio Molecular Potentials for the Prevision of Solvent Effects, *Chem. Phys.*, 1981, **55**, 117–129.
- 59 C. Gonzalez and H. B. Schlegel, An Improved Algorithm for Reaction Path Following, *J. Chem. Phys.*, 1989, **90**, 2154–2161.
- 60 K. Fukui, Formulation of the Reaction Coordinate, *J. Phys. Chem.*, 1970, **74**, 4161–4163.
- 61 H. Cartwright, Molecular Thermodynamics. By Donald A. McQuarrie and John D. Simon. University Science Books, 55D Gate Five Road, Sausalito CA 94965, USA, *Chem. Educ.*, 1999, **4**, 120–121.
- 62 E. Dabbish, F. Ponte, N. Russo and E. Sicilia, Antitumor Platinum(IV) Prodrugs: A Systematic Computational Exploration of Their Reduction Mechanism by l-Ascorbic Acid, *Inorg. Chem.*, 2019, **58**, 3851–3860.
- 63 X. Zhang, F. Ponte, E. Borfecchia, A. Martini, C. Sanchez-Cano, E. Sicilia and P. J. Sadler, Glutathione Activation of an Organometallic Half-Sandwich Anticancer Drug Candidate by Ligand Attack, *Chem. Commun.*, 2019, **55**, 14602–14605.
- 64 K. Aidas, C. Angeli, K. L. Bak, V. Bakken, R. Bast, L. Boman, O. Christiansen, R. Cimiraglia, S. Coriani, P. Dahle, E. K. Dalskov, U. Ekström, T. Enevoldsen, J. J. Eriksen, P. Ettenhuber, B. Fernández, L. Ferrighi, H. Fliegl, L. Frediani, K. Hald, A. Halkier, C. Hättig, H. Heiberg, T. Helgaker, A. C. Hennum, H. Hettema, E. Hjertenaes, S. Høst, I.-M. Høyvik, M. F. Iozzi, B. Jansík, H. J. Aa. Jensen, D. Jonsson, P. Jørgensen, J. Kauczor, S. Kirpekar, T. Kjaergaard, W. Klopper, S. Knecht, R. Kobayashi, H. Koch, J. Kongsted, A. Krapp, K. Kristensen, A. Ligabue, O. B. Lutnaes, J. I. Melo, K. V. Mikkelsen, R. H. Myhre, C. Neiss, C. B. Nielsen, P. Norman, J. Olsen, J. M. H. Olsen, A. Osted, M. J. Packer, F. Pawłowski, T. B. Pedersen, P. F. Provasi, S. Reine, Z. Rinkevicius, T. A. Ruden, K. Ruud, V. V. Rybkin, P. Sałek, C. C. M. Samson, A. S. de Merás, T. Saue, S. P. A. Sauer, B. Schimmelpfennig, K. Snegov, A. H. Steindal, K. O. Sylvester-Hvid, P. R. Taylor, A. M. Teale, E. I. Tellgren, D. P. Tew, A. J. Thorvaldsen, L. Thøgersen, O. Vahtras, M. A. Watson, D. J. D. Wilson, M. Ziolkowski and H. Ågren, *Wiley Interdiscip. Rev.: Comput. Mol. Sci.*, 2014, **4**, 269–284.
- 65 S. Koseki, M. W. Schmidt and M. S. Gordon, Effective Nuclear Charges for the First- through Third-Row Transition Metal Elements in Spin–Orbit Calculations, *J. Phys. Chem. A*, 1998, **102**, 10430–10435.

Electronic Supplementary Information

Mechanism of Action of the Curcumin *cis*-Diammineplatinum(II) Complex as Photocytotoxic Agent

Eslam Dabbish, Gloria Mazzone, Nino Russo, Emilia Sicilia*

Department of Chemistry and Chemical Technologies, Università della Calabria, 87036, Arcavacata di Rende (CS), Italy

Table of Contents

- **Table S1:** Vertical excitation energies, ΔE (eV), wavelength λ (nm), oscillator strengths (f) and main configuration (%) for curcumin and Platicur complex computed in water S3
- **Figure S1:** Energetic diagram of the highest occupied molecular orbitals (from H to H-3) and the lowest unoccupied molecular orbitals (from L to L+2) involved in the electronic transitions of Platicur S4
- **Figure S2:** Electron Density Difference Maps EDDMs between the excited singlet and ground states for Platicur complex (Purple and yellow colors represent a decrease and an increase in charge density, respectively). Natural Transition Orbitals NTOs for the corresponding states S5
- **Figure S3:** TDDFT singlet excited states S_n (with $n = 1-10$) energy from relaxed scan calculation along the Pt-O distance reaction coordinate, going from 2.0 to 3.0 Å, accounting for the detachment of the curcumin ligand S6
- **Figure S4:** Optimized structures (with selected geometric parameters) of ground and lowest singlet excited states (S_1 and S_2) and their adiabatic energy gaps S7
- **Figure S5:** Optimized structures and selected geometric parameters of the triplet excited states ($T_1 - T_4$) lying below the energy of S_1 S8

- **Figure S6:** Energy profile for the conversion of ADD₍₁₎ in ADD₍₄₎ and the optimized structure of the involved transition state S9
- **Figure S7:** Photophysical properties of curcumin: a) excited states adiabatic energies, b) SOC and $\Delta E(S_m-T_n)$, c) vertical electron affinity VEA and ionization potential VIP (Type I photoreactions), d) Molecular Orbitals counter plot S10
- **Figure S8:** Potential energy surface and a cut out of the optimized structures of all the stationary points intercepted along the GS curcumin release S11
- **References** S12

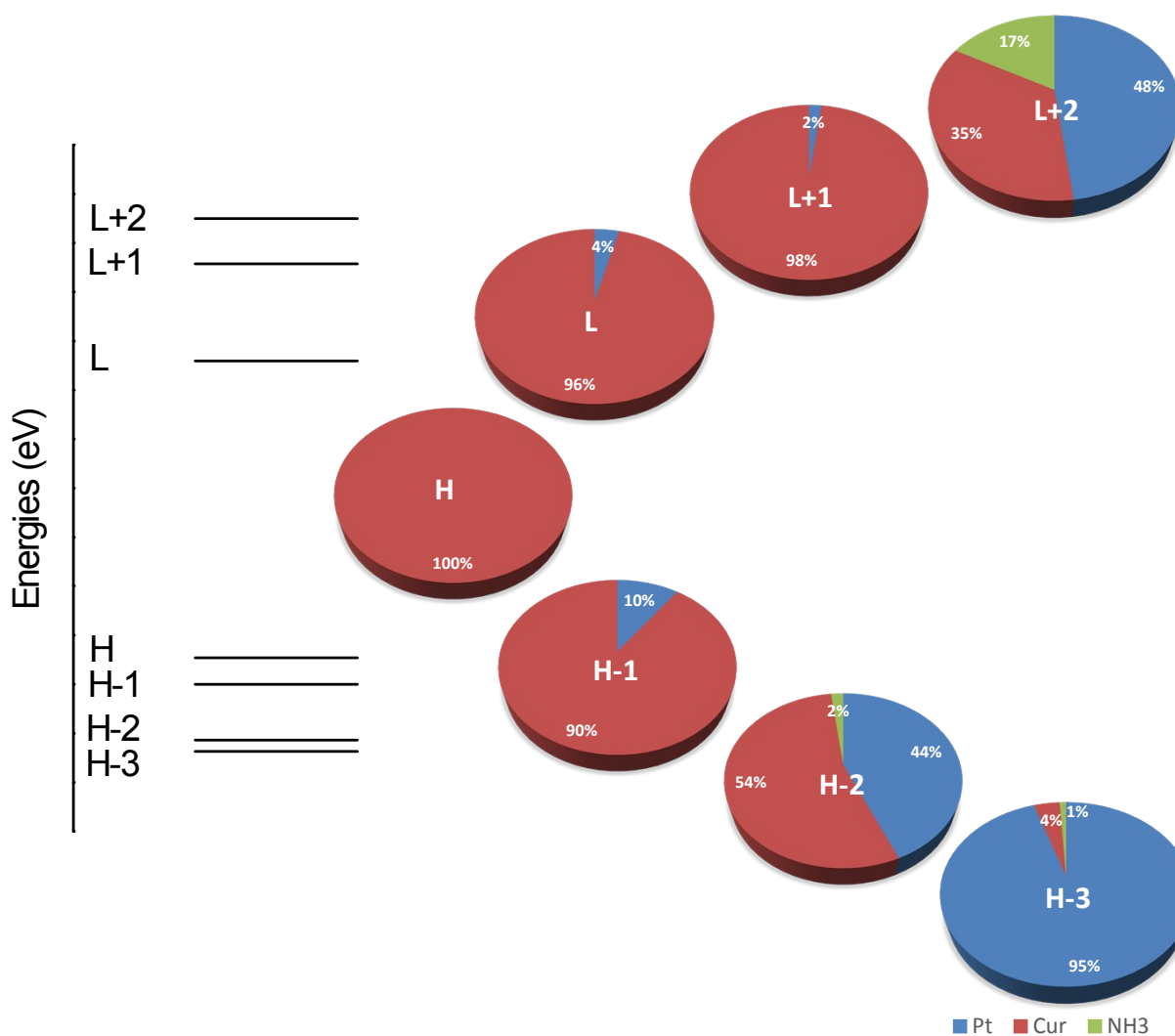
Table S1

Vertical excitation energies, ΔE (eV), wavelength λ (nm), oscillator strengths (f) and main configuration (%) for curcumin (HCur) and Platicur complex computed in water.

	λ	ΔE	Main Configuration, %	f^a	$\lambda^{exp,b}$	Assignment
HCur						
S ₁	452	2.74	H→L, 99	1.051	430	¹ $\pi\pi^*$
S ₂	385	3.22	H-1→L, 93	0.143		¹ $\pi\pi^*$
S ₃	334	3.71	H→L+1, 69	0.169	358	¹ $\pi\pi^*$
S ₄	309	4.01	H-1→L+1, 54	0.268		¹ $\pi\pi^*$
Platicur						
S ₁	473		H→L, 99	0.902	460	¹ LC/ ¹ LMCT
S ₂	411		H-1→L, 96	0.334	435	¹ LC/ ¹ MLCT
S ₃	330		H→L+1, 48; H-4→L, 23	0.468	385	¹ LC/ ¹ MLCT
S ₄	319		H-2→L+1, 82	0.235		¹ MLCT

a. Only transitions with oscillator strength greater than 0.1 were included, b. experimental spectrum from ref. [1]

Figure S1



Energetic diagram of the highest occupied molecular orbitals (from H to H-3) and the lowest unoccupied molecular orbitals (from L to L+2) involved in the electronic transitions of **Platicur**. The pie charts represent the percentage of participation of each portion of the complex, platinum (■ Pt), curcumin (■ Cur) and ammonia (■ NH₃) ligands, in the reported molecular orbitals.

Figure S2

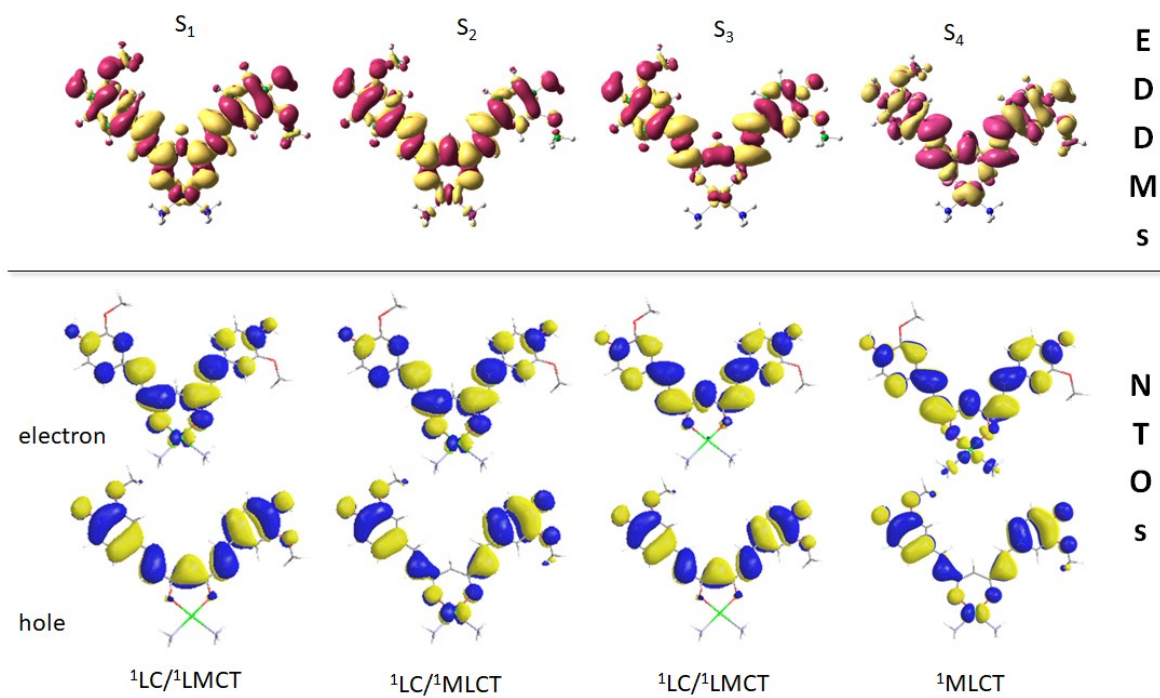


Figure S3

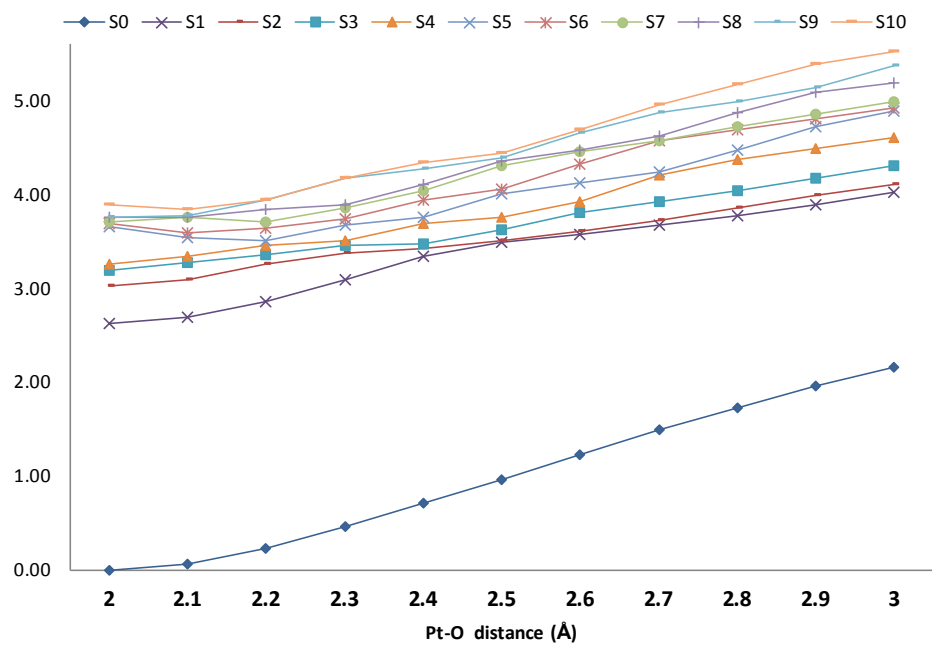
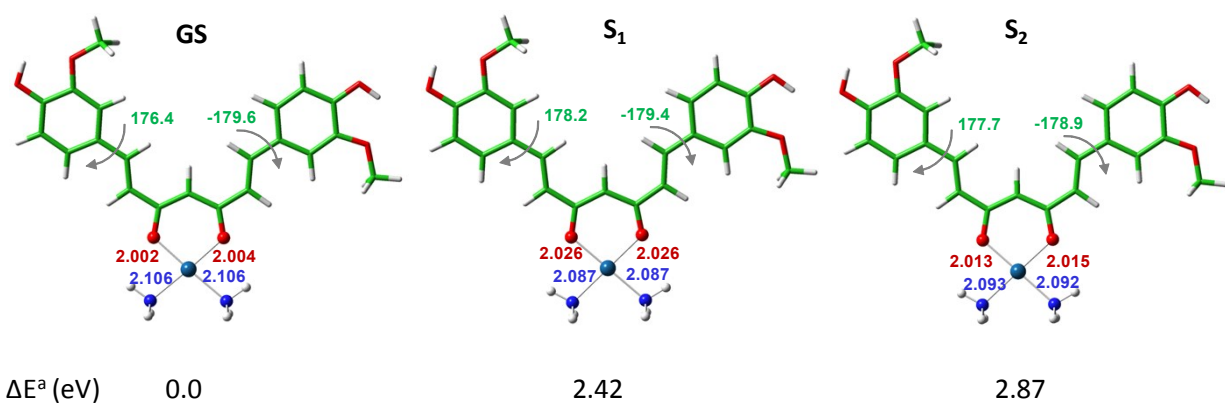


Figure S4



^aAdiabatic energies

Figure S5

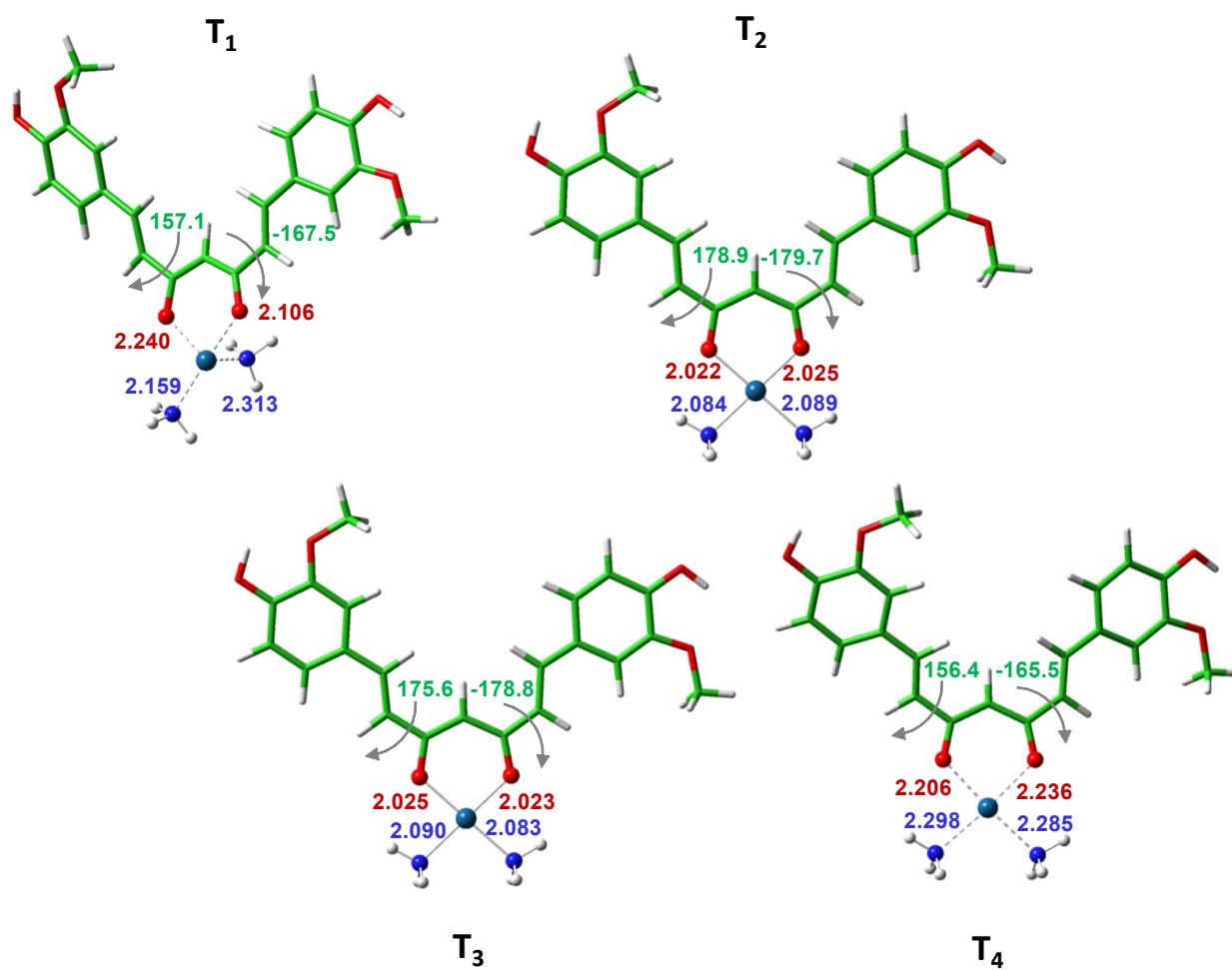


Figure S6

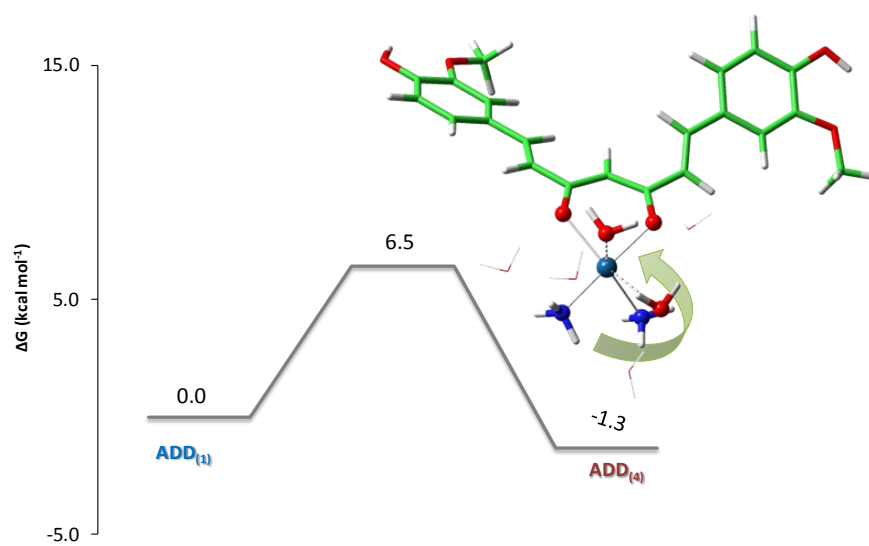




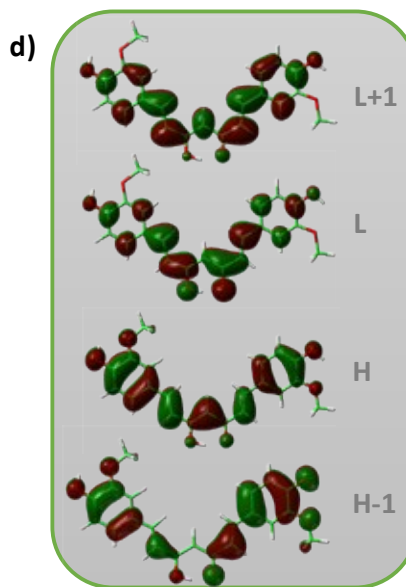


Figure S7

a)	ΔE (eV)	Main Configuration, %	Character
S_1	2.45	H→L, 99	$^1\pi\pi^*$
S_2	2.97	H-1→L, 93	$^1\pi\pi^*$
T_1	1.61^a	H→L, 47; H→L+1, 47	$^3\pi\pi^*$ $^3\pi\pi^*$
T_2	2.08	H→L, 51; H→L+1, 48	$^3\pi\pi^*$
T_3	2.74	H-1→L, 76	$^3\pi\pi^*$
T_4	2.87	H→L+1, 49	$^3\pi\pi^*$

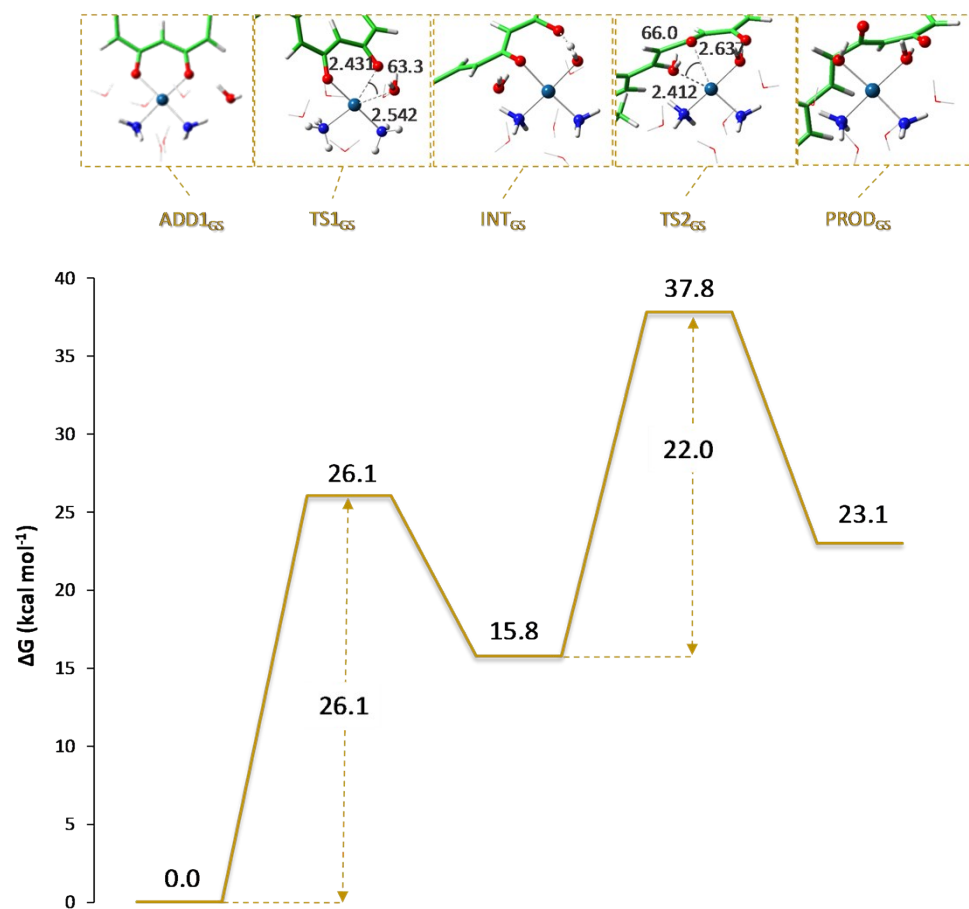
b)	m,n	SOC (cm ⁻¹)	$\Delta E S_m-T_n$ (eV)
	1,1	$5.4 \cdot 10^{-3}$	0.85
	1,2	$5.4 \cdot 10^{-3}$	0.37
	2,3	$5.2 \cdot 10^{-2}$	0.23
	2,4	$5.2 \cdot 10^{-2}$	0.11

c)	^b Photoprocess	Requirement	VEA	VIP	VEA(T_1)	VIP(T_1)
1.	$^3P_s + ^3O_2 \rightarrow P_s^{(+)} + O_2^{(-)}$	VEA (3O_2) + VIP (3P_s) < 0	 -2.83	5.67	-4.76	3.74
2.	$P_s^{(-)} + ^3O_2 \rightarrow ^1P_s + O_2^{(-)}$	VEA (3O_2) + VEA (1P_s) < 0				
3.	$^3P_s + ^1P_s \rightarrow P_s^{(+)} + P_s^{(-)}$	VEA (3P_s) + VIP (1P_s) < 0				
4.	$^3P_s + ^3P_s \rightarrow P_s^{(+)} + P_s^{(-)}$	VEA (3P_s) + VIP (3P_s) < 0			VEA(3O_2)	-3.16



^a sufficient energy to promote the molecular oxygen transition ($^3\Sigma_g^- \rightarrow ^1\Delta_g$); ^b computed in water B3LYP/6-311+G**.

Figure S8



References

- [1] Mitra, K.; Gautam, S.; Kondaiah, P.; Chakravarty, A. R. *Angew. Chem. Int. Ed.* **2015**, *54*, 13989-13993.

Chapter VII

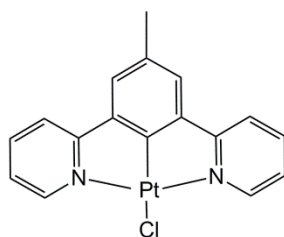
**Platinum drugs in
Photodynamic
Therapy (PDT)**

Chapter VII Platinum Drugs in Photodynamic Therapy (PDT)

7.1 Anticancer activity, DNA-binding and photodynamic properties of a N[^]C[^]N-coordinated Pt(II) complex

7.1.1 Introduction

Cyclometalated platinum(II) complexes containing tridentate π -conjugated organic ligands have been receiving an increase of interest as they display rich and diverse photoluminescent properties that are sensitively affected by local medium.¹ Alongside photoluminescent properties, such complexes have attracted, in the last few years, a lot of interest for application as potent anticancer agents and several groups have studied their antitumor properties.² These complexes can mediate their cytotoxic activity via either classical covalent binding to the DNA base pairs or reversible interactions such as intercalation. The planar motifs of these platinum(II) complexes can render them DNA metallointercalators inserting between adjacent DNA base pairs and establishing non-covalent ligand–ligand π – π stacking interactions. DNA interactions can also be electrostatic, groove-binding and hydrogen-bonding.



Complex (1)

Scheme 7.1 Structure of the investigated complex

The investigation of the luminescence properties of the Pt(II) complex of 1,3-di(2-pyridyl)benzene, acting as a terdentate N[^]C[^]N coordinating ligand cyclometalated at C2 of the benzene ring and substituted in 4 position by a methyl group (see Complex **1**, Scheme 7.1) has demonstrated that it is able

to intensely absorb light in the UV/visible region and possesses triplet excited states with significantly long, of the order of microseconds, lifetime and quantum yield.^{3,4} Recently, the investigation of the antiproliferative properties of complex **1** has demonstrated that it behaves as a promising photosensitizer under visible light capable to produce singlet oxygen in 70–80% yield in organic solvents.⁵ Moreover, due to the planarity of the ligand and polycyclic structure and aromaticity of the complex, binding to DNA by intercalation without direct metal coordination to DNA bases is very likely. The authors have suggested that intercalation protects the complex from oxygen and, therefore, other modes of interaction with DNA can be envisaged that might allow oxygen access to complex **1** causing DNA breaking as a result of ROS/singlet oxygen generation upon light mediated activation of the DNA bound complex.

7.1.2 Aim of study

We have undertaken a detailed theoretical investigation, using several computational tools, of the cytotoxic activity of complex (**1**), its modes of interaction with DNA, the effect on its spectroscopic properties of such interactions and the possibility that induced DNA damage is the consequence of its photosensitizer nature. DFT quantum mechanical calculations have been carried out to simulate the steps of the classical Pt(II) complexes mechanism of action for complexes **1**, that is aquation and interaction with guanine. Molecular dynamics (MD) simulations and free binding energy calculations have been carried out as starting point, to obtain information on the key intermolecular interactions between the intercalating complexes and DNA. TDDFT has been employed in order to analyze the spectroscopic properties of the investigated complex in its unperturbed, aquated and guanine bound forms and of the DNA intercalated complex aiming at both checking the suitability of complex **1** to act as a photosensitizer in

photodynamic therapy (PDT) and evaluating how the binding affects sensitization activity.

7.1.3 Highlighting results

The exploration of the key steps of the mechanism of action of traditional Pt(II) drugs shows that complex **1** can, in principle, be easily activated by aquation inside the cell and equally easily can bind nuclear DNA, whereas deactivating interactions with sulfur containing biomolecules is less thermodynamically favored.

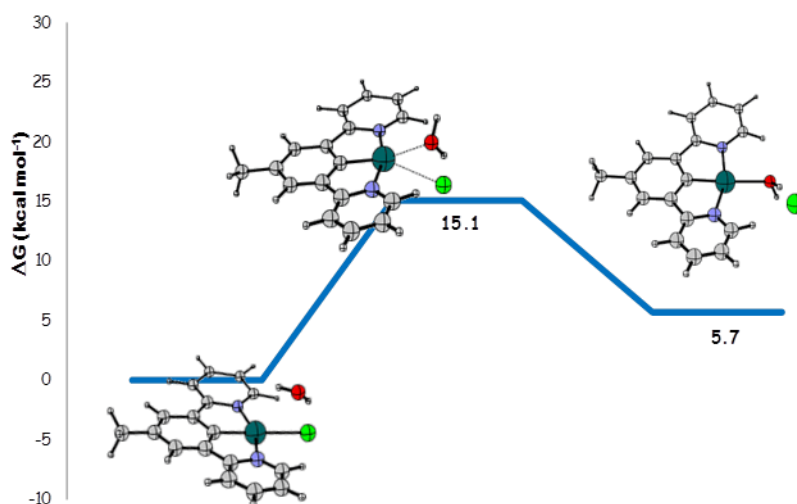


Figure 7.1 Free energy profiles in water describing the aquation reaction of complexes **1**. Geometrical structures of the stationary points intercepted along the path are also reported. Relative energies are in kcal mol⁻¹ and calculated with respect the zero reference energy of the initial adduct.

The photophysical properties for the intact complex **1**, its aquated **1_{wat}** and guanine bound **1_{gua}** form in water solvent have been computed. Calculated spectra and the corresponding frontier molecular orbitals are illustrated in **Figure 7.2** and **7.3** respectively.

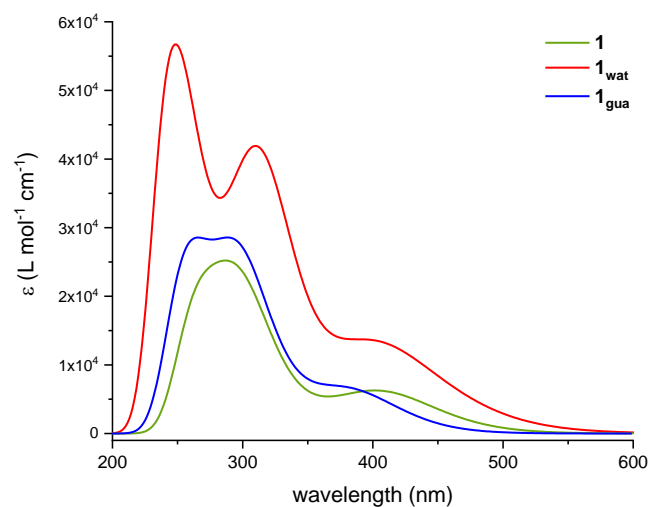


Figure 7.2 Computed absorption spectra of the intact complex **1** (green) and its aquated (red) and guanine bound (blue) forms.

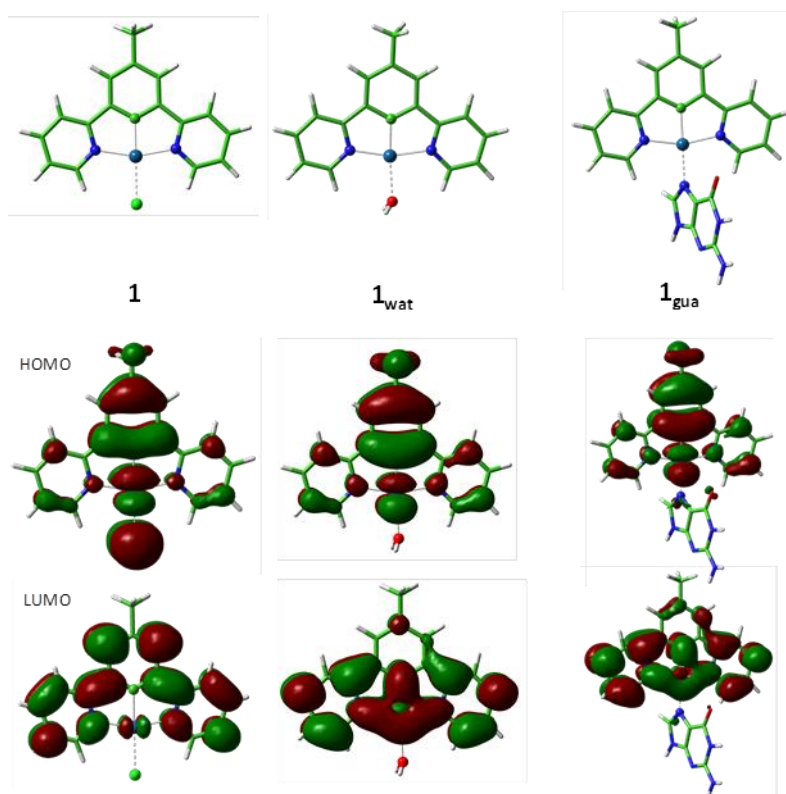


Figure 7.3 Contour plots for the frontier MOs of complex **1** and its aquated, **1_{wat}**, and guanine bound, **1_{gua}**, forms

The Simulated UV-vis spectrum of the complex shows that one electron absorption wavelengths are all not in the correct range of the PDT therapeutic window (600.0-800.0 nm). Blue-shift is caused by the displacement of the chlorido ligand by water and guanine.

Similarly, the photophysical properties of the aquated complex **1** that is intercalated at different sites of DNA (denoted as **1_{wat}(I)**, **1_{wat}(II)**, and **1_{wat}(III)** and obtained out of the molecular dynamics trajectory) is studied and compared to the separate aquated complex **1** (**1_{wat}**). A significant red-shifting of the bands as well as a strong effect on the absorption intensity is observed upon intercalation. The molecular orbitals analysis shows that the orbitals that are mainly involved in transitions are strongly affected by intercalation. Both HOMO and HOMO-1 orbitals have the character of the bases adjacent to the complex while the LUMO is localized on the complex.

The energy gaps between the ground-states and the first triplet excited states for all the possible photosensitizers examined for PDT application either the free or intercalated ones $\Delta E_{T_1, S_0}$ is larger than the 0.98 eV threshold corresponding to amount of energy that excited photosensitizer has to transfer to molecular oxygen (3O_2) for generating singlet oxygen species (1O_2) **Figure 7.4**. The efficiency of PDT application of complex **1** and its derivatives has been further verified calculating the values of the spin orbit coupling matrix element (\hat{H}_{SO} in cm^{-1}) which can reflect the intersystem crossing (ISC) probability. There are three excited triplet states (T_1 , T_2 and T_3) lying below the first excited singlet one for complex **1** and four for **1_{wat}** and **1_{gua}**. The excited triplet states lying below the first excited singlet state for all the examined species are shown in **Figure 7.4**. The magnitude of the computed spin orbit matrix elements associated with the first excited singlet state and the low lying triplet states indicate that the intersystem spin crossing processes are efficient for the intact complex and its water and guanine derivatives.

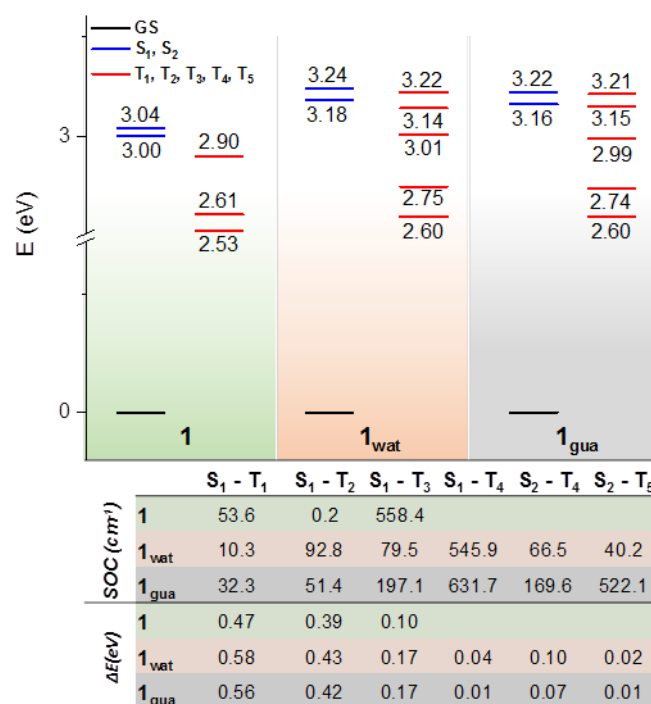


Figure 7.4 Lowest vertical singlet and triplet excitation energies (eV) of intact, aquated and guanine bound complex **1** and their spin orbit coupling (SOC) matrix element \hat{H}_{SO} , computed in water at TD-B3LYP-D3 level of theory.

References

- 1) J. G. Williams, *Chem. Soc. Rev.*, **2009**, 38, 1783–1801.
- 2) (a) R. W.-Y. Sun, A. L.-F. Chow, X.-H. Li, J. J. Yan, S. S.-Y. Chui, C.-M. Che, *Chem. Sci.*, **2011**, 2, 728-736; (b) R. Cortés, M. Crespo, L. Davin, R. Martín, J. Quirante, D. Ruiz, R. Messeguer, C. Calvis, L. Baldomà, J. Badia, M. Font-Bardía, T. Calvet, M. Cascante, *Eur. J. Med. Chem.*, **2012**, 54, 557–566; (c) S. D. Cummings, *Coord. Chem. Rev.*, **2009**, 253, 1495 – 1516; (d) R. W.-Y. Sun, H. L. Chan, D. L. Ma, M. Yang, C. M. Che, *ChemBioChem*, **2003**, 4, 62–68.
- 3) S. W. Botchway, S. W. et al. *P Natl Acad Sci*, **2008**, 105, 16071–16076.
- 4) J. G. Williams, A. Beeby, E. S. Davies, J. A. Weinstein, C. Wilson, *Inorg Chem*, **2003**, 42, 8609–8611.
- 5) R. E. Doherty, I. V. Sazanovich, L. K. McKenzie, A. S. Stasheuski, R. Coyle, E. Baggaley, S. Bottomley, J. A. Weinstein, H. E. Bryant, *Sci. Rep.*, **2016**, 6, 22668.

Paper VII

**Anticancer activity, DNA-binding and photodynamic properties of a
N[^]C[^]N-coordinated Pt(II) complex**

Eslam Dabbish, Stefano Scoditti, Nino Russo, Gloria Mazzone, Emilia Sicilia

Manuscript to be submitted (included)

Anticancer activity, DNA-binding and photodynamic properties of a N[^]C[^]N-coordinated Pt(II) complex

Eslam Dabbish, Stefano Scoditti, Nino Russo, Gloria Mazzone, Emilia Sicilia**

Department of Chemistry and Chemical Technologies, Università della Calabria, 87036, Arcavacata di Rende (CS), Italy

Abstract In the effort directed at the discovery of new targets as well as the improvement of therapeutic efficacy of metal containing anticancer compounds, transition metal complexes able to elicit cytotoxicity when irradiated by proper wavelength light and, then, candidates as potential photosensitizers (PS) for photodynamic therapy (PDT) treatment of cancers are actively being investigated. In the present work, the cytotoxicity in dark and the photophysical properties of the complex Pt(N[^]C[^]N)Cl, where the N[^]C[^]N ligand is 2,6-dipyrido-4-methyl-benzenechloride, are investigated in detail by means of DFT and its TD-DFT time-dependent extension together with Molecular Dynamics (MD) simulations. In dark cytotoxicity has been explored simulating the steps of the classical Pt(II) complexes mechanism of action. The suitability of the investigated complex to act as a photosensitizer has been verified calculating spectroscopic properties for both the unperturbed complex and its aquated and guanine bound forms. Furthermore, using MD simulation outcomes as starting point, DNA intercalated complex photophysical properties have been evaluated aiming at establishing how the intercalation affects sensitization activity.

1. Introduction

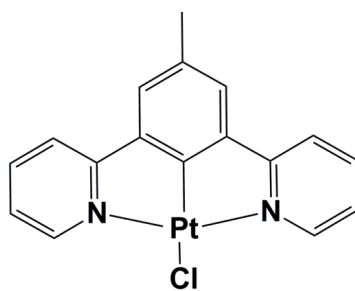
The fundamental discovery of the cytotoxic activity of cisplatin and the subsequent clinical approval of its carboplatin and oxaliplatin analogues^[1-3] has paved the way to worldwide efforts to develop new anti-cancer platinum(II) complexes. In cisplatin and its analogues, two coordination sites are occupied by labile ligands that can be displaced in the cytoplasm, allowing the formation of bifunctional intra- and inter-strand DNA crosslinks, mostly with guanine nucleobases.^[4-6] These crosslinks induce a conformational change to DNA which, through a series of events, ultimately leads to apoptosis.^[4] The clinical use of such complexes is well known to be seriously limited by severe shortcomings: side-effects (nephro-, neuro- and ototoxicity) and development of acquired or intrinsic resistance.^[7-10] These issues, have represented an impetus for the development of novel Pt-based anticancer chemotherapeutic drugs that, working with different modes, can have maximal curative potential and less systemic toxicity and internal resistance. Cyclometalated platinum(II) complexes containing tridentate π -conjugated organic ligands have been receiving an increase of interest as they display rich and diverse photoluminescent properties that are sensitively affected by local medium.^[11] Alongside photoluminescent properties, such complexes have attracted, in the last few years, a lot of interest for application as potent anticancer agents and several groups have studied their antitumor properties.^[12-14]

These complexes can mediate their cytotoxic activity via either classical covalent binding, both intra and inter strand crosslinkings, to the DNA base pairs or reversible interactions such as intercalation. Indeed, the planar motifs of these platinum(II) complexes can render them DNA metallointercalators inserting between adjacent DNA base pairs and establishing non-covalent ligand–ligand π – π stacking interactions. DNA interactions can also be electrostatic, groove-binding and hydrogen-bonding. As a function of their structural features, many of these Pt complexes show more than one mode of interaction.^[15-17]

The investigation of the luminescence properties of the Pt(II) complex of 1,3-di(2-pyridyl)benzene, acting as a terdentate N[^]C[^]N coordinating ligand cyclometalated at C2 of the benzene ring and substituted in 4 position by a methyl group has demonstrated that the complex, named from now on complex **1** (see Scheme 1), is able to intensely absorb light in the UV/visible region and possesses triplet excited states with significantly long, of the order of microseconds, lifetime and quantum yield.^[18,19] More recently, the investigation of the antiproliferative properties of complex **1** has demonstrated that it behaves as a promising photosensitizer under visible light capable to produce singlet oxygen in 70–80% yield in organic solvents.^[20] Moreover, due to the planarity of the ligand and polycyclic structure and aromaticity of the complex, binding to DNA by intercalation without direct metal coordination to DNA bases is very likely. The authors have suggested that intercalation

protects the complex from oxygen and, therefore, other modes of interaction with DNA can be envisaged that might allow oxygen access to complex **1** causing DNA breaking as a result of ROS/singlet oxygen generation upon light mediated activation of the DNA bound complex.

Inspired by such findings we have undertaken a detailed theoretical investigation, using several computational tools, of the cytotoxic activity of complex **1**, its modes of interaction with DNA, the effect on its spectroscopic properties of such interactions and the possibility that induced DNA damage is the consequence of its photosensitizer nature. DFT quantum mechanical calculations have been carried out to simulate the steps of the classical Pt(II) complexes mechanism of action for complexes **1**, that is aquation and interaction with guanine.



Complex **1**

Scheme 1. Structure of the investigated complex.

Molecular dynamics (MD) simulations and free binding energy calculations have been carried out as starting point, to obtain information on the key intermolecular interactions between the intercalating complexes and DNA. TDDFT has been employed in order to analyze the spectroscopic properties of the investigated complex in its unperturbed, aquated and guanine bound forms and of the DNA intercalated complex aiming at both checking the suitability of complex **1** to act as a photosensitizer in photodynamic therapy (PDT) and evaluating how the binding affects sensitization activity. (PDT) is a well-known alternative, less aggressive, treatment for fighting cancer based on the combined action of a drug, which is a photosensitizer, activating light of appropriate wavelength and molecular oxygen. Reactive oxygen species are produced, like excited singlet oxygen, as cytotoxic agents able to destroy diseased cells selectively. Absorption of light by the photosensitizer in its ground state (S_0) causes the excitation of one electron into a higher-energy orbital forming an excited singlet (S_1). A more stable excited triplet state (T_1) can be generated from such state by means of an ‘intersystem crossing’ (ISC). Due to the triplet state long lifetime, its energy can be transferred to molecular oxygen (O_2), which passes from its triplet ground state ($^3\Sigma_g$) to the singlet excited state ($^1\Delta_g$). The amplitude of the spin-orbit coupling singlet constants (SOC) determines the efficiency of the ISC,^[21] whereas molecular singlet oxygen can be produced only if the lowest triplet excited state (T_1) lies above the energy of the singlet by more than 0.98 eV, that is the

amount of energy needed to produce the singlet oxygen cytotoxic agent. In order to allow penetration into the tissue, the photosensitizer absorption wavelength should fall in the so called phototherapeutic window that is between 500 and 800 nm.

2. Computational Details

Gaussian 09 package has been used to perform quantum mechanical calculations.^[22] For the aquation, guanine and cysteine interaction studies of complex **1**, density functional theory has been employed using the hybrid Becke three parameter exchange functional^[23] and the Lee-Yang-Parr correlation functional,^[24] B3LYP. Grimme dispersion corrections for nonbonding interactions have been included using atom pair-wise additive scheme,^[25] DFT-D3 method. The def2TZVP effective core potential^[26] and corresponding split valence basis set have been used to describe platinum atom. 6-311+G** basis set has been employed to describe the rest of the atoms. Frequency calculations have been performed at the same level of theory for all located stationary points to confirm their nature of minima and transition states and for zero-point energy corrections calculations. More details are included in the Supporting Information (SI)

In order to study the drug intercalation into DNA, a B-DNA dodecamer, with Protein Data Bank code 1BNA,^[27] has been used. The aquated form of complex **1** has been manually introduced into the different potential intercalation sites. For the molecular dynamics study of the mentioned system, topology and coordinate files have been generated by means of tleap in Amber program^[28] using the standard DNA.bsc^[29] and gaff force fields^[30,31] together with the newly generated parameters for the aquated complex **1** (refer to SI). A TIP3P solvation model^[32-34] has been used to construct an octahedral box of explicit waters around the DNA complex with a 14 Å buffer distance around the DNA in each direction. Sodium ions have been added to neutralize the system. Minimization and heating have been conducted at constant volume periodic boundaries (details in the SI). Equilibration followed by production of molecular dynamics for 20 ns at 300 K have been ran under similar conditions with a 0.002 ps interval with no restraints on DNA. The SHAKE algorithm to constrain bonds involving hydrogen and the cutoff distance of 15.0 angstroms were all maintained. A constant pressure periodic boundary with an average pressure of 1 atm and an isotropic position scaling with a relaxation time of 2 ps were used. For evaluating the relative binding free energy between the aquated complex **1** at different intercalation sites and DNA, MM-GBSA method,^[35] as implemented by MMPBSA.py script in Amber 16 package, has been used evaluating the whole production trajectory of each intercalation position over 20ns. VMD program has been used to generate the figures out of the dynamics trajectory.^[36] More details are included in SI.

In order to accurately describe the photophysical properties, a preliminary benchmark study has been carried out on complex **1**. The optimized structure at B3LYP level has been used to compute the excitation energies employing several functionals: B3LYP, Cam-B3LYP,^[37] M06,^[38] PBE0,^[39] PW91^[40] and wB97XD,^[41] including the Grimme dispersion corrections (DFT-D3). Their performance has been evaluated comparing both calculated geometric parameters and T1 and S1 absorption peak wavelengths in acetonitrile. Thus a dielectric constant of 35.688 has been used in conjunction with 6-311+G(d,p) basis set for all the atoms except platinum, for which the def2QZVP effective core potential coupled with its valence basis set has been retained.

Out of the molecular dynamics trajectory of the intercalation of the aquated form of complex **1** at different DNA sites, the conformations including the drug and the four surrounding nucleotides that have shown the best Van der Waals interactions between the drug and the surrounding nucleotides are selected for further TDDFT analysis. The intercalated complex from the extracted conformation are optimized first while the DNA pair bases coordinates have been frozen in order to avoid the unrealistic distortion of the DNA portion included in the QM calculations because of the absence of the rest of the dodecamer used for the MD intercalation study. The optimization and, then, the absorption spectrum in water have been obtained maintaining B3LYP functional, the 6-311+G(d,p) basis set for all atoms (C, H, N, O) of the complex with the exception of platinum, again described by the def2QZVP pseudopotential, while all the atoms of the DNA portion were treated with the standard 6-31G(d) basis set. To ascertain the possibility of an intersystem spin crossing from a bright singlet state to a triplet one, spin-orbit matrix elements have been computed within the quadratic-response TD-DFT approach, as implemented in the Dalton code,^[42] (more details in SI). For this purpose, TD-B3LYP/cc-pVTZ in conjunction with the def2QZVP pseudopotential for Pt atom have been used in the framework of the spin-orbit coupling operators for effective core potentials with the effective nuclear charge.^[43]

3. Results and Discussion

3.1 Quantum mechanical simulation of in dark aquation, guanine binding and cysteine interaction.

Aquation, binding to guanine, as a model of a purine base site of DNA, and interaction with cysteine, as sulfur containing compound model, have been explored using quantum mechanical DFT calculations for complex **1**. Aquation reaction proceeds, as usual, by a second-order nucleophilic substitution (SN2) that leads to the exchange of the chlorido anion with a water molecule. The calculated energy profile in water is reported in Figure 1 along with the optimized

structures of the located stationary points. The transition state for the associative displacement of the chlorido ligand lies $15.1 \text{ kcal mol}^{-1}$ above the zero reference energy of the first formed adduct. Formation of aquated product, $\mathbf{1}_{\text{wat}}$, results to be endergonic by $5.7 \text{ kcal mol}^{-1}$.

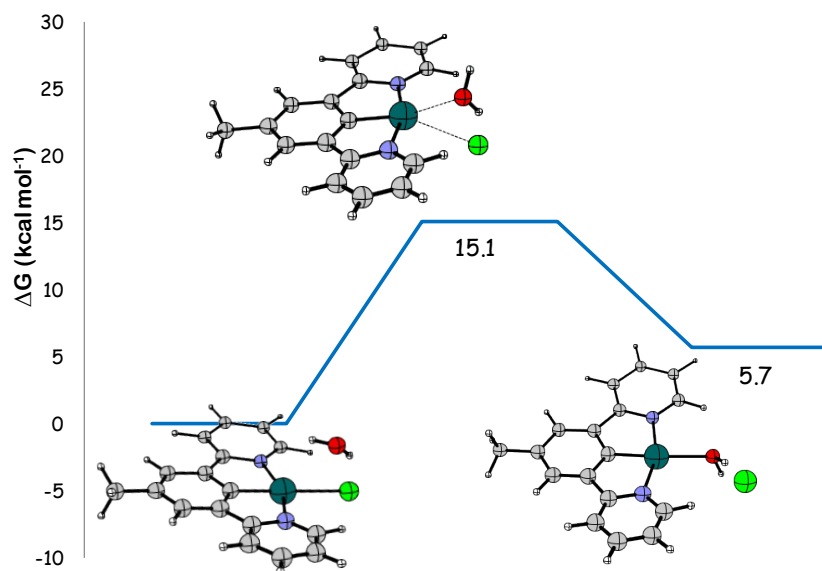


Figure 1. Free energy profiles in water describing the aquation reaction of complexes **1**. Geometrical structures of the stationary points intercepted along the path are also reported. Relative energies are in kcal mol^{-1} and calculated with respect the zero reference energy of the initial adduct.

Therefore, the calculated barrier height, compared with the range of the values^[44–47] previously calculated and experimentally estimated for cisplatin, confirms that the carbon atom in *trans* position to the chlorido leaving ligand is efficacious in favoring the dissociation^[48] and the activation by aquation occurs very quickly.

The aquation step is, for classical Pt(II) complexes, the prelude to DNA binding by coordination of the Pt atom to, mainly, the N7 positions of guanine bases. Then, the interaction of aquated complex $\mathbf{1}_{\text{wat}}$ with a guanine molecule as a model to simulate DNA binding has been explored and the calculated free energy profile is shown in Figure 2. Stationary point structures located along the pathway for have been also depicted in the same figure.

The very favorable nucleophilic attack occurs, in analogy with lots of examined situations, along a $\text{S}_{\text{N}}2$ mechanism pathway with the transition state assuming a pseudo bipyramidal trigonal geometry. The displacement of the water molecule is facilitated by the formation of a hydrogen bond between one of the water hydrogen atoms and the oxygen of the guanine base. Calculated barrier is $4.9 \text{ kcal mol}^{-1}$ and the displacement reaction is exergonic by $8.6 \text{ kcal mol}^{-1}$. The very

favorable nucleophilic attack occurs, in analogy with lots of examined situations, along a SN2 mechanism pathway with the transition state assuming a pseudo bipyramidal trigonal geometry.

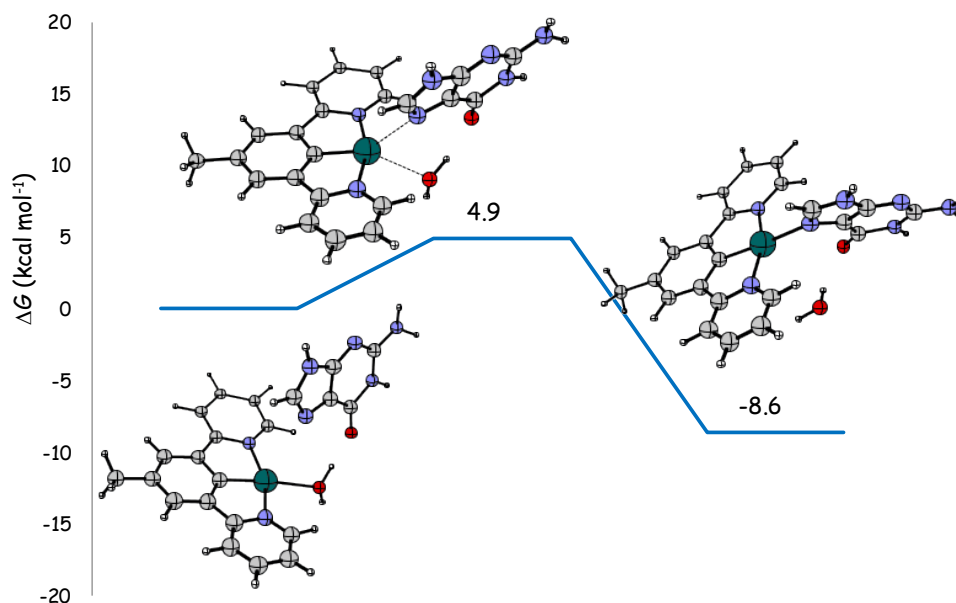


Figure 2. Free energy profile in water describing the attack of the aquated complex **1** on the N7 nitrogen of the guanine base together with geometrical structures of the intercepted stationary points. Relative energies are in kcal mol⁻¹ and calculated with respect the zero reference energy of the initial adduct.

The displacement of the water molecule is facilitated by the formation of a hydrogen bond between one of the water hydrogen atoms and the oxygen of the guanine base. Calculated barrier is 4.9 kcal mol⁻¹ and the displacement reaction is exergonic by 8.6 kcal mol⁻¹.

The possibility that the efficacy of the complex is decreased by the interaction with low-molecular-weight sulfur containing molecules, very abundant in human cells and having a high binding affinity for platinum, has been also checked. Using cysteine as a model compound, the calculation of the pathway that can lead to the inactivation of the complex by forming a stable adduct, thus preventing the drugs from reaching and binding to DNA, has been carried out. The corresponding free energy profile is shown in Figure 3 together with a sketch of the intercepted stationary point structures. As it clearly appears from Figure 3, some additional water molecules have been included to both save the zwitterionic nature of the cysteine and to avoid fictitious inappropriate hydrogen transfers. After the formation of the first adduct, the transition state for the SN2 substitution rearrangement that allows the displacement of the chlorido ligand by cysteine lies 16.1 kcal mol⁻¹ above the zero reference energy of the adduct. Formation of the water displacement product is endothermic by 6.7 kcal mol⁻¹. These values compared with those calculated for cisplatin, that is

16.7 kcal mol⁻¹ for the barrier and -4.9 kcal mol⁻¹ for the reaction energy, indicate that from a kinetic point of view complex **1** deactivation is viable as for cisplatin, but less favored from a thermodynamic point of view with respect to cisplatin.

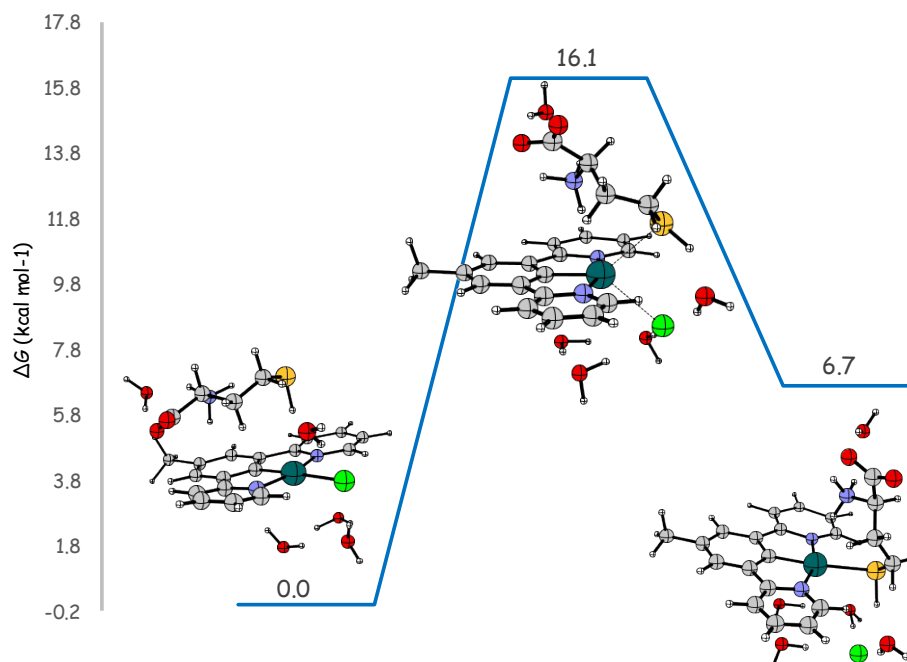


Figure 3. Free energy profile in water describing the chloride displacement by cysteine together with geometrical structures of the intercepted stationary points. Relative energies are in kcal mol⁻¹ and calculated with respect the zero reference energy of the initial adduct.

Therefore, the exploration of the key steps of the mechanism of action of traditional Pt(II) drugs shows that complex **1** can, in principle, be easily activated by aquation inside the cell and equally easily can bind nuclear DNA, whereas deactivating interactions with sulfur containing biomolecules is less thermodynamically favored. In the next paragraphs the outcomes of the exploration of the possible alternative modes of action of complex **1**, that should explain its superior cytotoxic activity with respect to cisplatin, will be illustrated.

3.2 MD simulation of complex **1** intercalation into DNA

Molecules can be non-covalently attached to DNA in three different binding modes,^[49,50] that is: electrostatic binding, groove binding, and intercalative binding. Intercalation is important for planar fused-ring aromatic molecules because DNA nucleic bases are arranged in an almost coplanar configuration, which allows strong π -stacking interactions with the drug. Intercalation stabilized by non-covalent interactions can induce conformational and functional changes,^[49,50] ultimately,

leading to inhibition of transcription and replication and DNA repair processes. Moreover, the stabilization energy of cationic intercalators is reported to be considerably larger than that of the uncharged species.^[51] Owing to the planar coordination, polycyclic structure and aromaticity of the compound, DNA intercalation is very likely. Therefore, molecular dynamics simulations have been used to study the intercalation of the aquated cationic complex **1** into the adopted dodecamer DNA model considering different sites in the major groove of the helix, with the NCN ligand located between two base pairs. The chosen intercalation sites, in which the drug has been manually placed, have been used in the study of photophysical properties. Several intercalation sites have been considered as in our previous study^[52] and the selected ones are shown in Figure 4 and are named **1_{wat(I)}**, **1_{wat(II)}**, **1_{wat(III)}**. In **1_{wat(I)}** the drug is stacked within the thymine-adenine (TA) and cytosine-guanine (CG) base pairs. **1_{wat(II)}** corresponds to the drug stacked within adenine-thymine (AT) and thymine-adenine (TA) base pairs and **1_{wat(III)}** to cytosine-guanine (CG) and guanine-cytosine (GC) base pairs stacking. Additionally, for such sites different arrangements of the aquated complex with respect to the surrounding nucleotides have been taken into consideration.

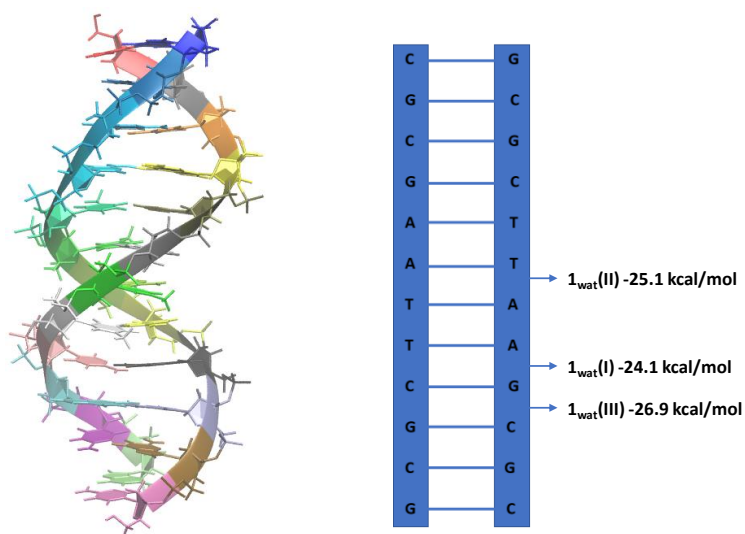


Figure 4. Selected intercalation positions in bare B-DNA dodecamer.

Binding free energy of the aquated complex **1_{wat}** at the different proposed intercalation sites as shown in Figure 5, has been calculated by means of the MM-GBSA approach.

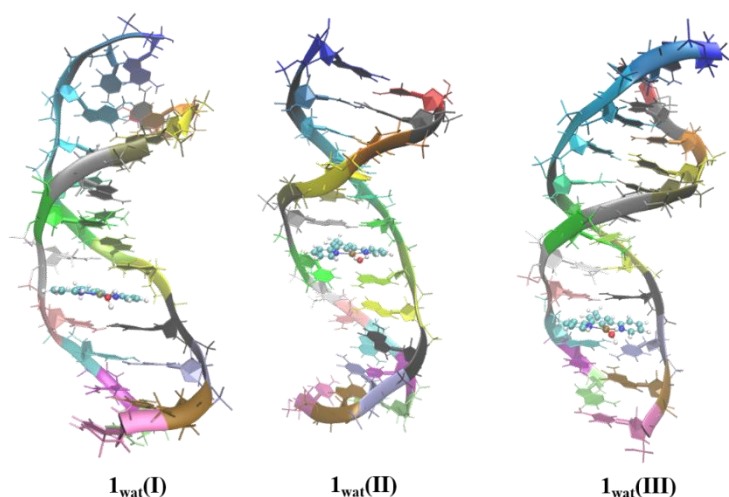


Figure 5. B-DNA dodecamer with complex **1** intercalated at the three most favored positions after 20 ns of dynamics simulation.

The different contributions to the binding energy are reported in Table S1 of the Supporting Information. Position labeled $1_{\text{wat}}(\text{III})$, having a binding energy of $-26.9 \text{ kcal mol}^{-1}$, is found to be the most preferred intercalation site. However, very close values of -24.1 and $-25.1 \text{ kcal mol}^{-1}$ for the $1_{\text{wat}}(\text{II})$ and $1_{\text{wat}}(\text{I})$ positions, respectively have been calculated. The intercalation of 1_{wat} induces a conformational distortion in the modeled DNA. The DNA length is calculated as the end-to-end distance of the helix, measured from the two terminal base pairs center of mass. The length change with respect to the drug-free DNA as a reference during the dynamics is also reported in Figure S1 of the SI. The observed oscillations in the DNA length are due to both the increased spacing between the base pairs at the intercalation site and the established interactions.

3.3 Photochemical properties

With the aim to select the most appropriate protocol, a preliminary investigation has been carried out of the performance of a series of exchange-correlation functionals in reproducing the most relevant spectroscopic features of complex **1**, whose structure and adsorption spectrum have been both characterized and computationally explored.^[19,20,52] The optimized structure at B3LYP level evidences a good agreement with the crystallographic structure (see Figure S2).ref Calculated values of the vertical excitation energies, obtained using several exchange–correlation functionals, for low-lying singlet (S_1) and triplet (T_1) states of complex **1**, together with corresponding oscillatory strengths and most significant molecular orbital (MO) contributions are collected in Table S2 of the SI and compared with the available experimental counterparts.^[53] For the comparison with experimental data, the UV-vis spectrum detected in acetonitrile solvent^[54] has

been used, being that solvent, among those reported in the literature, closer in behavior to water. From such comparison it appears that the B3LYP functional^[23] corrected for the Grimme's D3 dispersion correction^[25] allows the good reproduction of both geometrical and spectroscopic parameters and has been chosen therefore for all the calculations. Changes in spectrum induced by the displacement of the chlorido ligand by water and guanine together with intercalation have been explored. In particular, for the aquated DNA intercalated complex one frame for each more favored intercalative position coming from MD simulations has been examined.

3.3.1 Calculated electronic spectra for intact, aquated and guanine bound complex 1

Adopting the selected B3LYP-D3 approach, photophysical properties for the intact complex **1** in water solvent have been computed. Vertical excitation energies, maximum adsorption wavelength, oscillator strength and MO contributions for singlet excitations are reported in Table S3 together with those for the aquated and guanine bound complex. Lowest lying triplet excitation energies together with MO contributions are collected in Table S4. Calculated spectra and the corresponding frontier molecular orbitals are illustrated in Figure 6 and 7, respectively.

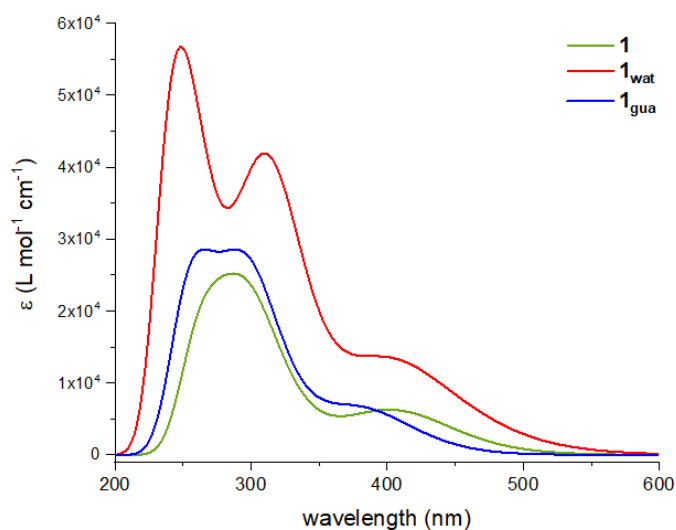


Figure 6. Computed absorption spectra of the intact complex **1** (green) and its aquated (red) and guanine bound (blue) forms.

The experimentally detected absorption spectrum in solution displays a very intense band at wavelengths below 300 nm. The absorption envelope in the range between 350 nm and 450 nm corresponds to absorptions towards singlet excited states with MLCT character. The lowest energy weak peaks, in the region 478-495 nm, are assigned to $S_0 \rightarrow T_1$ absorption by their mirror-symmetry relation with the emission peak. The computed spectrum reported in Figure 6 and Table S3 of the SI corresponds to such description.

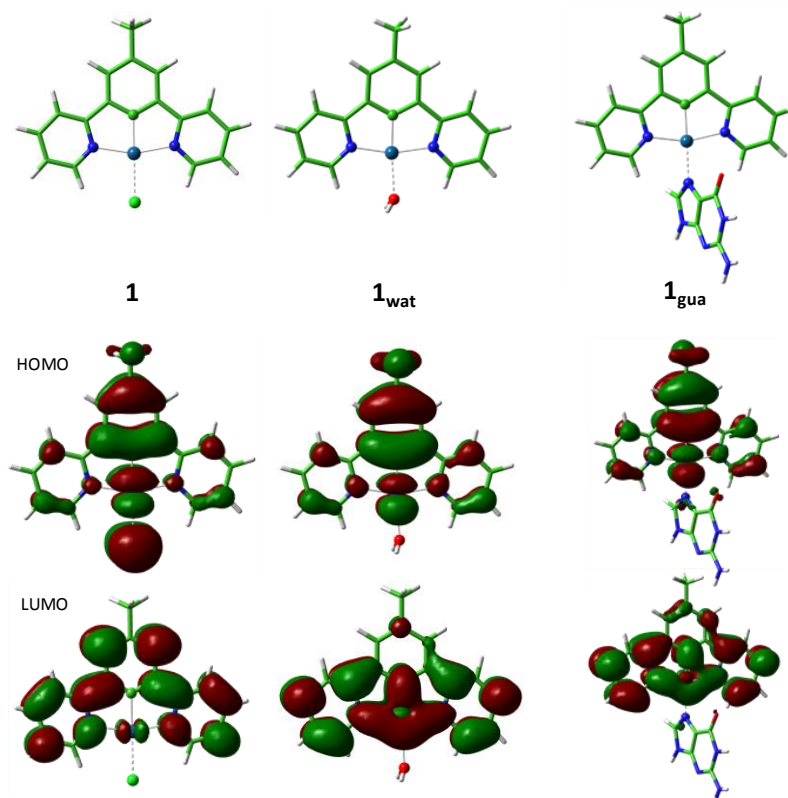


Figure 7. Contour plots for the frontier MOs of complex **1** and its aquated, **1_{wat}**, and guanine bound, **1_{gua}**, forms.

The lowest energy spin-allowed transitions in absorption, around 350-450 nm, can be attributed to the HOMO→LUMO and HOMO→LUMO+ 1 transitions. Similarly, the lowest-energy triplet state is seen to be comprised predominantly of HOMO→LUMO character (Table S3), and the calculated energy is remarkably close to that of the 0–0 band found in the experimental spectrum. In order to simplify the description of the nature of the MOs participating in the calculated transitions as occurring between an excited particle and an empty hole, natural transition orbitals, NTOs, are also provided in Figure S3 of the SI for both singlet and triplet lowest-energy transitions. Nevertheless, on the basis the mixed nature of the reported NTOs it can be concluded that for both singlet and triplet, the charge transfer that accompanies the formation of the excited state is mainly from Pt/, Cl and NCN ligand, especially phenyl, towards the tridentate ligand, especially pyridine rings. Transitions, then, have MLCT (metal to-ligand charge transfer) character mixed with ILCT (intra-ligand charge transfer) and LLCT (ligand-ligand charge transfer) character.

Analogous calculations have been performed for complex **1** both in its aquated form and bound to guanine by displacement of water. The corresponding calculated spectra are reported and compared with that of the intact complex in Figure 6. From such figure it is readily apparent that, when the aquated complex is examined, both lowest and highest-energy parts of the spectrum are blueshifted.

In addition, new peaks in the region between 322 and 399 nm generate a new band. The NTO contour plots show that the water ligand does not contribute to the orbitals involved in transitions. The charge transfer occurs mainly from the metal and phenyl towards the pyridine components of the terdentate ligand. A less pronounced redshifted spectrum has been calculated for the complex in which a new bond between the platinum center and the N7 of guanine is formed, while in that case the band below 300 nm is splitted. From the NTO analysis of the charge distributions responsible for the observed transitions it appears that the guanine ligand is not involved in transitions that, once again, are mainly due to a charge redistribution from the metal and the phenyl ring towards pyridine regions of the N⁺C⁻N ligand.

3.3.2 Calculated electronic spectrum of intercalated complex 1

Changes induced in the spectrum of the free complex upon DNA intercalation have been examined for each of the three most favorable intercalation positions. Calculated spectra are shown in Figure 8 and surfaces of MOs involved in transitions are depicted in Figure 9. The most relevant features of such spectra (Table S5) can be found in the SI together with the lowest lying triplet excitation energies (Table S6).

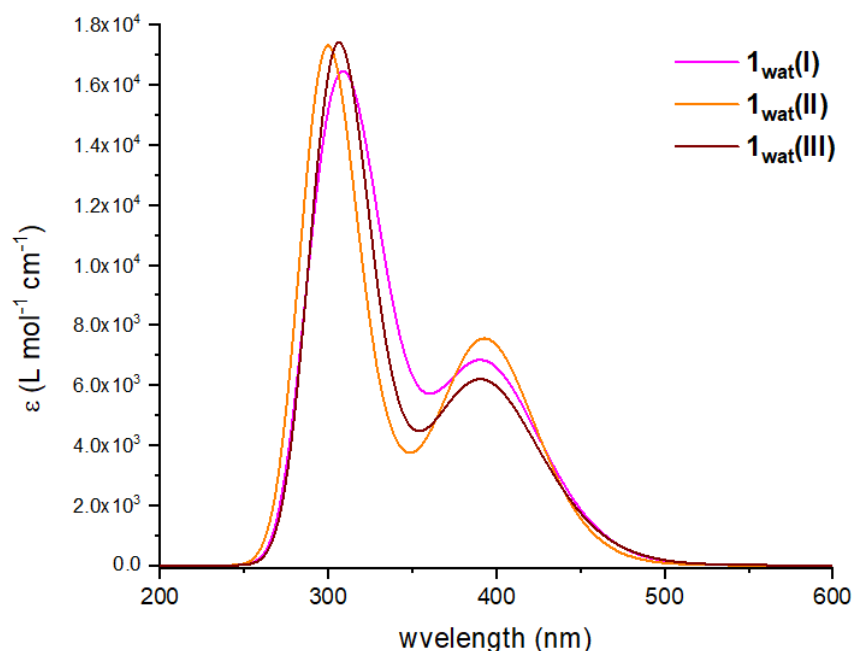


Figure 8. Computed absorption spectra of the intercalated complex **1** in the most favorable arrangements **1_{wat}(I)** (purple), **1_{wat}(II)** (orange) and **1_{wat}(III)** (brown).

According to the literature,^[55] DNA intercalative interaction should cause red shifting and significant hypochromism of the absorption bands. Compared to the spectrum in water (Figure 6)

the general shape of the spectrum is not totally altered, even if splitting of the in the region between 322 and 399 is not conserved. A significant shifting of the bands as well as a strong effect on the absorption intensity is observed upon intercalation. The molecular orbitals plot shows that the orbitals that are mainly involved in transitions are strongly affected by intercalation. Both HOMO and HOMO-1 orbitals have the character of the bases adjacent to the complex.

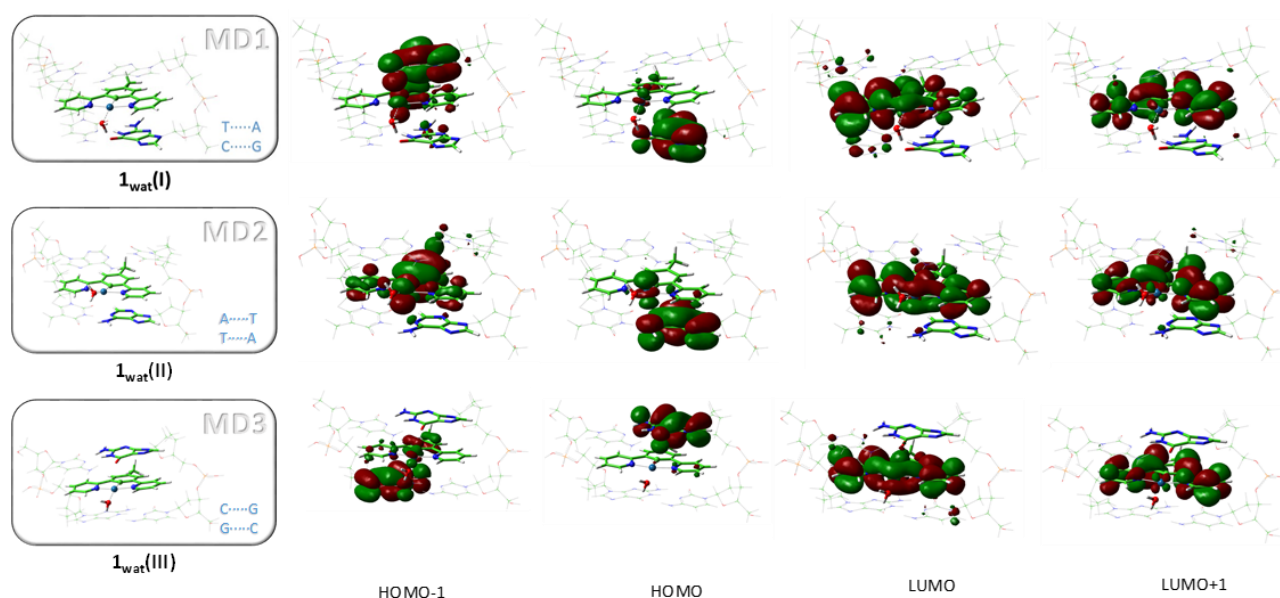


Figure 9. Contour plots of the two lowest unoccupied and the two highest occupied molecular orbitals for the intercalated complex adducts $\mathbf{1}_{\text{wat}}(\text{I})$, $\mathbf{1}_{\text{wat}}(\text{II})$ and $\mathbf{1}_{\text{wat}}(\text{III})$ extracted from MD simulations.

3.3.3 Excited states properties

The properties of the investigated complex **1** and its free and intercalated substituted forms have been further investigated for their application as photosensitizers. As it has been underscored in the introduction, the efficiency of photosensitizers in PDT depends on the triplet states energies as the energy gap between the first triplet energy and the ground state energy $\Delta E_{T_1-S_0}$ of the complexes should be not smaller than the threshold value 0.98 eV corresponding to amount of energy that excited photosensitizer has to transfer to molecular oxygen ($^3\text{O}_2$) for generating singlet oxygen species ($^1\text{O}_2$). Energy gaps between the ground-states and the first triplet excited states for all the possible photosensitizers examined here are reported in Figure 10 and from such values it appears that each $\Delta E_{T_1-S_0}$ is larger than the 0.98 eV threshold. This requirement is equally fulfilled by the

DNA intercalated complex as it appears from the values of energy of triplets reported in Table S6 of the SI.

The efficiency of PDT application of complex **1** and its derivatives has been further verified calculating the values of the spin orbit coupling matrix element (\hat{H}_{SO} in cm^{-1}) which can reflect the intersystem crossing (ISC) probability. There are three excited triplet states (T_1 , T_2 and T_3) lying below the first excited singlet one for complex **1** and four for **1_{wat}** and **1_{gua}**. The excited triplet states lying below the first excited singlet state for all the examined species are shown in Figure 9. Hence, the \hat{H}_{SO} between the initial state $\Psi(S_1)$ and final $\Psi(T_n, n = 1, 2, 3$ and $4)$ wave functions have been computed and presented in Figure 10. For complex **1** the largest $|\langle \Psi_{S_1} | \hat{H} | \Psi_{T_n} \rangle|$ spin orbit coupling matrix element has been calculated for the T_3 triplet state, whereas for **1_{wat}** and **1_{gua}** the largest value is calculated for the T_4 triplet state.

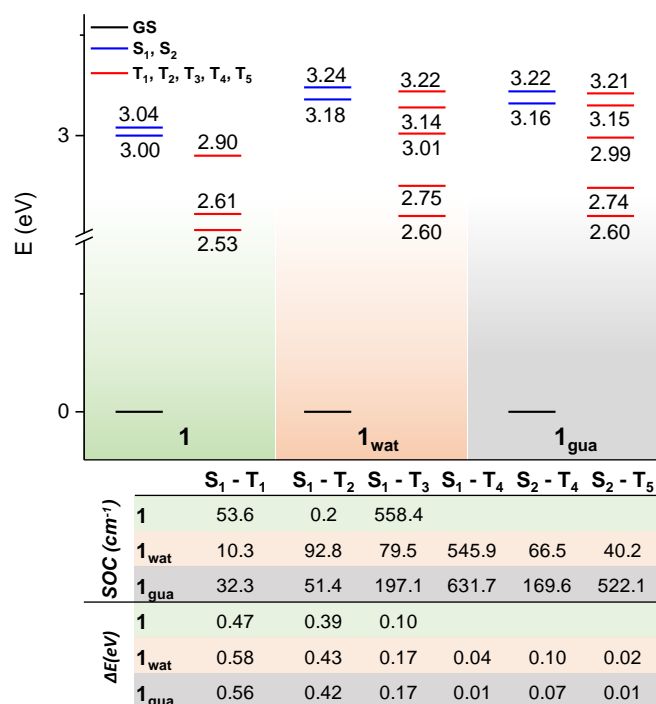


Figure 10. Lowest vertical singlet and triplet excitation energies (eV) of intact, aquated and guanine bound complex **1**, computed in water at TD-B3LYP-D3 level of theory.

Conclusions

In the present work, the cytotoxic properties of the Pt(N[^]C[^]N)Cl complex, with tridentate N[^]C[^]N pincer ligand 2,6-dipyrido-4-methyl-benzenechloride, both in dark and under proper wavelength light irradiation have been explored. On the basis of recent experimental findings, a detailed theoretical investigation has been carried out, using quantum mechanical DFT and TD-DFT

calculations accompanied by MD simulations, of the cytotoxic activity of complex **1**, its modes of interaction with DNA, the effect on its spectroscopic properties of such interactions and the possibility that induced DNA damage is the consequence of its photosensitizer nature. The steps of the mechanism of action of classical Pt(II) anticancer agents, that is aquation, guanine interaction and eventual deactivation due to sulfur containing molecules, have been tested. Both aquation and guanine binding are accessible when compared with analogous steps for cisplatin. Deactivation is viable even if less thermodynamically accessible with respect to cisplatin. Simulated UV-vis spectrum of the complex shows that one electron absorption wavelengths are all not in the correct range of the PDT therapeutic window (600.0-800.0 nm). Blue-shift is caused by the displacement of the chlorido ligand by water and guanine, whereas absorption wavelengths are red-shifted when the complex is intercalated. For the intact complex and all of its derived forms, the energy gaps between ground states and triplet excited states are larger than 0.98 eV, indicating that they can generate singlet oxygen for PDT via type II mechanism. Moreover, the magnitude of the computed spin orbit matrix elements associated with the first excited singlet state and the low lying triplet states indicate that the intersystem spin crossing processes are efficient for the intact complex and its water and guanine derivatives.

Acknowledgments

This research was supported by the project POR Calabria – FSE/FESR 2014-2020. University of Calabria and Calabria Region are acknowledged for financial support.

- [1] L. Kelland, *Nat Rev Cancer* **2007**, *7*, 573.
- [2] B. Rosenberg, L. Camp, T. Krigas, *Nature* **1965**, *205*, 698.
- [3] B. Rosenberg, L. Camp, J. Trosko, V. Mansour, *Nature* **1969**, *222*, 385.
- [4] Z. H. Siddik, *Oncogene* **2003**, *22*, 7265.
- [5] N. Pabla, Z. Dong, *Kidney International* **2008**, *73*, 994.
- [6] R. W. Gregg, J. M. Molepo, V. J. Monpetit, N. Z. Mikael, D. Redmond, M. Gadia, D. J. Stewart, *JCO* **1992**, *10*, 795.
- [7] C. F. Harrington, R. C Le Pla, G. D. Jones, A. L. Thomas, P. B. Farmer, *Chem. Res. Toxicol* **2010**, *23*, 1313.
- [8] S. Dasari, P. Bernard Tchounwou, *European Journal of Pharmacology* **2014**, *740*, 364.
- [9] B. Behmand, P. Cloutier, S. Girouard, J. R. Wagner, L. Sanche, D. J. Hunting, *J. Phys. Chem. B* **2013**, *117*, 15994.
- [10] E. R. Jamieson, S. J. Lippard, *Chem. Rev.* **1999**, *99*, 2467.
- [11] J. A. G. Williams, *Chem. Soc. Rev.* **2009**, *38*, 1783.
- [12] R. Wai-Yin Sun, A. Lok-Fung Chow, X.-H. Li, J. J. Yan, S. Sin-Yin Chui, C.-M. Che, *Chem. Sci.* **2011**, *2*, 728.
- [13] R. Cortés, M. Crespo, L. Davin, R. Martín, J. Quirante, D. Ruiz, R. Messeguer, C. Calvis, L. Baldomá, J. Badia, M. Font-Bardia, T. Calvet, M. Cascante, *European Journal of Medicinal Chemistry* **2012**, *54*, 557.

- [14] S. D. Cummings, *Coordination Chemistry Reviews* **2009**, 253, 1495.
- [15] S. Roy, K. D. Hagen, P. U. Maheswari, M. Lutz, A. L. Spek, J. Reedijk, G. P. van Wezel, *ChemMedChem* **2008**, 3, 1427.
- [16] A. D. Richards, A. Rodger, *Chem. Soc. Rev.* **2007**, 36, 471.
- [17] A. P. Rebolledo, M. Vieites, D. Gambino, O. E. Piro, E. E. Castellano, C. L. Zani, E. M. Souza-Fagundes, L. R. Teixeira, A. A. Batista, H. Beraldo, *Journal of Inorganic Biochemistry* **2005**, 9.
- [18] J. A. G. Williams, A. Beeby, E. S. Davies, J. A. Weinstein, C. Wilson, *Inorg. Chem.* **2003**, 42, 8609.
- [19] S. W. Botchway, M. Charnley, J. W. Haycock, A. W. Parker, D. L. Rochester, J. A. Weinstein, J. A. G. Williams, *Proceedings of the National Academy of Sciences* **2008**, 105, 16071.
- [20] R. E. Doherty, I. V. Sazanovich, L. K. McKenzie, A. S. Stasheuski, R. Coyle, E. Baggaley, S. Bottomley, J. A. Weinstein, H. E. Bryant, *Sci Rep* **2016**, 6, 22668.
- [21] J. R. Perumareddi, A. W. Adamson, *The Journal of Physical Chemistry*, **1968**, 72, 414.
- [22] Gaussian 09, Revision D.01, M. J. Frisch, G. W. Trucks, H. B. Schlegel, G. E. Scuseria, M. A. Robb, J. R. Cheeseman, G. Scalmani, V. Barone, B. Mennucci, G. A. Petersson, H. Nakatsuji, M. Caricato, X. Li, H. P. Hratchian, A. F. Izmaylov, J. Bloino, G. Zheng, J. L. Sonnenberg, M. Hada, M. Ehara, K. Toyota, R. Fukuda, J. Hasegawa, M. Ishida, T. Nakajima, Y. Honda, O. Kitao, H. Nakai, T. Vreven, J. A. Montgomery-Jr., J. E. Peralta, F. Ogliaro, M. Bearpark, J. J. Heyd, E. Brothers, K. N. Kudin, V. N. Staroverov, T. Keith, R. Kobayashi, J. Normand, K. Raghavachari, A. Rendell, J. C. Burant, S. S. Iyengar, J. Tomasi, M. Cossi, N. Rega, J. M. Millam, M. Klene, J. E. Knox, J. B. Cross, V. Bakken, C. Adamo, J. Jaramillo, R. Gomperts, R. E. Stratmann, O. Yazyev, A. J. Austin, R. Cammi, C. Pomelli, J. W. Ochterski, R. L. Martin, K. Morokuma, V. G. Zakrzewski, G. A. Voth, P. Salvador, J. J. Dannenberg, S. Dapprich, A. D. Daniels, O. Farkas, J. B. Foresman, J. V. Ortiz, J. Cioslowski, D. J. Fox, Gaussian, Inc., Wallingford CT, **2010**.
- [23] A. D. Becke, *The Journal of Chemical Physics* **1993**, 98, 1372.
- [24] C. Lee, W. Yang, R. G. Parr, *Phys. Rev. B* **1988**, 37, 785.
- [25] S. Grimme, J. Antony, S. Ehrlich, H. Krieg, *J. Chem. Phys.* **2010**, 132, 154104.
- [26] F. Weigend, R. Ahlrichs, *Phys. Chem. Chem. Phys.* **2005**, 7, 3297.
- [27] H. R. Drew, R. M. Wing, T. Takano, C. Broka, S. Tanaka, K. Itakura, R. E. Dickerson, *Proc. Natl. Acad. Sci.*, **1981**, 78, 2179.
- [28] D. A. Case, R. M. Betz, D. S. Cerutti, T. E. Cheatham, T. A. Darden, R. E. Duke, T. J. Giese, H. Gohlke, A. W. Goetz, N. Homeyer, S. Izadi, P. Janowski, J. Kaus, A. Kovalenko, T. S. Lee, S. LeGrand, P. Li, C. Lin, T. Luchko, R. Luo, B. Madej, D. Mermelstein, K. M. Merz, G. Monard, H. Nguyen, H. T. Nguyen, I. Omelyan, A. Onufriev, D. R. Roe, A. Roitberg, C. Sagui, C. L. Simmerling, W. M. Botello-Smith, J. Swails, R. C. Walker, J. Wang, R. M. Wolf, X. Wu, L. Xiao, P. A. Kollman, **2016**, AMBER 2016, University of California, San Francisco., .
- [29] I. Ivani, P. D. Dans, A. Noy, A. Pérez, I. Faustino, A. Hospital, J. Walther, P. Andrio, R. Goñi, A. Balaceanu, G. Portella, F. Battistini, J. L. Gelpí, C. González, M. Vendruscolo, C. A. Loughton, S. A. Harris, D. A. Case, M. Orozco, *Nat Methods* **2016**, 13, 55.
- [30] J. Wang, W. Wang, P. A. Kollman, D. A. Case, *Journal of Molecular Graphics and Modelling* **2006**, 25, 247.
- [31] J. Wang, R. M. Wolf, J. W. Caldwell, P. A. Kollman, D. A. Case, *J. Comput. Chem.* **2004**, 25, 1157.
- [32] M. W. Mahoney, W. L. Jorgensen, *The Journal of Chemical Physics* **2000**, 112, 8910.
- [33] M. W. Mahoney, W. L. Jorgensen, *J. Chem. Phys.* **2001**, 114, 363.
- [34] W. L. Jorgensen, J. Chandrasekhar, J. D. Madura, R. W. Impey, M. L. Klein, *The Journal of Chemical Physics* **1983**, 79, 926.

- [35] B. R. Miller, T. D. McGee, J. M. Swails, N. Homeyer, H. Gohlke, A. E. Roitberg, *J. Chem. Theory Comput.* **2012**, *8*, 3314.
- [36] W. Humphrey, A. Dalke, K. Schulten, *Journal of Molecular Graphics* **1996**, *14*, 33.
- [37] T. Yanai, D. P. Tew, N. C. Handy, *Chemical Physics Letters* **2004**, *393*, 51.
- [38] Y. Zhao, D. G. Truhlar, *Theor. Chem. Acc.* **2008**, *120*, 215.
- [39] C. Adamo, V. Barone, *J. Chem. Phys.* **1999**, *110*, 14.
- [40] K. Burke, J. P. Perdew, and Y. Wang, in *Electronic Density Functional Theory: Recent Progress and New Directions*, Ed. J. F. Dobson, G. Vignale, and M. P. Das (Plenum, 1998).
- [41] J.-D. Chai, M. Head-Gordon, *Phys. Chem. Chem. Phys.* **2008**, *10*, 6615.
- [42] K. Aidas, C. Angeli, K. L. Bak, V. Bakken, R. Bast, L. Boman, O. Christiansen, R. Cimiraglia, S. Coriani, P. Dahle, E. K. Dalskov, U. Ekström, T. Enevoldsen, J. J. Eriksen, P. Ettenhuber, B. Fernández, L. Ferrighi, H. Fliegl, L. Frediani, K. Hald, A. Halkier, C. Hättig, H. Heiberg, T. Helgaker, A. C. Hennum, H. Hettema, E. Hjertenaes, S. Høst, I.-M. Høyvik, M. F. Iozzi, B. Jansík, H. J. Aa. Jensen, D. Jonsson, P. Jørgensen, J. Kauczor, S. Kirpekar, T. Kjaergaard, W. Klopper, S. Knecht, R. Kobayashi, H. Koch, J. Kongsted, A. Krapp, K. Kristensen, A. Ligabue, O. B. Lutnaes, J. I. Melo, K. V. Mikkelsen, R. H. Myhre, C. Neiss, C. B. Nielsen, P. Norman, J. Olsen, J. M. H. Olsen, A. Osted, M. J. Packer, F. Pawłowski, T. B. Pedersen, P. F. Provasi, S. Reine, Z. Rinkevicius, T. A. Ruden, K. Ruud, V. V. Rybkin, P. Sałek, C. C. M. Samson, A. S. de Merás, T. Saue, S. P. A. Sauer, B. Schimmelpfennig, K. Snegov, A. H. Steindal, K. O. Sylvester-Hvid, P. R. Taylor, A. M. Teale, E. I. Tellgren, D. P. Tew, A. J. Thorvaldsen, L. Thøgersen, O. Vahtras, M. A. Watson, D. J. D. Wilson, M. Ziolkowski, H. Ågren, *WIREs Comput Mol Sci* **2014**, *4*, 269.
- [43] S. Koseki, M. W. Schmidt, M. S. Gordon, *J. Phys. Chem. A* **1998**, *102*, 10430.
- [44] R. N. Bose, R. E. Viola, R. D. Cornelius, *J. Am. Chem. Soc.* **1984**, *106*, 3336.
- [45] D. A. K. Vezzu, Q. Lu, Y.-H. Chen, S. Huo, *Journal of Inorganic Biochemistry* **2014**, *134*, 49.
- [46] K. Hindmarsch, D. A. House, M. M. Turnbull, *Inorg. Chem. Acta* **1997**, *257*, 11.
- [47] S. E. Miller, A. House, *Inorg. Chem. Acta* **1989**, *166*, 189.
- [48] L. S. Lerman, *J. Mol. Biol.* **1961** *3*, 18.
- [49] L. Streckowski, B. Wilson, *Mutation Research/Fundamental and Molecular Mechanisms of Mutagenesis* **2007**, *623*, 3.
- [50] H. Ihmels, D. Otto, *Top. Curr. Chem.* **2005**, *258*, 161.
- [51] W. Bauer, J. Vinograd, *J. Mol. Biol.* **1970**, *54*, 281.
- [52] M. L. D'Amico, V. Paiotta, F. Secco, M. Venturini, *J. Phys. Chem. B* **2002**, *106*, 12635.
- [53] E. Dabbish, N. Russo, E. Sicilia, *Chem. Eur. J.* **2020**, *26*, 259.
- [54] W. Sotoyama, T. Satoh, H. Sato, A. Matsuura, N. Sawatari, *J. Phys. Chem. A* **2005**, *109*, 9760.
- [55] W. I. Sundquist, S. J. Lippard, *Coord. Chem. Rev.* **1990**, *100*, 293.

Supporting Information

Anticancer activity, DNA-binding and photodynamic properties of a N[^]C[^]N-coordinated Pt(II) complex

Eslam Dabbish, Stefano Scoditti, Nino Russo, Gloria Mazzone, Emilia Sicilia**

Department of Chemistry and Chemical Technologies, Università della Calabria, 87036, Arcavacata di Rende (CS), Italy

Table of Contents

Computational details

S3-S5

Table S1. Contributions to the MM-GBSA binding free energy for the three selected positions of the intercalated drug in the DNA-complex **1** adduct. Van der Waals (VDWAALS), electrostatic (EEL), polar (EGB) and non-polar (ESURF) contributions to the solvation free energy, total gas phase (ΔG_{gas}) and solvation (ΔG_{solv}) binding energy, resulting MM-GBSA binding energy (ΔG_{TOTAL}) and the estimation of the entropy term by quasi-harmonic analysis are reported. All the values are in kcal mol⁻¹. S6

Figure S1. DNA length change due to the intercalation of the **1** complex calculated as the end-to-end distance of the helix, measured from the two terminal base pairs center of mass, taking the drug-free DNA as a reference. Changes for all the three selected positions are reported. S7

Figure S2. Comparison of selected geometrical parameters between the B3LYP-D3 optimized structure and the X-ray structure (in italic). Data from ref. [38] S8

Table S2. Main absorption wavelengths calculated in acetonitrile for band **I** of complex **1** by using the def2qzvp ecp for Pt coupled with its valence basis set and 6-311+G** basis set for the other atoms, employing different XC functionals. S9

Table S3. Vertical excitation energies, ΔE (eV), λ_{max} (nm), oscillator strengths, f , and main transitions computed in water (B3LYP/Pt:def2qzvp/C,H,N,O: 6-311+G**) of complex **1** and its aquated, **1_{wat}**, and guanine bound, **1_{gua}**, forms. S10

Table S4. Lowest lying triplet excitation energies together with MO contributions computed in water (B3LYP/Pt:def2qzvp/C,H,N,O:6-311+G**) of complex **1** and its aquated, **1_{wat}**, and guanine bound, **1_{gua}**, forms. S11

Figure S3. Natural Transition Orbitals, NTOs, for the singlet and triplet states transitions of complex **1** and its aquated, **1_{wat}**, and guanine bound, **1_{gua}**, forms. S12

Table S5. Vertical excitation energies, ΔE (eV), λ_{\max} (nm), oscillator strengths, f , and main transitions computed in water for the three frames extracted from the MD calculations for the preferred intercalation states. **S13**

Table S6. Lowest lying triplet excitation energies together with MO contributions computed in water for the three frames extracted from the MD calculations for the preferred intercalation states. **S14**

References **S15**

Computational details

Gaussian 09 package has been used to perform all quantum mechanical calculations.^[1] For the aquation, guanine and cysteine interaction studies of complex **1**, density functional theory has been employed using the hybrid Becke three parameter exchange functional^[2] and the Lee-Yang-Parr correlation functional,^[3] B3LYP. Grimme dispersion correction for nonbonding interactions has been included using atom pair-wise additive scheme,^[4] DFT-D3 method. The def2QZVP effective core potential^[5] and corresponding split valence basis set have been used to describe platinum atom. 6-311+G** basis set has been employed to describe the rest of the atoms. Frequency calculations have been performed at the same level of theory for all located stationary points to confirm their nature of minima and transition states and for zero-point energy corrections calculations. All the located transition states have been checked to be properly connected to the corresponding minima by means of intrinsic reaction coordinate (IRC) analysis.^[6,7] Solvent effect has been included by using Tomasi's implicit Polarizable Continuum Model (PCM) as implemented in Gaussian 09.^[8-10] The UFF set of radii has been used to build up the cavity in which the solute molecules are accommodated. The solvation Gibbs free energy have been calculated in implicit water ($\epsilon = 78.4$) at the same level, performing single point calculations on all stationary point structures obtained from vacuum calculations. Enthalpies and Gibbs free energies have been obtained at 298 K at 1 atm from total energies, including zero-point, thermal and solvent corrections, using standard statistical procedures.^[11]

In order to study the drug intercalation into DNA, a B-DNA dodecamer, with Protein Data Bank code 1BNA,^[12] has been used. The aquated form of complex **1** has been manually introduced into the different potential intercalation sites. For the molecular dynamics study of both of the above mentioned systems, hydrogens have been added to the model system using H++web-server.^[13-15] The platinum complex has been parametrized by using both Gaussian 09 and MCPB.py in Amber 16 package.^[1,16,17] Geometry optimization and frequency calculations of the platinum drug have been carried out using Gaussian 09 using Stuttgart/Dresden effective core potential^[18] and split valence basis set to describe platinum atom and 6-311G** basis set for the rest of the atoms. MCPB.py has been used to develop the parameters from the above quantum mechanical calculations using Seminario method. For the charges, Gaussian 09 has been used to calculate the Merz-Kollman ESP charge^[19,20] of the created metal center model. MCPB.py has been, then, used to perform RESP charge fitting.

Molecular dynamics topology and coordinate files have been generated by means of tleap in Amber¹⁵ using the standard DNA.bsc^[21] and gaff force fields^[22,23] together with the newly generated parameters for the aquated complex **1**. A TIP3P solvation model^[24-26] has been used to construct an octahedral box of explicit water around the DNA complex with a 14 Å buffer distance around the DNA in each direction. Sodium ions have been added to neutralize the system. The system has been relaxed prior to the molecular dynamics by a 1000 minimization steps with a cutoff distance of 15.0 Å and a constant volume periodic boundaries. The DNA has been held fixed during this initial minimization by using a force constant of 500 kcal mol⁻¹. This has been followed by 2500 minimization steps for the whole system including the DNA with the same cutoff distance and constant volume periodic boundaries. The system has been, then, heated from 0 K to 300 K over 10000 steps for a total of 20 ps. SHAKE algorithm has been implemented to constrain bonds involving hydrogen. During the heating, the DNA has been weakly restrained by a force constant of 10 kcal mol⁻¹ while keeping the constant volume periodic boundaries and same cutoff distance. Equilibration followed by production of molecular dynamics for 20 ns at 300 K were ran under similar conditions with a 0.002 ps interval with no restraints on DNA. The SHAKE algorithm to constrain bonds involving hydrogen and the cutoff distance of 15.0 angstroms were all maintained. A constant pressure periodic boundary with an average pressure of 1 atm and an isotropic position scaling with a relaxation time of 2ps were used.

For evaluating the relative binding free energy between the aquated complex **1** at different intercalation sites and DNA, MM-GBSA method,^[27] as implemented by MMPBSA.py script in Amber 16 package, has been used evaluating the whole production trajectory of each intercalation position over the 20ns. Calculation of the interaction energy and solvation free energies for the drug-DNA adducts and DNA and drug alone has been followed by results averaging to obtain an estimate of the binding free energy as implemented in the MM-GBSA method in Amber 16. A quasi harmonic approximation has been used for entropy calculation. Cpptraj^[28] in Amber 16 package has been used to generate data about the RMSD, distances between residues and conformational changes of the DNA in the drug-DNA complex either by taking the initial conformation or a simulated DNA alone without the bound drug as a reference. The electrostatic and vdW interactions have been also evaluated with the help of Cpptraj. VMD program has been used to generate the figures out of the dynamics trajectory.^[29]

To accurately describe the photophysical properties, a preliminary benchmark study has been carried out on complex **1**. The optimized structure at B3LYP level has been used to compute the excitation energies employing several functionals: B3LYP, Cam-B3LYP,^[30] M06,^[31] PBE0,^[32] PW91^[33] and wB97XD,^[34] including the Grimme dispersion corrections (DFT-D3). Their performances have been evaluated comparing both T₁ and S₁ absorption peak wavelengths in acetonitrile.^[35] Thus a dielectric constant of 35.688 has been used in conjunction with 6-311+G(d,p) basis set for all the atoms except platinum, for which the def2QZVP effective core potential coupled with its valence basis set has been retained. Then, B3LYP-D3 has been selected as most suitable exchange and correlation functional and it has been used for all the TDDFT calculations.

Out of the molecular dynamics trajectory of the intercalation of the aquated form of complex **1** at different DNA sites, the conformations including the drug and the four surrounding nucleotides that show the best Van der Waals interactions between the drug and the surrounding nucleotides are selected for further TDDFT analysis. The intercalated complex from the extracted conformation are optimized first while the DNA pair bases cartesian coordinates have been frozen in order to avoid the unrealistic distortion of the DNA portion included in the QM calculations because of the absence of the rest of the dodecamer used for the MD intercalation study. The optimization and then the absorption spectrum in water has been obtaining maintaining B3LYP functional, the 6-311+G(d,p) basis set for all atoms (C, H, N, O) of the complex with the exception of platinum, again described by the def2QZVP pseudopotential; while all the atoms of the DNA portion were treated with the standard 6-31G(d) basis set.

To ascertain the possibility of an intersystem spin crossing from a bright singlet state to a triplet one, spin-orbit matrix elements have been computed within the quadratic-response TD-DFT approach, as implemented in the Dalton code,^[36] as follow:

$$SOC_{nm} = \sqrt{\sum_i |\langle \psi_{T_{i,n}} | \hat{H}_{SO} | \psi_{S_m} \rangle|^2}; \quad i = x, y, z$$

where \hat{H}_{SO} is the spin-orbit Hamiltonian. For this purpose, TD-B3LYP/cc-pVTZ in conjunction with the def2-qzvp pseudopotential for Pt atom have been used in the framework of the spin-orbit coupling operators for effective core potentials with the effective nuclear charge.^[37]

Table S1

Energy component	MD1	MD2	MD3
VDWAALS	-43.9	-43.7	-44.2
EEL	-504.2	-522.8	-486.0
EGB	515.1	533.9	497.2
ESURF	-2.5	-2.55	-2.44
ΔG gas	-548.1	-566.6	-530.2
ΔG solv	512.6	531.4	494.7
ΔG TOTAL	-35.5	-35.2	-35.5
Quasi-harmonic entropy approximation	-11.4	-10.1	-8.6
ΔG binding	-24.1	-25.1	-26.9

Figure S1

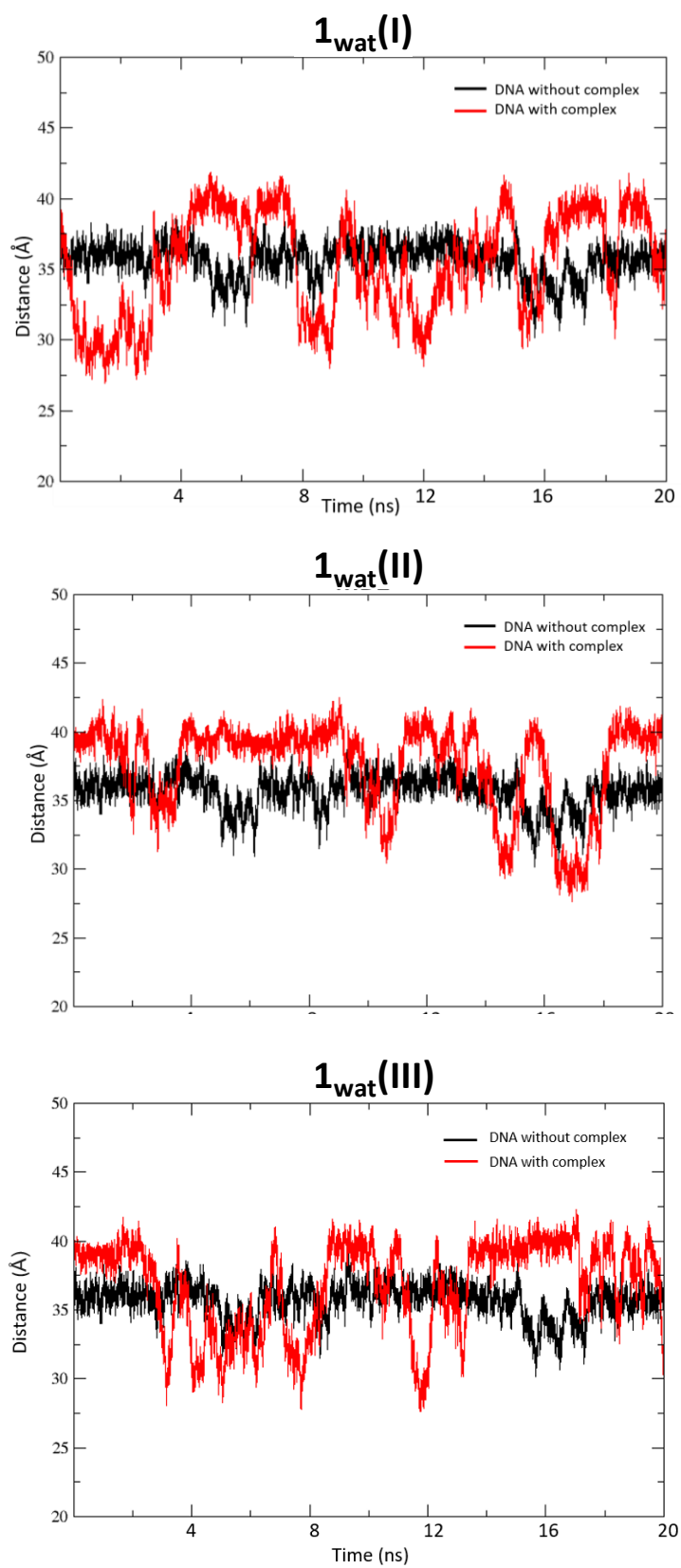
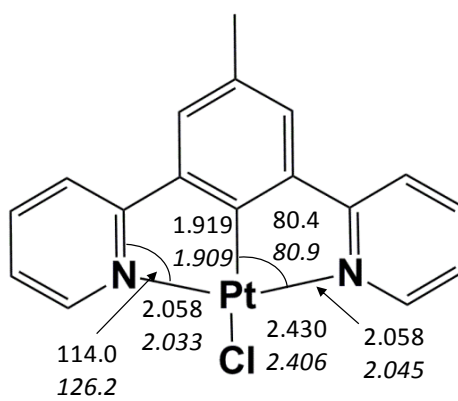


Figure S2



Complex 1

Table S2

		λ	f	MO contribution ^a	λ_{exp} ^b
B3LYP-D3	S1	414	0.004	H→L, 98%	408
	T1	491		H→L, 73%	
camB3LYP-D3	S1	353	0.220	H→L, 92%	
	T1	489		H→L, 42%; H→L+1, 32%	
M06-D3	S1	404	0.150	H→L, 96%	
	T1	494		H→L+1, 52%	
PBE0-D3	S1	395	0.004	H→L, 97%	
	T1	496		H→L, 51%	
PW91	S1	499	0.005	H→L, 97%	
	T1	564		H→L, 99%	
ω B97XD	S1	351	0.216	H→L, 91%	
	T1	467		H-1→L, 37%; H→L+1, 36%	

^aOnly contributions larger than 30% are reported; ^b data in acetonitrile from ref [39].

Table S3

	Band	ΔE	λ	f	MO contribution	Theoretical Assignment
1	I	3.00	414	0.004	H→L, 98%	¹ MLCT
		3.04	408	0.137	H→L+1, 96%	¹ MLCT/ ¹ LLCT
		3.50	354	0.027	H-1→L, 96%	
	II	4.09	303	0.019	H→L+3, 93%	¹ MLCT
		4.11	302	0.308	H-4→L, 87%	
		4.25	292	0.147	H-4→L, 63%	
		4.72	263	0.372	H-1→L+3, 80%	
1_{wat}	I	3.18	390	0.001	H→L, 97%	¹ MLCT
		3.24	382	0.133	H→L+1, 95%	
		3.41	364	0.008	H-2→L, 99%	
		3.51	353	0.017	H-1→L, 95%	
	II	3.85	322	0.068	H-1→L+1, 75%	¹ MLCT
		3.99	311	0.020	H→L+2, 85%	
		4.13	300	0.394	H-3→L, 76%	
	III	4.73	262	0.256	H-1→L+3, 81%	¹ MLCT
		4.97	249	0.020	H-5→L, 58%	
		5.02	247	0.216	H-5→L+1, 73%	
	5.04	246	0.066	H-4→L+2, 98%		
1_{gua}	I	3.16	392	0.007	H→L, 96%	¹ MLCT/ ¹ LLCT
		3.22	385	0.131	H→L+1, 94%	¹ MLCT
	II	4.13	301	0.348	H-4→L, 78%	¹ MLCT
		4.27	291	0.127	H-4→L+1, 60%	
	III	4.66	266	0.103	H-1→L+3, 74%	¹ LLCT
		4.70	250	0.153	H-6→L+1, 60%	

Table S4

	State	ΔE	MO contribution	Theoretical Assignment
1	T1	2.53	H \rightarrow L, 72% H-1 \rightarrow L+1 16%	³ MLCT
	T2	2.61	H \rightarrow L+1, 92%	³ MLCT
	T3	2.90	H-1 \rightarrow L+1, 61% H \rightarrow L, 23%	³ MLCT
1_{wat}	T1	2.60	H \rightarrow L, 58% H-1 \rightarrow L+1, 28%	³ MLCT
	T2	2.75	H \rightarrow L+1, 86%	
	T3	3.01	H-1 \rightarrow L+1, 52% H \rightarrow L, 37%	
	T4	2.14	H-1 \rightarrow L, 71%	
	T5	3.22	H-2 \rightarrow L, 97%	
1_{gua}	T1	2.36	H \rightarrow L, 55%	³ MLCT
	T2	2.45	H \rightarrow L+1, 84%	³ MLCT
	T3	2.62	H \rightarrow L, 37% H-2 \rightarrow L+1, 24% H-3 \rightarrow L+1, 23%	³ MLCT
	T4	2.68	H-2 \rightarrow L, 41% H-3 \rightarrow L, 24%	³ MLCT
	T5	2.72	H-3 \rightarrow L, 49% H-2 \rightarrow L, 39%	³ MLCT

Figure S3

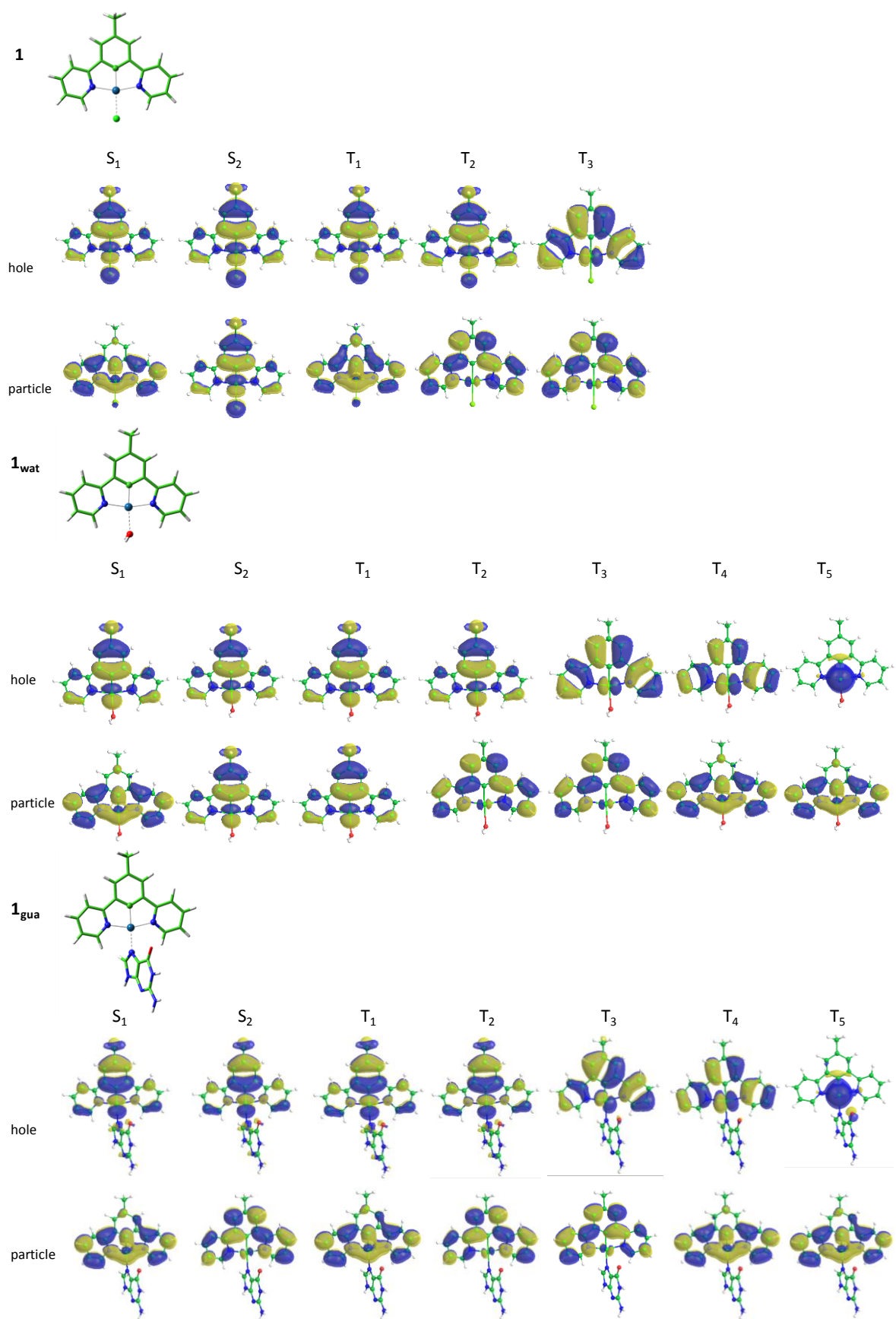


Table S5

	Band	ΔE	λ	f	MO contribution	Theoretical Assignment	
1_{wat}(I)	I	2.94	422	0.005	H→L, 77%	¹ CT _{Gua-NCN}	
		2.99	414	0.038	H→L+1, 81%		
		3.13	397	0.016	H-1→L, 82%		
		3.21	387	0.063	H-1→L+1, 93%		
	II	3.89	319	0.068	H-5→L, 73%		¹ CT _{Gua-NCN}
		3.90	318	0.078	H-6→L, 84%		
		4.12	301	0.092	H-7→L, 52%; H-5→L+1, 28%		
		4.13	300	0.015	H-6→L+1, 48%		
1_{wat}(II)	I	3.03	409	0.016	H→L, 60%; H-1→L, 20%	¹ CT _{Acc-NCN}	
		3.11	399	0.044	H→L+1, 41%; H→L, 28%		
		3.13	396	0.003	H-1→L, 57%; H→L+1, 26%		
		3.18	390	0.074	H-1→L+1, 74%		
	II	3.85	322	0.014	H-1→L+2, 25%; H-4→L+1, 20%		¹ CT _{Acc-NCN}
		3.91	317	0.007	H-5→L+1, 56%; H-6→L+1, 37%		
		3.95	314	0.010	H-6→L+1, 38%; H-4→L+1, 24%		
		3.99	310	0.024	H-6→L, 49%; H-5→L, 41%		
		4.10	302	0.039	H-1→L+2, 29%; H-7→L+1, 14%; H-7→L, 13%		
1_{wat}(III)	I	2.89	428	0.015	H→L, 73%	¹ CT _{Gua-NCN}	
		3.04	407	0.013	H-1→L, 73%		
		3.12	397	0.060	H-1→L+1, 66%		
		3.31	374	0.029	H-2→L+1, 76%		
	II	3.96	313	0.015	H-1→L+4, 78%		¹ CT _{Gua-NCN}
		4.00	310	0.076	H-1→L+2, 40%; H-5→L, 31%		
		4.13	300	0.067	H-6→L, 32%; H-5→L+1, 28%; H-5→L, 18%		

Table S6

	State	ΔE	MO contribution	Theoretical Assignment
1_{wat}(I)	T1	2.57	H-1→L+1, 21%; H-1→L, 18%; H→L, 10%	³ CT _{Gua-NCN}
	T2	2.67	H-1→L+1, 30%; H-1→L, 25%; H→L+1, 16%	³ CT _{Gua-NCN}
	T3	2.91	H-4→L, 22%; H→L, 18%; H→L+1, 15%	³ CT _{Gua-NCN}
	T4	2.99	H-1→L, 21%; H→L, 20%; H→L+1, 19%	³ CT _{Gua-NCN}
1_{wat}(II)	T1	2.57	H→L, 29%; H-1→L, 24%	³ CT _{Ace-NCN}
	T2	2.69	H→L+1, 55%; H-1→L+1, 20%	³ CT _{Ace-NCN}
	T3	2.90	H→L, 50%; H-1→L, 15%	³ CT _{Ace-NCN}
	T4	2.95	H-1→L+1, 38%; H-1→L, 20%	³ CT _{Ace-NCN}
	T5	3.08	H-1→L+1, 25%; H-3→L, 23%; H-1→L, 15%	³ CT _{Ace-NCN}
	T6	3.11	H-3→L+1, 17%; H-2→L, 15%; H-3→L, 15%	³ CT _{Ace-NCN}
1_{wat}(III)	T1	2.55	H-1→L+1, 27%; H-4→L+1, 18%; H-2→L, 18%	³ CT _{Gua-NCN}
	T2	2.71	H-2→L+1, 36%; H-1→L+1, 34%	³ CT _{Gua-NCN}
	T3	2.81	H→L, 51%; H→L+1, 27%	³ CT _{Gua-NCN}
	T4	2.93	H→L, 29%; H-1→L, 16%; H→L+1, 13%	³ CT _{Gua-NCN}
	T5	2.98	H-2→L, 35%; H→L+1, 24%; H-2→L+1, 13%	³ CT _{Gua-NCN}

Reference

- [1] Gaussian 09, Revision D.01, M. J. Frisch, G. W. Trucks, H. B. Schlegel, G. E. Scuseria, M. A. Robb, J. R. Cheeseman, G. Scalmani, V. Barone, B. Mennucci, G. A. Petersson, H. Nakatsuji, M. Caricato, X. Li, H. P. Hratchian, A. F. Izmaylov, J. Bloino, G. Zheng, J. L. Sonnenberg, M. Hada, M. Ehara, K. Toyota, R. Fukuda, J. Hasegawa, M. Ishida, T. Nakajima, Y. Honda, O. Kitao, H. Nakai, T. Vreven, J. A. Montgomery-Jr., J. E. Peralta, F. Ogliaro, M. Bearpark, J. J. Heyd, E. Brothers, K. N. Kudin, V. N. Staroverov, T. Keith, R. Kobayashi, J. Normand, K. Raghavachari, A. Rendell, J. C. Burant, S. S. Iyengar, J. Tomasi, M. Cossi, N. Rega, J. M. Millam, M. Klene, J. E. Knox, J. B. Cross, V. Bakken, C. Adamo, J. Jaramillo, R. Gomperts, R. E. Stratmann, O. Yazyev, A. J. Austin, R. Cammi, C. Pomelli, J. W. Ochterski, R. L. Martin, K. Morokuma, V. G. Zakrzewski, G. A. Voth, P. Salvador, J. J. Dannenberg, S. Dapprich, A. D. Daniels, O. Farkas, J. B. Foresman, J. V. Ortiz, J. Cioslowski, D. J. Fox, Gaussian, Inc., Wallingford CT, **2010**.
- [2] A. D. Becke, *The Journal of Chemical Physics* **1993**, *98*, 1372.
- [3] C. Lee, W. Yang, R. G. Parr, *Phys. Rev. B* **1988**, *37*, 785.
- [4] S. Grimme, J. Antony, S. Ehrlich, H. Krieg, *J. Chem. Phys.* **2010**, *132*, 154104.
- [5] F. Weigend, R. Ahlrichs, *Phys. Chem. Chem. Phys.* **2005**, *7*, 3297.
- [6] K. Fukui, *J. Phys. Chem.* **1970**, *74*, 4161.
- [7] C. Gonzalez, H. B. Schlegel, *J. Chem. Phys.* **1989**, *90*, 2154.
- [8] S. Miertuš, E. Scrocco, J. Tomasi, *Chem. Phys.* **1981**, *55*, 117.
- [9] S. Miertuš, E. Scrocco, J. Tomasi, *Chem. Phys.* **1982**, *65*, 239.
- [10] J. L. Pascual-Ahuir, E. Silla, I. Tuñón, *J. Comp. Chem.* **1994**, *15*, 1127.
- [11] D. A. McQuarrie, J. D. Simon, *Molecular Thermodynamics*, University Science Books: Sausalito, CA, 1999.
- [12] H. R. Drew, R. M. Wing, T. Takano, C. Broka, S. Tanaka, K. Itakura, R. E. Dickerson, *Proc. Natl. Acad. Sci.*, **1981**, *78*, 2179.
- [13] A. R. Anandakrishnan, B. Aguilar, A. V. Onufriev, *Nucleic Acids Res.* **2012**, *40*, 537.
- [14] J. Myers, G. Grothaus, S. Narayanan, A. Onufriev, *Proteins* **2006**, *63*, 928.
- [15] J. C. Gordon, J. B. Myers, T. Folta, V. Shoja, L. S. Heath, A. Onufriev, *Nucleic Acids Res.* **2005**, *33*, 368.
- [16] P. Li, K. M. Merz-Jr., *J. Chem. Inf. Model.* **2016**, *56*, 599.
- [17] D. A. Case, R. M. Betz, D. S. Cerutti, T. E. Cheatham, T. A. Darden, R. E. Duke, T. J. Giese, H. Gohlke, A. W. Goetz, N. Homeyer, S. Izadi, P. Janowski, J. Kaus, A. Kovalenko, T. S. Lee, S. LeGrand, P. Li, C. Lin, T. Luchko, R. Luo, B. Madej, D. Mermelstein, K. M. Merz, G. Monard, H. Nguyen, H. T. Nguyen, I. Omelyan, A. Onufriev, D. R. Roe, A. Roitberg, C. Sagui, C. L. Simmerling, W. M. Botello-Smith, J. Swails, R. C. Walker, J. Wang, R. M. Wolf, X. Wu, L. Xiao, P. A. Kollman, **2016**, AMBER 2016, University of California, San Francisco.
- [18] D. Andrae, U. Häussermann, M. Dolg, H. Stoll, H. Preuss, *Theor. Chim. Acta*, **1990**, *77*, 123.

- [19] U. C. Singh, P. A. Kollman, *J. Comp. Chem.* **1984**, *5*, 129.
- [20] B. H. Besler, K. M. Merz, P. A. Kollman, *J. Comput. Chem.* **1990**, *11*, 431.
- [21] I. Ivani, P. D. Dans, A. Noy, A. Pérez, I. Faustino, A. Hospital, J. Walther, P. Andrio, R. Goñi, A. Balaceanu, G. Portella, F. Battistini, J. L. Gelpí, C. González, M. Vendruscolo, C. A. Laughton, S. A. Harris, D. A. Case, M. Orozco, *Nat. Methods* **2016**, *13*, 55.
- [22] J. Wang, W. Wang, P. A. Kollman, D. A. Case, *J. Mol. Graph. Mod.*, **2006**, *25*, 247.
- [23] J. Wang, R. M. Wolf, J. W. Caldwell, P. A. Kollman, D. A. Case, *J. Comput. Chem.* **2004**, *25*, 1157.
- [24] M. W. Mahoney, W. L. Jorgensen, *J. Chem. Phys.* **2000**, *112*, 8910.
- [25] M. W. Mahoney, W. L. Jorgensen, *J. Chem. Phys.* **2001**, *114*, 363.
- [26] W. L. Jorgensen, J. Chandrasekhar, J. D. Madura, R. W. Impey, M. L. Klein, *J. Chem. Phys.*, **1983**, *79*, 926.
- [27] B. R. Miller, T. D. McGee Jr., J. M. Swails, N. Homeyer, H. Gohlke, A. E. Roitberg, *J. Chem. Theory Comput.* **2012**, *8*, 3314.
- [28] D. R. Roe, T. E. Cheatham, *J. Chem. Theory Comput.* **2013**, *9*, 3084.
- [29] W. Humphrey, A. Dalke, K. Schulten, *Journal of Molecular Graphics* **1996**, *14*, 33.
- [30] T. Yanai, D. P. Tew, N. C. Handy, *Chemical Physics Letters* **2004**, *393*, 51.
- [31] Y. Zhao, D. G. Truhlar, *Theor. Chem. Acc.* **2008**, *120*, 215.
- [32] C. Adamo, V. Barone, *J. Chem. Phys.* **1999**, *110*, 14.
- [33] K. Burke, J. P. Perdew, and Y. Wang, *Electronic Density Functional Theory: Recent Progress and New Directions*, Ed. J. F. Dobson, G. Vignale, M. P. Das, (Plenum 1998).
- [34] J.-D. Chai, M. Head-Gordon, *Phys. Chem. Chem. Phys.* **2008**, *10*, 6615.
- [35] W. Sotoyama, T. Satoh, A. Matsuura, N. Sawatari, *J. Phys. Chem. A* **2005**, *109*, 9760.
- [36] K. Aidas, C. Angeli, K. L. Bak, V. Bakken, R. Bast, L. Boman, O. Christiansen, R. Cimiraglia, S. Coriani, P. Dahle, E. K. Dalskov, U. Ekström, T. Enevoldsen, J. J. Eriksen, P. Ettenhuber, B. Fernández, L. Ferrighi, H. Fliegl, L. Frediani, K. Hald, A. Halkier, C. Hättig, H. Heiberg, T. Helgaker, A. C. Hennum, H. Hettema, E. Hjertenaes, S. Høst, I.-M. Høyvik, M. F. Iozzi, B. Jansík, H. J. Aa. Jensen, D. Jonsson, P. Jørgensen, J. Kauczor, S. Kirpekar, T. Kjaergaard, W. Klopper, S. Knecht, R. Kobayashi, H. Koch, J. Kongsted, A. Krapp, K. Kristensen, A. Ligabue, O. B. Lutnaes, J. I. Melo, K. V. Mikkelsen, R. H. Myhre, C. Neiss, C. B. Nielsen, P. Norman, J. Olsen, J. M. H. Olsen, A. Osted, M. J. Packer, F. Pawłowski, T. B. Pedersen, P. F. Provasi, S. Reine, Z. Rinkevicius, T. A. Ruden, K. Ruud, V. V. Rybkin, P. Salek, C. C. M. Samson, A. S. de Merás, T. Saue, S. P. A. Sauer, B. Schimmelpfennig, K. Sneskov, A. H. Steindal, K. O. Sylvester-Hvid, P. R. Taylor, A. M. Teale, E. I. Tellgren, D. P. Tew, A. J. Thorvaldsen, L. Thøgersen, O. Vahtras, M. A. Watson, D. J. D. Wilson, M. Ziolkowski, H. Ågren, *WIREs Comput Mol Sci* **2014**, *4*, 269.
- [37] S. Koseki, M. W. Schmidt, M. S. Gordon, *J. Phys. Chem. A* **1998**, *102*, 10430.

[38] S. J. Farley, D. L. Rochester, A. L. Thompson, J. A. K. Howard, J. A. G. Williams, *Inorg. Chem.* **2005**, *44*, 9690.

[39] W. Sotoyama, T. Satoh, H. Sato, A. Matsuura, N. Sawatari, *J. Phys. Chem. A*, **2005**, *109*, 9760.

Chapter VIII

**Iodido Platinum (IV)
and (II) Complexes as
Potential Anticancer
Agents**

Chapter VIII Iodido Platinum (IV) and (II) Complexes as Potential Anticancer Agents

8.1 A computational study of iodido equatorial ligands influence on the mechanism of action of Pt(IV) and Pt(II) anti-cancer complexes

8.1.1 Introduction

Platinum iodido complexes have been mainly considered for a long time as intermediates in the synthetic processes for the production of chlorido platinum-based drugs and the investigation of their biological and pharmacological properties and mechanism of action has been overlooked because iodido complexes have been regarded as unsuitable cytotoxic agents compared with cisplatin.¹

More recently, platinum (II) iodido complexes have been re-evaluated as possible anticancer drug candidates thanks to some promising results and for some of them it has been also suggested a different mechanism of action compared with their chlorido analogues. In addition, binding of cis-[Pt(NH₃)I₂] to histidine moieties of hen egg white lysozyme protein involving substituting of one of the ammonia groups instead of iodido ligands has been evidenced.²⁻⁵

On the other side, owing to severe side-effects and intrinsic and acquired resistance of Pt(II)-complexes, Pt(IV) complexes have been designed and synthesized as prodrugs. Pt(IV) complexes, having a low-spin d⁶ octahedral geometry, are more kinetically inert and, as a consequence, they can be administered orally, have diminished side effects and, very importantly, their reactivity can be modulated by means of the axial ligands.^{6,7}

Platinum(IV) pro-drugs require to be activated inside the cells by biological reducing agents that allow square planar active platinum(II) species to be formed by elimination of the axial ligands and the rates of reduction are one

of the most important parameters determining the efficacy of the Pt(IV) complexes as anticancer agents.⁸

Platinum (IV) iodido complexes have been considered also to be possible candidates for photoactivated drugs given the fact that diiodido-Pt(IV) diamines are capable of undergoing photolytic reduction to release the equivalent Pt(II) cytotoxic species. However, the dark stability of these complexes in presence of biological reducing agents is poor and the complexes show relatively high dark activity.^{9,10}

8.1.2 Aim of study

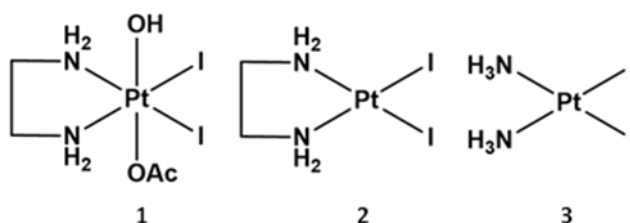


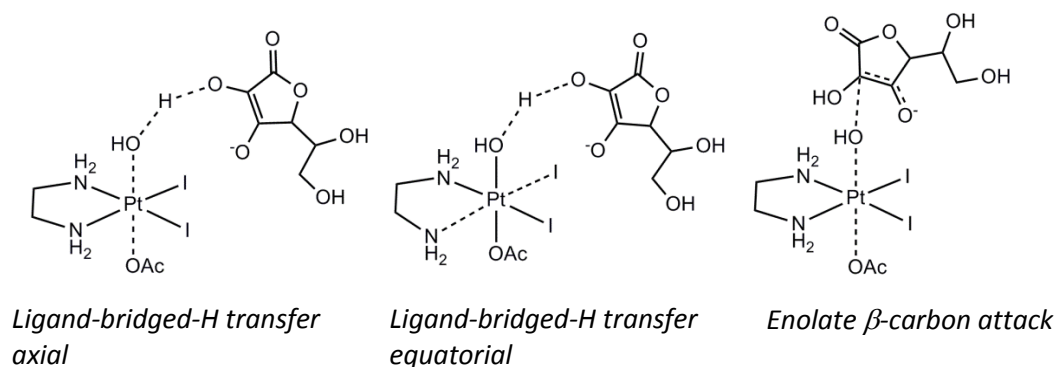
Figure 8.1 Drawing of the iodido Pt complexes under investigation

Motivated by the renewed interest in iodido-platinum (II) compounds and the known dark activity of iodido-platinum (IV) compounds, we have computationally explored the mechanism of action and differences in behaviour with respect to chlorido analogues of the following Pt(IV) and Pt(II) iodido complexes, *trans,-cis*-[Pt(en)(OH)(OAc)I₂] (**1**) (en=ethylenediamine), *cis*-[Pt(en)I₂] (**2**) and *cis*-[Pt(NH₃)I₂] (**3**).

This includes the Pt(IV) diiodido reduction mechanisms examination using monoanionic ascorbic acid and cysteine as reducing agents. Afterwards, the attention has been focused on Pt(II) active species. Aquation mechanism, interaction with guanine, sulfur containing compounds and histidine as a protein model have been explored.

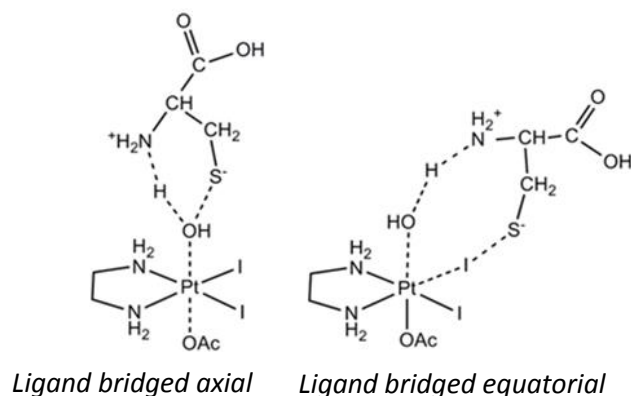
For the sake of comparison, the outcomes of this investigation have been compared with those for the chlorido Pt(IV) analogue *trans,cis*-[Pt(en)(OH)(OAc)Cl₂], and the Pt(II) leading compound cisplatin.

8.1.3 Highlighting results



Scheme 8.1 Schematic representation of the alternative inner-sphere reduction mechanisms by ascorbate (Asch⁻). Dashed lines indicate breaking and forming bonds.

When ascorbate is the reducing agent, the inner-sphere ligand-bridged-H transfer, involving a H⁻ unit transfer from the OH group of the ascorbate to the hydroxido axial ligand, is the preferred mechanism of reduction (**Scheme 8.1**). The low calculated energy barrier shows that reduction is facile.



Scheme 8.2 Schematic representation of the alternative inner-sphere reduction mechanisms by L-cysteine. Dashed lines indicate breaking and forming bonds.

In presence of L-cysteine the reduction follows a ligand bridging mechanism (**Scheme 8.2**). The OH group establishes a new bond with the zwitterionic cysteine sulfur atom leading to the formation of a sulfenylhydroxide overcoming an accessible energy barrier.

Comparison with the results for the reduction of the analogous chlorido Pt(IV) complex shows no significant difference in behavior. Differences appear when the cysteine attack occurs on one of the equatorial iodides or a new alternative ligand-bridged H-transfer mechanism assisted by ascorbate is taken into consideration. In both mechanisms increased bridging and leaving propensities of iodide over chloride lower the energy barriers that is necessary to overcome. Chloride appears to be less inclined both to work as a bridging ligand and to be displaced. It seems that the possibility for iodide to better delocalize both the negative and positive charge prevails in determining the final result.

The analysis of the aquation reaction and interaction with guanine and N-acetyl methionine of $[\text{Pt}(\text{en})\text{I}_2]$ and $\text{cis-}[\text{Pt}(\text{NH}_3)_2\text{I}_2]$ in comparison with cisplatin does not highlight any significant difference.

Only when the interaction of the $\text{cis-}[\text{Pt}(\text{NH}_3)_2\text{I}_2]$ complex with histidine is examined to model the reaction with hen egg white lysozyme a difference in behavior appears. Histidine interaction with the iodido complex is more favored with respect to cisplatin and, even if the preferred site of attack is the iodide, also the NH_3 substitution can be considered accessible. However, the suggestion that $\text{cis-}[\text{Pt}(\text{NH}_3)_2\text{I}_2]$ can retain iodido ligands has not been reproduced in spite of the different adopted strategies. Very likely, either a pH change or the specific environment of the protein and the interactions the drug can establish, which cannot be mimicked using our simplified histidine model system, can play a role in determining the final results.

References

- 1) M. J. Cleare, J. D. Hoeschele, *Bioinorganic Chemistry*, **1973**, 2 (3), 187–210-
- 2) D. Cirri, S. Pillozzi, C. Gabbiani, J. Tricomi, G. Bartoli, M. Stefanini, E. Michelucci, A. Arcangeli, L. Messori, T. Marzo, *Dalton Trans.*, **2017**, 46 (10), 3311–3317.
- 3) L. Messori, T. Marzo, C. Gabbiani, A. A. Valdes, A. G. Quiroga, A. Merlino, *Inorg. Chem.*, **2013**, 52 (24), 13827–13829.
- 4) M. Navarro, A. R. Higuera-Padilla, M. Arsenak, P. Taylor, *Transition Met Chem*, **2009**, 34 (8), 869–875.
- 5) M. Navarro, W. Castro, A. R. Higuera-Padilla, A. Sierralta, M. J. Abad, P. Taylor, R. A. Sánchez-Delgado, *Journal of Inorganic Biochemistry*, **2011**, 105 (12), 1684–1691.
- 6) X. Li, Y. Liu, H. Tian, *Bioinorganic Chemistry and Applications*, **2018**, 1–18.
- 7) S. H. van Rijt, P. J. Sadler, *Drug Discovery Today*, **2009**, 14 (23–24), 1089–1097.
- 8) K. Lemma, A. M. Sargeson, L. I. Elding, *J. Chem. Soc., Dalton Trans.*, **2000**, 1167-1172-
- 9) P. J. Bednarski, K. Korpis, A. F. Westendorf, S. Perfahl, R. Grünert, *Proc. R. Soc. A*, **2013**, 371 (1995), 20120118.
- 10) H. Shi, C. Imberti, P. J. Sadler, *Inorg. Chem. Front.*, **2019**, 6 (7), 1623–1638.

Paper VIII

**A computational study of iodido equatorial ligands influence on
the mechanism of action of Pt(IV) and Pt(II) anti-cancer
complexes**

Stefano Scoditti, Vincenzo Vigna, Eslam Dabbish and Emilia Sicilia

Manuscript submitted

A computational study of iodido equatorial ligands influence on the mechanism of action of Pt(IV) and Pt(II) anti-cancer complexes

Stefano Scoditti,^a Vincenzo Vigna,^a Eslam Dabbish^a and Emilia Sicilia*^a*

^a Department of Chemistry and Chemical Technologies, Università della Calabria, 87036, Arcavacata di Rende (CS), Italy

Abstract Recent findings in platinum drug design field on iodido Pt(II) complexes and very promising and surprising re-evaluation of their cytotoxic activity inspired us to undertake a detailed computational exploration of the most relevant steps of iodido Pt(IV) complexes reduction and Pt(II) drugs mechanism of action and eventual deactivation. *trans,-cis*-[Pt(en)(OH)(OAc)I₂] (en=ethylenediamine), *cis*-[Pt(en)I₂] and *cis*-[Pt(NH₃)₂I₂] have been investigated as model systems, whose behavior has been compared with that of the leading compound cisplatin and its Pt(IV) derivative. Both monodeprotonated ascorbic acid and L-cysteine, as a model of sulfur-containing bio-reductants, have been used as reducing agents involved in the inner-sphere reduction mechanism of Pt(IV) complexes. Aquation mechanism of iodido Pt(II) complexes, interaction with guanine and sulfur containing compounds and reaction with the model protein hen egg white lysozyme have been explored, having experimental studies proved for some aspects a different behavior with respect to classical platinum drugs. The elucidation of all the details of the examined reactions allows to shed light on the role that the increased *soft* character together with bridging and leaving abilities of iodide over chloride could play in determining the cytotoxic profile of iodido Pt drugs.

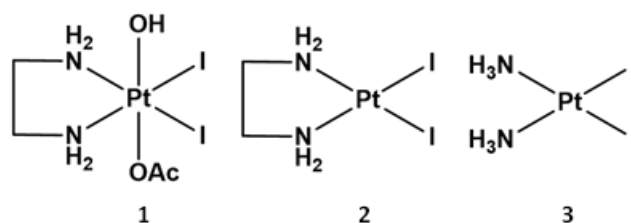
1. Introduction

The unique efficacy, on one hand, and the well-known shortcomings, on the other, of the anticancer drug cisplatin and its derivatives carboplatin and oxaliplatin, have inspired an intense search for platinum analogues with hopefully improved biological and pharmacological properties.^{1,2} Platinum iodido complexes have been mainly considered for a long time intermediates in the synthetic processes for the production of chlorido platinum-based drugs and the investigation of their biological properties and mechanism of action has been overlooked because iodido complexes have been regarded as biologically and pharmacologically unsuitable compared with chlorido analogues.³ More recently, platinum iodido complexes have been reconsidered as possible anticancer drug candidates and for some of them it has been also suggested a different mechanism of action compared with their chlorido analogues.⁴⁻⁷ Moreover, the investigation of the mechanism of action of these complexes has highlighted a significant and unexpected reactivity towards proteins,⁸ suggesting that proteins might be alternative important targets for iodido Pt(II) compounds. Owing to severe side-effects and intrinsic and acquired resistance of Pt(II)-complexes, Pt(IV) complexes have been designed and synthesized as prodrugs. Pt(IV) complexes, having a low-spin d^6 octahedral geometry, are more kinetically inert and, as a consequence, they can be administered orally, have diminished side effects and, very importantly, their reactivity can be modulated by means of the axial ligands.^{9,10} To overcome the side effects of and resistance to cisplatin, a variety of Pt(IV) prodrugs were designed and synthesized via different modifications including combination with lipid chains to increase hydrophobicity, conjugation with short peptide chains or nanoparticles to improve drug delivery, or addition of bioactive ligands to the axial positions of Pt(IV) complexes to exert dual-function effects. This review summarizes the recent progress in the development of Pt(IV) prodrugs conjugated with bioactive-targeting ligands, including histone deacetylase inhibitors, p53 agonists, alkylating agents, and nonsteroidal anti-inflammatory agents. Although Pt(IV)

complexes that conjugated with bioactive ligands show satisfactory anticancer effects, none has been approved for clinical use. Therefore, we hope that this review will contribute to further study and development of Pt(IV) complexes conjugated with bioactive and other ligands. Platinum(IV) pro-drugs require to be activated inside the cells by biological reducing agents that allow square planar active platinum(II) species to be formed by elimination of the axial ligands and the rates of reduction are one of the most important parameters determining the efficacy of the Pt(IV) complexes as anticancer agents.¹¹ One alternative approach to activate the pro-drug directly in tumors is by using light for inducing a photolytic reduction of a non-toxic but light-sensitive Pt(IV) complex to a cytotoxic Pt(II) species. This approach has been initially tried with diiodido-Pt(IV) diamines, which are activated by visible light to cytotoxic species that platinate DNA. However, the dark stability of these complexes in presence of biological reducing agents is poor and the complexes show relatively high dark activity.^{12,13} Motivated by the renewed interest in the design of novel, more efficacious and safer chemotherapeutics based on iodido-platinum compounds¹⁴ and the discontinuous experimental investigations, we have computationally explored their antitumor activity, mechanism of action and differences in behaviour with respect to chlorido clinically-used platinum complexes. *trans*-,*cis*-[Pt(en)(OH)(OAc)I₂] (**1**) (en=ethylenediamine), *cis*-[Pt(en)I₂] (**2**) and *cis*-[Pt(NH₃)I₂] (**3**), shown in Scheme 1, have been investigated as model systems.

Both inner- and outer Pt(IV) diiodido complexes reduction mechanisms have been examined initially by considering several mechanistic hypotheses. It is the first time, to our knowledge, that the details of the reduction assisted by a sulfur-containing reducing agent of a Pt(IV) complex having a OH axial ligand has been reported. Afterwards, the attention has been focused on Pt(II) active species. Aquation mechanism, interaction with guanine and sulfur containing compounds have been explored together with the reaction with the model protein hen egg white lysozyme, having experimental studies proved a different behaviour of iodido Pt(II) complexes with respect

to classical platinum drugs.^{8,15,16} Furthermore, also the possibility that chlorido ions substitute iodido ligands has been explored as it is well known that chlorido ions, due to their high concentration in blood plasma and extracellular fluid, can exchange with Pt(II) complex ligands. Both the *trans* effect and Pearson's Hard and Soft Acids and Bases (HSAB) principle have been invoked to rationalize observed peculiarities. Therefore, for the sake of comparison the outcomes of this investigation have been compared with those for the chlorido Pt(IV) analogue *trans,cis*-[Pt(en)(OH)(OAc)Cl₂], and the Pt(II) leading compound cisplatin.



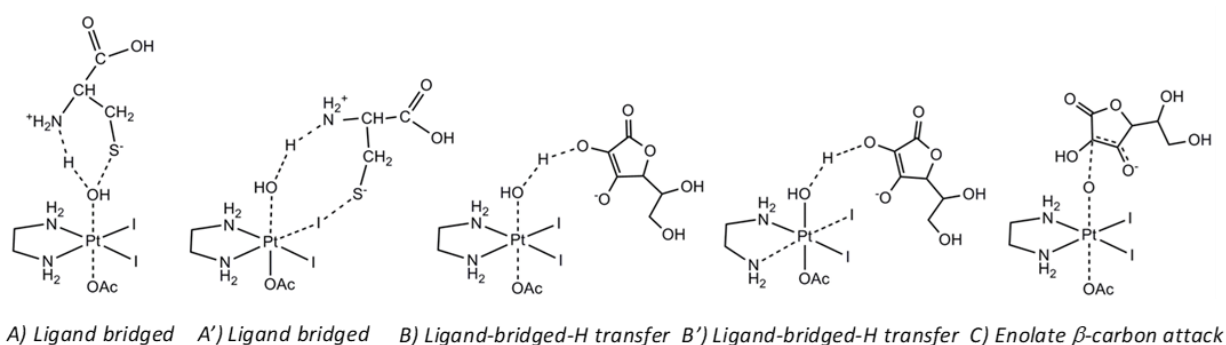
Scheme 1. Drawing of the iodido Pt complexes under investigation.

2. Results and discussion

2.1 Iodido Pt(IV) complexes reduction mechanism

Electron transfer mechanisms for the reduction of Pt(IV) complexes are commonly classified as inner- and outer-sphere. In the former case a direct contact, involving new bond formation, is established with the reducing agent, in the latter the electrons are transferred without any direct interaction. However, theoretical investigations carried out recently by some of us¹⁷ have allowed to further classify the reduction mechanisms of Pt(IV) prodrugs, when AscH⁻ is the reducing agent as *A) ligand bridged*, *B) ligand-bridged H-transfer* and *C) enolate β -carbon attack*. In both *A)* and *B)* mechanisms one of the axial ligands is able to form a bridge between the Pt(IV) center and the reductant mediating the flow of the electrons. However, in mechanism *B)* the electron transfer proceeds by the direct participation of the ligand, leading to the formation of dehydroascorbic acid (DHA), the oxidized form of ascorbic acid. Furthermore, as shown in Scheme 2, in the present case being iodide a good bridging leaving ligand,¹⁸ it has been taken into account the suggestion that the reducing agent can attack the iodido equatorial ligand

causing the temporary opening of the chelating ethylenediamine ligand (mechanism *A'*) *ligand bridged* in Scheme 2).¹⁹ Moreover, an alternative mechanism named *B'*) *ligand-bridged H-transfer* has been discovered that will be illustrated in the next paragraphs. A systematic examination of both inner- and outer-sphere reduction mechanisms for the iodido Pt(IV) complex **1** in Scheme 1 has been, therefore, carried out in presence of the monoanionic form of ascorbic acid (AscH^-), that is the most abundant at physiological pH (pka ca. 3.8), as reductant. Furthermore, L-Cysteine (Cys), as a model of sulfur-containing bioreductants, has been used as reducing agent involved in the inner-sphere mechanism.



Scheme 2. Schematic representation of the alternative inner-sphere reduction mechanisms by ascorbate (AscH^-) and L-cysteine. Dashed lines indicate breaking and forming bonds.

Therefore, all the three A), B) and C) mechanisms have been explored as a function of the identity of both the reducing agent and the involved ligand. Concerning the outer-sphere mechanism, the calculation of the standard redox potential of the examined complex has been performed adopting the decomposition scheme proposed by Baik and coworkers²⁰ and already tested^{17,21,22} assuming that reduction can take place through a two steps electron transfer encompassing formation of a metastable six-coordinate Pt(III) intermediate.

2.1.1 Inner-sphere reduction by AscH^-

The free energy profiles describing the A) *ligand bridged H-transfer* and B) *enolate β -carbon attack* reduction mechanisms of complex **1** in presence of AscH^- are shown in Figure 1. The geometries of the located stationary points are sketched in the same figure.

Along the pathway for the ligand bridged H-transfer mechanism (Figure 1, panel a) the adduct between complex **1** and the reducing agent rearranges to allow the transfer of the H⁻ unit from the OH group of the ascorbate to the bridging hydroxido ligands, to form the oxidized form of ascorbic acid, DHA. The formed water detaches inducing the concurrent release of the *trans* acetate ligand and the active complex **2** is formed. This rearrangement requires that a barrier of 19.3 kcal mol⁻¹ is overcome. The product, that is the adduct between complex **2** and the released ligands, lies 13.1 kcal mol⁻¹ below the entrance channel.

Enolate β-carbon attack mechanism (Figure 1, panel b) involves the nucleophilic attack of the enolate β-carbon of ascorbate on the OH ligand resulting in the formation of a new C-OH bond and the release of the other axial ligand. The height of the energy barrier, calculated with respect the first adduct is 24.3 kcal mol⁻¹ and the products are stabilized by 16.2 kcal mol⁻¹. Therefore, mechanism C) is calculated to be less kinetically favored, according to what previously reported,¹⁷ and the barrier of the second step of the process, leading to the formation of DHA through the elimination of a water molecule formed by the transferred OH⁻ with the abstraction of a proton from the geminal hydroxide, should be even higher.

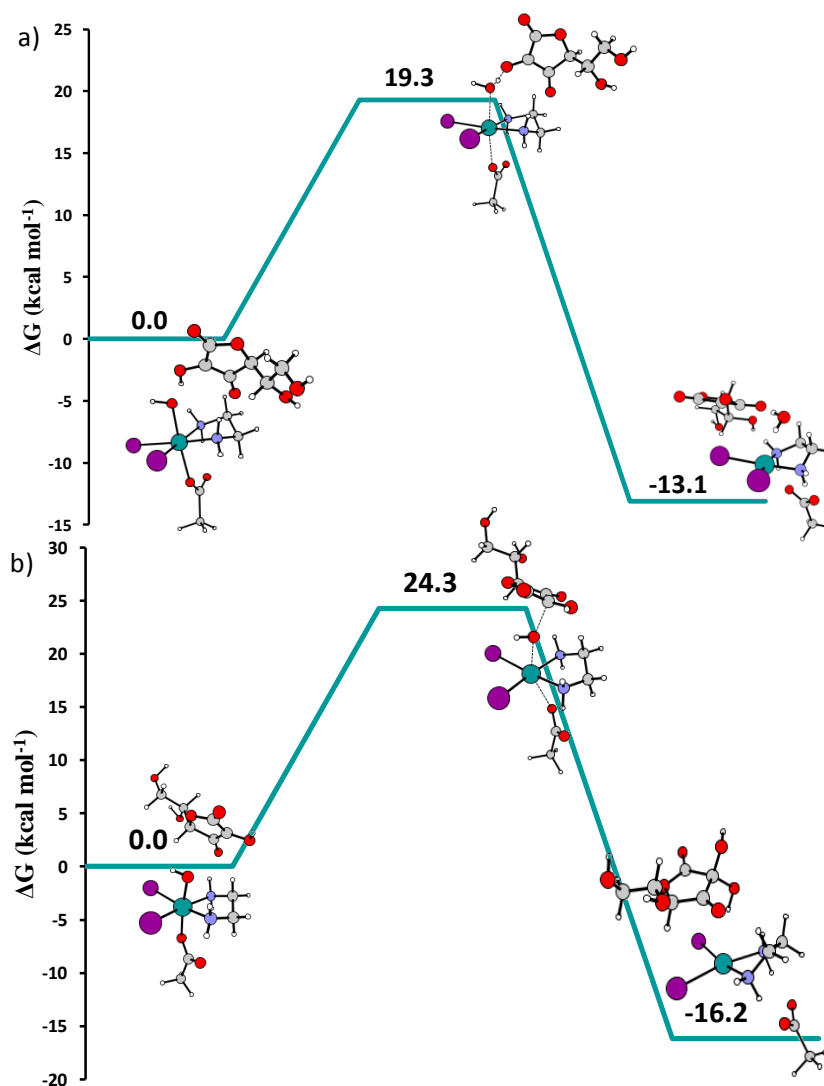


Figure 1. Free energy profiles describing the a) *B*) ligand-bridged-*H*-transfer and b) *C*) enolate β -carbon attack mechanisms for the reduction of complex **1** by ascorbate. Energies are in kcal·mol⁻¹ and relative to the first adduct.

Owing to the presence of equatorial iodido ligands in the complex under examination, the reaction following the ligand-bridged-*H* transfer mechanism should evolve also in a different way (mechanism *B'*) ligand-bridged-*H* transfer) as shown in panel a of Figure 2. Indeed, the formed water in axial position can migrate in equatorial position causing the release of one of the equatorial iodides along with the simultaneous detachment of one of the ends of the ethylenediamine chelating ligand in *trans* position. This rearrangement, involving a barrier of 20.2 kcal mol⁻¹, yields a square planar Pt(II) species in which one of the iodido ligands is

substituted by the formed water, whereas the acetate takes the place of the detached end of the en ligand. The reaction is nearly thermoneutral.

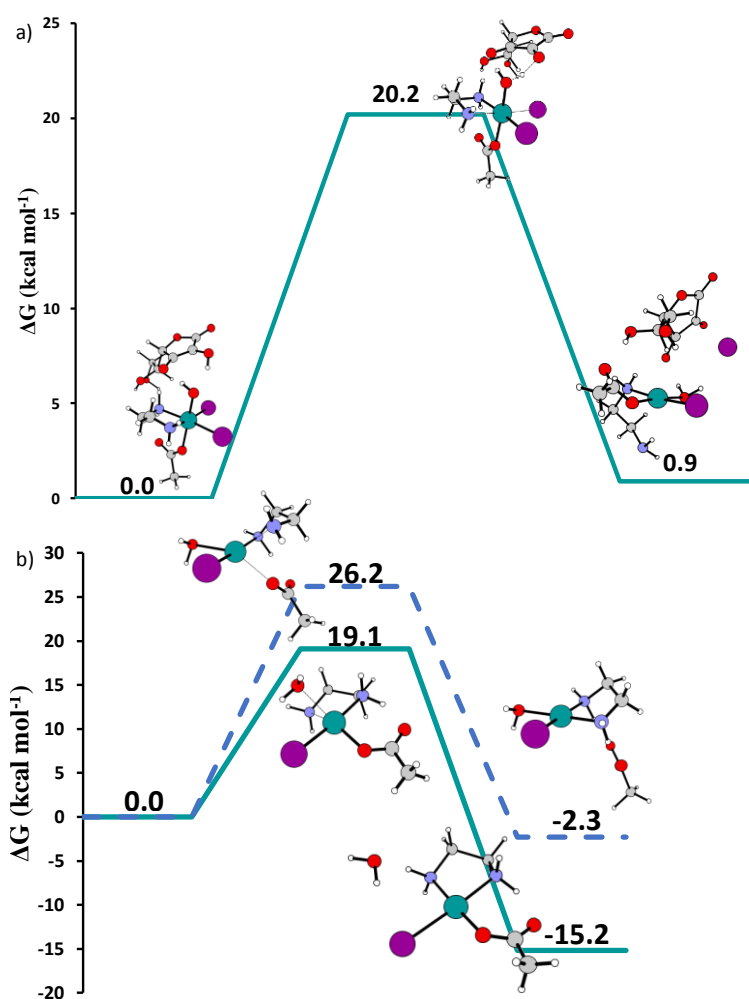


Figure 2. Free energy profiles describing the a) alternative B') *ligand-bridged-H transfer* mechanism for the reduction of complex 1 by ascorbate and b) two possible alternative reactions to close the en ring, that is water (green solid line) and acetate (blue dashed line) elimination. Energies are in kcal·mol⁻¹ and relative to the first adduct.

This pathway corresponds to what has been assumed to occur in presence of thiol reducing agents.¹⁹ The outcomes of the exploration of the ring closure mechanism are shown in panel b of Figure 2. Two possible alternatives have been examined. The elimination of water to restore the chelation requires that a barrier of 19.1 kcal mol⁻¹ has to be overcome and leads to the formation of a complex stabilized by 15.2 kcal mol⁻¹. For the acetate displacement it is necessary to

overcome a barrier of 26.2 kcal mol⁻¹ and the reaction results to be exergonic by 2.3 kcal mol⁻¹. When the acetate ligand is released the aquated [PtI(H₂O)(en)]⁺ complex is formed, which subsequently should interact with DNA.

For the sake of comparison, the ascorbate reduction of the chlorido analogue, *trans,cis*-[Pt(en)(OH)(OAc)Cl₂], of complex **1** has been explored. Corresponding free energy profiles are shown in Figures S1 and S2 of the Supporting Information (SI) for B), B') and C) mechanisms. With respect to the iodide complex, a barrier higher by about 2 kcal mol⁻¹ for mechanisms B) and the same height of 24.3 kcal mol⁻¹ for mechanism C), have calculated. This result is in line with the conclusion formerly drawn¹⁷ about the influence of the identity of the equatorial ligands on the reduction mechanisms when AscH⁻ is the reducing agent. On the contrary, the presence of chlorides in equatorial position instead of iodides introduces significant changes when the alternative B') mechanism is examined (see Figure S2 of the SI). This alternative ligand-bridged-H transfer path, that becomes viable once the formed water molecule in axial position provokes the elimination of one of the chlorido ligands together with the detachment of one end in *trans* position of the chelating ligand, the barrier is higher (31.6 kcal mol⁻¹ vs 20.2 kcal mol⁻¹). The barriers of the substitution reactions that allow to close the en ring for the chlorido complex are, instead, very similar to those for the iodido one and are 17.8 kcal mol⁻¹ for water and 26.2 kcal mol⁻¹ for acetate elimination.

2.1.2 Inner-sphere reduction by L-cysteine

Theoretical investigations of the inner-sphere reduction mechanism of Pt(IV) complexes involving thiol containing biological compounds as reducing agents are, to the best of our knowledge, very scarce^{23,24} even if, for a long time, sulfur containing reductants have been considered to be very active.^{18,25-27} The most accredited hypotheses suggest that the mechanism is of A) bridging ligand type (see Scheme 2) with

the sulfur atom forming a new bond with a good leaving group in axial position facilitating the electron flow and causing the release of the ligand in *trans* position.²⁸ As underlined above, for the particular case of complex **1**, it has been proposed that sulfur attacks one of the equatorial iodides (mechanism A') bridging ligand) causing the detachment of one of the ends of the chelating ligand and the temporary ring opening.¹⁹ The outcomes of the present computational analysis are reported in Figure 3 where the free energy profiles and the structures of the intercepted minima and transition states are shown for the attack to both axial OH (panel a) and equatorial iodido (panel b) ligands. According to what previously reported by Ariafard and coworkers,²³ lots of attempts carried out to select the most probable mechanism have shown that the reactive form of cysteine is the zwitterionic one that becomes even more active due to the migration of the proton form sulfur to one of the carboxylate oxygens. An additional water molecule has been added that, even if does not play any active role, avoids meaningless proton transfers.

Starting from the initial adduct formed between complex **1** and the active form of cysteine, the activation barrier for the reduction in axial position is 22.9 kcal mol⁻¹. The bridging OH group forms a new bond with the cysteine sulfur atom and the simultaneous release of the *trans* acetate liberates the active Pt(II) drug. The reaction is calculated to be exergonic by 3.3 kcal mol⁻¹. The formed sulfenylhydroxide can further react and afford the oxidized form of cysteine.

When the sulfur attack occurs on the equatorial iodide, the height of the barrier becomes 17.4 kcal mol⁻¹ and during the rearrangement one of the hydrogens of the NH₃⁺ group is transferred to the hydroxido ligand to form water. The result is the elimination of one of the iodido ligands that is accompanied by the en ring opening. The reaction is exergonic by 9.5 kcal mol⁻¹. The formed ring opened aquated Pt(II) complex can undergo ring closure as already described above (see panel b of Figure2), whereas the released reactive sulfenyl iodide might further react to give rise to the corresponding disulfide.

For the *trans,cis*-[Pt(en)(OH)(OAc)Cl₂] analogue (see Figure S3 of the SI) the sulfur attack to the OH axial group occurs involving an energy barrier of 22.9 kcal mol⁻¹. The release of the corresponding Pt(II) complex is exergonic by 3.3 kcal mol⁻¹. The equatorial chlorido ligand, instead, is significantly less keen

to act as a bridging ligand favoring the electron transfer. The barrier, indeed, is calculated to be 27.6 kcal mol⁻¹ and the process is almost thermoneutral.

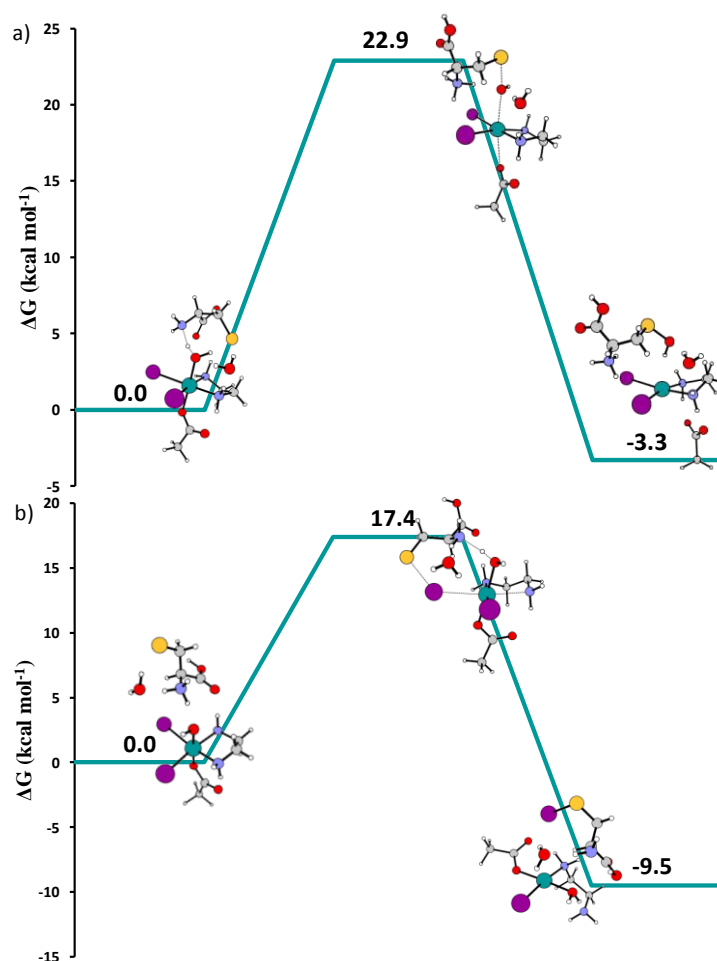


Figure 3. Free energy profiles describing the sulfur attack to the a) axial OH⁻ and b) equatorial I ligands in the A) and A') bridging ligand mechanisms for the reduction of complex 1 by cysteine. Energies are in kcal·mol⁻¹ and relative to the first adduct.

Some conclusions can be drawn on the basis of the results illustrated so far. The differences in behavior between iodido and chlorido complexes can be ascribed to the bridging/leaving propensity of the I⁻ ligand. Indeed, the iodido ligand works better as bridging ligand in mechanism A) according to the hypothesis that it is easier to form a I⁺ than a Cl⁺ during the reductive attack.²⁹ The hypothesis, instead, that the softer character of the iodide over chloride should strengthen the Pt-I bond is not supported by our calculations. Displacement of the I⁻ ligand is faster when the formed axial water migrates in equatorial

position. It seems that the possibility for iodide to better delocalize the negative charge prevails in determining the final result. Moreover, for iodido complex **1** the alternative *A'*) and *B'*) mechanisms appear to be viable and kinetically more favorable (in case of *A'*) and competitive (in case of *B'*) with respect to the normal *A*) and *B*) mechanisms. Finally, it is worth underlining that the low enough energy barriers for the reduction reaction confirm that such complexes are not stable in dark in presence of reducing agents and cannot be used as photoactivable prodrugs.¹³

2.1.3 Outer-sphere reduction mechanism

Cyclic voltammetry is routinely used to characterize the redox behavior of Pt(IV) antitumor compounds. However, due to the strong interconnection between electrochemical and chemical events, the two-electron redox process is commonly observed as a single irreversible reduction event, and the peak potential for the cathodic wave, determinedly dependent on the experimental conditions, is usually used instead of the standard redox potential. It is, therefore, matter of debate the possibility to estimate the standard reduction potential of Pt(IV) complexes from such measurements. Baik and coworkers²⁰ have proposed experimental and theoretical approaches that allow to bypass such limitations. In order to measure the propensity of complex **1** to be reduced by an outer-sphere mechanism, such approach has been adopted. On the basis of the proposed decomposition scheme, the reduction potential can be calculated as the energy change that accompanies the one electron transfer for the reduction of the six-coordinate Pt(IV) complex to the corresponding six-coordinate Pt(III) species with the axial ligand remaining in the coordination sphere of the metal center. The reduction potential is computed as $E^\circ = -\Delta G(\text{sol}) - E_{\text{ref}}$, where $\Delta G(\text{sol})$ is the Gibbs free energy change in solution for the one electron transfer to the Pt(IV) complex and E_{ref} is the absolute potential of the standard electrode used as a reference.

For the aim of comparison also the values of the standard redox potentials for the iodido *trans,cis*-[Pt(en)(OH)₂I₂] (**4**) and *trans,cis*- [Pt(en)(OAc)₂I₂] (**5**) complexes have been calculated and reported together with reduction potential measured using cyclic voltammetry,¹² The absolute potential of the

saturated calomel reference electrode has been used, that is the electrode used in experiments. Calculated and measured values have been collected in Table 1.

Table 1. Calculated standard redox potentials (E°_{comp}) (mV) for complexes **1**, **4** and **5** compared with the available experimental counterparts (E_{cp} =cathodic peak).

	E_{cp}	E°_{comp}
<i>trans,cis</i> -[Pt(en)(OH) ₂ I ₂] (4)	-287±17 ^a	-294
<i>trans,cis</i> -[Pt(en)(OH)(OAc)I ₂] (1)	-	-89
<i>trans,cis</i> -[Pt(en)(OAc) ₂ I ₂] (5)	-65±1 ^a	-53

^aRef. 12.

Calculated values very well reproduce the available measured values and show that the propensity to be reduced increases, as expected, in going from complex **4** to **1** to **5** in case an outer-sphere mechanism is operative. The values of the reduction potential, however, indicate, as expected for hydroxido and carboxylato ligands and according to values reported in ref. 12 for complexes coordinating chlorido axial ligands, a low propensity to be reduced. Very likely, an inner-sphere reduction is preferred as the values of the energy barriers calculated for complex **1** demonstrate. Reduction rate can be properly modulated and asymmetric compounds such as complex **1** seem to be well suited for the fine-tuning of Pt(IV) prodrug properties.³⁰ This is the reason why we have decided to investigate a Pt(IV) complex having hydroxido and acetato ligands in axial position.

2.2 Mechanism of action of iodido Pt(II) complexes

As it has been stressed above, the interest in iodido Pt(II) complexes that should be released as a result of the reduction of Pt(IV) iodido complexes has been awakened recently.¹⁴ Indeed, notable and surprising *in vitro* antiproliferative properties, in some cases superior to those of conventional Pt based drugs, have been disclosed, associated with peculiar mechanisms of action towards representative biomolecules. The attention, here, has been focused on diiodido-cisplatinum complexes *cis*-[PtI₂(NH₃)₂], **2**, and [Pt(en)I₂], **3**,

whose mechanism of action (MoA), just like cisplatin, involves iodido ligands substitution by water leading to formation of the corresponding “aquated” complexes able to act as transcription inhibitors by binding to nuclear DNA. Additionally, the interaction of *cis*-[Pt(I)₂(NH₃)₂] with other biological molecules such histidine and N-aceyl methionine residues as possible new targets has been explored.

As anticipated above, the possibility that iodido ligands could be substituted by chlorido ions has been also explored due to the high Cl⁻ concentration in blood plasma and extracellular fluid that inhibits hydrolysis. Nevertheless, all the attempts carried out to establish whether such exchange can occur have failed. The chlorido ions are able to displace only the ammonia molecules by overcoming a high energy barrier (27.2 kcal mol⁻¹ as shown in Figure S4 of the SI). The same results have been obtained even when, in order to better reproduce the environment, simulations have been carried out including water molecules and additional chlorido ions. Therefore, it can be concluded that chlorido ions are not competitive in altering the structure of the iodido drug in the extracellular fluids.

2.2.1 Aquation and interaction with guanine

The results of the computational exploration of the aquation and guanine binding two key steps are collected in Table 2. Activation and reaction free energies calculated for both first and second aquation processes of **2** and **3** complexes are reported together with the analogous values calculated for the reference cisplatin.

Table 2. Calculated activation (ΔG^\ddagger) and reaction (ΔG_{rxn}) free energies in water describing the first and second aquation process and guanine interaction. Relative energies are in kcal mol⁻¹ and calculated with respect to the first encounter complex.

	1° Aquation		2° Aquation		Guanine Attack	
	ΔG^\ddagger	ΔG_{rxn}	ΔG^\ddagger	ΔG_{rxn}	ΔG^\ddagger	ΔG_{rxn}
<i>cis</i> -[Pt(en)I ₂]	24.5	12.0	25.2	11.2	19.1	-9.6
<i>cis</i> -[Pt(NH ₃) ₂ I ₂]	23.0	5.4	27.8	14.7	18.0	-9.8
<i>cis</i> -[Pt(NH ₃) ₂ Cl ₂]	22.9	2.3	29.8	12.5	18.9	-10.5

The reaction proceeds, as usual, by the water molecule attack, both first and second, to the platinum centre replacing the iodido ligand in a SN2 fashion leading through a pseudo trigonal bipyramid platinum transition state to the formation of the corresponding aquated species. The first aquation process is hampered by an energy barrier of 24.5 and 23.0 kcal mol⁻¹ and endergonic by 12.0 and 5.4 kcal mol⁻¹ for **2** and **3** complexes, respectively. Values calculated for the aquation of reference cisplatin are 22.9 kcal mol⁻¹ for the barrier and 2.3 kcal mol⁻¹ for the reaction energy. Transition states intercepted along the pathways for the second aquation lie 25.2 kcal mol⁻¹ for **2** and 27.8 kcal mol⁻¹ for **3** above the corresponding encounter complex zero reference energy. Free reaction energies are 11.2 and 14.7 kcal mol⁻¹ for **2** and **3**, respectively. Second cisplatin aquation involves an energetic cost of 29.8 kcal mol⁻¹ and is calculated to be endergonic by 12.5 kcal mol⁻¹. From such results can be deduced that first aquation of iodido Pt(II) complexes is less favorable by both kinetic and thermodynamic points of view, according with the literature.³¹ The barriers for the second hydrolysis of iodide complexes are slightly lower than that of cisplatin, but in all cases the reactions are strongly endergonic according to the hypothesis, even today controversial, that diaquated species are not involved in the anticancer activity of cisplatin and its derivatives.³²⁻³⁴ It is worth underlining that, even if the debate on the proper computational strategy to be used to investigate hydrolysis of cisplatin and its derivatives is still open, here the focus is the comparison between chlorido and iodido Pt(II) drugs to highlight similarities and differences investigated using the same tools and under the same operative conditions.

DNA platination process by complex **2** and **3** has been investigated through the interaction of the guanine nucleobases, as a model, with mono-aquated complexes. The attack occurs in a monodentate fashion at the N7 position following a SN2 associative mechanism. The free energy changes that describe the interaction of the aquated form of the studied complexes with guanine are collected in Table 1. The magnitude of the energy barrier is very similar for the two complexes, 19.1 and 18.0 kcal mol⁻¹ for **2** and **3**, respectively as well as are very close the stability values of the formed products, -9.6 and -9.8 kcal mol⁻¹. Moreover, such values do not differ from those calculated for cisplatin that are 18.9 kcal mol⁻¹ for the

barrier and $-10.5 \text{ kcal mol}^{-1}$ the reaction energy. The present outcomes demonstrate that the rate of the reaction is not influenced either by the identity of the halogen atom or by the nature of the inert ligands, when they are not very different amongst them. It is, therefore, confirmed, in agreement with the literature dealing with this subject,³⁵ that iodido Pt(II) complexes exhibit an interaction mode very similar to that of cisplatin and some relevant differences in behavior observed when *in vitro* experiments are taken into consideration can be, very likely, the consequence of ‘second order’ effects such as degree of induced distortion or thermal stability of platinated DNA.

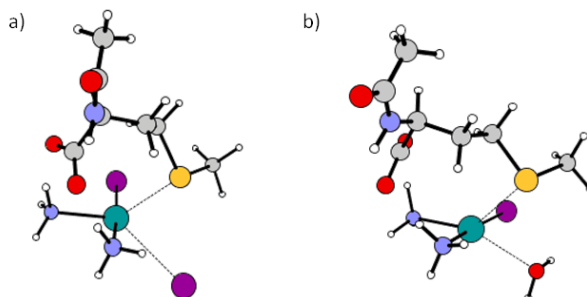
2.2.2 Interaction with N-Acetyl methionine

It is well known that the abundant sulfur containing biological molecules, due to the soft nature of the platinum center, can cause the deactivation of Pt containing complexes forming stable adducts and, thus, preventing the drug from reaching the DNA target. N-acetyl methionine (NAM) has been used here as a model to study the tendency of the examined complexes, in both non-aquated and mono-aquated forms, to interact with sulfur containing species. Free energy barriers and reaction energies are gathered in Table 3 together with those calculated for cisplatin and its mono-aquated form. Geometrical structure of the intercepted transition states in the case of intact and mono-aquated complex **2** are drawn in Figure 4. Optimized geometries of stationary points sketched along the corresponding pathways for all the complexes under investigation can be found in Figures S5-S7 of the ESI.

Table 3. Calculated B3LYP-D3 activation (ΔG^\ddagger) and reaction (ΔG_{rxn}) free energies in water for the NAM substitution. Relative energies are in kcal mol^{-1} and calculated with respect to the first encounter complex.

	NAM attack	
	ΔG^\ddagger	ΔG_{rxn}
<i>cis</i> -[Pt(en)I ₂]	16.3	-6.2
<i>cis</i> -[Pt(NH ₃) ₂ I ₂]	18.1	0.0
<i>cis</i> -[Pt(NH ₃) ₂ Cl ₂]	16.7	-4.9
<i>cis</i> -[Pt(en)(H ₂ O)I] ⁺	17.0	-8.5
<i>cis</i> -[Pt(NH ₃)(H ₂ O)I] ⁺	19.3	-2.0
<i>cis</i> -[Pt(NH ₃)(H ₂ O)Cl] ⁺	18.0	-3.3

Figure 4. Geometrical structure of the transition states intercepted along the pathways for the a) NAM/iodide and b) NAM/H₂O exchange in intact and aquated complex **3**, respectively.



The iodido ligand displacement by NAM occurs, once again, following a S_N2 mechanism. The transition states for the associative displacement of the iodido ligand lie 16.3 and 18.1 kcal mol⁻¹ above the first adduct reference energy for complex **2** and **3**, respectively. The NAM substitution is exergonic by 6.2 kcal mol⁻¹ for complex **2**, while for complex **3** is thermoneutral. The analogous values for cisplatin are: 16.7 kcal mol⁻¹ for the barrier and -4.9 kcal mol⁻¹ for the reaction energy. Therefore, complex **3** with respect to the analogous chlorido cisplatin complex appears to be less prone to be deactivated by sulfur-containing biomolecules. The barrier for the mono-aquated forms increases by about 1 kcal mol⁻¹. The values of the barrier and the reaction energy for the mono-aquated cisplatin are 18.0 and -3.3 kcal mol⁻¹, respectively. That is, an analogous barrier increase of about 1 kcal mol⁻¹ is calculated. Summarizing, it appears that the interaction of iodido complexes **2** and **3** with NAM is faster than the aquation reaction and, likewise, the interaction of their aquated forms with NAM is more favorable, at least from a thermodynamic point of view, with guanine. Therefore, substitution reaction by sulfur containing biomolecules contribute to deactivate the drug interfering with key reactions leading to cell apoptosis.

2.2.3 Binding to histidine

Hen egg white lysozyme (HEWL) is often employed as a model system to investigate the interaction between proteins and metallodrugs. A lot of attention has been focused on the interaction with HEWL of the iodido complex **3**. Several investigations revealed the peculiar and different mode of interaction toward this model protein in comparison with cisplatin, in particular the possibility to release different Pt ligands at diverse pHs.^{8,16,36} Platination occurs at the ND1 atom of the imidazole ring of His15. However, cisplatin typically affords protein platination through substitution of chlorido ligands, whereas *cis*-[Pt(NH₃)₂I₂] can give rise to a protein-bound species in which, in the proper environment, both iodido ligands are retained. This behavior has been considered to be at the origin of different pharmacological profiles for the two drugs.

The interaction of complex **3**, *cis*-[Pt(NH₃)₂I₂], with histidine, therefore, has been investigated. The results of the exchange reaction between both iodido and ammonia ligands in complex **3** with histidine are shown in Figure 5. Along the pathways are also sketched the structures of the located stationary points and in parentheses are reported the values for the analogous cisplatin drug.

Aiming at better reproducing the environmental conditions, two additional water molecules have been added. One that allows to save the zwitterionic form of the histidine molecule and one as a spectator. Calculations show that the barrier for the displacement of the iodido ligand (21.6 kcal mol⁻¹) is lower than that for the ammonia substitution (28.6 kcal mol⁻¹). A similar trend has been recently reported using imidazole as a model for histidine.³⁶ The analogous barriers for cisplatin are 25.5 and 29.9 kcal mol⁻¹ for chlorido and ammonia substitution, respectively.

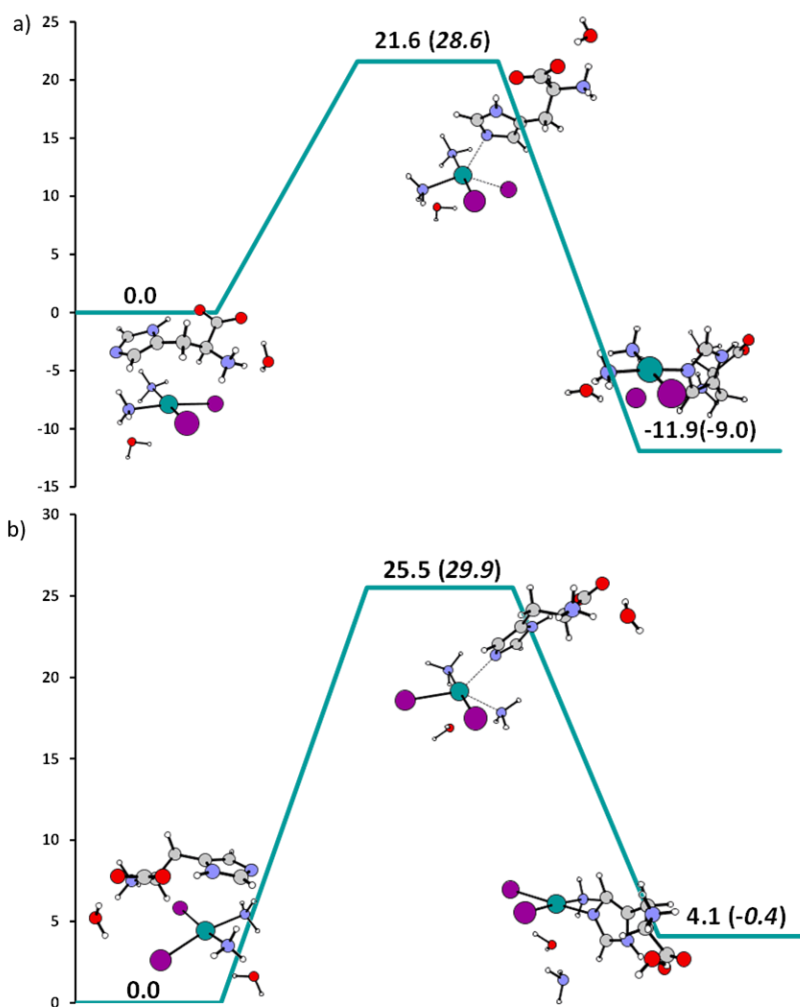


Figure 5. Free energy profiles describing histidine displacement of a) one iodido and b) one ammonia ligand in *cis*-[Pt(NH₃)₂I₂] complex. Values in parentheses are those calculated for the analogous cisplatin complex. Energies are in kcal·mol⁻¹ and relative to the first adduct.

The information coming from such data is that histidine interaction with the iodido complex is more favored and, even if the preferred site of attack is the iodide also the NH₃ substitution can be considered accessible. Substitution of one of the ammonia ligands by histidine could also occur in two steps. That is, after the halogenido/histidine exchange occurs, the eliminated I⁻ and Cl⁻ ions can re-coordinate to the metal center displacing one the ammonia ligand in *trans* to the histidine. This possibility has been explored and the results are summarized in Figure S8 of the ESI where the energy profiles for the two-steps displacement are shown for both *cis*-[Pt(NH₃)₂I₂] and *cis*-[Pt(NH₃)₂Cl₂]. The energetic cost for the substitution of the ammonia in *trans* position to histidine is 29.1 kcal mol⁻¹ for the iodido and 33.1 kcal

mol⁻¹ for the chlorido ligands. The process is more favorable when the iodido complex is involved, but direct substitution in the intact complex is the preferred pathway. The viable pathways explored here can lead to draw the conclusion that the [*cis*-Pt(NH₃)₂I₂] complex has a higher affinity for histidine. However, the atypical observed behavior can be due either to a pH change or to the specific environment of the protein and the interactions the drug can establish, which are not reproduced using the histidine portion for the whole molecule.

The outcomes of our computational analysis, at least for the aspects investigated here, do not corroborate the suggestion, very often underlined, that iodido Pt-based complexes are less reactive due to the strengthening of the Pt-I bond with respect to the Pt-Cl one as a consequence of the soft nature of both the metal center and iodido ligand.

Conclusions

Motivated by the recent renewed interest in iodido Pt anticancer drugs, we present here the outcomes of a complete computational exploration of the most relevant steps of iodido Pt(IV) complexes reduction and the mechanism of action and eventual deactivation of iodido Pt(II) drugs. Results reported here allow to shed light on the role that should be played by the increased *soft* character of iodide with respect to chloride together with its leaving and bridging abilities in delineating the cytotoxic activity of iodido platinum compounds. The reduction of the model system *trans,cis*-[Pt(en)(OH)(OAc)I₂] by both monodeprotonated ascorbic acid and L-cysteine, as a model of sulfur-containing bioreductants, has been investigated. When ascorbate is the reducing agent, the inner-sphere ligand-bridged-H transfer, involving a H unit transfer from the OH group of the ascorbate to the hydroxido axial ligand, is the preferred mechanism of reduction. The low calculated energy barrier shows that reduction is facile. In presence of L-cysteine the reduction follows a ligand bridging mechanism. The OH group establishes a new bond with the zwitterionic cysteine sulfur atom leading to the formation of a sulfenylhydroxide overcoming an accessible energy barrier. The calculated value of the standard redox potential indicates, instead, a low

propensity to be reduced by an outer-sphere mechanism. Comparison with the results for the reduction of the analogous cisplatin Pt(IV) derivative shows no significant difference in behavior. Differences appear when the cysteine attack occurs on one of the equatorial iodides or a new alternative ligand-bridged H-transfer mechanism assisted by ascorbate is taken into consideration. In both mechanisms increased bridging and leaving propensities of iodide over chloride lower the energy barriers that is necessary to overcome. Chloride appears to be less inclined both to work as a bridging ligand and to be displaced. It seems that the possibility for iodide to better delocalize both the negative and positive charge prevails in determining the final result.

The analysis of the aquation reaction and interaction with guanine and N-acetyl methionine of $[\text{Pt}(\text{en})\text{I}_2]$ and *cis*- $[\text{Pt}(\text{NH}_3)_2\text{I}_2]$ in comparison with cisplatin does not highlight any significant difference. Only when the interaction of the *cis*- $[\text{Pt}(\text{NH}_3)_2\text{I}_2]$ complex with histidine is examined to model the reaction, extensively experimentally investigated, with hen egg white lysozyme a difference in behavior appears. Histidine interaction with the iodido complex is more favored with respect to cisplatin and, even if the preferred site of attack is the iodide, also the NH_3 substitution can be considered accessible. However, the suggestion that cisplatin undergoes usual substitution of chlorido ligands, whereas *cis*- $[\text{Pt}(\text{NH}_3)_2\text{I}_2]$ can retain iodido ligands has not been reproduced in spite of the different adopted strategies. The atypical experimentally observed behavior, likely, can be due to either a pH change or to the specific environment of the protein and the interactions the drug can establish, which cannot be mimicked using the histidine portion for the whole molecule. Finally, all the data reported here do not support the hypothesis that the *soft* nature of the iodido ligand should strengthen, on the basis of the HSAB principle, the bond with the soft Pt center, likely because the bridging and leaving abilities of the I ligand prevail.

Computational Details

All molecular geometry optimizations have been performed by employing the B3LYP hybrid exchange–correlation functional^{37,38} as implemented in the Gaussian09 software package in gas phase.³⁹ Grimme dispersion corrections⁴⁰ for non-bonding interactions have been included using atom pairwise additive scheme denoted as D3. In order to select the most appropriate computational protocol preliminary test calculations have been carried out using numerous combinations of xc functionals and basis sets. In particular, for the halogen atoms, and mainly iodine, several basis sets have been tested for their influence on the final results. The adopted computational protocol has been chosen as it represents a proper compromise between accuracy and computational costs. The relativistic compact Stuttgart/Dresden (SDD) effective core potential⁴¹ and the corresponding split valence basis set have been used to describe platinum atom. For a better description of iodine atom to the SDD pseudopotential, used for the core electrons, the 6-311G** basis set for the valence electrons has been associated. The same 6-311G** basis set has been employed to describe all the other atoms except for oxygen and sulfur atoms directly participating in the platinum(IV) reduction process, for which a diffuse function has been included. The located stationary points have been checked by vibrational analysis at the same level of theory to confirm their nature of minima or transition states. The involved transition states have been carefully checked by intrinsic reaction coordinate (IRC) analysis.⁴² Enthalpies and Gibbs free energies have been calculated using standard statistical procedures at 298 K and 1 atm from total energies, including zero-point and thermal corrections.⁴³ Explicit water molecules, as underlined in the text, have been added, when appropriate, to better simulate the behavior of the investigated compounds. To better refine the obtained energies, single point calculations on the optimized gas phase geometries of all stationary points have been performed employing the def2QZVP⁴⁴ effective core potential and its related valence basis set for both Pt and I atoms and a the 6-311+G** basis set for the rest of atoms. To evaluate the water solvent ($\epsilon = 78.4$) impact on the energetics of the reaction, the above mentioned larger basis sets have been used to carry out single point calculations on the gas phase optimized geometries with the Tomasi's implicit

polarizable continuum model (PCM) as implemented in Gaussian09.⁴⁵⁻⁴⁶ The UFF set of radii has been chosen to build up the cavity.

Conflicts of interest

There are no conflicts to declare.

Acknowledgements

This research was supported by the project POR Calabria – FSE/FESR 2014-2020. University of Calabria and Calabria Region are acknowledged for financial support.

References

- (1) Kelland, L. R.; Sharp, S. Y.; O'Neill, C. F.; Raynaud, F. I.; Beale, P. J.; Judson, I. R. Mini-Review: Discovery and Development of Platinum Complexes Designed to Circumvent Cisplatin Resistance. *Journal of Inorganic Biochemistry* **1999**, *77* (1–2), 111–115. [https://doi.org/10.1016/S0162-0134\(99\)00141-5](https://doi.org/10.1016/S0162-0134(99)00141-5).
- (2) Galanski, M.; Yasemi, A.; Slaby, S.; Jakupec, M. A.; Arion, V. B.; Rausch, M.; Nazarov, A. A.; Keppler, B. K. Synthesis, Crystal Structure and Cytotoxicity of New Oxaliplatin Analogues Indicating That Improvement of Anticancer Activity Is Still Possible. *European Journal of Medicinal Chemistry* **2004**, *39* (8), 707–714. <https://doi.org/10.1016/j.ejmech.2004.04.003>.
- (3) Cleare, M. J.; Hoeschele, J. D. Studies on the Antitumor Activity of Group VIII Transition Metal Complexes. Part I. Platinum (II) Complexes. *Bioinorganic Chemistry* **1973**, *2* (3), 187–210. [https://doi.org/10.1016/S0006-3061\(00\)80249-5](https://doi.org/10.1016/S0006-3061(00)80249-5).
- (4) Cirri, D.; Pillozzi, S.; Gabbiani, C.; Tricomi, J.; Bartoli, G.; Stefanini, M.; Michelucci, E.; Arcangeli, A.; Messori, L.; Marzo, T. PtI₂ (DACH), the Iodido Analogue of Oxaliplatin as a Candidate for Colorectal Cancer Treatment: Chemical and Biological Features. *Dalton Trans.* **2017**, *46* (10), 3311–3317. <https://doi.org/10.1039/C6DT03867K>.
- (5) Messori, L.; Cubo, L.; Gabbiani, C.; Álvarez-Valdés, A.; Michelucci, E.; Pieraccini, G.; Ríos-Luci, C.; León, L. G.; Padrón, J. M.; Navarro-Ranninger, C.; Casini, A.; Quiroga, A. G. Reactivity and Biological Properties of a Series of Cytotoxic PtI₂ (Amine)₂ Complexes, Either *Cis* or *Trans* Configured. *Inorg. Chem.* **2012**, *51* (3), 1717–1726. <https://doi.org/10.1021/ic202036c>.
- (6) Navarro, M.; Higuera-Padilla, A. R.; Arsenak, M.; Taylor, P. Synthesis, Characterization, DNA Interaction Studies and Anticancer Activity of Platinum–Clotrimazole Complexes. *Transition Met Chem* **2009**, *34* (8), 869–875. <https://doi.org/10.1007/s11243-009-9276-y>.
- (7) Navarro, M.; Castro, W.; Higuera-Padilla, A. R.; Sierraalta, A.; Abad, M. J.; Taylor, P.; Sánchez-Delgado, R. A. Synthesis, Characterization and Biological Activity of Trans-Platinum(II)

- Complexes with Chloroquine. *Journal of Inorganic Biochemistry* **2011**, *105* (12), 1684–1691. <https://doi.org/10.1016/j.jinorgbio.2011.09.024>.
- (8) Messori, L.; Marzo, T.; Gabbiani, C.; Valdes, A. A.; Quiroga, A. G.; Merlino, A. Peculiar Features in the Crystal Structure of the Adduct Formed between *Cis*-Pt(II)(NH₃)₂ and Hen Egg White Lysozyme. *Inorg. Chem.* **2013**, *52* (24), 13827–13829. <https://doi.org/10.1021/ic402611m>.
- (9) Li, X.; Liu, Y.; Tian, H. Current Developments in Pt(IV) Prodrugs Conjugated with Bioactive Ligands. *Bioinorganic Chemistry and Applications* **2018**, *2018*, 1–18. <https://doi.org/10.1155/2018/8276139>.
- (10) van Rijt, S. H.; Sadler, P. J. Current Applications and Future Potential for Bioinorganic Chemistry in the Development of Anticancer Drugs. *Drug Discovery Today* **2009**, *14* (23–24), 1089–1097. <https://doi.org/10.1016/j.drudis.2009.09.003>.
- (11) Lemma, K.; Sargeson, A. M.; Elding, L. I. Kinetics and Mechanism for Reduction of Oral Anticancer Platinum(IV) Dicarboxylate Compounds by L-Ascorbate Ions †. *J. Chem. Soc., Dalton Trans.* **2000**, No. 7, 1167–1172. <https://doi.org/10.1039/a909484i>.
- (12) Bednarski, P. J.; Korpis, K.; Westendorf, A. F.; Perfahl, S.; Grünert, R. Effects of Light-Activated Diazido-Pt^{IV} Complexes on Cancer Cells *in Vitro*. *Proc. R. Soc. A* **2013**, *371* (1995), 20120118. <https://doi.org/10.1098/rsta.2012.0118>.
- (13) Shi, H.; Imberti, C.; Sadler, P. J. Diazido Platinum(IV) Complexes for Photoactivated Anticancer Chemotherapy. *Inorg. Chem. Front.* **2019**, *6* (7), 1623–1638. <https://doi.org/10.1039/C9QI00288J>.
- (14) Štarha, P.; Vančo, J.; Trávníček, Z. Platinum Iodido Complexes: A Comprehensive Overview of Anticancer Activity and Mechanisms of Action. *Coordination Chemistry Reviews* **2019**, *380*, 103–135. <https://doi.org/10.1016/j.ccr.2018.09.017>.
- (15) Ferraro, G.; De Benedictis, I.; Malfitano, A.; Morelli, G.; Novellino, E.; Marasco, D. Interactions of Cisplatin Analogues with Lysozyme: A Comparative Analysis. *Biometals* **2017**, *30* (5), 733–746. <https://doi.org/10.1007/s10534-017-0041-y>.
- (16) Tanley, S. W. M.; Schreurs, A. M. M.; Kroon-Batenburg, L. M. J.; Helliwell, J. R. Room-Temperature X-Ray Diffraction Studies of Cisplatin and Carboplatin Binding to His15 of HEWL after Prolonged Chemical Exposure. *Acta Crystallogr F Struct Biol Cryst Commun* **2012**, *68* (11), 1300–1306. <https://doi.org/10.1107/S1744309112042005>.
- (17) Dabbish, E.; Ponte, F.; Russo, N.; Sicilia, E. Antitumor Platinum(IV) Prodrugs: A Systematic Computational Exploration of Their Reduction Mechanism by L-Ascorbic Acid. *Inorg. Chem.* **2019**, *58* (6), 3851–3860. <https://doi.org/10.1021/acs.inorgchem.8b03486>.
- (18) Shi, T.; Berglund, J.; Elding, L. I. Kinetics and Mechanism for Reduction of *Trans*-Dichlorotetracyanoplatin(IV) by Thioglycolic Acid, L-Cysteine, DL-Penicillamine, and Glutathione in Aqueous Solution. *Inorg. Chem.* **1996**, *35* (12), 3498–3503. <https://doi.org/10.1021/ic951598s>.
- (19) Kratochwil, N. A.; Guo, Z.; del Socorro Murdoch, P.; Parkinson, J. A.; Bednarski, P. J.; Sadler, P. J. Electron-Transfer-Driven *Trans*-Ligand Labilization: A Novel Activation Mechanism for Pt(IV) Anticancer Complexes. *J. Am. Chem. Soc.* **1998**, *120* (32), 8253–8254. <https://doi.org/10.1021/ja980393q>.
- (20) McCormick, M. C.; Keijzer, K.; Polavarapu, A.; Schultz, F. A.; Baik, M.-H. Understanding Intrinsically Irreversible, Non-Nernstian, Two-Electron Redox Processes: A Combined Experimental and Computational Study of the Electrochemical Activation of Platinum(IV) Antitumor Prodrugs. *J. Am. Chem. Soc.* **2014**, *136* (25), 8992–9000. <https://doi.org/10.1021/ja5029765>.
- (21) Tolbatov, I.; Coletti, C.; Marrone, A.; Re, N. Insight into the Electrochemical Reduction Mechanism of Pt(IV) Anticancer Complexes. *Inorg. Chem.* **2018**, *57* (6), 3411–3419. <https://doi.org/10.1021/acs.inorgchem.8b00177>.

- (22) Ponte, F.; Russo, N.; Sicilia, E. Insights from Computations on the Mechanism of Reduction by Ascorbic Acid of Pt^{IV} Prodrugs with Asplatin and Its Chlorido and Bromido Analogues as Model Systems. *Chem. Eur. J.* **2018**, *24* (38), 9572–9580. <https://doi.org/10.1002/chem.201800488>.
- (23) Ejehi, Z.; Ariafard, A. A Computational Mechanistic Investigation into the Reduction of Pt(IV) Prodrugs with Two Axial Chlorides by Biological Reductants. *Chem. Commun.* **2017**, *53* (8), 1413–1416. <https://doi.org/10.1039/C6CC07834F>.
- (24) Dobrogorskaia-Méreau, Ia. I.; Nemukhin, A. V. Quantum Chemical Modeling of the Reduction of Cis-Diammineplatinum(IV) Tetrachloride [Pt(NH₃)₂Cl₄] by Methyl Thiolate Anion. *J. Comput. Chem.* **2005**, *26* (9), 865–870. <https://doi.org/10.1002/jcc.20224>.
- (25) Hall, M. D.; Hambley, T. W. Platinum(IV) Antitumour Compounds: Their Bioinorganic Chemistry. *Coordination Chemistry Reviews* **2002**, *232* (1–2), 49–67. [https://doi.org/10.1016/S0010-8545\(02\)00026-7](https://doi.org/10.1016/S0010-8545(02)00026-7).
- (26) Dong, J.; Huo, S.; Shen, S.; Xu, J.; Shi, T.; Elding, L. I. Reactivity of the Glutathione Species towards the Reduction of Ormaplatin (or Tetraplatin). *Bioorganic & Medicinal Chemistry Letters* **2016**, *26* (17), 4261–4266. <https://doi.org/10.1016/j.bmcl.2016.07.046>.
- (27) Dong, J.; Ren, Y.; Huo, S.; Shen, S.; Xu, J.; Tian, H.; Shi, T. Reduction of Ormaplatin and Cis-Diamminetetrachloroplatinum(IV) by Ascorbic Acid and Dominant Thiols in Human Plasma: Kinetic and Mechanistic Analyses. *Dalton Trans.* **2016**, *45* (28), 11326–11337. <https://doi.org/10.1039/C6DT01804A>.
- (28) Wexselblatt, E.; Gibson, D. What Do We Know about the Reduction of Pt(IV) pro-Drugs? *Journal of Inorganic Biochemistry* **2012**, *117*, 220–229. <https://doi.org/10.1016/j.jinorgbio.2012.06.013>.
- (29) Zhang, J. Z.; Wexselblatt, E.; Hambley, T. W.; Gibson, D. Pt(IV) Analogs of Oxaliplatin That Do Not Follow the Expected Correlation between Electrochemical Reduction Potential and Rate of Reduction by Ascorbate. *Chem. Commun.* **2012**, *48* (6), 847–849. <https://doi.org/10.1039/C1CC16647F>.
- (30) Yap, S. Q.; Chin, C. F.; Hong Thng, A. H.; Pang, Y. Y.; Ho, H. K.; Ang, W. H. Finely Tuned Asymmetric Platinum(IV) Anticancer Complexes: Structure-Activity Relationship and Application as Orally Available Prodrugs. *ChemMedChem* **2017**, *12* (4), 300–311. <https://doi.org/10.1002/cmdc.201600577>.
- (31) Marzo, T.; Pillozzi, S.; Hrabina, O.; Kasparkova, J.; Brabec, V.; Arcangeli, A.; Bartoli, G.; Severi, M.; Lunghi, A.; Totti, F.; Gabbiani, C.; Quiroga, A. G.; Messori, L. Cis-Pt I₂(NH₃)₂: A Reappraisal. *Dalton Trans.* **2015**, *44* (33), 14896–14905. <https://doi.org/10.1039/C5DT01196E>.
- (32) Bancroft, D. P.; Lepre, C. A.; Lippard, S. J. Platinum-195 NMR Kinetic and Mechanistic Studies of Cis- and Trans-Diamminedichloroplatinum(II) Binding to DNA. *J. Am. Chem. Soc.* **1990**, *112* (19), 6860–6871. <https://doi.org/10.1021/ja00175a020>.
- (33) Davies, M. S.; Berners-Price, S. J.; Hambley, T. W. Slowing of Cisplatin Aquation in the Presence of DNA but Not in the Presence of Phosphate: Improved Understanding of Sequence Selectivity and the Roles of Monoaquated and Diaquated Species in the Binding of Cisplatin to DNA. *Inorg. Chem.* **2000**, *39* (25), 5603–5613. <https://doi.org/10.1021/ic000847w>.
- (34) Vinje, J.; Sletten, E.; Kozelka, J. Influence of DT20 and [d(AT)₁₀]₂ on Cisplatin Hydrolysis Studied by Two-Dimensional [¹H,¹⁵N] HMQC NMR Spectroscopy. *Chem. Eur. J.* **2005**, *11* (13), 3863–3871. <https://doi.org/10.1002/chem.200500002>.
- (35) Musumeci, D.; Platella, C.; Riccardi, C.; Merlino, A.; Marzo, T.; Massai, L.; Messori, L.; Montesarchio, D. A First-in-Class and a Fished out Anticancer Platinum Compound: Cis-[PtCl₂(NH₃)₂] and Cis-[PtI₂(NH₃)₂] Compared for Their Reactivity towards DNA Model Systems. *Dalton Trans.* **2016**, *45* (20), 8587–8600. <https://doi.org/10.1039/C6DT00294C>.
- (36) Tolbatov, I.; Marzo, T.; Cirri, D.; Gabbiani, C.; Coletti, C.; Marrone, A.; Paciotti, R.; Messori, L.; Re, N. Reactions of Cisplatin and Cis-[PtI₂(NH₃)₂] with Molecular Models of Relevant Protein

- Sidechains: A Comparative Analysis. *Journal of Inorganic Biochemistry* **2020**, 111096. <https://doi.org/10.1016/j.jinorgbio.2020.111096>.
- (37) Becke, A. D. Density- functional Thermochemistry. III. The Role of Exact Exchange. *The Journal of Chemical Physics* **1993**, 98 (7), 5648–5652. <https://doi.org/10.1063/1.464913>.
- (38) Lee, C.; Yang, W.; Parr, R. G. Development of the Colle-Salvetti Correlation-Energy Formula into a Functional of the Electron Density. *Phys. Rev. B* **1988**, 37 (2), 785–789. <https://doi.org/10.1103/PhysRevB.37.785>.
- (39) M. Frisch, G. T.; H. Schlegel. Gaussian 09 Citation | Gaussian.com (accessed May 31, 2020).
- (40) Grimme, S.; Antony, J.; Ehrlich, S.; Krieg, H. A Consistent and Accurate *Ab Initio* Parametrization of Density Functional Dispersion Correction (DFT-D) for the 94 Elements H-Pu. *The Journal of Chemical Physics* **2010**, 132 (15), 154104. <https://doi.org/10.1063/1.3382344>.
- (41) Andrae, D.; Haussermann, U.; Dolg, M.; Stoll, H.; Preuss, H. Energy-Adjusted *ab Initio* Pseudopotentials for the Second and Third Row Transition Elements. *Theoret. Chim. Acta* **1990**, 77 (2), 123–141. <https://doi.org/10.1007/BF01114537>.
- (42) Fukui, K. Formulation of the Reaction Coordinate. *J. Phys. Chem.* **1970**, 74 (23), 4161–4163. <https://doi.org/10.1021/j100717a029>.
- (43) McQuarrie, D.A.; Simon, J. D. *Molecular Thermodynamics*, University Science Books: Sausalito, CA, **1999**.
- (44) Weigend, F.; Ahlrichs, R. Balanced Basis Sets of Split Valence, Triple Zeta Valence and Quadruple Zeta Valence Quality for H to Rn: Design and Assessment of Accuracy. *Phys. Chem. Chem. Phys.* **2005**, 7 (18), 3297.
- (45) Miertuš, S.; Tomasi, J. Approximate evaluations of the electrostatic free energy and internal energy changes in solution processes. *Chem. Phys.* **1982**, 65, 239-245.
- (46) Miertuš, S.; Scrocco, E; Tomasi J. Electrostatic interaction of a solute with a continuum. A direct utilization of *ab initio* molecular potentials for the prevision of solvent effects. *Chem. Phys.* **1981**, 55, 117-129.

For Table of Contents Only

Iodido Pt(II) and Pt(IV) complexes reactivity in comparison with cisplatin and its Pt(IV) derivative has been computationally explored, with the aim to highlight the aspects at the origin of a possible difference in behavior. All the reported data do not support the hypothesis that the *soft* nature of the iodido ligand, on the basis of the HSAB principle, should strengthen the bond with the soft Pt center, likely because the bridging and leaving abilities of the I⁻ ligand prevail.

TOC graphics



Supporting Information

A computational study of iodido equatorial ligands influence on the mechanism of action of Pt(IV) and Pt(II) anti-cancer complexes

Stefano Scoditti,^a Vincenzo Vigna,^a Eslam Dabbish*^a and Emilia Sicilia*^a

^a Department of Chemistry and Chemical Technologies, Università della Calabria, 87036, Arcavacata di Rende (CS), Italy

Figure S1. Free energy profiles describing the a) ligand-bridged-H transfer and b) enolate β -carbon attack mechanisms for the reduction of chlorido analogue of complex **1** by ascorbate. Energies are in kcal·mol⁻¹ and relative to the first adduct.
S2

Figure S2. Free energy profiles describing the a) ligand-bridged-H transfer leading to the elimination of one chloride and detachment of one end of the ethylene diamine ligand. In the same figure are reported the two alternative pathways restoring the chelating ligand by elimination of b) water and c) acetate. Energies are in kcal·mol⁻¹ and relative to the first adduct.
S3

Figure S3. Free energy profiles describing the sulphur attack to the a) axial OH⁻ and b) equatorial I⁻ ligands in the ligand-bridged mechanism for the reduction of cisplatin by cysteine. Energies are in kcal·mol⁻¹ and relative to the first adduct.
S4

Figure S4. Free energy profile describing the chloride attack to chlorido ligands of complex **3** that results in ammonia displacement. Energies are in kcal·mol⁻¹ and relative to the first adduct.
S5

Figure S5. Free energy profile describing the NAM attack to the a) intact and b) aquated complex **2**. Energies are in kcal·mol⁻¹ and relative to the first adduct.
S6

Figure S6. Free energy profiles describing the NAM attack to the a) intact and b) aquated complex **3**. Energies are in kcal·mol⁻¹ and relative to the first adduct.
S7

Figure S7. Free energy profiles describing the NAM attack to the a) intact and b) aquated cisplatin. Energies are in kcal·mol⁻¹ and relative to the first adduct.
S8

Figure S8. Free energy profiles describing the two-step histidine attack to complex **3** leading to the final elimination of an ammonia ligand for a) **3** and b) cisplatin complexes.
S9

Figure S1.

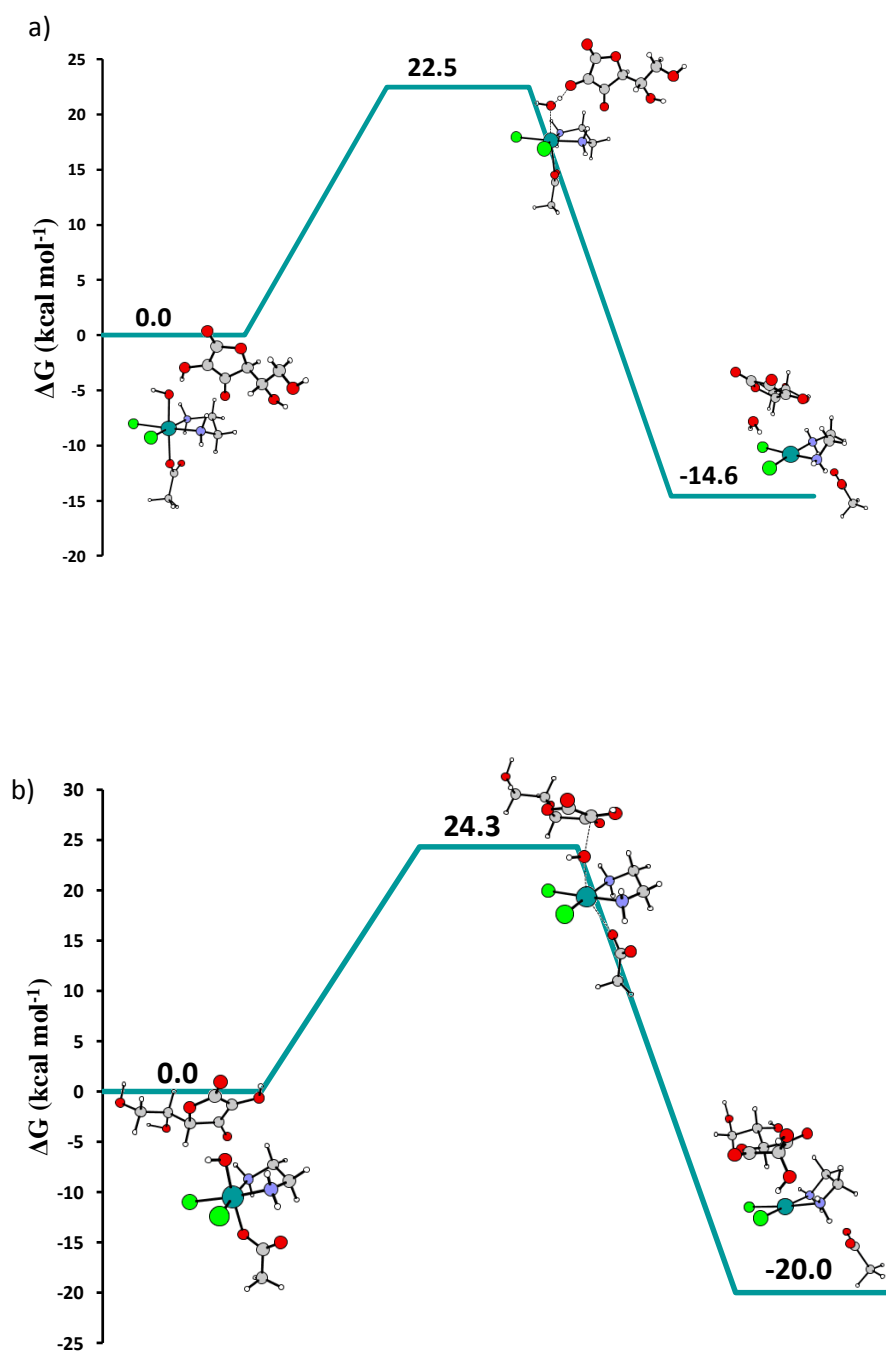


Figure S2.

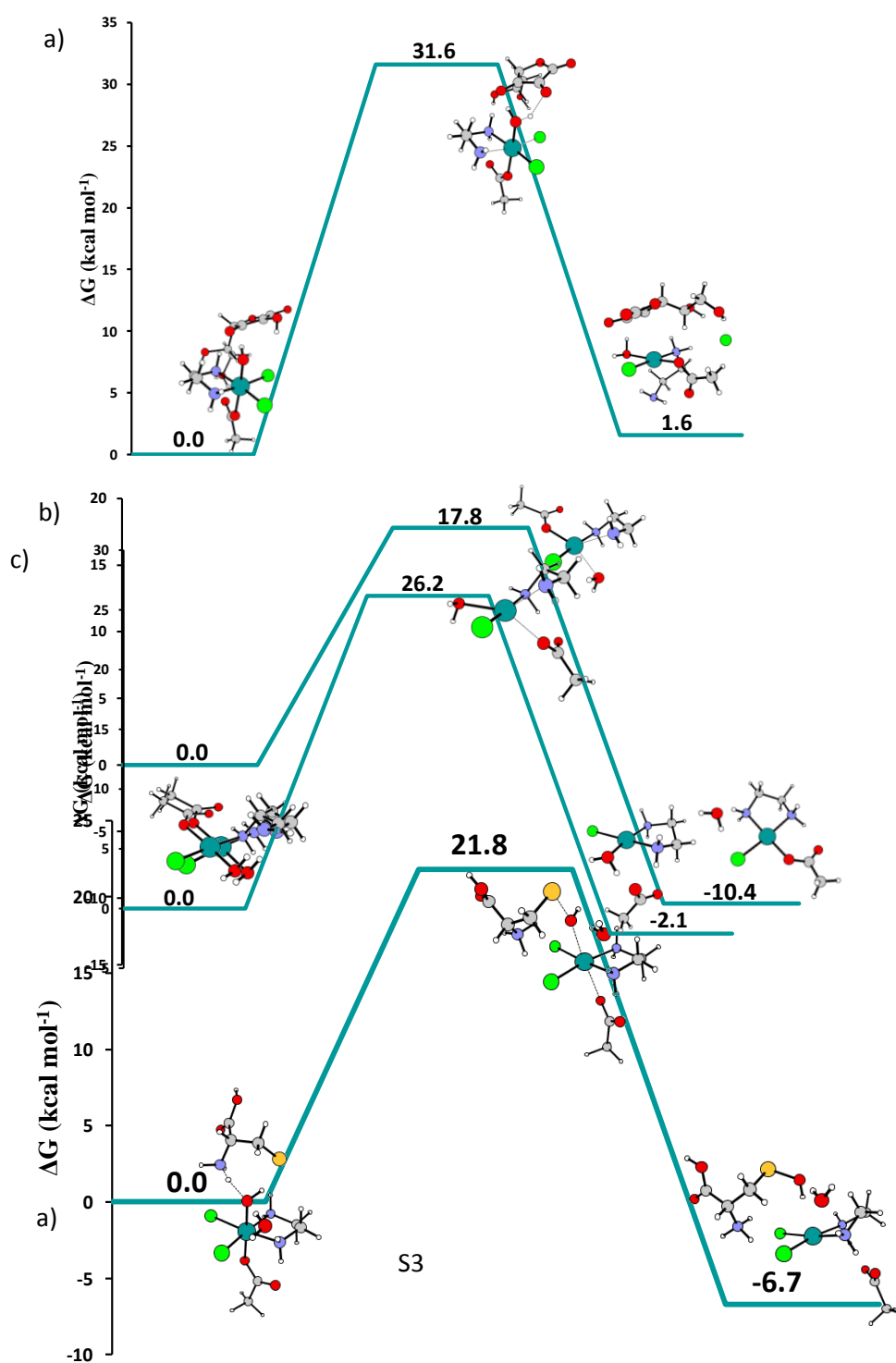


Figure S3.

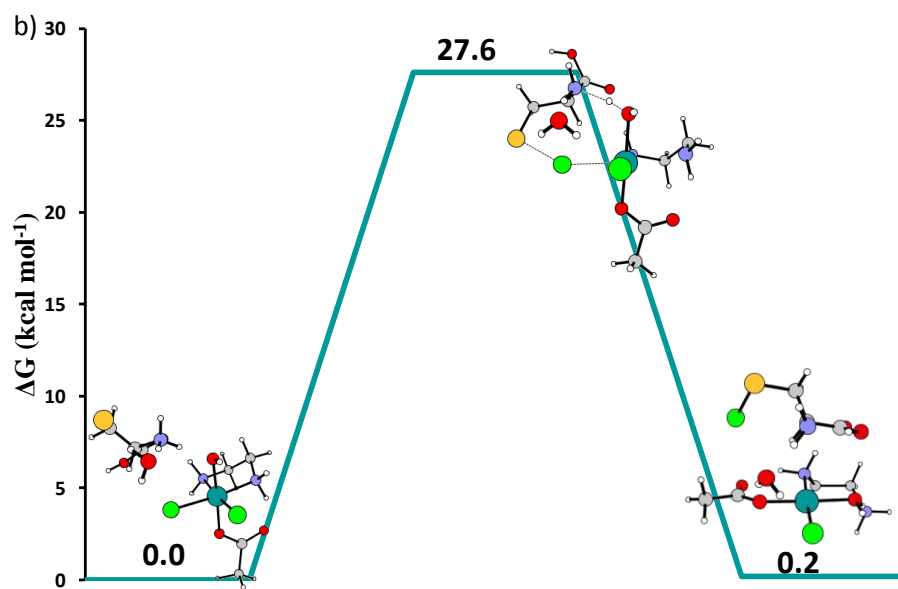


Figure S4.

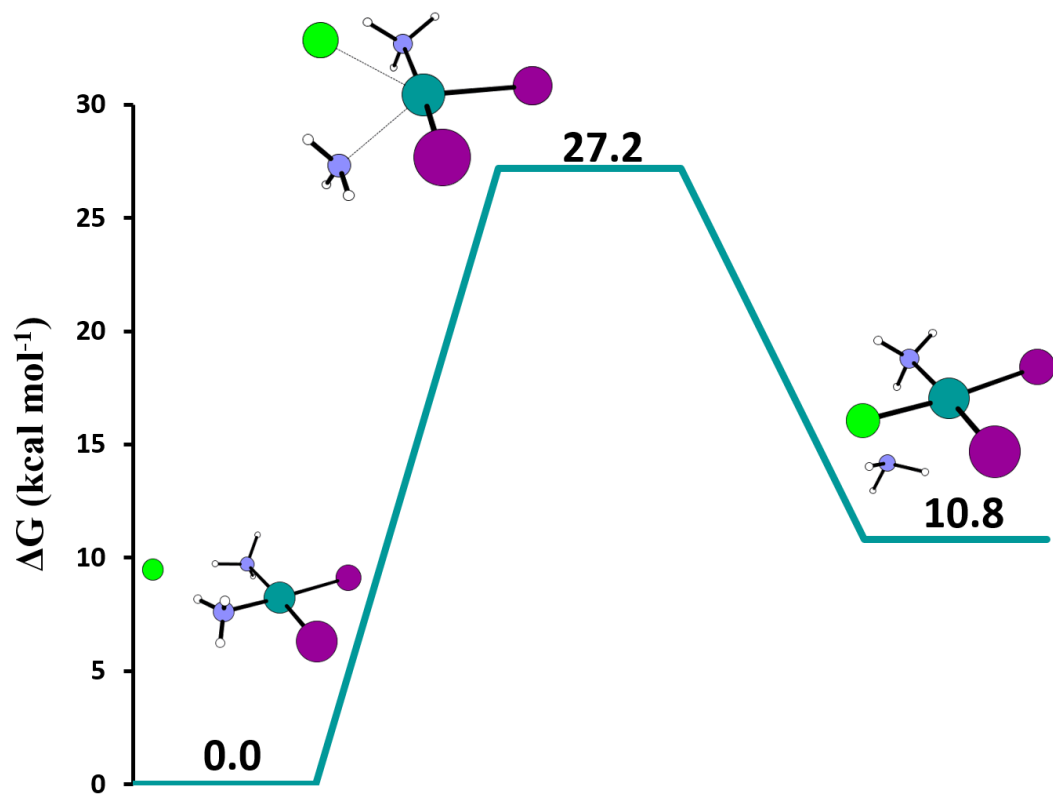


Figure S5.

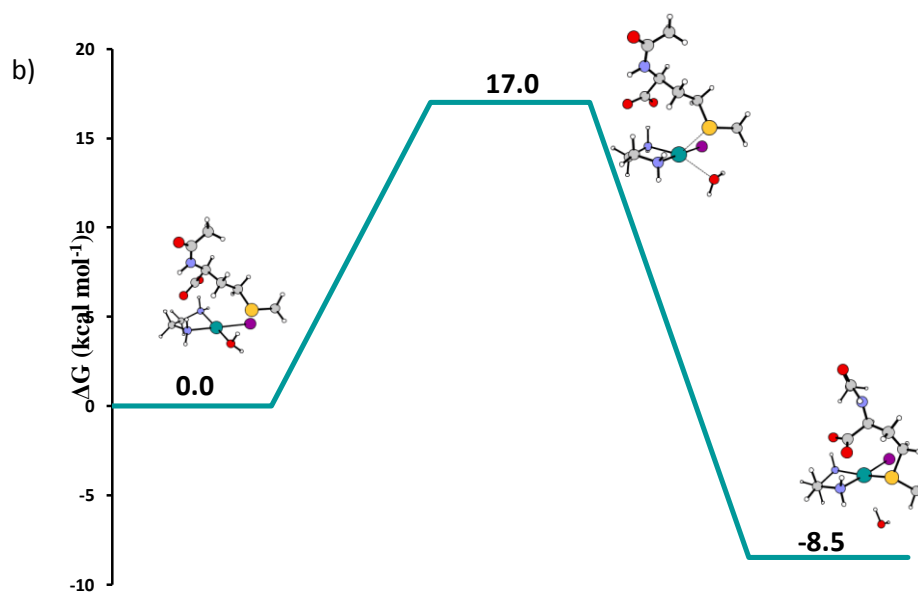
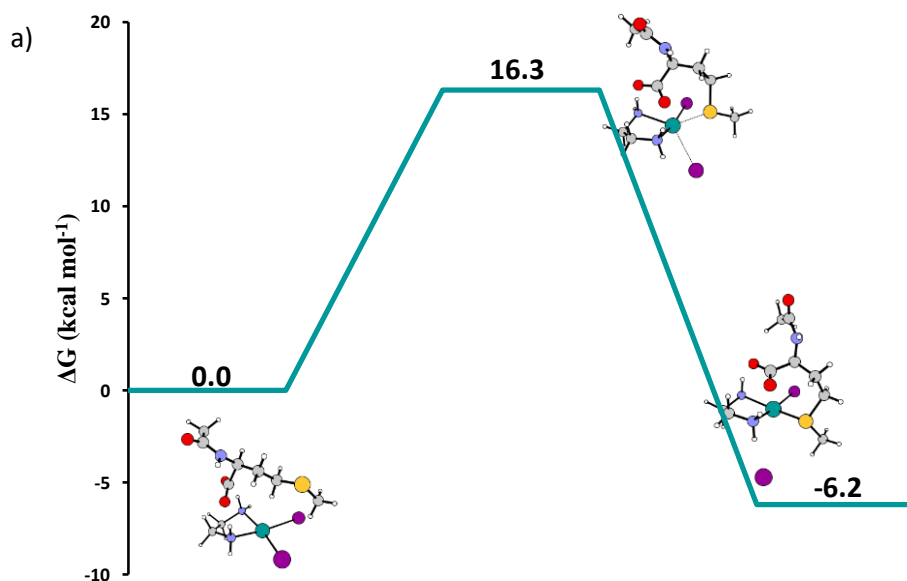
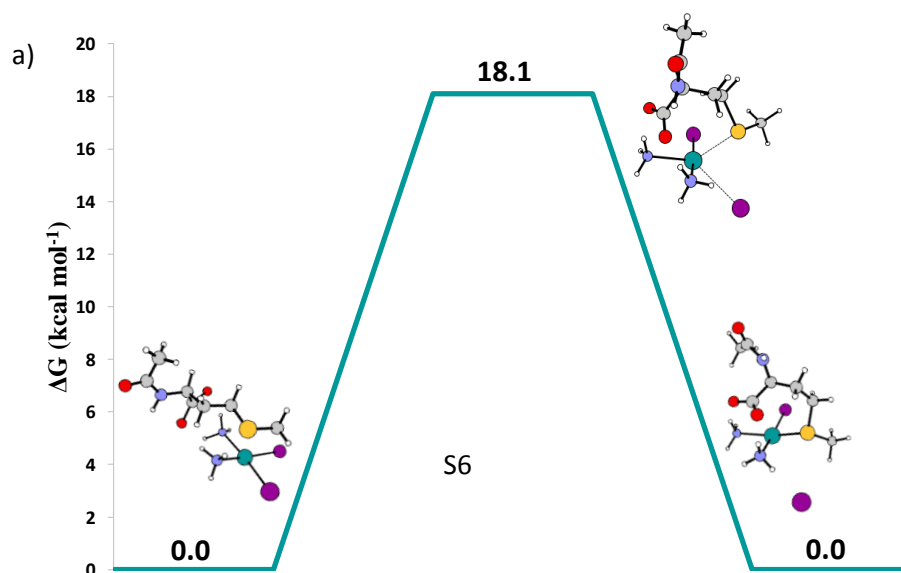
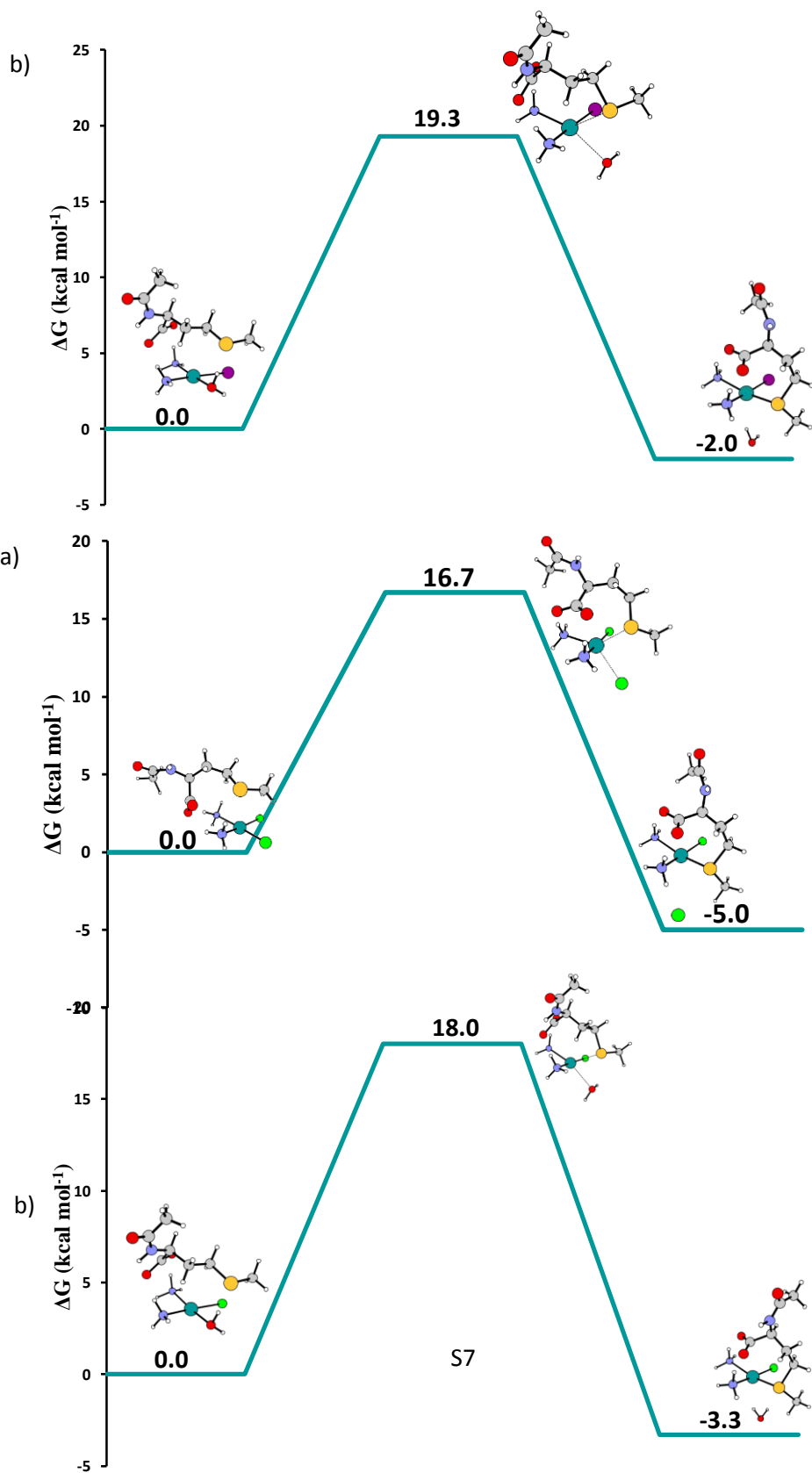


Figure S6.

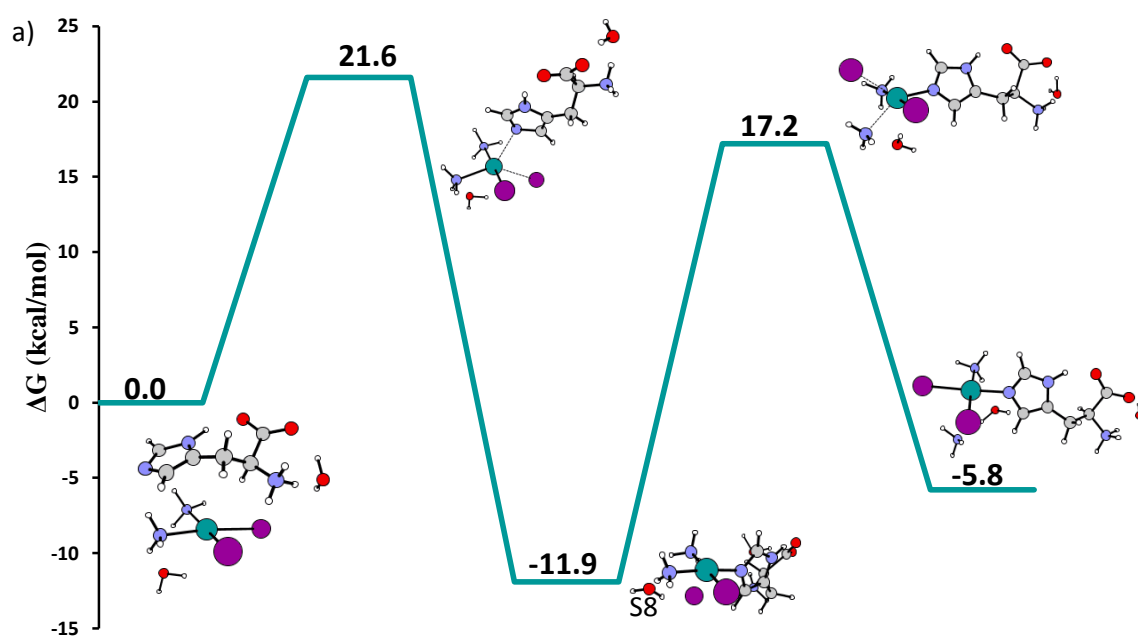


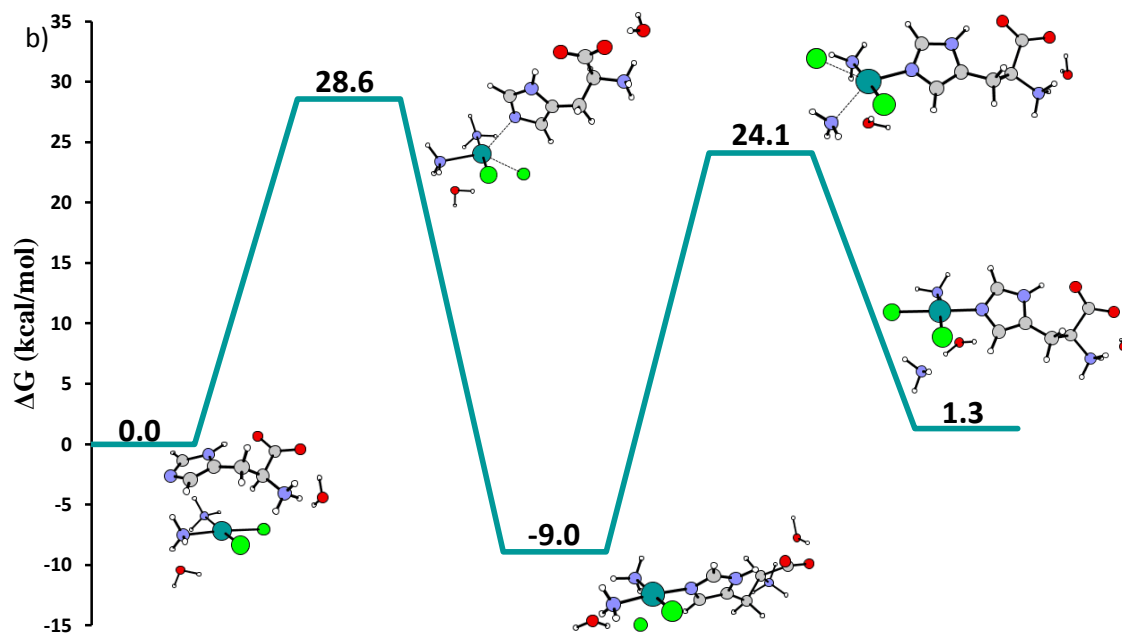
Figure



S7.

Figure
S8.





Chapter IX

Bioorthogonal

Photocatalytic

Reduction system of

Pt(IV) Prodrugs

Chapter IX Bioorthogonal Photocatalytic Reduction system of Pt(IV) Prodrugs

9.1 Riboflavin as a bioorthogonal photocatalyst for Pt(IV) reduction

9.1.1 Introduction

Salassa and co-workers have demonstrated that flavins (FL) under light irradiation of 460 nm can catalyse the reduction of Pt(IV) complexes in the presence of electron donors like NADH.¹⁻⁴ With further detailed studies, it turned out that upon light excitation FL excited singlet state undergo an intersystem crossing to the excited triplet state that is reductively quenched by NADH to give the reduced form of FL (FLH⁻) and NAD⁺. The doubly reduced FL can then undergo Pt(IV) reduction. The released Pt(II) is now ready to exert its anticancer effect while the oxidised form of FL can then repeat the catalytic cycle by a new molecule of NADH electron donor. See (Figure 9.1 and Scheme 9.1)

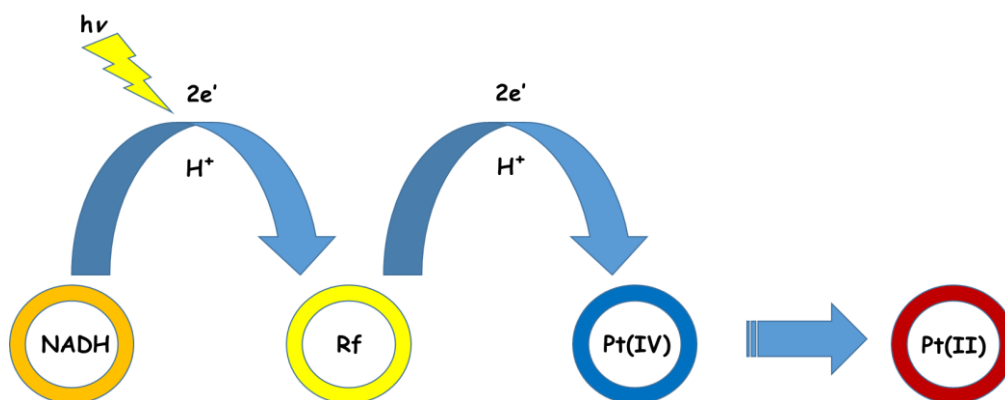
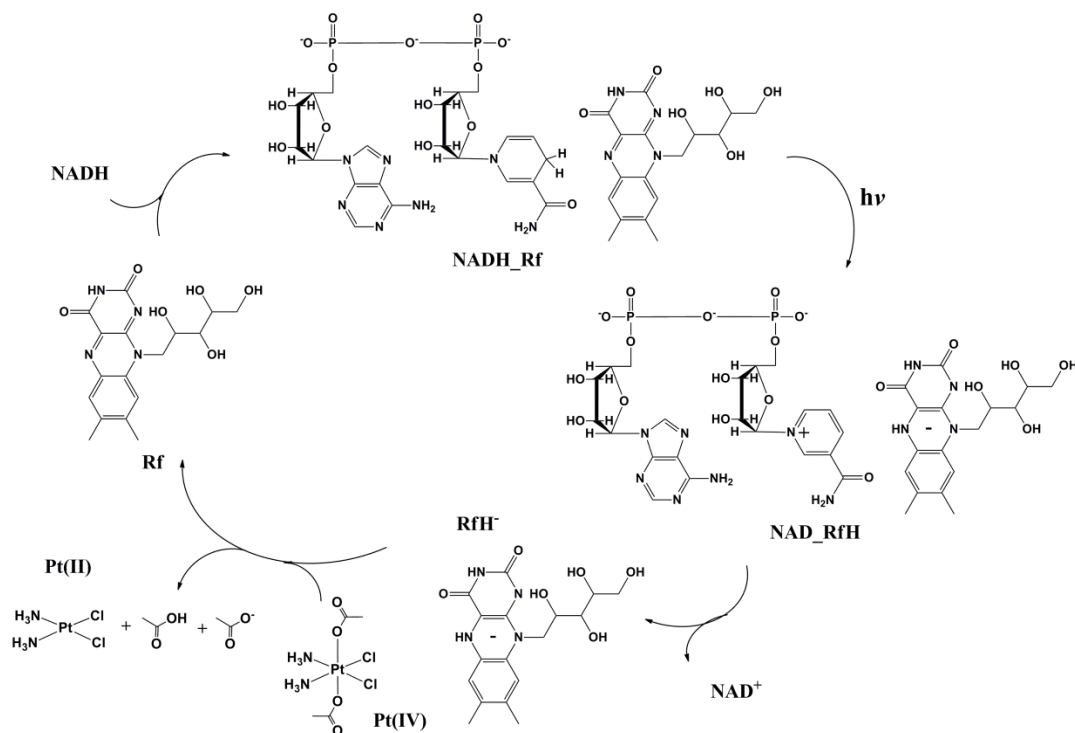


Figure 9.1 A schematic representation of the NADH/Rf/Pt(IV) photoreduction system



Scheme 9.1 A detailed representation of the NADH/Rf/Pt(IV) catalytic cycle

Several FL like riboflavin (**Rf**), tetraacetylriboflavin (**TARf**), lumiflavin (**Lf**), Flavin phosphate (**FMN**) and FL containing protein miniSOG were evaluated for their catalytic behaviour for a set of Pt(IV) complexes (Figure 9.2). The selected Pt(IV) complexes 1-4 were all of the dicarboxylate type that are known to be relatively stable against reduction in darkness with ascorbate a NADH or NADH/FL system reducing agents which is experimentally supported as well (**Scheme 9.2**).¹⁻⁴

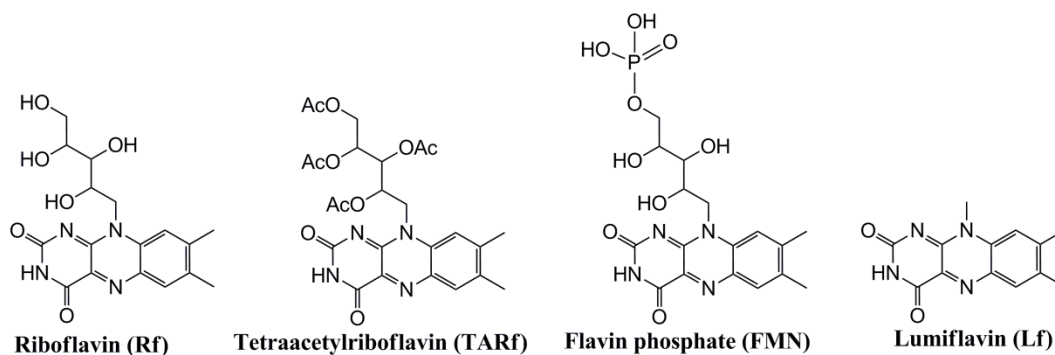
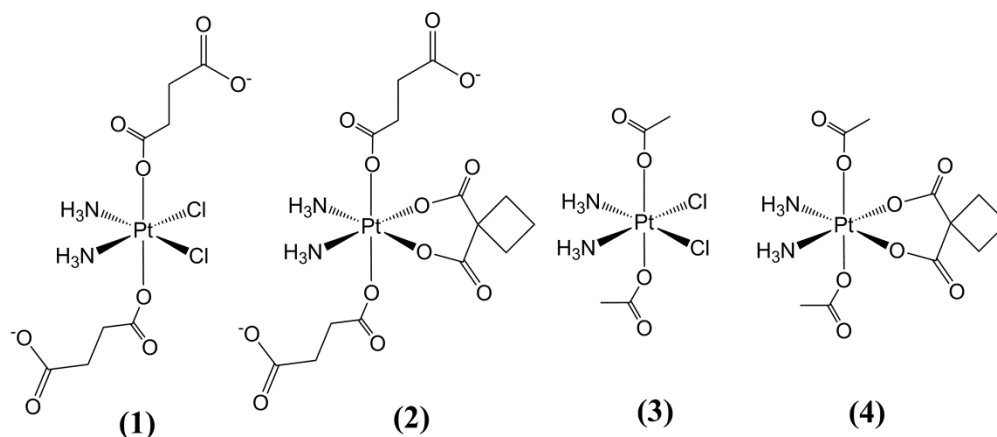


Figure 9.2 Chemical structures of different types of flavins



Scheme 9.2 Chemical structures of the four studied Pt(IV) dicarboxylate complexes $\text{cis,cis,trans-[Pt(NH}_3)_2(\text{Cl})_2(\text{O}_2\text{CCH}_2\text{CH}_2\text{CO}_2)_2]^{2-}$ (1), $\text{cis,cis,trans-[Pt(NH}_3)_2(\text{O}_4\text{C}_6\text{H}_6)(\text{O}_2\text{CCH}_2\text{CH}_2\text{CO}_2)_2]^{2-}$ (2), $\text{cis,cis,trans-[Pt(NH}_3)_2(\text{Cl})_2(\text{O}_2\text{CCH}_3)_2]$ (3), and $\text{cis,cis,trans-[Pt(NH}_3)_2(\text{O}_4\text{C}_6\text{H}_6)(\text{O}_2\text{CCH}_3)_2]$ (4)

9.1.2 Aim of study

Our aim is to computationally study the mechanism and energetics of the reaction between NADH and riboflavin both in darkness and in light. In addition, we further studied the mechanism of reduction of the four different Pt(IV) 1-4 complexes using the reduced form of riboflavin as the reducing agent in supported by the available experimental data about the relative rate of reduction of the four complexes.

9.1.3 Highlighting results

NADH is reported to undergo a charge transfer complex formation with FL containing molecules particularly in protein surrounding atmosphere of enzymes which is then followed by a process of proton coupled electron transfer to give the reduced form of flavin FLH^- and NAD^+ . In analogy, we have computationally identified a complex formation between the NADH and Rf with a clear π - π interaction between the nicotinic and isoalloxazine rings of

NADH and Rf respectively with the HOMO located on the nicotinic ring and LUMO located on the isoalloxazine rings making the complex ready to undergo the electron transfer process, see **Figure 9.3**.

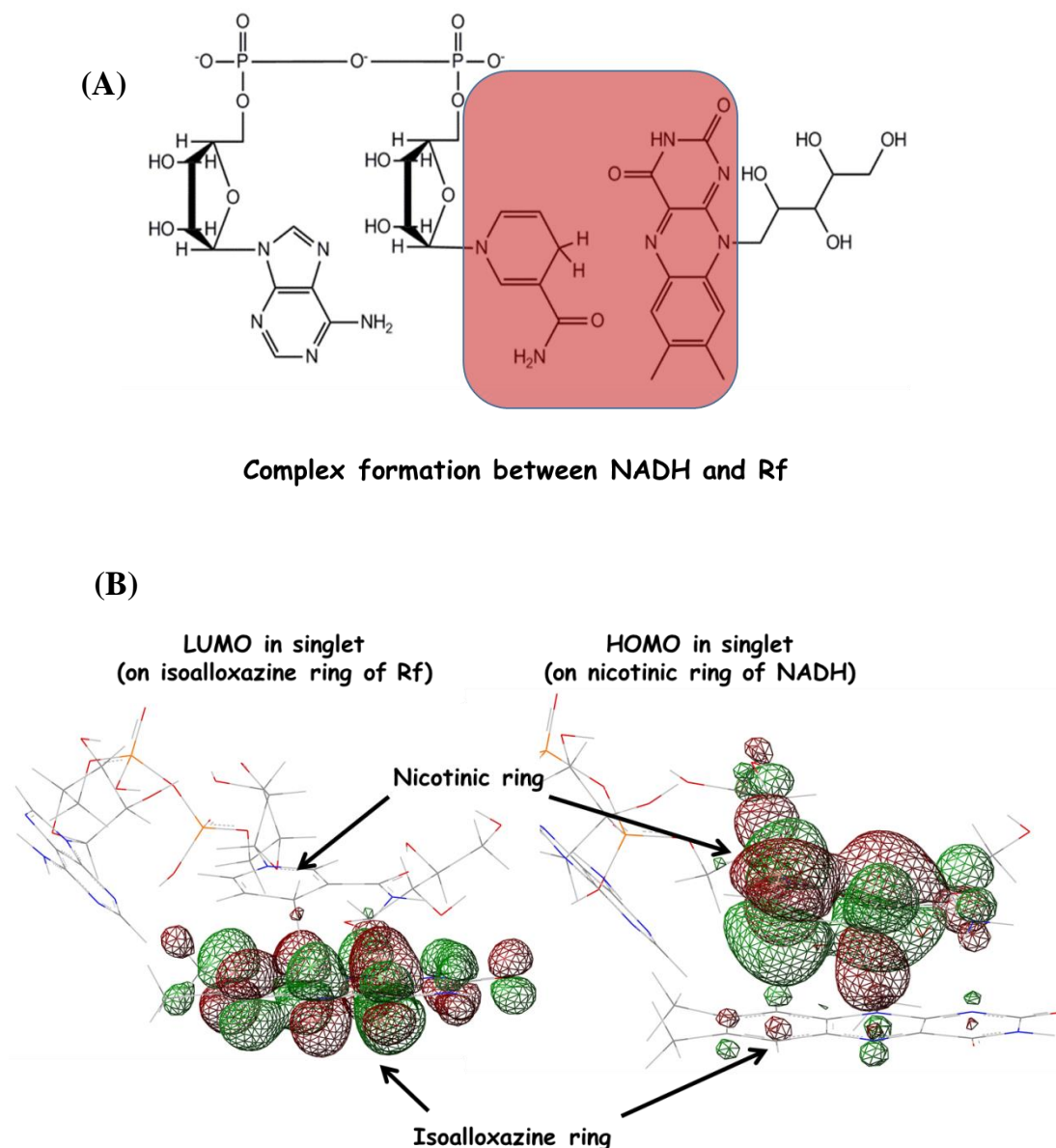


Figure 9.3 (A) Shows the adduct formation between the nicotinic ring of NADH and isoalloxazine ring of Rf (B) The HOMO and LUMO distribution over the formed adduct in singlet state and the π - π interaction between the nicotinic and isoalloxazine rings.

In **Figure 9.4**, we are reporting the potential energy surface (PES) of the reaction between NADH and Rf in both singlet and triplet states. The singlet

PES which corresponds to the reaction in darkness involves a transition state that is 17.7 kcal higher than the entrance channel with a clear proton movement from NADH to Rf with a calculated rate constant of $7.8 \times 10^{-1} \text{ s}^{-1}$. The formed product which is an adduct of NAD^+ and RfH^- is endergonic by about 2 kcal with a backward reaction rate constant of $2.3 \times 10^1 \text{ s}^{-1}$ and overall equilibrium constant of 3.4×10^{-2} indicating the possibility of a competitive backward reaction. Indeed, this is agreeing with the experimental finding that in absence of light the reaction between NADH and FL is recognised by the formation of FLH^- however significantly less efficient than in presence of light.

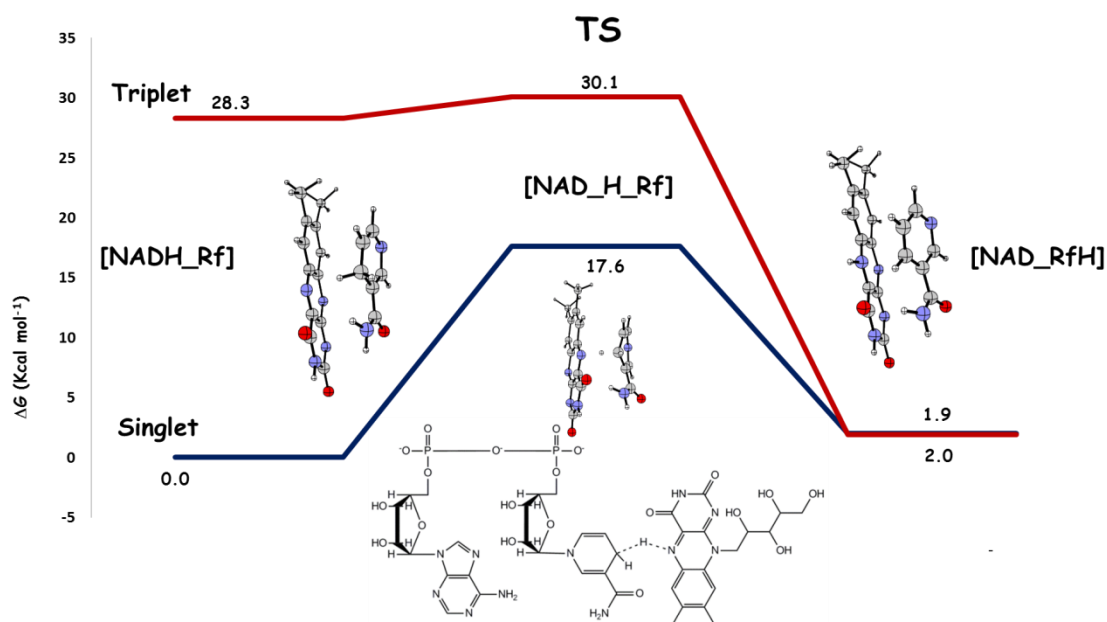


Figure 9.4 Free energy profiles describing the reaction between NADH and Riboflavin (Rf) in both singlet and triplet states. A reduced model (for simplification) and schematic representation of the singlet transition state, adduct and product are reported. Relative energies are in kcal mol^{-1} and calculated with respect to the zero reference energy of the initial adduct in singlet.

We have further supported this by modelling the reaction in triplet state that corresponds to the light excited state supported by the reported fact that it is the triplet form of the FL that is involved in the reaction which rules out the possibility of the reaction going on in the excited singlet state. Upon light

excitation to the triplet state and with HOMO/LUMO distribution as clarified in the ground state, one electron is expected to be re-localised to the isoalloxazine ring of Rf. The triplet state adduct can then undergo a proton coupled electron transfer process that is almost barrier less giving a product that is highly stabilised by 26.4 kcal relative to the triplet state entrance channel. The reaction in triplet state got a calculated rate constant of $3.0 \times 10^{11} \text{ s}^{-1}$ with an equilibrium constant of 2.3×10^{19} clearly indicating a much faster and more favourable reaction compared to the singlet state.

In the second step, we have turned our attention to the reduction step of Pt(IV) complexes using the NADH/Rf photoactivated system. As previously pointed out, it was proved that it is the FLH⁻ moiety that undergoes the catalytic reduction process of Pt(IV). Based on this fact and on the experimental finding of the extent of reduction of a four different studied Pt(IV) complexes 1-4, we have started investigating the mechanism of the reduction process of Pt(IV) with RfH⁻ to try rationalising our previous experimental results. Pt(IV) reduction is a two electron reduction process that can involve either an outer sphere or an inner sphere mechanism.

The reduction potential of the complexes 1-4 were calculated as per reported Baik et al. approach which depends on splitting the reduction process into electron accepting and ligand departure events where the first electron acceptance step is used to calculate the theoretical reduction potential. This approach was adopted owing to the known experimental challenge of determining the reduction potential of Pt(IV) complexes because of the irreversibility of the reduction when undergoing cyclic voltammetry measurements since the reduction is accompanied by a chemical change and an axial ligands leave. The calculated reduction potential reported in Table 9.1 implies that complexes are readily reduced in the descending order of $4 > 2 > 3 > 1$ which contradicts the experimentally measured rate of reduction using the

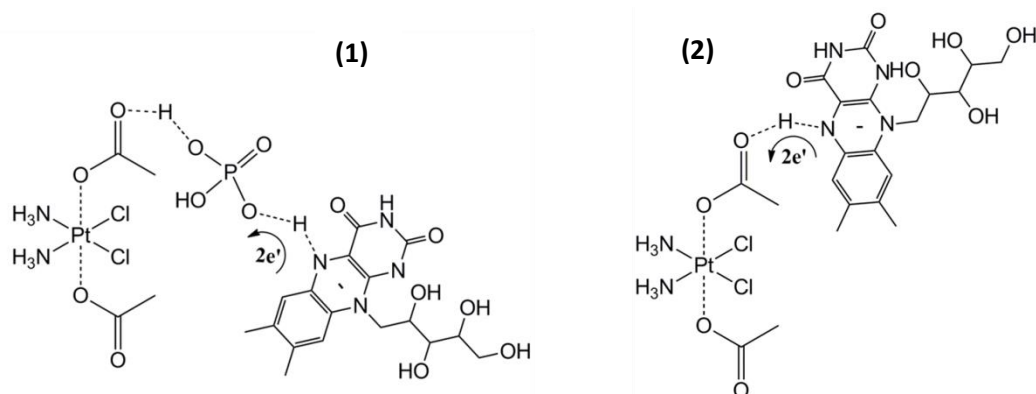
NADH/Rf photoactivated system which is $3 > 1 > 4 > 2$. This can rule out the possibility of a typical outer sphere mechanism.

complex	1	2	3	4
E°	-0.128	-0.069	-0.076	-0.0104

Table 9.1 Standard reduction potentials, in eV, calculated as the energy change that accompanies the first step one-electron transfer for the reduction of the six-coordinate Pt(IV) complexes in the proposed by Baik et al. decomposition scheme

When considering the inner sphere mechanism, we have taken monodeprotonated dehydroascorbate as benchmark reducing agent that are known to act on Pt(IV). This helps to verify our experimental findings about the stability of reduction of the studied Pt(IV) complexes to ascorbate reduction as well as understanding the efficiency of the NADH/Rf photoactivated system relative to a known benchmark. The suggested mechanism involves a hydride transfer from ascorbate to the carboxylate oxygen of the axial acetate group together with the detachment of the corresponding acetate group leading to the formation of cisplatin, dehydroascorbic acid, acetate and acetic acid. The calculated free energy barrier for the reduction of complex 3 with ascorbate was calculated to be 24.2 kcal/mol which is relatively high compared to our previously reported studies of a set of Pt(IV) complexes reduction by ascorbate. This can explain the stability of complex 1-4 of the dicarboxylate type to reduction by ascorbate.

Taking the RfH⁻ as the reducing agent to study the reduction mechanism of the four complexes 1-4, two different inner sphere mechanisms were suggested 1) buffer assisted ligand-bridged H transfer mechanism and 2) Regular ligand-bridged H transfer mechanism (Scheme 9.3).



Scheme 9.3 Two suggested mechanisms (1) buffer assisted ligand-bridged H transfer (2) Regular ligand-bridged H transfer mechanism

In mechanism (1), a dihydrogen phosphate molecule that is abundant in the used buffer medium was used as an assisting molecule that helps the transfer of the H^+ from the RfH^+ molecule to one of the axial carboxylate leaving groups. The metal centre is reduced with the leave of the two axial carboxylate ligands. Compared to the ascorbate benchmark, all the reported transition state free energy barrier in Figure 9.5 shows a dramatic decrease suggesting that the process is extremely feasible with complex 2 having the highest energy barrier of 14.5 kcal/mol out of 1-4 complexes that is 10 kcal less than that of ascorbate. All the products are strongly thermally stabilised with up to 51.6 exergonic stabilisation for complex 3. It is worth mentioning that the extent of stabilisation of the reduction products as per mechanism (1) is very prominent compared to ascorbate case that is only 6.3 kcal stabilised agrees with the detected experimental order for the extent of reduction of the studied complexes with the order of $3 > 1 > 4 > 2$.

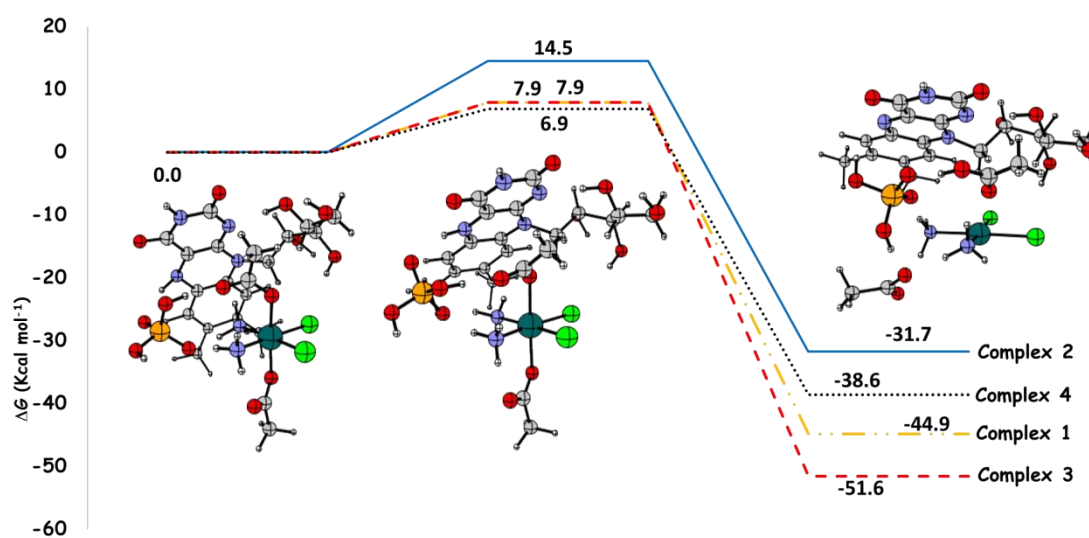


Figure 9.5 Free energy profile describing the reaction of complexes 1-4 with Rf as per the buffer assisted ligand-H⁻ transfer mechanism.

In mechanism (2), the H⁻ is directly transferred from RfH⁻ to the axial carboxylate. In Figure 9.6, although the calculated transition state free energy barrier do not show a particular trend among the studied complexes but they all seem accessible. The transition state geometry are stabilised by a group of a direct hydrogen bondings between the Rf molecule and Pt(IV) complex in which the ribityl tail of the RfH⁻ helps in the structure stabilisation shedding light on a possible role that might be played by the substituent on FL molecule as reported by our group to have an effect on the extent of reduction upon using different FL with different substituents. On the other hand, the formed products that are again strongly stabilised follows the experimental trend of the extent of the complexes 1-4 reduction.

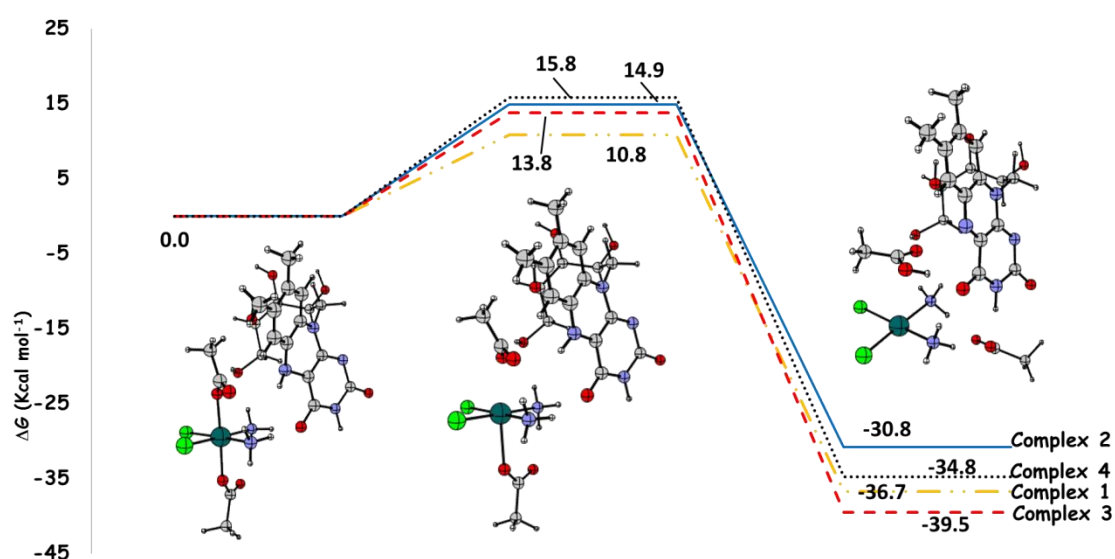


Figure 9.6 Free energy profile describing the reaction of complexes 1-4 with Rf as per the regular ligand-H⁻ transfer mechanism.

The results of both mechanisms (1) and (2) and its comparison with the experimental findings for the extent of reduction of complexes 1-4 gives an indication that the reaction might be more thermodynamically controlled than being kinetically controlled. In addition, although mechanism (1) seems to be more energetically favourable but this can't rule out the possibility of mechanism (2) given the direct interaction of RfH⁻ molecule with the Pt(IV) complex in which the FL substituent group got a direct impact.

Indeed, the experimental and mechanistic findings agrees with our previously suggested theoretical explanation for the extent of reduction complexes 1-4 by NADF/FL photoactivated systems. Complexes 1 and 3 with a cisplatin equatorial backbone is expected to be easily reduced compared to carboplatin backbone complexes owing to the weaker electrostatic interaction between Pt and equatorial ligands in cisplatin compared to carboplatin. On the other hand, when comparing complex (1 and 3) and (2 and 4), acetate groups are a better leaving groups compared to succinates, making complex 3 easier to be reduced compared to 1.

References

- 1) S. A.-de Castro, E. Ruggiero, A. R.-de-Angulo, E. Rezabal, J. C. M.- Rivas, X. Lopez, F. L. Gallego, L. Salassa, *Chem. Sci.*, **2017**, 8, 4619-4625.
- 2) S. A.-de Castro, A. Terenzi, S. Hager, B. Englinger, A. Faraone, J. C. Martinez, M. Galanski, B. K. Keppler, W. Berger, L. Salassa, *Scientific Reports*, **2018**, 8, 17198.
- 3) S. A.-de Castro, A. L. Cortajarena, F. L. Gallego, L. Salassa, *Angew. Chem. Int. Ed.*, **2018**, 57, 3143-3147.
- 4) J. G. Pereda, V. M. Martinez, E. Rezabal, X. Lopez, C. Garino, F. Mancin, A. L. Cortajarena, L. Salassa, *ACS Catal.*, **2020**, 10, 1, 187-196.

Paper IX

**Bioorthogonal Photocatalytic Reduction system of Pt(IV)
Prodrugs**

Riboflavin as a bioorthogonal photocatalyst for Pt(IV) reduction

Manuscript under preparation
